

GEOLOGY, GEOCHEMISTRY AND METALLOGENY  
OF THE BURNT LAKE AREA, CENTRAL MINERAL BELT  
LABRADOR, CANADA

CENTRE FOR NEWFOUNDLAND STUDIES

**TOTAL OF 10 PAGES ONLY  
MAY BE XEROXED**

(Without Author's Permission)

LEONARD M. MACKENZIE, B.Sc., (Honours)







National Library  
of Canada

Bibliothèque nationale  
du Canada

Canadian Theses Service

Service des thèses canadiennes

Ottawa, Canada  
K1A 0N4

## NOTICE

The quality of this microform is heavily dependent upon the quality of the original thesis submitted for microfilming. Every effort has been made to ensure the highest quality of reproduction possible.

If pages are missing, contact the university which granted the degree.

Some pages may have indistinct print especially if the original pages were typed with a poor typewriter ribbon or if the university sent us an inferior photocopy.

Reproduction in full or in part of this microform is governed by the Canadian Copyright Act, R.S.C. 1970, c. C-30, and subsequent amendments.

## AVIS

La qualité de cette microforme dépend grandement de la qualité de la thèse soumise au microfilmage. Nous avons tout fait pour assurer une qualité supérieure de reproduction.

S'il manque des pages, veuillez communiquer avec l'université qui a conféré le grade.

La qualité d'impression de certaines pages peut laisser à désirer, surtout si les pages originales ont été dactylographiées à l'aide d'un ruban usé ou si l'université nous a fait parvenir une photocopie de qualité inférieure.

La reproduction, même partielle, de cette microforme est soumise à la Loi canadienne sur le droit d'auteur, S.R.C. 1970, c. C-30, et ses amendements subséquents.

**GEOLOGY, GEOCHEMISTRY AND METALLOGENY**  
**OF**  
**THE BURNT LAKE AREA, CENTRAL MINERAL BELT**  
**LABRADOR, CANADA**

**BY**

**LEONARD M. MACKENZIE, B.Sc., (Honours)**

**A thesis submitted to the School of Graduate  
Studies in partial fulfilment of the  
requirements for the degree of  
Master of Science**

**Department of Earth Science  
Memorial University of Newfoundland**

**April, 1991**

**St. John's**

**Newfoundland**





National Library  
of Canada

Bibliothèque nationale  
du Canada

Canadian Theses Service    Service des thèses canadiennes

Ottawa, Canada  
K1A 0N4

The author has granted an irrevocable non-exclusive licence allowing the National Library of Canada to reproduce, loan, distribute or sell copies of his/her thesis by any means and in any form or format, making this thesis available to interested persons.

The author retains ownership of the copyright in his/her thesis. Neither the thesis nor substantial extracts from it may be printed or otherwise reproduced without his/her permission.

L'auteur a accordé une licence irrévocable et non exclusive permettant à la Bibliothèque nationale du Canada de reproduire, prêter, distribuer ou vendre des copies de sa thèse de quelque manière et sous quelque forme que ce soit pour mettre des exemplaires de cette thèse à la disposition des personnes intéressées.

L'auteur conserve la propriété du droit d'auteur qui protège sa thèse. Ni la thèse ni des extraits substantiels de celle-ci ne doivent être imprimés ou autrement reproduits sans son autorisation.

ISBN 0-315-68265-5

Canada



**Frontispiece: Scenery of the Burnt Lake area. White Bear Mountain in the background.**

**ABSTRACT**

The Burnt Lake area, located within the central region of the Central Mineral Belt of Labrador, is underlain by the Early Proterozoic (1855 Ma) supracrustal sequence of the Upper Aillik Group felsic volcanic and associated sedimentary rocks. Intruded into this volcanic pile is the 1650 Ma Burnt Lake Granite, a high level, leucocratic, post-tectonic granite.

The area was the focus of uranium exploration in the late 1970's and hosts open pit reserves of 140,000 tonnes grading 0.082%  $U_3O_8$ .

Uranium was originally deposited (1855 Ma) by subvolcanic leaching of volcanic glasses and concentration during K-metasomatic alteration of the felsic volcanic rocks (Burnt Lake Potassic Showing) and later upgraded during a period of magmatic and metamorphic activity between 1800 Ma - 1740 Ma (Burnt Lake Sodic, Emben and Aurora River Showings). This produced uranium enrichments associated with intense Na-metasomatism and is characterized as epigenetic-hydrothermal.

Base metal (and possibly some uranium) mineralization was later superimposed on the Burnt Lake uraniferous occurrences which originated as magmatic fluids from the Burnt Lake Granite (1650 Ma). The mineralization is characterized as epigenetic magmatic-hydrothermal (granophile) with potassium, lead, zinc, copper, fluorite and molybdenite enrichments.



Model ages from a galena separate from Burnt Lake, hosted in felsic volcanic rocks of the Upper Aillik Group (1855 Ma) are 1651 Ma for the lower crust-type reservoir. This indicates an age of 1651 Ma for at least some of the lead mineralization derived from a magmatic source.

An Rb/Sr isocron for the Burnt Lake Granite has produced an age of  $1651 \pm 140$  Ma, however, the isotopic signature has been disturbed by fluid effects and a partial re-setting of the isotopic clock during the Grenville Orogeny.

Significant concentrations of molybdenite occur near the contact of the Burnt Lake Granite and the meta-felsic volcanic rocks. Differentiation trends in geochemical data for this granite indicate vapour phase concentration towards the top of the pluton.

### ACKNOWLEDGEMENTS

The author acknowledges financial support provided by a Memorial University of Newfoundland graduate fellowship and teaching assistantships. The field work was funded by the Geological Survey of Canada (GSC) through a contract from a Canada-Newfoundland Mineral Development Agreement (MDA), a NSERC Operating Grant, a NSERC Northern Supplement to Dr. D.H.C. Wilton and a grant from the Northern Science Training Program to the author. Logistical support for the field work was provided by the Newfoundland Department of Mines and Energy (NDME) through W. Tuttle, K. O'Quinn, R.J. Wardle, A. Kerr and M. Batterson, and P. Hum of Brinex Exploration Ltd.

Dr. Derek Wilton is gratefully thanked for his supervision, discussions and continued encouragement during the course of this study.

C. MacDougall, J. North and C. Pumphrey are thanked for countless discussions and memorable experiences throughout this study. L. Fiander provided able field assistance while enduring the wilds of Labrador.

Other individuals that are thanked for their discussions and comments include R.J. Wardle, A. Kerr, S.S. Gandhi, T. Birkett and D. Kontak.

L. Stockley is owed a special thanks for her encouragement through the completion of this thesis.

## TABLE OF CONTENTS

	page
Abstract.....	(iii)
Acknowledgements.....	(v)
List of Figures .....	(ix)
List of Tables .....	(xix)
List of Maps .....	(xx)
 <b>CHAPTER 1            INTRODUCTION</b>	
1.1 Introduction.....	1
1.2 Location, Access and Physiography.....	2
1.3 Exploration History.....	5
1.4 Previous Geological Work.....	8
1.5 Methodology of Present Study.....	10
 <b>CHAPTER 2            REGIONAL GEOLOGY</b>	
2.1 Introduction.....	12
2.1.1 Central Mineral Belt.....	12
2.1.2 Nain Province .....	13
2.1.3 Makkovik Province.....	16
2.2 Tectonic Evolution of Labrador.....	17
2.2.1 Introduction.....	17
2.2.2 Hudsonian Orogeny.....	17
2.2.3 Makkovikian Orogeny.....	19
2.2.4 Labradorian Orogeny.....	19
2.2.5 Grenvillian Orogeny.....	20
2.2.6 The Grenville Front in Labrador.....	20
2.3 Proterozoic Supracrustal Rocks.....	22
2.3.1 Lower and Upper Aillik Groups.....	22
2.3.2 Lower Aillik Group.....	22
2.3.3 Upper Aillik Group.....	24
2.3.4 Moran Lake Group.....	26
2.3.5 Bruce River Group.....	27
2.3.6 Trans-Labrador Magmatism.....	28
2.4 Property Geology.....	29
2.4.1 Unit 1.....	30
2.4.2 Unit 2.....	33
2.4.3 Unit 3.....	36
2.4.4 Unit 4.....	36
2.4.4.1 Unit 4a.....	40
2.4.4.2 Unit 4b.....	40
2.4.4.3 Unit 4c.....	42
2.4.4.4 Unit 4d.....	42
2.4.4.5 Unit 4e.....	43



2.5	Intrusive Rocks.....	50
2.5.1	Unit 5a.....	50
2.5.2	Unit 5b.....	51
2.5.3	Unit 5c.....	52
2.5.4	Unit 6 .....	52
2.5.5	Unit 7 .....	53
2.6	Structural Geology .....	60
2.6.1	Regional Structural Geology .....	60
2.6.2	Local Structural Geology .....	60

### CHAPTER 3 LITHOGEOCHEMISTRY

3.1	Upper Aillik Group .....	63
3.1.1	Methodology .....	63
3.1.2	Major Element Patterns and Classification..	64
3.1.2.1	Upper Aillik Group.....	65
3.1.3	Trace Element Patterns and Classification..	85
3.1.3.1	Classification.....	93
3.1.4	Rare-Earth-Element Patterns.....	99
3.2	Granitoids in the Burnt Lake Area.....	101
3.2.1	Introduction.....	101
3.2.2	Major and Trace Element Patterns and Classification.....	101
3.2.3	Rare-Earth-Patterns.....	119
3.2.4	Chemical Zonation in the Burnt Lake Granite (BLG). .....	125
3.3	Geochronology.....	127
3.3.1	Rb-Sr isotopic data from the BLG.....	127

### CHAPTER 4 MINERALIZATION

4.1	Introduction.....	134
4.2	Uranium Mineralization in the Burnt Lake Area..	135
4.2.1	Burnt Lake North (Main) Zone.....	136
4.2.2	Burnt Lake Central Zone.....	137
4.2.3	Burnt Lake Northwest Zone.....	147
4.2.4	Burnt Lake Southwest Zone.....	149
4.2.5	Emben Main Zone.....	156
4.2.6	Emben South Zone.....	161
4.2.7	Aurora River Zone.....	168
4.3	Base-Metal Sulphide Mineralization .....	172
4.3.1	Burnt Lake Main Zone .....	172
4.3.2	Burnt Lake Northwest Zone .....	173
4.3.3	Burnt Lake Southwest Zone .....	175
4.3.4	Emben South Zone .....	176
4.4	Granite-Hosted Mineralization .....	179

**CHAPTER 5 GEOCHEMISTRY OF MINERALIZED SHOWINGS**

5.1	Introduction .....	183
5.2	Burnt Lake Showings .....	184
5.2.1	Major Element Patterns .....	184
5.2.2	Trace Element Patterns .....	197
5.3	Emben Showings .....	206
5.3.1	Major Element Patterns .....	206
5.3.2	Trace Element Patterns .....	212
5.4	Aurora River Showing .....	216
5.4.1	Major and Trace Element Patterns .....	216
5.5	Geochemical Comparison between the Radioactive Zones .....	221
5.5.1	Major Element Patterns .....	229
5.5.2	Trace Element Patterns .....	233
5.5.3	Statistical Interpretation .....	241
5.6	Comparison with Non-Mineralized Aillik Group ..	247
5.6.1	Rare-Earth-Element Patterns .....	256
5.7	Pb Isotope Data .....	260
5.8	Sulphur Isotope Data .....	264
5.9	Summary of the Radioactive Zones. ....	265

**CHAPTER 6 DISCUSSION AND CONCLUSIONS**

6.1	Uranium Ore Genesis .....	268
6.2	Ore Forming Models .....	272
6.3	Conclusions .....	283

<b>REFERENCES</b> .....	288
-------------------------	-----

<b>APPENDIX I</b> .....	304
<b>APPENDIX II</b> .....	352
<b>APPENDIX III</b> .....	365
<b>APPENDIX IV</b> .....	378
<b>APPENDIX V</b> .....	379
<b>APPENDIX VI</b> .....	380
<b>References Cited in Appendices</b> .....	381

## LIST OF FIGURES

	Page
Frontispiece: Scenery of the Burnt Lake area. ....	(ii)
Figure 1-1: Location and extent of study area. ....	3
Figure 1-2: General geology of the Central Mineral Belt..	4
Figure 2-1: Regional Geology of Labrador. ....	14
Figure 2-2: Geology of the Central Mineral Belt. ....	15
Figure 2-3: Grenville Province Boundary in Eastern Labrador. ....	21
Figure 2-4: Generalized stratigraphic section at Burnt Lake .....	31
Figure 2-5: (A): Recrystallized arkosic sandstone with thin bands of magnetite. (B): Bands and clots of aegirine within tuffaceous sediments. ....	35
Figure 2-6: (A): Well bedded volcanoclastic siltstone (B): Interbedded volcanoclastic siltstone and sandstone of unit 2. (C): Bedded volcanoclastic siltstone of unit 2. (D): Pink and green bedded volcanoclastic siltstone of Unit 2 .....	38
Figure 2-7: Close-up photograph of maroon volcanoclastic siltstone of unit 3 .....	39
Figure 2-8: (A): Banded ash tuff of the Upper Aillik Group in the Burnt Lake area. (B): Contact between welded ash tuff and feldspar porphyry. (C): Contact between a grey quartz-feldspar porphyry and a pink quartz porphyry .....	45
Figure 2-9: (A): Welded quartz-feldspar porphyry of Unit 4b. (B): Explosive breccia of quartz-feldspar porphyry fragments in a finer grained ash tuff matrix. (C): Ash tuff containing mafic lithic fragments. ....	47
Figure 2-10: (A): Contact between lapilli tuff and a bluish- grey feldspar porphyry. (B): Close-up photo of feldspar porphyry (unit 4d). (C): Sheared and brecciated outcrop of andesite near the Aurora River radioactive showings. ....	49



- Figure 2-11: (A) Fine grained leucocratic Burnt Lake Granite. (B): Biotite-rich phase of the Burnt Lake Granite. (C): Intrusive contact between the Burnt Lake Granite and felsic tuff of the Upper Aillik Group. .... 55
- Figure 2-12: (A): Pegmatite dyke at the contact with felsic tuff of the Upper Aillik Group. Dashed lines outline the pegmatite dyke. (B): Foliated hornblende-biotite granite of Unit 5b. (C): Coarse-grained hornblende-biotite granite of Unit 5c. .... 57
- Figure 2-13: (A): Amphibolite dyke showing refolded folds. (B): Metadiabase showing sharp intrusive contacts with the felsic volcanic tuff of the Upper Aillik Group. .... 59
- Figure 2-14: Equal area contoured stereographic projection of mineral stretching lineations as measured in the Burnt Lake area. .... 62
- Figure 3-1: (a) Histogram of weight percent  $\text{SiO}_2$  in the Upper Aillik Group samples (based on 2% intervals). (b):  $\text{K}_2\text{O}$  versus  $\text{SiO}_2$  plot showing classification fields by Pecerillo and Taylor (1976). (c):  $\text{K}_2\text{O} + \text{Na}_2\text{O}$  versus  $\text{SiO}_2$  plot showing classification fields by Cox et al; 1979. .... 68
- Figure 3-2: Harker variation diagrams of major elements in the Upper Aillik Group samples from the Burnt Lake area. .... 71
- Figure 3-3:  $\text{K}_2\text{O}$  versus  $\text{SiO}_2$  plot showing classification of andesites by Gill, 1981. .... 74
- Figure 3-4: Igneous spectrum of Hughes (1973) distinguishing between igneous and metasomatised chemical compositions. .... 76
- Figure 3-5: Total alkalis versus silica plot (weight percent) for the Upper Aillik Group in the Burnt Lake area. Fields from Irvine and Baragar (1971). .... 78
- Figure 3-6:  $\text{Na}_2\text{O}$  versus  $\text{K}_2\text{O}$  plot for rocks of the Upper Aillik Group in the Burnt Lake area. .... 79
- Figure 3-7: Total Alkalies versus Silica diagram of the Upper Aillik Group. Fields from Irvine and Baragar, (1971). .... 81

- Figure 3-8: AFM diagram with Irvine and Baragar's (1971) calc-alkaline trend. .... 82
- Figure 3-9: Jensen (1976) cation plot of unmineralized Upper Aillik Group rocks in the Burnt Lake area. .. 84
- Figure 3-10: Harker variation diagrams of trace elements versus Zr in samples of the Upper Aillik Group from the Burnt Lake area. .... 89
- Figure 3-11: Variation diagrams of incompatible elements versus Nb. Shaded fields represent average values for metasedimentary rocks of the Lower Aillik Group. .... 92
- Figure 3-12a:  $Zr/TiO_2$  versus Nb/Y diagram showing distribution of the Upper Aillik Group meta-volcanic suite of the Burnt Lake area. Fields from Winchester and Floyd (1977)..... 94
- Figure 3-12b:  $SiO_2$  versus  $Zr/TiO_2$  diagram showing distribution of the Upper Aillik Group meta-volcanic suite of the Burnt Lake area. Fields from Winchester and Floyd (1977)..... 95
- Figure 3-13: Tectonic discrimination diagrams (after Pearce et al., 1984) for samples from the Upper Aillik Group meta-volcanic suite in the Burnt Lake area. .... 96
- Figure 3-14: Lithotectonic Ti-Zr-Y discrimination diagram (after Pearce and Cann, 1973) data for andesitic rocks from the Upper Aillik Group in the Aurora River area. .... 97
- Figure 3-15: Lithotectonic Zr-Nb-Y discrimination diagram (after Meschede, 1986) for andesitic rocks from the Upper Aillik Group in the Aurora River area. .... 98
- Figure 3-16: Chondrite-normalized REE patterns for non-mineralized felsic volcanic rocks of the Upper Aillik Group in the Burnt Lake area. .... 100
- Figure 3-17: Harker variation diagrams of major elements in the Burnt Lake area granitoids. .... 104
- Figure 3-18: Harker variation diagrams of trace elements versus Zr in the Burnt Lake area granitoids. 106
- Figure 3-19: Modal classification of granitic rocks after O'Conner (1965). .... 112

- Figure 3-20: AFM diagram with Irvine and Baragar (1971) calc-alkaline trend. .... 113
- Figure 3-21: Major element variation diagram of total alkalis ( $\text{Na}_2\text{O} + \text{K}_2\text{O}$ ) versus  $\text{SiO}_2$ . Field boundary from Irvine and Baragar (1971). .... 114
- Figure 3-22: Tectonic discrimination diagrams for the Burnt Lake area granitoids (Pearce *et al.*, 1984). .... 116
- Figure 3-23a:  $\text{Na}_2\text{O}$  versus  $\text{K}_2\text{O}$  diagram for classification of I-A-S type granites. Fields from White and Chappell (1983). .... 118
- Figure 3-23b: Ga versus  $\text{Al}_2\text{O}_3$  diagram for classification of I-A-S type granites. Fields from White and Chappell (1983). .... 118
- Figure 3-24: SUN-normalized REE plot of samples that are considered to represent a standard for the Burnt Lake Granite. .... 121
- Figure 3-25: Extended trace element variation diagram for standard samples of the BLG ratioed to primitive mantle values (PRIM). .... 122
- Figure 3-26: SUN-normalized REE plot of samples from the BLG that are transitional from the main body to the volatile-rich margin. .... 122
- Figure 3-27: Extended trace element variation diagram for transitional samples of the BLG ratioed to PRIM. .... 123
- Figure 3-28: SUN-normalized REE plot of samples from the BLG that are closest to the volatile-rich margin. .... 123
- Figure 3-29: Extended trace element variation diagram for the most fractionated samples of the BLG ratioed to PRIM. .... 124
- Figure 3-30: SUN-normalized REE plot of the synkinematic Makkovikian granite. .... 124
- Figure 3-31: Extended trace element variation diagram for the synkinematic Makkovikian granite. .... 125
- Figure 3-32: Contour plot of  $\text{SiO}_2$  for the Burnt Lake Granite. Contour interval is 2%  $\text{SiO}_2$ . .... 126



Figure 3-33:	Rb/Sr isochron generated for whole rock samples of the Burnt Lake Granite. ....	129
Figure 3-34:	Rb-Sr isocron plot for the BLG. ....	133
Figure 4-1:	Geology and sample location map of the Burnt Lake Main Zone. ....	138
Figure 4-2:	Simplified drillcore log section through the Burnt Lake Main Zone (looking southwest)....	139
Figure 4-3:	(A): Photograph of Trench #6 from the Main Zone showing a pink hematized radioactive zone (hammer) adjacent to a breccia zone (lens cap). (B): Photograph of typical volcanic breccia from Trench #8A (Main Zone). (C): Felsic ash tuff lense within a felsic crystal tuff (Trench #12). ....	141
Figure 4-4:	(A): Mafic clots in a hematized radioactive lapilli tuff (Trench #13). (B): Outcrop of quartz-feldspar porphyry with characteristic mafic banding (Trench #16). (C): Hematized radioactive quartz-feldspar porphyry with mafic banding and clots. ....	143
Figure 4-5:	Scanning Electron Microscope (SEM) back scatter images of uraninite intergrown with zircon in a potassium feldspar matrix. ....	144
Figure 4-6:	SEM back scatter image of uraninite intergrown with monazite in a silicate gangue matrix. ....	145
Figure 4-7:	SEM energy dispersive spectra for monazite associated with uranium mineralization in the Burnt Lake Main Zone. ....	145
Figure 4-8:	SEM back scatter image of chalcopryrite intergrown with quartz gangue matrix and a uraninite veinlet (white). ....	146
Figure 4-9:	SEM back scatter image of magnetite (small white grains) rimming recrystallized feldspar porphyroblasts in a non-mineralized quartz-feldspar porphyry unit. ....	146
Figure 4-10:	SEM back scatter image of an intergrowth of uraninite, ilmenite, apatite and zircon in a silicate gangue matrix. ....	147

Figure 4-11: Geology of and sample locations from the Burnt Lake Northwest Zone. ....	148
Figure 4-12: Geology and sample locations of the Burnt Lake Southwest Zone. ....	151
Figure 4-13: Diamond drill section (DDH 77.11) of the Burnt Lake Southwest Zone (looking east). ....	152
Figure 4-14: Outcrop of volcanic breccia (tuffisite) from the Southwest Zone. ....	153
Figure 4-15: SEM back scatter image of a uraninite and sphene intergrowth in a potassium feldspar matrix..	154
Figure 4-16: SEM back scatter image of intergrown uraninite and a Ti-Fe-Mn oxide in a feldspar matrix. .	154
Figure 4-17: SEM back scatter image of sphalerite intergrown with pyrite and sphene in a silicate gangue matrix. Small bright grains at the top of the photograph are uraninite. ....	155
Figure 4-18: SEM back scatter image of galena stringers transecting silicate gangue. Uraninite and sphalerite are intergrown with galena. ....	155
Figure 4-19: Location of radioactive occurrences in the Emben area. ....	157
Figure 4-20: Geology and sample locations of the Emben Main Zone. ....	158
Figure 4-21: SEM back scatter image of a high concentration of uraninite within a large ragged sphene grain. The host gangue is sodic feldspar. ....	159
Figure 4-22: SEM back scatter image of uraninite occurring as veinlets, fracture fillings and individual discrete grains in a plagioclase matrix. ....	159
Figure 4-23: SEM back scatter image of barite grains in a matrix of plagioclase and potassium feldspar. ....	160
Figure 4-24: Geology and sample locations of the Emben South Zone. ....	162
Figure 4-25: Radioactive dyke from Trench #1, Emben South Zone. ....	163

- Figure 4-26: (A): Close-up of a dark green pyroxene vein in an amphibolite dyke from the Emben South Zone which assayed at 2 wt% U. (B): Contact between radioactive dyke and unmineralized felsic volcanic host. The highest radioactivity was obtained from pyroxene veins within the dyke. (C): Recrystallized felsic tuff from the Emben South Zone with disseminated purple fluorite and molybdenite. .... 165
- Figure 4-27: SEM back scatter image of uraninite grain in a K-Si-Fe matrix. Alteration mineral in centre of photo contains U, Nb, W, Ti, and Ca. .... 166
- Figure 4-28: Energy dispersive X-ray spectra for uranium-bearing Nb-W alteration mineral from the Emben South showing. .... 166
- Figure 4-29: SEM back scatter image of euhedral galena and zircon grains in an interlocking mosaic of plagioclase. A calcite veinlet occurs in the lower left corner of the photo. .... 167
- Figure 4-30: (A): Banded quartz-feldspar porphyry dyke from the Aurora River Zone.(B): Sheared brecciated and hematized andesite from Trench #3, Aurora River Zone. Note infilling of carbonate (white).(C): Hematized radioactive andesite from Trench #4, Aurora River Zone. .... 171
- Figure 4-31: SEM back scatter images of intergrown galena and chalcopyrite in a plagioclase gangue. .... 173
- Figure 4-32: Recrystallized felsic tuff with a narrow veinlet of sphalerite. .... 174
- Figure 4-33: SEM back scatter image of coarse sphalerite mineralization and finely disseminated uraninite. .... 175
- Figure 4-34: SEM back scatter image of intergrown galena and chalcopyrite in a potassium feldspar gangue. .... 176
- Figure 4-35: A cut section through extensive sulphide mineralization hosted by an altered mafic dyke. .... 177
- Figure 4-36: SEM back scatter image of an intergrowth of sphalerite, chalcopyrite and galena in a quartz-plagioclase gangue. .... 178

- Figure 4-37: SEM back scatter image of intergrowth of galena, pyrite, sphalerite and sphene in a Na-Ca-Mg-Fe-Si gangue matrix. .... 178
- Figure 4-38: Discovery outcrop of molybdenite mineralization in the Burnt Lake Granite. .... 180
- Figure 4-39: Close-up photo of disseminated molybdenite mineralization in the Burnt Lake Granite.... 181
- Figure 4-40: SEM back scatter image of fibrous molybdenite intergrown with quartz and feldspar in the leucocratic contact zone of the Burnt Lake Granite. .... 182
- Figure 5-1: Frequency distribution of Log(U) in felsic volcanic rocks of the Burnt Lake Showings... 185
- Figure 5-2: Harker variation diagrams of major elements of the Burnt Lake mineralized samples. .... 188
- Figure 5-3: Na<sub>2</sub>O versus K<sub>2</sub>O plot for mineralized rocks from the Burnt Lake showings. Fields are based on apparent metasomatic intensities. .... 190
- Figure 5-4: Harker variation diagrams of major elements versus Log(Rb). .... 192
- Figure 5-5: Plots of Na<sub>2</sub>O versus Rb and K<sub>2</sub>O versus Rb for mineralized rocks from the Burnt Lake showings. Fields are based on apparent metasomatic intensities. .... 194
- Figure 5-6: Harker variation diagrams of major elements versus uranium for mineralized rocks from the Burnt Lake showings..... 195
- Figure 5-7: Harker variation diagrams of trace elements versus Rb for mineralized rocks from the Burnt Lake showings. .... 200
- Figure 5-8: Harker variation diagrams of trace elements versus uranium for mineralized rocks from the Burnt Lake showings..... 203
- Figure 5-9: Harker variation diagrams of major elements of the Emben mineralized samples. .... 208
- Figure 5-10: Harker variation diagrams of major elements versus uranium for mineralized rocks for the Emben Showings ..... 210

- Figure 5-11: Harker variation diagrams of trace elements versus uranium for mineralized rocks for the Emben Showings. .... 213
- Figure 5-12: Harker variation diagrams of major elements for the Aurora River Showing ..... 217
- Figure 5-13: Harker variation diagrams of trace elements versus uranium for mineralized rocks for the Aurora River Showing ..... 219
- Figure 5-14:  $\text{Na}_2\text{O} + \text{K}_2\text{O}$  versus  $\text{SiO}_2$  diagram of mineralized rocks of the Upper Aillik Group. Fields from Irvine and Baragar (1971)..... 224
- Figure 5-15: AFM diagram with Irvine and Baragar (1971) calcalkaline trend. .... 225
- Figure 5-16:  $\text{Zr}/\text{TiO}_2$  versus  $\text{Nb}/\text{Y}$  diagram showing distribution of mineralized samples of the Upper Aillik Group. Fields from Winchester and Floyd (1977). .... 226
- Figure 5-17:  $\text{SiO}_2$  versus  $\text{Zr}/\text{TiO}_2$  diagram of mineralized samples of the UAG. Fields from Winchester and Floyd (1977). .... 227
- Figure 5-18:  $\text{K}_2\text{O} + \text{Na}_2\text{O}$  versus  $\text{SiO}_2$  plot showing classification fields by Cox et al., 1979. .... 228
- Figure 5-19: Harker variation diagrams of major elements of mineralized samples from the Burnt Lake area of the UAG. .... 230
- Figure 5-20:  $\text{K}_2\text{O}$  versus  $\text{Na}_2\text{O}$  plot for mineralized rocks of the UAG in the Burnt Lake area. .... 232
- Figure 5-21: Frequency distribution of uranium in: (A) all mineralized samples; (B) Burnt Lake potassic suite; (C) Burnt Lake sodic suite; (D) Emben Main suite; (E) Emben South suite; (F) Aurora River suite. .... 236
- Figure 5-22: Harker variation diagrams of trace elements versus uranium for all mineralized rocks from the Burnt Lake area of the UAG. .... 237
- Figure 5-23: K versus Rb plot of mineralized samples of the UAG in the Burnt Lake area. .... 240
- Figure 5-24: Harker variation diagrams for selected trace elements versus uranium. .... 250

Figure 5-25: $K_2O$ versus $Na_2O$ plot of the UAG in the Burnt Lake area. ....	251
Figure 5-26: $Na_2O$ versus Rb plot of the UAG in the Burnt Lake area. ....	252
Figure 5-27: K versus Rb plot of the UAG in the Burnt Lake area. ....	253
Figure 5-28: K/Rb versus Rb plot of the UAG in the Burnt Lake area. ....	254
Figure 5-29: K/Rb versus U plot of the UAG in the Burnt Lake area. ....	255
Figure 5-30: Chondrite-normalized REE patterns for non-mineralized felsic volcanic rocks of the UAG in the Burnt Lake area. ....	258
Figure 5-31: Chondrite-normalized REE patterns for mineralized felsic volcanic rocks of the UAG in the Burnt Lake area. ....	259
Figure 5-32: Chondrite-normalized REE patterns for samples from the Emben Main Showing (both mineralized and non-mineralized). ....	259
Figure 5-33: Chondrite-normalized REE patterns for samples from the Emben South Showing. ....	260
Figure 5-34: $^{207}Pb/^{204}Pb$ versus $^{206}Pb/^{204}Pb$ diagram for three galena separates from the Burnt Lake radioactive occurrences. ....	262
Figure 5-35: $^{208}Pb/^{204}Pb$ versus $^{206}Pb/^{204}Pb$ diagram for three galena separates from the Burnt Lake radioactive occurrences. ....	263
Figure 6-1 : Schematic diagram representing a syngenetic model for uranium mineralization within the Upper Aillik Group in the Burnt Lake area.....	276
Figure 6-2 : Schematic diagram representing an epigenetic model for uranium mineralization within the Upper Aillik Group in the Burnt Lake area.....	280
Figure 6-3 : Schematic diagram representing a model for base-metal mineralization within the Upper Aillik Group in the Burnt Lake area. ....	282

## LIST OF TABLES

page

Table 3-1 :	Rare-earth-element data for the Upper Aillik Group in the Burnt Lake area. ....	100
Table 3-2 :	Average chemical compositions of granitoids in the Burnt Lake area. ....	102
Table 3-3 :	Rb-Sr data for samples of the Burnt Lake Granite used for geochronology. ....	128
Table 5-1 :	Average major and trace element compositions of mineralized rocks from the Burnt Lake area. ....	223
Table 5-2 :	Correlation matrix of selected major and trace elements for the Burnt Lake Sodic rock suite. ....	243
Table 5-3 :	Correlation matrix of selected major and trace elements for the Emben Main rock suite. ....	244
Table 5-4 :	Correlation matrix of selected major and trace elements for the Emben South rock suite. ....	245
Table 5-5 :	Correlation matrix of selected major and trace elements for the Aurora River rock suite. ..	246
Table 5-6 :	Varimax Rotated Factor Matrix for the Burnt Lake Potassic rock suite .....	247
Table 5-7 :	Rare-earth-element data for the Upper Aillik Group in the Burnt Lake area. ....	257
Table 5-8 :	Pb isotope ratios, calculated u and model ages for galena separates from the Burnt Lake area.....	261
Table 5-9 :	Sulphur isotope data for sulphide separates from the Burnt Lake area. ....	265
Table 5-10:	General characteristics of the five mineralized rock suites of the Burnt Lake area. ....	266



xx

**LIST OF MAPS (back pocket)**

Map 1 : Geology of the Burnt Lake Area, Labrador (1:30,000).

Map 1B: Sample Location Map of the Burnt Lake Area, Labrador  
(1:30,000).

Map 2 : Geology and Mineral Occurrences of the Burnt Lake  
Radioactive Showings (1:3,000).

Map 2B: Sample Locations of the Burnt Lake Radioactive  
Showings (1:3,000).

Map 3 : Geology of the Aurora River Radioactive Showings.

## CHAPTER 1

### 1.1 Introduction

This thesis is a study of the geology, geochemistry and mineralization in the Burnt Lake area in Central Labrador. The area is underlain by Early Proterozoic felsic volcanic and volcanoclastic sedimentary rocks of the supracrustal Upper Aillik Group (Figure 1). The Burnt Lake area became a focus for uranium exploration in the 1970's and is located 20 km east of the partially developed Michelin Uranium deposit (7,366,000 t at 0.10 % U) and 45 km southwest of the Kitts deposit (347,000 t at 0.449 % U) (Gower et al. 1982). The Burnt Lake Uranium deposit has had 1851 m of diamond drilling and extensive trenching which indicated reserves of 146,000 t with an average grade of 0.067 %  $U_3O_8$ .

Approximately 80 km<sup>2</sup> was mapped for this current study during the 1985 field season and for four days in 1986. The area mapped also included the smaller Emben Main and South radioactive zones in the east, and Aurora River showings in the north. The objectives of this thesis were to study the geology and the styles of mineralization in the Burnt Lake area.

Geochemical, petrographic, and geochronological studies suggest that the main mineralizing event in the Burnt Lake area was accompanied by alkali metasomatism of the felsic

volcanic rocks at ~ 1800 Ma, however, it is also apparent that later events (i.e. magmatism during the Labrador Orogeny (~1650 Ma) and Grenvillian tectonism (~1000 Ma)) have affected the area by partially resetting isotopic signatures and remobilizing and reconcentrating uranium and base-metal mineralization.

### **1.2 Location , Access and Physiography**

The study area is located within the Central Mineral Belt (CMB) of Labrador (Figure 2). The area is wholly contained within the early Proterozoic, wedge-shaped fold belt known as the Makkovik Structural Province (Wardle *et al.* 1986), an apparent extension of the Ketilidian Mobile Belt of southern Greenland (Gower and Ryan, 1986). Burnt Lake is located approximately 150 km north-northeast of the town of Goose Bay (population 5000) and 30 km due south of the coastal community of Postville (pop. 300). Access into the remote area is confined to float-equipped fixed wing aircraft (e.g. Cessna, Beaver or Otter) or helicopter; all of which are based in Goose Bay. Goose Bay is serviced by daily jet and turboprop service from St. John's, Nfld. The nearby coastal communities of Makkovik and Postville have year-round gravel landing strips, and Labrador Airways of Goose Bay has a regularly scheduled passenger/mail service to these northern communities. In addition, Marine Atlantic provides an

inexpensive passenger/freight service during ice-free months (generally June to November). Coastal marine vessels sail from St. John's and Lewisporte, Newfoundland to Goose Bay with stops at the coastal communities. Expediting services for field work in these isolated areas is available from Goose Bay, although limited grocery items can be purchased from the government-operated stores in Postville or Makkovik.

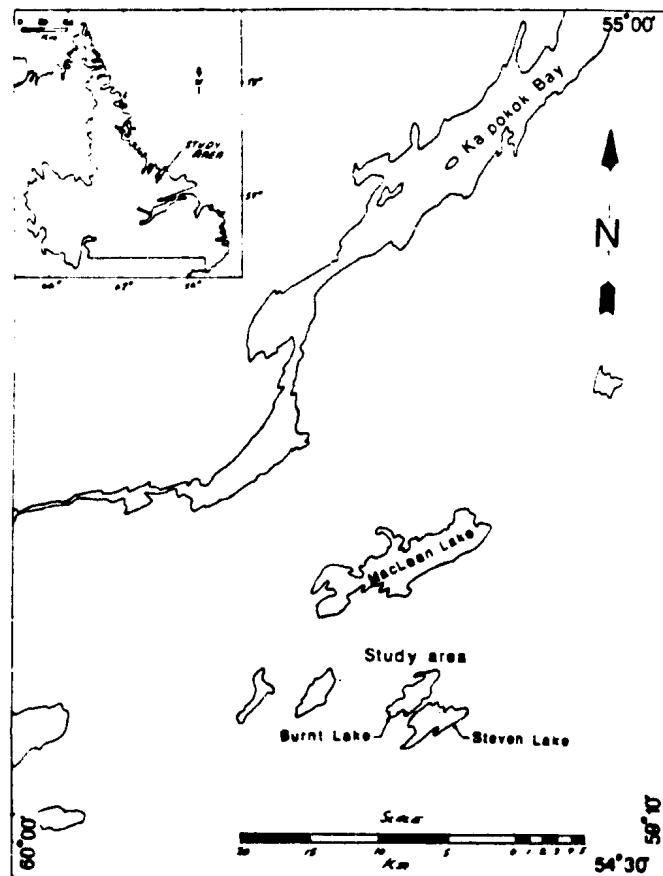
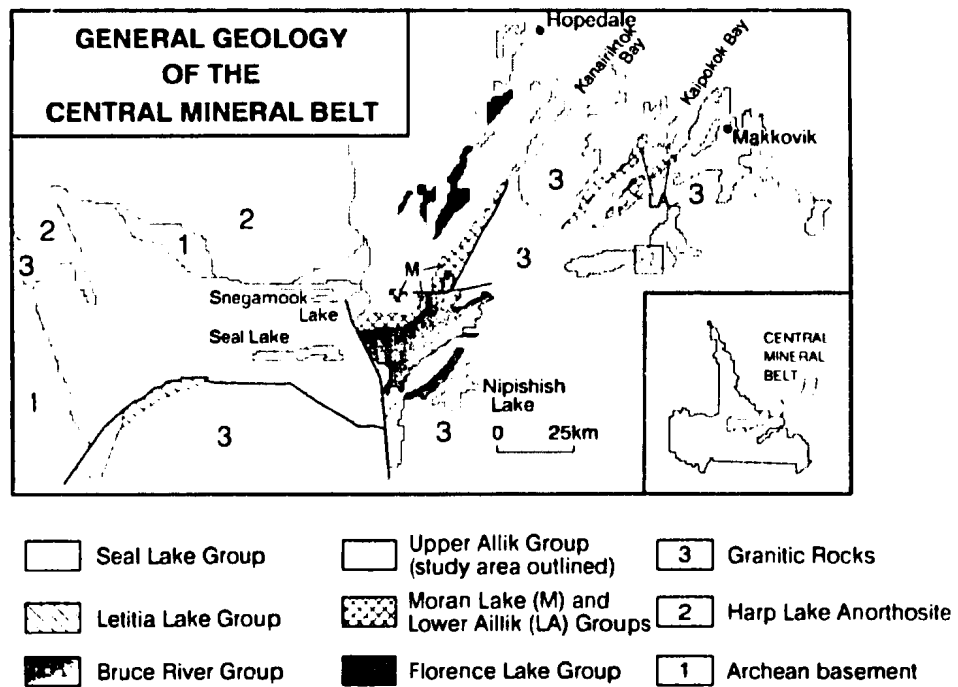


Figure 1-1: Location and extent of study area.



**Figure 1-2: General geology of the Central Mineral Belt. The study area is outlined by a small square on the map.**

Physiographically, the Burnt Lake area has low to moderate relief (150-400m elevation) and is extensively covered by glacial till and boulders. Outcrop usually occurs as SW-NE trending linear ridges which mimic the stratigraphy and numerous faults in the area. Much of the immediate area is covered with burnover (hence the name Burnt Lake), which shows no sign of rejuvenation. Dense coniferous tree growth occurs in the northern portions of the study area which is divided by marshy draws and string bogs connecting the numerous small ponds. A prolific growth of mosses and lichens is ubiquitous on rock outcrops and must be scraped away.

Climatic conditions in Labrador can be quite severe and changeable. Field work can begin after spring breakup which occurs around mid-June in central Labrador. The weather deteriorates in early September, restricting a comfortable field season to three months. Black flies, mosquitoes and deer flies are a close companion in their peak season which one must learn to work with.

### **1.3 Exploration History**

The Central Mineral Belt has had a varied and sporadic exploration history (see Ryan, 1984 Appendix II; Wilton, 1991a). The discovery of uranium mineralization in Labrador in 1954 by Piloski (Piloski, 1955) and the subsequent recognition of the area as a uraniferous province (Beavan,

1958) spurred explorationists to look for this metal with some success. The first discovery of uranium in the Burnt Lake area was made in 1957 by Turcott and Roberts, two prospectors working for British Newfoundland Exploration Limited (BRINEX). This initial discovery was made two kilometres north of Burnt Lake. The uranium mineralization was described as fault-hosted within what was then thought to be quartzite (Beavan, 1958).

Ten years later in 1967, geologists with BRINEX returned to Burnt Lake and conducted airborne gamma-ray spectrometer, EM and magnetometer surveys with follow-up ground geophysics over the original Turcott showing (Beavan, 1968). A major result of this preliminary work was the discovery of a larger, more important occurrence now known as the Burnt Lake North showing, which was also mapped and geophysically surveyed the same year. In 1969, regional geological mapping was carried out at a scale of 1:24,000 with limited soil geochemistry over the Burnt Lake North showing which led to the discovery of new, significant uranium mineralization in bedrock eight kilometres to the east (the Emben occurrences). Three separate showings were discovered by Matthew Ben Andrews and described by Gandhi et al. (1969) who recommended immediate detailed follow-up. A grid was established, and in September 1969 detailed exploration of the Emben showings involved geological mapping, soil sampling, a radiometric survey and the blasting of four trenches at the Emben Main showing and three trenches at the Emben South showing (Janecek, 1969). Due to the thick

Pleistocene drift cover in the area a boulder tracing and drift study was undertaken and significant uranium mineralization was discovered in boulder trains near the Emben Central and South Zones (Doak and MacCallum, 1970). In 1970, Bundrock (1970) mapped a small area near the Emben Main showing on a scale of 1:4,800. In 1976, the focus returned to the Burnt Lake North showing and eleven mineralized zones were mapped and trenched. As well, Krajewski (1976) carried out regional mapping in the McLean Lake area (five kilometres to the north) on a scale of 1:25,000.

In 1977, a reconnaissance grid was established over the Burnt Lake showings with detailed mapping, magnetometer and radiometric surveys at a scale of 1:3,000. Twenty trenches were blasted and the mineralization was tested below surface in seventeen diamond drill holes with a combined depth of 1851 metres. Indicated reserves of uranium are in the order of 140,000 tonnes with an average grade of 0.082 %  $U_3O_8$  reported for a 40 m by 300 m zone (Sharpley, 1978). In 1978, a detailed grid was established and soil geochemical and magnetometer orientation surveys were carried out. One Winkie diamond drill hole tested to a depth of 25.6 m (Sharpley, 1978).

Kontak (1978) mapped a small area concentrating on the Burnt Lake Main zone as part of a larger regional study. Bailey (1978) carried out 1:50,000 scale regional mapping which incorporated the Burnt Lake region. In 1978, Davidson visited the Emben area as part of a comparison study



with other radioactive showings (Davidson and Gentile, 1978). In 1980, R. Cote (1980) mapped the Aurora-McLean-Burnt-Emben Lakes area on a scale of 1:10,000. In July, 1984 a two-man BRINEX crew carried out prospecting and geological investigations over the Burnt Lake Main Showing in an attempt to subdivide the felsic pyroclastic rocks into sub-units (Hum, 1984). During that same summer R.J. Wardle and D.H.C. Wilton sampled both the Burnt Lake and Emben showings as part of a reconnaissance sampling program for precious metals (Wardle and Wilton 1985). BRINEX geologists were on the property again in the summer of 1985 to conduct a two week soil sampling program (Hum, 1985).

#### **1.4 Previous Geological Work**

The earliest geological observations in Labrador were made only on coastal exposures (e.g. Packard, 1891 and Daly, 1902). The reports were descriptive in nature but nevertheless make for interesting reading. Serious geological consideration was not given to the interior portions of Labrador because the ruggedness of the terrain and a poorly navigable river system prevented many of the early attempted investigations. Krank (1939) was the first to name the "sedimentary" rocks in coastal sections of the Aillik and Makkovik areas as the Aillik Formation; these rocks were subsequently defined as the Aillik Series (Krank, 1953 and Douglas, 1953).

The division of the Canadian Shield into structural provinces was initiated by Stockwell (1964). The boundaries of these structural provinces in Labrador were redefined as a result of regional mapping by Taylor (1971, 1972), who proposed that a wedge of Lower Proterozoic rocks on the coast be termed the Makkovik Subprovince. It has been recently suggested that the Makkovik Belt should be raised to independent status as an orogenic province (Gower and Ryan, 1986).

The Central Mineral Belt (CMB) has been the focus of numerous studies by exploration companies and government geologists since the construction of a military air base in Goose Bay during the mid 1940's. The first discovery of significant mineralization in the CMB was made in 1946 by geologists with Norancon Exploration Limited who found native copper in the Adeline Lake area (Evans, 1952). Extensive exploration continued in the early 1950's which led to the discovery of the numerous copper occurrences in the Seal Lake and Bruce River Groups, (Brummer and Mann, 1961; MacPherson, 1954), and uranium in the Upper Aillik Group (Beavan, 1958). The CMB was defined by these early exploration geologists to include a large belt of Proterozoic supracrustal sequences that extends from Makkovik on the coast to the Smallwood Reservoir in the west. The earliest work of the exploration companies (eg. BRINEX, Beavan (1958)) coincided with the first regional studies by the Geological Survey of Canada (Christie

et al., 1953 ; Fahrig, 1959; Stevenson, 1970; and Roscoe and Emslie, 1973). The regional studies included the first stratigraphic subdivisions of the supracrustal sequences of the CMB. Ryan (1984) produced a comprehensive report on the supracrustal sequences comprising the central CMB. Gower et al. (1982) described the geology of the eastern CMB, and Wilton (1991a) described the metallogeny of the entire CMB.

The earliest published work describing the geology and genetic interpretation of the uranium mineralization in the CMB was carried out by Gandhi et al. 1969. Other important studies involving various aspects of uranium in the CMB include Minatidis (1976), Watson-White (1976), Kontak (1978, 1980), Gandhi (1978, 1986), Evans (1980), White and Martin (1980), Gower et al. (1982), Payette and Martin (1986), and MacKenzie and Wilton (1987a).

### 1.5 Methodology of Present Study

The present study was initiated in the summer of 1985, with a field program of approximately two months duration. The study area was visited briefly in 1986 for some follow-up work. An 80 km<sup>2</sup> area was mapped at a scale of 1:30,000 utilizing enlarged black and white airphotos. The area immediately surrounding the Burnt Lake uranium occurrences was mapped at a scale of 1:3000 using the BRINEX grid for control. Most of the BRINEX trenches were located, mapped and

sampled. Drill core from fourteen diamond drill holes was re-logged and mineralized sections were sampled. All lithological units identified in the field were sampled and analyzed for major, trace and rare-earth elements. Selected mineralized samples were analyzed for precious metals at Chemex Laboratories in Vancouver, B.C. Analytical procedures and techniques are given in Appendix I. A thin section was cut for each sample analyzed and each rock suite was studied petrographically; in all 181 thin sections were made. Polished sections (3 samples) and polished thin sections (26 samples) were prepared from mineralized samples and were studied using a Scanning Electron Microscope (SEM). Mafic minerals were identified by XRD and microprobe techniques.

A Rb/Sr geochronological study was undertaken of samples of the Burnt Lake Granite using whole rock powders and mineral separates. Isotope analyses of Pb from galena separates were completed by Geospec Consultants Ltd. of Edmonton, Alberta using the techniques outlined by Swinden et al. (1988). Sulphur isotope analyses of sulphide separates were completed at the Ottawa-Carleton Centre for Geoscience Studies - Geological Survey of Canada stable isotope facility in Ottawa, Ontario.

**CHAPTER 2****REGIONAL GEOLOGY****2.1 Introduction**

The regional geology of Labrador is illustrated on Figure 2-1. Labrador contains five geological provinces of the Canadian Shield, viz: the Superior, Churchill, Nain and Grenville provinces (Taylor, 1971) and the Makkovik province (Gower and Ryan, 1986). The last province comprises a sequence of early Proterozoic supracrustals and reworked Archean rocks, considered to be distinct from the adjoining Nain and Grenville Provinces. The Makkovik Subprovince was recognized by Sutton *et al.* (1972) as a continuation of the Ketilidian Mobile Belt of Greenland.

**2.1.1 Central Mineral Belt**

The Central Mineral Belt (CMB) of Labrador (Figure 2-2) is the informal name given to an easterly-northeasterly trending belt of Aphebian to Neohelikian supracrustal rocks in central Labrador. The CMB covers an area 260 km long and up to 75 km wide, from the Smallwood Reservoir in the west, to Makkovik on the coast. The majority of the rocks contained within coastal portions of this belt are part of the 1.8 Ga

Makkovikian structural province. The Moran Lake and Bruce River Groups are in the central portions of the belt, whilst the Aillik Groups are in the east (Figure 2-2). The CMB contains numerous metallic occurrences and has been sporadically explored for iron ore, base metals and uranium (Ryan, 1984; Wilton, 1991a).

#### **2.1.2 Nain Province**

The Nain Province of Labrador was first sub-divided into eastern and western sub-provinces by Stockwell (1964), but was later redefined by Taylor (1971) whose nomenclature has been retained. The northern portion of the Nain Province is comprised of high grade Archean gneisses deformed during the Kenoran Orogeny (2560 Ma) (Wardle et al., 1986). To the southwest, the most common rock type is the ~2800 Ma (Grant et al., 1983) trondhjemitic granitoids of the Kanairiktok Intrusive Suite (Ermanovics and Raudsepp, 1979). The Moran Lake Group unconformably overlies these granitoids. On the coast the Archean comprises the ca. 2300 Ma (Scharer et al., 1988) Island Harbour Pond-Iggiuk Bight Complex (Ryan et al., 1983). The contact between the gneissic complex and the Lower Aillik Group is a mylonitized tectonic slide zone (Marten, 1977) in Kaipokok Bay. In the southern portion of the province these Archean granitoids are overlain by supracrustal rocks of Aphebian age. The Aillik and Moran Lake Groups have been

affected by the Makkovikian Orogeny (1800 Ma) that produced NE-SW structural trends (Gower and Ryan, 1986).

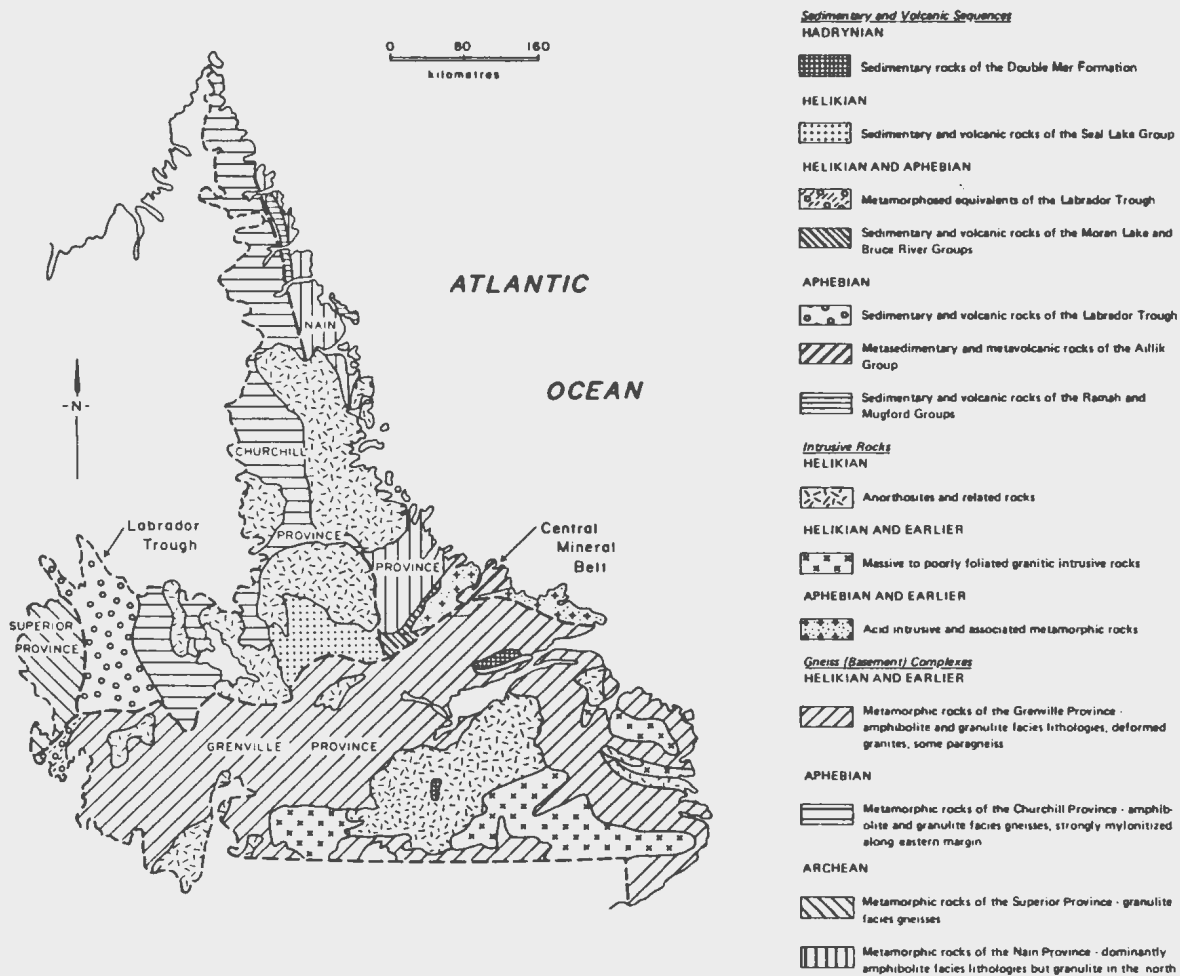
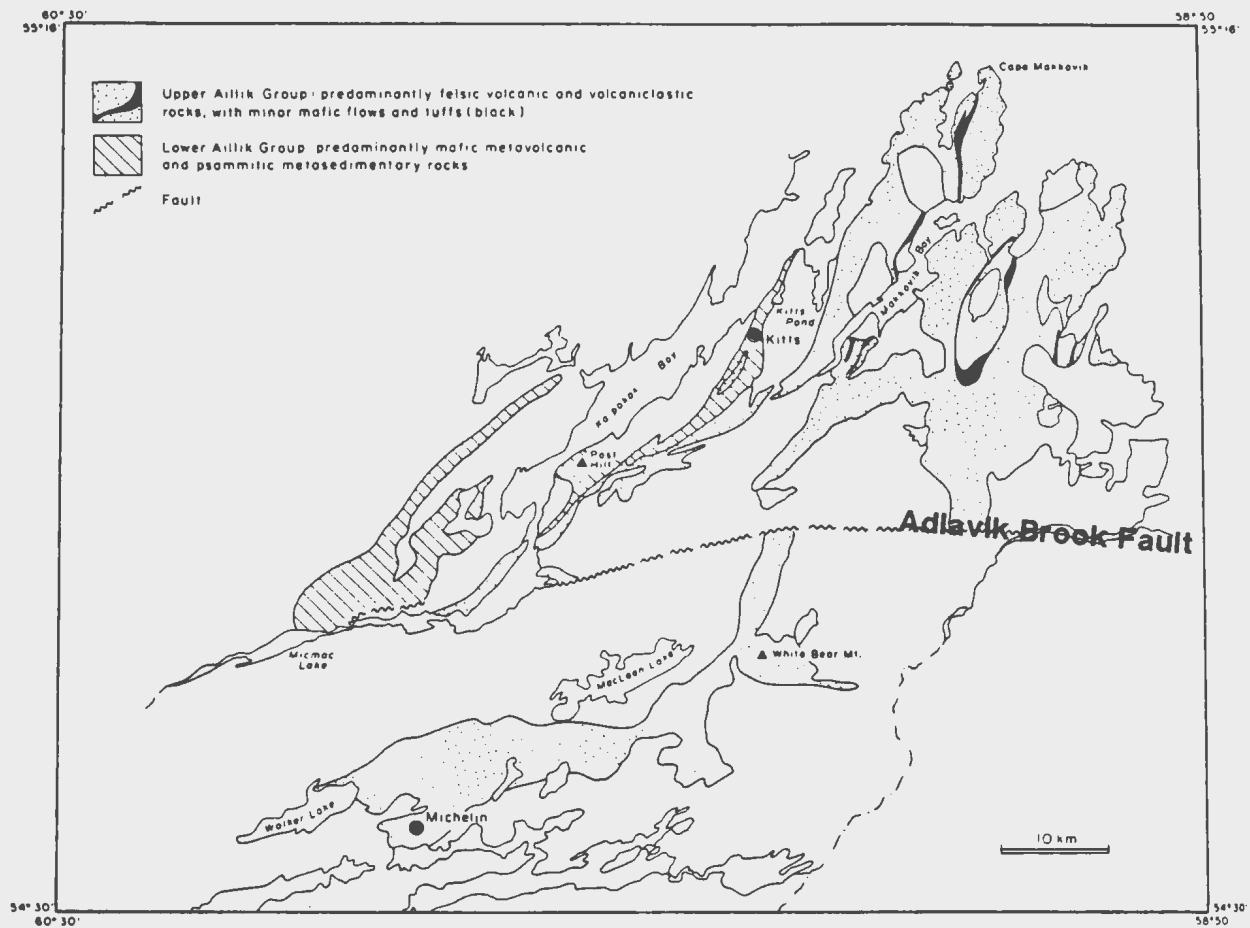


Figure 2-1: Regional Geology of Labrador (from Ryan, 1984).



**Figure 2-2: Geology of the Central Mineral Belt, Labrador (after Ryan, 1984).**



### 2.1.3 Makkovik Province

The major supracrustal sequences within the Makkovik Province (which also includes most of the eastern CMB), are the Moran Lake, Aillik and Bruce River Groups. Each sequence will be dealt with in more detail later. This province is bounded to the north by the Archean Nain Province and structurally to the south by the Grenville Province.

The lowermost supracrustal rocks of the Makkovik Province include the sedimentary and mafic volcanic rocks of the Lower Aillik and Moran Lake Groups which are overlain by the primarily felsic volcanic assemblages of the Upper Aillik and Bruce River Groups.

The Lower Aillik Group in the Kaipokok Bay area is comprised of amphibolite overlain by a metasedimentary unit of psammite, phyllitic schists, semipelite, quartz-muscovite schist and biotite schist (Marten, 1977). The uppermost unit of the Lower Aillik Group consists of pillowed mafic volcanic rocks intercalated with argillite and oxide-silicate iron formation (Gower et al. 1982).

The Upper Aillik Group consists predominantly of a variable assemblage of felsic volcanic and volcanoclastic sedimentary rocks with minor mafic volcanic and tuffaceous rocks and occurs in two distinct belts (the Makkovik and Michelin Zones) separated by the Adlavi Brook Fault (Figure 2-2).

Deposition and deformation of the Aillik and Moran Lake Groups occurred during the Makkovikian Orogeny (1850-1750 Ma) (Gower and Ryan, 1986). Synkinematic granitoid rocks (i.e. Island Harbour Bay Plutonics) are also related to this orogenic event (Gower et al. 1982). Scharer et al., (1988) have been able to constrain the high grade metamorphism associated with the termination of the orogeny to between 1794 and 1761 Ma from high precision U-Pb dates on zircon separates from felsic volcanic and granitic rocks. Previously, the timing of the deformation from this event was only constrained by the 1650 Ma Trans-Labrador Batholith (Wardle et al., 1986) which had not suffered Makkovikian deformation.

## **2.2 TECTONIC EVOLUTION OF LABRADOR**

### **2.2.1 Introduction**

The tectonic evolution of Labrador, and more specifically that of the Central Mineral Belt, from the Early Proterozoic has involved the Hudsonian, Makkovikian - Ketilidian, Labradorian and finally Grenvillian orogenies.

### **2.2.2 Hudsonian Orogeny**

This orogenic cycle (1850-1750 Ma, Stockwell, 1973) deformed and metamorphosed the Trans Hudsonian Orogen (or

Churchill Province) (Hoffman, 1988) in the western portion of the CMB to produce north-south structural trends and fold-thrust belts on the orogen margins. The grade of metamorphism is from lower greenschist to upper amphibolite in the interior of the orogen.

Prior to the recognition of the Makkovikian orogeny in Labrador (Wardle et al., 1986), the principal deformation (and possibly re-mobilization of uranium) in the Aillik Group was considered to be Hudsonian (Stockwell, 1973). The tectonic evolution of the Aillik Group is poorly constrained as some contend that deposition of the volcanic rocks occurred in a classic non-orogenic continental rift environment (e.g. Gandhi, 1978; White and Martin, 1980). Wardle and Bailey (1980) suggested the transition from basic to felsic volcanism (i.e. Lower to Upper Aillik Groups) was the result of a major tectonic change from rifting to an ensialic orogeny, and that an unconformity must therefore occur between the lower and upper divisions of the Aillik Group because of the differences in the intensity of Hudsonian deformation and grade of metamorphism between the divisions.

The rocks of the Aillik Group have had a polydeformational history (Hudsonian) with tight folding and NE-SW structural trends. Metamorphism ranges from greenschist facies in the western portion to amphibolite grade in the east (Wardle et al., 1986).

### 2.2.3 Makkovikian Orogeny

The recently recognized Makkovikian Orogeny is considered to be correlative to the Ketilidian Orogeny of southern Greenland and is wholly contained within central Labrador (Gower and Ryan, 1986). Metamorphism ranges from greenschist facies in the northwest to amphibolite facies in the southeast. Deformation and uplift during the orogeny are poorly constrained in Labrador but appear to have occurred between 1850-1750 Ma.

### 2.2.4 Labradorian Orogeny

The Labrador Orogeny is a recently recognized orogenic event that occurred from 1700 to 1600 Ma (Thomas et al., 1986; Wardle et al., 1986) in what is now mainly the Grenville Province. The orogeny produced a polydeformed paragneiss belt known as the Labrador High Grade Terrane, (Wardle et al., 1986) with intrusion of associated calc-alkaline granitoids, charnockitic and gabbroic rocks collectively known as the Trans-Labrador batholith (Kerr; 1986, 1987). The northern boundary of the batholith is relatively undeformed, whereas the southern boundary lies within the Grenville province and is generally foliated and gneissic to almost migmatitic.

#### **2.2.5 Grenvillian Orogeny**

The Grenvillian Orogeny was the final tectonic event to affect much of southern Labrador and it overprints the earlier tectonic fabrics (Wardle et al., 1986; Gower and Ryan, 1986). Subdivision of the 1000 Ma orogen was previously based on various structural and lithological features as well as metamorphic and geophysical characteristics (Wynne-Edwards, 1972). The most recent interpretation of the Grenville Province is based upon the recognition of allochthonous elements throughout the southern portion of eastern and western Labrador-Quebec (Rivers and Chown, 1986). The autochthon of Labrador includes the southern portion of the CMB and is adjacent to the parautochthon, representing the northerly limit of Grenvillian ductile shearing and metamorphism.

#### **2.2.6 The Grenville Front in Labrador**

The criteria used to define the northern boundary of the Grenville front (Figure 2-3) have been structural and lithological features, along with metamorphic and geophysical characteristics (Wynne-Edwards, 1972). The boundary was defined by Gower et al. (1980) as the northern extent of widespread Grenvillian brittle deformation coinciding with major regional faults. The boundary has also been described

as the northernmost limit of the Michael Gabbro intrusions (e.g. Gower and Ryan, 1986). Gower et al. (1980, 1982) and Wardle et al. (1986) placed the boundary along the Adlavik Brook Fault system north of the Burnt Lake area. Stevenson (1970), Kerr (1987), Gower and Ryan (1986), and Owen et al. (1986) described the boundary as being along the Benedict Fault System south of Burnt Lake (i.e. south of the Upper Aillik Group) within the Trans-Labrador Batholith. The Grenville front boundary is discussed below based on new isotopic and structural data generated during this study.

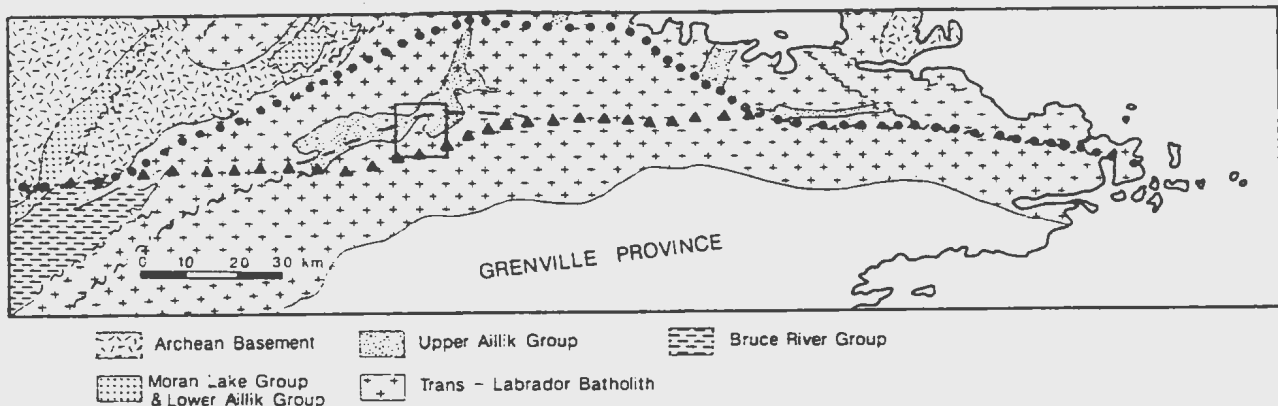


**Figure 2-3: Grenville Province boundaries in Eastern Labrador.** The line defined by the solid triangles indicates the location of the northern Grenville Front boundary along the Benedict Fault system as defined by Gower and Ryan (1986), Owen et al. (1986) and Kerr (1987); the dashed line (through the middle of the Burnt Lake area) indicates the boundary of Gower and Owen (1984) and Scharer et al. (1986); and the line of solid circles indicates the boundary (along the Adlavik Brook Fault) of Gower et al. (1980, 1982) and Wardle et al. (1986).

## 2.3 PROTEROZOIC SUPRACRUSTAL ROCKS

### 2.3.1 Lower and Upper Aillik Groups

The Aillik Group of Labrador was first described as the Aillik Series (Kranck, 1939; Beavan, 1958; King, 1963; Gandhi et al., 1969) and was originally defined as a sedimentary sequence of mainly quartzite. Sutton et al. (1971) recognized that the rocks were actually the products of felsic volcanism. The group has been divided into a lower unit of mafic volcanic and metasedimentary rocks (the Lower Aillik Group), and an upper unit of felsic volcanic and volcanoclastic sedimentary rocks (the Upper Aillik Group).

### 2.3.2 Lower Aillik Group

The Lower Aillik Group is well exposed in the Kaipokok Bay region (Figure 2-2). The basal unit of the sequence overlies the migmatitic Archean gneisses and granitoids of the Island Harbour Pond-Iggiuk Bight Complex (ca. 2300 Ma, Scharer et al., 1988) which is part of the Hopedale Complex, Nain Province (Marten, 1977). The contact with the basement is considered to be a tectonized slide zone with ductile shearing (Marten, 1977). The basal unit is the Post Hill Amphibolite (metamorphosed mafic volcanics) (Gower et al., 1982) which is conformably overlain by 1000 m of

metasedimentary rocks, including micaceous schists and pelites with pyritic and graphitic members. On top is 900 m of massive to pillowed basalt and mafic tuffs with silicate-oxide iron formation and chert. The uppermost portion of the Lower Aillik Group is a 50 m thick argillaceous - tuffaceous unit which Gandhi (1984) suggests represents the beginning of felsic volcanism and associated sedimentation. This conformable unit is the main host rock for uranium mineralization at the Kitts uranium deposit and at various other smaller occurrences in the Kitts-Post Hill Uranium Belt (Gandhi, 1978). U-Pb ages on pitchblende from the uranium occurrences range from 1730 to 1659 Ma (Gandhi, 1978; Kontak, 1980). Wilton *et al.* (in press) have suggested that the Lower Aillik uranium occurrences are related to granitic sources therefore the 1730-1650 Ma ages are reasonable.

The Lower Aillik Group has undergone a polydeformational history with upper greenschist to amphibolite grade metamorphism (Marten, 1977). The earliest fabric developed in the Lower Aillik rocks resulted from the tectonic ductile shearing on the contact with the Archean basement which produced subhorizontal thrusts. These subhorizontal sheets were later deformed into upright folds with shearing developed along the subvertical axial planes.



### 2.3.3 Upper Aillik Group

The contact between the lower and upper divisions of the Aillik Group has been variously described as disconformable (Marten, 1977) or conformable (Evans, 1980; Gandhi, 1978). The structural contact is, however, a zone of strong cataclasis and since the depositional contact has never been found, Wilton and Wardle (1987) consider the break a tectonic shear zone with interleaving of the two divisions.

The Upper Aillik Group is exposed in two separate belts (Figure 2-2), one disposed near the coast and centered around Makkovik, and the other an inland belt which includes the Michelin and Burnt Lake uranium deposits. Separating the two belts is the Adlavik Brook Fault. The inland Michelin belt was thought to be younger and related to the 1650 Ma Trans - Labrador batholith (Gower and Ryan, 1987) and also believed to be chemically distinct from the coastal belt. The coastal Aillik rocks have suffered more intense deformation and recrystallization of felsic volcanics when compared to the inland Aillik rocks (MacDougall, 1988). However, Scharer et al. (1988) have produced U-Pb zircon ages of  $1856 \pm 2$  Ma for rhyolites in the Michelin zone (Michelin Ridge) and  $1861 \pm 9/-3$  Ma for rhyolites in the Makkovik area, thus relating both belts to the same Makkovikian orogeny.

The Upper Aillik Group consists mainly of a variable assemblage of felsic volcanic and volcanoclastic rocks with

minor mafic volcanics (flows and tuffs). Various stratigraphic schemes for the Upper Aillik Group have been developed (Bailey, 1979; Gandhi, 1978, 1986; Gower *et al.*, 1982; Wilton and Wardle, 1987). Due to the apparent complexity of felsic volcanism and sedimentation, certain generalizations must be made. The basal units are arkose, conglomerate and tuffaceous sandstone with minor limestone, tuffs and silicate-iron formation. Lying on top is a thin mafic unit, primarily tuffaceous with minor pillow lava, breccia and flows. This is the marker horizon which Gower and Ryan (1986) used to distinguish between the early and late parts of the Upper Aillik Group. According to Gower and Ryan, this is overlain by a thick sequence of rhyolitic ash-flow and ash fall tuffs (welded and non-welded), quartz and/or feldspar porphyries, lapilli tuffs, rhyolitic breccias, tufficites and hypabyssal intrusives.

The volcanoclastic and sedimentary rocks (sandstone, conglomerate, limestone and iron formation) of the early portion of the Upper Aillik Group indicate deposition in a shallow marine environment with some marine incursions. There is some debate over the origin of the later sequence, consisting predominantly of rhyolites and tuffs, and various authors have placed the felsic volcanic rocks in pre-, syn- and anorogenic environments (e.g. Gower and Ryan, 1986; White and Martin, 1980). The volcanic rocks of the earlier portion of the Upper Aillik Group (Michelin ridge and Makkovik areas)

have been dated around 1860 Ma (Scharer et al., 1988) and apparently represent the first of two periods of felsic magmatism. The second pulse of felsic magmatic activity occurred around 1807 Ma (Scharer et al., 1988) with the formation of the quartz-feldspar porphyry in the White Bear Mountain area. This latter subvolcanic intrusion is probably equivalent to the synkinematic granitoids (Kerr, 1987) in the area.

Previous Rb-Sr geochronological studies on the rhyolitic rocks in the Michelin Ridge area yielded ages from 1659 to 1767 Ma (Gandhi, 1978; White, 1976; and Kontak, 1980). The Rb-Sr systematics in the felsic volcanic rocks must have undergone resetting (or partial resetting) due to regional metamorphism.

Upper Aillik Group rocks are relatively undeformed in the Walker Lake - Burnt Lake area. Deformation is considered to be much less intense with only a single planar fabric; a schistosity axial planar to tight isoclinal folds (Bailey, 1979). The folds have been overturned with the hinges of the anticlines reactivated as shear zones. Metamorphism is from lower to middle greenschist facies (Bailey, 1978).

#### **2.3.4 Moran Lake Group**

The Moran Lake Group has been broadly correlated with the Lower Aillik Group (Marten, 1977; Smyth et al., 1978;

Ryan, 1984) however some notable differences were outlined by Wilton et al. (1987b). The Moran Lake Group lies unconformably on only slightly deformed Archean granite of the Kanairiktok Intrusive Suite (Ryan, 1984). The basal Warren Creek Formation is comprised of a dolomitic regolith which grades into a succession of arkose, slate, chert, siltstone and minor mafic volcanics. The overlying Joe Pond Formation is a pillow lava unit with minor iron formation. The Moran Lake Group rocks underwent at least two periods of deformation prior to deposition of the 1649 Ma (Scharer et al., 1988) Bruce River Group. The first deformation produced a slaty cleavage and isoclinal folding plunging steeply to the east and overturned towards the north. The second deformation overprints the first and is represented by open asymmetric folding to tight crenulations (Smyth et al., 1975; North and Wilton, 1988).

#### **2.3.5 Bruce River Group**

The Bruce River Group was deposited unconformably on the polydeformed Moran Lake Group in the western portion of the Central Mineral Belt. The 1649 Ma Bruce River Group is bounded to the south by the Otter Lake Granite of the Trans-Labrador batholith which may be the subvolcanic equivalent to the Bruce River felsic rocks (Ryan et al., 1986). The unit has a basal conglomerate and fluviatile arkosic sedimentary rocks overlain by volcanoclastic arkoses which are in turn overlain by an

upper sequence of felsic ash tuffs and mafic flows (Ryan, 1984). The volcanic rocks are generally felsic, welded ash-flow tuffs with an approximate thickness of 8000 m (Ryan et al., 1987).

#### 2.3.6 Trans-Labrador Magmatism

The granitoid rocks of the CMB can be broadly assigned to either the 1.79-1.85 Ma Makkovikian Intrusive (Kerr, 1986; Kerr and Fryer, 1989) or the 1.65 Ga Trans-Labrador Batholith (Thomas et al., 1986). The granitoids of the Makkovikian Suite range in composition from granodiorite to quartz monzonite and have north-northeast trending fabrics which were produced during the Makkovikian orogeny (1.85 Ma). The granitoids have a synkinematic relationship in terms of deformation and metamorphism with the Aillik Group (i.e. Long Island Gneiss,  $1832 \pm 58$  Ma, Gandhi et al., 1988; Island Harbour Bay Plutonic Suite,  $1843 \pm 90$  Ma, Grant et al., 1983). Kerr (1987) sub-divided the Makkovikian suite into five units forming a discontinuous belt across the CMB.

The granitoids of the Trans-Labrador Batholith were emplaced during the Labradorian Orogeny, (Thomas et al., 1986). The intrusive rocks, which are post-tectonic with respect to the deformation in the Aillik Group, range in composition from pyroxenite to alkali-feldspar granite and have recently been divided into three divisions, based on

regional setting, size, and distribution which reflect different exposure levels within the batholith (Kerr, 1987).

Various geochronological studies on the time of emplacement for the Trans-Labrador Batholith range between 1795 Ma (Kerr, 1987) to 1500 Ma (Kontak, 1980). However, recent U/Pb and Rb/Sr geochronological data of Kerr and Krogh (1990) have indicated that most plutonic rocks of the Trans-Labrador Batholith are readily separated into the 1800 Ma post-tectonic Makkovikian or the 1650 Ma Labradorian plutonic suites. The younger ages (1500 Ma) obtained by Kontak (1980) are associated with the granitic rocks in the vicinity of the Grenville tectonic front that could have suffered some isotopic disturbance during Grenvillian metamorphism.

#### **2.4 Property Geology**

The geology of the Burnt Lake area, as shown on Maps 1 and 2 (back pocket) is dominated by rhyolitic volcanic and sedimentary rocks of the Upper Aillik Group. The rocks are mainly pink to grey varieties of subaerial tuffaceous rocks with varying proportions of quartz and feldspar phenocrysts-porphyroclasts that are both welded and non-welded. There are relatively minor amounts of non-porphyritic rhyolite, ash flow tuff, tuffaceous sandstones and siltstones, pyroclastic breccias and lapilli tuffs. The sedimentary rocks are

typically shades of blue, green and pink to maroon well-bedded, tuffaceous sandstones and siltstones.

Intrusive into the volcanic sequence in the vicinity of the Burnt Lake and Emben uranium showings is a ca. 1650 Ma fine to medium-grained leucocratic quartz monzonite to granite called the Burnt Lake Granite (This granite has also been called the Walker Lake Granite by Bailey (1979) and constitutes part of Kerr's (1987) Trans Labrador Batholith).

Both units were subsequently intruded by metadiabase and metadiorite dykes, and even later by northeast trending, coarse-grained gabbroic dykes of the ca. 1450 Ma Michael Gabbro Suite (Bailey, 1979).

Mapping was complicated by the highly variable felsic volcanic rocks and problems developed in defining an accurate stratigraphy of the area, however, a generalized stratigraphic section is presented in Figure 2-4 . The lithological subdivisions of Bailey (1979) were generally followed because of the more regional nature of his study.

#### 2.4.1 Unit 1

Unit 1 underlies much of the western portion of the map area (Map 1). Gower et al. (1982) considered Unit 1 to be the base of the Upper Aillik Group. In the map area this unit (which hosts high grade uranium mineralization at the Emben Main and Emben South Zones) has limited exposure east of Burnt

Lake as heavy drift cover obscures its relationships with other units. The rocks in the Emben area have been named feldspathic quartzite by Gandhi *et al.* (1969), meta-rhyolite by Krajewski (1976), arkosic sandstone by Bailey (1978), volcaniclastic sandstone by Cote (1980) and granulite by Harder (1981).

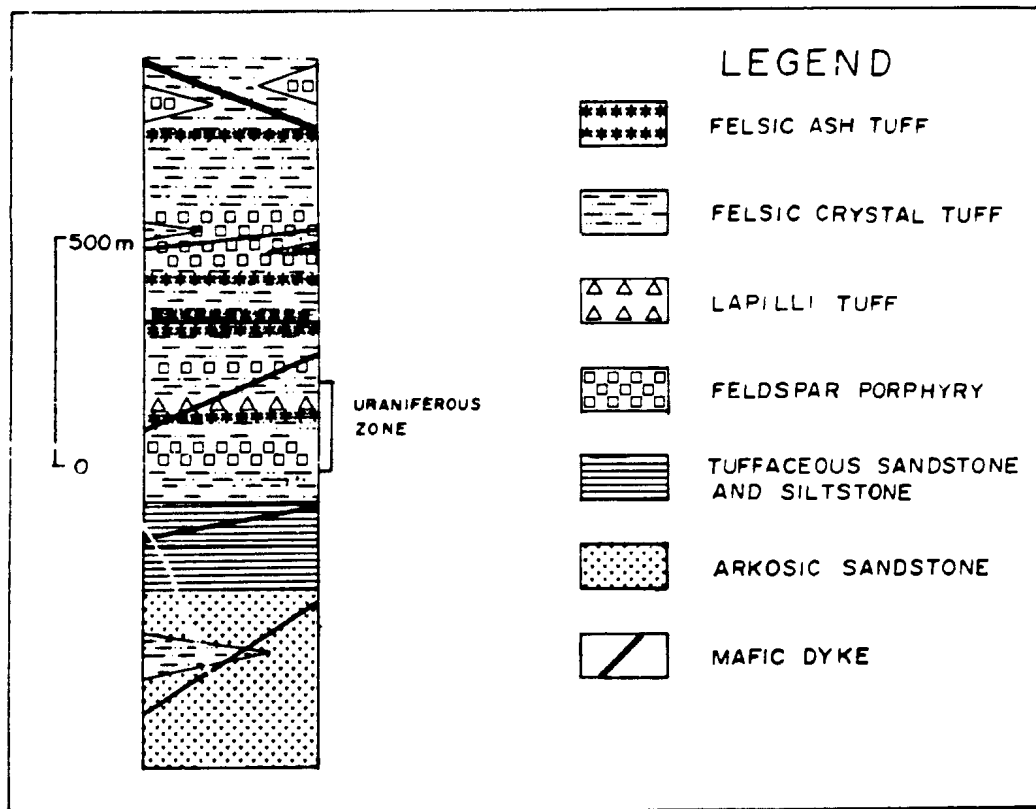


Figure 2-4: Generalized stratigraphic section at Burnt Lake



The Emben Main Zone is underlain by metamorphosed arkosic sandstone (Figure 2-5A) that is predominantly pink to grey, and composed of 65-85 % plagioclase forming aggregates of grains with an interlocking to mosaic texture and a slight parallel fabric due to the flattening of the individual grains. Some of the larger plagioclase grains show undulatory extinction. Quartz is generally not present in most sections, however, quartz segregations do sometimes occur parallel to the foliation and are coarser grained than plagioclase and partially recrystallized. Garnet is present as anhedral blebs in distinct bands parallel to the plagioclase foliation. Microcline grains and light green actinolite prisms were seen in close association with the garnet bands and are smaller than the plagioclase. Sphene occurs as evenly distributed euhedral to subhedral grains. Accessory minerals include epidote, zircon, magnetite, hematite, uraninite, chalcopyrite and galena. In some outcrops, relict bedding planes (1-2 cm thick) are outlined by the alignment of <1 mm thick mafic bands (up to 5% magnetite). Intercalated with this sedimentary unit are minor porphyritic tuffs, indicating the increasingly proximal nature of volcanism.

A notable difference in the mineralogy at the Emben South Zone compared to the Emben Main Zone is the common occurrence of the ferromagnesium mineral aegirine, forming clumps and single anhedral grains with minor riebeckite prisms (Figure 2-5B). In some sections pyrrhotite occurs as large aggregates

of anhedral grains associated with the aegirine. Accessory minerals include sphene, apatite, magnetite, pyrite, uraninite, zircon, chalcopyrite and galena.

#### 2.4.2 Unit 2

Unit 2 is well exposed just south of Maclean Lake in a broad east-west trending belt (Map 1). Its actual relationship with Unit 1 is unknown but Bailey (1979) assumed that it overlies Unit 1. The rocks in this formation are composed of well bedded, volcanoclastic siltstone and sandstone in shades of pink, green and grey, probably indicative of changing depositional conditions (Figure 2-6). Bedding and/or laminations are well preserved with a general east-west strike and southerly dip. Generally, bedding is continuous, but occasionally cross-bedding was observed.

In thin section, the rock has a very fine-grained quartzo-feldspathic matrix. Coarser layers have minor quartz and feldspar phenocrysts, while most grains are embayed and subrounded. Accessory minerals include epidote and magnetite.

**Figure 2-5:**

**(A):** Recrystallized (sugary) arkosic sandstone with thin bands of magnetite. Sample is from the Emben Central showing. Scale bar is in centimetres. **(B):** Bands and clots of aegirine within tuffaceous sediments. Photograph was taken at the Emben South showing.



#### 2.4.3 Unit 3

This unit forms an east-west trending belt across the map area and is disrupted by faults (Map 1). The unit consists of red to maroon volcanoclastic siltstone and sandstone. It conformably overlies Unit 2 with similar bedding attitudes, and is probably the regressive equivalent of Unit 2 (i.e. indicating very shallow water to terrestrial depositional conditions). In thin section, the rock has a very fine-grained quartzo-feldspathic matrix that shows greater deformation than Unit 2. The rock has a strong foliation with abundant cross-cutting calcite-rich veinlets (Figure 2-7). Bedding is defined by mafic-rich layers and coarser quartz and feldspar bands.

#### 2.4.4 Unit 4

Unit 4 is the most important rock type with respect to mineralization, yet, it is also the most difficult to unravel. The outcrop pattern is generally confined to northeasterly trending linear ridges separated and overlain by abundant drift cover. Unit 4 is grouped into several subunits, including a felsic pyroclastic unit and an underlying feldspar porphyry. A subdivision of the felsic pyroclastic unit is shown on Map 2 because of its close association with uranium mineralization, and includes felsic ash flow tuff, felsic crystal tuff, lapilli tuff and

**Figure 2-6:**

**(A): Well bedded volcaniclastic siltstone of Unit 2. Lens cap for scale. (B): Interbedded volcaniclastic siltstone and sandstone of Unit 2. Lens cap for scale. (C): Close-up photograph of bedded volcaniclastic siltstone of Unit 2. Scale bar is in centimetres. (D): Close-up photograph of pink and green bedded volcaniclastic siltstone of Unit 2. Scale bar is in centimetres.**





agglomerate. Occasionally, contacts between the various subunits were observed, however, the sub-members interdigitate and transitions were generally not documented.



**Figure 2-7: Close-up photograph of maroon volcaniclastic siltstone of Unit 3. Note calcite (white) infilling cross-cutting fractures. Scale is in centimeters.**



#### **2.4.4.1 Unit 4a: Felsic Ash Tuff**

The felsic ash flow tuff (Figure 2-8A,B) is pink to grey, fine to medium-grained and generally massive with local green banding (amphibole and pyroxene). The mafic banding wraps around the phenocrysts in an eutaxitic texture. Locally, the rock contains minor 1-2 mm size blue quartz eyes.

In thin section the quartz phenocrysts are recrystallized and form a coarse granoblastic texture. The mafic bands consist of acmite and augite that sometimes occur as aggregates. The matrix is generally fine-grained quartzofeldspathic showing a granoblastic-polygonal texture.

#### **2.4.4.2 Unit 4b: Undivided Felsic Crystal Tuff, Ash Tuff and Lapilli Tuff**

This unit was not divided in the field because of the complex and discontinuous nature of the felsic units. However, the rock types are described separately below.

The felsic crystal tuff (Figure 2-8C) is fine to medium grained with a pink to greenish-grey colour. The rock has a wide range of quartz/feldspar phenocryst ratios and sizes with 5-15%, 4-10 mm white feldspar and 1-10%, 1-5 mm blue quartz eyes set in a fine grained tuffaceous matrix. The quartz-feldspar porphyry is sometimes welded as shown in Figure 2-9A. Locally, the unit is brecciated as shown in Figure 2-9B,

where angular fragments of quartz-feldspar porphyry are set in a finer grained tuffaceous matrix.

In thin section, the quartz phenocrysts are recrystallized and form a granoblastic texture. Some quartz grains are intensely corroded and show undulose extinction. The feldspar phenocrysts, usually subhedral with a rectangular shape, are 2-10 mm in size and include orthoclase and plagioclase with varying secondary alterations. Orthoclase is commonly perthitic along its margins due to secondary alteration. Plagioclase occurs as anhedral grains with a variable replacement by chessboard albite. The matrixes generally has granoblastic-polygonal texture composed of quartz and feldspar with lesser plagioclase. Mafic minerals include amphibole, pyroxene, and biotite. From SEM probe work, accessory minerals identified include ilmenite, sphene, zircon and magnetite. Rarely, ash flow tuffs, both welded and non-welded contain both crystal and lithic components (Figure 2-9C).

#### **2.4.4.3 Unit 4c: Lapilli Tuff**

The lapilli tuff (Figure 2-10A) is greenish-grey to pink and consists of 40-70% elliptical white feldspar fragments of 1-4 cm size with minor quartz in a fine grained greenish quartz-crystal ash matrix. A distinct cleavage is developed in the rocks.

In thin section the rock possesses irregular shaped recrystallized quartz phenocrysts and feldspars in a groundmass of polygonal, recrystallized quartz and feldspar (granoblastic). Accessory minerals include chlorite, biotite, augite and riebeckite.

#### **2.4.4.4 Unit 4d: Feldspar Porphyry**

The feldspar porphyry (Figure 2-10B) has a dark purplish-grey color, is generally massive, and is locally flow banded with up to 50% euhedral feldspar phenocrysts in the 1-10 mm size range and 1-5% blue quartz eyes in the 1-4 mm range.

In thin section the rock looks similiar to the felsic crystal tuff with feldspar phenocrysts in a polygonal granoblastic matrix of quartz and feldspar. Coarser quartz and feldspar lenses are common indicating that the unit was probably welded. The feldspars are commonly corroded and poikilitic and have been invariably replaced by perthitic

microcline. Accessory minerals identified by SEM include magnetite, ilmenite, sphene and zircon.

#### **2.4.4.5 Unit 4e: Mafic Tuffs and Intermediate Flows**

Mafic and intermediate tuffs and flows occur as lenses within the feldspar porphyry unit in the northwestern corner of the study area (see map 3: Aurora River). The andesite is light green-grey to dark green-grey and is commonly flow banded with epidote, chlorite and sericite alteration. The banding was identified as tremolite by the X-ray diffraction method. Cutting the unit are abundant (0.1-0.5 m wide) quartz-carbonate veins which carry fibrous tremolite and specular hematite pods. The andesite is commonly highly sheared and brecciated especially at lithological contacts (Figure 2-10C).

**Figure 2-8:**

**(A): Banded ash tuff of the Upper Aillik Group in the Burnt Lake area. Lens cap for scale. (B): Contact between welded ash tuff and feldspar porphyry. Lens cap for scale. (C): Contact between a grey quartz-feldspar porphyry and a pink quartz porphyry. Marker on contact for scale.**



A



B



C

**Figure 2-9:**

**(A): Welded quartz-feldspar porphyry of Unit 4b. Scale is in centimetres. (B): Explosive breccia of quartz-feldspar porphyry fragments in a finer grained ash tuff matrix. (C): Ash tuff containing mafic lithic fragments. Lens cap for scale.**



A



B



C

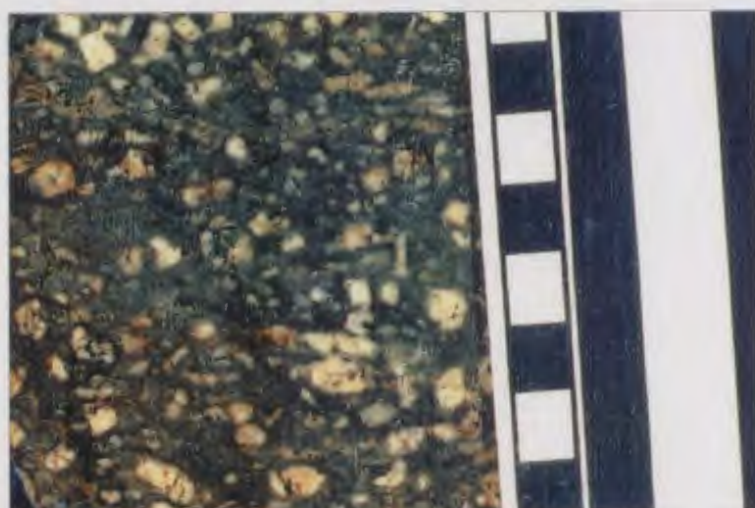


**Figure 2-10:**

(A): Contact between lapilli tuff and a bluish-grey feldspar porphyry. Pencil for scale. (B): Close-up photo of feldspar porphyry (Unit 4d). Note euhedral feldspar phenocrysts and smaller blue quartz eyes in a blue-grey matrix. (C): Sheared and brecciated outcrop of andesite near the Aurora River radioactive showings. Hammer in bottom left-hand corner of photo for scale.



A



B



C

## 2.5 INTRUSIVE ROCKS

Granitoid rocks of the Burnt Lake area are disposed in three separate areas as seen in Map 1. Units 5b and 5c crop out in the extreme northwest and southeast corners of the map sheet, respectively. Unit 5a crops out sporadically throughout the central portion of the map, however, the western intrusive contact is fairly well exposed with some drift cover.

The granitoids are divided into two groups based on field, petrographic and chemical evidence (discussed later). Units 5b and 5c are considered to be part of the synkinematic Makkovikian suite (1.8-1.7 Ga), while the post-tectonic granitoids of unit 5a belong to the younger Trans-Labrador batholith (1.65 Ga). The differences between the granitoids is evident in the rock type, petrology, texture and chemical signatures.

### 2.5.1 Unit 5a

This unit comprises the Burnt Lake Granite and has limited surface exposure in the area. The rock unit comprises a suite of fine to medium grained, pink to grey, muscovite-bearing leucogranite to quartz monzonite (Figure 2-11A). Mafics (biotite and hornblende) are usually less than 2%, however, the eastern portion of the intrusive contains up to 15% biotite (Figure 2-11B). In thin section the granite is

composed of 20-30 % quartz, 40-50% potassium feldspar and 20% plagioclase. The groundmass is a complex intergrowth of quartz and feldspar in an almost granular texture. The potassium feldspar is usually orthoclase with lesser microcline. The plagioclase is commonly rimmed by another feldspar and/or magnetite, and has irregular boundary contacts. Accessories include epidote, sphene, and chlorite,  $\pm$  tremolite. In general, mafic minerals (biotite and hornblende) are only minor constituents.

The western intrusive contact with Unit 4 is quite sharp (Figure 2-11C) as the undeformed granite cuts meta-felsic volcanic rocks that have a definite fabric without an obvious contact aureole. The lack of extensive contact metamorphism in addition to rare miarolitic cavities in the granite suggests that the intrusion was high level and only a small temperature differential existed between it and the wall rocks. Pegmatite dykes (0.1 to 1 m wide) occur near the contact with the felsic volcanic rocks which suggests aqueous vapour phase accumulation occurred at the contact (Figure 2-12A). Bailey (1979), however, described the contact as a transitional pluton-hypabyssal volcanic relationship.

#### **2.5.2 Unit 5b**

This granitic phase crops out in the northern section of the area in a steep cliff exposure. It is composed of a pink,

medium to coarse-grained hornblende-biotite granite that is foliated and almost gneissic in places (probably pre-dates 5a) (Figure 2-12B). The rock is composed mainly of fractured plagioclase with lesser potassium feldspar and quartz, all of which has been recrystallized. Accessory minerals include epidote, sphene, zircon, pyrite, sphalerite and ilmenite.

#### **2.5.3 Unit 5c**

This unit crops out in the southeastern corner of the map area. The rock is a grey, medium to coarse-grained hornblende-biotite granite (Figure 2-12C). This unit is much fresher looking than Unit 5b with anhedral twinned plagioclase (50 % of the rock), microcline (20-25 %), and interstitial quartz (10-15 %). Besides abundant hornblende and biotite, accessory minerals include epidote, sphene, calcite and magnetite.

#### **2.5.4 Unit 6**

This unit is comprised of various metadiabase and metadiorite dykes which cut all previous units. The dykes have been classified as early or late depending upon the degree of deformation. The earlier dykes (Figure 2-13A) are generally 0.5 m to 3 m wide and demonstrate multiphase deformation in the form of refolded folds and crenulations. The dykes are

generally greenish in colour and are fine grained. The lamprophyre dykes have been classified as vogesites by Kontak (1980). In thin section the dykes contain 50% riebeckite, 10% biotite, 20-25% orthoclase, 15% plagioclase, 5% quartz and 2-3% opaques. The feldspars occur as coarser phases with the amphiboles and quartz forming a finer grained matrix. The orthoclase has been altered to sericite and epidote. The plagioclase is commonly rimmed by orthoclase.

The later dykes are generally 5-20 m wide and have an easterly to northeasterly strike (Figure 2-12B).

#### 2.5.5 Unit 7

Northeast trending gabbro dykes are exposed in the northeast and southwest portions of the map area and cut both the volcanic and granitic rocks. The Michael Gabbro, as it is known (Fahrig and Larochelle, 1972) has a K-Ar age of 1000 Ma (Gandhi et al., 1969). In outcrop the rock has a fine grained strongly foliated chill margin, while towards the centre the dyke is medium to coarse grained with euhedral pyroxenes and plagioclase up to several centimeters long with a very weak foliation. The rock has a grey to green-black weathered surface and forms prominent linear ridges.

**Figure 2-11:**

**(A) Fine grained leucocratic Burnt Lake Granite. Scale bar is in centimetres. (B): Biotite-rich phase of the Burnt Lake Granite. Scale bar is in centimetres. (C): Intrusive contact between the Burnt Lake Granite (bottom half) and felsic tuff of the Upper Aillik Group. Pencil at contact.**

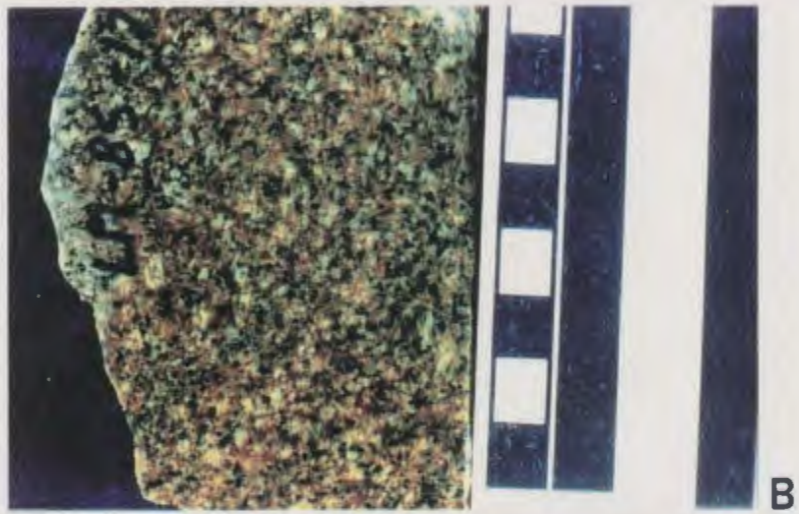
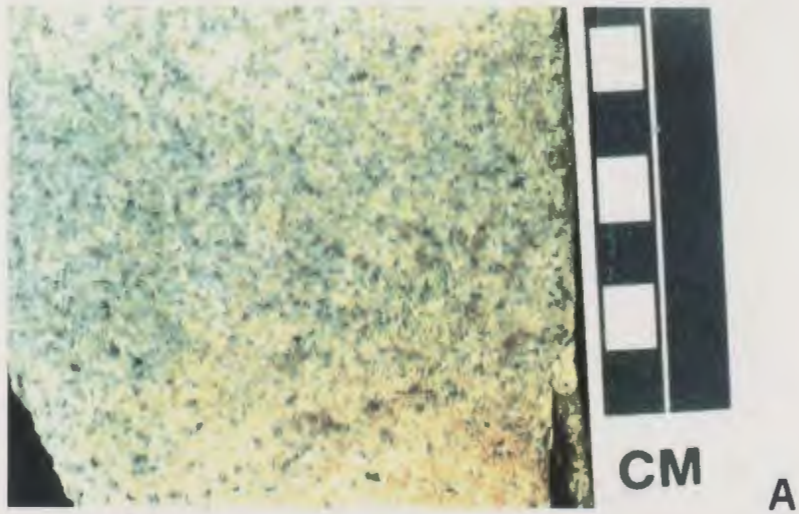
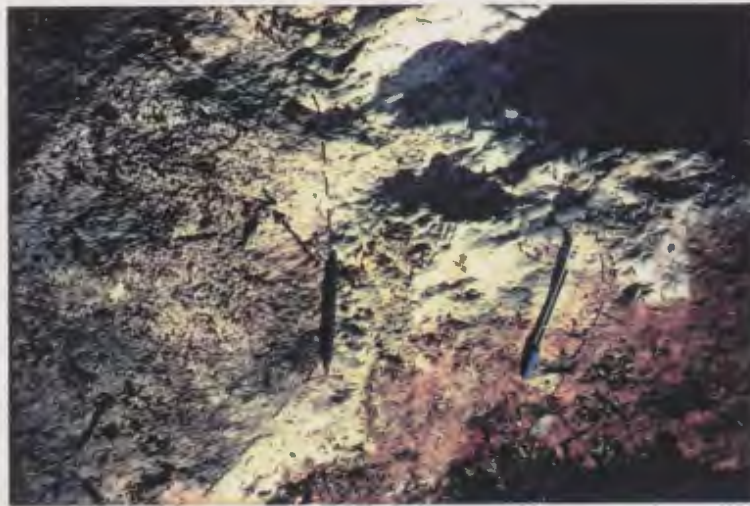


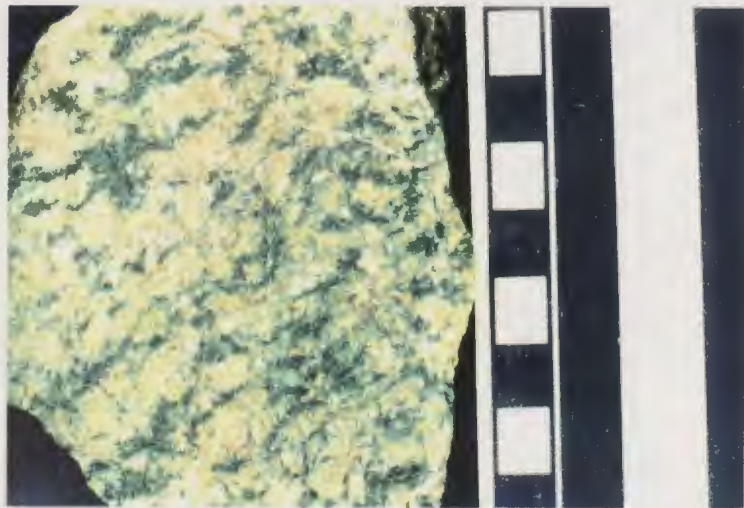


**Figure 2-12:**

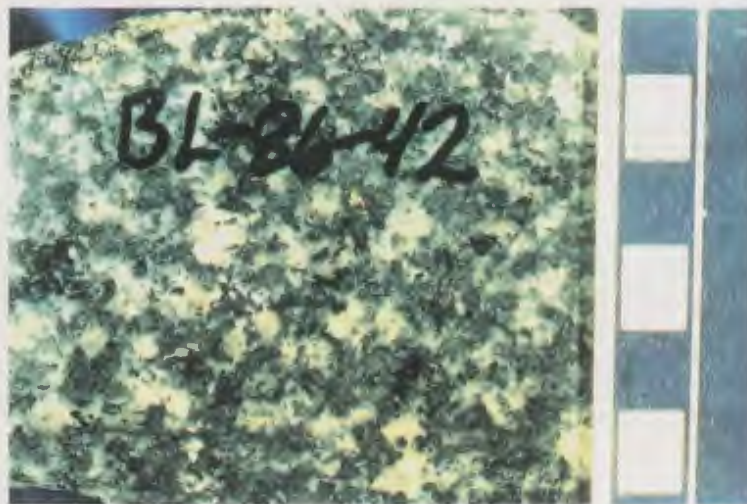
(A): Pegmatite dyke at the contact with felsic tuff of the Upper Aillik Group. Dashed lines outline the pegmatite dyke. Pencils for scale. (B): Foliated hornblende-biotite granite of Unit 5b. (C): Coarse grained hornblende-biotite granite of Unit 5c. Scale bar is in centimetres.



A



B



C

**Figure 2-13:**

**(A): Amphibolite dyke showing refolded folds. Photograph was taken next to the Burnt Lake Camp. Width of photo is approximately 2 m. (B): Metadiabase showing sharp intrusive contacts with the felsic volcanic tuffs of the Upper Aillik Group.**

**A****B**

## **2.6 Structural Geology**

### **2.6.1 Regional Structural Geology**

The White Bear Mountain - Walker Lake area has undergone polyphase deformation. Structural trends are predominantly east-northeast with foliations commonly dipping to the south-southeast. The earliest deformation produced overturned, tight to isoclinal folds and low angle thrusts (Gower and Ryan, 1986). The latest deformation produced upright folding, subvertical planar structures, and subhorizontal stretching lineations.

### **2.6.2 Local Structural Geology**

Changes in lithology, as mapped in the Burnt Lake area, are usually attributable to faulting, however, the extent of the deformation affecting the lower sedimentary and upper volcanic sequences is similar. In general, the sedimentary rocks in the Burnt Lake area have well-developed northeasterly striking, southeast-dipping bedding, while the volcanic rocks have a northeasterly striking, south dipping cleavage with southeasterly plunging mineral lineations.

The main phases of Hudsonian and Makkovikian deformations which affected the Burnt Lake area produced isoclinal, southwesterly plunging antiform-synform pairs, with the

antiforms generally sheared along their axes (Bailey, 1979). Bailey also mentions the presence of L-fabrics (mineral lineations) in granitic rocks. Bailey (1978) states that lineations are developed along fault (mylonitic) and/or shear planes perpendicular to the shear fabric.

Bailey (1979) and Gower et al. (1982) ascribe L-fabric development to shearing/faulting during Grenvillian deformation. Figure 2-14 is an equal area contoured stereographic projection of mineral stretching lineations as measured in the Burnt Lake area. The diagram indicates that the lineations mainly have a steep southeastern plunge, with minor examples of northwestern plunges, suggesting a fold with a NE-SW strike. Gower et al. (1982) stated that folds were overturned to the north-northwest during the Grenvillian deformation, concurrent with the L-fabric development. If the linear fabrics, as shown in Figure 2-14, were produced during the Grenvillian orogeny, then this event obviously had a great effect on rocks in the Burnt Lake area, enough to suggest that the area lies within the Grenville Province.



**Figure 2-14: Equal area contoured stereographic projection of mineral stretching lineations as measured in the Burnt Lake area.**

**CHAPTER 3****LITHOGEOCHEMISTRY****3.1 UPPER AILLIK GROUP****3.1.1 Methodology**

Forty-two samples out of a total of one hundred and six samples of the Upper Aillik Group volcanic and volcanoclastic sedimentary rocks were analyzed for both major and trace element contents. The remaining sixty-four samples of this group were analysed for trace elements only. Five samples were analysed for rare earth elements. A brief rock and/or petrographic description of each sample is given in Appendix II.

Analytical methods, precision and accuracy are described in Appendix I. Major oxides were analysed by atomic absorption spectrometry methods (AA). The trace elements were determined on pressed whole-rock powder pellets by X-ray Fluorescence (XRF) techniques (Longerich and Veinott, 1986). Other trace elements including Ag, As, Bi, Cd, Co, Mn, Mo, and P were determined in 44 samples by Nitric-Acid-Aqua-Regia digestion and ICP emission spectroscopy techniques at Chemex Labs Ltd., Vancouver. Gold analyses in 37 samples were determined by Fire Assay and Atomic Absorption methods by



Chemex Labs Ltd.. REE contents were determined by a thin film XRF technique (after Fryer, 1977).

The geochemical data and normative mineralogies are also presented in Appendix I. Sample locations are shown on Map 1B (back pocket). Most of the samples were collected in the vicinity of the radioactive occurrences which led, therefore, to a sampling bias for these areas. Only those samples with < 50 ppm U are considered as being unmineralized and are described in this section.

The data obtained from the geochemical analyses have been plotted on a series of standard variation and discrimination diagrams in an attempt to classify the Upper Aillik Group with respect to established volcanic rock suites. The original analyses are recalculated to 100% anhydrous; samples having >5% loss on ignition (LOI) are considered to be suspect and have, therefore, been omitted. The symbols used for the various diagrams correspond to the lithological subdivisions shown in Appendix I and on Maps 1 and 2 (back pocket).

### **3.1.2 Major Element Patterns and Classification**

A frequency distribution diagram (Figure 3-1a) of  $\text{SiO}_2$  in the samples indicates a bimodal distribution with a wide range of values, the majority of samples falling in the rhyolite range ( $\geq 70\% \text{SiO}_2$ ). The relative proportions of rock types in the data base may reflect a sampling bias towards the

felsic end due to the availability of more resistant outcrop exposures. However, the lack of rock samples with intermediate compositions has been noted by previous workers (e.g. White, 1976; Gandhi, 1984).

Using the classification scheme of Pecerillo and Taylor (1976) on a  $K_2O$  versus  $SiO_2$  diagram (Figure 3-1b), the vast majority of samples plot as high-K rhyolites. Arkosic sandstone and felsic tuff samples of unit 1 plot as low-K rhyolites and one sample plotted in the andesite field. Intermediate samples from the Aurora River area (Unit 4f) plot in the basalt to basalt-andesite fields.

On Cox *et al.*'s (1979) plot of total alkalis versus silica (Figure 3-1c), the vast majority of felsic volcanic samples plot on the diagram as rhyolites, while the intermediate volcanic rocks plot as trachyandesites, and the diabase dykes as mugearites.

#### **3.1.2.1 Upper Aillik Group**

Harker diagrams for major element distributions in the Upper Aillik Group volcanic rocks from the Burnt Lake area are shown on Figure 3-2. Chemical trends can be observed between some elements, however, the scatter in others may be attributable to widespread alteration. A single source for both the mafic and felsic rocks is probably not valid because of the non-linear chemical trends between the two groups. Of

all elements plotted, only  $\text{Al}_2\text{O}_3$  has a definitive correlation with  $\text{SiO}_2$  in the felsic volcanic rocks (typical of a normal differentiation trend).

**Unit 1: Arkosic Sandstone and Felsic Tuff:**

This unit is characterized by high  $\text{SiO}_2$  (>70%), enriched  $\text{Na}_2\text{O}$  (7-9%) and depleted  $\text{K}_2\text{O}$  (0.1-0.9%) contents which are possibly the effects of Na metasomatism. The high  $\text{SiO}_2$  contents and geochemical trends similar to those observed in the other felsic volcanic rocks in the area support a derivation from a felsic volcanic source.

**Units 2 and 3: Volcaniclastic Sandstone:**

Only one sample was analysed for major elements from Unit 2 and it plots with the felsic volcanic group. No samples from Unit 3 were analysed for major elements.

**Units 4a, 4b and 4c: Felsic Ash Tuff, Felsic Crystal Tuff,  
Lapilli Tuff:**

Banded ash tuffs, crystal tuffs and lapilli tuffs of Unit 4 exhibit considerable geochemical variation. Variations in  $\text{Na}_2\text{O}$ ,  $\text{K}_2\text{O}$  and  $\text{Al}_2\text{O}_3$  are most prevalent. Two geochemically distinct groups (a low  $\text{Na}_2\text{O}$ -high  $\text{K}_2\text{O}$  group and a low  $\text{K}_2\text{O}$ -high  $\text{Na}_2\text{O}$  group) are evident as a result of metasomatic alteration. Analyses reported here are comparable to those reported by Kontak (1980).

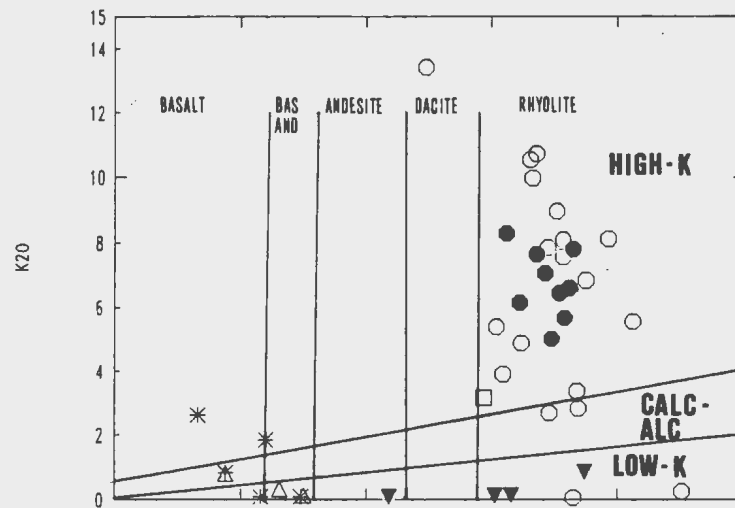
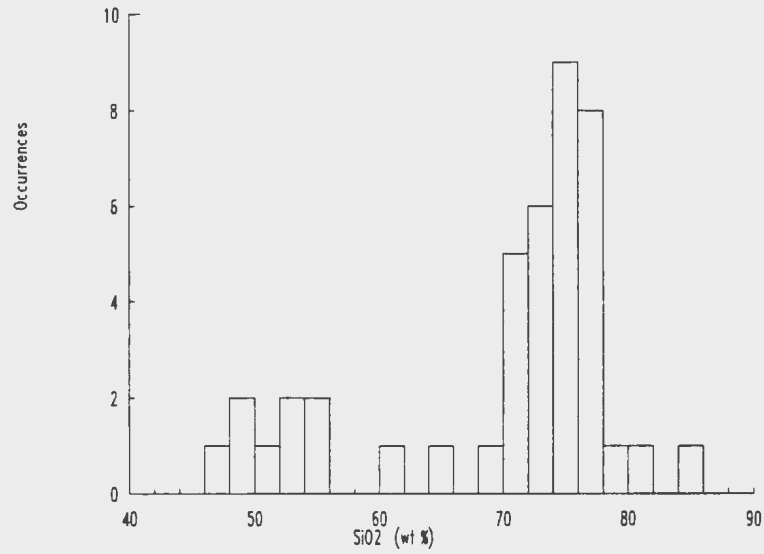
Figure 3-1a: Histogram of weight percent  $\text{SiO}_2$  in the Upper Aillik Group samples (based on 2% intervals).

Figure 3-1b:  $\text{K}_2\text{O}$  vs  $\text{SiO}_2$  plot showing classification fields by Peczerillo and Taylor (1976). Symbols are as follows; Solid inverted triangle: arkosic sandstone and felsic tuff (Unit 1a); Open triangle: diabase dykes (Unit 1b); Open square: volcanoclastic sedimentary rocks (Units 2 and 3); Open circle: felsic volcanic crystal tuff, ash tuff, and minor lapilli tuff (Units 4a, 4b, 4c); Solid circle: feldspar porphyry with minor quartz (Unit 4d); Asterisk: andesite (Unit 4f).

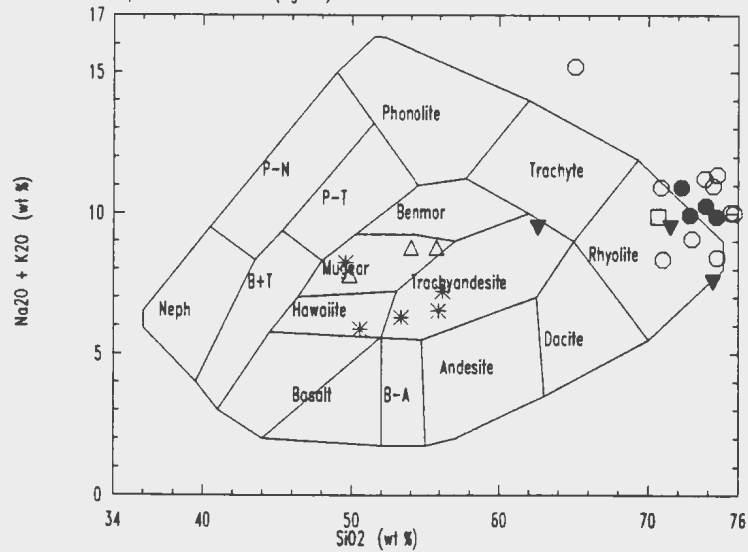
Figure 3-1c:  $\text{K}_2\text{O} + \text{Na}_2\text{O}$  vs  $\text{SiO}_2$  plot showing classification fields by Cox et al, 1979. Note that most of the rocks plot in the rhyolite or trachyandesite fields. Symbols are as in Figure 3-1b.

Distribution of Silica in Upper Aillik

No. of Samples: 106



Aillik Group Cox et al 1979 (fig 2.2)



**Unit 4d: Feldspar Porphyry:**

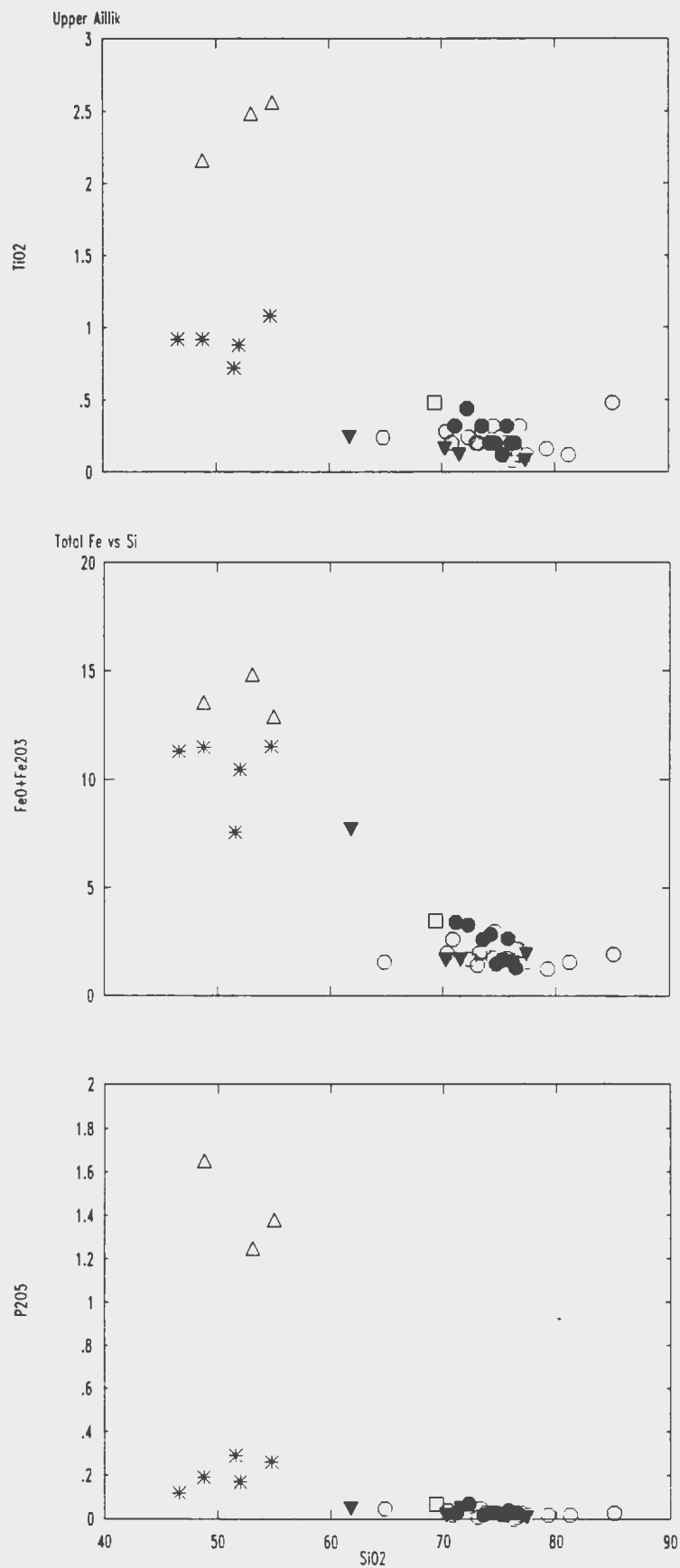
Major element geochemistry patterns for the feldspar porphyry unit are very similiar to other felsic volcanic rocks of Unit 4 and follow the same gross geochemical trends. These rocks appear to be transitional between the two  $\text{Na}_2\text{O}$ - $\text{K}_2\text{O}$  groups in Units 4a-4e and, therefore, Unit 4d represents the most pristine group.

**Unit 4f and Unit 1b: Intermediate to Mafic Rocks:**

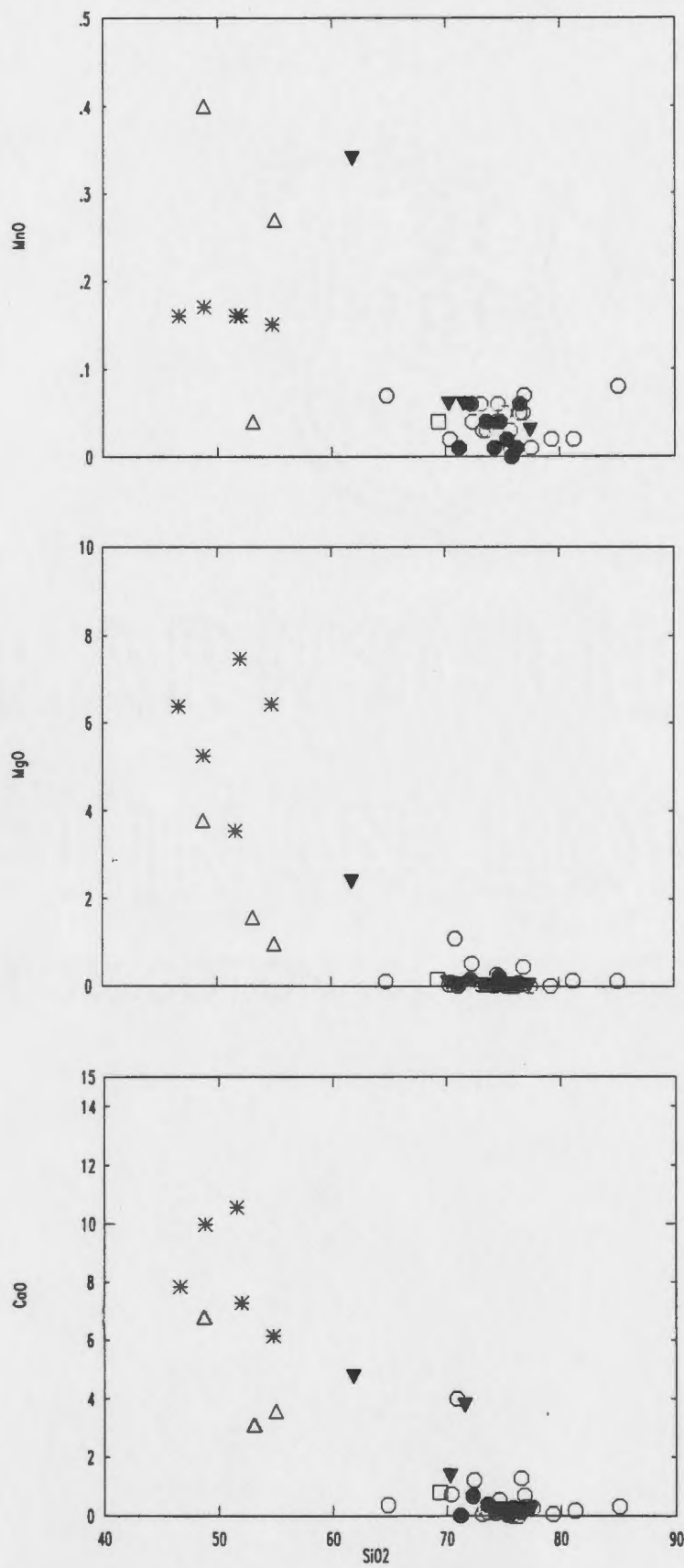
The mafic rocks show a narrow range of values (12-16 wt %  $\text{Al}_2\text{O}_3$ ) and are separated from the felsic volcanic trend. The mafic dyke samples from Emben have elevated values of  $\text{P}_2\text{O}_5$ ,  $\text{TiO}_2$  and  $\text{FeO}$  when compared to the felsic rocks and the andesitic rocks of the Aurora River area. On the  $\text{K}_2\text{O}$  and  $\text{Na}_2\text{O}$  versus  $\text{SiO}_2$  plots, all rocks have a wide scatter indicating the relative mobility of these elements. The mafic rocks can be characterized as being high soda, low potassium rocks.

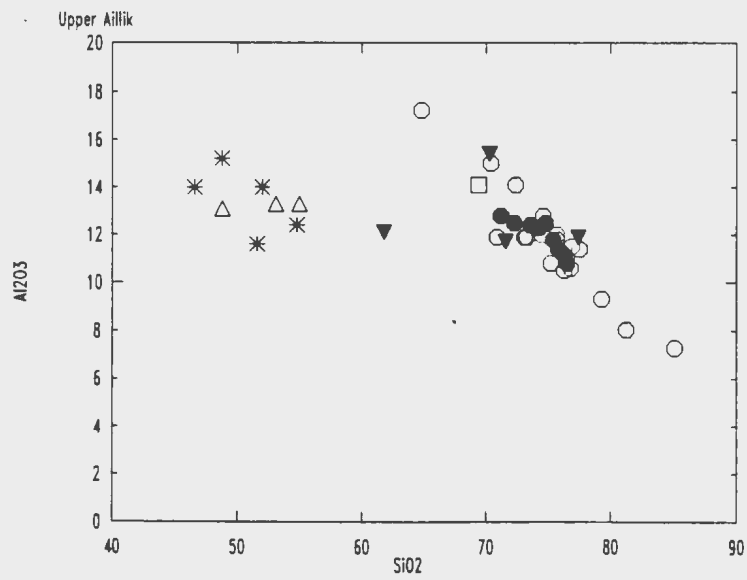
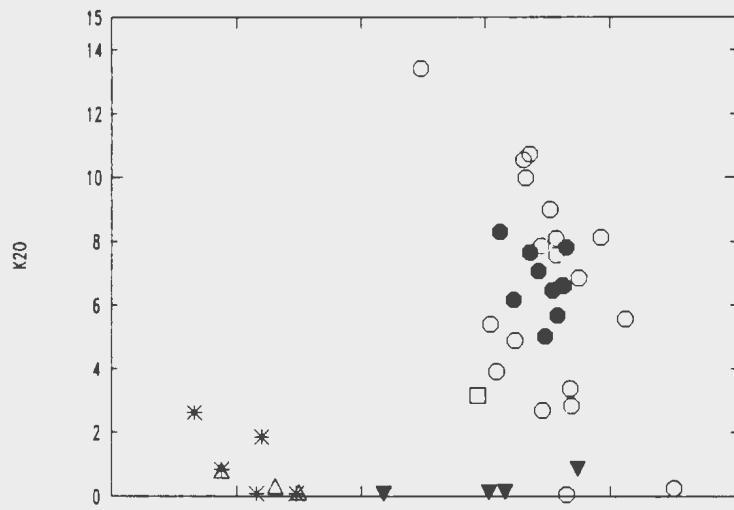
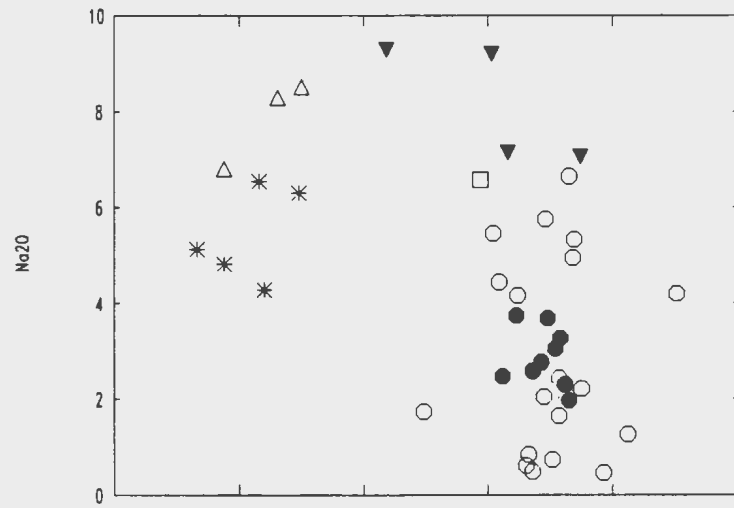
The  $\text{K}_2\text{O}$  versus  $\text{SiO}_2$  plot of Gill (1981 - Figure 3-3) for andesites shows a wide variation in  $\text{K}_2\text{O}$  for andesites from the Aurora River area reflecting probable metasomatic activity, however, all the samples plot in the basic field of the diagram.

Figure 3-2: Harker variation diagrams of major elements in the Upper Aillik Group samples from the Burnt Lake area. Oxides are in weight percent. Symbols are as follows; Solid inverted triangle: arkosic sandstone and felsic tuff (Unit 1a); Open triangle: diabase dykes (Unit 1b); Open square: volcaniclastic sedimentary rocks (Unit 2); Open circle: felsic volcanic crystal tuff, ash tuff, and minor lapilli tuff (Units 4a, 4b, 4c); Solid circle: feldspar porphyry with minor quartz (Unit 4d); Asterisk: andesite (Unit 4f).









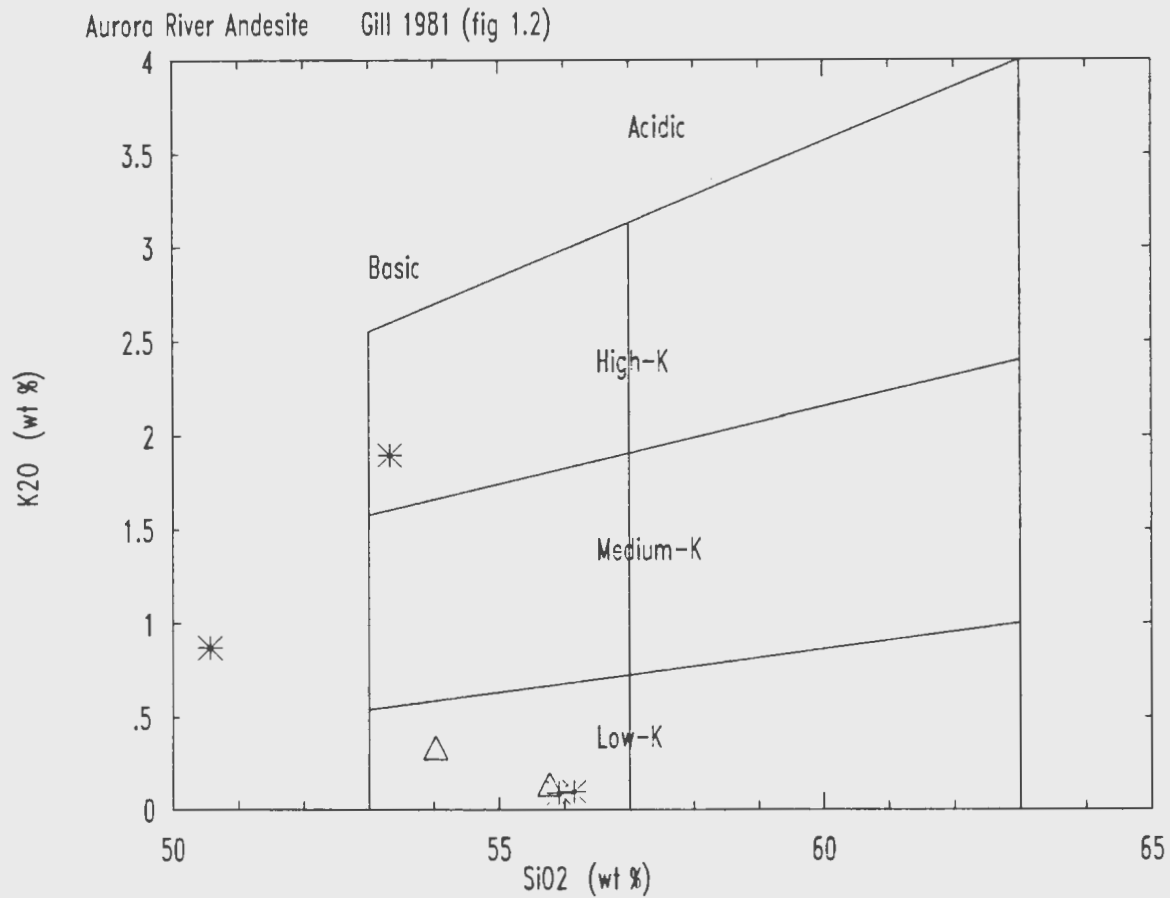


**Figure 3-3:  $K_2O$  vs  $SiO_2$  plot showing classification of andesites by Gill, 1981. Symbols as in Figure 3-2.**

According to Hughes' (1973) method of distinguishing between igneous and metasomatised chemical compositions (Figure 3-4), only about one third of the Upper Aillik Group samples fall within the igneous spectrum. Approximately one third of the samples fall into the Na metasomatised field and the remaining third in the potassic metasomatised field (i.e. high  $K_2O$  relative to  $Na_2O$ ). However, it should be noted that rocks which lie within the "igneous spectrum" may still have undergone considerable change in  $K_2O/Na_2O$  and this must be considered when examining lithogeochemistry. The diagram suggests that the suite of rocks has suffered alkali metasomatism and any classification involving the alkalis should be viewed with caution. White and Martin (1980) were the first to document the soda enrichment as a metasomatic event within the felsic volcanic rocks, and they attributed the Na metasomatism to circulation of synvolcanic magmatic or meteoric fluids. Evans (1980) attributed the Na metasomatism to be a result of an interaction with sea water. Although a major synvolcanic metasomatic event occurred, it is also possible that local alkali leaching/enrichment processes occurred (discussed below).

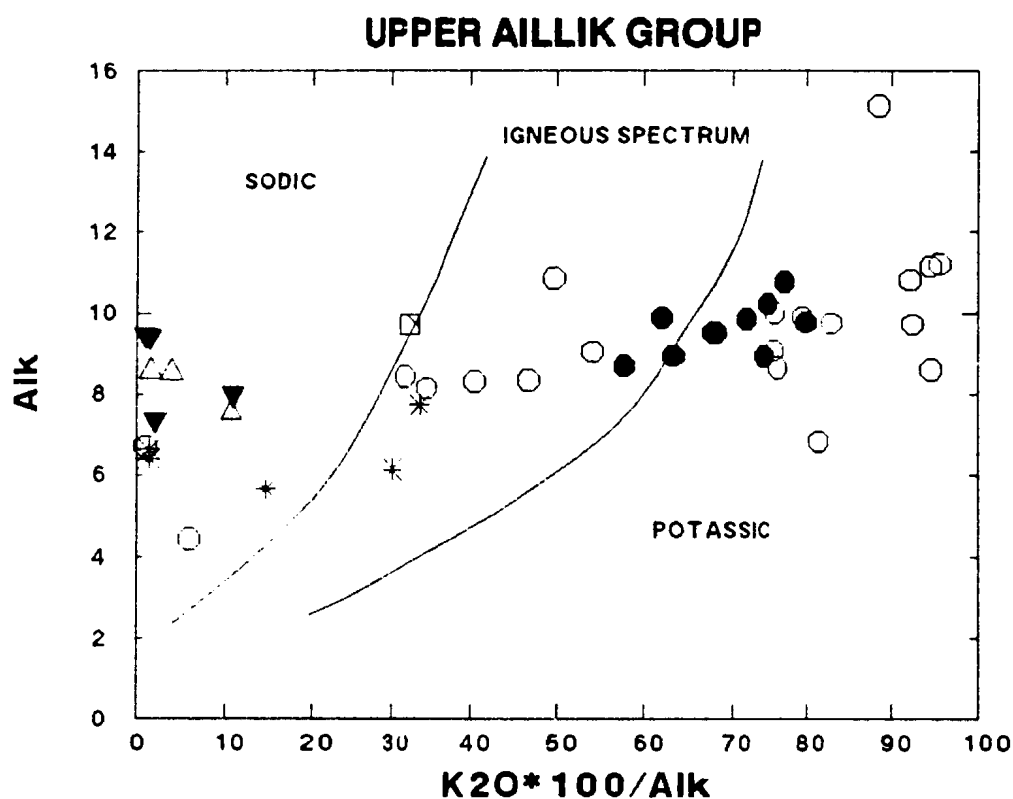


**Figure 3-4: Igneous spectrum of Hughes (1973) distinguishing between igneous and metasomatised chemical compositions. Symbols as in Figure 3-2.**

Regardless of the metasomatic overprint, most of the Upper Aillik Group felsic volcanic samples appear to exhibit a calc-alkaline affinity while the mafic samples are alkaline to sub-alkaline (Figure 3-5). According to the geochemical data, the Upper Aillik Group is characterized by a high total alkali content of between 7-10%. The mafic/intermediate rocks (andesite and dykes) have a roughly positive correlation between total alkalis and  $\text{SiO}_2$  while the felsic rocks (rhyolites) yield a negative correlation between total alkalis and  $\text{SiO}_2$  contents. This negative correlation is not evident in the Harker diagrams of  $\text{Na}_2\text{O}$  and  $\text{K}_2\text{O}$  vs  $\text{SiO}_2$  (Figure 3-2), suggesting a superimposed, metasomatic cation exchange between the alkalis. The plot  $\text{Na}_2\text{O} - \text{K}_2\text{O}$  (Figure 3-6) shows a direct inverse relationship between the two alkalis. The feldspar porphyry unit (4d) occupies a gap of 2-4%  $\text{Na}_2\text{O}$  and 4.5-8%  $\text{K}_2\text{O}$  between other felsic volcanic samples. The clustering of samples in this narrow range is interpreted to approximate the least effected composition of the felsic volcanic rocks and the scatter in the diagram is a result of the subsequent disturbance of one or the other alkali.

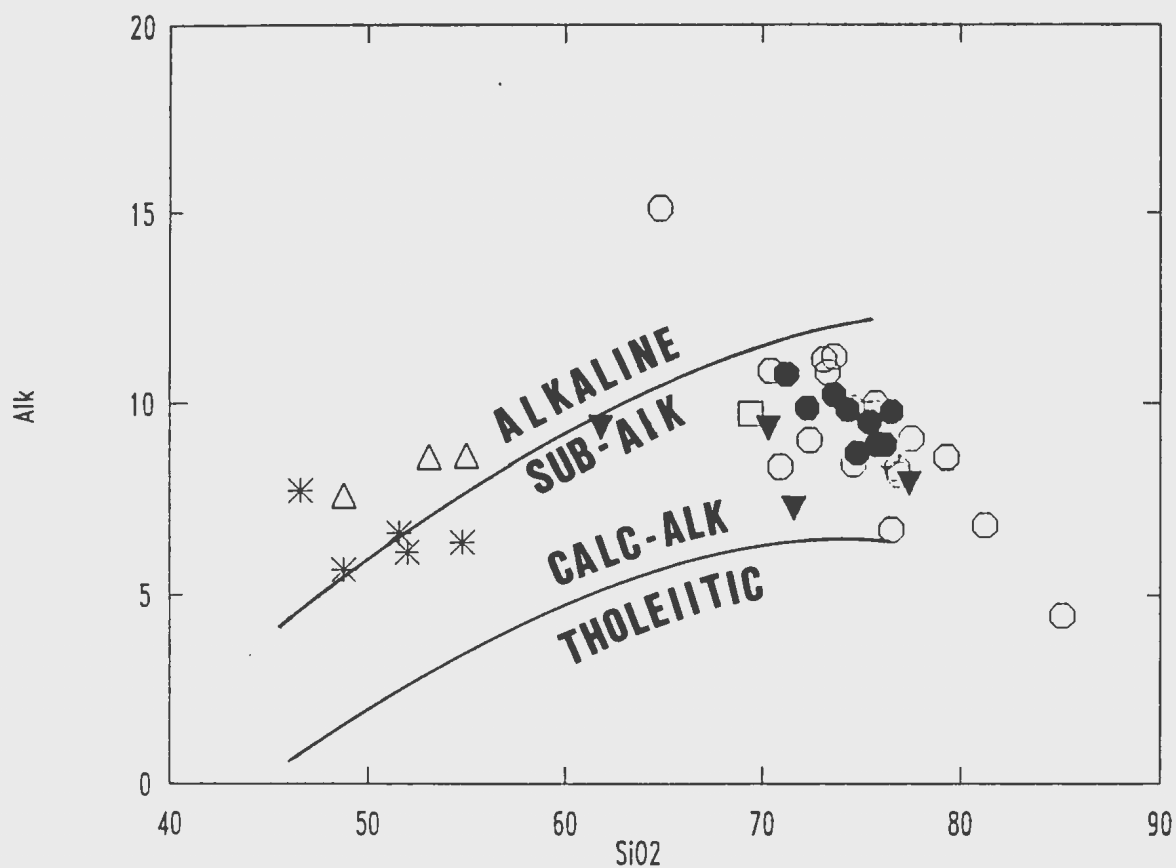
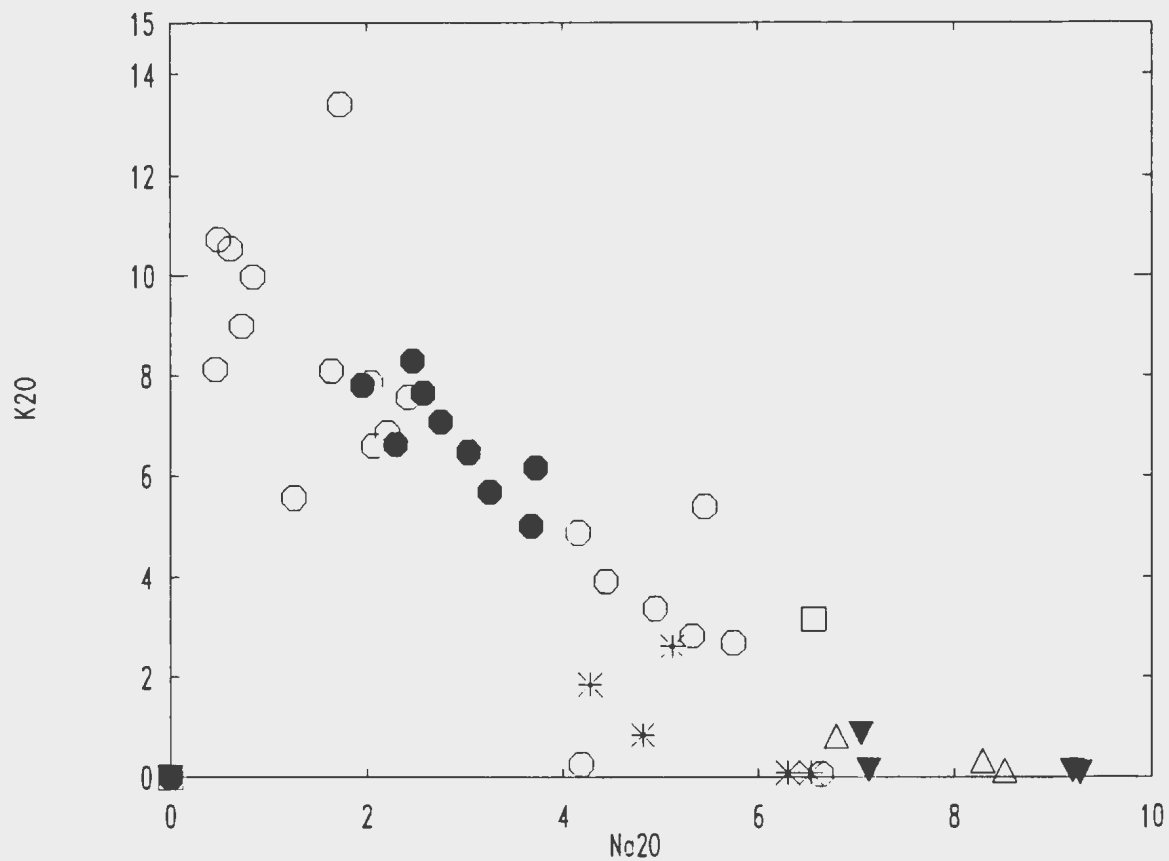


Figure 3-5: Total alkalis vs. silica plot (weight percent) for the Upper Aillik Group in the Burnt Lake area. Symbols as in Figure 3-2. Fields from Irvine and Baragar (1971).



**Figure 3-6: Na<sub>2</sub>O vs K<sub>2</sub>O plot for rocks of the Upper Aillik Group in the Burnt Lake area. Oxides in weight percent. Note negative slope of the felsic compositions and general low K<sub>2</sub>O contents of mafic and intermediate rocks. Symbols are as in Figure 3-2.**



The Upper Aillik Group volcanic rocks have been classified as having a calc-alkaline affinity by Bailey (1979) and Evans (1980). Other workers suggest that the rhyolites are alkaline to mildly peralkaline and state that the general calc-alkaline signature was produced metasomatically (Gandhi, 1978, White and Martin, 1980). Payette and Martin (1986) studied glass inclusions in a quartz-feldspar porphyry and concluded that the felsic magmas which formed the Upper Aillik Group were of alkaline affinity.

The majority of samples from the Upper Aillik Group in the Burnt Lake area plot as subalkaline rocks (Figure 3-7) on Irvine and Baragar's (1971)  $\text{Na}_2\text{O} + \text{K}_2\text{O} - \text{SiO}_2$  diagram. Those samples plotting in the alkaline field are intermediate to mafic volcanic rocks. On an AFM diagram (Figure 3-8) the rocks are predominantly calcalkaline but some samples plot in the tholeiitic field. Those samples plotting in the tholeiitic field (EMS86-TR1D, TR1E and TR5A) were collected from a mafic dyke near the Emben South Showing.

The data from this study, therefore, seem to suggest that the rocks were originally calcalkaline and that the peralkaline signature of the rocks is a result of metasomatic alteration.

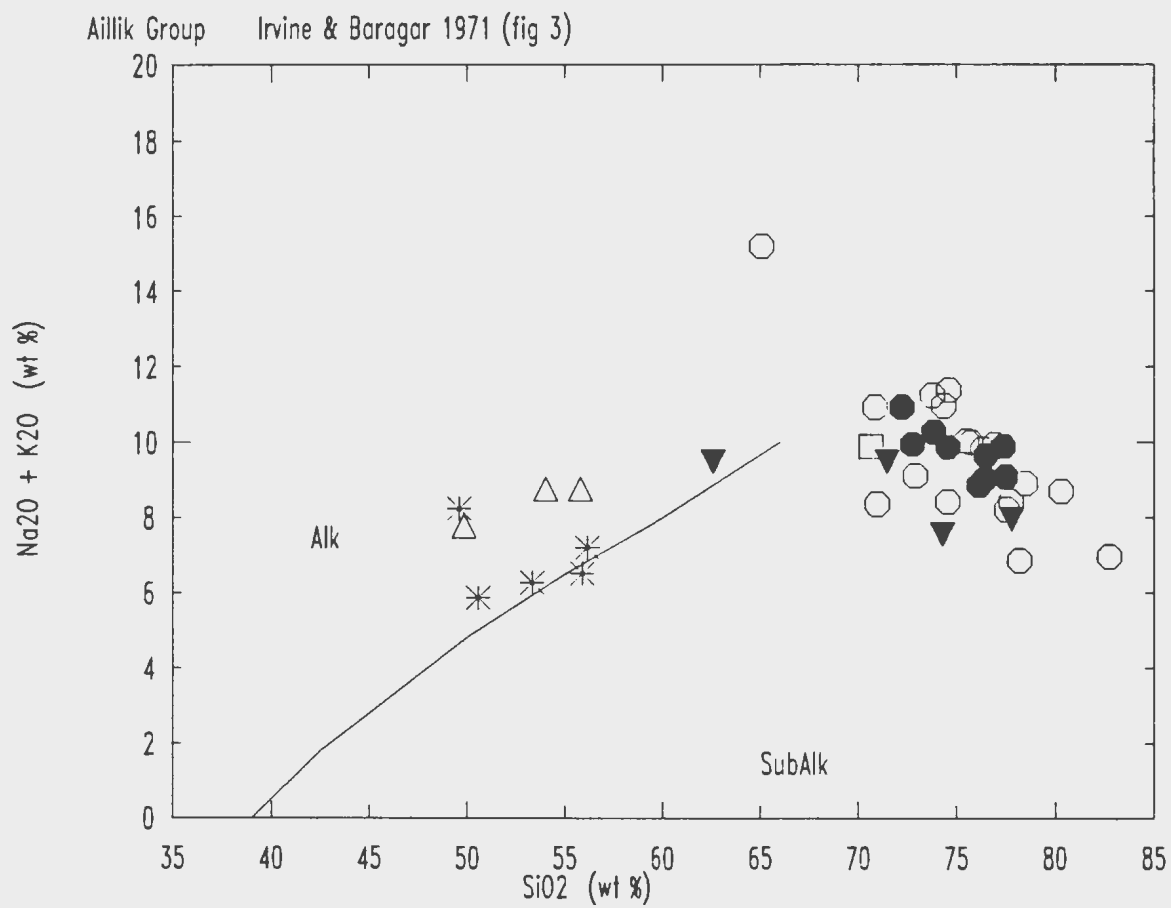


**Figure 3-7: Total Alkalies vs Silica diagram of the Upper Aillik Group. Fields from Irvine and Baragar, 1971.**

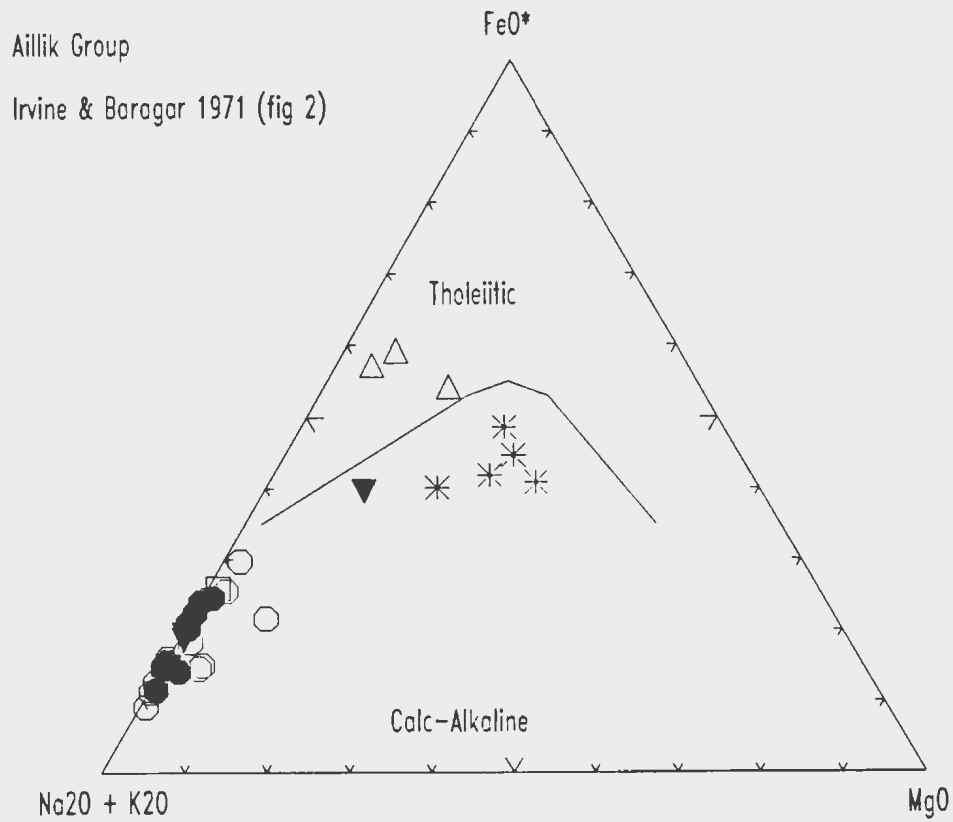


**Figure 3-8: AFM diagram with Irvine and Baragar (1971) calc-alkaline trend. Symbols as in Figure 3-2. A = Na<sub>2</sub>O + K<sub>2</sub>O; F = FeO + 0.8998 Fe<sub>2</sub>O<sub>3</sub>; M = MgO; all in weight percent.**

### Discussion:

The Upper Aillik Group was subjected to intense metasomatism (Bailey, 1980 and White and Martin, 1980) as shown by the Hughes diagram in Figure 3-3. The linear trend between  $\text{Na}_2\text{O} + \text{K}_2\text{O}$  (Figure 3-6) probably demonstrates the ionic substitution described by White and Martin (1980) in the Michelin area, whereby an ionic exchange occurs rapidly between Na and K with no change in the Al/Si ratio. Evans (1980) has shown that in the Upper Aillik Group in the Michelin area there is a progressive depletion of K and Si and an enrichment of Al, Na and  $\text{Fe}^{3+}$  followed by an exchange of K and Na and a substitution of Na-Al for Si. In the Burnt Lake data, there is an inverse relationship between Al and Si in a plot of  $\text{Al}_2\text{O}_3$  vs  $\text{SiO}_2$  (Figure 3-2) and possibly an exchange of total alkalis for  $\text{SiO}_2$  (Figure 3-7), however, neither Na or K show a linear relationship with  $\text{SiO}_2$  (Figure 3-2), demonstrating that ionic exchange between Na and K during metasomatism was independent of Si.

It is thus suggested that these discrimination diagrams are not applicable to highly metasomatised Upper Aillik Group rocks as sampled in the Burnt Lake area, and that diagrams using LIL elements are suspect in determining petrochemical affinities and classifications. Therefore, diagrams using immobile elements, such as those of Winchester and Floyd (1977), should be used for discrimination purposes.

Figure 3-9 indicates that the rocks in the Burnt Lake

area are predominantly tholeiitic. Other trace element plots using trace elements generally regarded as immobile (i.e. Zr, Ti, Y, Nb) confirm a tholeiitic classification (see later for discussion).

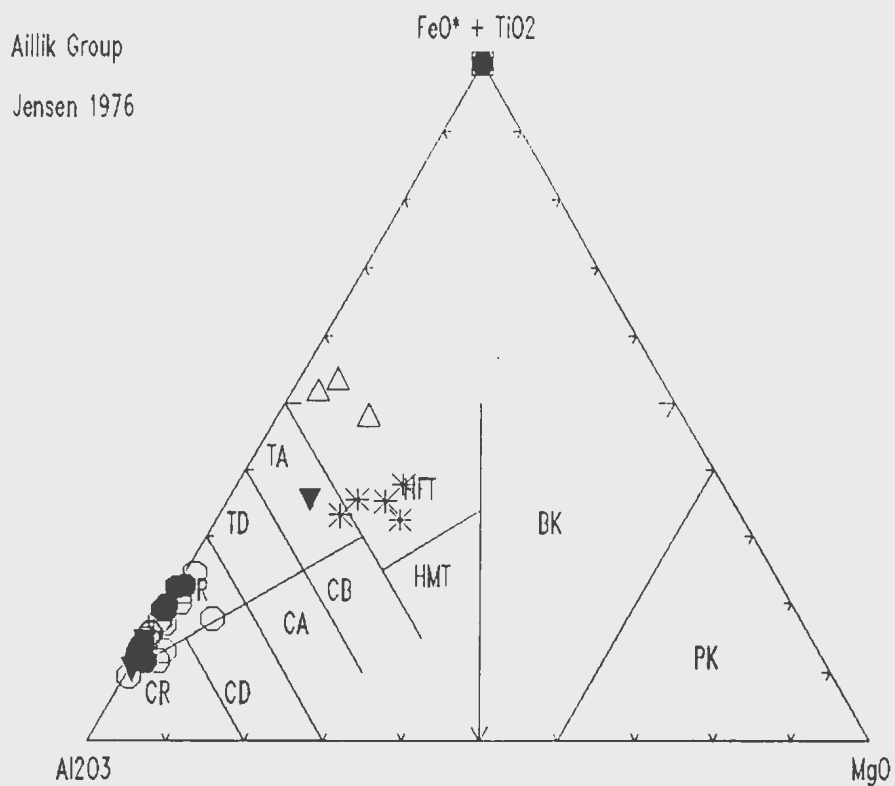


**Figure 3-9: Jensen (1976) cation plot of unmineralized Upper Aillik Group rocks in the Burnt Lake area.**

### 3.1.3 Trace Element Patterns and Classification

Variation diagrams for trace elements have been plotted against zirconium and are shown as Figure 3-10. Zr was chosen because of its relative immobility and because half the data set was not analysed for major elements. Two samples are omitted from the following diagrams because they seemed to have experienced a high degree of hydrothermal alteration as shown by the exceptionally high Zr values (LM85-110: 1050 Zr, LM85-50: 1575 Zr).

#### **Unit 1a: Arkosic Sediment and Felsic Tuff (solid inverted triangle)**

Geochemically Unit 1 follows very closely the general geochemical trend of other Upper Aillik Group volcanic rocks in the Burnt Lake area, however, the unit as a whole shows an overall enrichment in Ga and a depletion in Rb reflecting a greater feldspar content of the rocks. Some of the samples were taken near mineralized zones and are slightly enriched in Cu, Zn, Pb and U.

#### **Unit 1b: Mafic Dykes (open triangle)**

The mafic dyke samples from the Emben area are geochemically similar to other mafic dykes in the area and are further discussed below.

**Units 2 & 3: Volcaniclastic Sediments (open square)**

Trace element patterns for the volcaniclastic sedimentary rocks (Units 2 & 3) are chemically distinct from those of the predominantly felsic volcanic rocks of the Upper Aillik Group. The rocks are distinguished from the felsic volcanic rocks by higher Ba, Cr, Ni, Ti and Sr and lower La, Th, Y and Nb. Distinctive separations between the different rock types can be seen on the plots of Nb versus U, Nb versus Zr or Y versus Nb (Figure 3-11). It is apparent that the volcaniclastic sedimentary rocks were not derived directly from weathering of the Upper Aillik Group based on the geochemical differences. Chemical fields for representative rocks of the Lower Aillik Group (after Wilton, 1991a) show striking geochemical similarities to those of the volcaniclastic sedimentary rocks in this study and, therefore, seem to be correlative.

**Units 4a, 4b, 4c and 4e: Felsic Ash Tuff, Felsic Crystal Tuff, Lapilli Tuff and Volcanic Breccia (open circle)**

These rock types can be easily identified in the field, however, geochemically they are very similar to each other and are therefore grouped together. The immobile elements follow typical fractionation trends and have good positive correlations with Zr.

**Unit 4d: Feldspar Porphyry (solid circle)**

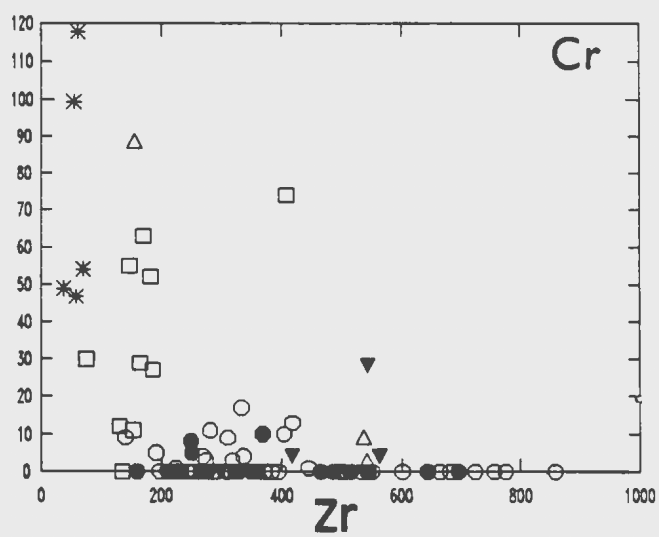
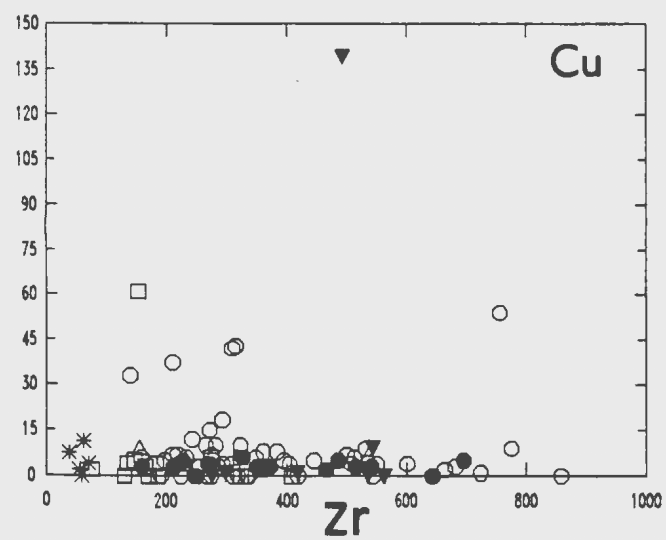
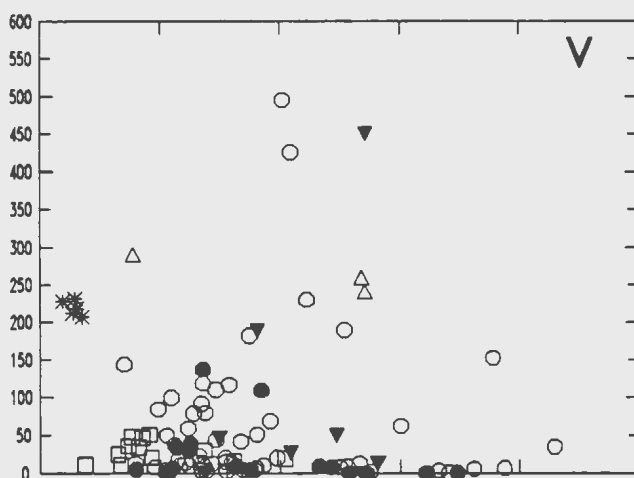
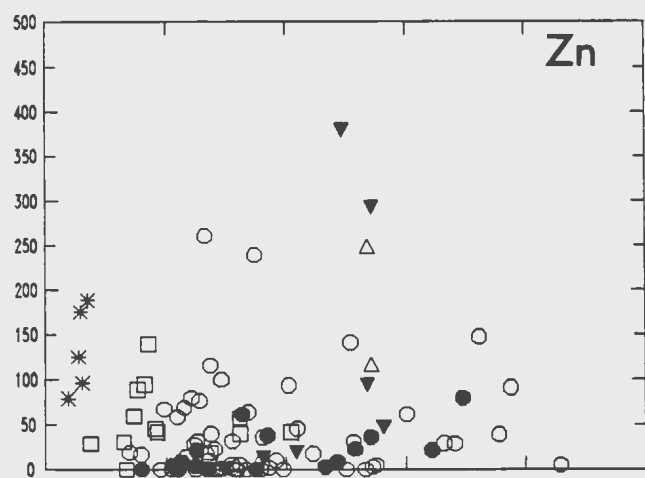
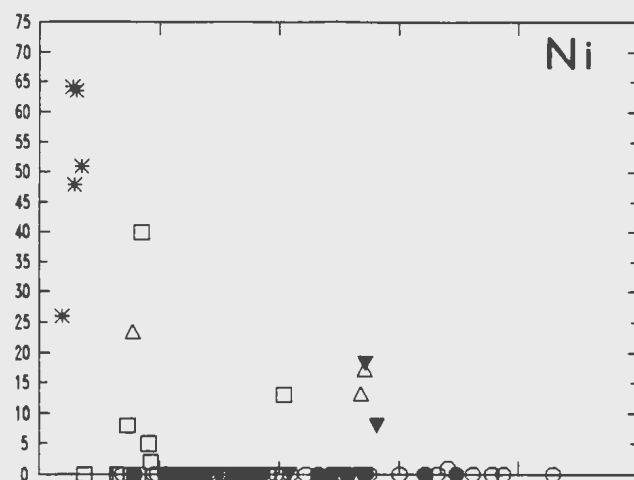
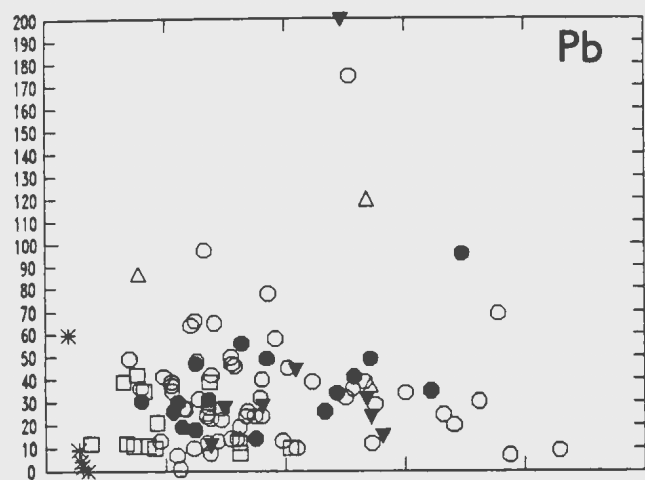
The data from the feldspar porphyry samples show some evidence for both fractionation and disturbance of the compatible elements. The immobile elements Y, Nb and Ga show a good positive correlation with Zr. The data show a scatter in Ba, Rb, V, La, U, Th and Pb and low contents of Sr, Cr, Ti, Ni, Cu and Zn.

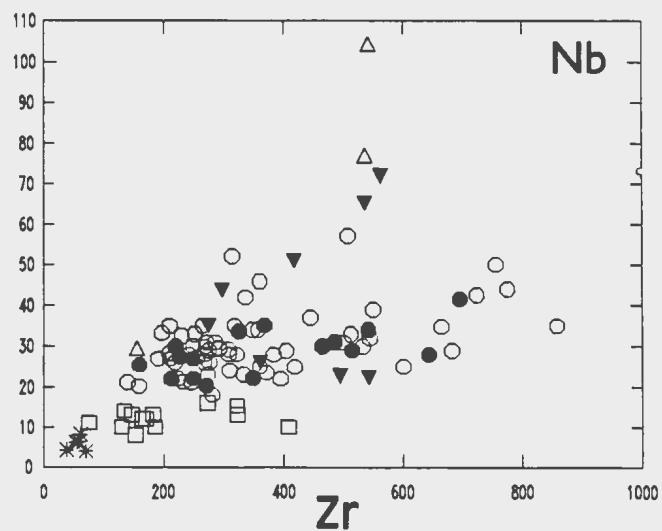
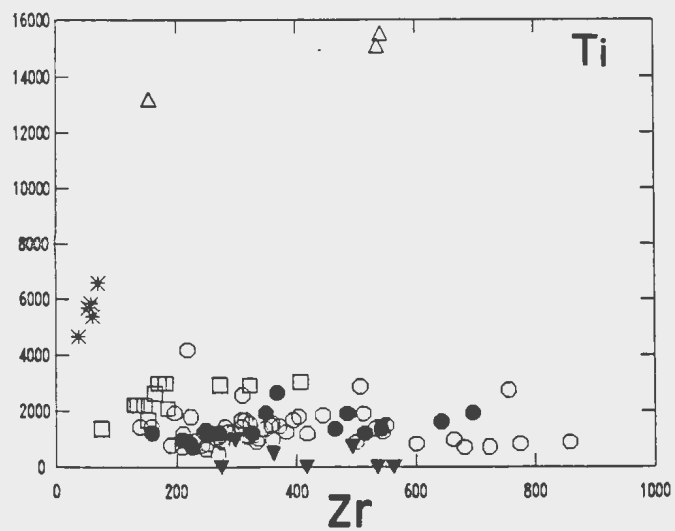
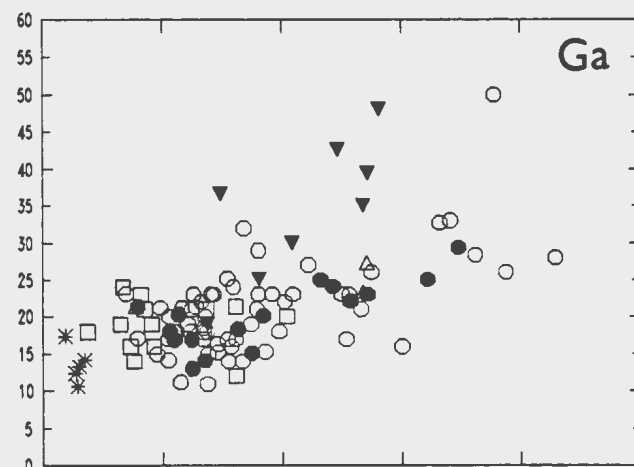
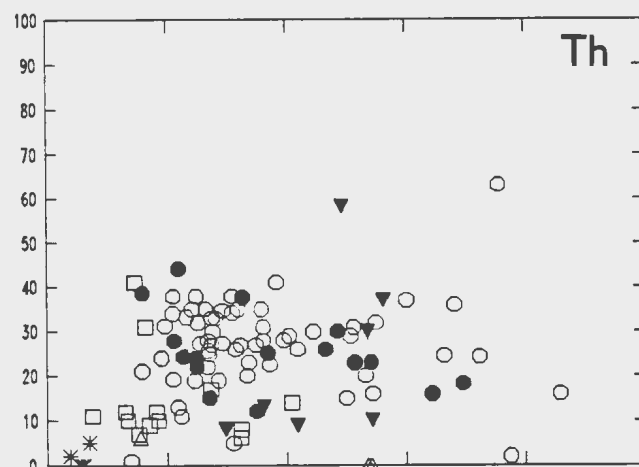
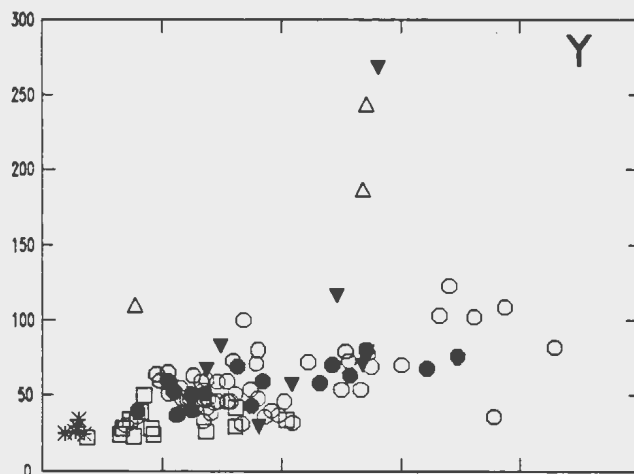
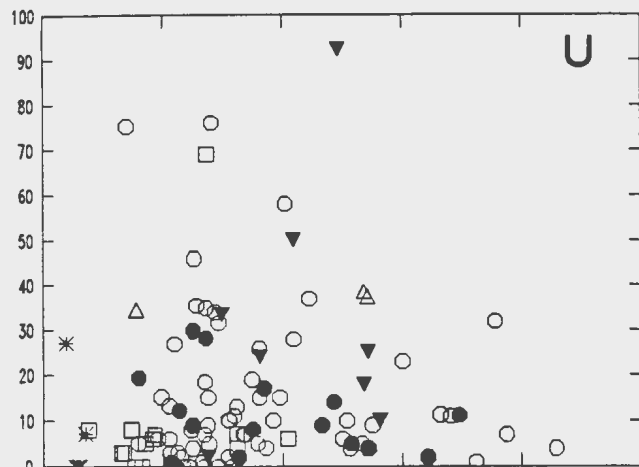
**Unit 4f: Andesite (asterisk)**

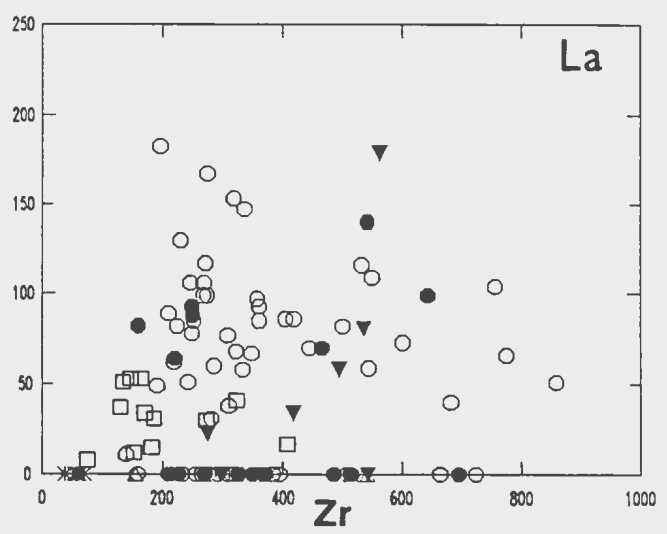
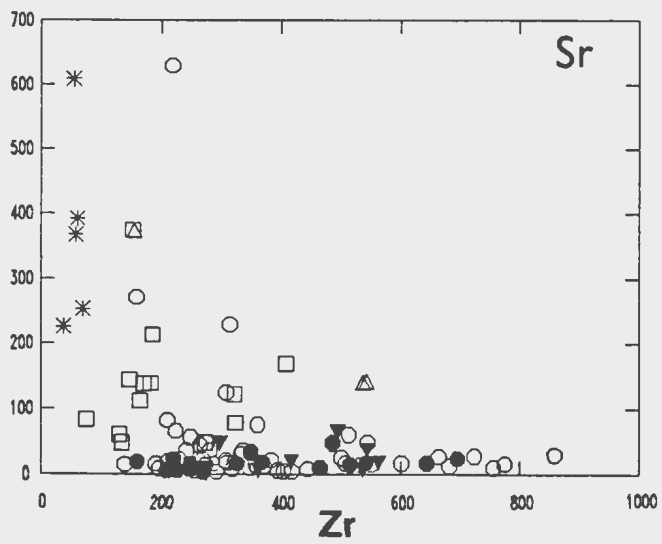
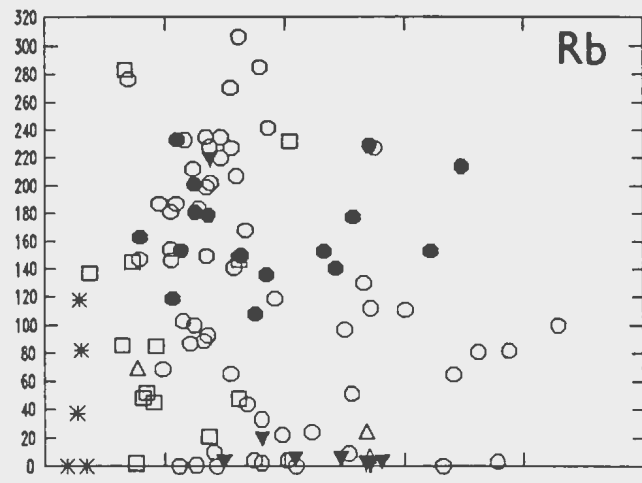
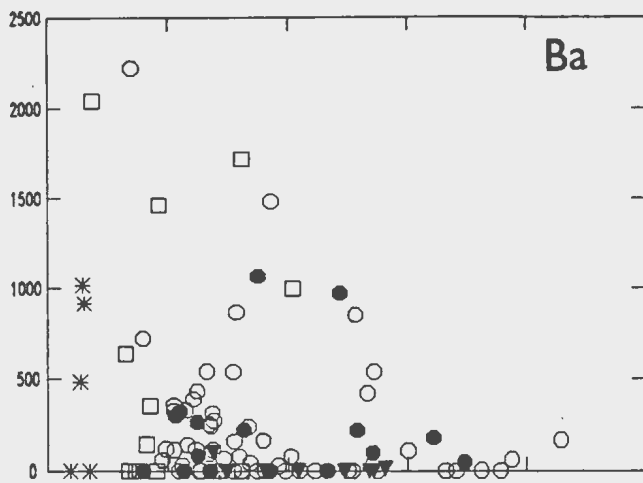
The andesitic samples have very low Zr contents and have little geochemical variation. The rocks are generally enriched in Sr, Cr, Ti and Ni and depleted in the high field strength (HFS) elements Ga, Nb, and Y, as well as Th and U. There is a little variation in the V contents with a tight cluster between 200-240 ppm. The base metals (Cu and Pb) are generally very low, however, Zn shows some scatter from 75-175 ppm Zn. Rb and Ba also show some scatter in the data.

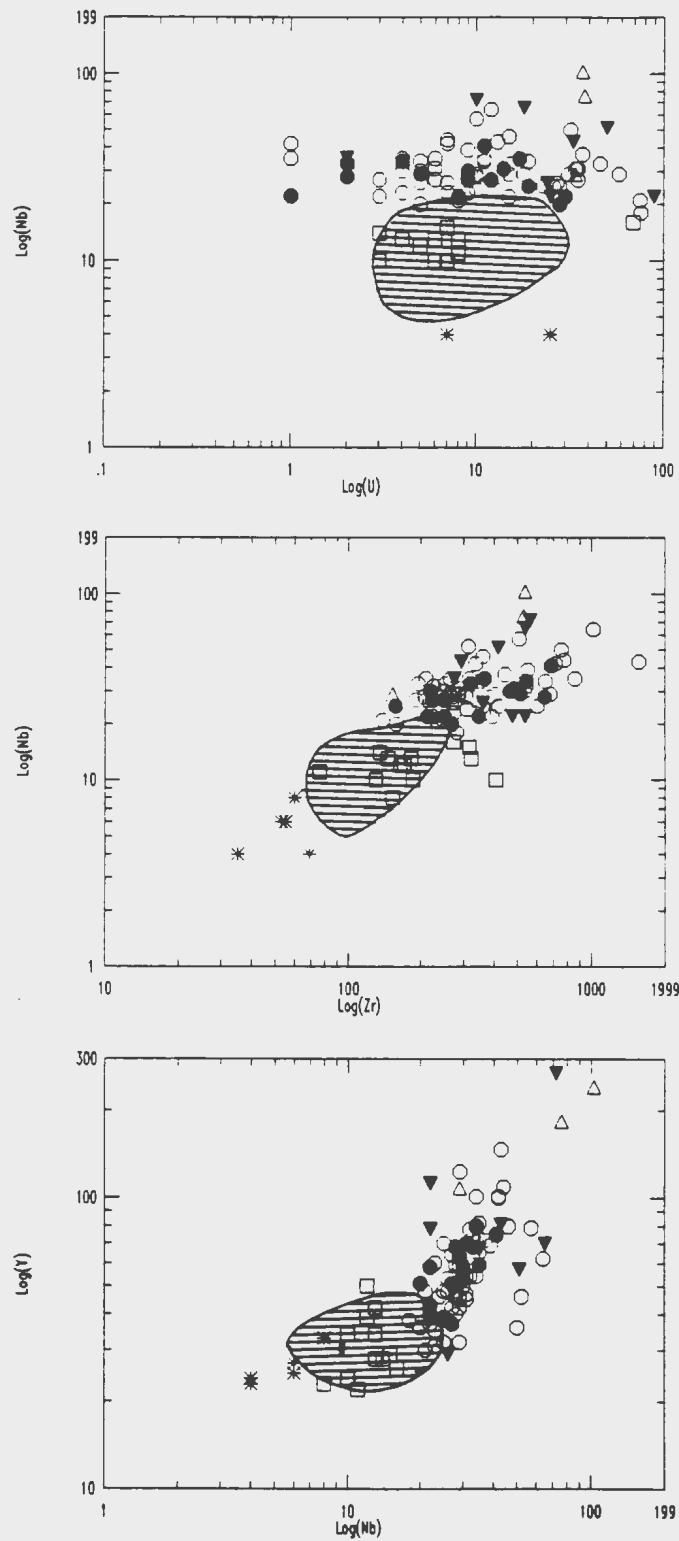


Figure 3-10: Harker variation diagrams of trace elements vs Zr in samples of the Upper Aillik Group from the Burnt Lake area. Symbols are as follows; Solid inverted triangle: arkosic sandstone and felsic tuff (Unit 1a); Open triangle: diabase dykes (Unit 1b); Open square: volcaniclastic sedimentary rocks (Units 2 and 3); Open circle: felsic volcanic crystal tuff, ash tuff, and minor lapilli tuff (Units 4a, 4b, 4c); Solid circle: feldspar porphyry with minor quartz (Unit 4d); Asterisk: andesite (Unit 4f).









**Figure 3-11: Variation diagrams of incompatible elements vs Nb. Shaded fields represent average values for metasedimentary rocks of the Lower Aillik Group (from Wilton, 1991a).**

### 3.1.3.1 Classification

On the Winchester and Floyd's (1977)  $Zr/TiO_2$  -  $Nb/Y$  and  $SiO_2$  -  $Zr/TiO_2$  diagrams (Figures 3-12a&b) the majority of felsic volcanic samples plot within the rhyolite field with some overlap into the comendite/pantellerite field. A second grouping is within the rhyodacite/dacite field and consists of the volcanoclastic rocks, and the third grouping is the Aurora River andesites which plot in the Andesite/Basalt field. There is, however, some spread of values into the peralkaline fields (Figure 3-12b).

Trace element tectonic diagrams commonly used to classify granitoid rocks (Figure 3-13a and 3-13b) have been constructed for the data from Upper Aillik Group rocks in the Burnt Lake area. On a  $Nb$  versus  $Y$  diagram (Figure 3-13a) a clear separation of the various rock units is evident. All of the felsic volcanic rocks plot in the "within-plate" environment. The volcanoclastic sedimentary rocks (units 2 and 3) exhibit lower  $Nb$  and  $Y$  contents and plot in the volcanic-arc environment. The andesitic rocks (Unit 4f) have the lowest values of  $Nb$  and  $Y$  and all plot in the lower left hand corner of the diagram. These rocks are strongly sub-alkaline and have low  $Nb/Y$  ratios.

A similar distribution can be seen on a  $Rb$  versus ( $Y + Nb$ ) diagram (Figure 3-13b) except with a greater disturbance in the  $Rb$  contents.

Figure 3-9 indicates that the andesitic rocks in the Burnt Lake area are predominantly tholeiitic. Other plots using trace elements generally regarded as immobile (i.e. Zr, Ti, Y, Nb) confirm a tholeiitic classification (see Figures 3-14, 3-15)

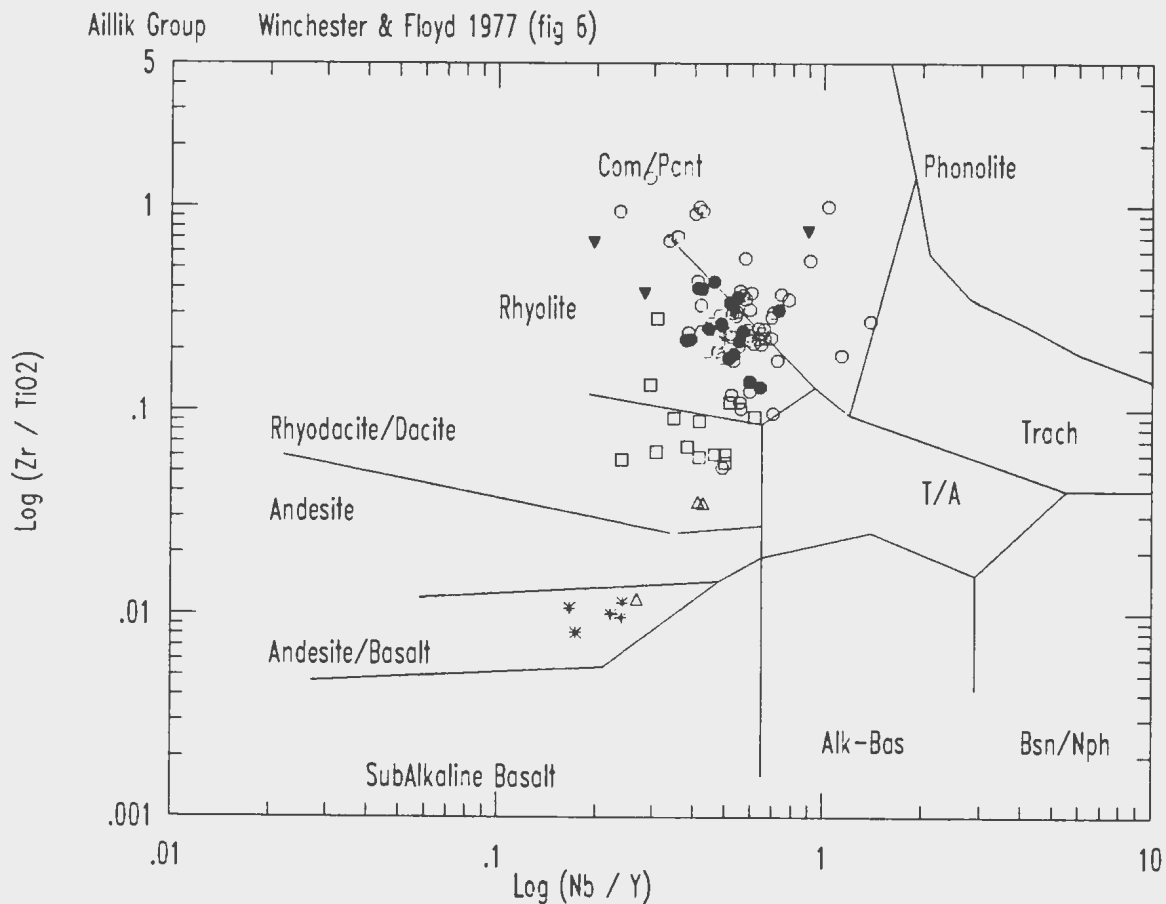


**Figure 3-12a: Zr/TiO<sub>2</sub> vs Nb/Y diagram showing distribution of the Upper Aillik Group meta-volcanic suite of the Burnt Lake area. Fields from Winchester and Floyd (1977). Symbols as in Figure 3-2.**

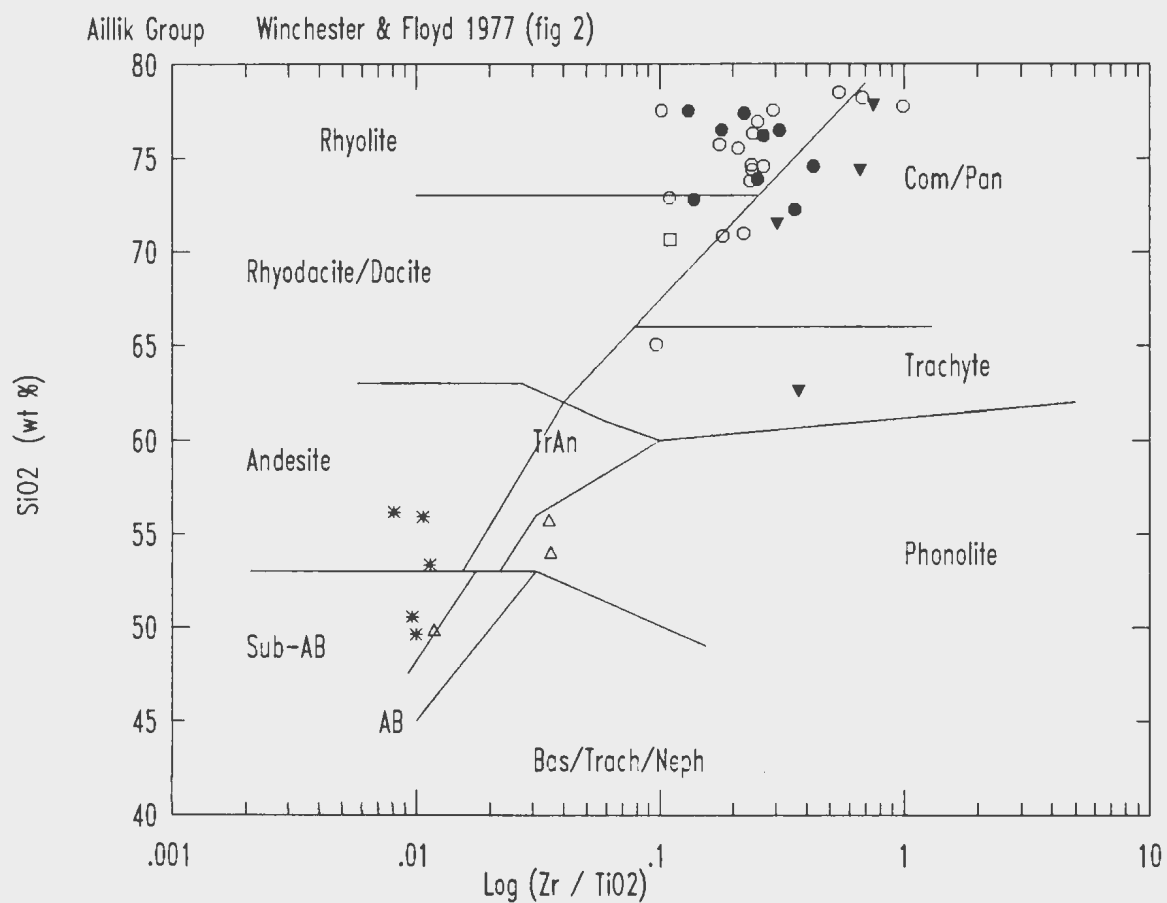


**Figure 3-12b: SiO<sub>2</sub> vs Zr/TiO<sub>2</sub> diagram showing distribution of the Upper Aillik Group meta-volcanic suite of the Burnt Lake area. Fields from Winchester and Floyd (1977). Symbols as in Figure 3-2**



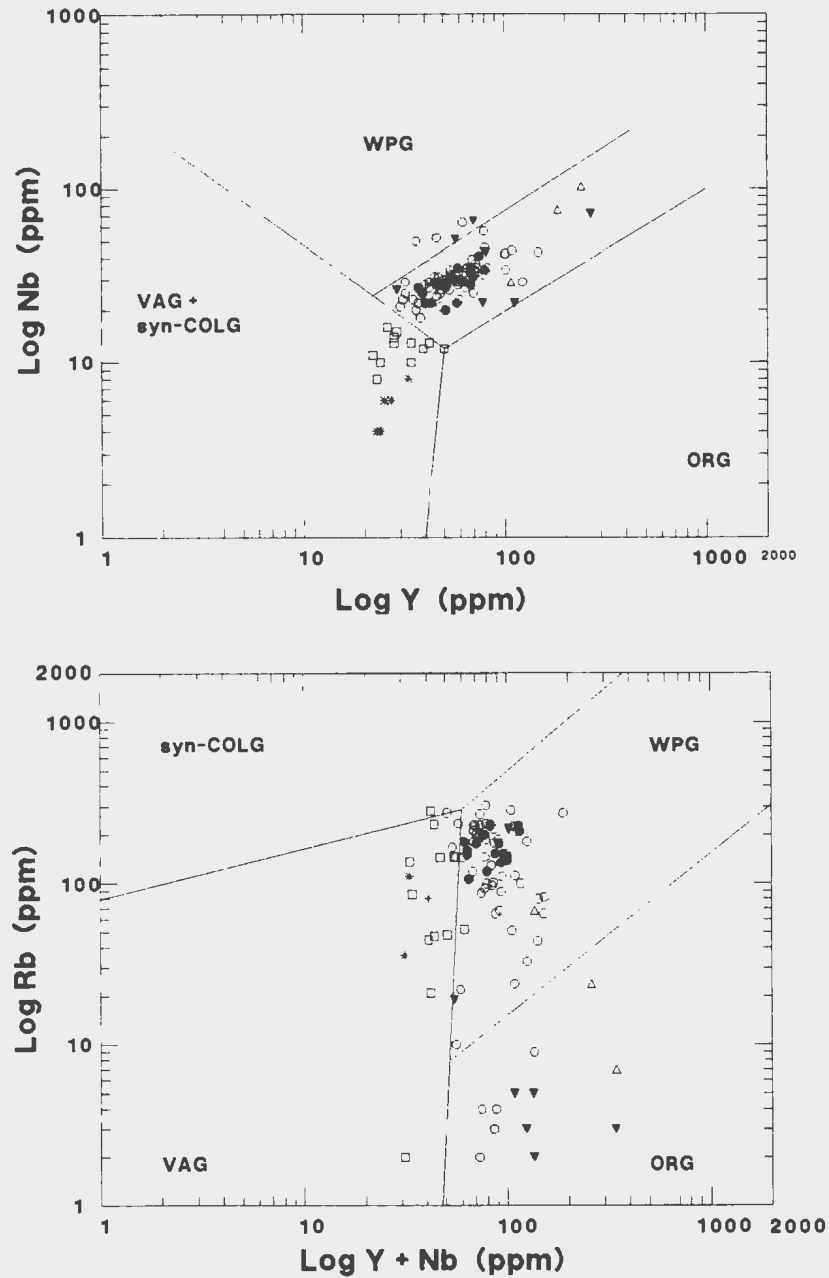


**Figure 3-13: Tectonic discrimination diagrams (after Pearce et al., 1984) for samples from the Upper Aillik Group meta-volcanic suite in the Burnt Lake area.**

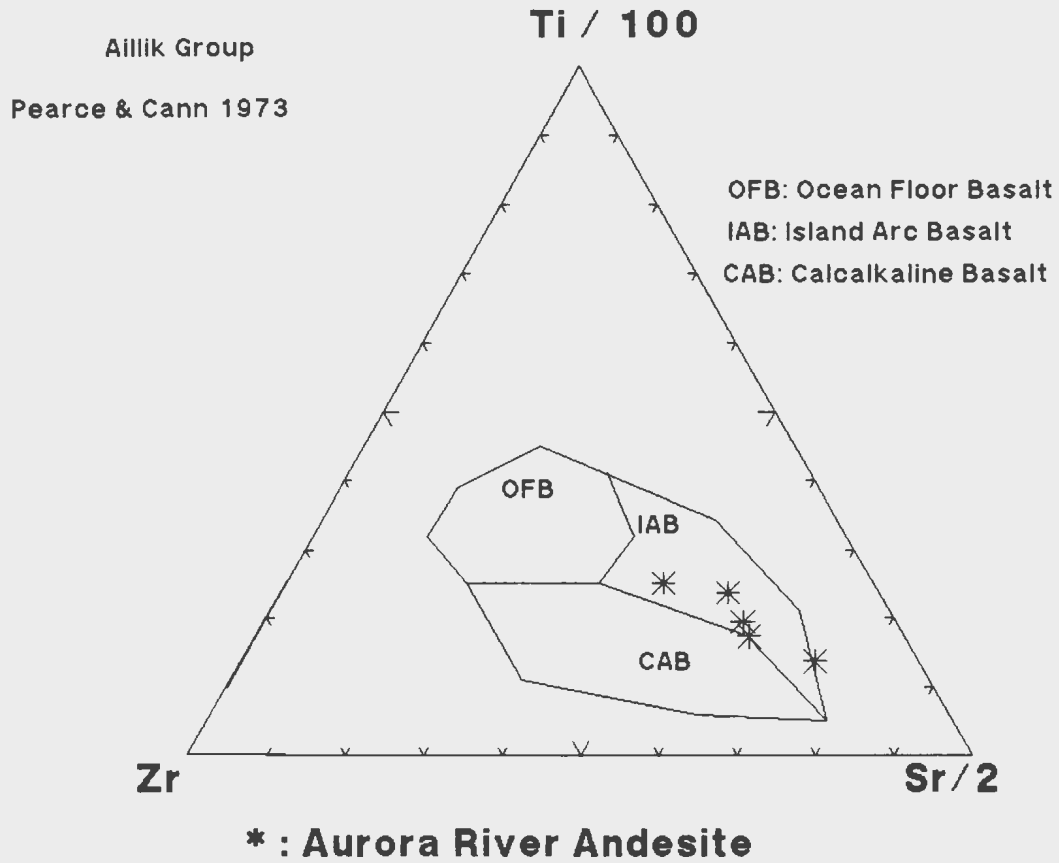


**Figure 3-14: Lithotectonic Ti-Zr-Sr discrimination diagram (after Pearce and Cann, 1973) data for andesitic rocks from the Upper Aillik Group in the Aurora River area.**

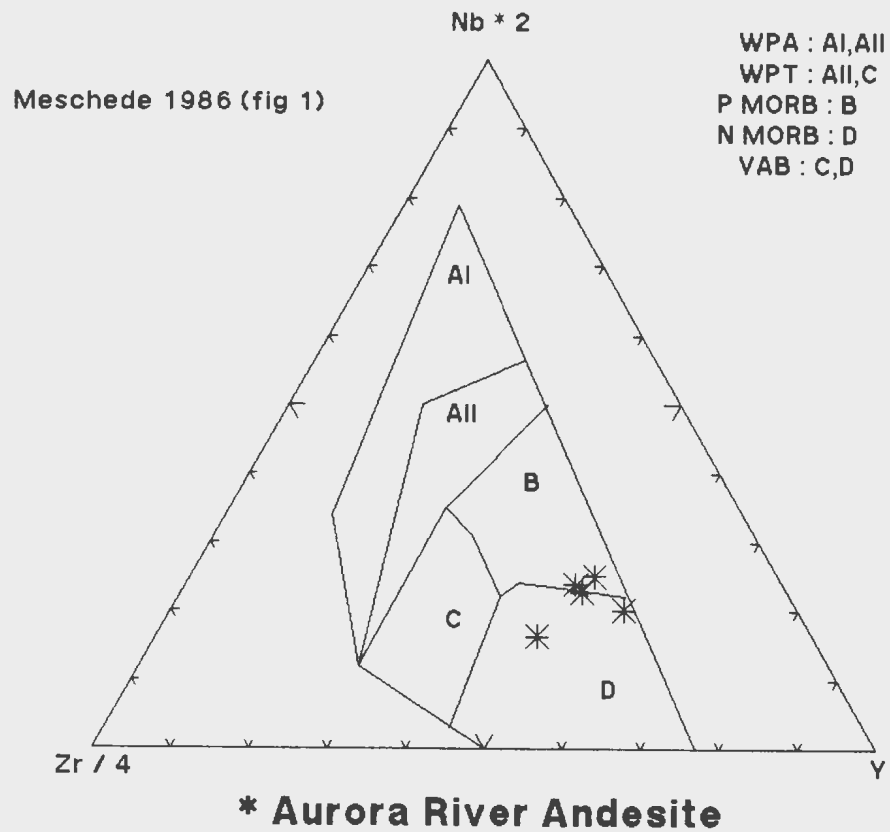


**Figure 3-15: Lithotectonic Zr-Nb-Y discrimination diagram (after Meschede, 1986) for andesitic rocks from the Upper Aillik Group in the Aurora River area.**

#### 3.1.4 Rare Earth Element Patterns

Rare earth element (REE) data for the UAG are listed in Table 3-1 and the chondrite-normalized REE patterns are illustrated on Figure 3-16. Overall, unmineralized Upper Aillik Group felsic volcanic rocks possess enriched REE contents (up to 400x chondrite), extreme LREE/HREE fractionation which is typical of some rhyolitic rocks (LREE enriched relative to HREE), and a pronounced negative Eu anomaly reflecting extreme plagioclase and K-feldspar fractionation. Samples LM85-32 and LM85-60 are consistent with other unmineralized Upper Aillik Group rhyolitic rocks in the coastal exposures (Wilton and Wardle, 1987, MacDougall, 1988) and in the Michelin deposit to the west (White and Martin, 1980). Samples LM85-14 and LM85-37 are hydrothermally altered with traces of disseminated pyrite and show slightly enriched HREE's and a reduced negative Eu anomaly. Wilton and Wardle (1987) and MacDougall (1988) reported similar REE patterns associated with mineral occurrences hosted in UAG rocks near the coast.

**Table 3-1: Rare earth element data for the Upper Aillik Group  
in the Burnt Lake Area.**

EL(ppm)	LM85-14	LM85-32	LM85-37	LM85-60
LA	62.1	107.9	107.2	89.8
CE	139.5	211.8	227.0	185.0
PR	11.7	16.9	19.1	16.2
ND	52.9	73.2	87.0	67.6
SM	10.6	11.7	15.0	10.5
EU	0.2	0.0	0.7	0.0
GD	9.3	8.5	11.4	6.6
DY	11.9	7.4	11.0	4.7
ER	6.9	4.5	7.2	2.7
YB	6.5	4.1	6.7	1.9

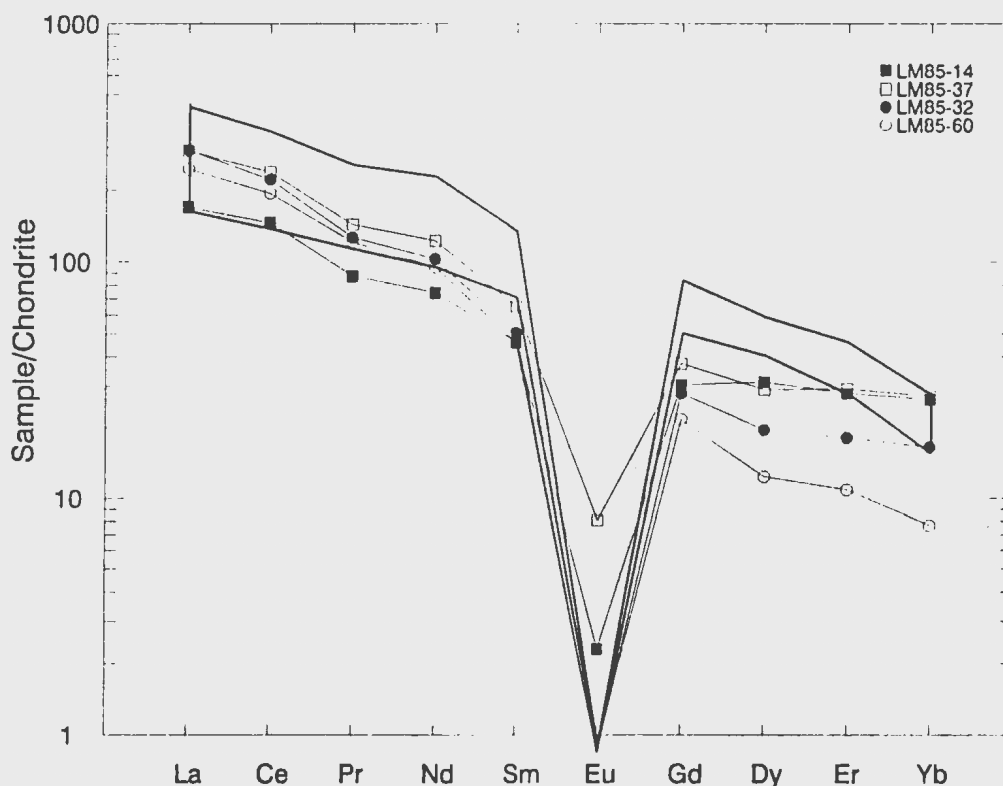


**Figure 3-16: Chondrite-normalized REE patterns for non-mineralized felsic volcanic rocks of the Upper Aillik Group in the Burnt Lake area with a field for the UAG felsic volcanic rocks in the Makkovik area (from Wilton and Wardle, 1987).**

### **3.2 Granitoids in the Burnt Lake Area**

#### **3.2.1 Introduction**

Based on petrography and field relationships (described in Chapter 2) there are two distinct granitoid suites in the Burnt Lake area; viz. a synkinematic Makkovikian suite and a post-tectonic Labradorian suite (the Burnt Lake Granite) (Kerr and Krogh, 1990).

A total of 24 samples of granite were analyzed for major and trace elements (seventeen from the Burnt Lake Granite and seven from the Makkovikian suite). The average geochemical data are listed in Table 3-2 and normative compositions are listed in Appendix I. A further 12 samples were analyzed for trace elements only and REE were analyzed for 12 samples. A brief rock description for each sample is given in Appendix II. Analytical methods, precision and accuracy are described in Appendix I.

#### **3.2.2 Major and Trace Element Patterns and Classification**

Harker variation diagrams for the major and trace elements of the Burnt Lake Granite constitute Figures 3-17 and 3-18. The symbols used in the diagrams correspond to subdivisions of the granitoids as shown on Map 1.

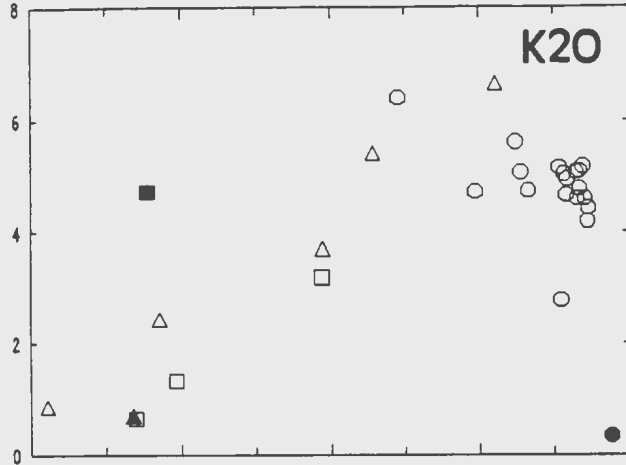
**Table 3-2: Average Chemical Compositions of Granitoids in the  
Burnt Lake Area.**

Burnt Lake Granite					Makkovikian Granite			
	n=17					n=7		
	Mean	SD	Min	Max		Mean	SD	Min
Max								
SiO <sub>2</sub>	73.90	4.49	62.02	79.30	51.88	7.41	39.79	62.02
TiO <sub>2</sub>	0.17	0.20	0.04	0.92	1.39	0.61	0.76	2.63
Al <sub>2</sub> O <sub>3</sub>	13.66	1.67	12.03	19.34	16.81	1.56	15.11	18.93
FeO*	1.38	1.61	0.35	7.62	10.96	4.84	6.16	18.70
MnO	0.04	0.03	0.01	0.12	0.16	0.06	0.11	0.28
MgO	0.22	0.18	0.03	0.62	4.72	2.87	0.41	8.61
CaO	1.33	1.01	0.24	4.85	7.15	3.01	2.14	11.56
Na <sub>2</sub> O	4.25	0.63	3.54	6.3	3.66	0.81	2.24	4.72
K <sub>2</sub> O	4.84	0.67	2.92	6.33	2.46	1.56	0.74	5.33
P <sub>2</sub> O <sub>5</sub>	0.03	0.03	0.0	0.11	0.38	0.31	0.06	0.83

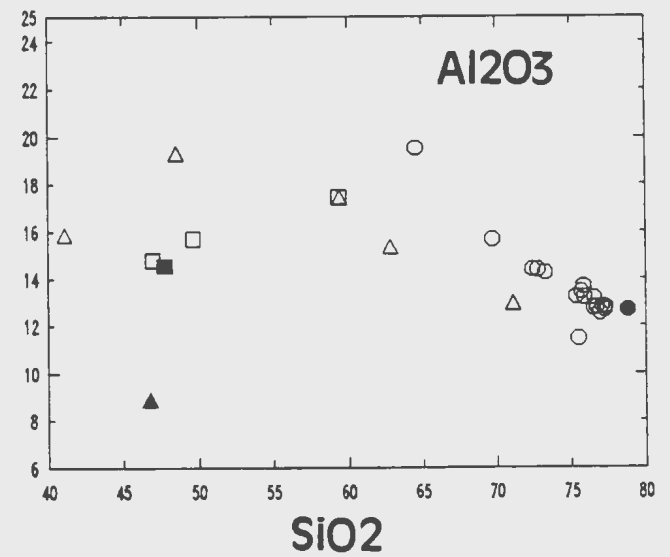
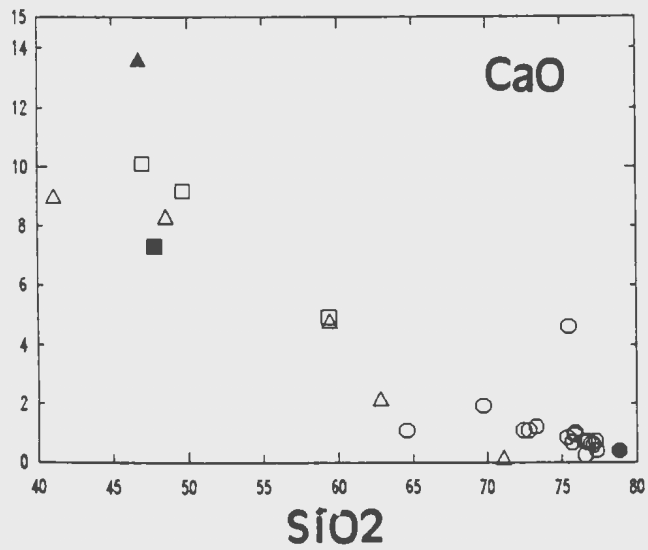
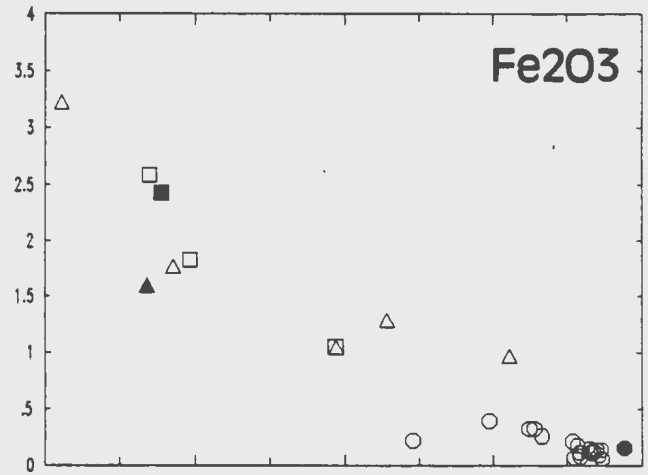
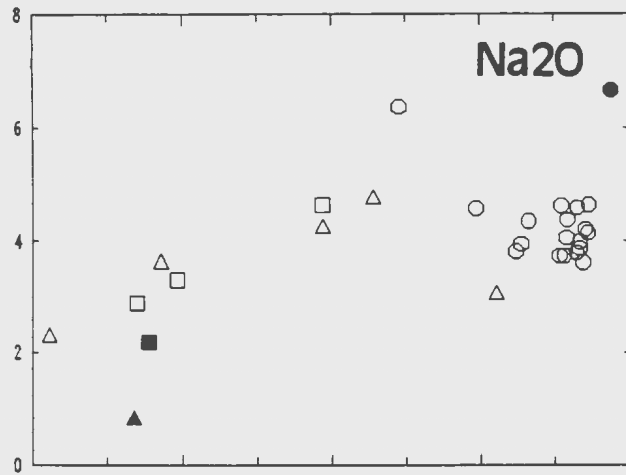
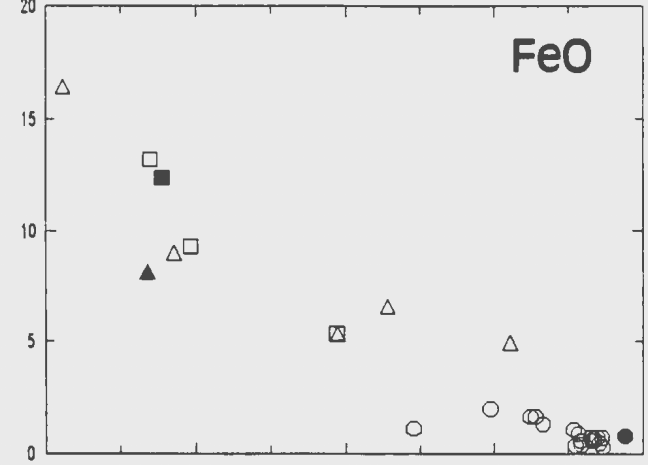
Figure 3-17: Harker variation diagrams of major elements in the Burnt Lake area granitoids. Oxides are in weight percent. Symbols are as follows; Open Circle: Burnt Lake Granite (Unit 5a); Solid Circle: Pegmatite Dyke; Open Triangle: North Granite (Unit 5b); Open Box: South Granite (Unit 5c); Solid Box: Mafic Dykes (Unit 6); Solid Triangle: Michael Gabbro (Unit 7).



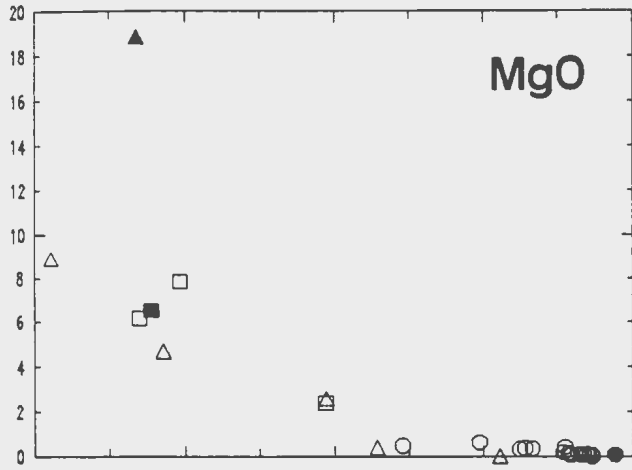
Burnt Lake Area Granitoids



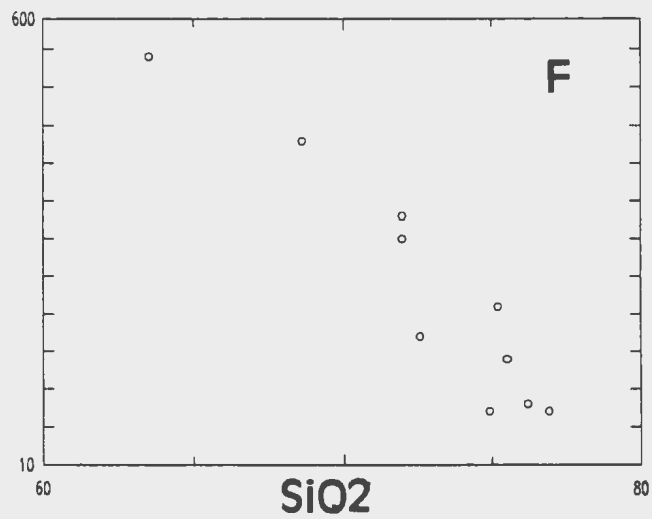
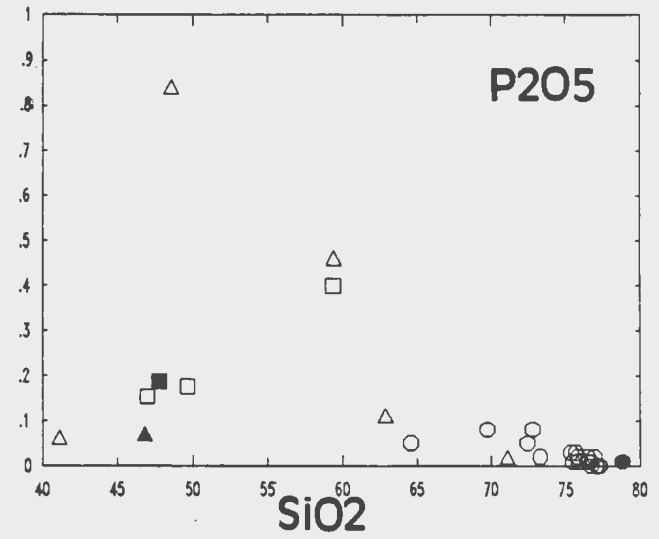
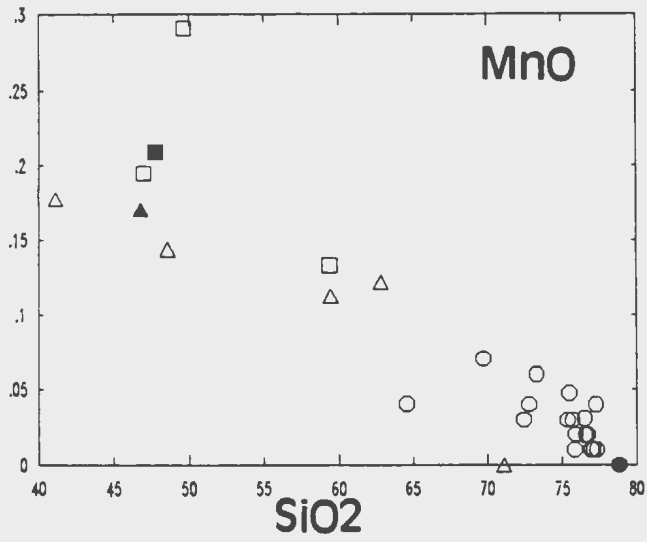
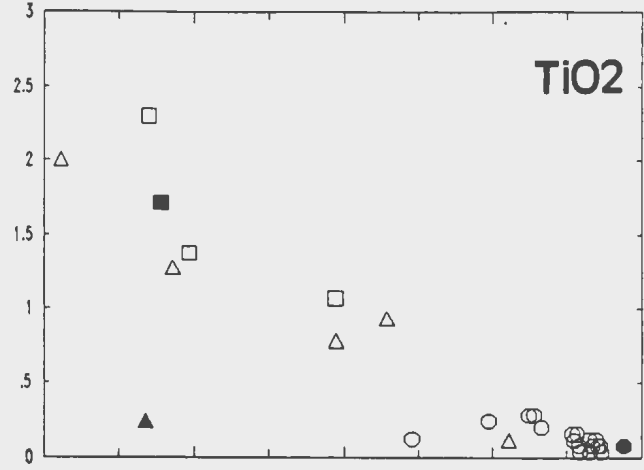
Burnt Lake Area Granitoids

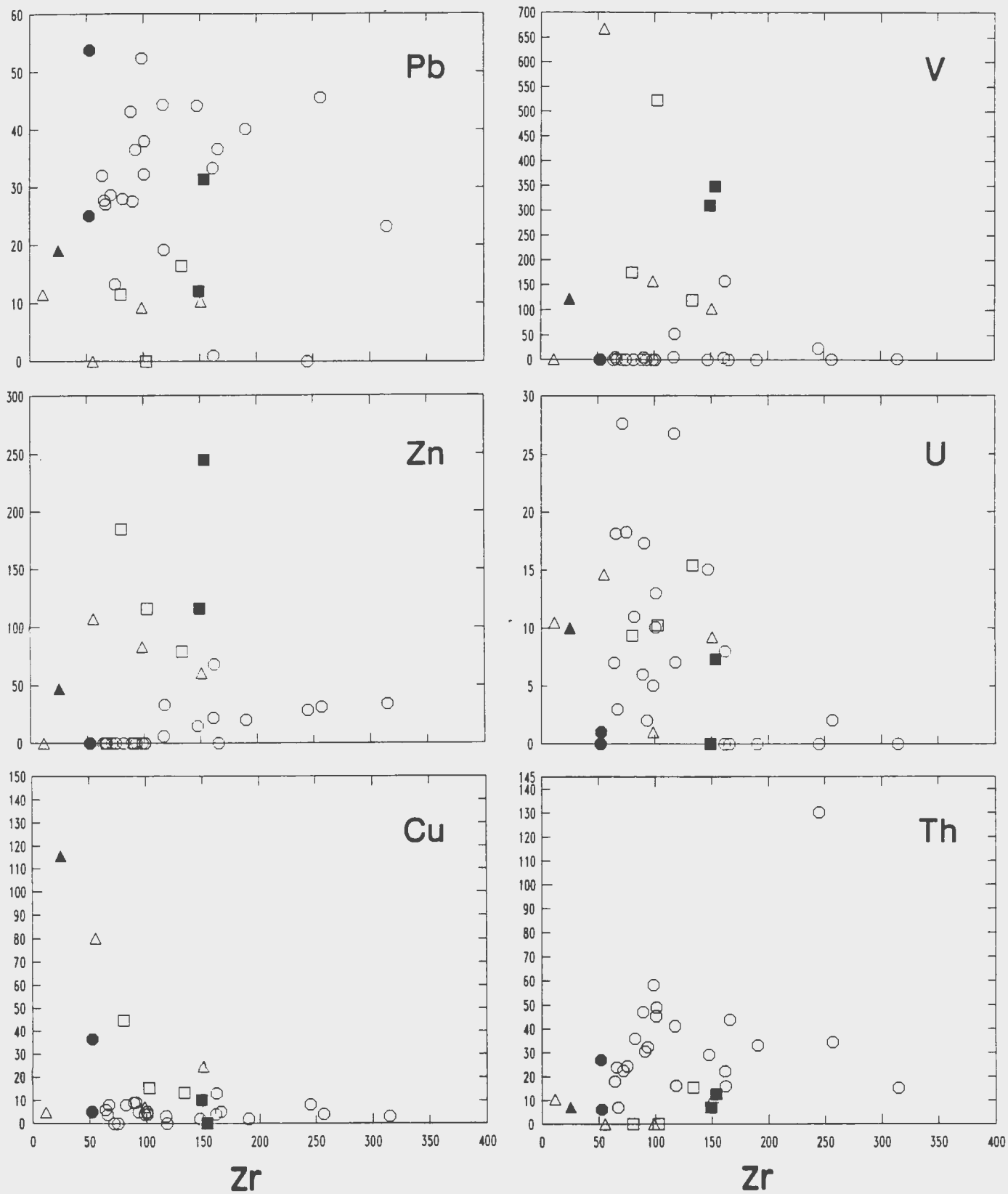


Burnt Lake Area Granitoids



Burnt Lake Area Granitoids





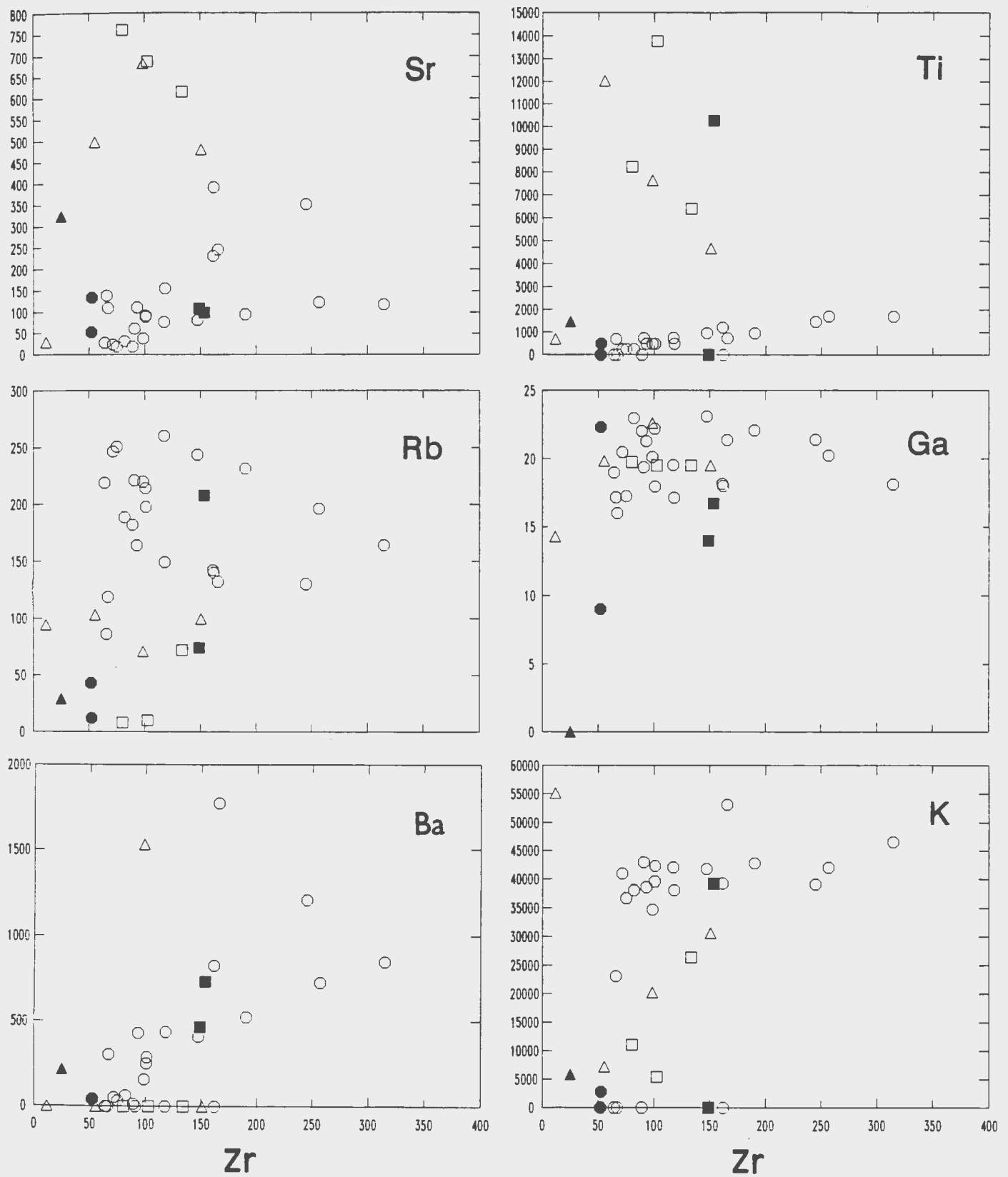


Figure 3-18: (Continued)

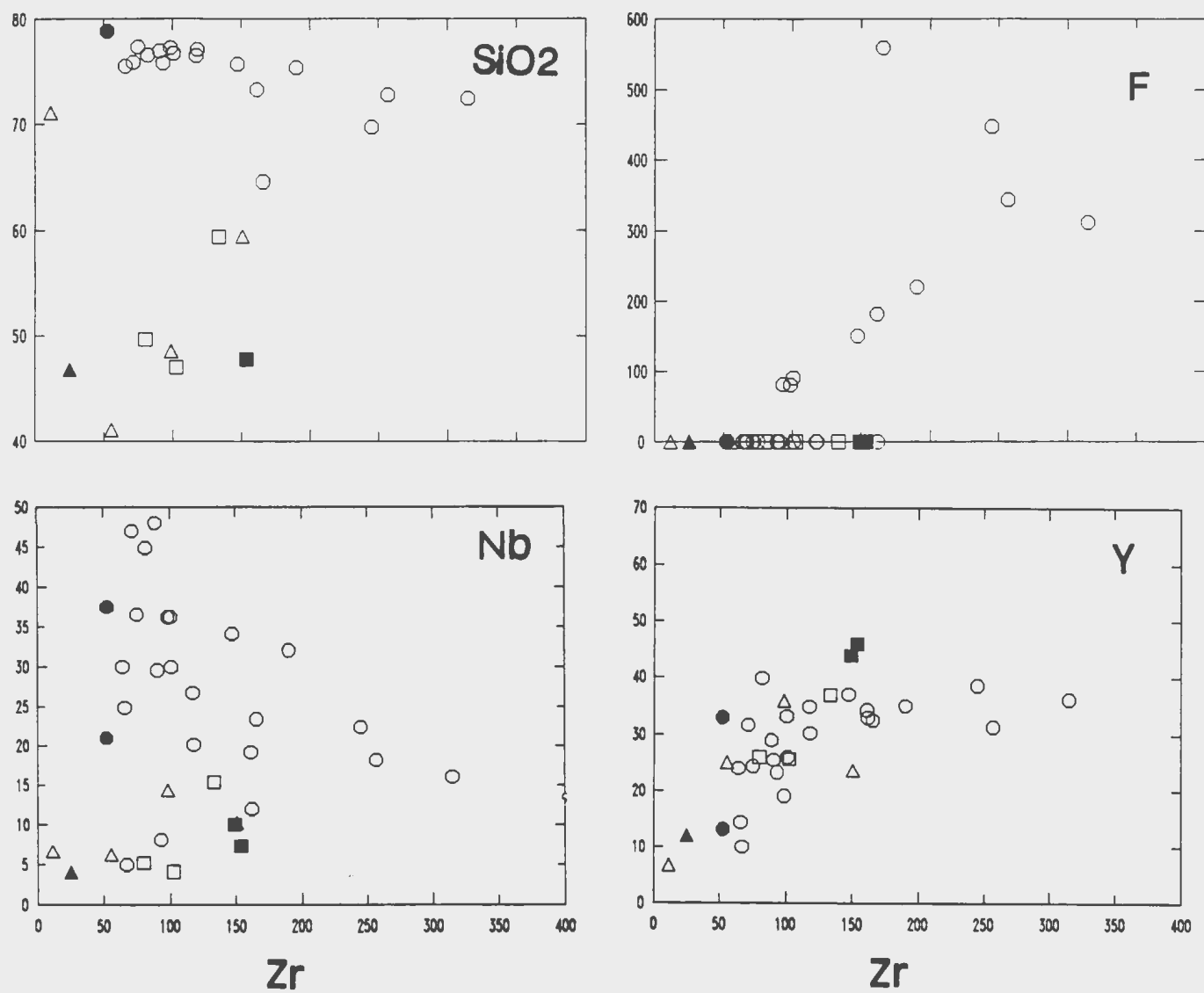


Figure 3-18: (Continued)

The Burnt Lake granite (unit 5a) is a high silica (averaging 73.9 wt%), highly differentiated, peraluminous granite. CIPW normative compositions are listed in Appendix I. The granitic body has low CaO, averaging just over 1%. K<sub>2</sub>O dominates slightly over Na<sub>2</sub>O, averaging 4.84% and 4.25% respectively. Combined total iron averages 1.38%, MgO averages 0.22% and TiO<sub>2</sub> at 0.17%. The western intrusive contact is much more differentiated, possessing higher SiO<sub>2</sub> and lower CaO contents.

Harker-type variation diagrams illustrate typical differentiation trends with respect to increasing SiO<sub>2</sub>. The major element patterns are typical of evolved granites and suggest the possibility of "specialized granites" as outlined by Tischendorf (1977), Strong (1981) and Taylor and Strong (1985). Some of the features of "specialized granites" are as follows:

- (1) High SiO<sub>2</sub> contents, generally >72%, with extreme depletion of CaO, MgO and total iron.
- (2) Enrichment in LIL trace elements (i.e. Rb, Pb, Li, U and Th) and sometimes HFS elements (i.e. Zr, Nb, Y and Ga).
- (3) Extreme depletion in compatible trace elements (i.e. Cr, Ni and V) and also in LIL elements such as Ba and Sr, which behave as compatible elements due to incorporation in feldspars.
- (4) Evidence of hydrothermal activity and volatile activity in the form of enrichment of F, B and Cl.

(5) Finally, an extreme variation in lithophile element concentrations which contrast with a very restricted major element compositional range. This indicates a decoupling of trace element behaviour from major element variations produced by fractional crystallization.

The Burnt Lake granite shows many of the characteristics of a "specialized granite" with respect to the major element contents such as high silica and depletion of CaO, MgO and total iron. However, trace element patterns are quite variable and not consistent with the specialized granite criteria. There is only minor to variable enrichment in the LIL (Rb, U, Pb and Th) and HFS elements (Zr, Nb, Y and Ga). Compatible elements (Cr, Ni and V) are depleted as well as the LIL elements of Ba and Sr.

Fluorine contents are low when compared to averages for low - Ca granites (Turekian and Wedepohl, 1961) and show an inverse relationship with  $\text{SiO}_2$  (Figure 3-17).

The decoupling of major and trace element variations is present to some degree and indicates the influence of such magmatic-differentiation processes such as fractional crystallization or thermogravitational diffusion (Hildreth, 1981). These processes are important controls on the enrichment of ore minerals in high silica magma chambers, however, to fully evaluate each process would require a much larger regional study which is beyond the scope of this thesis.

The two granitoid suites (synkinematic and post-tectonic) demonstrate different fractionation/differentiation trends. For example, the Burnt Lake granite has a negative correlation of  $\text{SiO}_2$  with  $\text{Al}_2\text{O}_3$ ,  $\text{CaO}$  and  $\text{K}_2\text{O}$ , whereas the Makkovikian suite has negative correlations in  $\text{TiO}_2$ ,  $\text{FeO}$ ,  $\text{MnO}$ ,  $\text{MgO}$  and  $\text{CaO}$  and positive correlations with  $\text{K}_2\text{O}$  and  $\text{Na}_2\text{O}$ .

According to O'Conner's (1965) normative mineral classification scheme for granitic rocks (Figure 3-19), the biotite-hornblende-bearing synkinematic granitoids (5b and 5c) are granodiorite to tonalite in composition while, in contrast, the Burnt Lake granitoids are readily classified as granites.

On the AFM projection (Figure 3-20) of Irvine and Baragar (1971) the Burnt Lake granite samples (unit 5a) plot as a dense grouping at the alkali corner. The Makkovikian suite forms a separate grouping due to its higher Fe and Mg contents and plots near the calc-alkaline - tholeiitic boundary.

In a plot of  $(\text{Na}_2\text{O}+\text{K}_2\text{O})$  vs  $\text{SiO}_2$  (Figure 3-21) the high silica end of the Burnt Lake granite plots within the subalkaline field, while the Makkovikian suite with low to intermediate silica contents plots near the boundary and into the alkaline field.



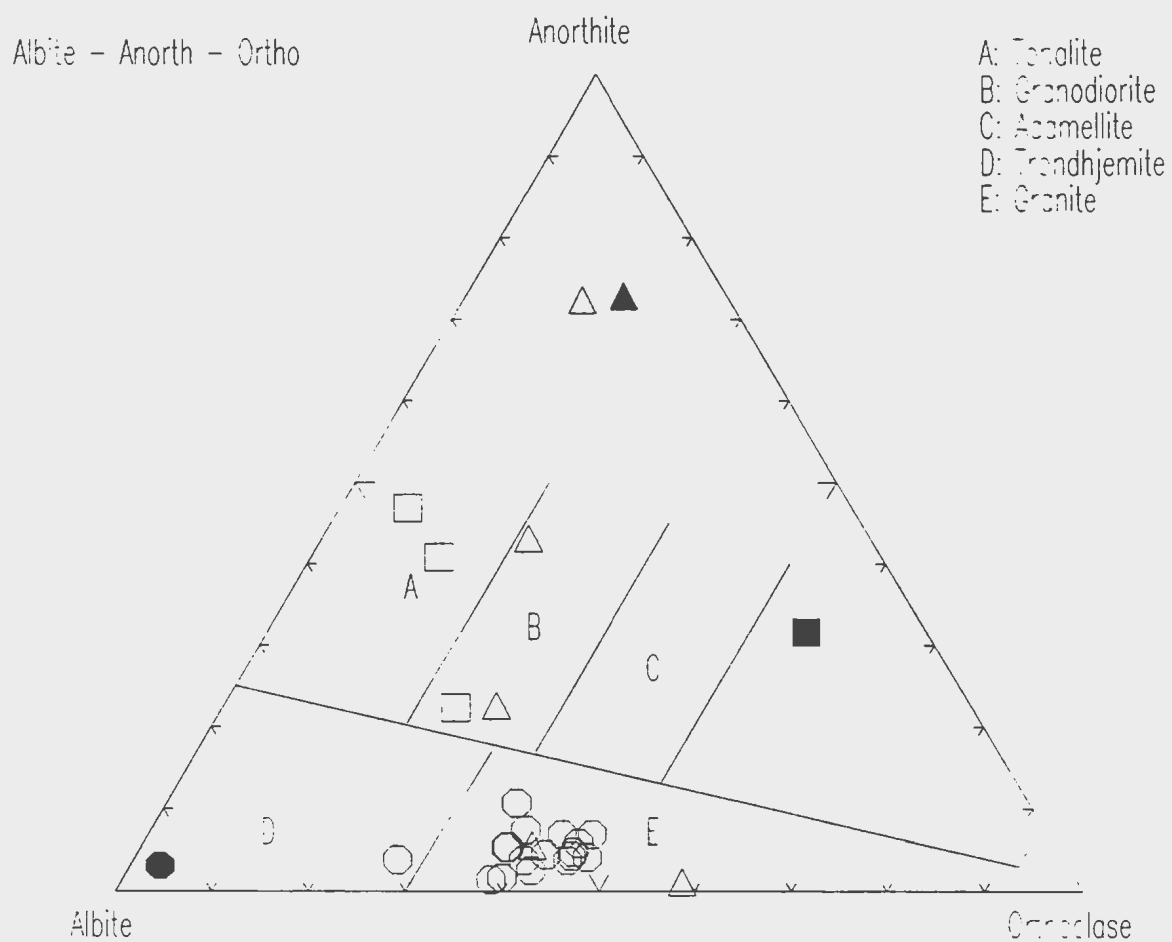


**Figure 3-19: Modal classification of granitic rocks after O'Conner, 1965. Symbols as in Figure 3-17**

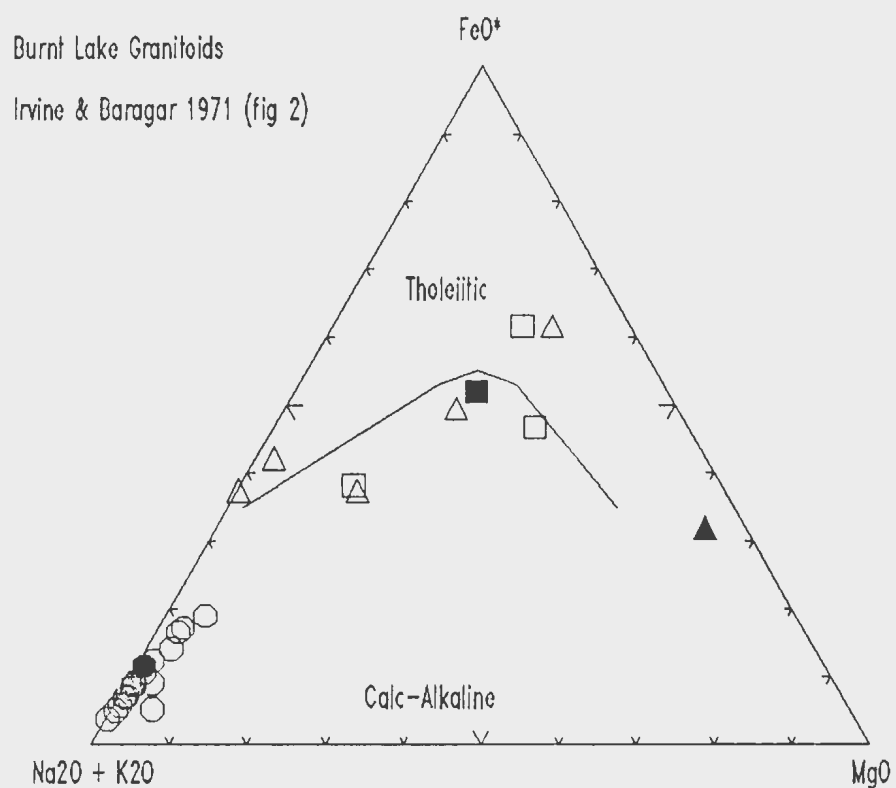


**Figure 3-20: AFM diagram with Irvine and Baragar (1971) calc-alkaline trend. Symbols as in Figure 3-17. A =  $\text{Na}_2\text{O} + \text{K}_2\text{O}$ ; F =  $\text{FeO} + 0.8998 \text{Fe}_2\text{O}_3$ ; M =  $\text{MgO}$ ; all in weight percent.**

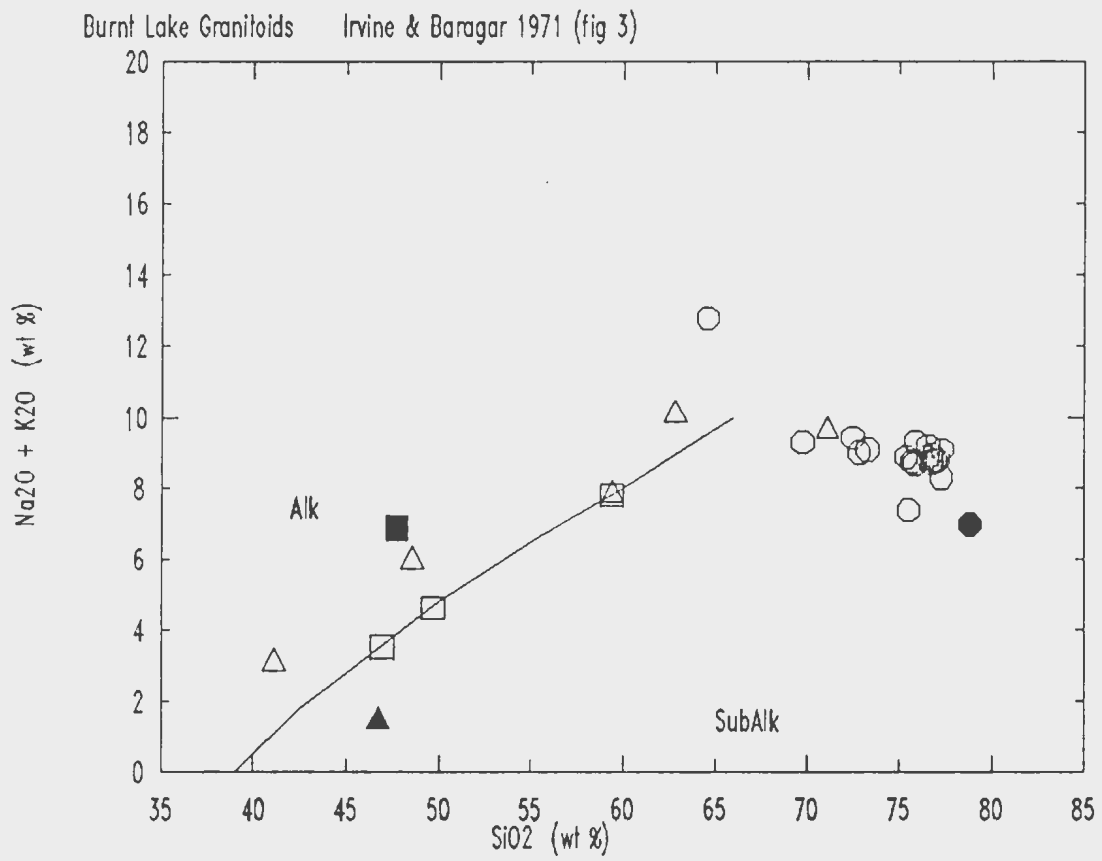


**Figure 3-21: Major element variation diagram of total alkalis ( $\text{Na}_2\text{O} + \text{K}_2\text{O}$ ) vs  $\text{SiO}_2$ . Field boundary from Irvine and Baragar (1971). Symbols as in Figure 3-17.**

On Pearce et al.'s (1984) Rb-(Y+Nb) discrimination diagram (Figure 3-22a), half of the Burnt Lake granite samples plot in the volcanic-arc granite field (VAG) with the other samples plotting in the within-plate granite (WPG). These data plot within the field from Kerr and Krogh (1990) for a large data set of Labradorian (1650 Ma) granitoid rocks. The Makkovikian (ca. 1800 Ma and older) granitoid rocks from Kerr and Krogh's (1990) study mostly plot in the within-plate granite (WPG) field while the Makkovikian granitoid rocks from the Burnt Lake area plot mainly in the volcanic-arc granite (VAG) field. This difference could be a result of the small sample suite used for this study as compared to the regional study of Kerr (1990).

In the Nb versus Y discrimination diagram (Figure 3-22b) of Pearce et al. (1984), the Burnt Lake Granite rocks plot mostly in the WPG field with some overlap into the VAG field. The Makkovikian granitoid rocks from this study have lower Nb and Y contents and plot mainly in the VAG field.

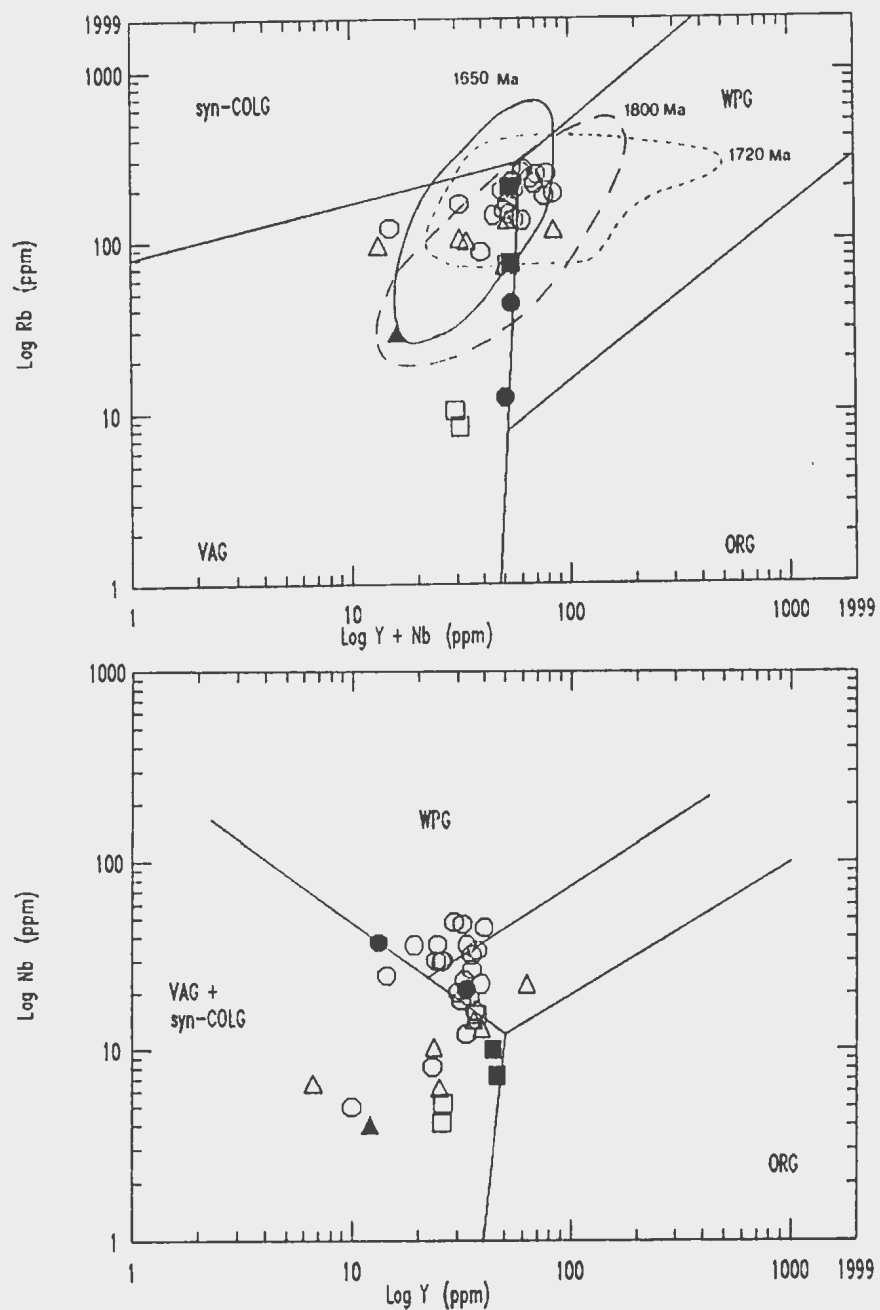


**Figure 3-22: Tectonic discrimination diagrams for the Burnt Lake area granitoids (after Pearce et al., 1984). Syn-COLG = syn-collisional granite, WPG = within plate granite, VAG = volcanic arc granite, ORG = orogenic granite. Fields of synkinematic Makkovikian (1800 Ma), posttectonic Makkovikian (1720 Ma) and Labradorian granitoids (1650 Ma) are from Kerr and Krogh (1990) in Figure 3-22a. Symbols as in Figure 3-17.**

A genetic classification scheme for granitic rocks (Figure 3-23) outlined by White and Chappell (1983) is based on the lithogeochemical compositions of the source materials from which the granites were derived as partial melts. I-type (igneous source) granites are produced in post-orogenic, uplift regimes, S-type (sedimentary source) granites are the product of continental collisions and A-type (anorogenic) granites are produced by post-tectonic melting of an anhydrous lower crust from which an orogenic granite had been previously extracted. On the  $K_2O$  versus  $Na_2O$  diagram, the Burnt Lake Granite plots as an A-type granite with one sample plotting in the I-type field. The Makkovikian suite on the other hand plots mainly in the I-type field while two samples plot within the A-type boundary. Ga versus  $Al_2O_3$  shows a clearer separation, with the Burnt Lake Granite plotting as A-type and the Makkovikian suite plotting as I-type granitoids. The classification of the Burnt Lake Granite as an A-type granite is consistent with a post-tectonic intrusion. A-type granitoids have also been associated with Pb-Zn, Sn, W, Mo and F mineralization (Tuach et al., 1986). The I-type classification for the Makkovikian synkinematic suite is consistent with the orogenic intrusion.

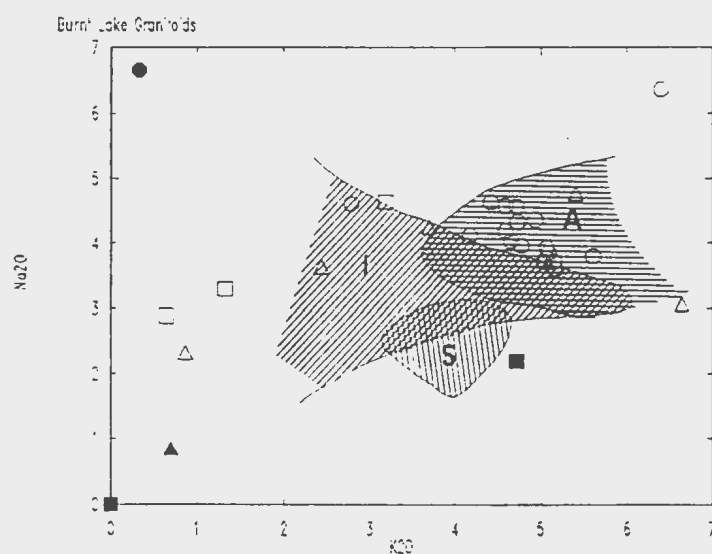


**Figure 3-23a:  $\text{Na}_2\text{O}$  versus  $\text{K}_2\text{O}$  diagram for classification of I-A-S type granites. Fields from White and Chappell (1983).**

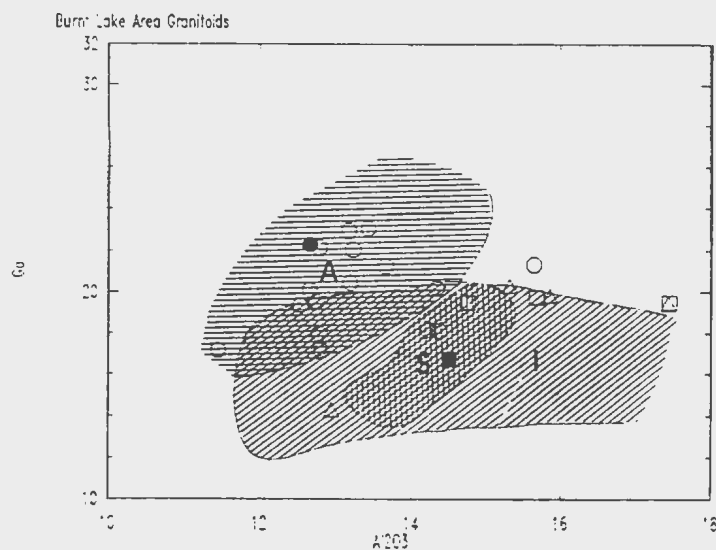


**Figure 3-23b : Ga versus  $\text{Al}_2\text{O}_3$  diagram for classification of I-A-S type granites. Fields from White and Chappell (1983).**

### 3.2.3 Rare Earth Patterns

Analytical procedures and data tables for rare earth element (REE) analysis are given in Appendix I. Normalized REE patterns for the post-tectonic Burnt Lake Granite are illustrated on Figures 3-24 to 3-29, while the REE pattern for one sample of the synkinematic Makkovikian granite is shown on Figure 3-30. Generally, the patterns have LREE>HREE and a negative Eu anomaly. REE concentrations decrease with increasing  $\text{SiO}_2$  (*i.e.* fractionation - sample LM-23 has 75.5 %  $\text{SiO}_2$ ; and LM-165 has 76.9 %  $\text{SiO}_2$ ). Also the patterns have a "saucer-shape" with increasing HREE from Dy to Yb. Such shapes have been interpreted by Taylor *et al.*, (1981) to indicate the presence of  $\text{F}^-$  or  $\text{CO}_3^{2-}$  rich volatile phases in high level granitoids (the  $\text{F}^-$  or  $\text{CO}_3^{2-}$  ions supposedly complex and thus enrich the HREE). This is plausible in the Burnt Lake Granite as there are demonstrated upper level volatile concentrations (shown by the pegmatite and molybdenite) in the contact zone and fluorite is present in the vicinity of the contact.

Samples GEO-1, GEO-2 and LM85-174, taken from the centre of the Burnt Lake Granite (BLG), represent a standard for the BLG and show typical REE patterns with HREE depletion over LREE and negative Eu anomalies (Figure 3-24). An extended plot (Figure 3-25) shows a slight increase in U with depletions in Nb, Sr and Ti. LM85-167 and 168 are an intermediate distance from the molybdenum-bearing western intrusive contact. The



samples have increased silica contents and show an overall decrease in REE's with a stronger negative Eu anomaly (Figure 3-26). These samples are transitional from the main body to the volatile-rich margin and show an overall decrease in all elements below K on an extended plot (Figure 3-27). Sample LM85-24 is from a pegmatite dyke within the BLG and shows extreme depletion in all REE's. The group of samples closest to the molybdenum mineralization (LM85-23, 34, 164, 165, 166) show even greater depletions in REE's, with Eu totally stripped from samples LM85-164 and 165 (Figure 3-28). An extended plot (Figure 3-29) shows an overall decrease in all elements below K but a slight enrichment in U and Th in samples near the contact zone.

Loss of REE's in an exsolved volatile-rich vapour phase has been suggested to account for REE depletion in highly differentiated granitic rocks (Muecke and Clarke, 1981). As mentioned earlier, the saucer-shaped profiles have been interpreted as indicating the presence of a  $F^-$  and/or  $CO_3^{2-}$ -volatile-rich phase (Taylor *et al.*, 1981) which results in the depletion of the HREE. Taylor and Fryer (1982, 1983) have suggested that in general  $Cl^-$  can complex and transport the LREE, while a phosphate-rich volatile phase (i.e.  $PHO_4$ ) could effectively complex and transport the MREE.

It is therefore possible that a combination of complexing species were available in a volatile-rich phase which effectively concentrated and removed REE as complexes from the

coexisting magma/vapour phase in the granitic melt.

Sample LM85-134 is from the synkinematic suite to the north and shows an overall increase in REE's with a moderate negative Eu anomaly (Figure 3-30). The extended plot (Figure 3-31) shows a lower U content with strong Nb, Ti and Sr depletions.

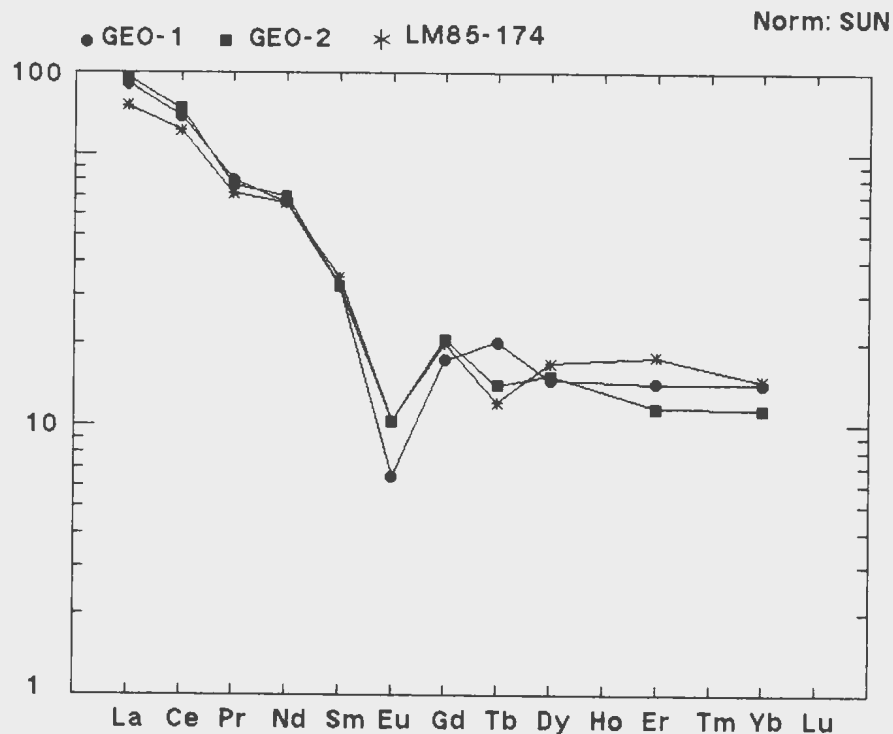


**Figure 3-24: SUN-normalized REE plot of samples that are considered to represent a standard for the BLG.**

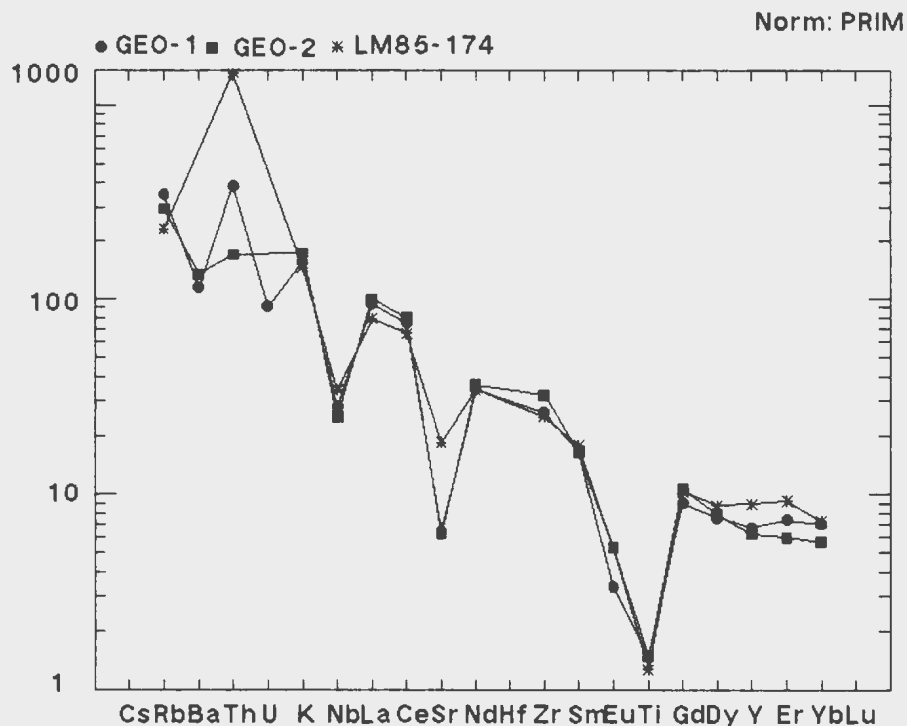


**Figure 3-25: Extended trace element variation diagram for standard samples of the BLG ratioed to primitive mantle values (PRIM).**

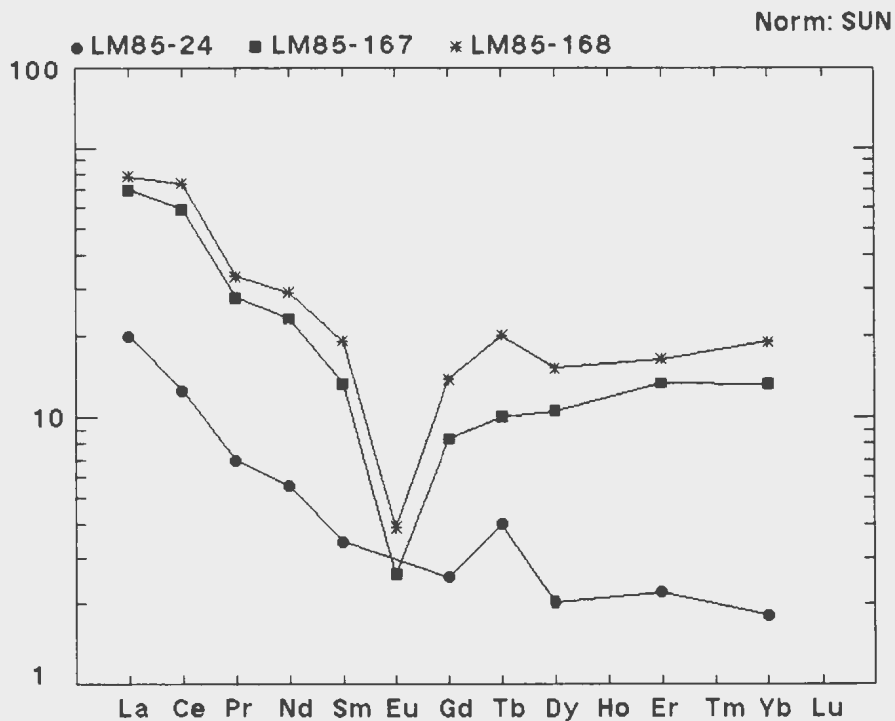


**Figure 3-26: SUN-normalized REE plot of samples from the BLG that are transitional from the main body to the volatile-rich margin.**

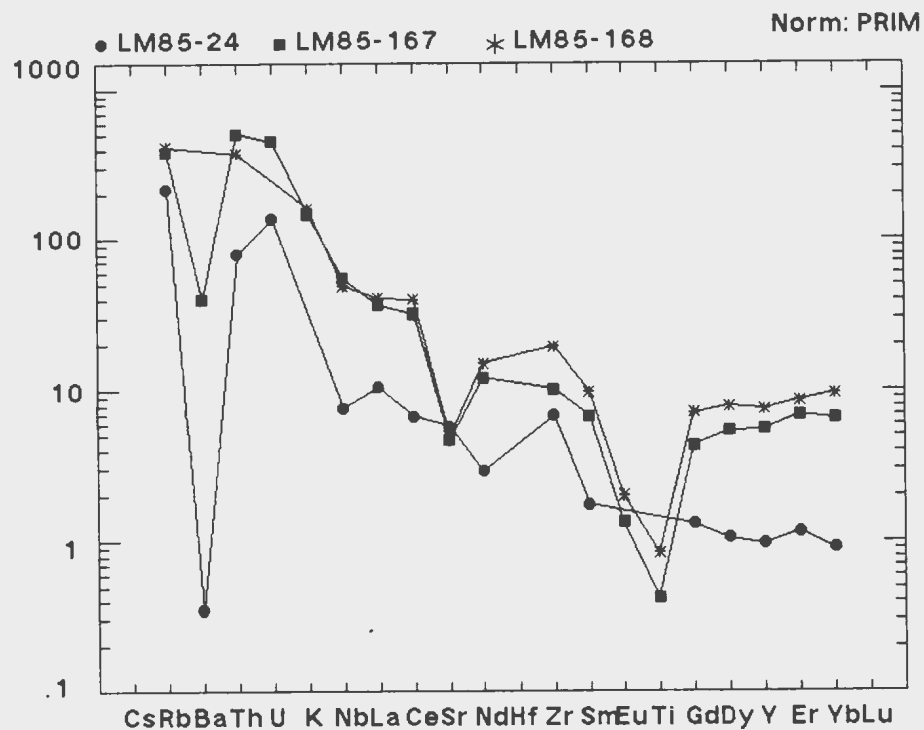


**Figure 3-27: Extended trace element variation diagram for transitional samples of the BLG ratioed to PRIM.**

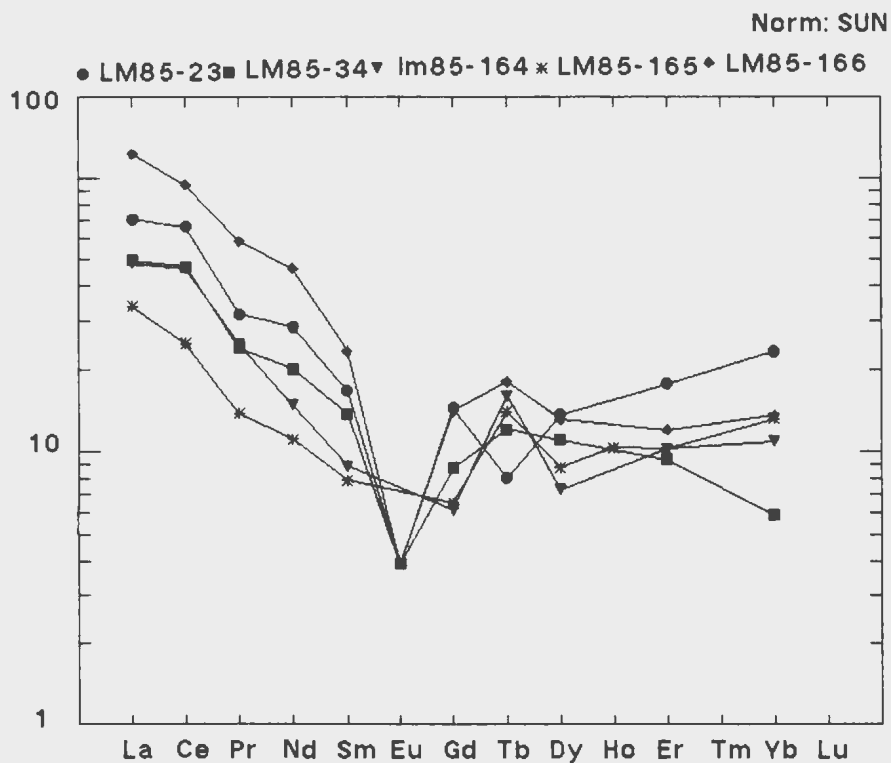


**Figure 3-28: SUN-normalized REE plot of samples from the BLG that are closest to the volatile-rich margin.**

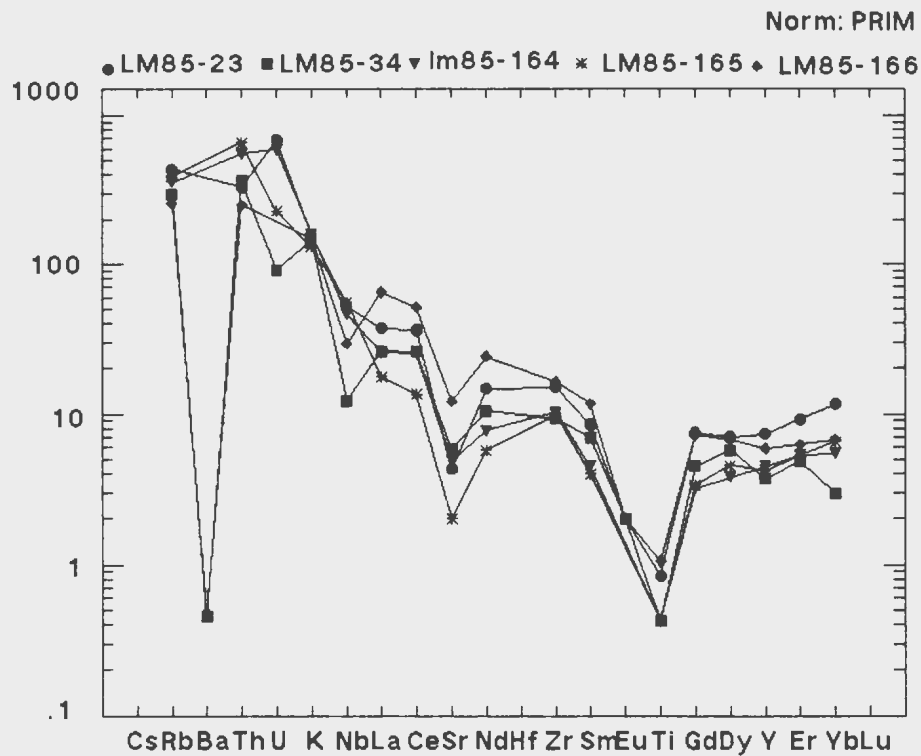


**Figure 3-29: Extended trace element variation diagram for the most fractionated samples of the BLG ratioed to PRIM.**

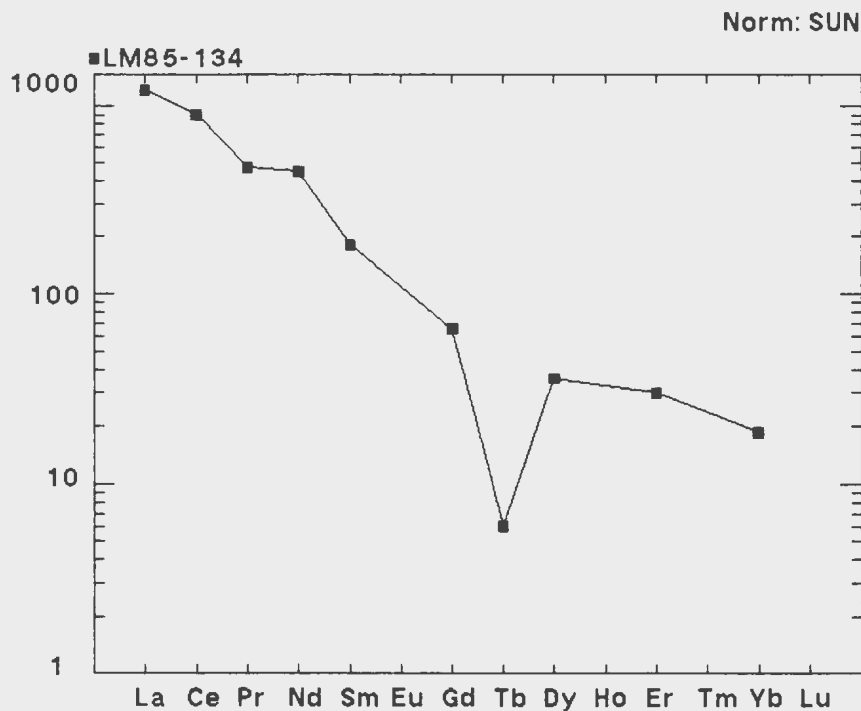


**Figure 3-30: SUN-normalized REE plot of the synkinematic Makkovikian granite.**

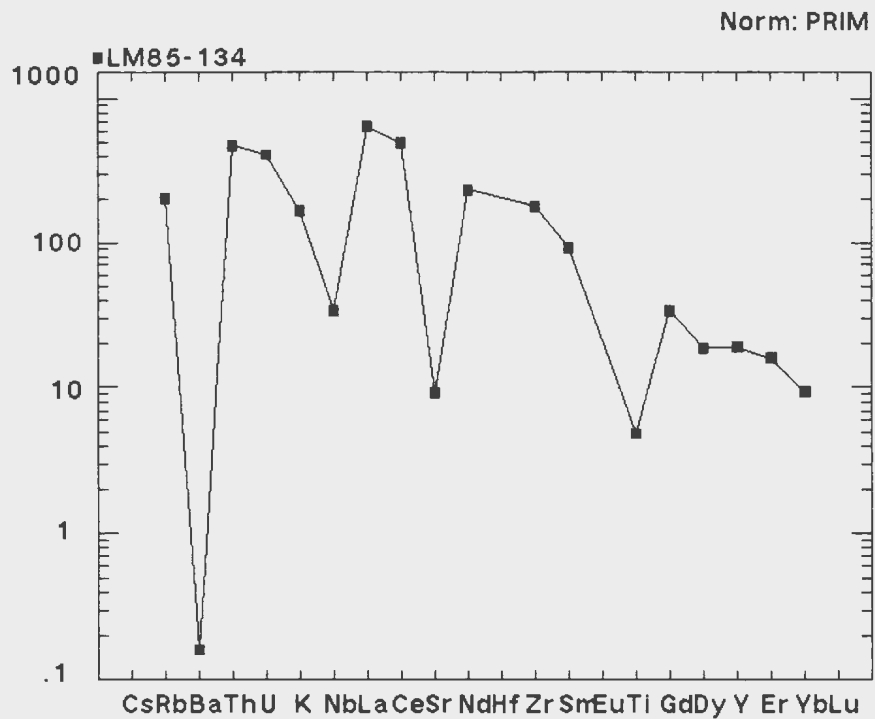


**Figure 3-31: Extended trace element variation diagram for the synkinematic Makkovikian granite.**

#### **3.2.4 Chemical Zonation in the Burnt Lake Granite (Unit 5a)**

The wide variation of  $\text{SiO}_2$  values (from 63 to 79%) in the Burnt Lake Granite reflects successive fractionation, in fact there is a rough zonation in which the  $\text{SiO}_2$  content increases toward the western intrusive contact of this granite with the Upper Aillik Group (Figure 3-32). High grade molybdenite mineralization located at and near this intrusive contact is associated with the highest silica values and represents the most differentiated portion of the pluton. The chemical zonation of silica and lithophile elements towards

an upper or sidewall contact is characteristic of high silica and specialized granitic systems (Tuach et al., 1986, Hildreth, 1981)

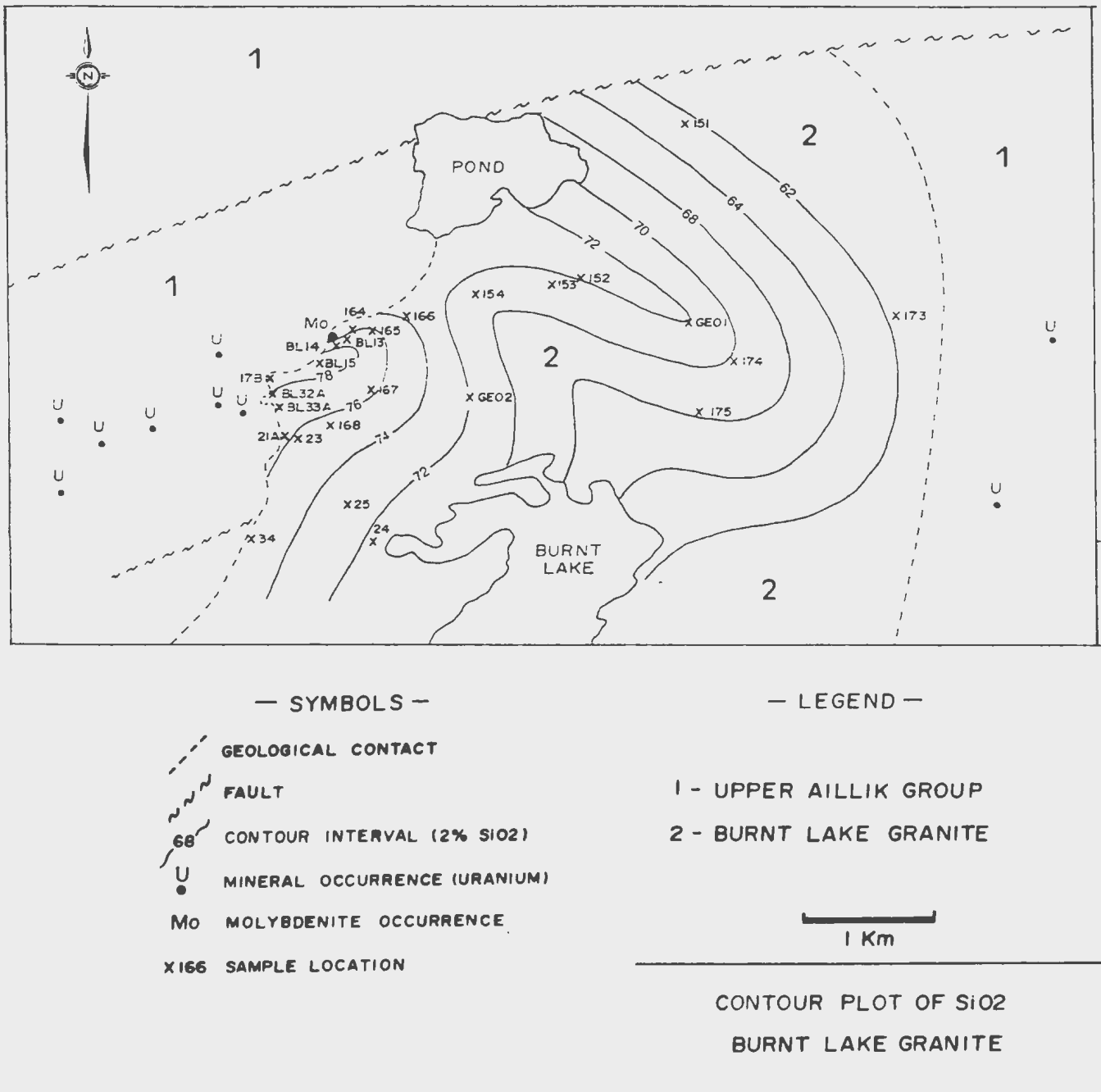


Figure 3-32: Contour plot of SiO<sub>2</sub> for the Burnt Lake Granite. Contour interval is 2% SiO<sub>2</sub>.

### 3.3 Geochronology

#### 3.3.1 Rb-Sr isotopic data from the Burnt Lake Granite

Rb/Sr isochrons have been generated for whole rock samples and mineral separates of the Burnt Lake Granite. Data used to construct the diagrams are listed in Table 3-4, while methods and techniques are outlined in Appendix V. All of the samples appear to be fresh except for sample LM85-164 which shows noticeable alteration in the form of thin epidote veinlets and sample GEO1 which contains minor amounts of pyrite associated with locally developed clusters of biotite. Samples are leucocratic and undeformed except for GEO2 which contains 10-15% biotite and shows a strong foliation.

A Rb/Sr isochron generated for whole rock samples of the Burnt Lake Granite is shown as Figure 3-33. The "isotopic" age of  $1548 \pm 90$  Ma (with a MSWD of 86.5) approximates previously derived Rb-Sr whole rock ages of  $1548 \pm 73$  Ma and  $1498 \pm 46$  Ma (Kontak, *in* Ryan, 1984) for the Otter Lake - Walker Lake Granite which Kontak defined as being part of the same pluton as the Burnt Lake Granite. The Rb/Sr age for the Burnt Lake Granite is younger than (by ~ 100 Ma) a more accurate U-Pb zircon date of  $1647 \pm 2$  Ma for the same granitoid unit (Kerr and Krogh, 1990). This new geochronological information includes the Burnt Lake Granite as part of the Trans-Labrador Granitoid Belt (TLGB) which is dated at ca. 1620-1650 Ma on



the coast and ca. 1654 Ma in central Labrador (Thomas et al., 1986). The 1548 Ma age for this granite might be correct if the granite represents a later (or terminal) phase of the Trans-Labradorian granitoid magmatism (1660-1650 Ma - after Thomas et al., 1986). However it seems to represent a partial re-setting of the Rb/Sr isotope systematics by a later metamorphic event (i.e. loss of radiogenic Sr or gain of Rb) giving the Burnt Lake Granite an apparent 100 Ma younger age.

TABLE 3-3

Summary of Rb-Sr data for samples of the Burnt Lake Granite used for geochronology.

Sample	$^{87}\text{Rb}/^{86}\text{Sr}$	$^{87}\text{Sr}/^{86}\text{Sr}$
LM85-23	8.62228	.899094
LM85-34	4.33228	.804451
LM85-174	1.007	.727062
LM85-134	1.91288	.755078
LM85-151	1.48726	.739702
LM85-165	18.73069	1.10089
LM85-164	6.52262	.838619
LM85-166	1.69933	.742412
LM85-167	7.32835	.869538
LM85-168	6.78367	.861691
LM85-GEO2	3.72831	.804056
LM85-GEO1	4.31142	.788475
GEO1-BIO	20.6222	1.574489
GEO1-SPHENE	.786	.760408
GEO2-FELD	3.8525	.800091
GEO2-BIO	86.9909	1.657088
GEO1-FELD	---	.800136

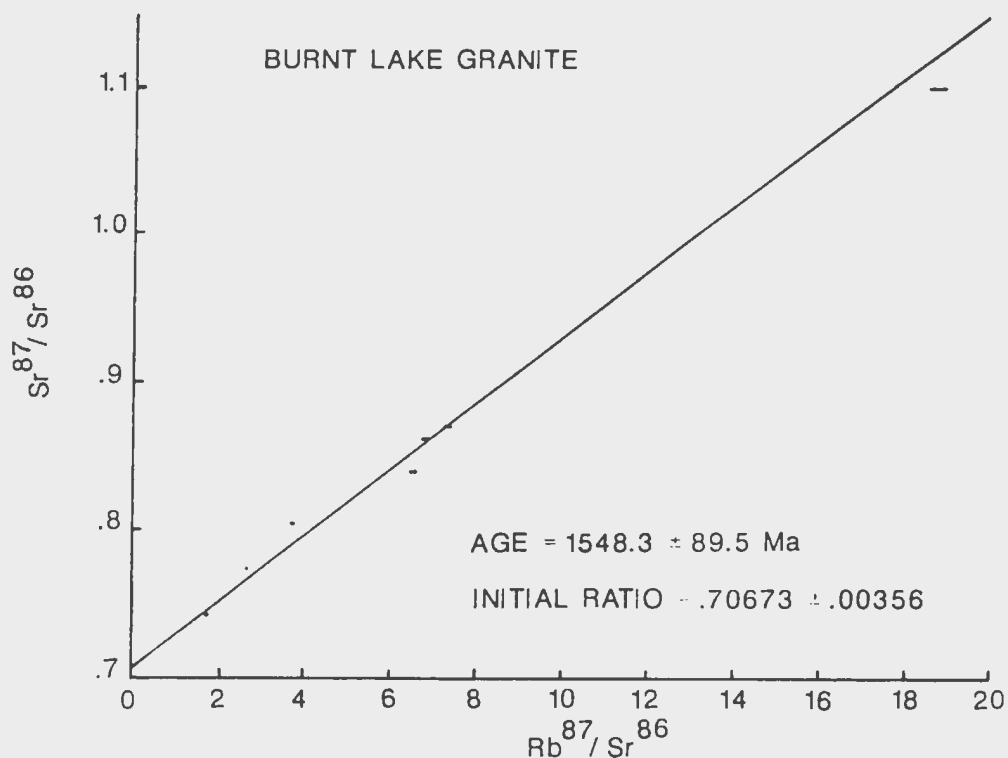


**Figure 3-33: Rb/Sr isochron generated for whole rock samples of the Burnt Lake Granite.**

The large scatter obtained may also be attributed to other factors including: an incomplete homogenization of the  $^{87}\text{Sr}/^{86}\text{Sr}$  ratio if the rocks were formed from partial melts or assimilation of older material through anatexis. Mineral separates from sample LM85-GEO1 (sample was taken in the middle of the granite, see Figure 3-32 for sample location)(GEO1-Bio, GEO1-sphene and GEO1-epidote) gave a Model 3 Yorkfit age of  $2810 \pm 620$  Ma. Obviously the isotopic signature for this sample has been affected by a superimposed

event whereby Sr was added and/or Rb was removed in the minerals.

Sample GEO2 is located approximately 2 km east of the western intrusive contact with the Upper Aillik Group and shows a strong fabric with an alignment of the mafic minerals. The sample contains 10-15% biotite compared to the other samples which generally contain < 5%. In thin section the biotite is anhedral to subhedral in shape and is badly corroded and variably altered to chlorite which formed along the cleavage direction. A Model 3 Yorkfit for GEO2, GEO2-Feld and GEO2-Bio indicates an age of  $720 \pm 110$  Ma, indicating that this system has also been affected by later fluids (possibly during the Grenvillian). The biotites had Rb stripped and Sr added.

An isochron without GEO1, GEO1-Bio, GEO1-Sphene, GEO2-Feld, GEO2-Bio and LM85-164 gives a Model 1 Yorkfit age of  $1650 \text{ Ma} \pm 140 \text{ Ma}$  with a MSWD of 61.6 and a Model 3 age of  $1470 \text{ Ma} \pm 70 \text{ Ma}$  (Figure 3-34).

A similar Rb-Sr isotope "re-setting" has occurred in Upper Aillik Group felsic volcanic rocks in this same Michelin Zone (i.e. that portion of the Aillik Group which occurs south of the Adlavik Brook Fault). Kontak (1980) reported a well fitted Rb/Sr whole rock isochron of  $1767 \pm 4 \text{ Ma}$  for a rhyolite unit on Michelin Ridge (just to the NW of the Michelin deposit). Kontak later revised the age to  $1786 \pm 38 \text{ Ma}$  (Ryan, 1984) and stated that this date reflected Hudsonian orogenic

events rather than the true volcanic age. The interpretation that Kontak's Rb/Sr isochron does not indicate the primary magmatic age has been borne out by a U/Pb zircon age of 1855 Ma (Scharer et al., 1988) from the same outcrop area sampled by Kontak.

Heaman et al., (1986) studied the U-Pb zircon, U-Pb sphene and Rb-Sr whole rock ages from granites in the Central Metasedimentary Belt of Ontario and found similar isotopic complexities. They concluded that the Rb-Sr disturbance giving an incorrect younger age (compared with the more accurate U-Pb zircon age) was the result of late stage-fracturing and alkali metasomatism. The most interesting feature of the apparent isotopic re-setting in the Burnt Lake area is that it has apparently thoroughly affected both the older volcanic rocks and the post-tectonic granitoids on a very broad regional scale (i.e., the isochron re-setting is not attributable to single samples, thus, all samples must have undergone the same isotopic alteration), and the effect in both cases has been to reduce the "real age" by about 60-90 Ma. Since the post-Hudsonian granites were equivalently affected, the isotopic disturbance in the felsic volcanic rocks was not a result of Hudsonian deformation. The only major subsequent deformation of rocks in the area was Grenvillian.

Walraven et al. (1986) reported similar "disturbances" in Rb-Sr isotope systematics that have produced a consistent lowering in the whole rock Rb/Sr age dates of granites from

the Bushveld Complex. These authors described the phenomenon as having resulted from the preferential removal of radiogenic Sr ( $^{87}\text{Sr}$ ) from potassium feldspar. The widespread, cross-unit age date lowering in the Burnt Lake area might have resulted from a similar mechanism. The Sr removal could have conceivably been initiated by Grenvillian tectonics.

Kontak (1980) reported that two pitchblende separates from the Burnt Lake Showing gave discordant Pb isotope ages of 1770 and 1680 Ma. Kontak (1980) and Gandhi (1986) thought that these dates resulted from Grenvillian disturbance of the lead isotope system. If the age of the Burnt Lake Showing is assumed to be 1855 Ma (U-Pb zircon date for the Upper Aillik Group, Scharer et al., 1988), a regression of the Pb isotope data of galena separates from this showing (reported in Wilton et al., 1986a and discussed in Chapter 4) through this point indicates a 950 Ma (Grenvillian) age for the extraction of radiogenic lead from uranium and subsequent deposition as galena.

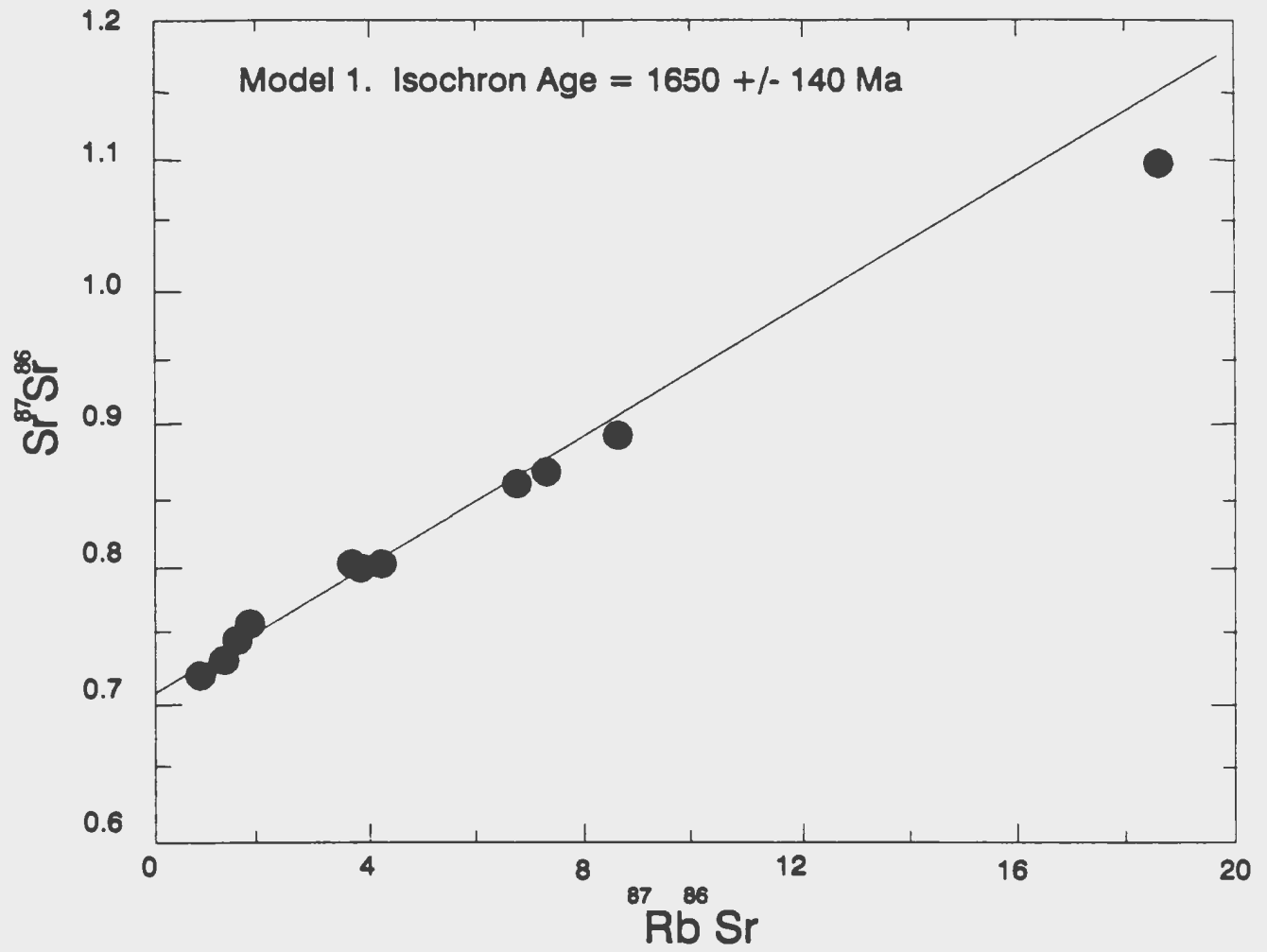


Figure 3-34: Rb-Sr isocron plot for the Burnt Lake Granite.

## CHAPTER 4

## MINERALIZATION

## 4.1 Introduction

The Burnt Lake area is characterized by numerous, widely distributed radioactive zones (Maps 1 and 2) and has open pit reserves of 140,000 tonnes grading 0.082%  $U_3O_8$  for a 40m by 300m zone (Sharpley, 1978). Four styles of mineralization have been identified in the area which include:

- (1) Uranium mineralization associated with alkalic metasomatism and hematization.
- (2) Uranium mineralization associated with structural features (i.e. fractures, faults and dyke contacts) and granophile minerals (i.e. fluorite and molybdenite) indicating possible relationship to granitoid magmatism.
- (3) Pb-Zn-Cu sulphide (+ Ag and Au) stringers and veinlets associated with potash metasomatism (granite-related).
- (4) Significant concentrations of molybdenite in a high level, leucocratic, post-tectonic granite (Burnt Lake Granite) near the contact with the felsic volcanic country rocks (Upper Aillik Group).

#### 4.2 Uranium Mineralization in the Burnt Lake Area

In the Burnt Lake area there are four main areas of uranium mineralization viz. the Burnt Lake Main, Burnt Lake Central, Burnt Lake Northwest, and the Burnt Lake Southwest. Five kilometres to the west are the Emben Main, Emben Central and Emben South showings. The Aurora River occurrence is located 4 kilometres north of the Burnt Lake prospects (see Map 1, back pocket).

According to Krajewski et al. (1977), uranium mineralization in the Burnt Lake area, "is associated with chlorite and hematite alteration, pyrite, magnetite and minor amounts of fluorite, sphalerite, galena and molybdenum with traces of gold and silver".

Uranium mineralization in the Burnt Lake area occurs in narrow and sporadic zones within the volcanic rocks of the Upper Aillik Group. The main mineralizing event was associated with intense hydrothermal alteration and alkali metasomatism (both Na and K, i.e. Burnt Lake showings). Uranium has also been remobilized and concentrated along structural weaknesses such as fractures and faults, along mafic dykes (e.g. Emben showings) and along lithological boundaries (e.g. Aurora River). The showings are described separately in the following section.



#### 4.2.1 Burnt Lake North (Main) Zone

This is the main ore zone at Burnt Lake and contains 17 trenches and 8 diamond drill holes with patchy and discontinuous uranium mineralization over an area of 50m x 500m (Map 2). Figure 4-1 shows several typical trenches through the radioactive zone (see Map 2 for location). A typical drill section through the radioactive zone is shown in Figure 4-2. The drill logs from this zone are given in Appendix III.

Lithologies generally present in the trenches include a pink to grey coarse-grained felsic crystal tuff, quartz-feldspar porphyry that is often brecciated (see Figures 4-3A,B), coarse-grained feldspar porphyry, banded felsic ash tuff, and lapilli tuff (Figures 4-3A and 4-4A). Mafic clots and pods are abundant and commonly wrap around feldspar and quartz phenocrysts in a eutaxitic texture (Figures 4-4B and 4-4C). The mafic bands and clots were identified petrographically as acmite and aegirine-augite. Mineral lineations defined by quartz rodding in the quartz-feldspar porphyry have a steep southeastern to northeastern plunge.

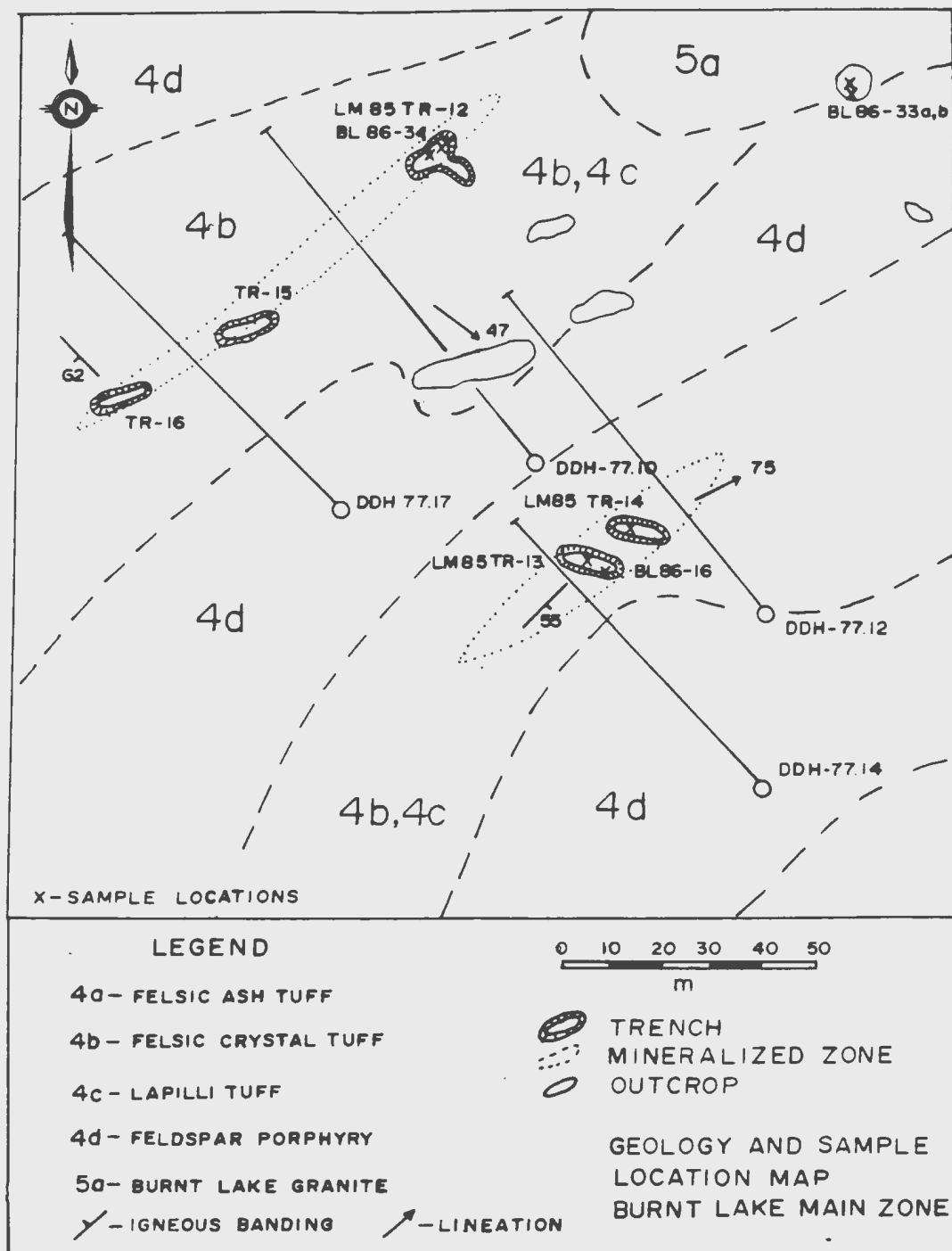
Uraninite is generally disseminated in the banded felsic ash tuff, felsic crystal tuff and lapilli tuff and is associated with the mafic clots and pods. In thin section uraninite also occurs with zircon (Figure 4-5) and is rarely intergrown with monazite and a Ti-Fe-Mn oxide. Other accessory minerals include sphene, ilmenite, barite, apatite and

monazite (Figures 4-6 and 4-7). Uranium mineralization also occurs as veinlets (Figure 4-8) or as fracture-fillings intergrown with specular hematite cutting the host felsic volcanic rocks. Alteration associated with uraninite includes hematization and uranophane staining as well as some chloritization and epidotization. Ore mineralogy includes galena, sphalerite and minor chalcopyrite (+Ag) (see base metal section below).

#### **4.2.2 Burnt Lake Central Zone**

Mineralization in the central zone is generally narrow and of low grade, but has a discontinuous lateral extent of approximately 700 m containing 6 trenches and 6 diamond drill holes (Map 2). Diamond drill logs are in Appendix II. The lithologies in the trenches vary from coarse-grained feldspar porphyry, to fine-grained quartz-feldspar porphyritic rhyolite, to sugary quartz crystal tuff, to breccia composed of feldspar porphyry fragments in a fine-grained grey ash matrix. A peculiar alteration of the feldspar phenocrysts in the non-mineralized quartz-feldspar porphyry is present as partial rimming to total replacement of the feldspar with a greenish-black mineral that was identified as magnetite from a SEM qualitative probe analysis of sample LM85-14 (Figure 4-9). The mineralized areas are strongly hematized, resulting from the oxidation of magnetite and contain abundant

uranophane staining.

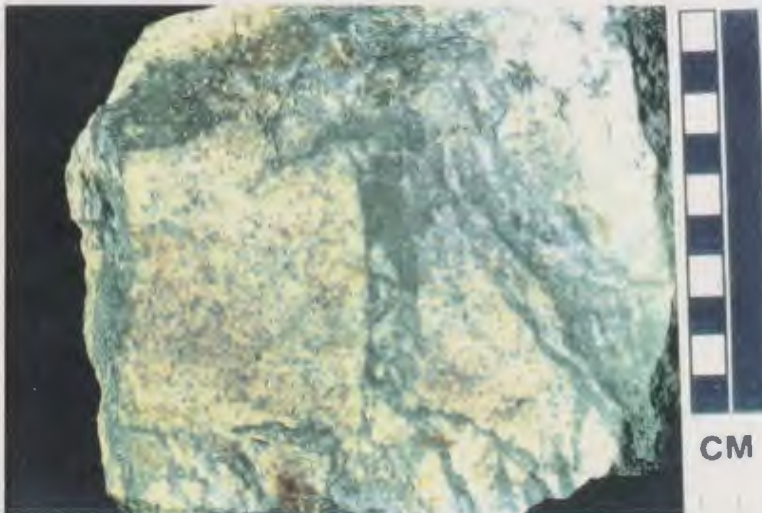


**Figure 4-1: Geology and sample location map of the Burnt Lake Main Zone.**



**Figure 4-3:**

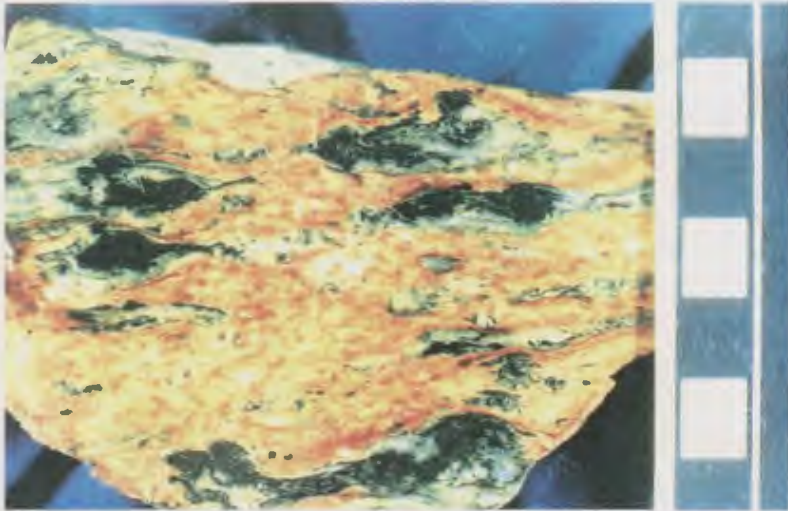
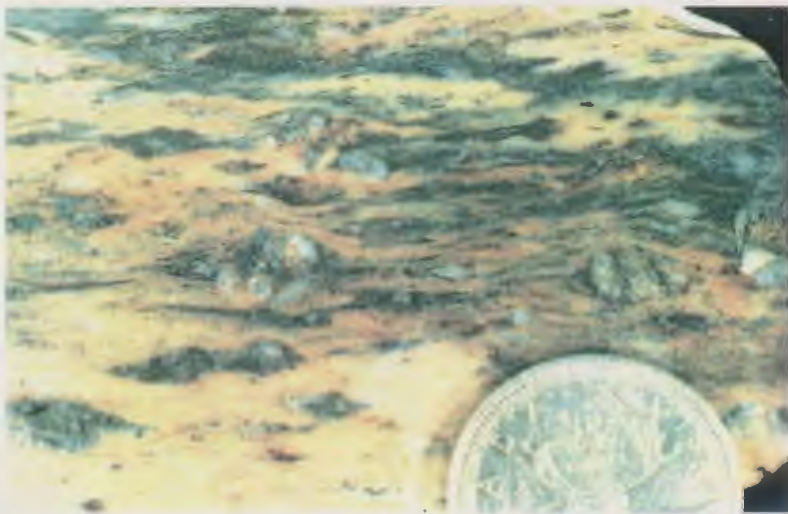
(A): Photograph of Trench #6 from the Main Zone showing a pink hematized radioactive zone (hammer) adjacent to a breccia zone (lens cap). (B): Photograph of typical volcanic breccia from Trench #8A (Main Zone). Breccia is composed of pink quartz-feldspar porphyry fragments set in a fine grained greenish volcanic ash matrix. (C): Felsic ash tuff lens within a felsic crystal tuff (Trench #12).

**A****B****C**

**Figure 4-4:**

**(A): Mafic clots in a hematized radioactive lapilli tuff (Trench #13). (B): Outcrop of quartz-feldspar porphyry with characteristic mafic banding (Trench #16). Lens cap for scale. (C): Hematized radioactive quartz-feldspar porphyry with mafic banding and clots.**



**A****B****C**



There is an association between uranium and amphibole pods and veinlets in the quartz-feldspar porphyry and quartz crystal tuff. Uraninite occurs as disseminations within the host-rocks and uraniferous amphiboles or as individual grains associated with ilmenite, apatite and zircon (Figure 4-10). Pyrite is common in the non-radioactive areas associated with fractures. Base metal mineralization is generally absent in the central zone.

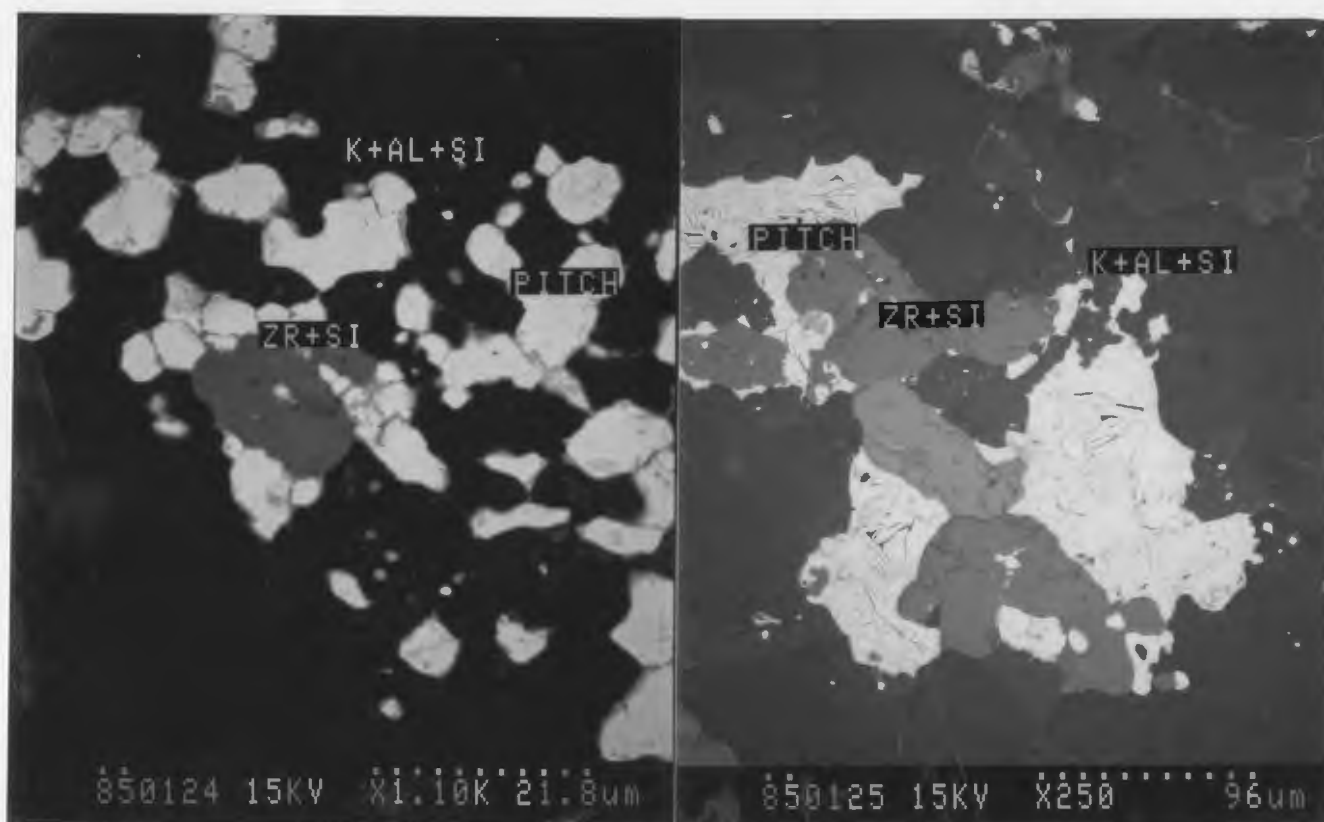


**Figure 4-5:** (850124,125) Scanning Electron Microscope (SEM) back scatter images of uraninite (pitch) intergrown with zircon (ZR+SI) in a potassium feldspar (K+AL+SI) matrix.

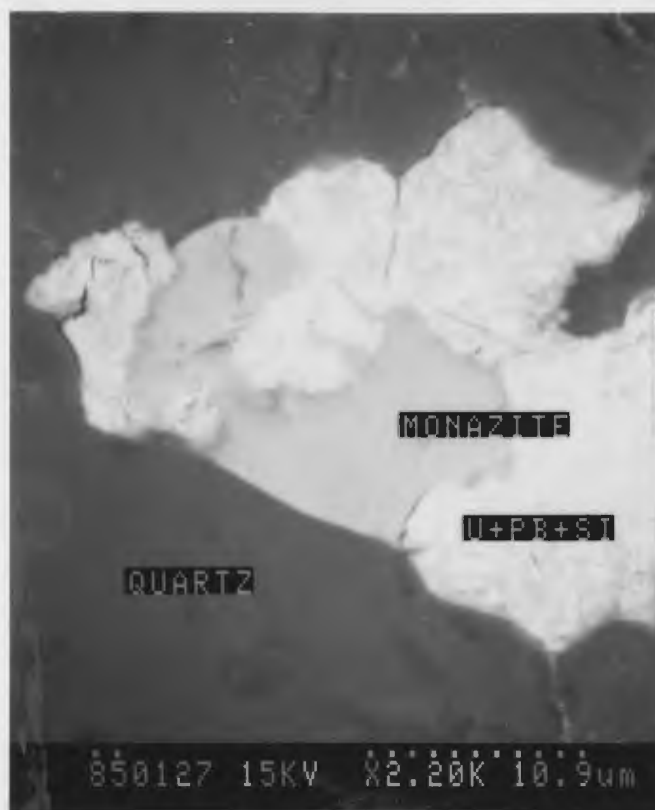


**Figure 4-6:** (850127) SEM back scatter image of uraninite intergrown with monazite in a silicate gangue matrix.

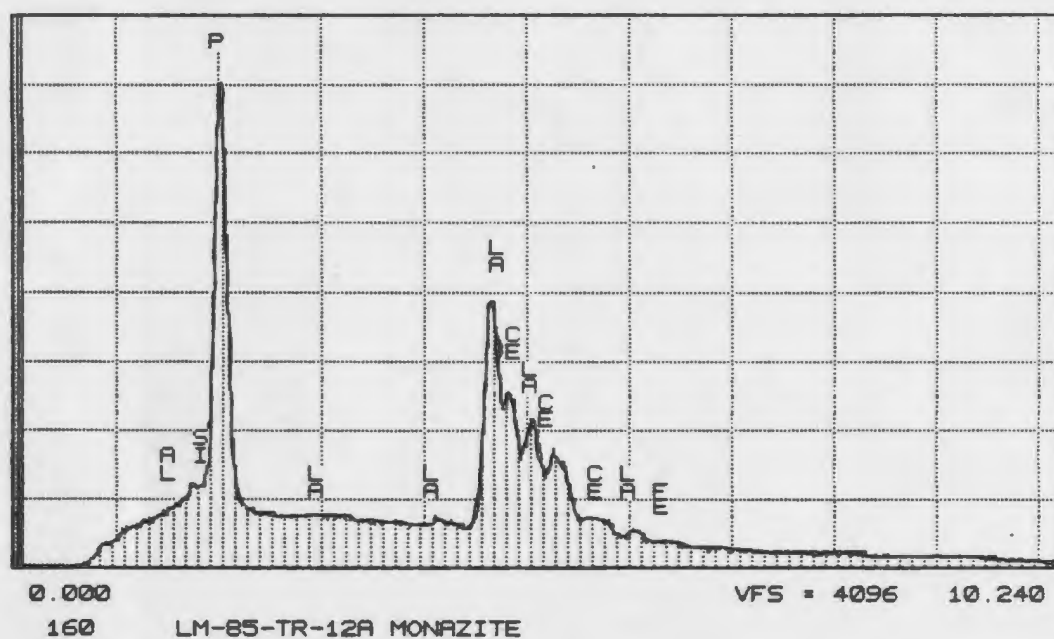


**Figure 4-7:** SEM energy dispersive spectra for monazite associated with uranium mineralization in the Burnt Lake Main Zone.



**Figure 4-8:** (850126) SEM back scatter image of chalcopyrite (FE+CU+S) intergrown with quartz (QUARTZ) gangue matrix and a uraninite (U+PB) veinlet (white).



**Figure 4-9:** (850142) SEM back scatter image of magnetite (small white grains) rimming recrystallized feldspar porphyroblasts in a non-mineralized quartz-feldspar porphyry unit.

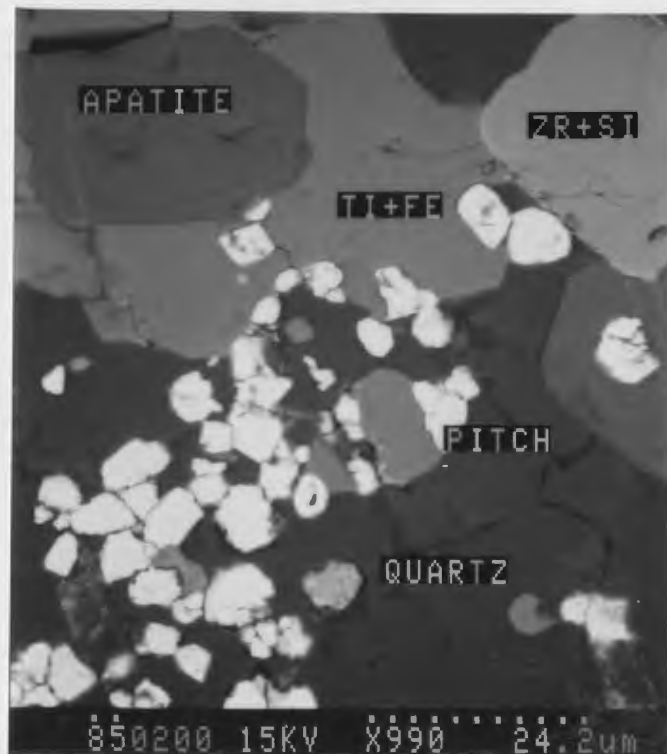


**Figure 4-10: (850200) SEM back scatter image of an intergrowth of uraninite (PITCH), ilmenite (TI+FE), apatite (APATITE) and zircon (ZR+SI) in a silicate (QUARTZ) gangue matrix.**

#### **4.2.3 Burnt Lake North West Zone**

The area contains 3 trenches exposing narrow discontinuous radioactive zones. Figure 4-11 shows the three trenches through the radioactive zone (see Map 2 for location). The radioactive zone is extensively altered by hematite and chlorite giving the host felsic crystal tuff a dark red to almost black colour. Within the radioactive area, there is an increase in mafic pods and veinlets as well as common yellow uranophane staining. The uranium mineralization occurs as disseminated uraninite grains and uraninite-bearing amphiboles.

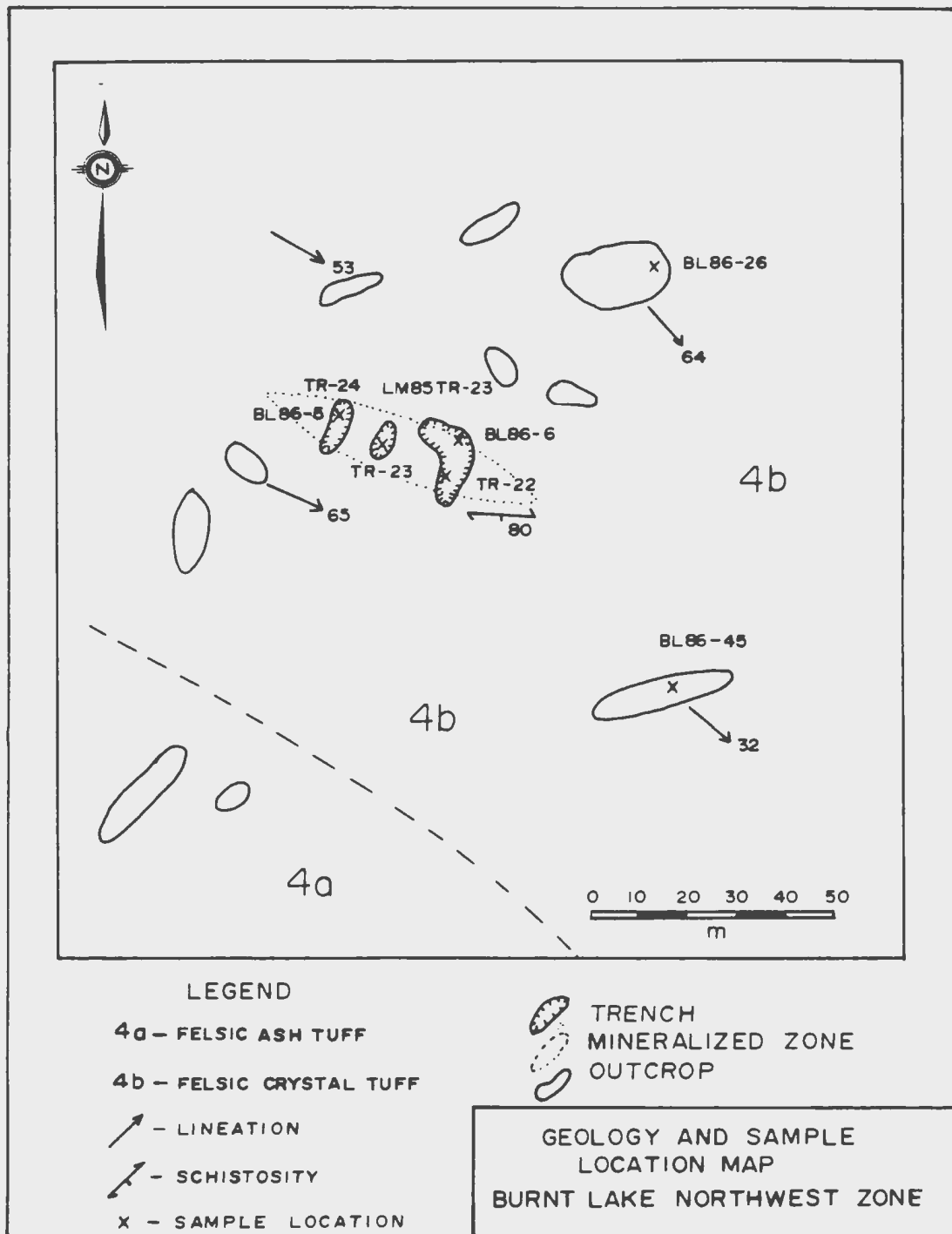


**Figure 4-11: Geology of and sample locations from the Burnt Lake Northwest Zone.**

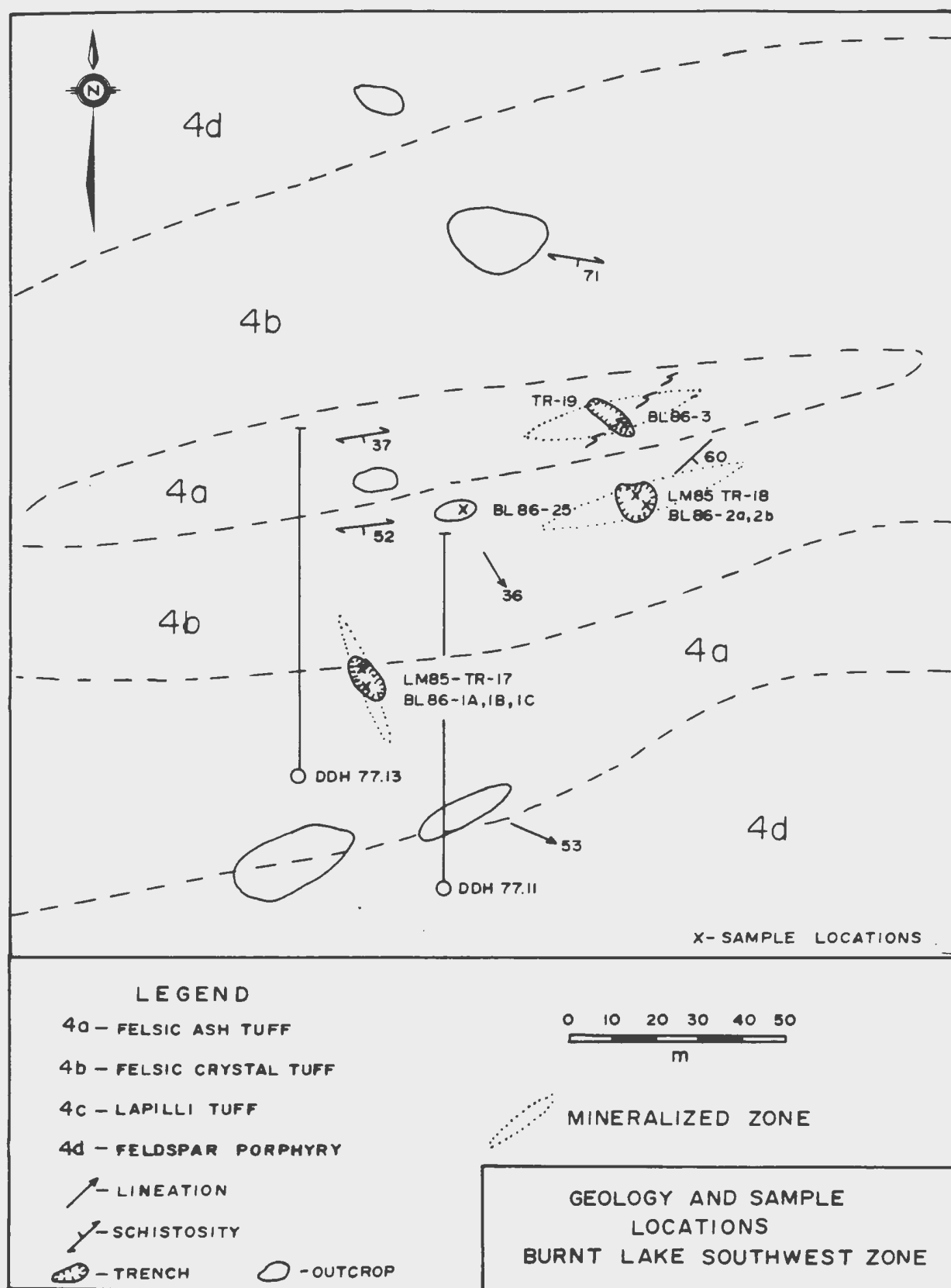
Galena, sphalerite and chalcopryrite are present as veins, disseminations and fracture-fillings over a distance of approximately 13 m in trench 22, however, base metal veins are generally not present in the highly radioactive zone. Disseminated pyrite is present throughout the trenches but has been oxidized to hematite in the radioactive areas. The mineralized zone is subparallel to the regional cleavage having an east-west strike and a steep southerly dip. Uranium mineralization appears to predate the base metal mineralization because of the cross-cutting relationship of the Pb-Zn-Cu sulphide veinlets and postdates the disseminated pyrite mineralization which probably provided a reducing environment to precipitate uraninite. The host rocks underwent intense potassic alteration (K-metasomatism) which accompanied the formation of Pb-Zn-Cu sulphides in stringers and veinlets (MacKenzie and Wilton, 1987).

#### **4.2.4 Burnt Lake South West Zone**

This zone is comprised of three trenches and two diamond drill holes (Map 2). The area is moderately radioactive in a 1-2 m wide zones that appears to be discontinuous. A trench map and drill section are shown on Figures 4-12 and 4-13 respectively, and drill logs can be found in Appendix III. The host lithology varies from a coarse-grained feldspar  $\pm$  quartz porphyry and felsic crystal tuff (unit 4b) to a

non-porphyritic felsic ash tuff (unit 4a) and tuffisite. Igneous banding in places is present as alternating pink and grey layers. The quartz-feldspar porphyry is often brecciated resembling tuffisite (Figure 4-14) and fractured in places with a strong cleavage and lineation.

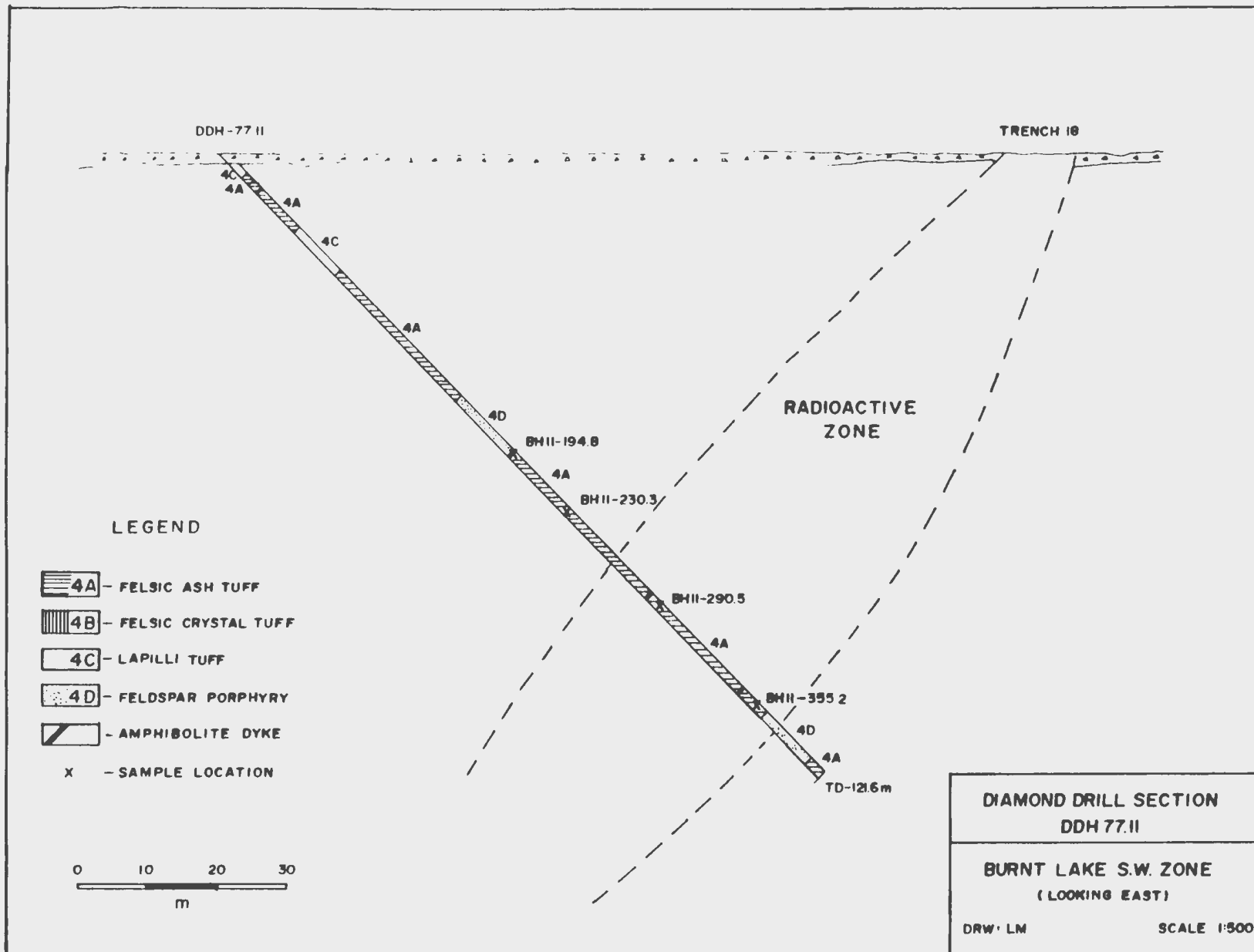
The radioactive zone is identified by pink to red hematitic alteration accompanied by minor yellow uranophane staining. Uranium mineralization occurs as discrete grains of uraninite or as uraninite intergrowths with sphene and a Ti+Fe+Mn oxide (see Figures 4-15 and 4-16) that are disseminated throughout hematized zones or concentrated as grain aggregates in discordant fracture-fillings. Uraninite is locally associated with stringers of sphalerite and galena in a silicate gangue matrix (Si-Al-Mg) (Figures 4-17 and 4-18) which has been linked to the Burnt Lake Granite, two kilometres to the east of the showings (see later for discussion). Discordant pegmatite-like carbonate veins contain galena, sphalerite and minor chalcopyrite (+Ag), including abundant amphibole, biotite, pyrite and rare fluorite, cross cut the regional fabric and radioactive zones.



**Figure 4-12: Geology and sample locations of the Burnt Lake Southwest Zone.**

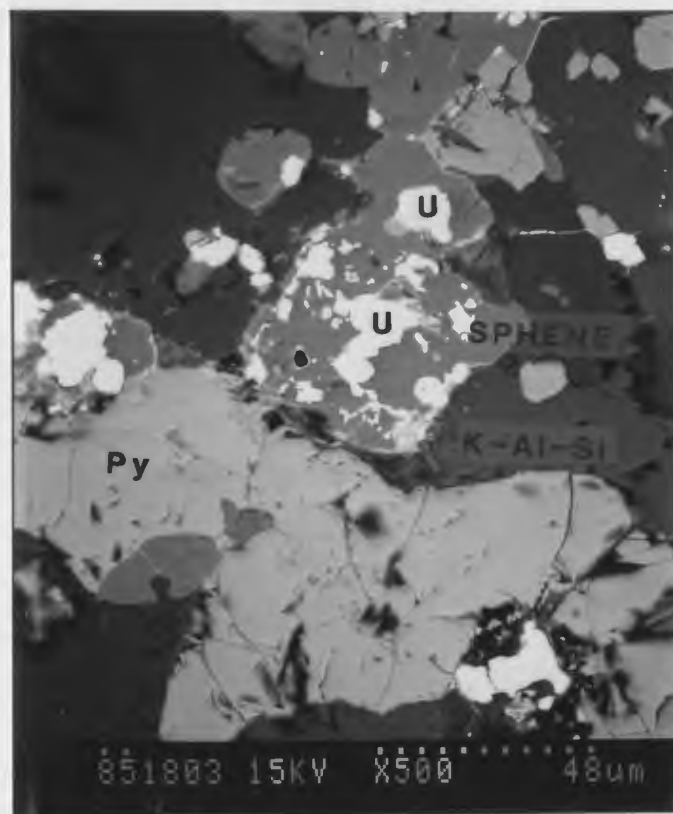


Figure 4-13: Diamond drill section (DDH 77.11) of the Burnt Lake Southwest Zone (looking east).





**Figure 4-14: Outcrop of volcanic breccia (tuffisite) from the Southwest Zone.**



**Figure 4-15:** (851803) SEM back scatter image of a uraninite (U-white) and sphene (dark grey) intergrowth in a potassium feldspar (K+Al+Si) matrix (centre of photo). Large pyrite grain (Py) at the bottom of the photo.

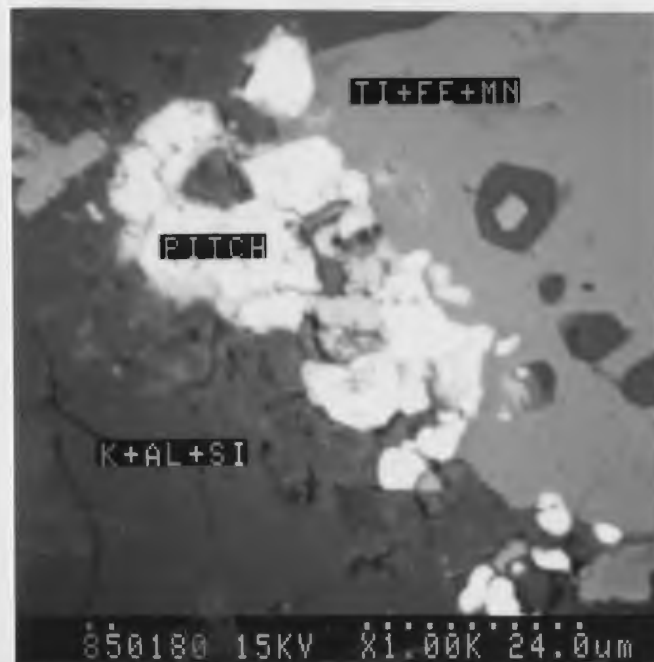


**Figure 4-16:** (850180) SEM back scatter image of intergrown uraninite (PITCH) and a Ti-Fe-Mn oxide (medium grey) in a feldspar (K+AL+SI) matrix (dark grey).



**Figure 4-17:** (851701) SEM back scatter image of sphalerite (ZN) intergrown with pyrite and sphene in a silicate gangue matrix (Si+Al+Mg). Small bright grains at the top of the photograph are uraninite (PITCH).

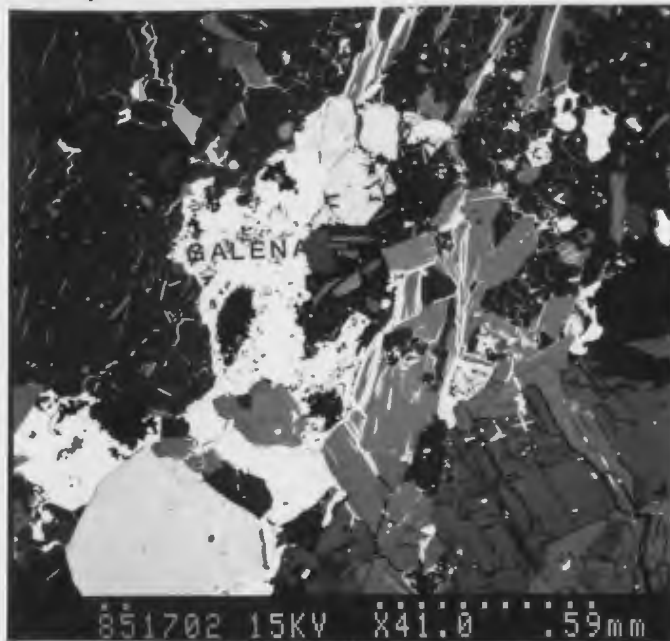


**Figure 4-18:** (851702) SEM back scatter image of galena stringers transecting silicate gangue. Uraninite (small bright grains throughout photograph) and sphalerite (medium grey) are intergrown with the galena.

#### 4.2.5 Emben Main Zone

The locations of radioactive occurrences in the Emben area are shown on Figure 4-19 (see Map 1 for location).

The radioactive zone at the Emben Main showing is small and of low grade. Figure 4-20 shows the geology and sample locations of the radioactive zone. The host rocks are tuffaceous sediments (arkosic) and banded felsic tuff with occasional volcanic porphyritic layers. The banding in the tuffaceous sedimentary rocks is defined by 2-3 mm thick alternating pink and grey layers separated by 0.5 mm laminations of magnetite. Uranium mineralization generally occurs as individual discrete grains or intergrowths with sphene, garnet, plagioclase and Ti-Fe-Mn oxides (Figure 4-21), that are disseminated throughout hematized zones, or concentrated along fractures associated with hematization and uranophane staining (Figure 4-22). The contact between the tuffaceous sediments and a small greenish amphibolite dykelet is also radioactive and hematized. The best assay from this zone was from Trench #2 and yielded 0.162%  $U_3O_8$  (Harder, 1981). Accessory minerals include ilmenite and barite (Figure 4-23). In Trench #3 anomalous gold values of up to 215 ppb were obtained from a grab sample of a well banded felsic tuff adjacent to the amphibolite dyke.

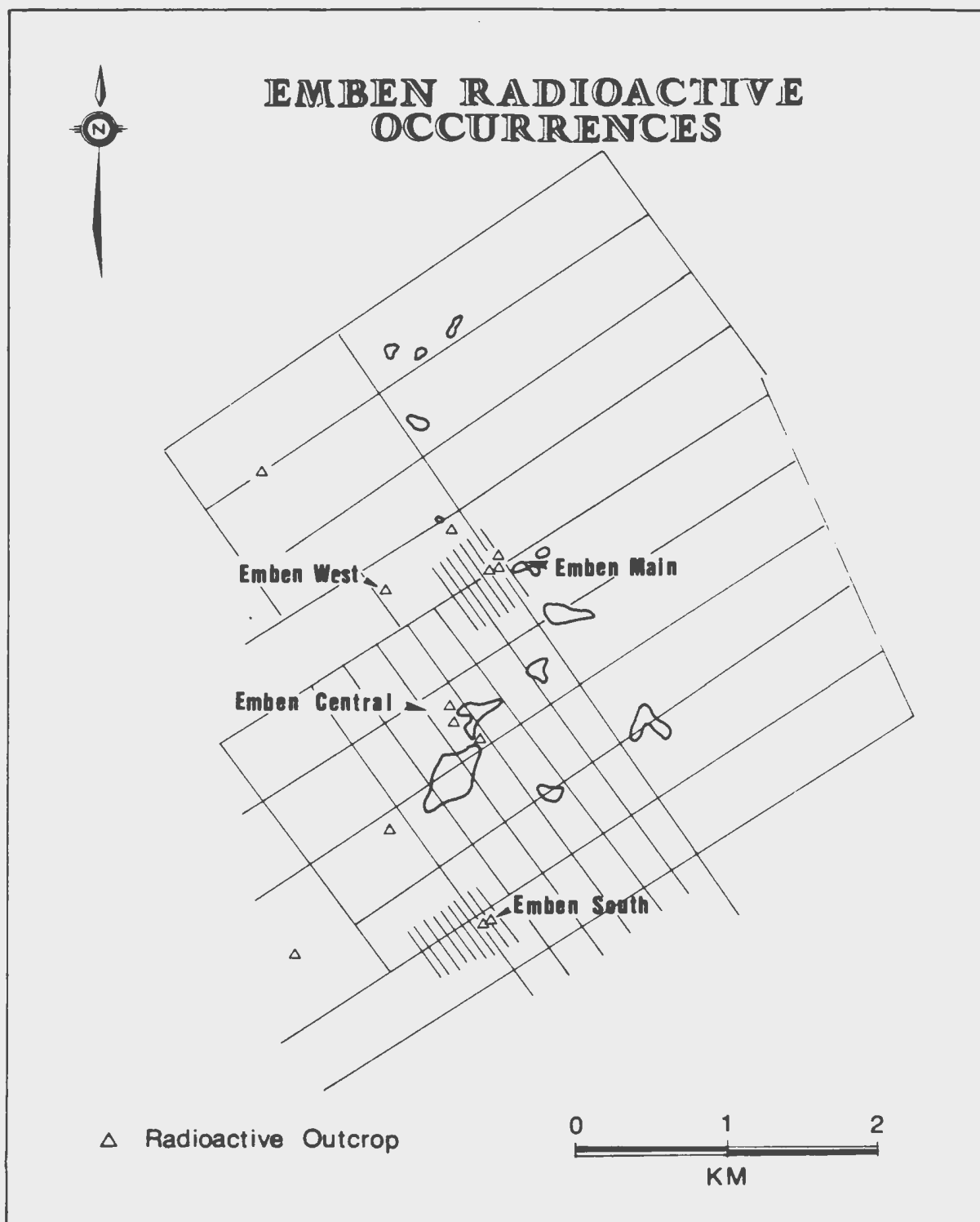


**Figure 4-19: Location of radioactive occurrences in the Emben area.**

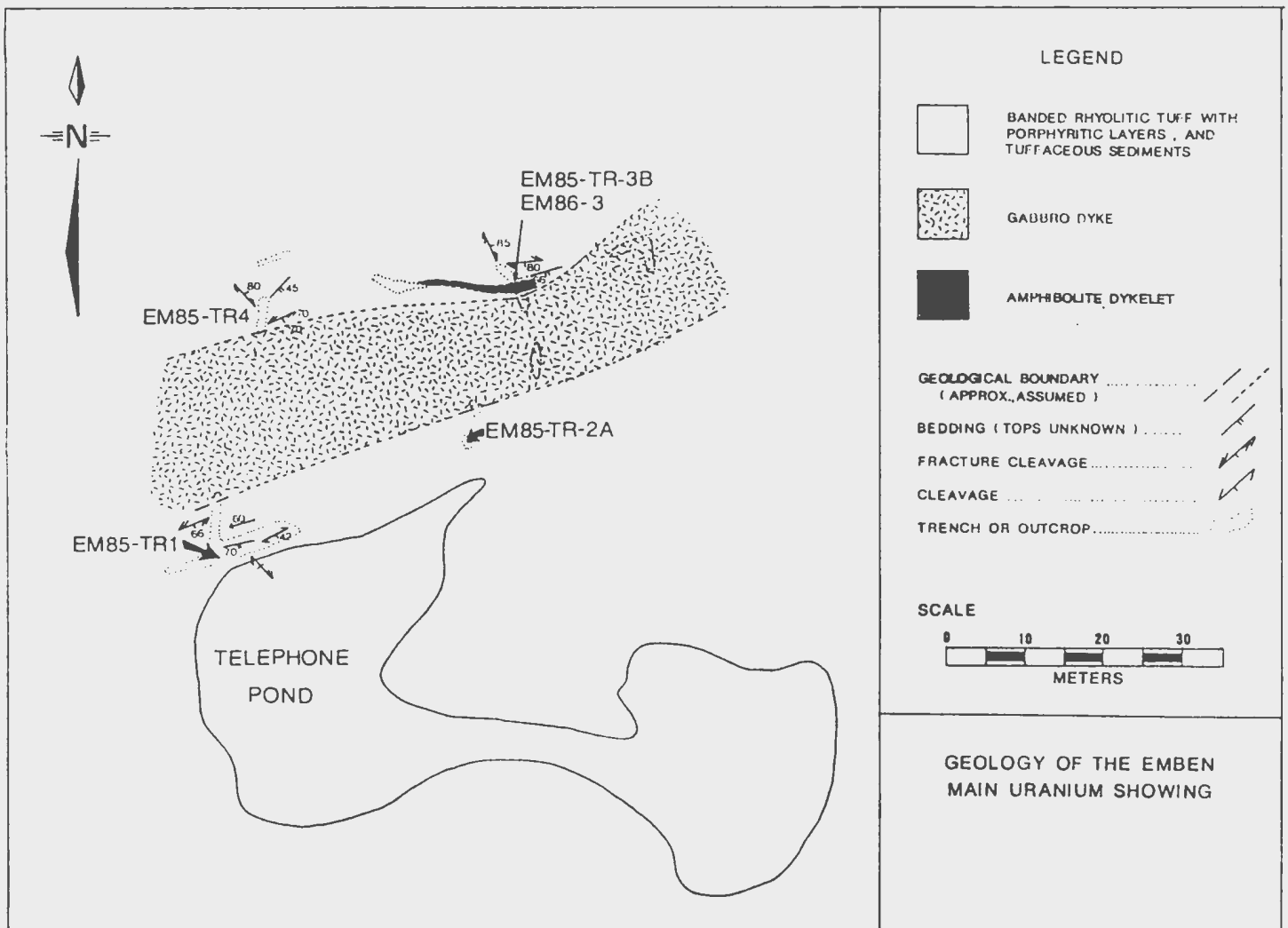


**Figure 4-20: Geology and sample locations of the Emben Main Zone.**

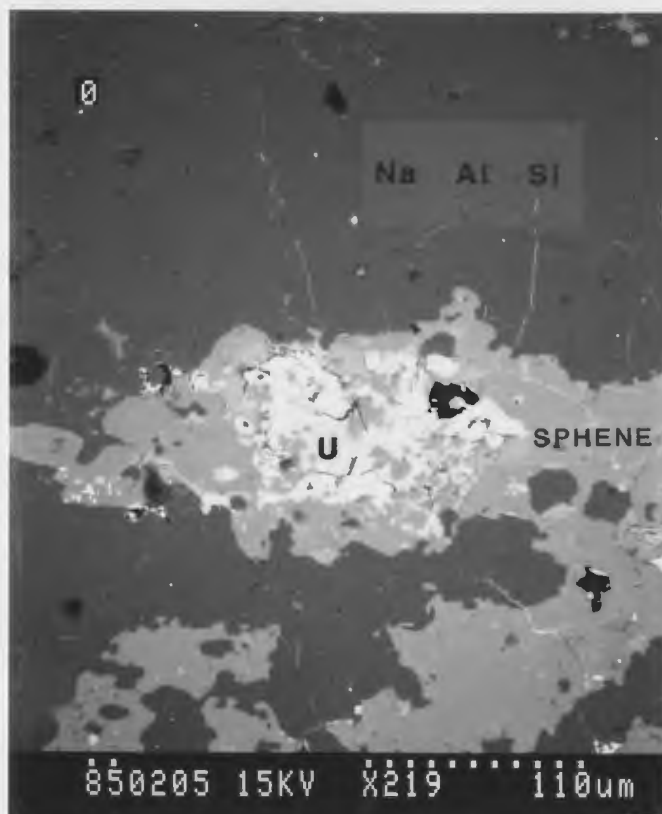


**Figure 4-21:** (850205) SEM back scatter image of a high concentration of uraninite (U) within a large ragged sphene grain (light grey). The host gangue is sodic feldspar (Na+Al+Si).

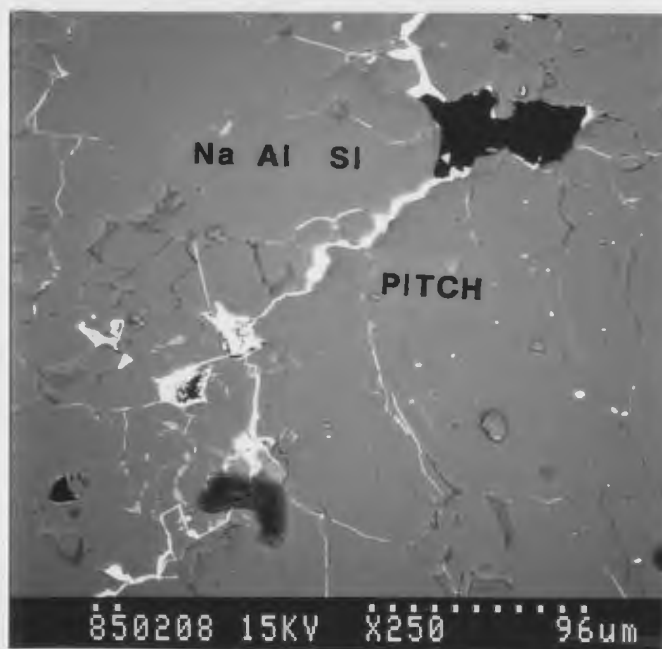


**Figure 4-22:** (850208) SEM back scatter image of uraninite (PITCH-white) occurring as veinlets, fracture fillings and individual discrete grains in a plagioclase matrix (Na+Al+Si-grey).



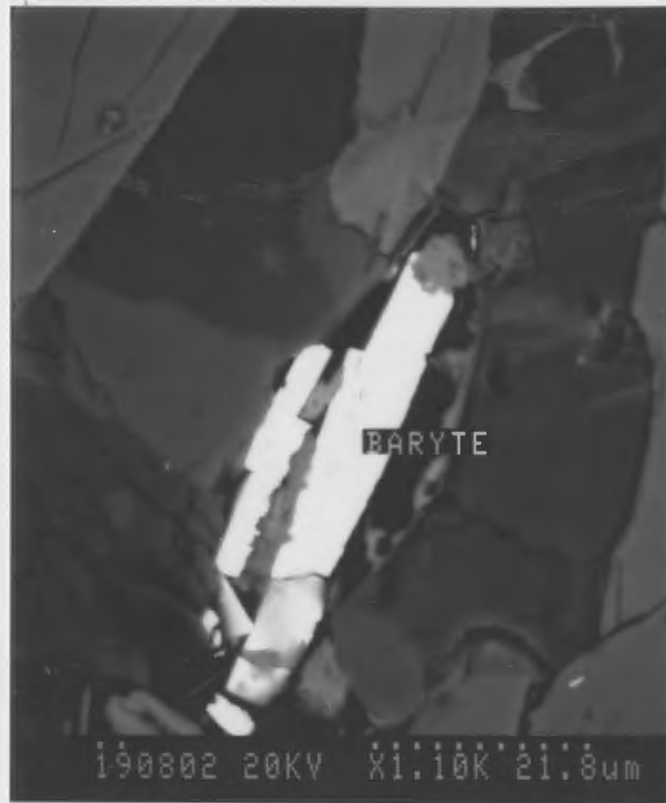


**Figure 4-23:** (19082) SEM back scatter image of barite grains (labelled BARYTE - white) in a matrix of plagioclase (dark grey) and potassium feldspar (light grey). Sample is a banded felsic tuff from trench #3.

#### 4.2.6 Emben South Zone

This zone is the most interesting of the radioactive occurrences in the area because of the high uranium grade (0.2% U from a grab sample), the style of mineralization and the accompanying mineral assemblage. Radioactivity is patchy and discontinuous over an area 3 m x 50 m (Figure 4-24). The scarcity of outcrop in the area prevented the complete tracing of this zone. The trenches are in dominantly metasedimentary and metavolcanic tuffs that are cut by two biotite-feldspar-bearing mafic dykes (biotitic feldspathic amphibolitic schist) (Figure 4-25). The radioactivity is confined to the dykes and is greatest in tightly folded bands of coarse amphibole or pyroxenes within the dykes (Figure 4-26A). The radioactivity falls off rapidly from both sides of the intrusives (Figure 4-26B). The best assay result from the BRINEX Ltd. survey was obtained from Trench #5 which graded 0.432%  $U_3O_8$  over 3 m (Harder, 1981).

Uranium mineralization is associated with fine grained sodic pyroxenes, amphiboles or occurs as inclusions or intergrowths with fine-grained plagioclase. The ore mineral assemblage includes uraninite with Nb and Ti, galena, sphalerite, chalcopryite, molybdenum and scheelite (+Ag) (see Figures 4-26C, 4-27 and 4-28). Accessory phases include sphene, zircon (with Hf), garnet (andradite), calcite and fluorite. Figure 4-29 shows a SEM image of euhedral galena and zircon grains in an interlocking mosaic of plagioclase.

Figure 4-24: Geology and sample locations of the Emben South Zone.

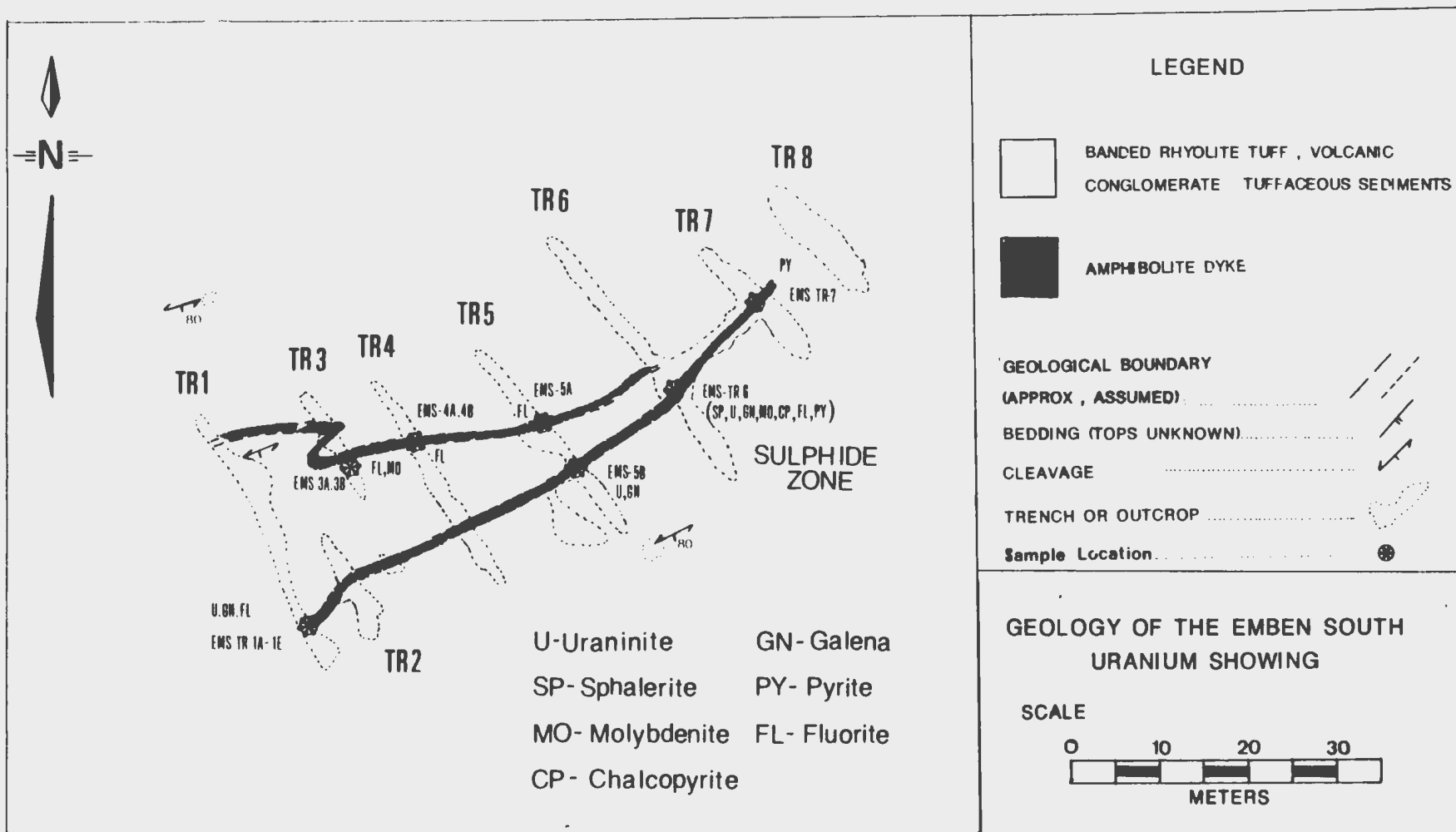
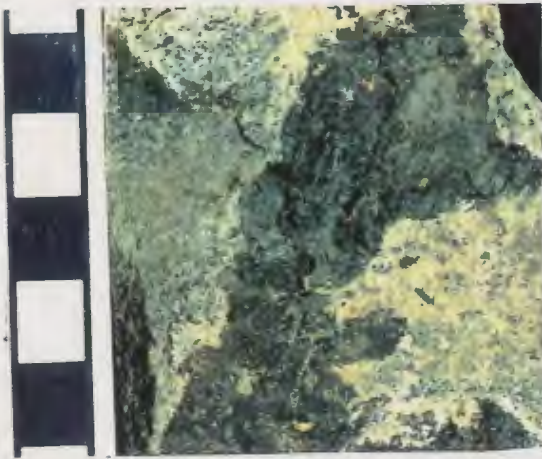




**Figure 4-25: Radioactive dyke from Trench #1, Emben South Zone (the dyke is outlined by dashed lines).**

**Figure 4-26:**

**(A):** Close-up of a dark green pyroxene vein in an amphibolite dyke from the Emben South Zone which assayed at 2% U. (Scale bars are 1 cm). **(B):** Contact between radioactive dyke (top) and unmineralized felsic volcanic host (bottom half). The highest radioactivity was obtained from pyroxene veins (black in upper left) within the dyke. **(C):** Recrystallized felsic tuff from the Emben South Zone with disseminated purple fluorite and molybdenite. (Scale bars are 1 cm each).



**A**



**B**



**C**



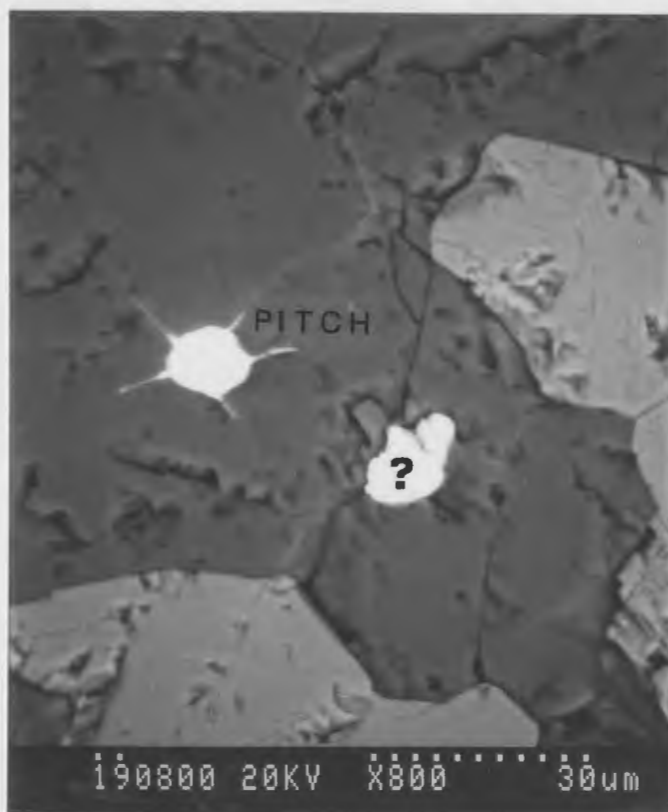


**Figure 4-27: (190800) SEM back scatter image of uraninite (PITCH) grain in a K-Si-Fe matrix. Alteration mineral (?) in centre of photo contains U, Nb, W, Ti, and Ca.**

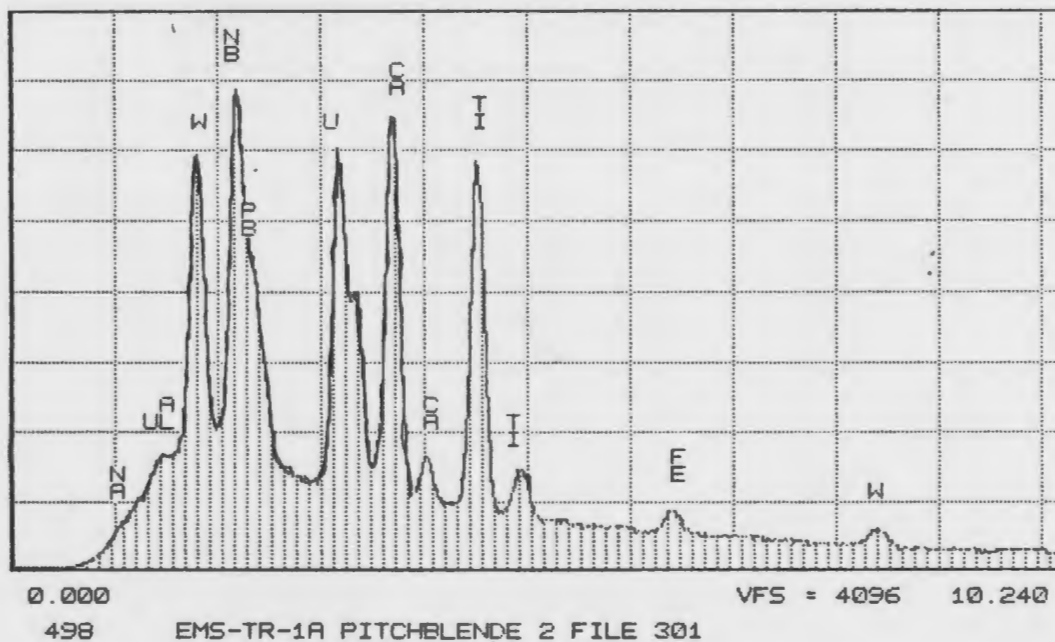


**Figure 4-28: Energy dispersive X-ray spectra for uranium-bearing Nb-W alteration mineral from the Emben South showing.**



**Figure 4-29: (850001) SEM back scatter image of euhedral galena and zircon (ZR) grains (white) in an interlocking mosaic of plagioclase (dark grey). A calcite veinlet occurs in the lower left corner of the photo (light grey).**



#### 4.2.7 Aurora River Zone

The Aurora River uranium occurrences are in the northwest corner of the study area and comprise six trenches with radioactive mineralization, five of which were located and sampled for this study. The mineralization occurs within mixed rhyolite/tuff and andesite near the contact with a 100m-150m wide northeast-trending feldspar  $\pm$  quartz porphyry dyke (Map 3, see Map 1 for location). The lithologies in the trenches vary somewhat, however, generally consisting of reddish rhyolite/tuff (brecciated in places) intermixed with a fine-grained greenish intermediate volcanic (andesite) rock that is sheared and contains bluish-green bands. The bands have been identified by X-ray diffraction methods (XRD) as tremolite. The fabric (banding) strikes from  $80^{\circ}$  to  $90^{\circ}$  N and dips steeply to the southeast. Chlorite is the most pervasive alteration mineral in the andesite, however, epidote and sericite commonly occur as thin stringers within 0.1m-0.5m wide quartz-carbonate veins that also contain tremolite and specular hematite.

The feldspar-quartz porphyry contains 5-15%, 2-5 mm rounded to subrounded feldspar  $\pm$  quartz phenocrysts in a pink to grey matrix (see Figure 4-30A). The porphyry is generally banded with alternating pink and brownish 5-10mm bands. Thin (1-2mm) magnetite bands are commonly sub-parallel to an east-west trending foliation. The porphyry is generally more

fractured near its contacts.

The mineralization consists of several moderately radioactive zones averaging 0.5-1.0 m in width which are discontinuous over approximately 700 metres. The mineralization is of a low grade, however, Sharpley and Cote (1980) reported an average grade from one of the trenches of 0.164%  $U_3O_8$  over 3 m. Radioactivity is confined to extensively hematized breccia and shear zones within the andesite suggesting fluid flow and uraninite precipitation in zones of structural weakness (Figure 4-30B). Mineralization occurs as disseminated uraninite within the andesite or occurs along the rhyolite/andesite contact where the host rocks are extensively hematized, giving the rocks a dark reddish colour (Figure 4-30C). Radioactivity also occurs in thin veins and fractures within the rhyolite and within thin shear zones in brecciated andesite. Quartz-carbonate veins with fibrous tremolite, pods of specular hematite, minor bornite and uranophane staining are also associated with the hematized shear zones.

**Figure 4-30:**

**(A):** Banded quartz-feldspar porphyry dyke from the Aurora River Zone. Scale bars are 1 cm long. **(B):** Sheared brecciated and hematized andesite from Trench #3, Aurora River Zone. Note infilling of carbonate (white). Scale bars are 1 cm long. **(C):** Hematized radioactive andesite from Trench #4, Aurora River Zone. Note the extensive chlorite alteration (green blebs) and thin, slightly discordant pyrite veinlets (lower half of photo).



#### **4.3 Base metal sulphide mineralization**

Base metal sulphide mineralization in the Burnt Lake area generally occurs as narrow veinlets and disseminations within recrystallized felsic volcanic rocks of the Upper Aillik Group and is low grade over narrow widths.

##### **4.3.1 Burnt Lake Main Zone**

Base metal concentrations within the Burnt Lake Main Zone are generally low. Sulphide mineralization consists of thin stringers of galena that correspond to an increase in uranium mineralization. Pb isotope data from a galena separate from this zone (sample LM85-TR13) indicate a radiogenic lead origin (Wilton, 1991b). Rare stringer chalcopyrite and bornite are present in some trenches and have been documented through SEM work to be associated with galena (Figure 4-31). An assay from one grab sample (BL86-16 from trench #13) returned 0.14% Pb, 0.53% U, 0.12% Cu, 26 ppm Ag and 70 ppb Au.

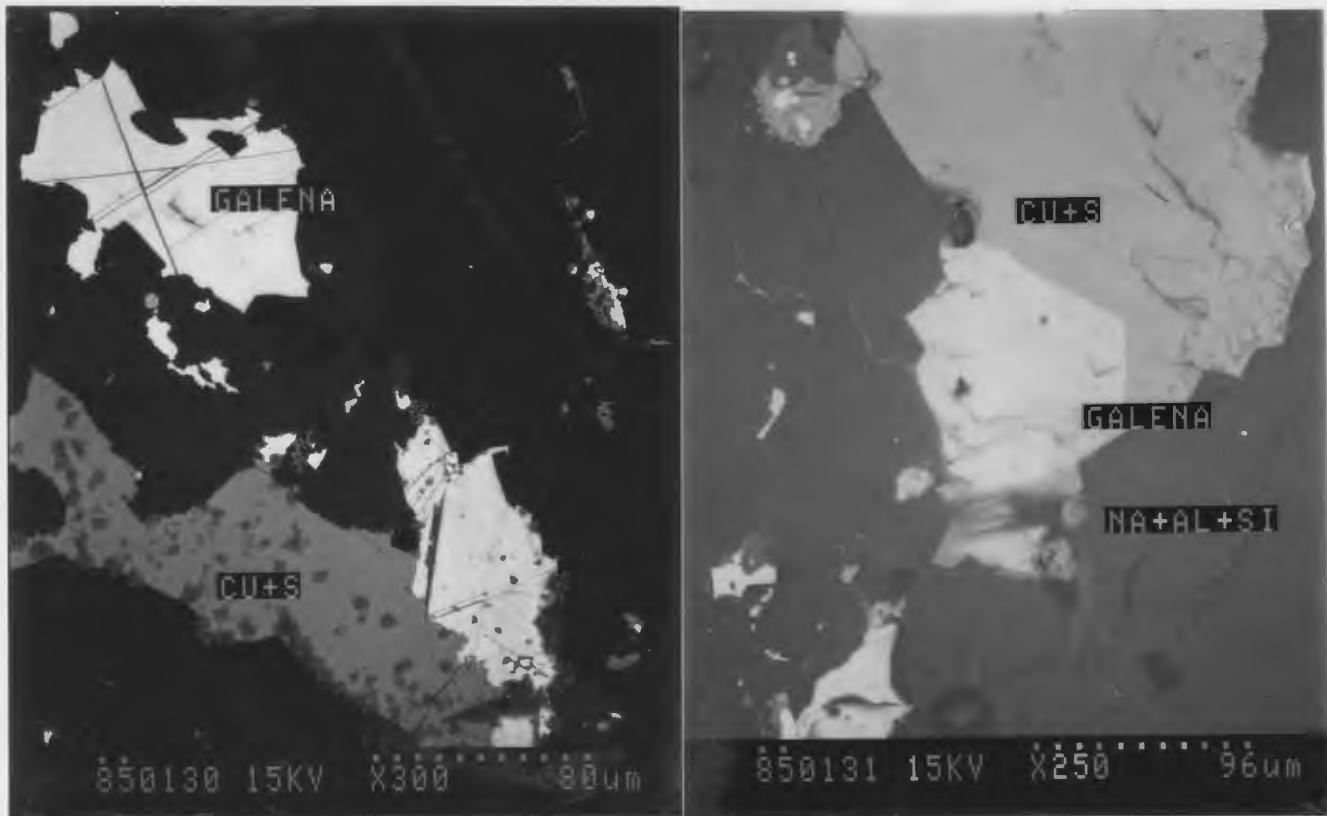


**Figure 4-31: (850130,31) SEM back scatter images of intergrown galena (bright) and chalcopyrite (CU+S) (grey) in a plagioclase (NA+AL+SI) gangue.**

#### **4.3.2 Burnt Lake Northwest Zone**

Significant base metal mineralization has been traced for over 13 m at the Burnt Lake Northwest zone (trench #22). The mineralization consists of stringer and disseminated pyrite, sphalerite and galena (Figure 4-32). Chalcopyrite occurs as small pods while bornite occurs mainly along fractures. The host lithology is generally medium-grained, pink to grey quartz-feldspar porphyry (see Figure 4-11). The hematized radioactive zone is about 1 m wide and contains only



disseminated pyrite and magnetite. A grab sample (BL86-6) assayed 1.1% Pb and 3.8% Zn with a relatively low uranium concentration (709 ppm U). Pb isotope data from galena separates of this sample (BL86-6) have indicated a magmatic origin for the lead mineralization (Wilton, 1991b) Analyses for precious metals were generally low with the highest being 5.2 ppm Ag and 120 ppb Au.



**Figure 4-32: Recrystallized felsic tuff with a narrow veinlet of sphalerite. Scale bar is in centimetres.**

#### 4.3.3 Burnt Lake Southwest Zone

The Burnt Lake southwest zone (trench #17) hosts base metal mineralization within 0.2-0.4 m wide carbonate veins that contain uraninite, sphalerite, galena and chalcopryrite (Figure 4-33). Also associated with the carbonate veins are quartz, biotite and amphibole. In trench #18, galena, sphalerite, chalcopryrite and pyrite are concentrated along fractures. Figure 4-34 shows the close association between galena and chalcopryrite as veinlets in a K-feldspar and quartz matrix. Within the trench there is a pegmatite containing calcite, quartz and amphibole with rare fluorite and molybdenite. A grab sample (LM85-TR18A) assayed 1.3% Zn, 0.5% Pb and 0.2% U. Anomalous silver and gold are also present (18.2 ppm Ag, 390 ppb Au).

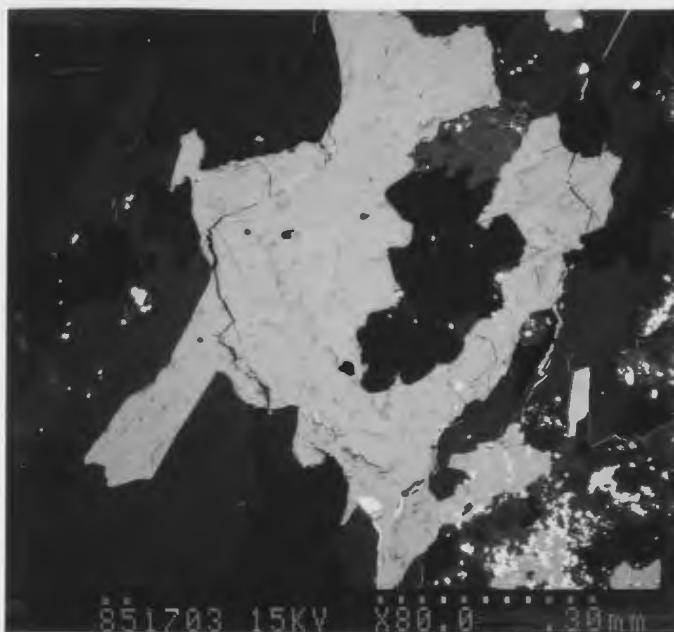


**Figure 4-33:** (851703) SEM back scatter image of coarse sphalerite mineralization (grey) and finely disseminated uraninite (small bright grains lower right corner of photo).



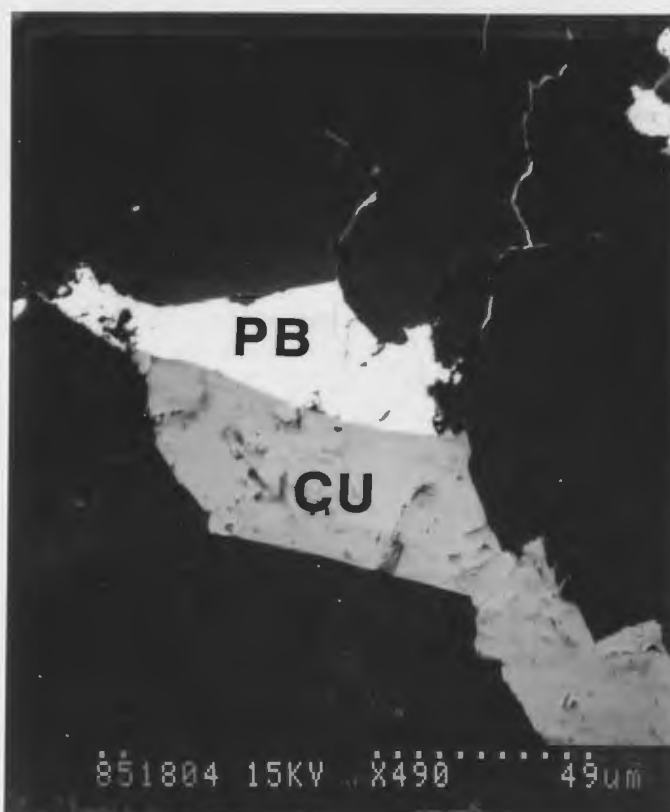


**Figure 4-34: (851804) SEM back scatter image of intergrown galena (PB) and chalcopyrite (CU) in a potassium feldspar gangue.**

#### **4.3.4 Emben South Zone**

Extensive sulphide mineralization occurs over a length of 15 m in a strongly radioactive biotite-feldspar dyke (see Figure 4-24). The mineralization ranges from disseminations and stringers to semi-massive pyrite, pyrrhotite, sphalerite, galena, chalcopyrite and molybdenite (Figures 4-35 to 37). A grab sample (EMS86-TR6) from the mineralized zone assayed 2.0% Zn, 0.58% Pb, 0.10% Cu, 0.43% U and 0.14% Mo. Precious metals are present with values ranging up to 32 ppm Ag and 55 ppb Au.

The style of mineralization and the observed mineralogical association of U, Pb, Zn, Cu, Mo and F may suggest an influence of hydrothermal fluids of magmatic derivation. The Burnt Lake Granite is located approximately 800 m west of the Emben South showing.



**Figure 4-35:** A cut section through extensive sulphide mineralization hosted by an altered mafic dyke. Sample EMS86-TR6 assayed 2.0% Zn, 0.58% Pb, 0.10% Cu, 0.43% U, 0.14% Mo and 22 ppm Ag. Note the tight fold in the lower righthand corner.



**Figure 4-36:** (850003) SEM back scatter image of an intergrowth of sphalerite (ZNS), chalcopyrite (CUS) and galena (PBS) in a quartz-plagioclase (SI+CA+FE) gangue. Note the small zircon (ZR) grain in the lower righthand corner.



**Figure 4-37:** (190801) SEM back scatter image of intergrowth of galena, pyrite (FE), sphalerite and sphene in a Na-Ca-Mg-Fe-Si gangue matrix.

#### 4.4 Granite Hosted Mineralization

In the Burnt Lake area, significant concentrations of molybdenite occur in a high level, leucocratic, post-tectonic granite (Burnt Lake Granite) near the contact with the felsic volcanic country rocks (Upper Aillik Group). The prospect was discovered in 1984 during a helicopter reconnaissance of the Burnt Lake area by Wilton and Wardle (1985). The discovery outcrop covers an area of approximately 20 m x 20 m and is located 800m northeast of the Burnt Lake camp (see Map 2 and Figure 4-38). The unmineralized Burnt Lake Granite has been previously described in Chapter 2 as a fine-grained, grey to pink leucogranite containing biotite, chlorite, muscovite and rare garnet. The mineralized zone is highly oxidized on its weathered surface and is easily broken. Mineralization consists of rosettes and pods, up to 2 cm in diameter, with finer disseminated molybdenite throughout the outcrop (Figure 4-39 and 40). Low grade mineralization has been traced along the intrusive contact in outcrop for over 200 m southwest of the prospect. The molybdenite showing may indicate vapour phase accumulation in the apical portions of the Burnt Lake Granite. The differentiation of the magma chamber could have occurred by convection driven thermogravitational diffusion producing a high silica, volatile-rich zone at the top of the chamber (Mutschler et al., 1981). A zonation pattern of silica is evident in the BLG where it culminates near the endocontact



molybdenum mineralization (Chapter 3).



**Figure 4-38: Discovery outcrop of molybdenite mineralization in the Burnt Lake Granite.**

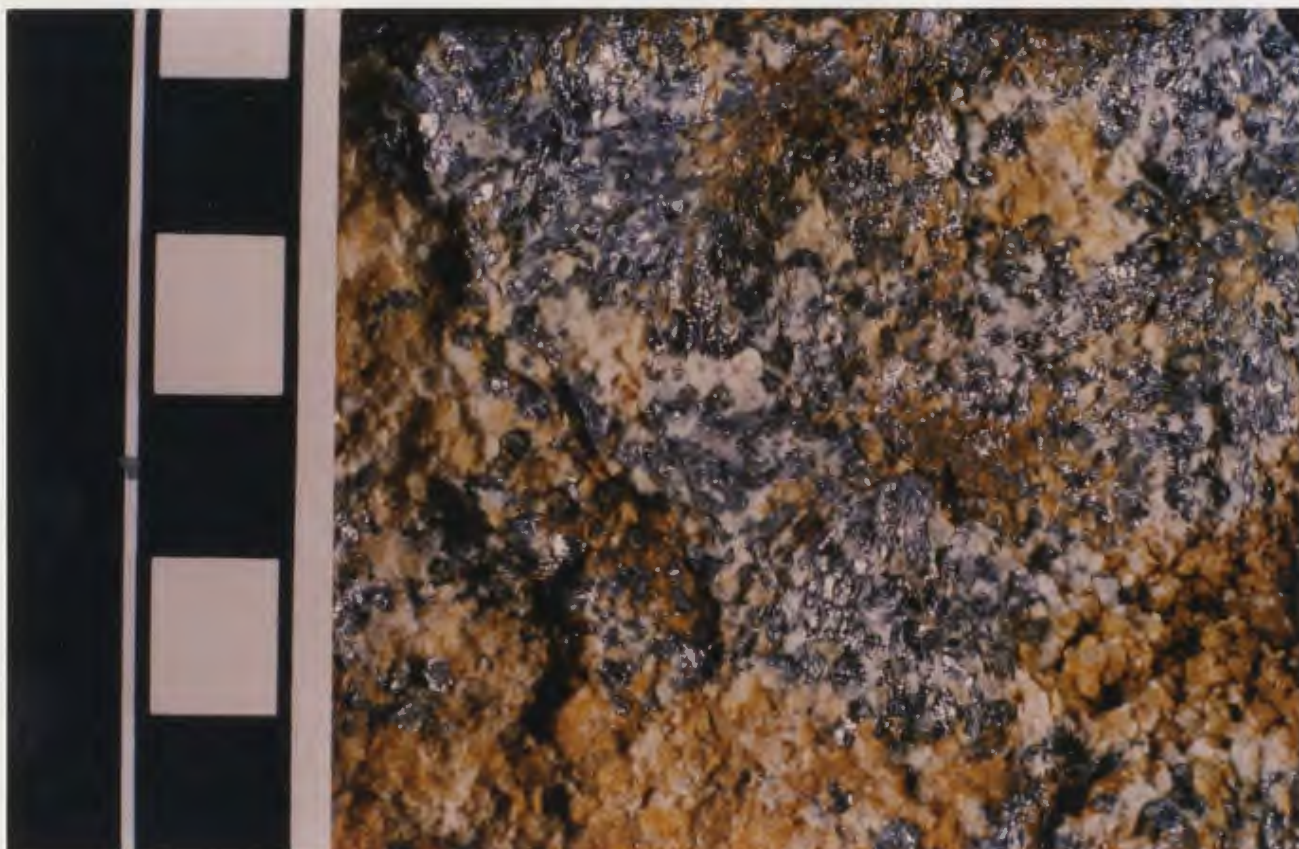


**Figure 4-39: Close-up photo of disseminated molybdenite mineralization in the Burnt Lake Granite. Scale is in centimetres.**



**Figure 4-40: (850122) SEM back scatter image of fibrous molybdenite (MO-light grey) intergrown with quartz and feldspar in the leucocratic contact zone of the Burnt Lake Granite.**

## CHAPTER 5

## GEOCHEMISTRY OF MINERALIZED SHOWINGS

## 5.1 Introduction

A total of 78 samples of mineralized rocks were collected from the Burnt Lake, Aurora River, and Emben radioactive showings. Of this, 54 samples were analyzed for major and trace elements, while the remaining 24 samples were analyzed for trace elements only. Sixteen samples were analyzed for REE. A brief rock and/or petrographic description for each sample is given in Appendix II. Analytical methods, precision and accuracy are described in Appendix I. The geochemical data are presented in Appendix I.

The rhyolitic rocks of the Upper Aillik Group in the Burnt Lake and Emben areas, along with the andesites at the Aurora River showing, host numerous hematized radioactive occurrences. Regional background geochemical analyses for these lithologies have been discussed in Chapter 3. It is the purpose of this chapter to document the geochemistry of the mineralized showings, present a comparison between the showings, and compare the mineralized lithologies with the unmineralized host rocks in the Burnt Lake area.



## 5.2 Burnt Lake Showings

Representative samples were taken from 29 mineralized trenches and 11 diamond drill holes. Uranium concentrations within the Burnt Lake radioactive zones vary considerably. A histogram plot of uranium contents from the Burnt Lake area (Figure 5-1) indicates a log normal distribution with a mean of 950 ppm.

### 5.2.1 Major Element Patterns

Figure 5-2 shows major oxide distributions plotted against silica for mineralized samples. Generally, there is no systematic variation with the oxides versus silica as would be the case with normal differentiated volcanic rocks. The wide scattering in the data is thus attributable to widespread metasomatic alteration which has affected all lithologies to some degree.

Uranium mineralization in the Burnt Lake area was accompanied by alkali metasomatism of the host volcanic rocks. This phenomenon is common in other felsic volcanic and igneous rocks elsewhere in the Central Mineral Belt, (White and Martin, 1980; Kontak, 1980) and in uranium deposits from other parts of the world (e.g. Smellie and Laurikko, 1984; Stuckless and Troeng, 1984; Cathelineau, 1983; White and Martin, 1980; Kontak, 1980; Leroy, 1978; Smirnov, 1977; Hoeve, 1974;

Zinchenko and Rakovich, 1972). White and Martin (1980) documented K-metasomatism in unmineralized porphyritic flows from the Michelin area through petrographic studies and microprobe analysis of feldspar phenocrysts. According to White and Martin (1980) the ore zone at Michelin is, however, comprised entirely of Na-metasomatised tuffs. At Burnt Lake both sodic and potassic metasomatic effects are associated with uranium mineralization.

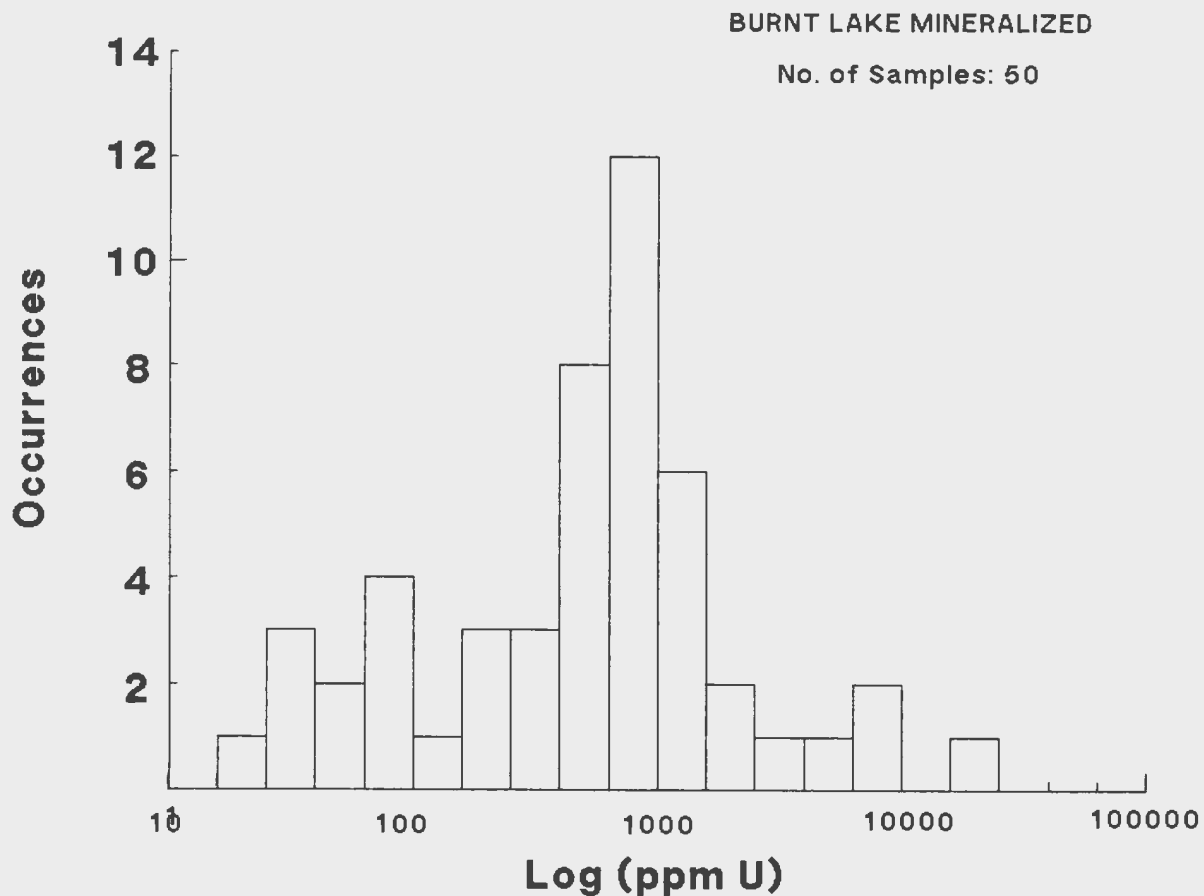


**Figure 5-1: Frequency distribution of Log(U) in felsic volcanic rocks of the Burnt Lake Showings.**

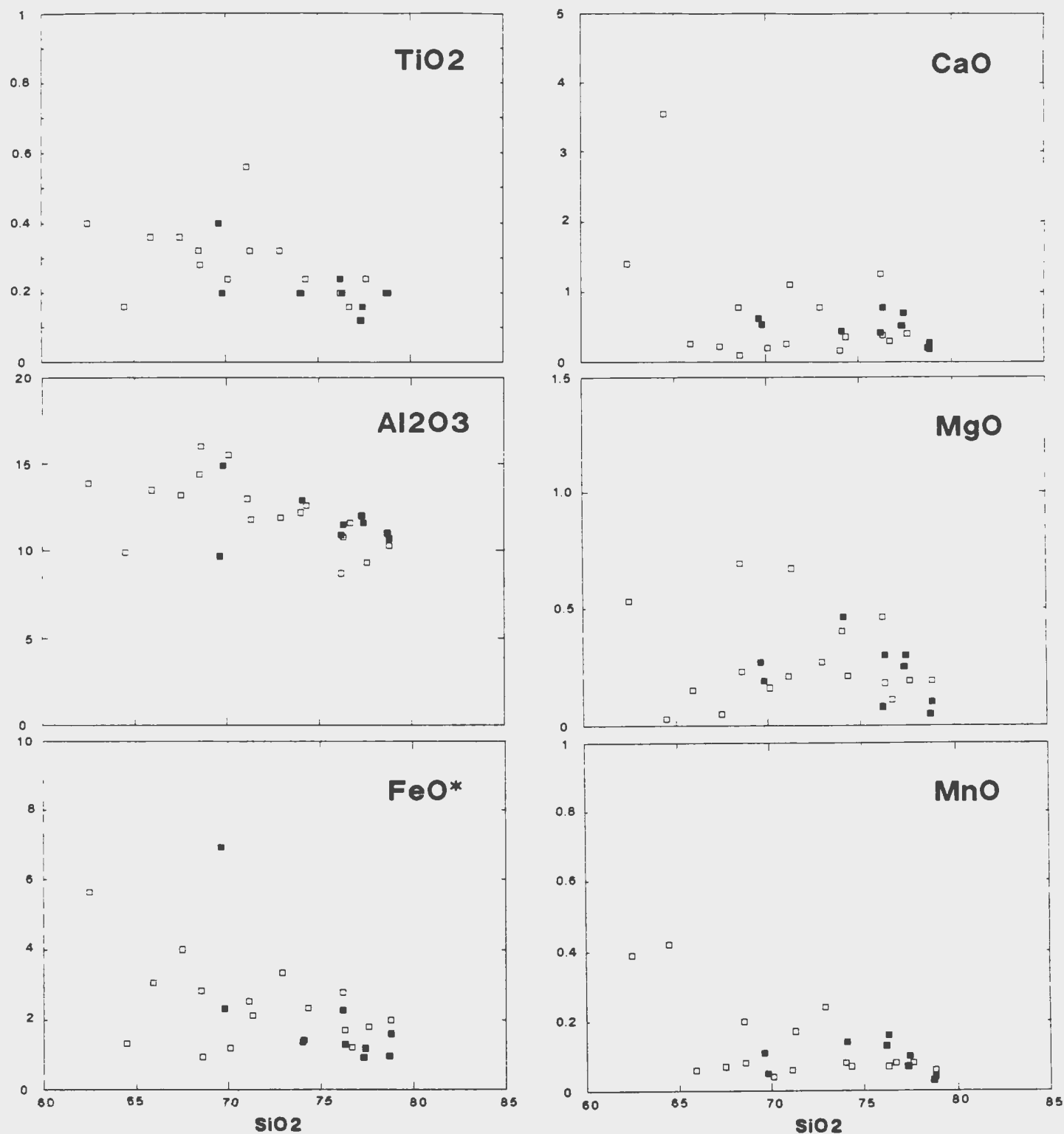
Na-metasomatism in the Burnt Lake area has previously been documented by Bailey (1979); Gandhi (1978, 1984); Gower et al. (1982); Kontak (1980); and White and Martin (1980). The metasomatic event is recognized by  $\text{Na}_2\text{O}$  enrichments to >6.5 wt% with complete to partial albitization of feldspars and replacement of the matrices by albite, as well as by the presence of metasomatic silicate phases such as chlorite, riebeckite and aegirine augite. Na-metasomatism was accompanied by apparent enrichments of  $\text{Al}_2\text{O}_3$  and  $\text{TiO}_2$  and depletions in  $\text{K}_2\text{O}$  (<0.2%),  $\text{SiO}_2$ , and  $\text{P}_2\text{O}_5$ . Similar major element variations have been reported from uranium deposits in granites (Leroy, 1978) and felsic volcanic rocks (Smellie and Laurikko, 1984).

K-metasomatism is demonstrated in the major element geochemistry by apparent enrichments of  $\text{K}_2\text{O}$  (>6%),  $\text{TiO}_2$ ,  $\text{Al}_2\text{O}_3$  and in some cases  $\text{FeO}^*$  and  $\text{CaO}$ , with depletions of  $\text{Na}_2\text{O}$  (<3%) and  $\text{SiO}_2$ . In the most strongly K-metasomatised samples, the groundmass contains only microcline and quartz, while the feldspar phenocrysts show exsolution textures of perthite (microcline and albite) and K-feldspar mantles or occur as patches within plagioclase.

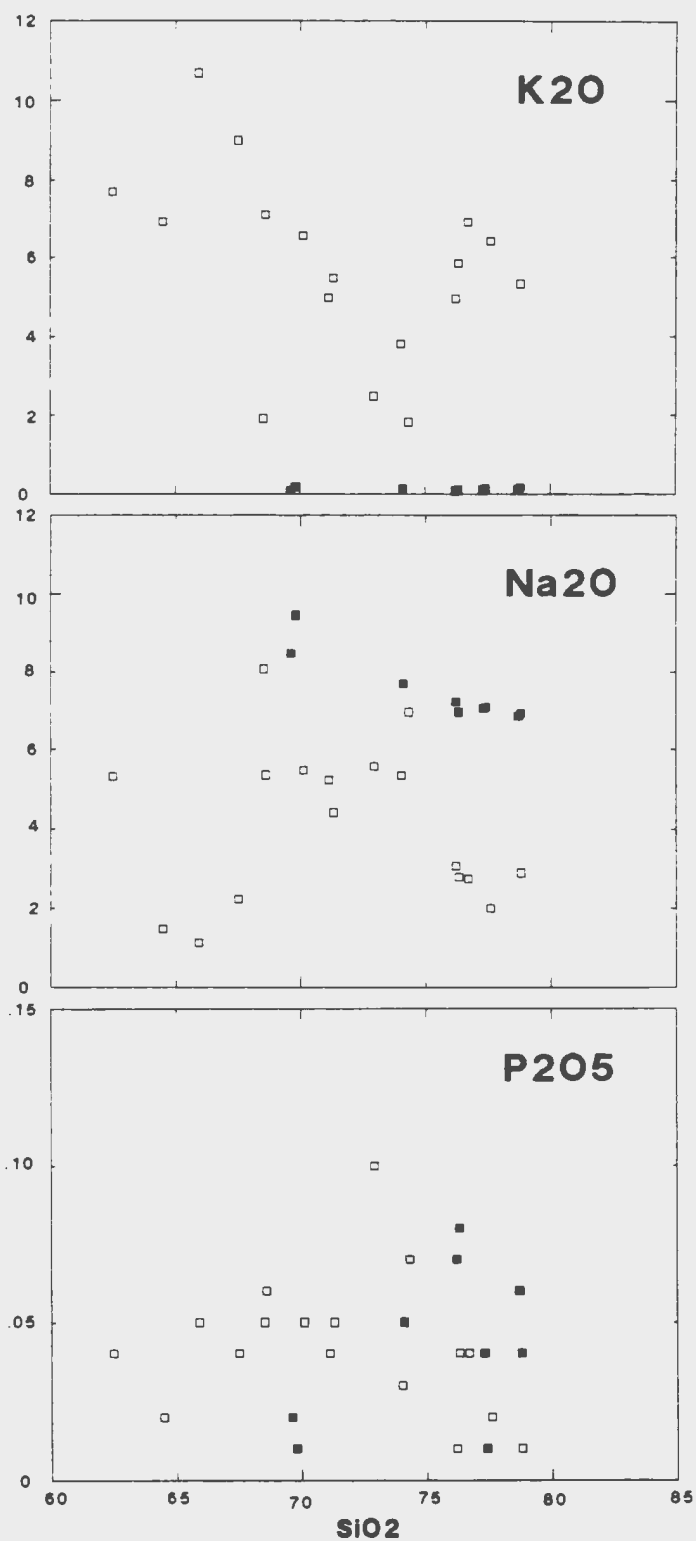
The effects of the metasomatic alteration are largely a function of the permeability variations and grain size of the host lithology. The Na-metasomatised samples are generally fine to medium-grained, non-porphyritic to slightly porphyritic ash tuffs with bedded ash tuff. The rocks are

commonly brecciated or located within shear zones. On the other hand, the K-metasomatised samples are generally medium to coarse-grained quartz and feldspar porphyritic rhyolites.

White and Martin (1980) identified several intensities of metasomatism in the Michelin area. They suggested that mild metasomatism involved a simple cation exchange from a Na enriched solution during which the  $K^+$  cation in the K-bearing minerals (feldspars) was replaced with  $Na^{2+}$ , while intense alteration (Na-metasomatism) resulted from Na+Al substituting for Si. Silica is apparently depleted during Na metasomatism because of its high solubility. On a  $K_2O$  versus  $Na_2O$  plot (Figure 5-3) the mineralized rocks from the Burnt Lake showings can be subdivided into five fields based on the apparent metasomatic intensity. The average field on Figure 5-3 represents a small group of samples which are the least mineralized and hydrothermally altered.



**Figure 5-2: Harker variation diagrams of major oxide distribution in the Burnt Lake mineralized samples. Oxides are in weight percent. Symbols are as follows; open square: medium to coarse-grained quartz and feldspar porphyritic rhyolites; solid square: fine to medium-grained, non-porphyritic to slightly porphyritic ash tuffs with bedded ash tuff.**

**Figure 5-2: (Continued)**

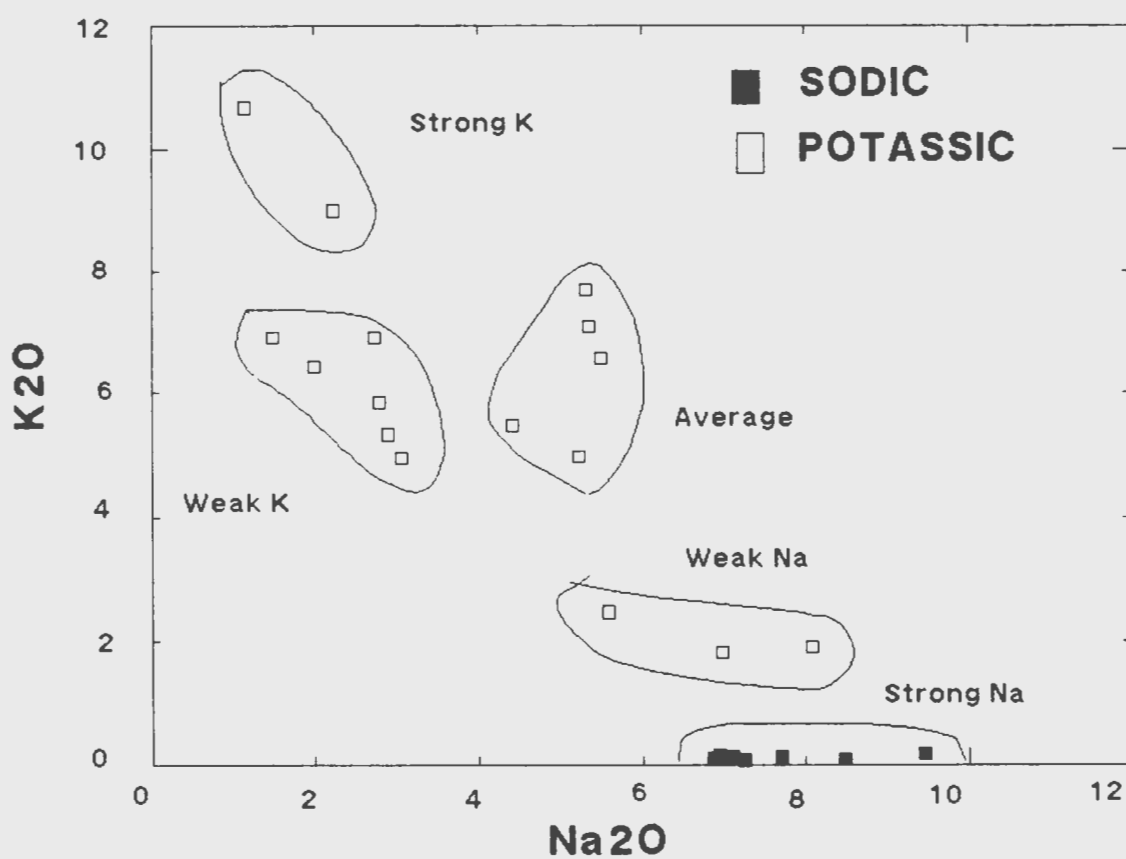
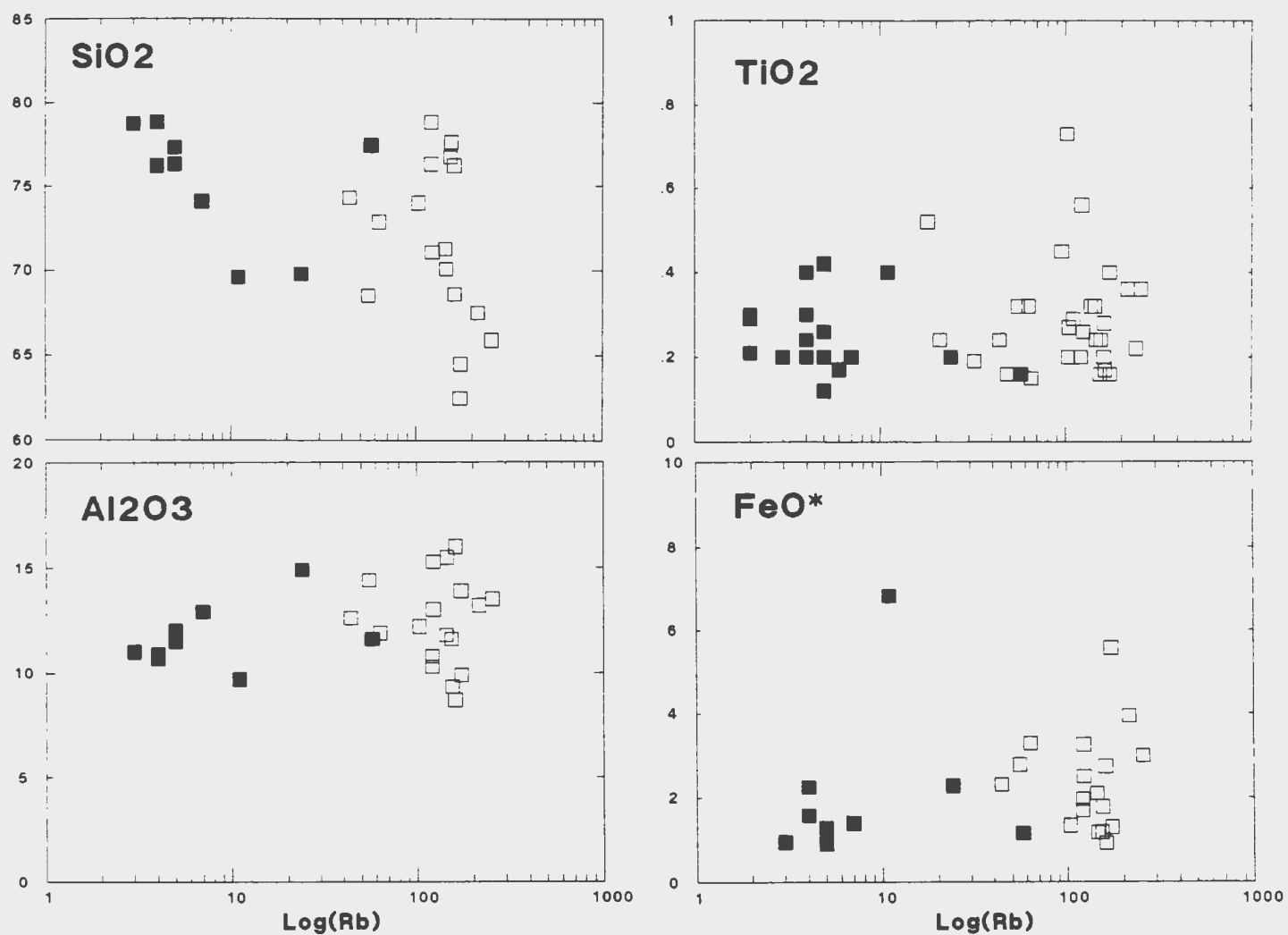


Figure 5-3:  $\text{Na}_2\text{O}$  vs  $\text{K}_2\text{O}$  plot for mineralized rocks from the Burnt Lake showings. Fields are based on apparent metasomatic intensities. Symbols as in Figure 5-2.

The best indicator of the bimodal metasomatic overprints in the Burnt Lake area is Rb. Figure 5-4 shows the variation of major elements versus Log(Rb). Strong linear correlations are visible on Na<sub>2</sub>O and K<sub>2</sub>O versus Rb plots (Figure 5-5) indicating that Rb was systematically enriched during the different metasomatic alterations. K and Rb are usually highly correlated in mineralized and altered rocks (Kerrick, 1990) and their observed relationship must have resulted from a coenrichment by hydrothermal solutions. A positive correlation between Na<sub>2</sub>O and Rb for the Na-metasomatised rocks reaches a peak at 9.46% Na<sub>2</sub>O (0.18% K<sub>2</sub>O) and 24 ppm Rb. In the potassic suite, K is substituted for Na, with even more Rb added to the system. Potassic metasomatism reaches a limit at 10.68% K<sub>2</sub>O (1.14% Na<sub>2</sub>O) and 254 ppm Rb. Rb readily substitutes for potassium (having a similar ionic radius) in potassic minerals. However, Rb is concentrated in late-stage magmatic fluids because of its larger ionic radius.

Major elements have been plotted against U to relate the uranium mineralization to major element geochemistry, however, most are not correlated with uranium. On the K<sub>2</sub>O versus U plot (Figure 5-6) the potassic suite is separated into two groups of samples that are positively correlated with U. The significance of these contrasting trends are discussed later. On a Na<sub>2</sub>O versus U plot the sodic samples have a positive correlation with uranium while the potassic suite have a wide range of Na values and show no positive correlation with U.





**Figure 5-4: Variation diagrams of major elements vs Rb. Oxides in weight percent, Rb in ppm; symbols as in Figure 5-2.**

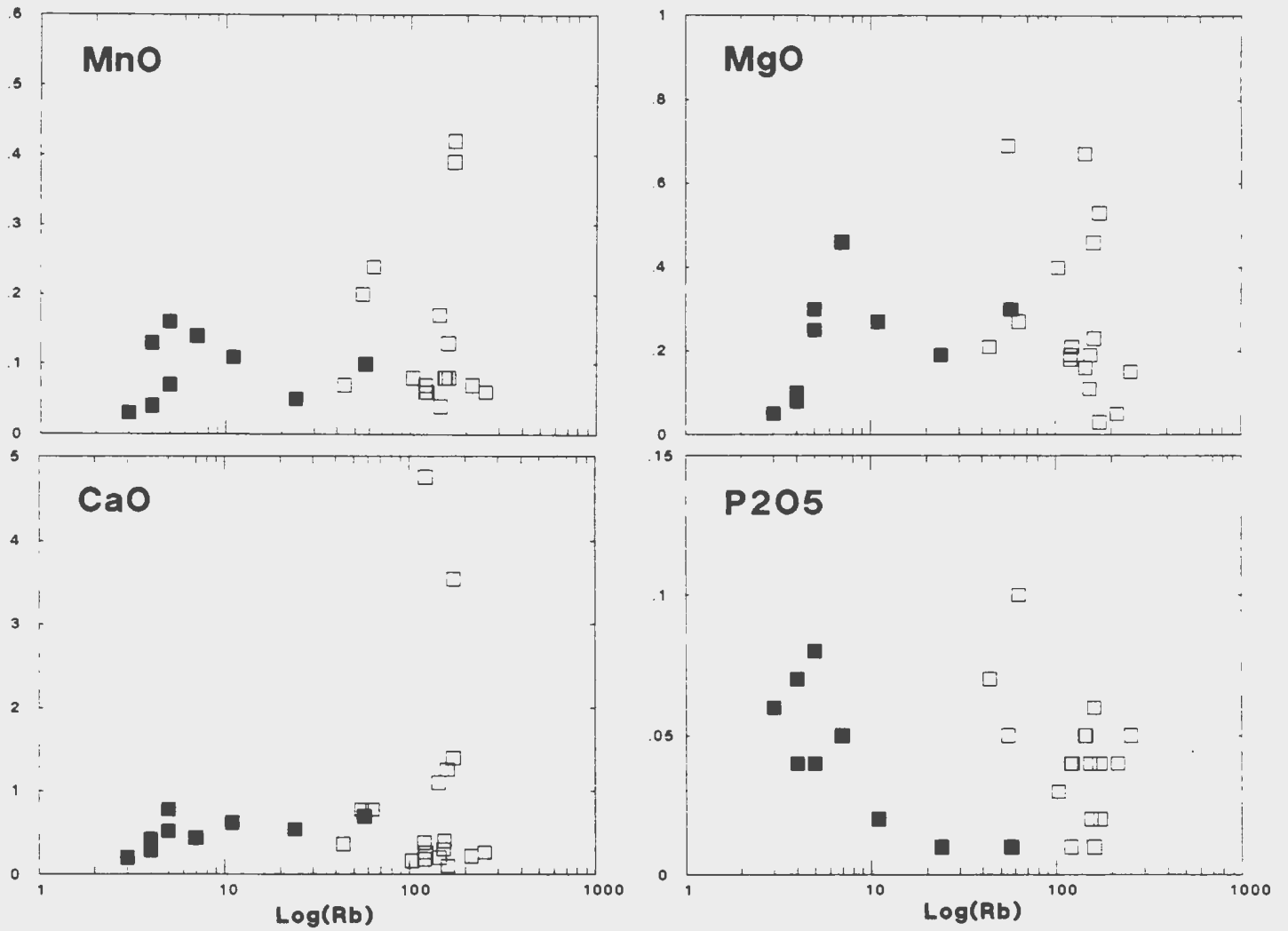


Figure 5-4: (Continued).

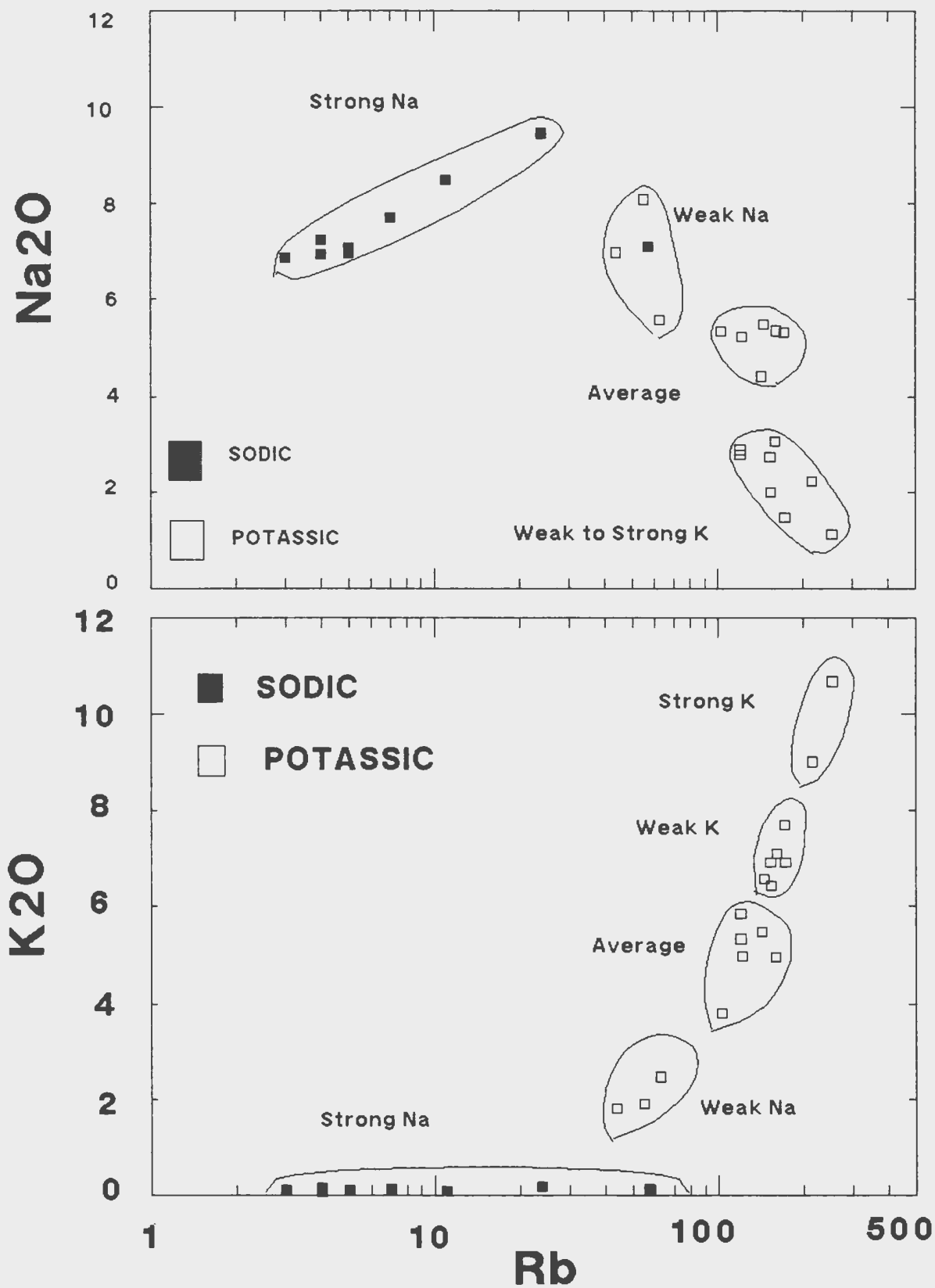
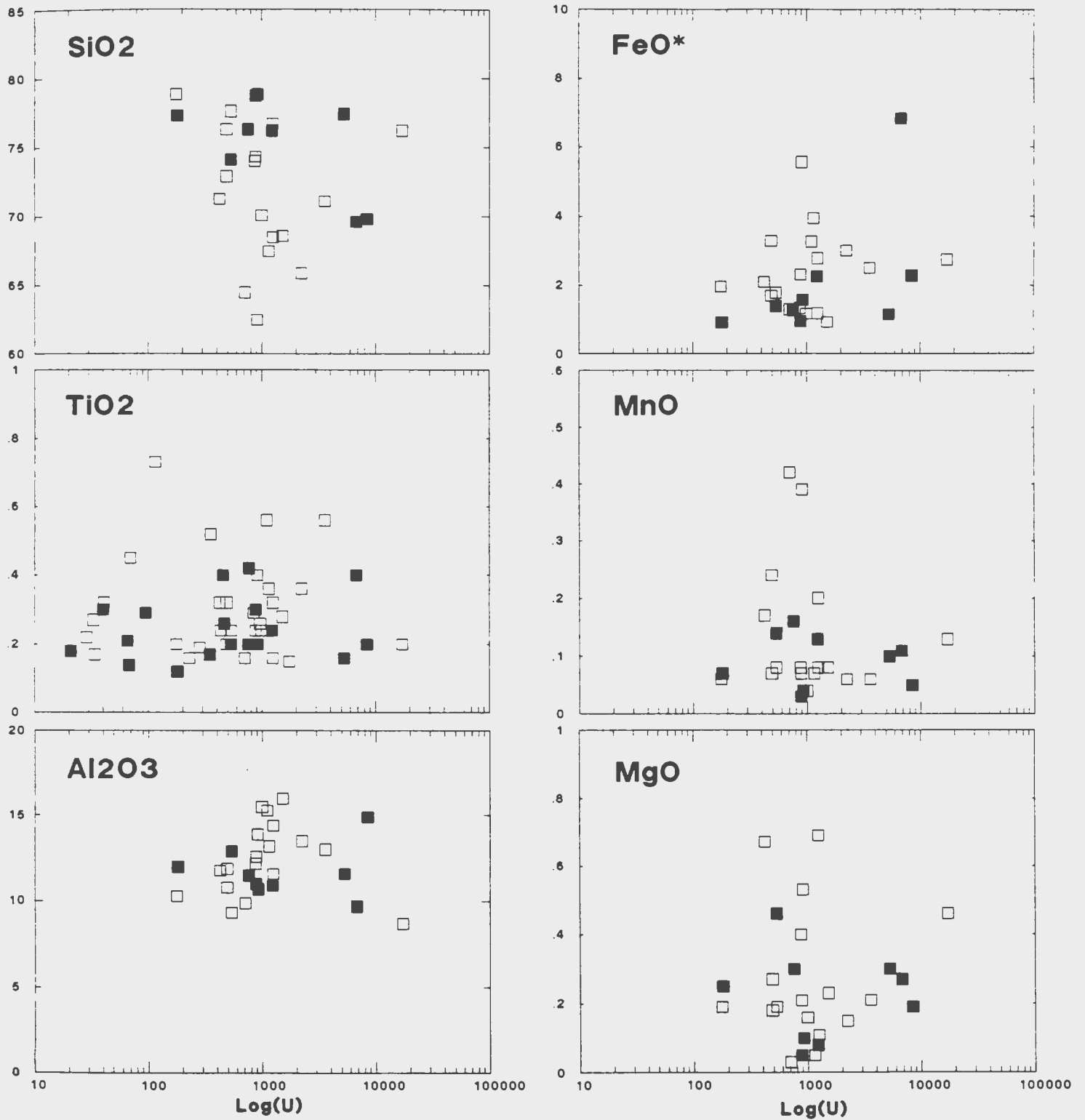


Figure 5-5: Plots of Na<sub>2</sub>O vs Rb and K<sub>2</sub>O vs Rb for mineralized rocks from the Burnt Lake showings. Fields are based on apparent metasomatic intensities. Symbols as in Figure 5-2.



**Figure 5-6: Variation diagrams of major elements vs U. Oxides in weight percent, U in ppm; symbols as in Figure 5-2.**

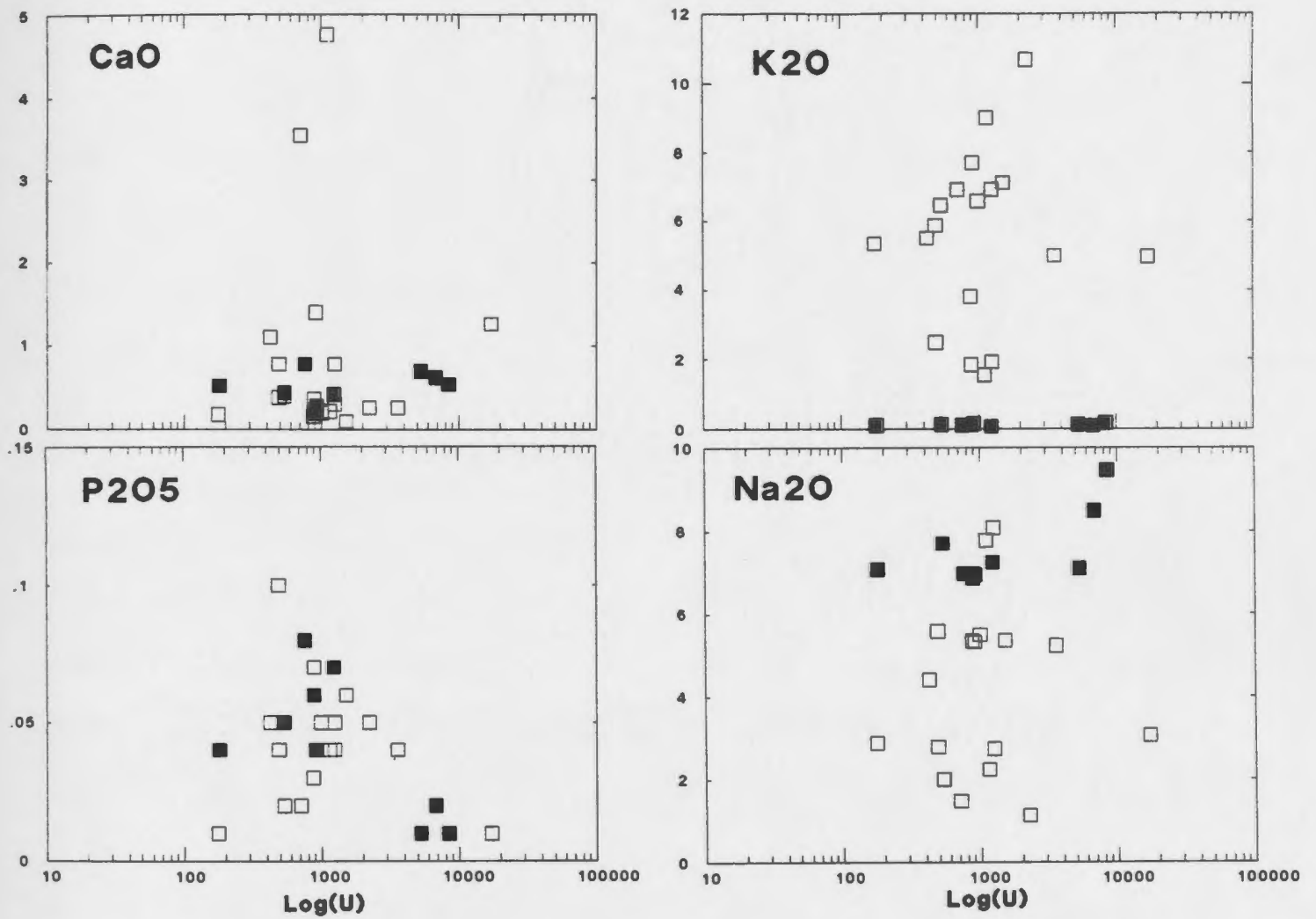


Figure 5-6: (Continued).

### 5.2.2 Trace Element Patterns

Trace elements have also been used to document element associations in the Upper Aillik Group mineralized samples. Trace element geochemistry also reflects the metasomatic processes associated with mineralized zones.

Trace elements have been plotted against Rb (Figure 5-7) which is thought to be the best indicator of metasomatic intensity. Pb has a good correlation with Rb in the potassic suite and is slightly disturbed in the sodic samples. Zn has an excellent positive correlation with Rb for the potassic while showing no correlation in the sodic samples. Cu and Ag are well correlated with Rb in the sodic suite while showing some scatter in the potassic suite. Sr values are highly scattered over a wide range of Rb abundances indicating that Sr was neither enriched nor depleted with respect to Rb. Generally, the potassic samples show positive correlations of Pb, U, As, Zn, Ag, Au, Mo, Ga and Ce vs Rb. The sodic samples show positive correlations of Pb, U, Ag and Cu vs Rb.

Trace elements plotted against uranium are shown in Figure 5-8. On the U versus Pb plot, an excellent positive correlation exists indicating that most of the lead is of radiogenic origin. However, four of the K-metasomatized samples which fall off the straight line have a non-radiogenic lead component or possibly have undergone uranium loss as a result of later remobilization (i.e. during the Grenville).

The Th versus U plot shows little correlation at grades <3000 ppm U, while at higher grades, (i.e. >5000 ppm U) Th is apparently mobilized and selectively removed from the depositional environment. Perhaps this suggests that the physiochemical conditions were suitable for selectively mobilizing Th and not U (i.e. high enough temperature to mobilize Th and a pH too low to complex U).

The plot of Zn versus U shows some scattering in the data, however, the highest zinc contents are in the strongly potassic altered rocks and are not always correlated with uranium. The plot of Cu versus U shows that a broad positive correlation with uranium and the highest copper values exists within the sodic metasomatized rocks. As and Ag have roughly positive correlations with U. Au and Mo are enriched in only a few samples, the mostly highly potassic. Y, V, Ba and Sr have weak positive correlations with U. The Zr versus U plot shows some scatter in the data but has a rough positive correlation which suggests that some uranium occurs within zircon (as proven by SEM studies on mineralized samples). There is little variation in the incompatible elements (Nb and Ga) with increasing uranium contents, indicating that these elements were not mobile during uranium mineralization. La is depleted in highly radioactive samples (>2000 ppm U). U is independent of Ce and nearly independent of Ti. On a Rb versus U plot there is a positive correlation between Rb and U in the sodic samples and slightly positive correlation in the

potassic. Also the three highest U samples in the sodic group have separated from the main Rb group. This decoupling of Rb from K commonly occurs during late stage magmatic processes (Kerrick, 1990).



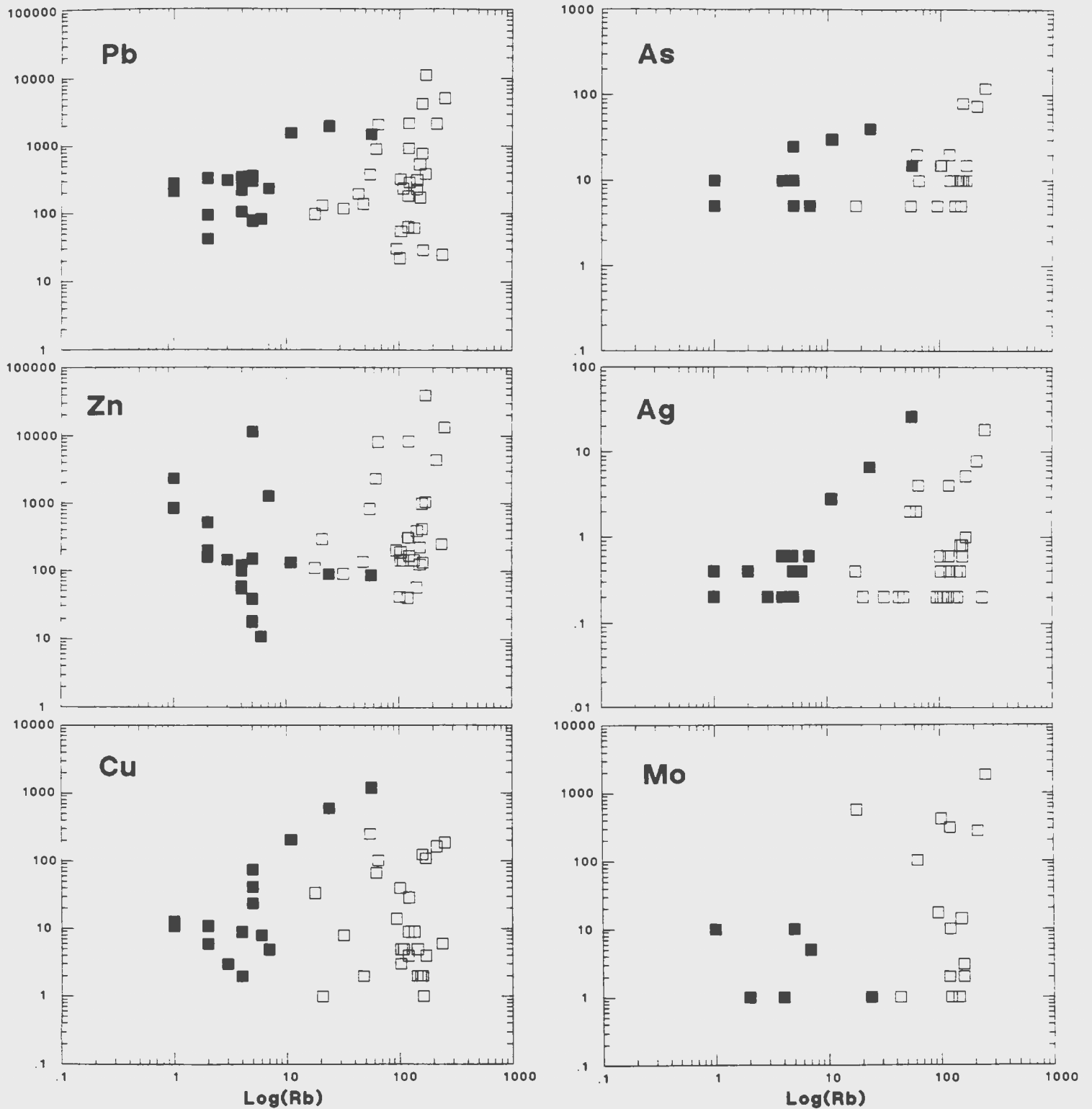


**Figure 5-7: Harker variation diagrams of trace elements vs Rb for mineralized rocks from the Burnt Lake showings. Symbols as in Figure 5-2.**

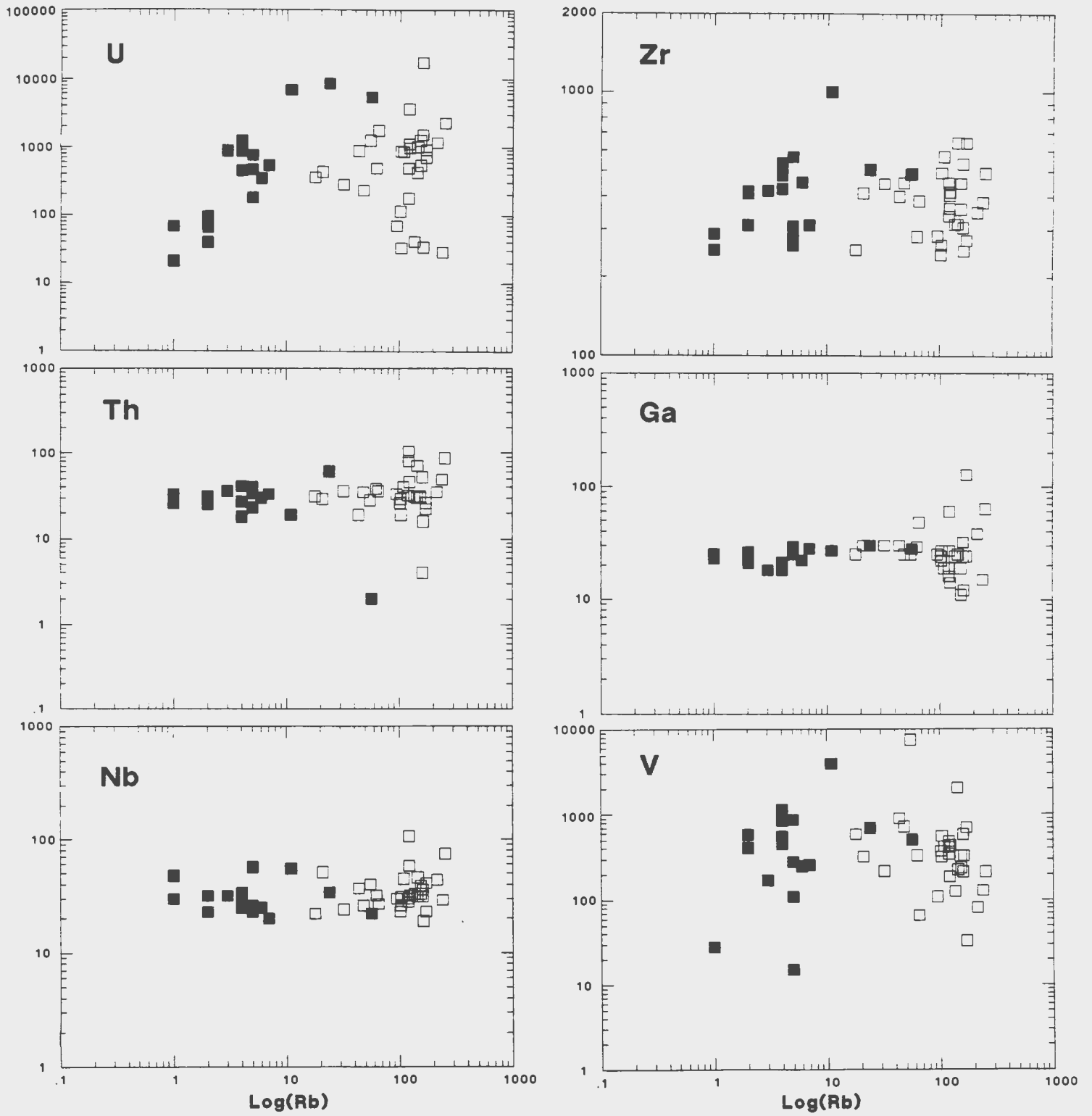


Figure 5-7: (Continued).

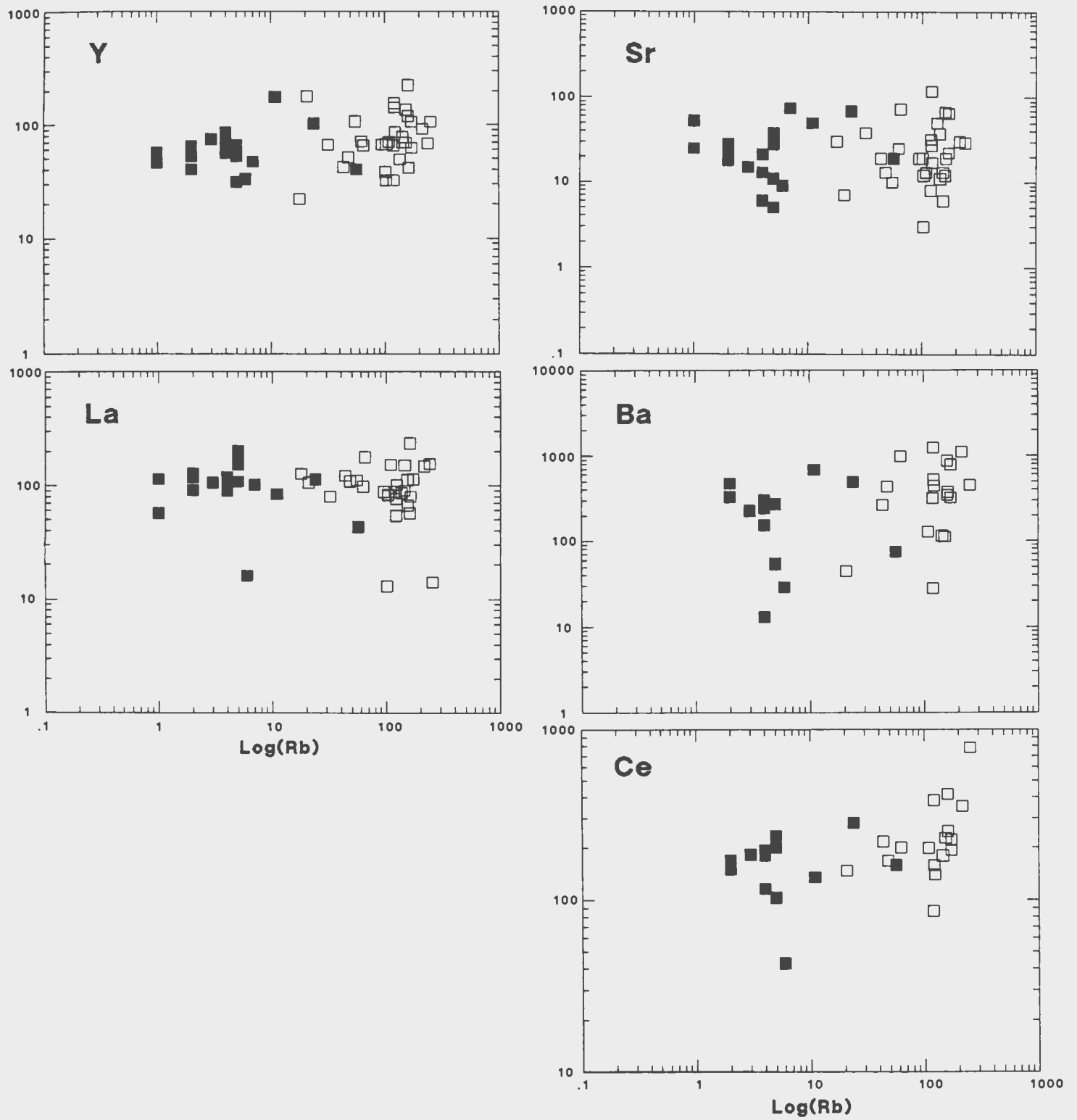
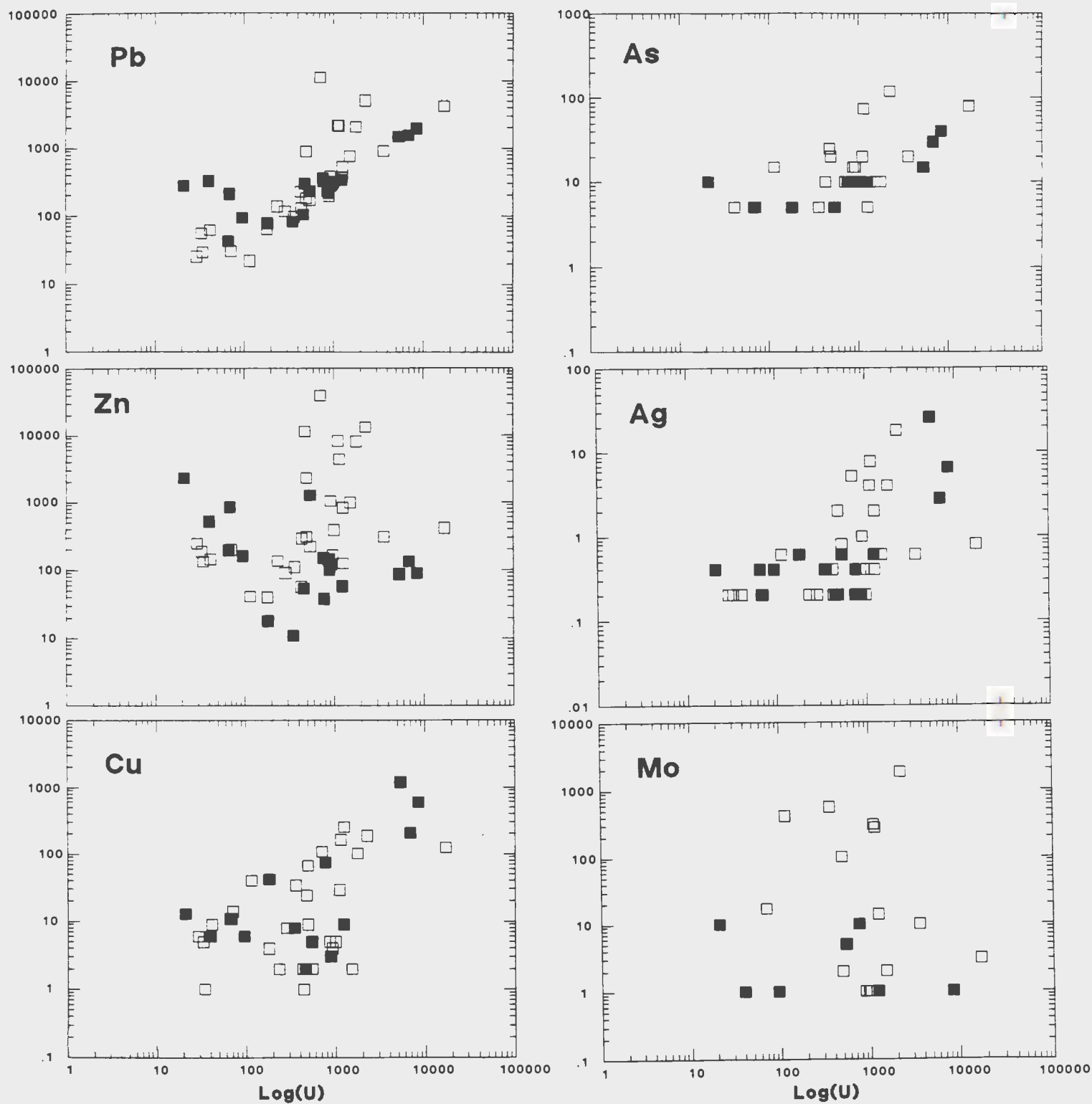


Figure 5-7: (Continued).



**Figure 5-8: Harker variation diagrams of trace elements vs uranium for mineralized rocks from the Burnt Lake showings. Symbols as in Figure 5-2.**

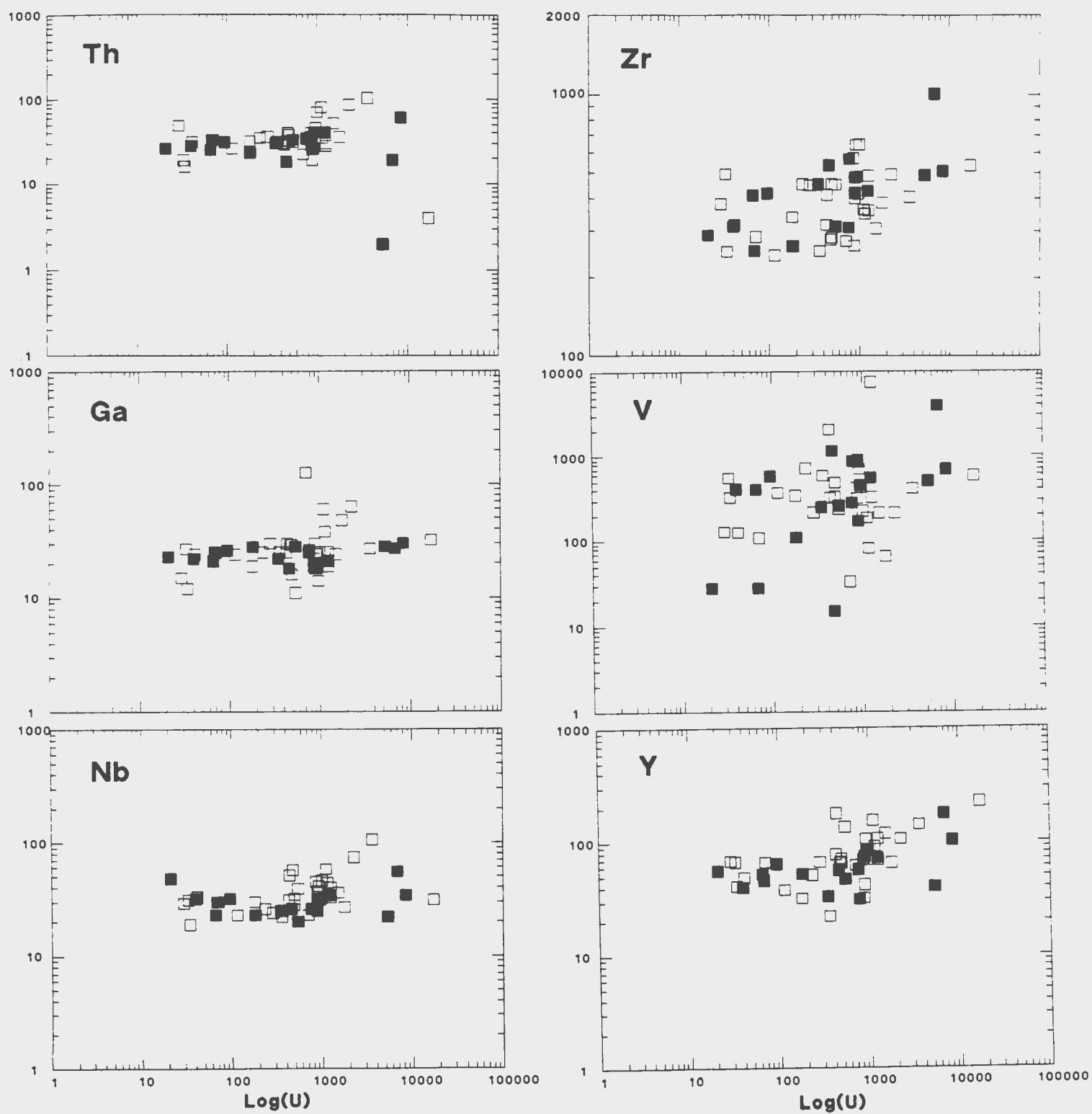


Figure 5-8: (Continued)

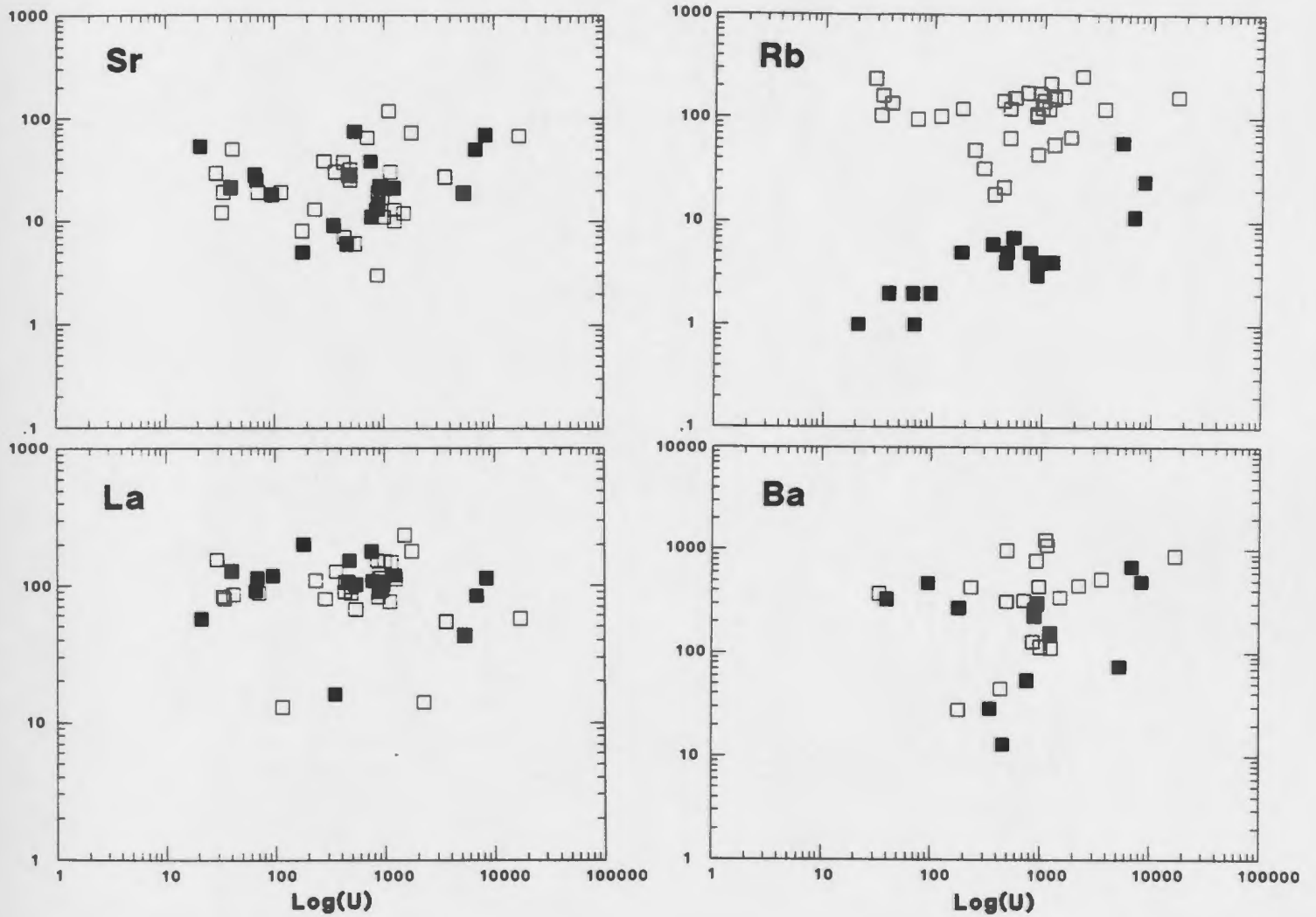


Figure 5-8: (Continued)

### 5.3 Emben Showings

Uranium mineralization has been discovered in four areas of the Emben region, namely the Emben South, Emben Main, Emben Central and Emben West showings. For this section the Emben Main, Central and West showings are grouped together because of the similarities of host rock and mineralization style. Samples from the Emben South Zone are treated separately.

#### 5.3.1 Major Element Patterns

Major element distributions compared to silica are shown in Figure 5-9. The mineralized samples from the Emben South Zone can be characterized as containing elevated  $\text{TiO}_2$ ,  $\text{FeO}^*$  and  $\text{CaO}$  contents, reflecting the presence of significant pyrite, ilmenite, sphene, calcic amphiboles and pyroxenes. The high  $\text{P}_2\text{O}_5$  contents probably reflect primary enrichment of apatite or from increased volatile content. Fluorite has been noted in the Emben South zone, however, F was not analysed. The Emben showings have undergone strong alkali metasomatism with  $\text{Na}_2\text{O}$  enrichments ( $\text{Na}_2\text{O}$  between 6-11 wt%) and extreme  $\text{K}_2\text{O}$  depletions (usually <0.2 wt%).  $\text{Na}_2\text{O}$  has an excellent positive correlation with silica within the mineralized mafic dykes from Emben South (<65 wt%  $\text{SiO}_2$ ), while having a negative correlation in the felsic rocks from the other Emben showings and Emben South. Sodium enrichments accompanying silica and

potassium depletions have been shown to be the result of Na-metasomatism elsewhere in the region (White and Martin, 1980).

The mafic dykes from Emben South are different on the  $\text{TiO}_2$  and  $\text{P}_2\text{O}_5$  diagrams.  $\text{Al}_2\text{O}_3$  has the same positive and negative correlations as  $\text{Na}_2\text{O}$  while  $\text{Fe}_2\text{O}_3$  shows good negative correlation with  $\text{SiO}_2$ . Most of the elements  $\text{TiO}_2$ ,  $\text{Al}_2\text{O}_3$ ,  $\text{Fe}_2\text{O}_3$ ,  $\text{CaO}$  and  $\text{Na}_2\text{O}$  reflect primary magmatic chemistry while only  $\text{K}_2\text{O}$  is disturbed. This contrasts with the Burnt Lake felsic volcanics where none of the samples have a magmatic (ie. differentiated) signature (therefore the dykes are not related to the felsic volcanics).

Majors elements plotted against U are shown as Figure 5-10 and demonstrate broad differences between the mafic dykes from the Emben South Showing and the felsic tuffaceous rocks from all the Emben showings. Silica and sodium show weak positive correlations with uranium in the mafic dykes, while  $\text{FeO}^*$  and  $\text{TiO}_2$  are negatively correlated with U in these same samples. The tuffaceous rocks do not show any linear correlation between major elements and uranium.



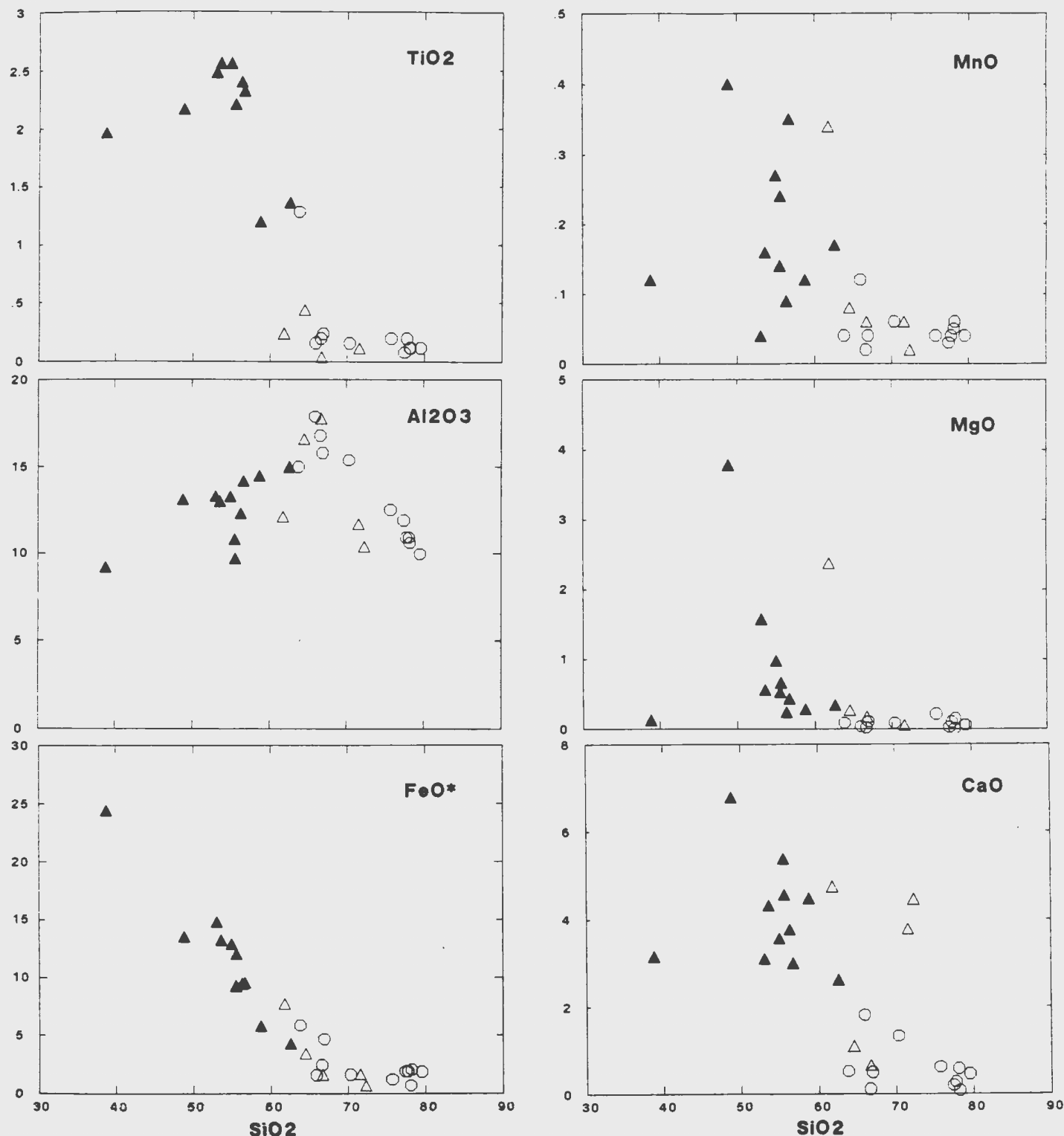


**Figure 5-9: Harker variation diagrams for the mineralized samples from the Emben Showings. Oxides are in weight percent. Symbols are as follows; open circle: tuffaceous sedimentary rocks and rhyolite tuff from the Emben Main, Emben Central and Emben West Showings; solid triangle: biotite-feldspar dykes from the Emben South Showing; open triangle: tuffaceous rocks from the Emben South Showing.**

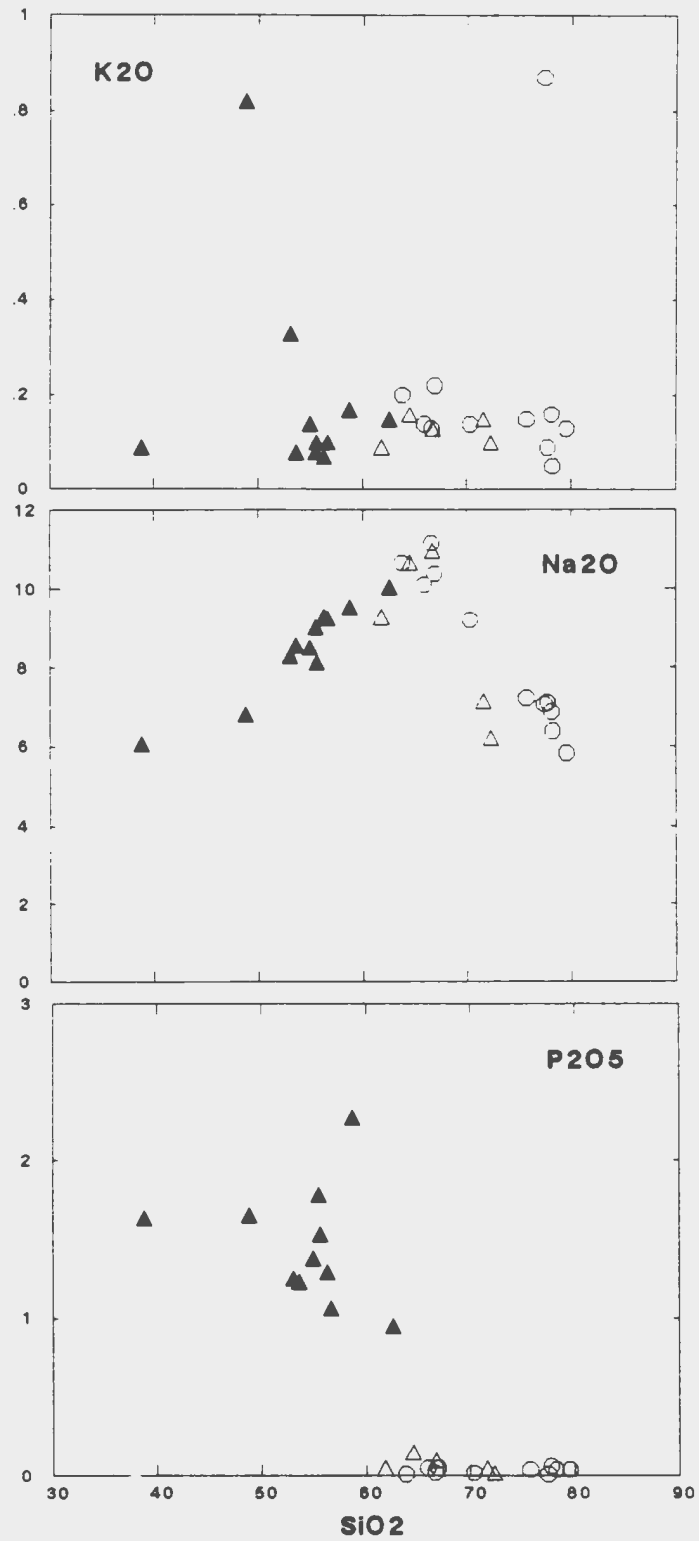
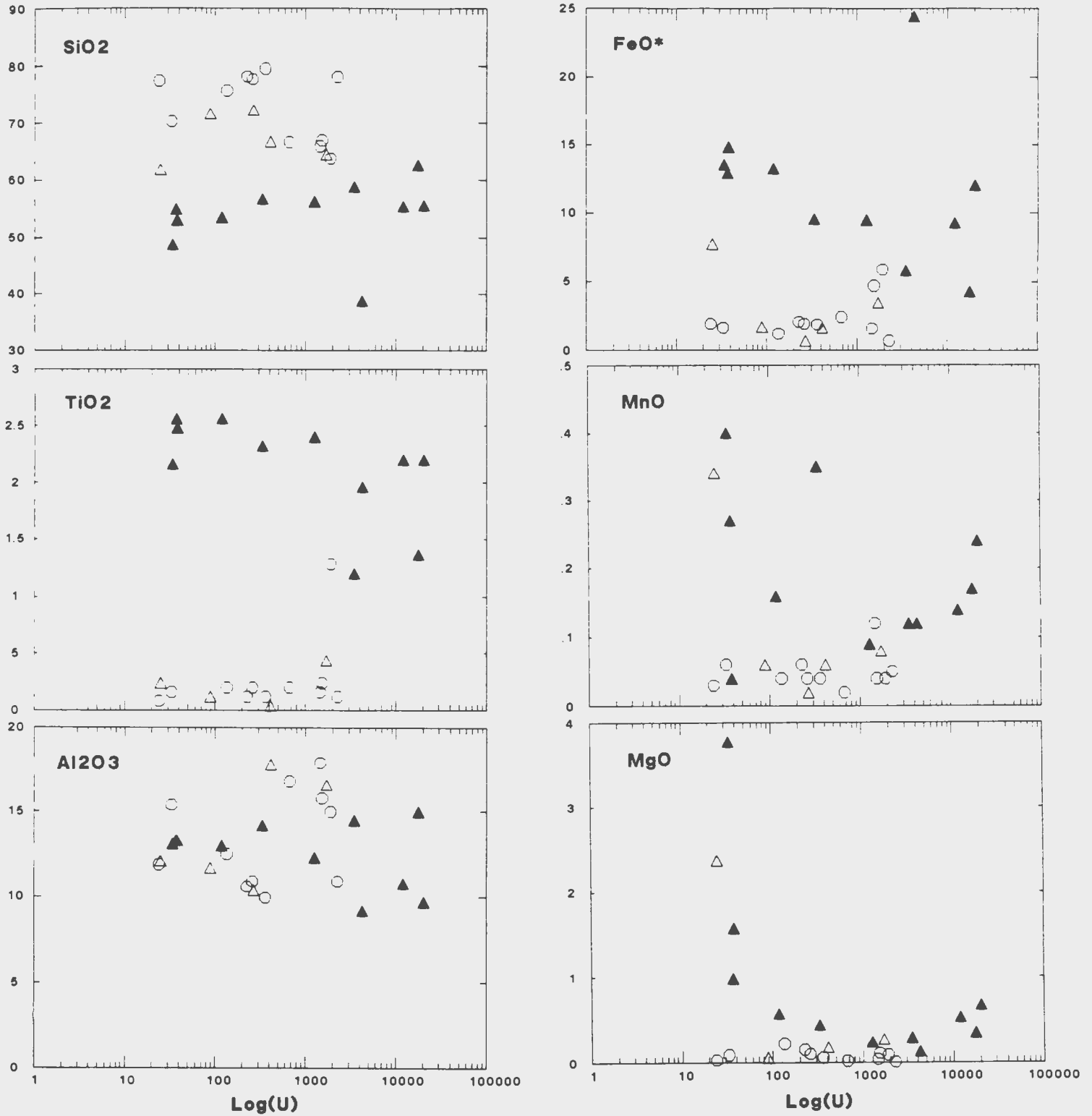


Figure 5-9: (Continued).



**Figure 5-10: Variation diagrams of major elements vs uranium for the Emben Showings. Symbols as in Figure 5-9.**

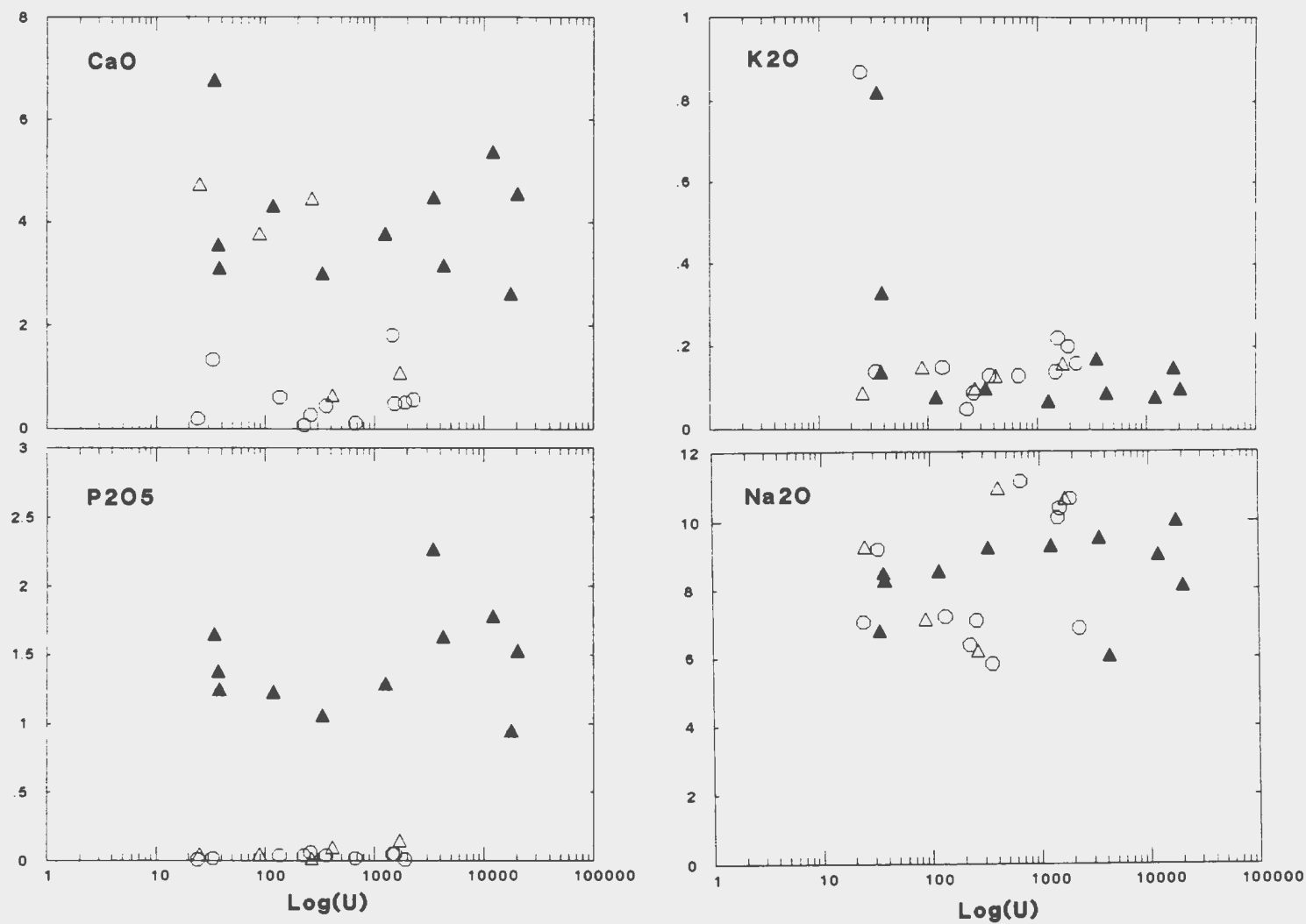
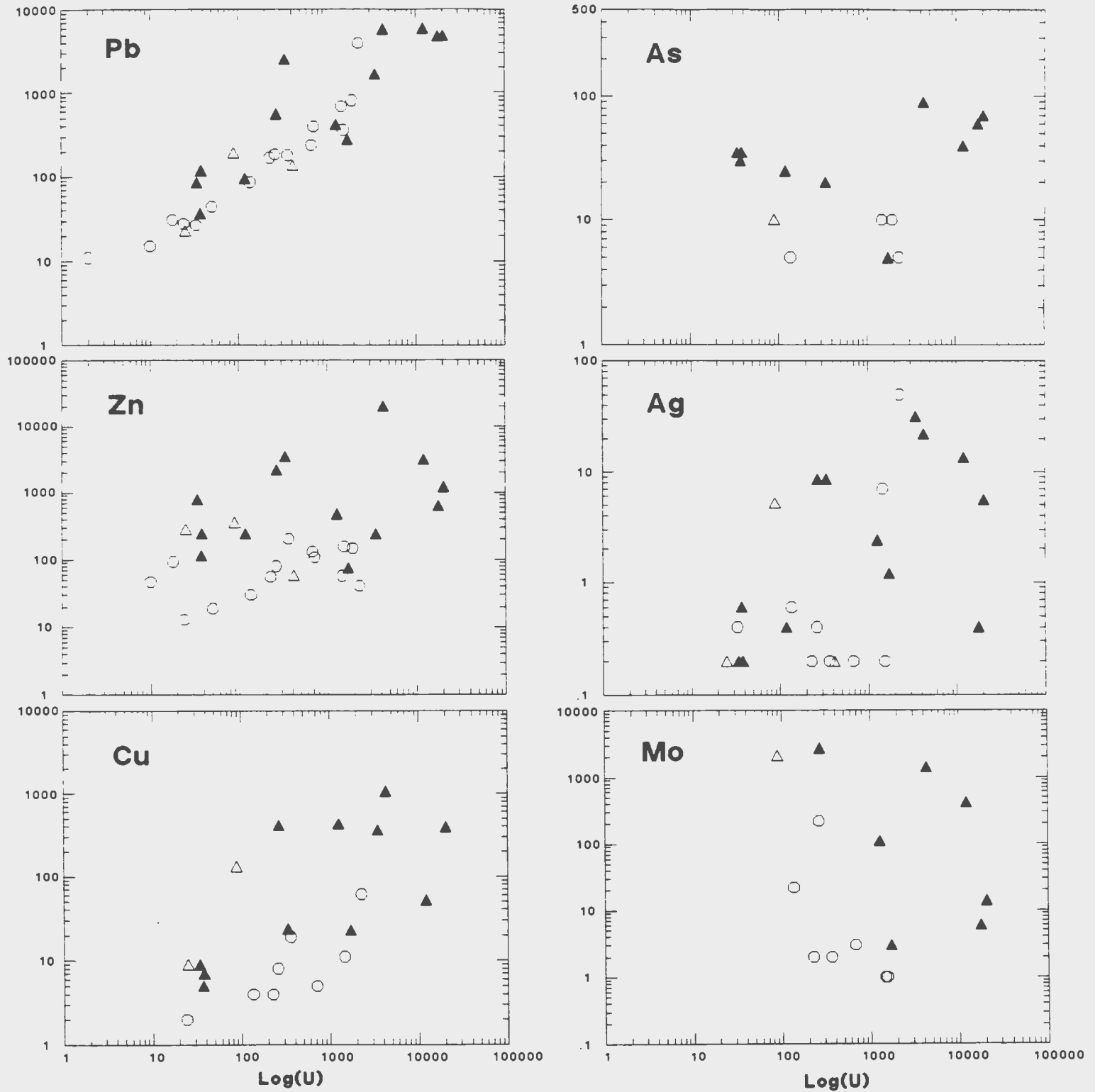


Figure 5-10: (Continued)

### 5.3.2 Trace Element Patterns

Trace element concentrations were plotted against uranium (Figure 5-11) in an attempt to document the trace element distributions associated with the uranium mineralization in the Emben Showings.

U has an excellent positive correlation with Pb indicating that most of the Pb is radiogenic. Zn, Cu, As, Ag and Mo versus U have a lot of scatter in the data but show enrichments exclusively in the Emben South dyke samples. Th, V and Ni show broad positive relationships with uranium. Y, Nb, Ga and Rb show enrichment with uranium reflecting mobility of these incompatible elements during mineralization. Sr, Zr and Cr show a broad scattering indicating that Sr and Zr were neither depleted nor enriched during mineralization. There is no correlation of U with As, Ag, Mo, Zr and Cr while only slight positive correlation with Sr and V. Zn and Cu contents are enriched only in the mafic dyke samples and show broad positive correlations with uranium. Th versus U shows linear correlations in both sample suites. A good positive correlation exists between Sm and U and possibly indicates the association of uranium with feldspars. Ni is enriched exclusively in the mafic dykes and shows a slight positive correlation with uranium.



**Figure 5-11: Harker variation diagrams of trace elements vs uranium for mineralized rocks from the Emben showings. Symbols as in Figure 5-8.**

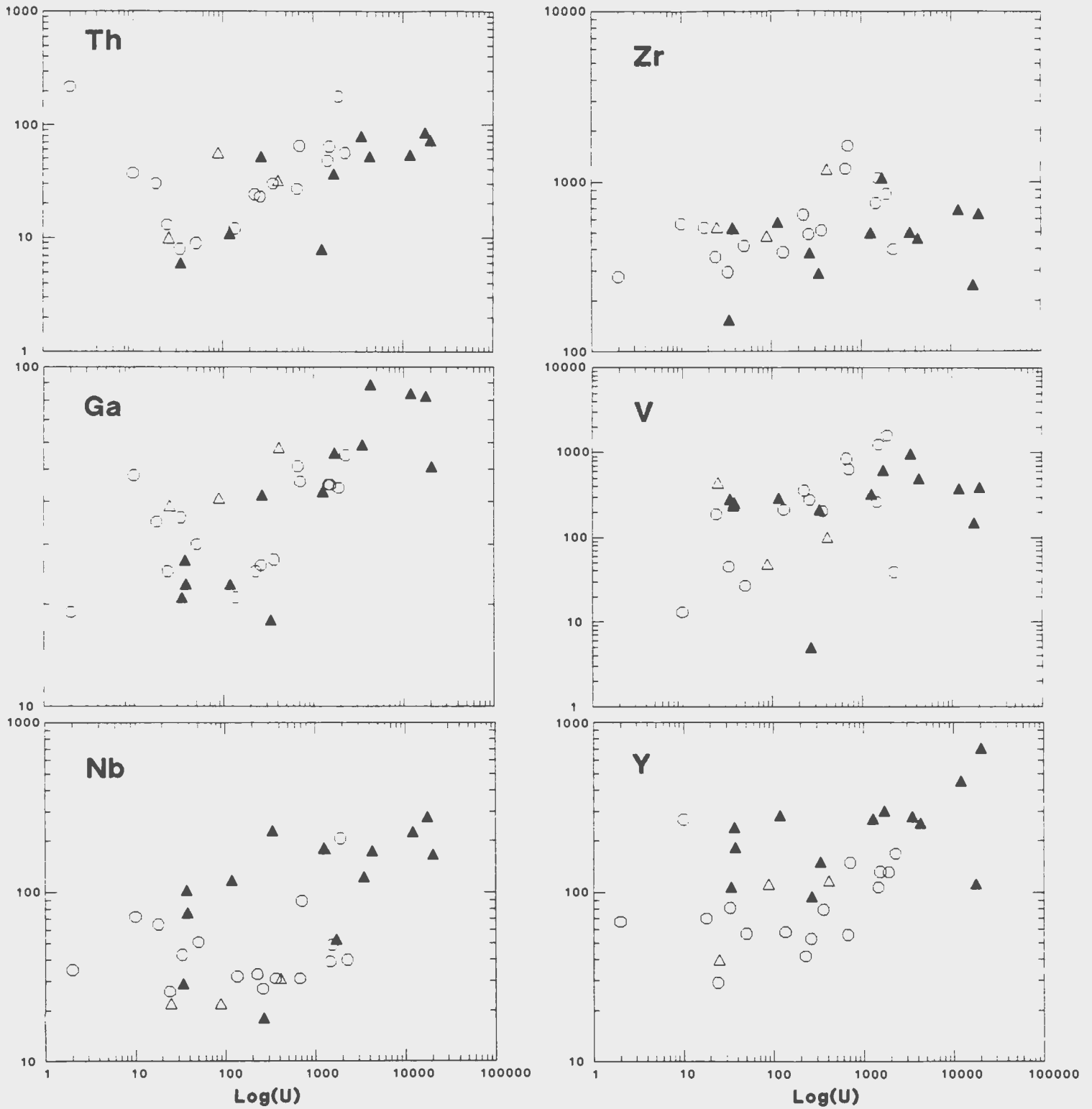


Figure 5-11: (Continued)

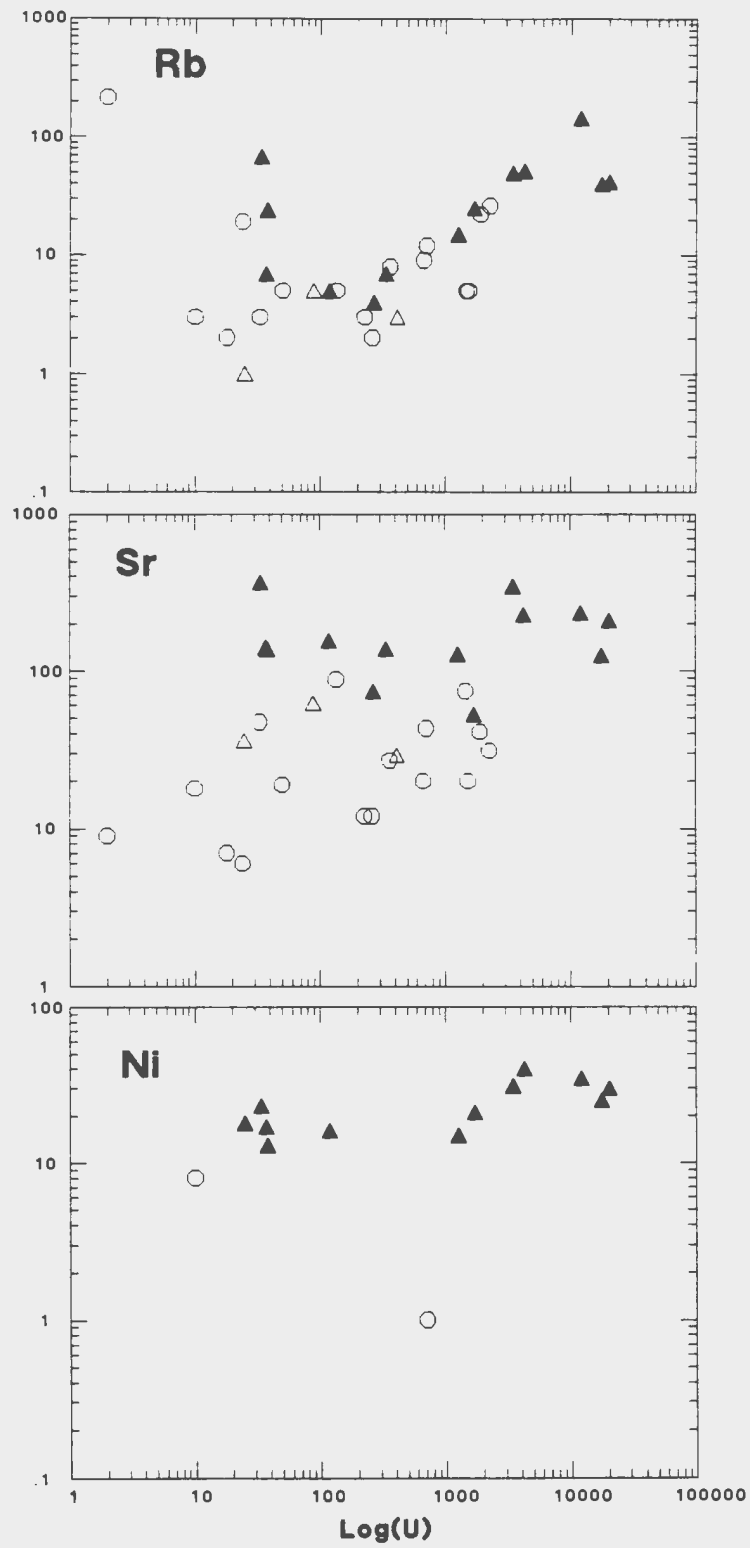


Figure 5-11: (Continued)



## 5.4 Aurora River Showing

### 5.4.1 Major and Trace Element Patterns

The mineralized andesitic rocks of the Aurora River Showing exhibit strong alkali metasomatic effects involving the enrichment of  $\text{Na}_2\text{O}$  ( $>6\%$ ) and depletion of  $\text{K}_2\text{O}$  ( $<0.3\%$ ). When compared to the unmineralized samples the mineralized samples (Figures 5-12 and 5-13) show some enrichment in  $\text{SiO}_2$ ,  $\text{Na}_2\text{O}$ ,  $\text{P}_2\text{O}_5$ , V, Pb, Bi, As, Au, Ba, Ga, Nb, Zr and Y and depletions in  $\text{TiO}_2$ ,  $\text{Al}_2\text{O}_3$ ,  $\text{FeO}^*$ , MgO,  $\text{K}_2\text{O}$ , Cr, Ni, Co, Sr and Rb. MnO, CaO, Zn and Th are relatively unchanged in both sample suites. Both the mineralized and unmineralized rocks have high contents of CaO which average 8.45% for the mineralized samples suggesting that the uraniferous mineralization was preceded by strong carbonate alteration. Pb shows a good correlation with U indicating that the lead is radiogenic. Rb and Ga are strongly correlated with uranium suggesting the association of uraninite with feldspars. Th contents are extremely low, but average 14 ppm due to one high value of 103 ppm, while most samples were below detection.

Trace element data from the area indicate an interesting correlation between uranium and vanadium. The unmineralized samples (0-10 ppm U) contain  $<200$  ppm V while the mineralized samples (700-2000 ppm U) contain between 500-1500 ppm V. The presence of enriched vanadium at Aurora River may indicate the co-precipitation of carnotite with uraninite from the

mineralizing solutions (e.g. Langmuir, 1978) or may just reflect local mobility of V in the mineralized andesites rather than a common origin for V and U.

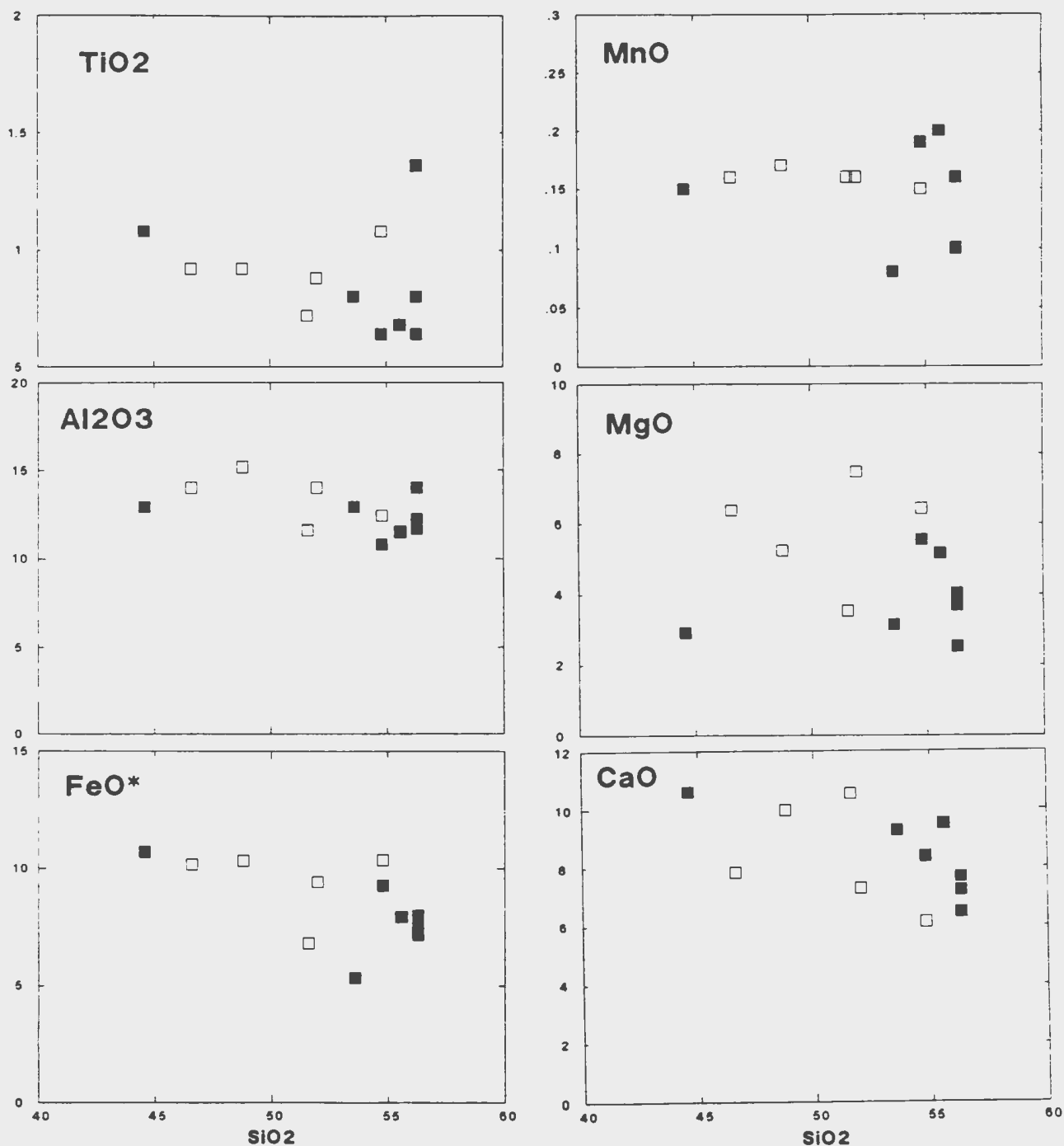


**Figure 5-12: Harker variation diagrams for samples from the Aurora River Showing. Oxides are in weight percent. Symbols are as follows; open box: unmineralized andesite; solid box: mineralized andesite.**

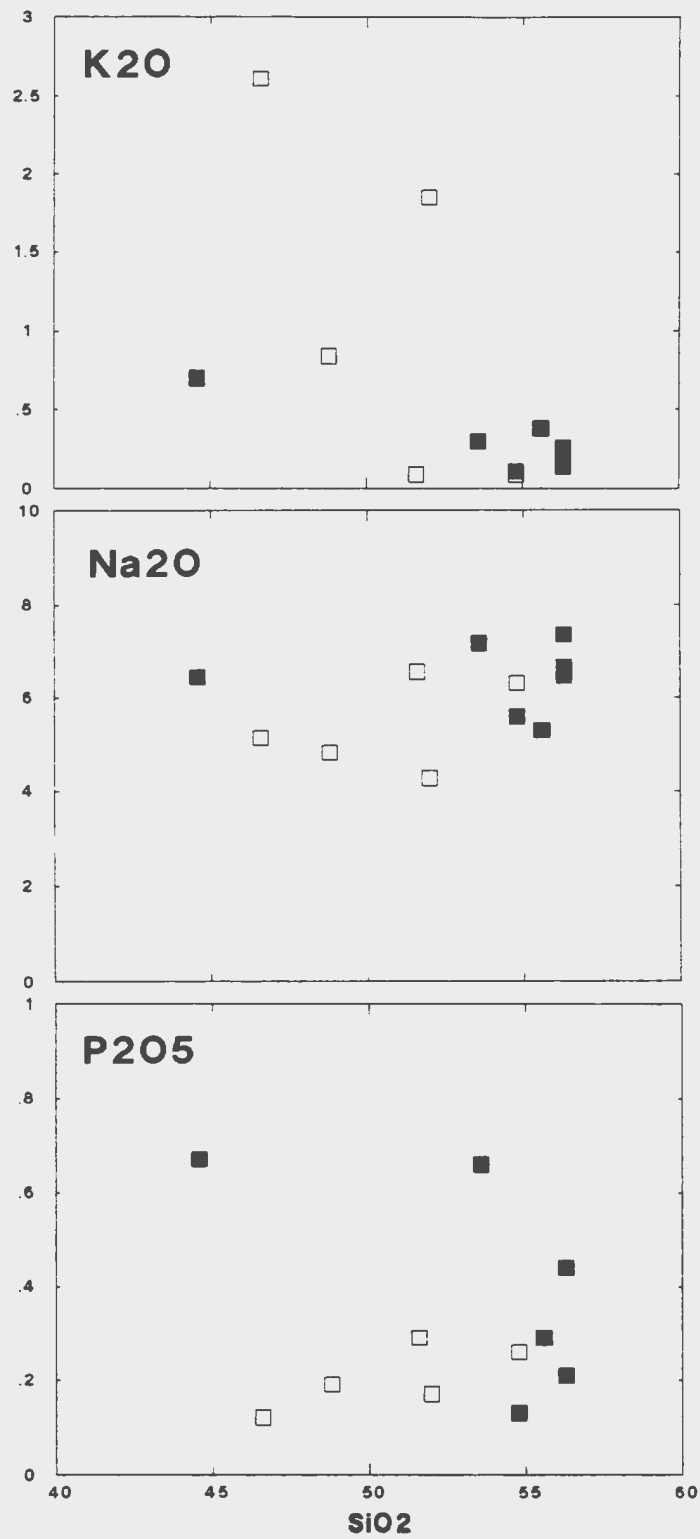


**Figure 5-12: (Continued).**

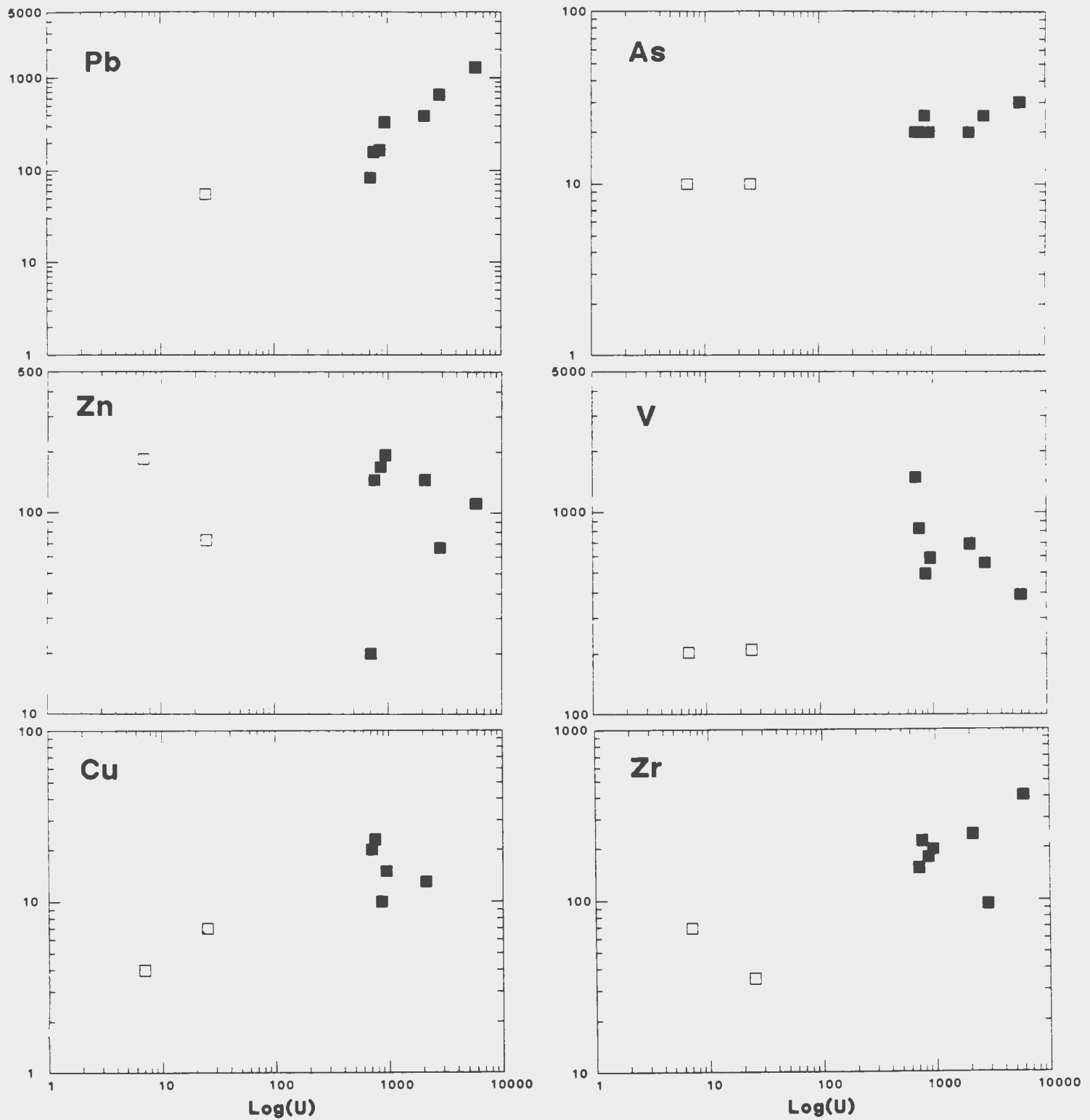


**Figure 5-13: Harker variation diagrams of trace elements vs uranium for rocks from the Aurora River Showing. Symbols as in Figure 5-12.**

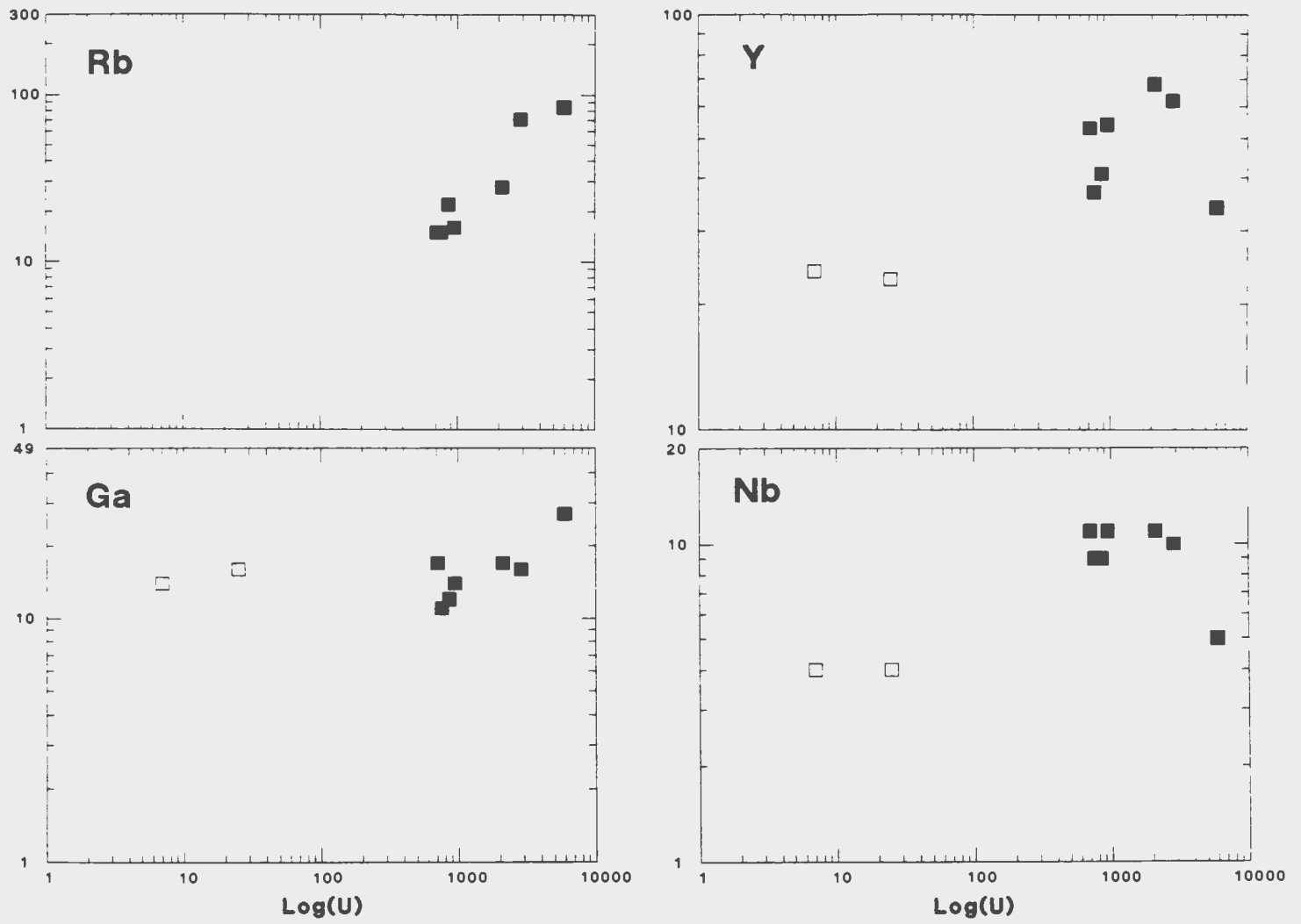


Figure 5-13: (Continued).

### 5.5 Geochemical Comparisons Between the Radioactive Zones

A comparison of the various radioactive zones in the Burnt Lake area was attempted in order to document the similarities and differences within these zones. Table 5-1 lists the average compositions of the five mineralized zones, namely: Burnt Lake (sodic), Burnt Lake (potassic), Emben Main, Emben South and Aurora River. On Figure 5-14, a  $\text{Na}_2\text{O} + \text{K}_2\text{O}$  vs  $\text{SiO}_2$  diagram, mineralized samples in the Burnt Lake area plot as two groups; low silica with a positive correlation between silica and total alkalies and high silica with negative correlation between silica and total alkalies. The samples of mafic dykes from Emben South and andesitic rocks from Aurora River plot in the alkaline field. On an AFM diagram (Figure 5-15) the rocks are dominantly calcalkaline except for the mafic dykes from Emben South which plot in the tholeiite field, suggesting that the dykes are not part of the chemical continuum with the Upper Aillik Group. The Burnt Lake and Emben Main samples plot mainly in Winchester and Floyd's (1977) rhyolite field on a  $\text{Zr}/\text{TiO}_2$  vs  $\text{Nb}/\text{Y}$  diagram (Figure 5-16) with a lot of scatter in the peralkaline comendite/pantellerite field. The Emben South samples plot in the rhyolite/dacite field with minor scattering into the trachyandesite field. The unmineralized Aurora River samples plot entirely within the andesite/basalt field, while the mineralized equivalent plot in the rhyolite/dacite field with

minor scattering into the trachyandesite field. This is a result of an enrichment in Zr and a depletion in  $\text{TiO}_2$  during mineralization. On Winchester and Floyd's (1977)  $\text{SiO}_2$  vs  $\text{Zr/TiO}_2$  diagram (Figure 5-17) there is a spread of values into the alkaline or peralkaline comendite/pantellerite, phonolite and trachyte fields. These samples are highly mineralized and hence reflect that the peralkaline geochemical signature is a result of metasomatic alteration. The Aurora River samples plot in the subalkaline basalt field, while the mineralized samples plot in the alkaline phonolite field. Na-metasomatism is generally accompanied by a depletion in  $\text{SiO}_2$ , as shown in the other mineralized suites from the area, however, the mineralized samples from Aurora River have enriched silica and sodium contents reflecting a different style of mineralization. On a  $\text{K}_2\text{O} + \text{Na}_2\text{O}$  versus  $\text{SiO}_2$  plot showing Cox et al.'s (1979) classification fields, most of the Burnt Lake and Emben Main samples plot in the rhyolite field with the highly metasomatised and mineralized samples (i.e. less silica) plotting as trachytes. The Emben South samples plot in several fields from benmorite to trachyte, while the Aurora River samples plot in the trachyandesite field.

A comparison of total Fe between the mineralized and non-mineralized samples indicates that iron is fairly constant, therefore, most of the  $\text{Fe}^{+2}$  has been oxidized to  $\text{Fe}^{+3}$  in the uraniferous samples. Evans (1980) recognized areas surrounding radioactive zones where high  $\text{Fe}^{+3}/\text{Fe}^{+2}$  ratios are

associated with Na metasomatism (Na content increases towards the mineralized areas as Si decreases). The red hematitic alteration that is commonly found associated with uranium mineralization suggests that pitchblende precipitation resulted from the reduction of  $U^{+6}$  to  $U^{+4}$  by the oxidation of the reduced iron ( $Fe^{+2}$  to  $Fe^{+3}$ ) in the wall rocks adjacent to the ore fluids channelways.

**Table 5-1: Average major and trace-element compositions of mineralized rocks from the Burnt Lake area.**  
(n.d. = not detected, n.a. = not analysed)

	Oxide weight percent	BURNT LAKE Potassic		BURNT LAKE Sodc		EMDEN MAIN		EMDEN SOUTH		AURORA RIVER	
		n=17 MEAN	S.D.	n=9 MEAN	S.D.	n=9 MEAN	S.D.	n=11 MEAN	S.D.	n=7 MEAN	S.D.
	SiO <sub>2</sub>	71.58	4.84	75.36	3.50	72.49	6.47	58.31	8.65	53.93	4.23
	TiO <sub>2</sub>	0.28	0.10	0.21	0.08	0.29	0.37	1.52	0.97	0.86	0.27
	Al <sub>2</sub> O <sub>3</sub>	12.27	2.07	11.69	1.51	13.37	3.02	13.04	2.85	12.29	1.07
	FeO*	2.33	1.18	2.07	1.85	2.49	1.68	8.55	6.71	8.88	1.87
	MnO	0.14	0.12	0.22	0.13	0.05	0.03	0.14	0.09	0.15	0.04
	MgO	0.28	0.20	0.09	0.05	0.09	0.07	0.33	0.20	3.86	1.14
	CaO	0.69	0.84	0.5	0.19	0.55	0.51	3.41	1.49	8.45	1.44
	Na <sub>2</sub> O	4.12	2.00	7.54	0.88	8.40	2.11	8.88	1.59	6.41	0.76
	K <sub>2</sub> O	5.76	2.38	0.12	0.03	0.14	0.05	0.11	0.03	0.29	0.2
	P <sub>2</sub> O <sub>5</sub>	0.04	0.02	0.04	0.03	0.03	0.02	1.09	0.74	0.37	0.22
	LOI	0.72	0.57	0.46	0.32	0.31	0.15	1.33	2.35	2.91	2.19
ppm	Cr	5.9	9.3	22.4	58.5	5.1	9.4	5.8	10.5	53.7	15.4
	Ni	0.1	0.2	n.d.	---	n.d.	---	19.4	14.5	28.4	6.9
	Co	32.2	16.0	33.9	9.1	34.4	14.0	56.5	103.5	13.6	4.2
	V	879.1	1775.9	773.8	1209.8	562.1	543.8	360.9	271.5	718.7	363.9
	Cu	54.8	80.9	228.6	411.4	11.9	19.5	252.0	331.2	11.6	9.0
	Pb	1633.6	2830.1	726.3	709.8	736.9	1220.1	2467.7	2430.7	436.9	418.0
	Zn	3735.8	9597.8	230.7	393.6	101.2	61.7	2910.2	5844.4	121.7	60.6
	Bi	1.9	5.3	1.6	4.7	n.d.	---	10.0	14.5	n.d.	---
	Cd	2.7	8.3	n.d.	---	n.d.	---	6.5	15.6	n.d.	---
	Mo	131.6	443.0	1.9	3.4	27.9	72.4	429.9	882.6	n.d.	---
	As	23.8	34.1	13.9	12.9	3.3	1.4	28.2	32.4	22.9	3.9
	Ag	2.4	4.6	4.2	8.5	6.5	16.5	8.6	10.3	0.2	0.2
ppb	Au	44.4	103.9	9.4	23.2	60.0	94.8	8.6	17.9	n.d.	---
	Rb	138.7	54.2	13.3	17.6	9.4	8.6	35.4	41.3	35.9	29.1
	Ba	365.6	369.8	249.9	219.9	6.8	12.8	9.9	15.4	582.7	996.4
	Sr	22.8	19.4	34.8	24.8	36.1	27.3	156.2	92.3	261.3	168.9
	Ga	32.7	26.8	24.8	4.6	37.7	12.8	55.0	23.4	16.3	5.3
	Nb	41.0	20.3	30.8	10.5	54.3	57.6	145.6	85.5	9.4	2.2
	Zr	412.1	119.3	468.4	72.9	696.2	288.4	594.0	295.8	212.9	97.9
	Y	1678.5	617.2	78.22	41.2	91.8	44.4	310.0	200.9	49.9	12.9
	Th	39.4	25.5	32.2	16.5	51.3	50.5	43.9	29.1	14.7	38.9
	U	2045.4	4000.9	2784.9	3158.9	977.1	812.9	5649.6	7409.3	2033.0	1916.3
	La	90.8	59.1	115.2	47.6	85.8	29.6	n.a.	---	n.a.	---
	Ce	193.2	198.2	166.0	79.5	115.3	123.6	n.a.	---	n.a.	---



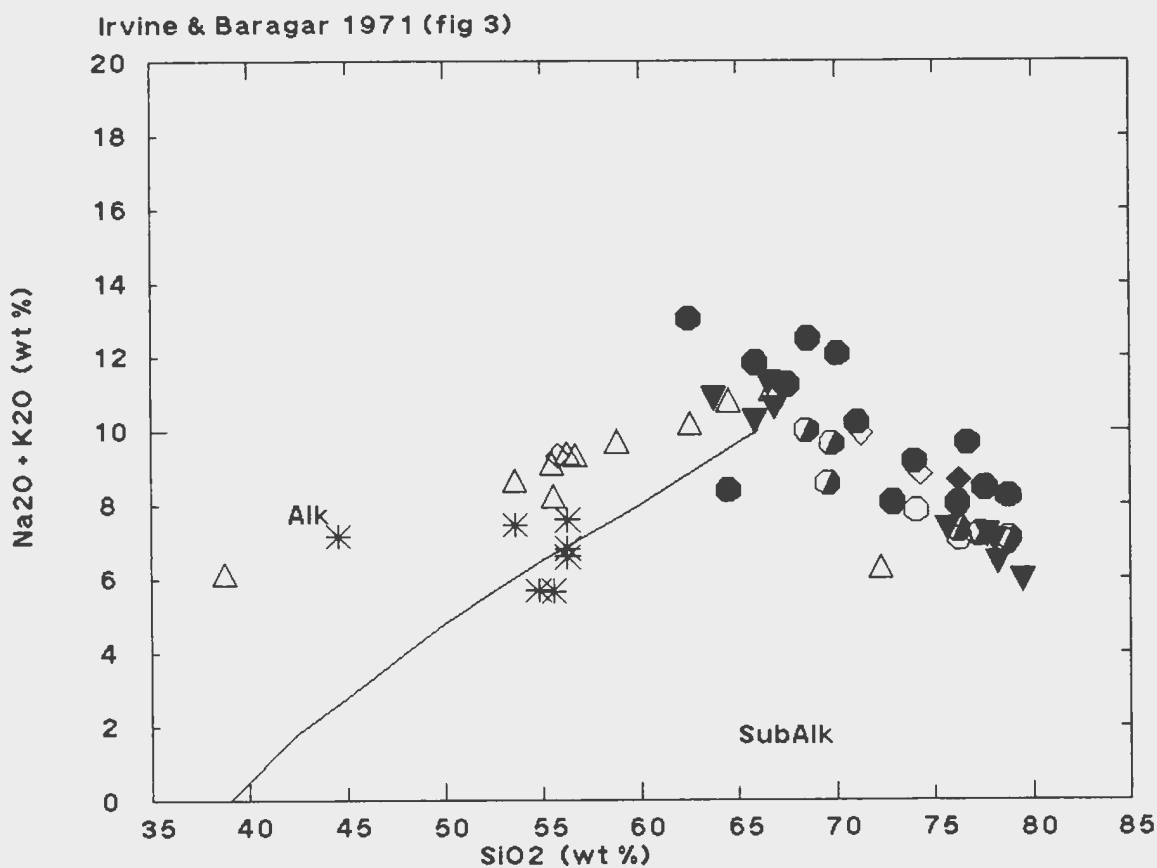


**Figure 5-14: Total alkalis (Na<sub>2</sub>O + K<sub>2</sub>O) vs SiO<sub>2</sub> diagram for mineralized rocks from the Upper Aillik Group, Burnt Lake region with fields from Irvine and Baragar (1971). Symbols as follows: solid triangle: tuffaceous sedimentary rocks and rhyolite tuff from the Emben Main, Emben Central and Emben West showings; open triangle: biotite-feldspar dykes and tuffaceous rocks from the Emben South showing; asterisk: andesite from Aurora River; open circle: bedded ash tuff from the Burnt Lake Showings; half-filled circle: non-porphyritic to slightly porphyritic ash tuff (Burnt Lake); solid circle: quartz and feldspar porphyritic rhyolite (Burnt Lake); open diamond: tufficite, breccia (Burnt Lake); solid diamond: feldspar porphyry (Burnt Lake).**

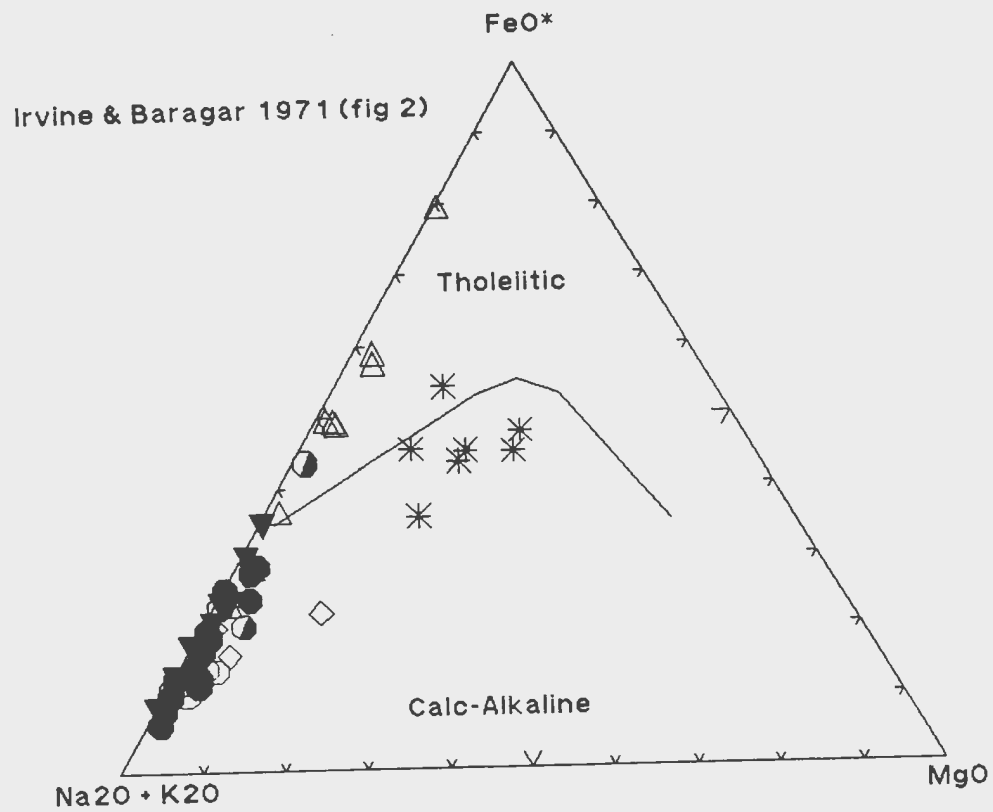


**Figure 5-15:** A (Na<sub>2</sub>O + K<sub>2</sub>O) F (total FeO) M (MgO) diagram with Irvine and Baragar's (1971) fields. Symbols as in Figure 5-14.

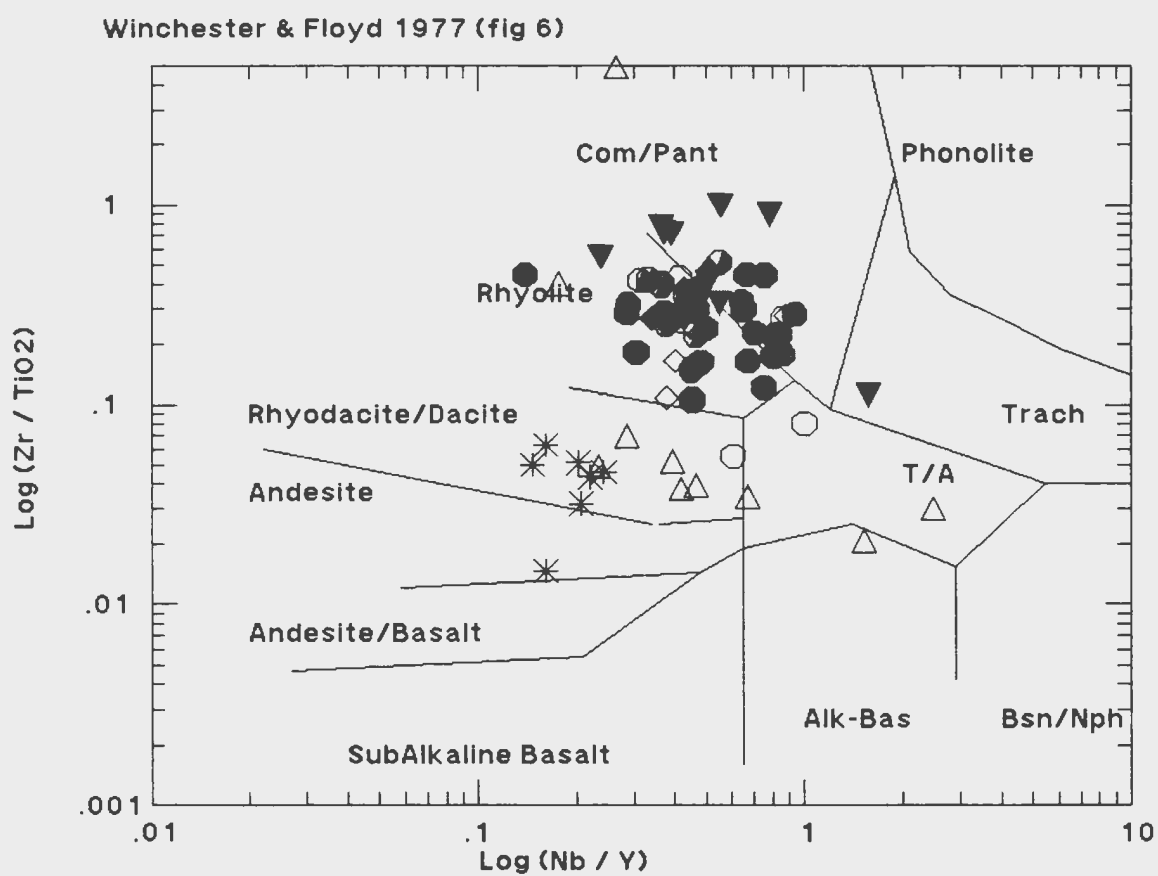


**Figure 5-16:  $\text{Zr/TiO}_2$  vs  $\text{Nb/Y}$  diagram showing distribution of mineralized samples of the Upper Aillik Group. Fields from Winchester and Floyd (1977). Symbols as in Figure 5-14.**

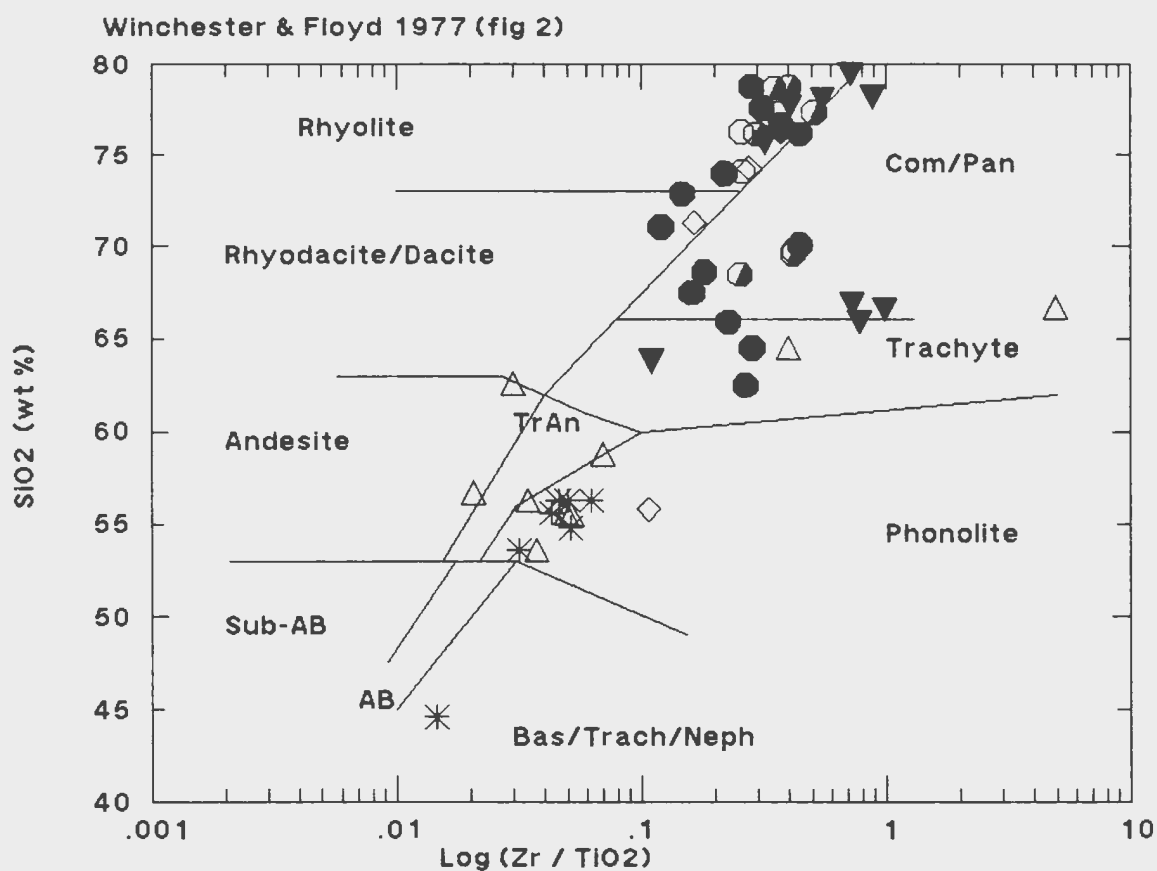


**Figure 5-17: SiO<sub>2</sub> vs Zr/TiO<sub>2</sub> diagram of mineralized samples of the UAG. Fields from Winchester and Floyd (1977). Symbols as in Figure 5-14.**

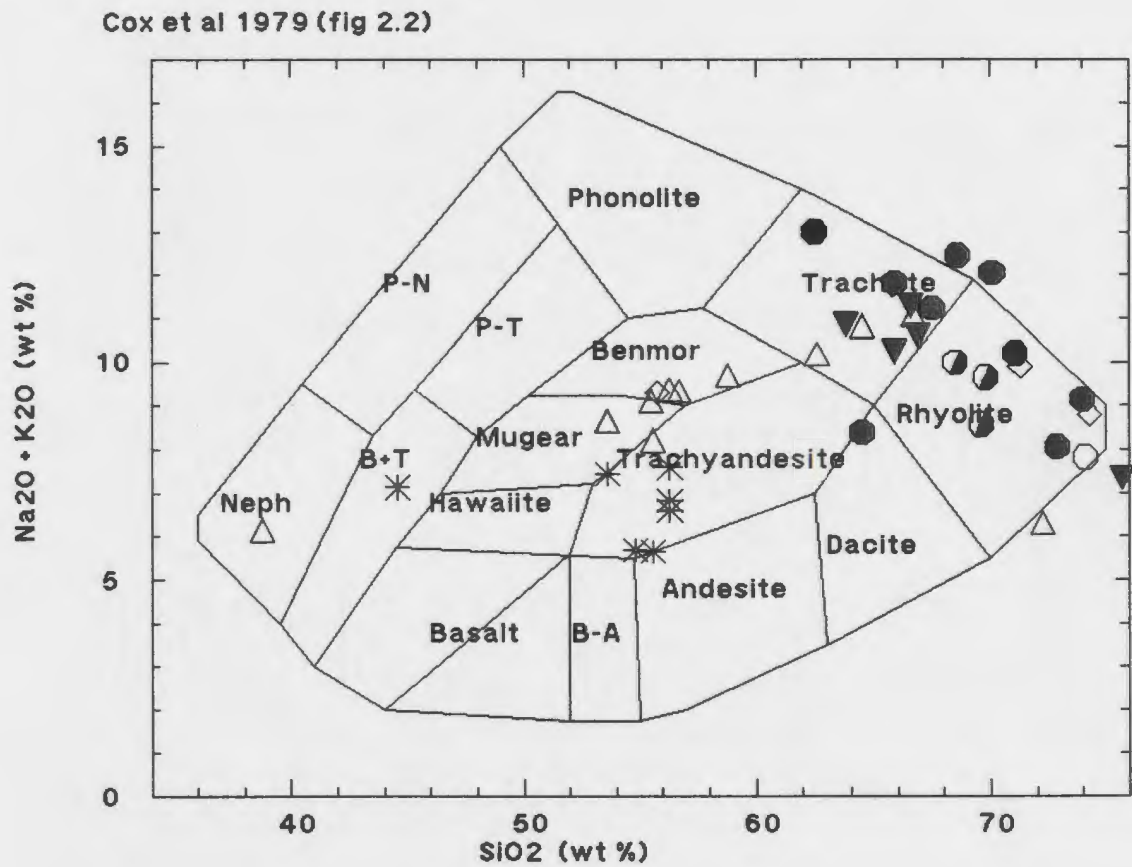
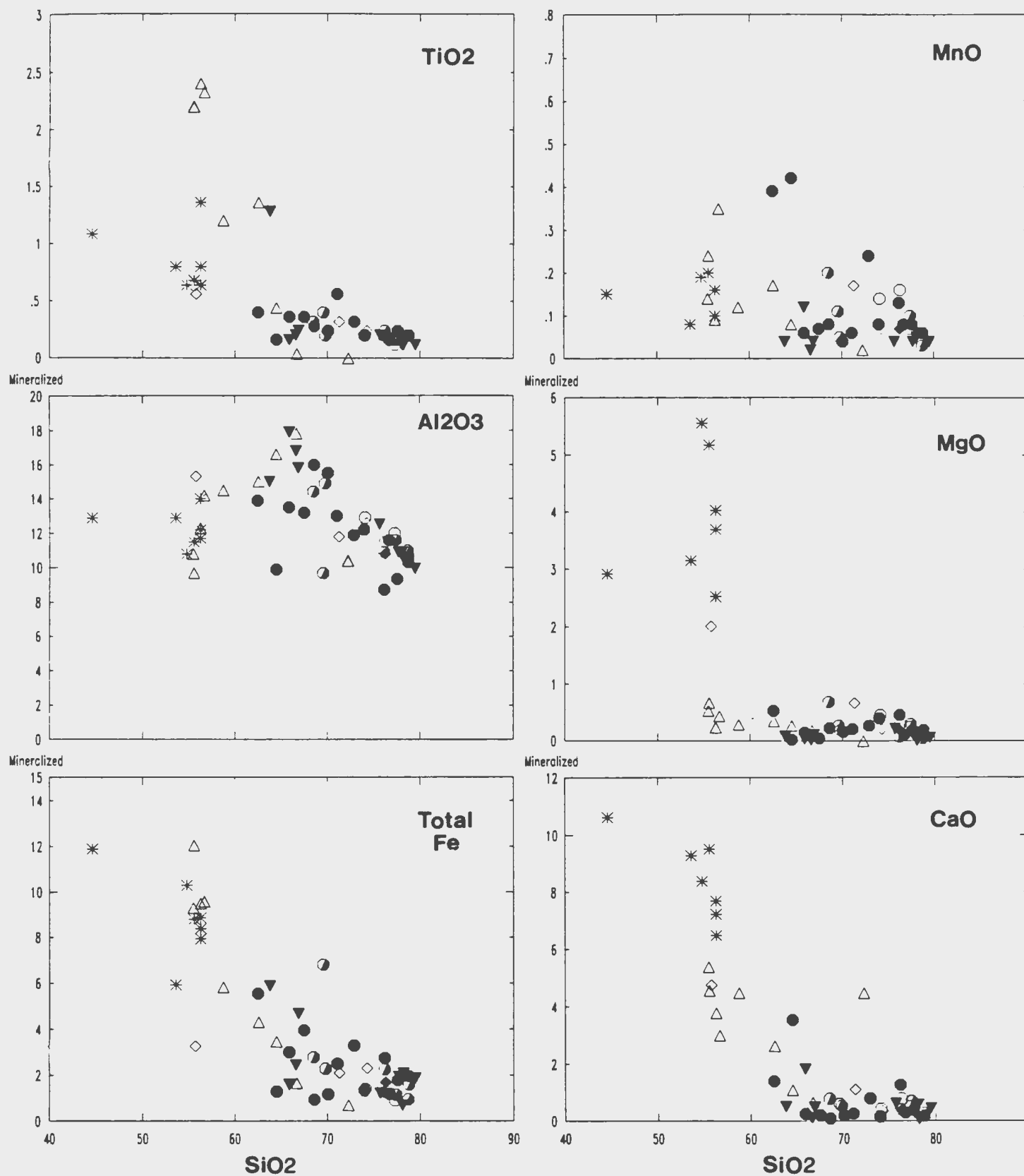


Figure 5-18:  $K_2O + Na_2O$  vs  $SiO_2$  plot showing classification fields of Cox et al., 1979. Symbols as in Figure 5-14.

### 5.5.1 Major Element Patterns

Figure 5-19 shows the distribution of major elements versus silica for all mineralized samples. Differences in major element geochemistry between the various mineralized units are sometimes subtle. The Burnt Lake (sodic) samples have the highest average  $\text{SiO}_2$  contents (75.36%) followed by Emben Main (72.49 wt.%) and Burnt Lake Potassic (71.58 wt.%). Emben South and Aurora River have the lowest mean  $\text{SiO}_2$  values and the highest  $\text{CaO}$ ,  $\text{FeO}$ ,  $\text{TiO}_2$  and  $\text{P}_2\text{O}_5$  values reflecting their mafic to intermediate compositions. Excluding the Burnt Lake Potassic samples, all mineralized samples have elevated  $\text{Na}_2\text{O}$  values (typically > 7%) and extremely low  $\text{K}_2\text{O}$  values (< 0.2%). Generally,  $\text{MgO}$  values are similar (< 0.3%) in all showings except for Aurora River showing with mean values of nearly four weight percent.

The  $\text{K}_2\text{O}$  versus  $\text{Na}_2\text{O}$  plot of the mineralized samples (Figure 5-20) shows an inverse relationship between the two alkalies in the quartz-feldspar porphyries from the Burnt Lake Showings (unit 4b, Map 2). This wide range of values is attributable to different intensities of metasomatic alteration. On the other hand, all other mineralized rock suites have suffered intense Na-metasomatism with a near total loss of potassium.



**Figure 5-19: Harker variation diagrams of mineralized samples from the Burnt Lake area of the UAG. Oxides are in weight percent. Symbols as in Figure 5-14.**

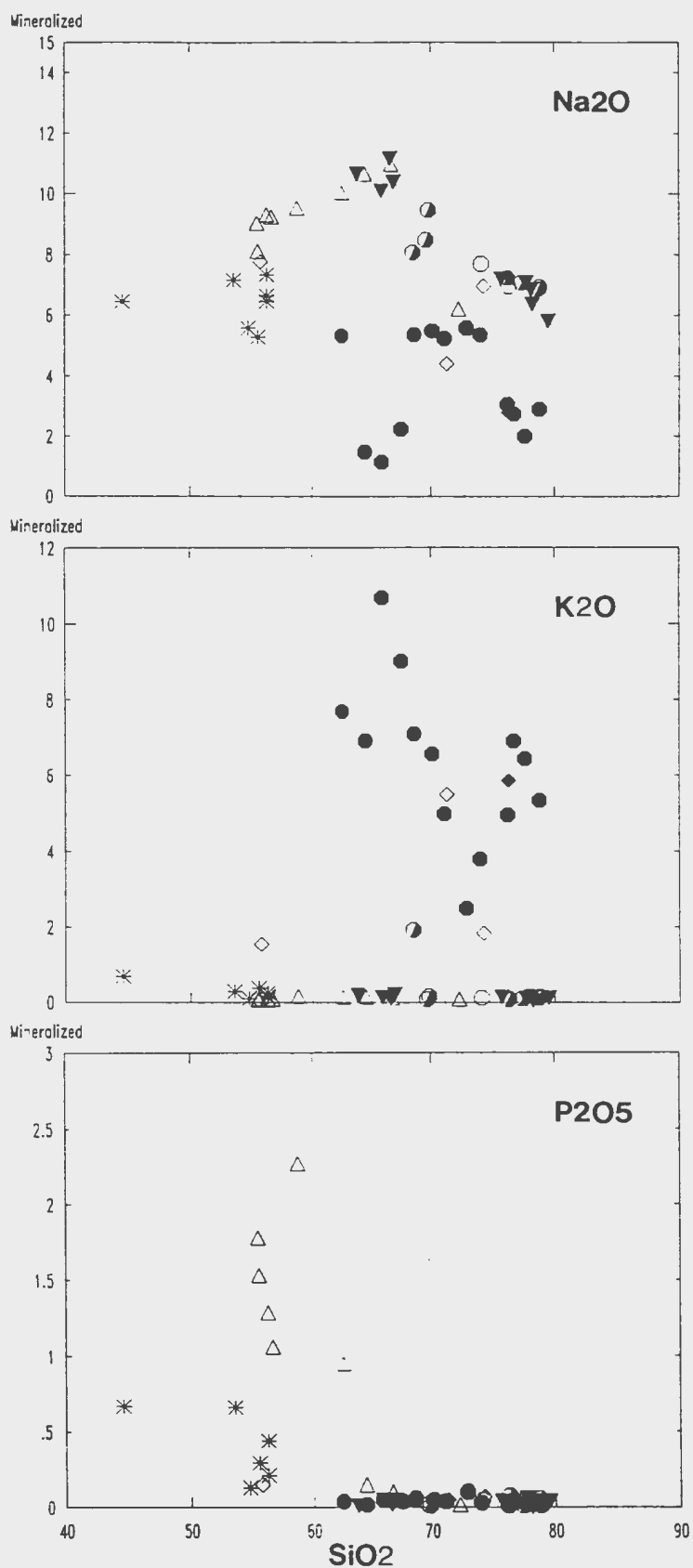


Figure 5-19: (Continued)



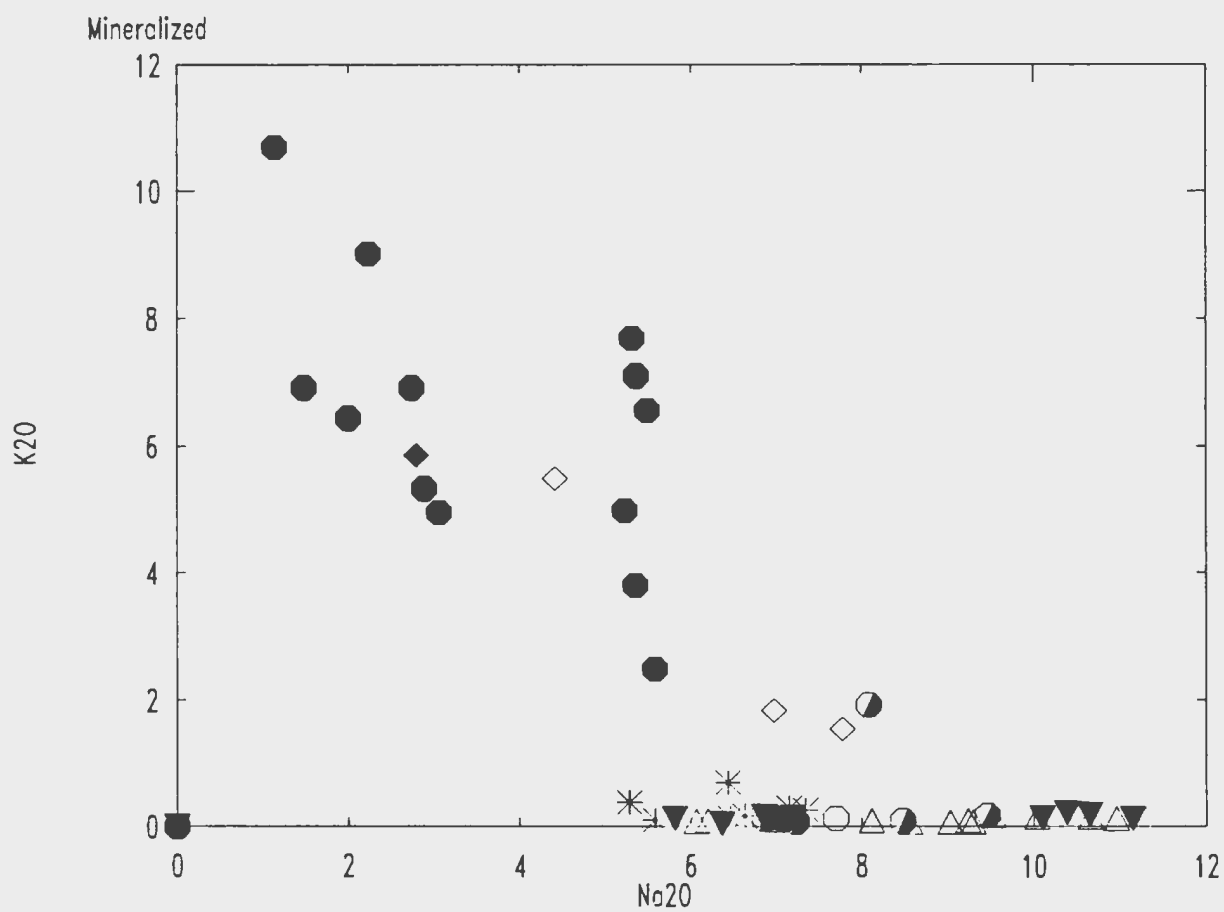


Figure 5-20:  $K_2O$  vs  $Na_2O$  plot for mineralized rocks of the UAG in the Burnt Lake area. Oxides in weight percent. Symbols as in Figure 5-14.

### 5.5.2 Trace Element Patterns

The variability of uranium contents in the five mineralized suites is shown as a frequency distribution of uranium on Figure 5-21. Figure 5-21A shows a log-normal distribution for all mineralized samples. Figure 5-21B shows at least two populations in the potassic suite, a minor population with low values and the main population with high values. Figures 5-21C and 5-21D both show two populations. Figure 5-21E is skewed to the right reflecting anomalous higher grade samples. Figure 5-21F shows a bimodal population with the minor population of low values and a larger population of higher values. The diagrams show that uranium mineralization is more intense in the Emben Main (D) and Aurora River (F) showings than in Emben South (E). The potassic suite (B) is slightly more U-enriched than the sodic suite (C).

Table 5-1 lists the average values for 24 trace elements from the different showings. The trace elements were plotted against uranium in an attempt to compare chemical associations within each of the radioactive occurrences (Figure 5-22). Some trace distributions are different in each of the mineralized rock suites. There is a positive correlation in all showings between Pb and U suggesting that Pb is radiogenic (discussed further in the Pb isotope section below). The Burnt Lake Potassic and Emben South samples have the highest average Pb,

Zn, and Mo values. The potassic suite also has the highest Rb and Y values. Ni and Sr contents are the highest in Emben South and Aurora River Showings. Cu is most concentrated in Burnt Lake Sodic and Emben South suites. V is the lowest in Emben South and Emben Main samples. There is little variation in the incompatible elements (Y, Zr, Ga, Th and Nb) with increasing uranium contents, indicating that these elements were not mobile during uranium mineralization, however, Nb and Y are highest in Emben South and lowest in Aurora River.

There appears to be two separate geochemical trends in K, Rb and Ba distributions with respect to uranium mineralization indicating two different metasomatic trends. Interelement trends between Rb, K, Ba and Sr can characterize partitioning trends of a late-stage magmatic system. The K/Rb ratio is widely used as a differentiation index for granitic rocks and shows a distinction between the suites (Figure 5-23) (Taylor, 1965). The cluster of samples in the top of the diagram comprise predominantly quartz-feldspar porphyries of the Burnt Lake Potassic suite and K/Rb ratio ranges between 300 to 450 and resembles a normal volcanic/magmatic signature (Taylor, 1965). The cluster of samples in the middle of the diagram comprises the Burnt Lake Sodic, Emben South, Emben Main and Aurora River Showings and has K/Rb ratios ranging from 450 to 10 reflecting Rb enrichment over K. The two groups define two separate chemical trends (i.e. evolutions) that do not appear to be related. Kerrich (1989) has related similar geochemical

trends involving crystal fractionation of biotite, K-feldspar and plagioclase to late-stage magmatic processes.

Therefore, the potassic suite plots as a normal granite trend, while the sodic suite, which shows Rb decoupled from K, reflects trends similar to magmatic fluids derived from a late-stage granite. Wilton (1985) suggested that volatile rich magmas (late-stage) would plot off the normal granite trend (Taylor, 1965).

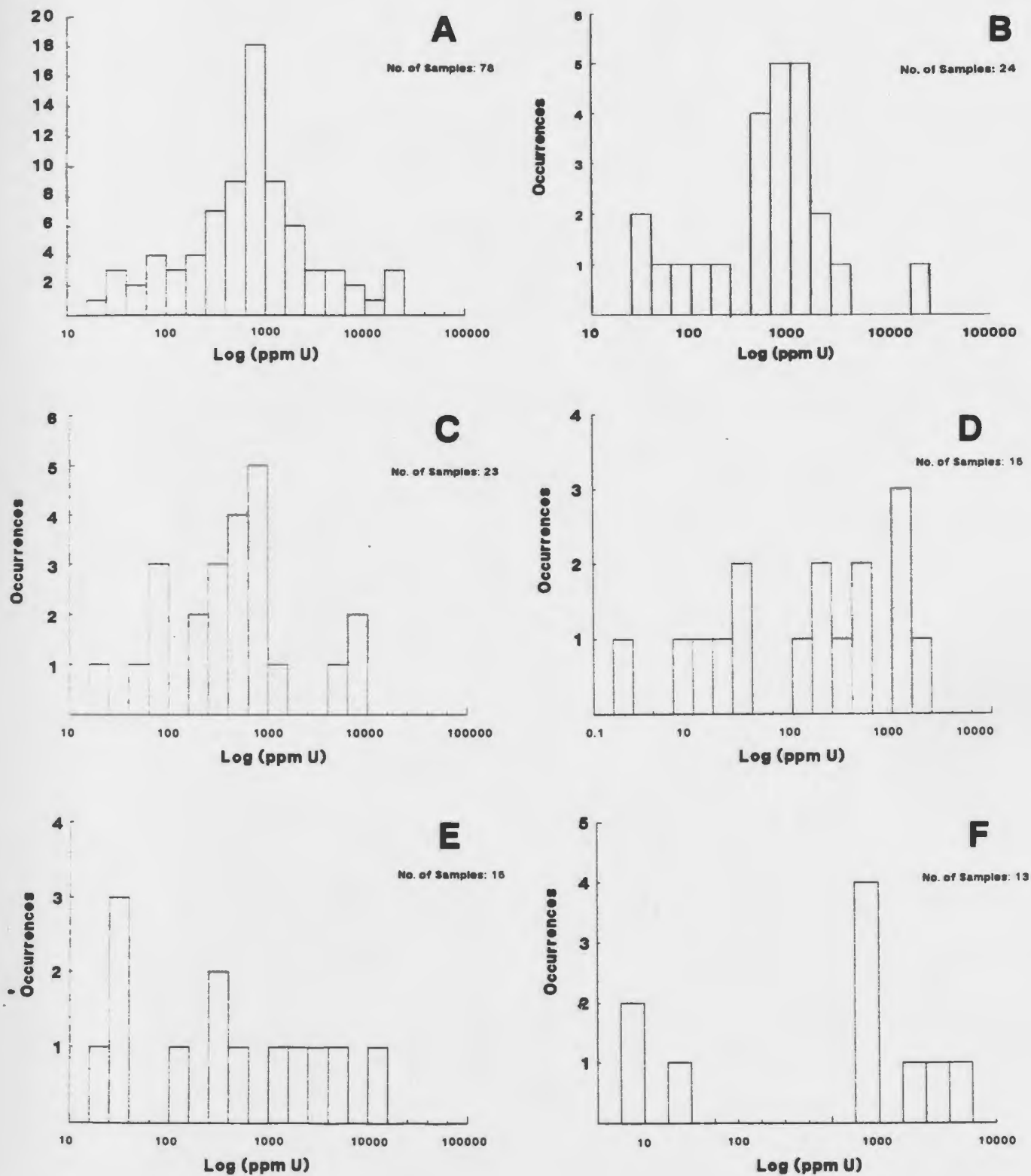


**Figure 5-21: Frequency distribution of uranium in: (A) all mineralized samples; (B) Burnt Lake potassic suite; (C) Burnt Lake sodic suite; (D) Emben Main suite; (E) Emben South suite; (F) Aurora River suite.**

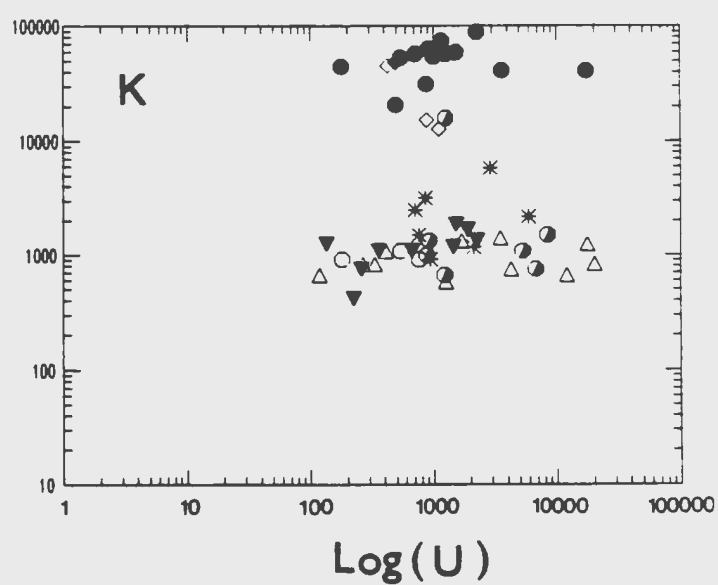
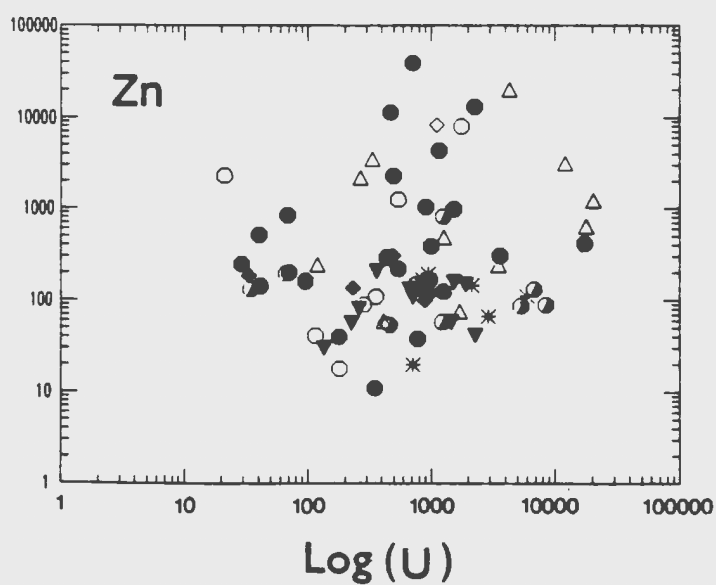
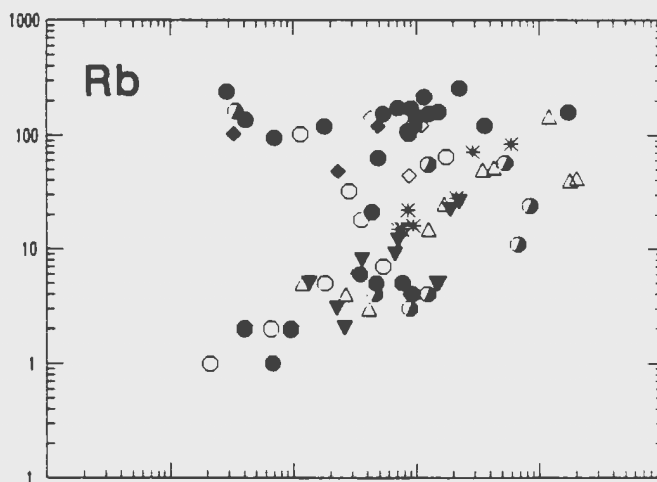
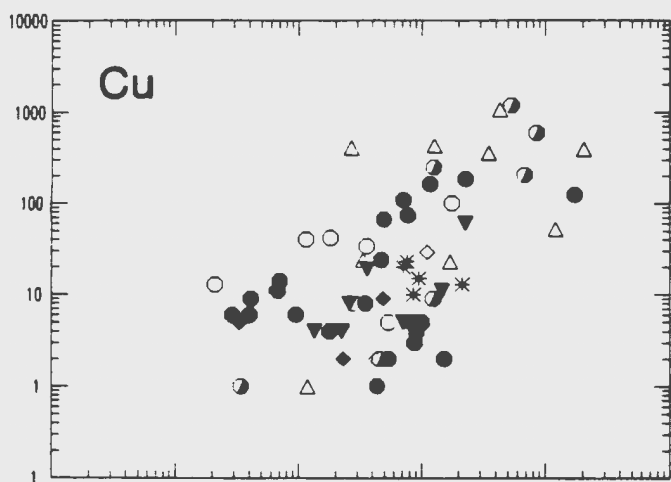
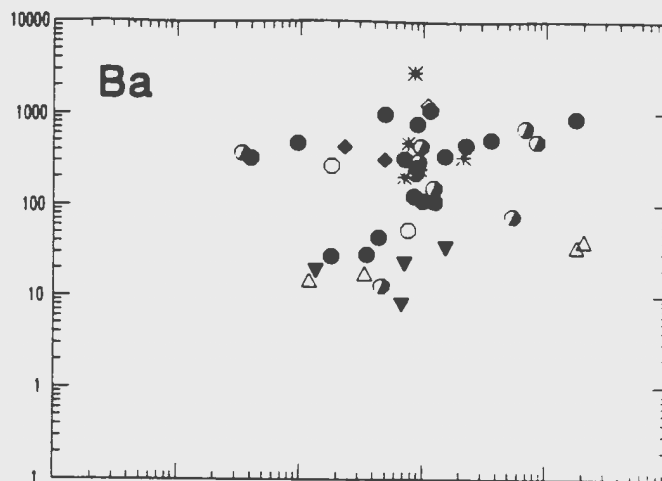
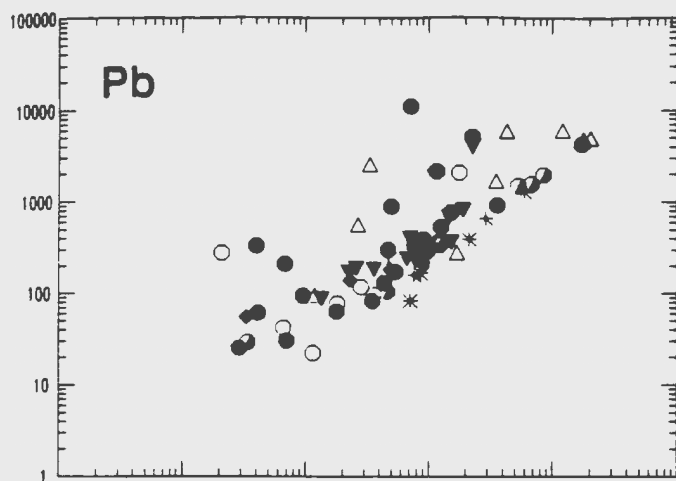
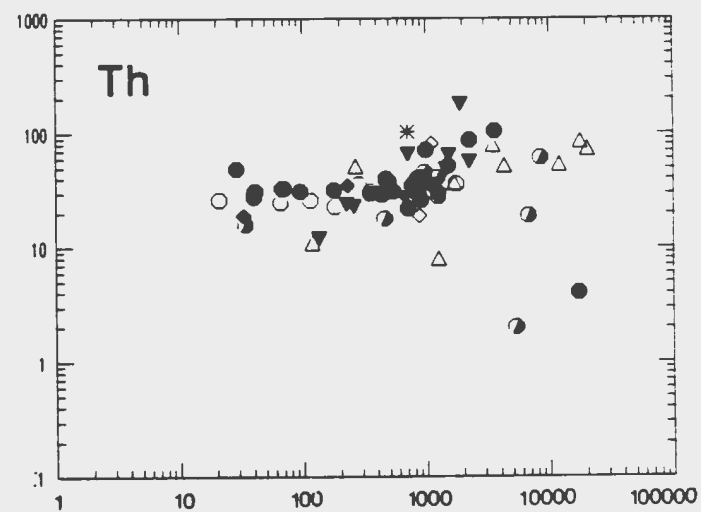
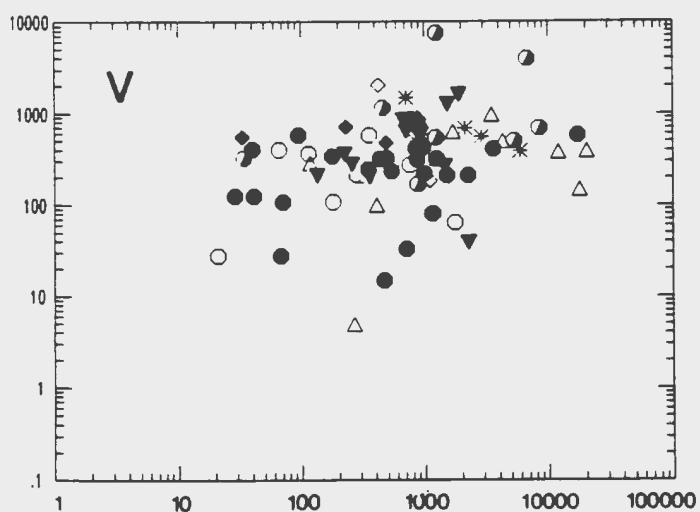
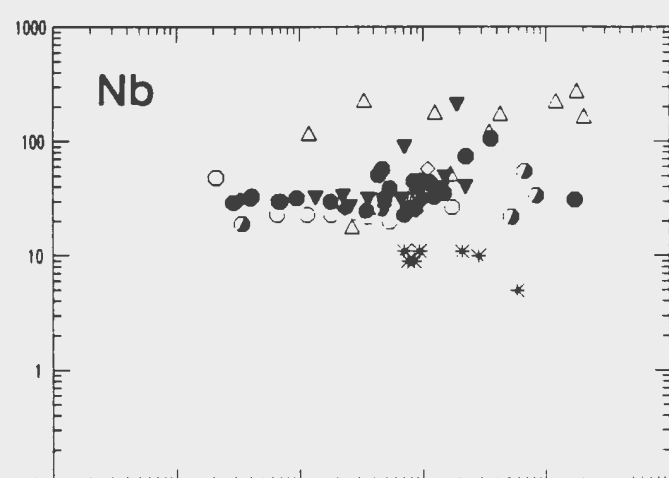
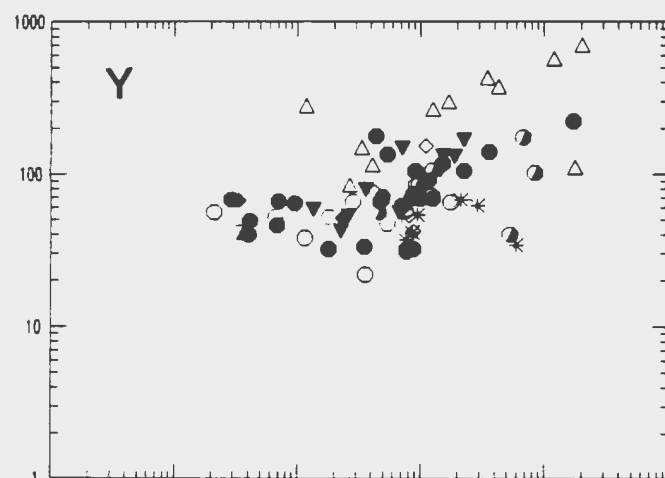
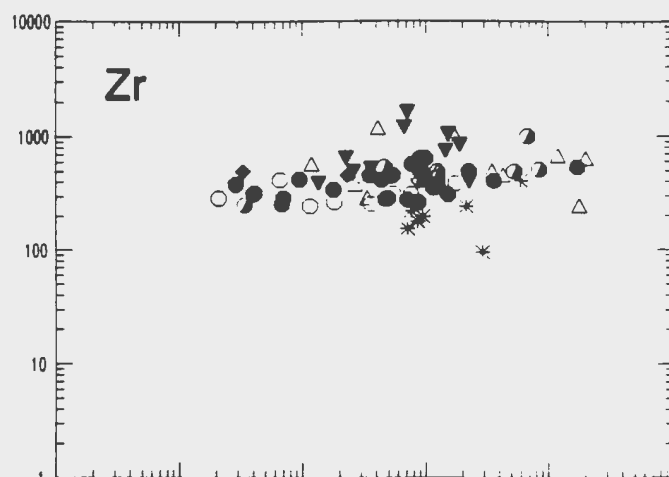
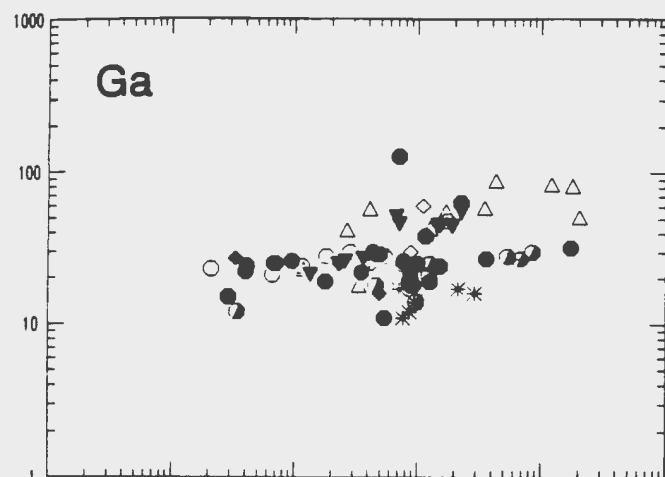


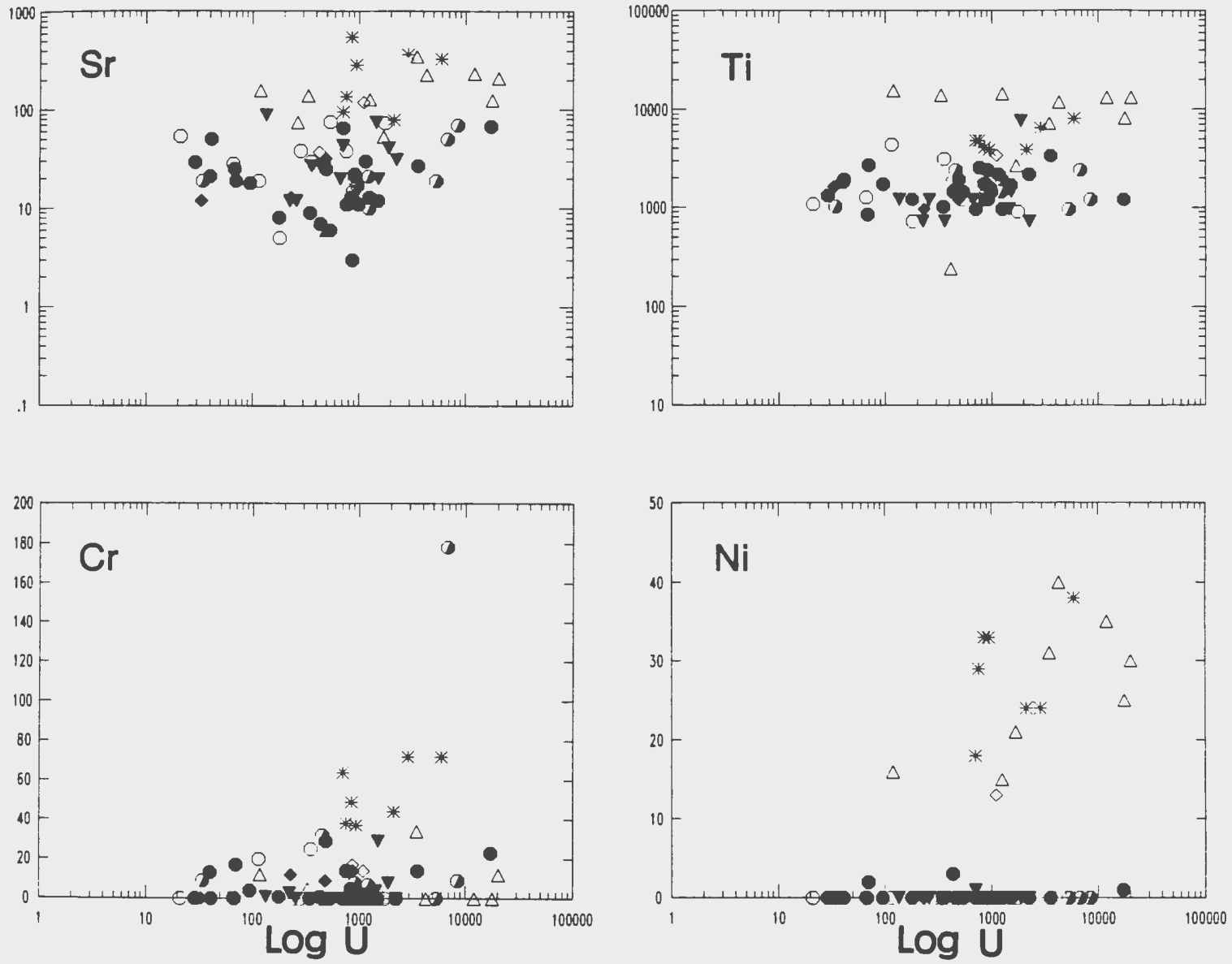
**Figure 5-22: Harker variation diagrams of trace elements vs uranium for all mineralized rocks from the Burnt Lake area of the UAG. Symbols as in Figure 5-14.**



Log(U)

Log(U)

**Figure 5-22: (Continued)**

**Figure 5-22: (Continued)**



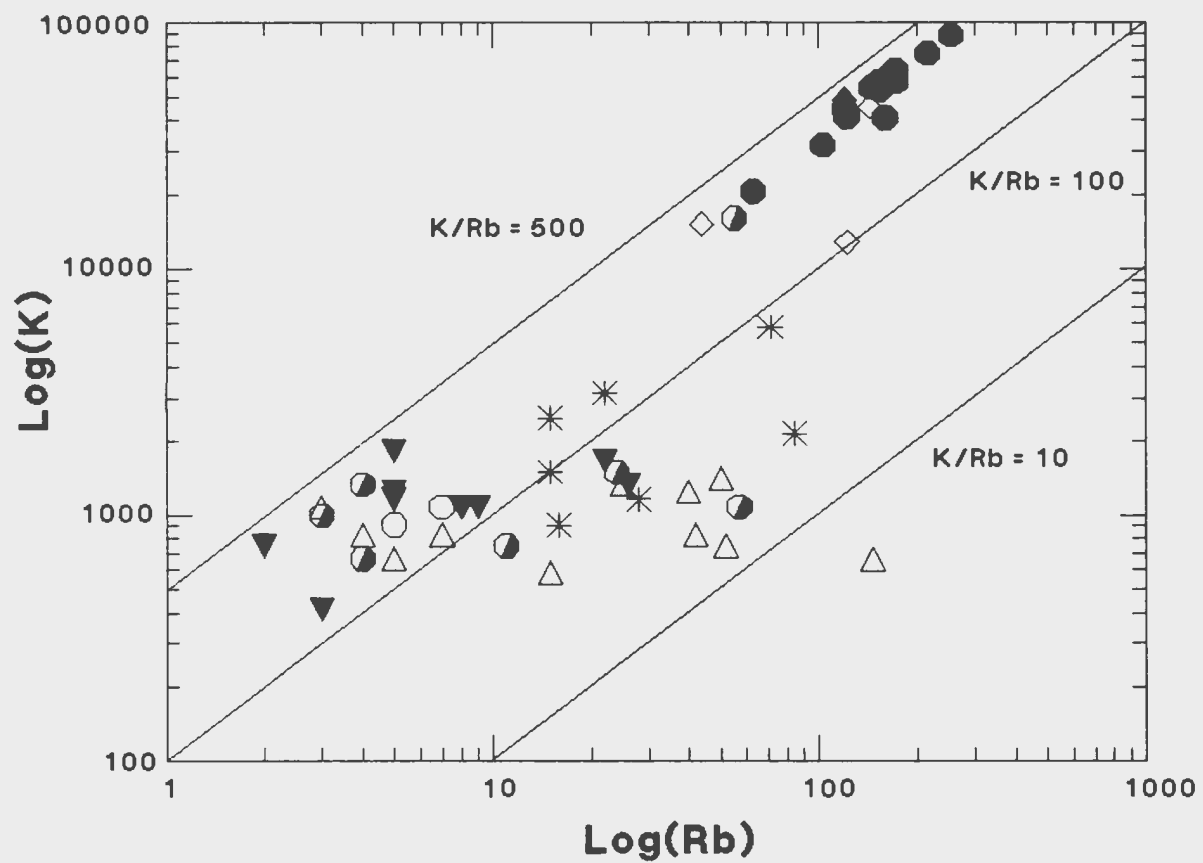


**Figure 5-23: K vs Rb diagram for mineralized samples from the UAG in the Burnt Lake area. Symbols as in Figure 5-14.**

### 5.5.3 Statistical Interpretation

General geochemical behaviour between elements can be described by simple linear correlation for the Burnt Lake (Sodic), Emben South, Emben Main and Aurora River showings as listed in Tables 5-2 to 5-5. The Burnt Lake Sodic suite shows strong correlations between U,  $\text{Na}_2\text{O}$ , Pb and As and negative correlations with  $\text{SiO}_2$  and  $\text{P}_2\text{O}_5$ . These element associations reflect the sodium metasomatism and uranium mineralization. The Emben Main suite shows a different association of uranium with Rb, Ga, Y and Pb reflecting the association of uranium with feldspars. In the Emben South suite, uranium is only directly correlated Th and Pb, however, Pb is also positively correlated with Rb, Ga and Ni (the association of uranium with feldspars). The other base metals (Cu and Zn) are negatively correlated with  $\text{Na}_2\text{O}$  and  $\text{SiO}_2$  and show no correlation with uranium. Uranium in the Aurora River suite is positively correlated with  $\text{TiO}_2$ , Pb, As, Rb and Ga and negatively correlated with Cu.

The Burnt Lake (potassic) data set (9 samples) has, however, been treated by factor analysis and varimax rotation (using SPSS statistics program) to subdivide the various inter-element relationships (Table 5-4). The trace element data were log-transformed to compensate for asymmetric frequency distribution. The four-factor model explains 87% of the total variance within the data set.

Factor 1 (CaO, Pb, Zn, Ga, MnO, Sr) accounts for 40% of the total variance within the data set and represents the enrichments that accompanied the base metal mineralizing event that is possibly related to carbonate alteration.

Factor 2 ( $K_2O$ , Rb, Ag, -  $Na_2O$ ) accounts for 22% of the total variance and represents the potash metasomatism affecting these rocks and the resulting mineralization.

Factor 3 (Cu, Mo, Ag, -  $SiO_2$ ) accounts for 15% of the total variance and is of uncertain significance. Mo and Ag are part of Factor 2 association, but Cu is not present in other associations. The negative correlation with  $SiO_2$  is similar to Factor 1 association.

Factor 4 (U, Y, Sr) only accounts for 10% of the total variance and probably represents the remaining influence of an earlier uraniferous mineralizing event. Sr is also part of the Factor 1 association and represents a disturbance in the feldspars during mineralization.

**Table 5-2: Correlation matrix of selected major and trace elements for the Burnt Lake Sodic rock suite. Values greater than 0.75 are significant at the 2% level.**

Sample Correlations														
Na2O	K2O	P2O5	FeO	Cu	V	Zr	Rb	Ga	Nb	Y	As	Pb	U	
-.9373 ( 9) .0002	-.0876 ( 9) .8226	.4749 ( 9) .1964	-.7292 ( 9) .0258	-.1725 ( 9) .6572	-.6749 ( 9) .0461	-.6099 ( 9) .0811	-.0957 ( 9) .8066	-.6355 ( 9) .0659	-.5894 ( 9) .0949	-.6879 ( 9) .0405	-.8507 ( 9) .0036	-.7135 ( 9) .0309	-.7629 ( 9) .0168	SiO2
1.0000 ( 9) .0000	.3700 ( 9) .3270	-.5959 ( 9) .0904	.5466 ( 9) .1278	.2761 ( 9) .4721	.4840 ( 9) .1867	.4943 ( 9) .1762	.1766 ( 9) .6495	.5955 ( 9) .0907	.4778 ( 9) .1933	.5952 ( 9) .0908	.9035 ( 9) .0008	.7724 ( 9) .0147	.8235 ( 9) .0064	Na2O
	1.0000 ( 9) .0000	-.4775 ( 9) .1936	-.3269 ( 9) .3905	.3273 ( 9) .3900	-.3287 ( 9) .3877	-.1638 ( 9) .6737	.2803 ( 9) .4651	.1345 ( 9) .7301	-.2718 ( 9) .4793	-.1128 ( 9) .7727	.3463 ( 9) .3613	.3260 ( 9) .3918	.3201 ( 9) .4011	K2O
		1.0000 ( 9) .0000	-.3441 ( 9) .3645	-.7427 ( 9) .0219	-.3948 ( 9) .2930	-.5096 ( 9) .1611	-.6890 ( 9) .0401	-.5407 ( 9) .1328	-.2319 ( 9) .5482	-.3503 ( 9) .3553	-.6767 ( 9) .0453	-.7968 ( 9) .0101	-.8008 ( 9) .0095	P2O5
			1.0000 ( 9) .0000	-.0048 ( 9) .9901	.9868 ( 9) .0000	.9356 ( 9) .0002	-.0522 ( 9) .8939	.1890 ( 9) .6262	.9173 ( 9) .0005	.9303 ( 9) .0003	.6116 ( 9) .0801	.5185 ( 9) .1527	.5734 ( 9) .1065	FeO
				1.0000 ( 9) .0000	.0632 ( 9) .8717	.2096 ( 9) .5883	.9903 ( 9) .0000	.4967 ( 9) .1738	-.1117 ( 9) .7749	-.0929 ( 9) .8121	.4651 ( 9) .2071	.7492 ( 9) .0201	.6820 ( 9) .0430	Cu
					1.0000 ( 9) .0000	.9539 ( 9) .0001	.0242 ( 9) .9508	.2020 ( 9) .6022	.8926 ( 9) .0012	.9087 ( 9) .0007	.5741 ( 9) .1059	.5319 ( 9) .1405	.5764 ( 9) .1043	V
						1.0000 ( 9) .0000	.1598 ( 9) .6813	.0789 ( 9) .8402	.9073 ( 9) .0007	.9131 ( 9) .0006	.6297 ( 9) .0691	.6427 ( 9) .0619	.6789 ( 9) .0443	Zr
							1.0000 ( 9) .0000	.4785 ( 9) .1926	-.1869 ( 9) .6301	-.1736 ( 9) .6551	.3663 ( 9) .3322	.6736 ( 9) .0467	.5965 ( 9) .0900	Rb
								1.0000 ( 9) .0000	-.1044 ( 9) .7893	.0214 ( 9) .9565	.5305 ( 9) .1417	.5419 ( 9) .1318	.5319 ( 9) .1405	Ga
									1.0000 ( 9) .0000	.9721 ( 9) .0000	.5674 ( 9) .1111	.4586 ( 9) .2144	.5245 ( 9) .1472	Nb
										1.0000 ( 9) .0000	.6530 ( 9) .0565	.5154 ( 9) .1556	.5871 ( 9) .0965	Y
											1.0000 ( 9) .0000	.9040 ( 9) .0008	.9350 ( 9) .0002	As
												1.0000 ( 9) .0000	.9930 ( 9) .0000	Pb
													1.0000 ( 9) .0000	U

SiO<sub>2</sub>[illegible]

**Table 5-4: Correlation matrix of selected major and trace elements for the Emben South rock suite. Values greater than 0.68 are significant at the 2% level.**

Table Correlations														
	Na2O	K2O	P2O5	TiO2	Rb	Th	Ga	Ni	Y	Cu	Zn	Pb	U	
0	.3833	.4237	-.6865	-.7332	-.3278	.0781	-.2631	-.6474	-.4763	-.5912	-.7477	-.5571	-.1246	SiO2
1	( .11)	( .11)	( .11)	( .11)	( .11)	( .11)	( .11)	( .11)	( .11)	( .11)	( .11)	( .11)	( .11)	
9	.2446	.1941	.0196	.0102	.3251	.8194	.4344	.0313	.1386	.0554	.0082	.0750	.7152	
0	.2244	-.2049	.4683	.6799	.3323	-.0043	-.1872	.3031	.6138	-.4010	-.2897	.3386	.5369	MgO
0	( .11)	( .11)	( .11)	( .11)	( .11)	( .11)	( .11)	( .11)	( .11)	( .11)	( .11)	( .11)	( .11)	
0	.5071	.5456	.1462	.0214	.3180	.9899	.5816	.3649	.0446	.2217	.3875	.3084	.0886	
	1.0000	.5240	-.1685	-.1707	-.0477	-.1127	-.0532	-.1854	-.1509	-.7496	-.6502	-.3189	.0070	Na2O
	( .11)	( .11)	( .11)	( .11)	( .11)	( .11)	( .11)	( .11)	( .11)	( .11)	( .11)	( .11)	( .11)	
	.0000	.0980	.6204	.6157	.8893	.7414	.8766	.5853	.6578	.0079	.0303	.3392	.9837	
		1.0000	-.1506	-.6040	-.1039	.5109	.2279	.0578	-.1706	-.2658	-.2977	-.1616	.0732	K2O
		( .11)	( .11)	( .11)	( .11)	( .11)	( .11)	( .11)	( .11)	( .11)	( .11)	( .11)	( .11)	
		.0000	.6586	.0491	.7611	.1082	.5002	.8659	.6160	.4295	.3739	.6351	.8307	
			1.0000	.7064	.5666	.2742	.2421	.7201	.6735	.3408	.2609	.5403	.3455	P2O5
			( .11)	( .11)	( .11)	( .11)	( .11)	( .11)	( .11)	( .11)	( .11)	( .11)	( .11)	
			.0000	.0151	.0692	.4145	.4733	.0124	.0231	.3050	.4383	.0862	.2980	
				1.0000	.2899	-.2681	-.1447	.3963	.4717	.1293	.2074	.4198	.2591	TiO2
				( .11)	( .11)	( .11)	( .11)	( .11)	( .11)	( .11)	( .11)	( .11)	( .11)	
				.0000	.3871	.4254	.6712	.2276	.1430	.7048	.5406	.1987	.4416	
					1.0000	.4425	.6720	.7162	.6458	.0643	.2105	.7243	.5181	Rb
					( .11)	( .11)	( .11)	( .11)	( .11)	( .11)	( .11)	( .11)	( .11)	
					.0000	.1730	.0235	.0132	.0319	.8510	.5344	.0117	.1026	
						1.0000	.6839	.5801	.3562	.2064	.0589	.5307	.6986	Th
						( .11)	( .11)	( .11)	( .11)	( .11)	( .11)	( .11)	( .11)	
						.0000	.0203	.0614	.2823	.5425	.8634	.0930	.0168	
							1.0000	.7014	.2795	.3405	.4501	.6656	.5028	Ga
							( .11)	( .11)	( .11)	( .11)	( .11)	( .11)	( .11)	
							.0000	.0162	.4053	.3055	.1647	.0254	.1149	
								1.0000	.7370	.4370	.4343	.7017	.5633	Ni
								( .11)	( .11)	( .11)	( .11)	( .11)	( .11)	
								.0000	.0097	.1790	.1820	.0161	.0712	
									1.0000	.2573	.1258	.5346	.5465	Y
									( .11)	( .11)	( .11)	( .11)	( .11)	
									.0000	.4450	.7124	.0902	.0820	
										1.0000	.7981	.3376	-.0198	Cu
										( .11)	( .11)	( .11)	( .11)	
										.0000	.0032	.3099	.9539	
											1.0000	.5419	-.0371	Zn
											( .11)	( .11)	( .11)	
											.0000	.0851	.9137	
												1.0000	.7495	Pb
												( .11)	( .11)	
												.0000	.0079	
													1.0000	U
													( .11)	
													.0000	

**Table 5-5: Correlation matrix of selected major and trace elements for the Aurora River rock suite. Values greater than 0.80 are significant at the 2% level.**

Correlations													
	MgO	Na2O	K2O	Cr	V	Cu	Pb	As	Rb	Ga	Nb	Zr	U
TiO2	-.7661 ( 7) .0446	.6452 ( 7) .1176	.4229 ( 7) .3446	.8119 ( 7) .0266	-.3013 ( 7) .5113	-.7094 ( 7) .0742	.8756 ( 7) .0098	.8274 ( 7) .0216	.9136 ( 7) .0040	.7836 ( 7) .0371	-.7984 ( 7) .0313	.4935 ( 7) .2604	.8836 ( 7) .0083
Al2O3	-.9228 ( 7) .0030	.8522 ( 7) .0149	.3867 ( 7) .3915	.8561 ( 7) .0139	.0771 ( 7) .8695	-.4751 ( 7) .2813	.6665 ( 7) .1020	.6449 ( 7) .1179	.7399 ( 7) .0573	.7498 ( 7) .0523	-.6637 ( 7) .1040	.4108 ( 7) .3599	.7339 ( 7) .0604
MgO	1.0000 ( 7) .0000	-.8978 ( 7) .0061	-.3861 ( 7) .3922	-.8020 ( 7) .0300	-.1774 ( 7) .7035	.4182 ( 7) .3505	-.5778 ( 7) .1743	-.4279 ( 7) .3382	-.6853 ( 7) .0893	-.6920 ( 7) .0849	.4079 ( 7) .3637	-.2723 ( 7) .5547	-.6627 ( 7) .1048
Na2O		1.0000 ( 7) .0000	.0072 ( 7) .9878	.5771 ( 7) .1749	.3863 ( 7) .3921	-.0794 ( 7) .8657	.4521 ( 7) .3084	.2096 ( 7) .6520	.4345 ( 7) .3300	.6691 ( 7) .1003	-.3873 ( 7) .3907	.4262 ( 7) .3404	.5328 ( 7) .2182
K2O			1.0000 ( 7) .0000	.6895 ( 7) .0866	-.1215 ( 7) .7953	-.6010 ( 7) .1535	.1855 ( 7) .6904	.4382 ( 7) .3254	.5276 ( 7) .2236	.0107 ( 7) .9818	-.0489 ( 7) .9171	-.5074 ( 7) .2450	.1869 ( 7) .6882
Cr				1.0000 ( 7) .0000	.0196 ( 7) .9668	-.6988 ( 7) .0806	.6150 ( 7) .1417	.6911 ( 7) .0855	.7869 ( 7) .0358	.6827 ( 7) .0910	-.4397 ( 7) .3236	.0916 ( 7) .8451	.6590 ( 7) .1074
V					1.0000 ( 7) .0000	.6720 ( 7) .0982	-.5869 ( 7) .1660	-.6076 ( 7) .1479	-.5316 ( 7) .2194	-.1963 ( 7) .6731	.5045 ( 7) .2482	-.3759 ( 7) .4059	-.5184 ( 7) .2332
Cu						1.0000 ( 7) .0000	-.8178 ( 7) .0246	-.8543 ( 7) .0144	-.9146 ( 7) .0039	-.6142 ( 7) .1423	.5282 ( 7) .2229	-.2390 ( 7) .6058	-.7987 ( 7) .0312
Pb							1.0000 ( 7) .0000	.8278 ( 7) .0215	.9289 ( 7) .0025	.8724 ( 7) .0104	-.7754 ( 7) .0405	.6806 ( 7) .0924	.9870 ( 7) .0000
As								1.0000 ( 7) .0000	.8567 ( 7) .0138	.6760 ( 7) .0955	-.8589 ( 7) .0133	.5074 ( 7) .2451	.8310 ( 7) .0206
Rb									1.0000 ( 7) .0000	.7600 ( 7) .0474	-.6791 ( 7) .0934	.4036 ( 7) .3692	.9270 ( 7) .0027
Ga										1.0000 ( 7) .0000	-.6585 ( 7) .1078	.7227 ( 7) .0665	.9078 ( 7) .0047
Nb											1.0000 ( 7) .0000	-.7836 ( 7) .0371	-.7886 ( 7) .0351
Zr												1.0000 ( 7) .0000	.7046 ( 7) .0771
U													1.0000 ( 7) .0000

TABLE 5-6

Varimax Rotated Factor Matrix for the  
Burnt Lake (Potassic) data set. Values greater  
than 0.56 are significant at the 2% level.

(% Var)	(40)	(22)	(15)	(10)
Factor	1	2	3	4
Element				
SiO <sub>2</sub>	-0.484	-0.041	-0.635	0.160
CaO	0.975	-0.012	-0.031	0.110
MnO	0.830	-0.222	0.085	-0.052
Na <sub>2</sub> O	-0.205	-0.915	0.099	-0.105
K <sub>2</sub> O	0.037	0.891	0.238	-0.043
Cu	0.230	-0.038	0.795	0.310
Pb	0.822	0.386	0.254	0.180
Zn	0.869	0.330	0.221	-0.140
Mo	-0.135	0.544	0.742	-0.049
Ag	0.106	0.560	0.790	-0.045
Rb	0.103	0.883	0.276	0.140
Sr	0.706	0.024	-0.250	0.560
U	0.032	0.037	-0.022	0.958
Y	-0.047	0.092	0.145	0.896
Ga	0.863	0.289	0.297	-0.063

## 5.6 Comparison with Non-Mineralized Aillik Group

Studies by others in the area, Watson-White (1976), Minatidis (1976) and Bailey (1978) have indicated that sodium metasomatism was responsible for altering the whole rock geochemistry where uranium mineralization occurred.

Selected trace elements have been plotted against uranium for all samples from the Burnt Lake area and are shown as Figure 5-24. Generally, Pb shows a good correlation with uranium with only a few samples falling off the linear trend, indicating that the lead in rocks >10 ppm U is predominantly



radiogenic. Zn and Cu tend to be positively correlated with uranium but with much more scattering in the data. V is positively correlated with U in the unmineralized rocks but shows no correlation in the mineralized samples. K and Rb are elevated in the unmineralized rocks (i.e. U <10 ppm) while in the mineralized samples (>10 ppm U) both K and Rb separate the data into two fields (Figure 5-24).

It is suggested that alkali metasomatism has altered the UAG rocks regionally (i.e. all rocks have been affected). This is shown by the inverse relationship on a  $K_2O$  versus  $Na_2O$  plot (Figure 5-25) for both mineralized and unmineralized rocks in the Burnt Lake area. It is suggested that the uraniferous mineralization was preceded by Na-metasomatism during an extensive period of metamorphism and granitoid intrusion between 1800 Ma and 1719 Ma (Kerr and Krogh, 1990 and Scharer et al., 1988). The extent and intensity of metasomatic alteration is related in a large part to the permeability of the host rocks and distance from vent areas. The Burnt Lake uranium mineralization was previously dated at 1770 Ma (U-Pb method on uraninites, Kontak, 1980) although this age has since been modified to reflect a resetting event during the Hudsonian (see Kontak in Ryan, 1984). Another period of plutonism and metasomatism occurred at 1650 Ma and produced granophile (Pb, Zn, Mo) mineralization associated with potash metasomatism.

Other diagrams have been constructed to show the two separate metasomatic trends. Figure 5-26 is a plot of  $\text{Na}_2\text{O}$  vs Rb and shows a wide scattering of values for the "sodic" rocks, while for the "potassic suite"  $\text{Na}_2\text{O}$  is inversely correlated with Rb. At the same time, K is strongly correlated with Rb for the "potassic" rocks while showing no correlation in the "sodic suite" (Figure 5-27). The K/Rb ratio clearly demonstrates the two metasomatic trends (i.e. evolutions) and mineralizing events in the Burnt Lake area. Figures 5-28 and 5-29 separate the data set into two groups: the first group is associated with potassic metasomatism and mineralization is related to syngenetic leaching of the host felsic volcanic rocks. The second group shows a disturbance in the K/Rb ratio and mineralization is associated with sodic metasomatism related to magmatic fluids derived from a late-stage granite.

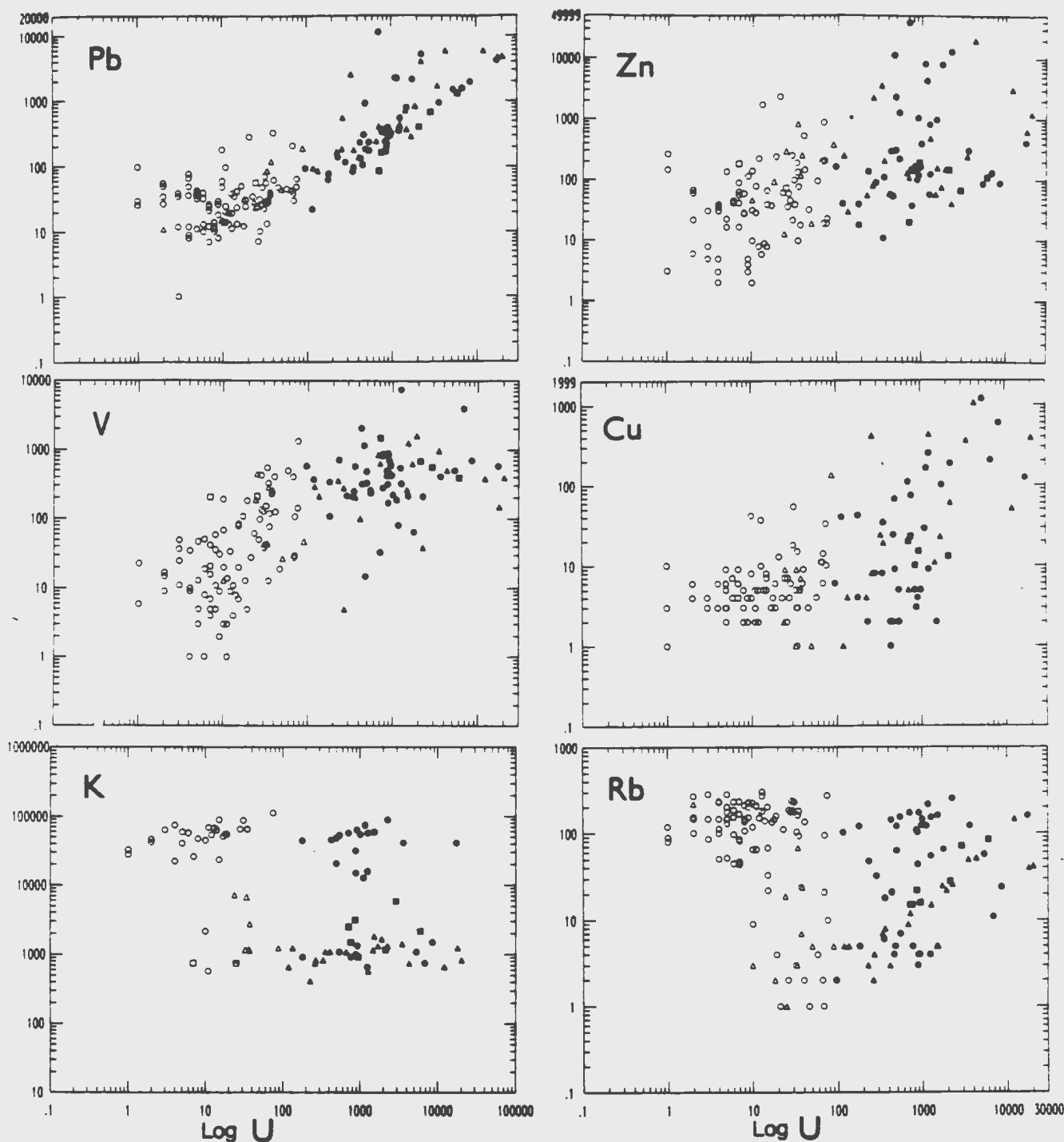


**Figure 5-24: Harker variation diagrams for selected trace elements vs uranium. Symbols as follows: open circle: unmineralized felsic volcanic rocks from the Burnt Lake area; solid circle: mineralized rocks from the Burnt Lake Showings; open triangle: unmineralized rocks from the Emben area; solid triangle: mineralized rocks from the Emben Showings; open box: unmineralized andesite from the Aurora River Showings; solid box: mineralized andesite from the Aurora River Showings.**

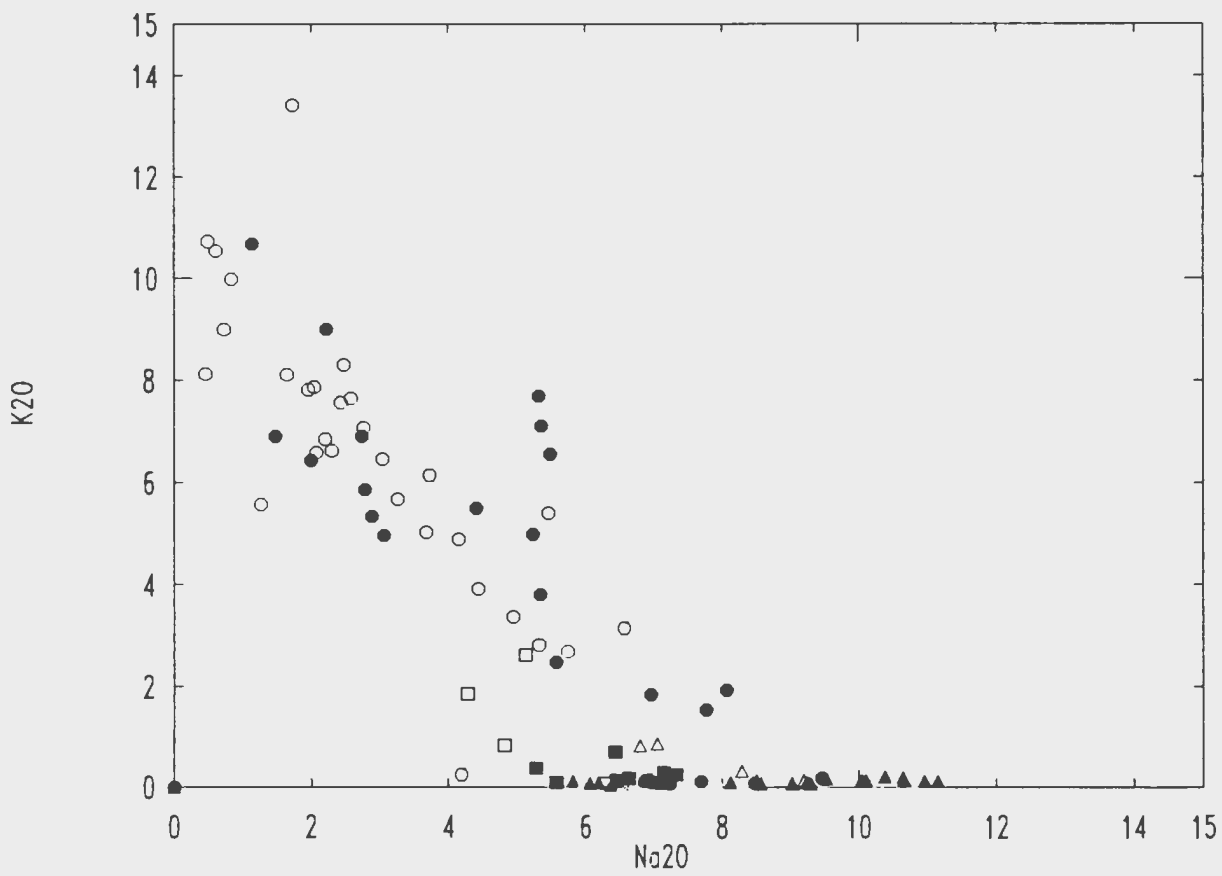


Figure 5-25:  $K_2O$  vs  $Na_2O$  plot of the UAG in the Burnt Lake area. Symbols as in Figure 5-20.

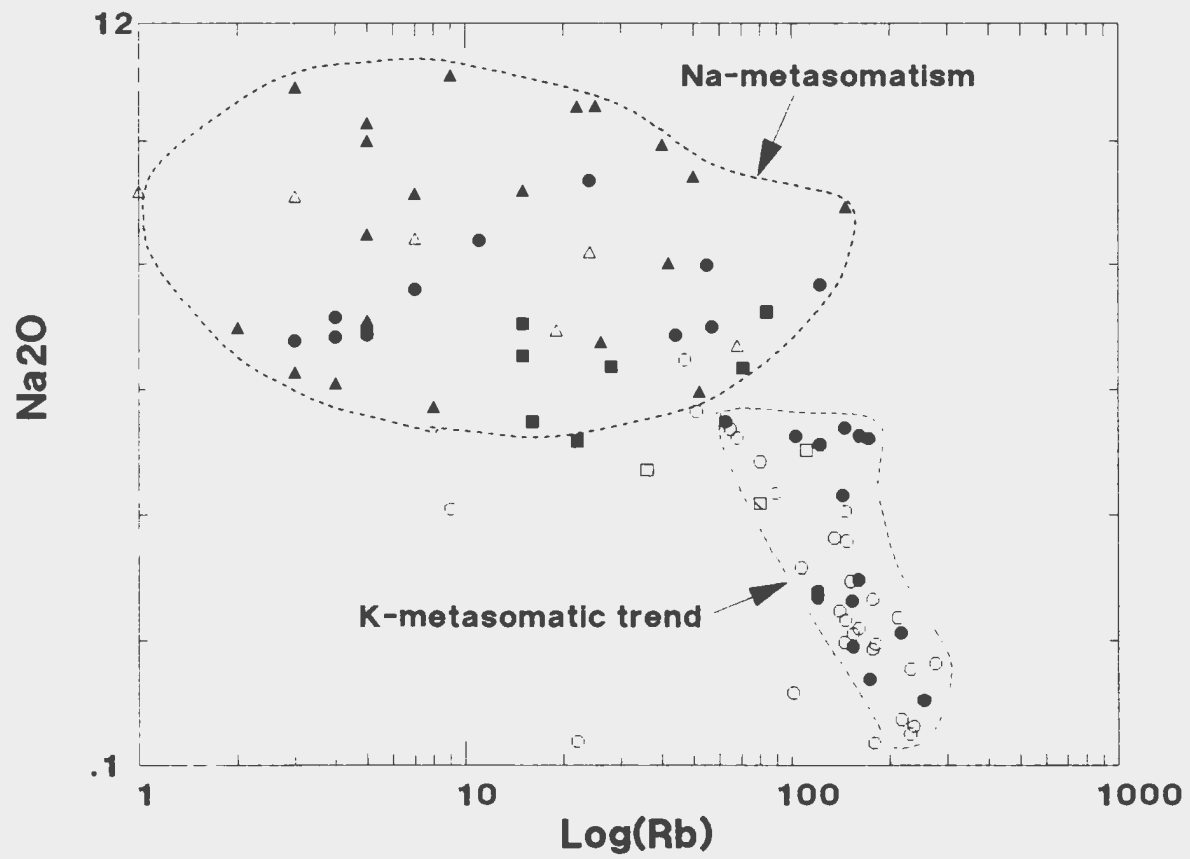


Figure 5-26:  $\text{Na}_2\text{O}$  vs Rb plot of the UAG in the Burnt Lake area. Symbols as in Figure 5-20.

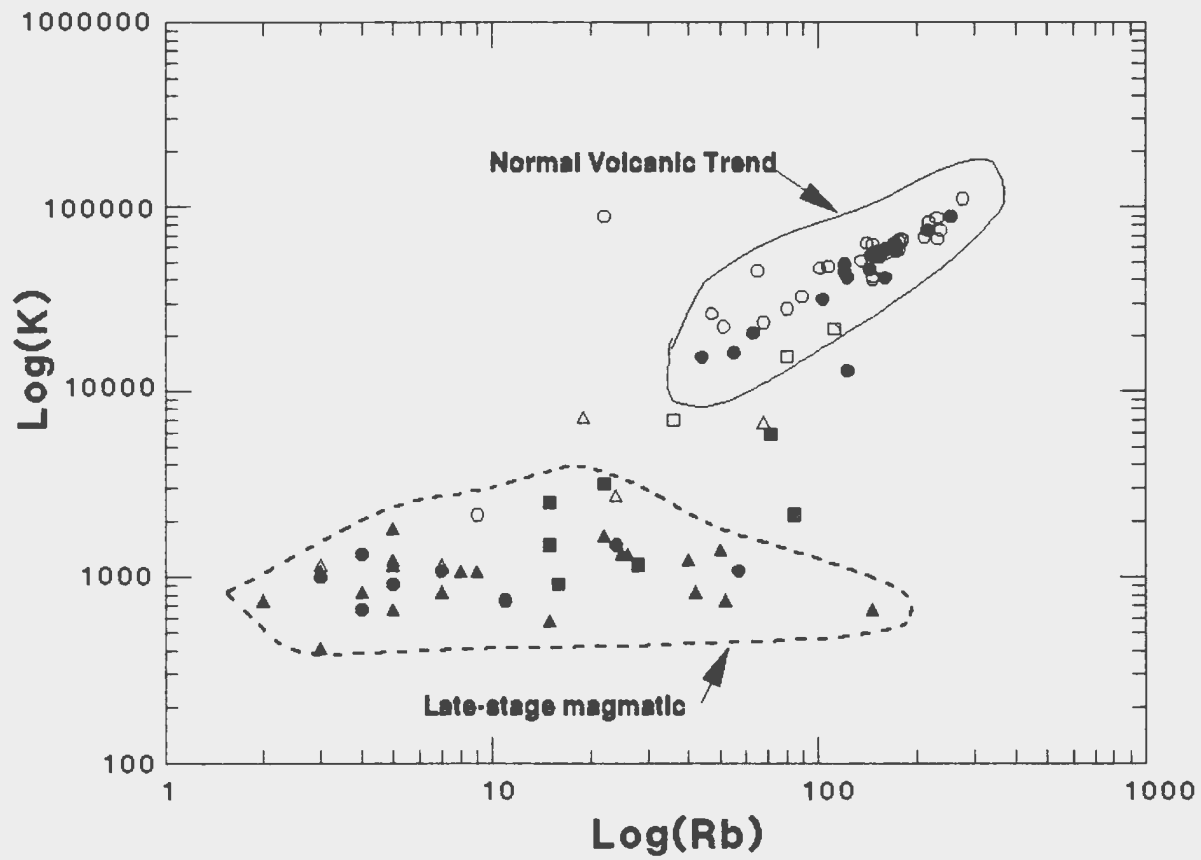
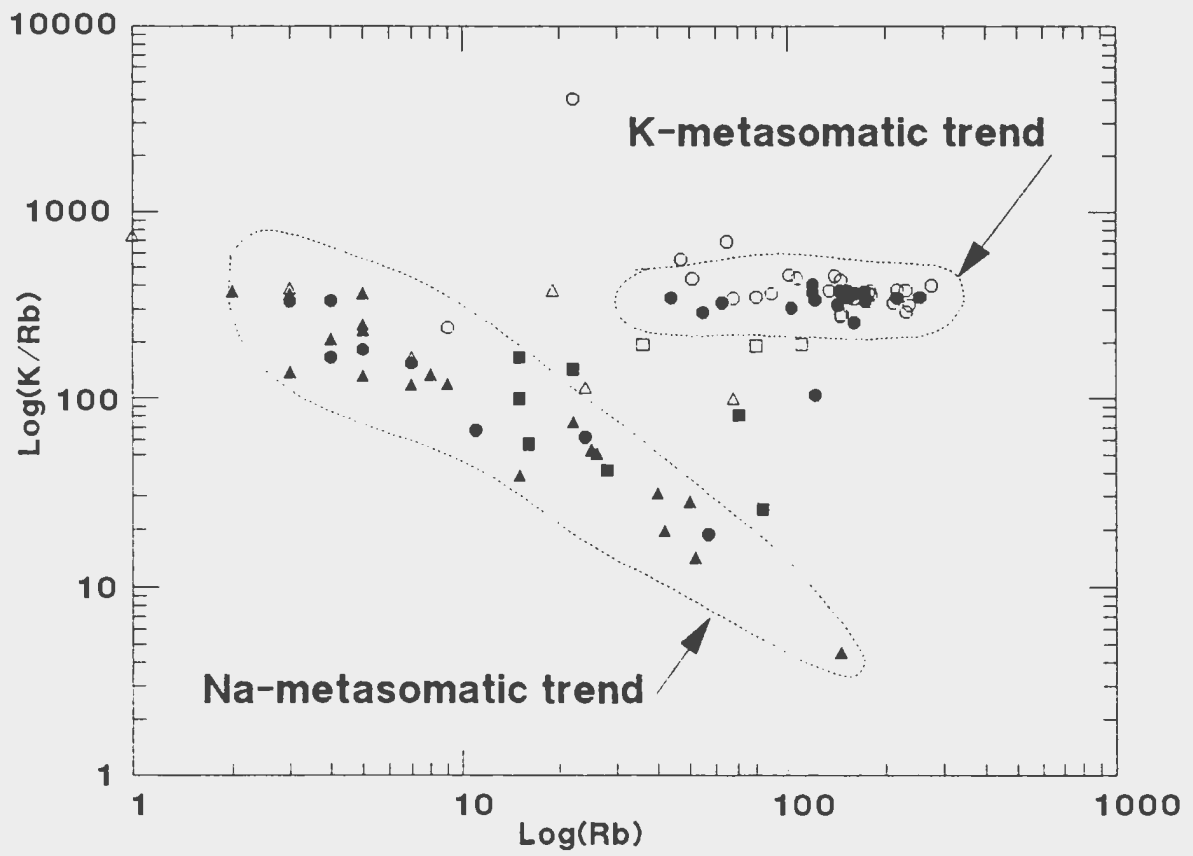
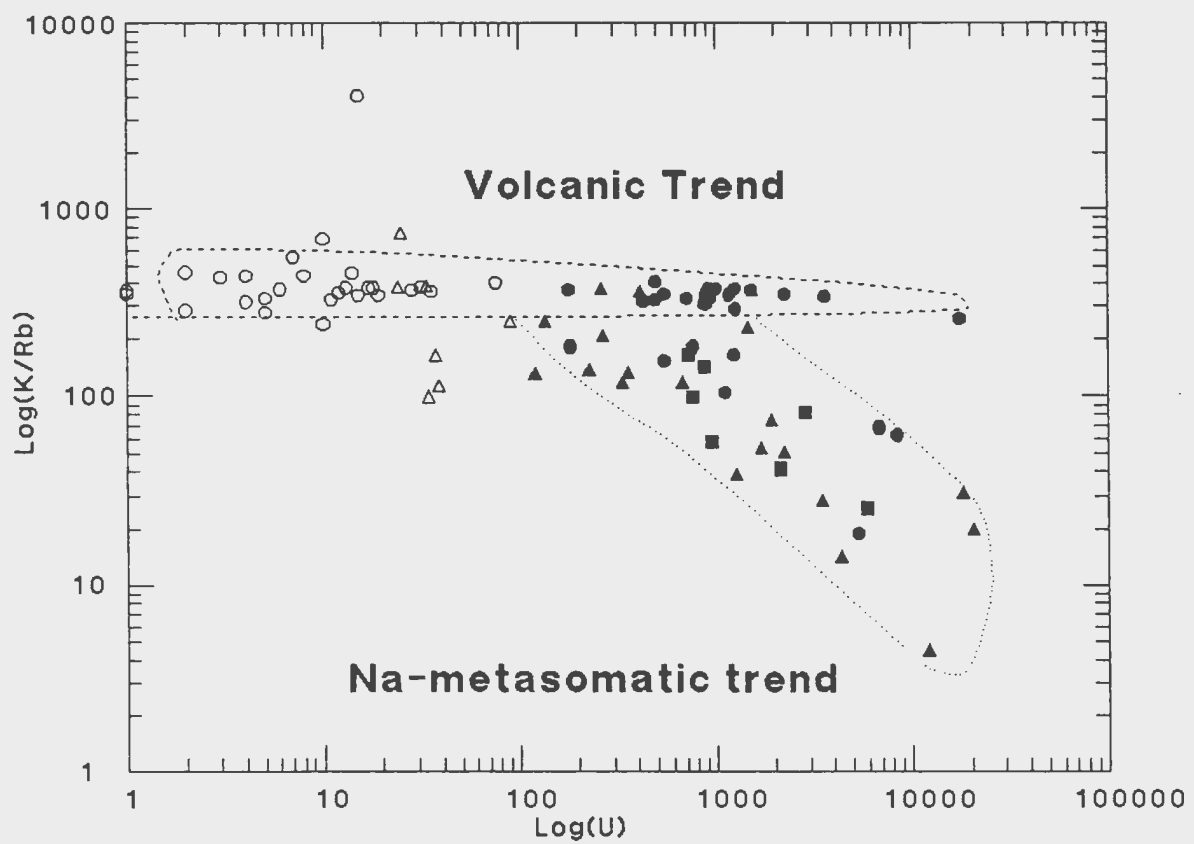


Figure 5-27: K vs Rb plot of the UAG in the Burnt Lake area.  
Symbols as in Figure 5-20.



**Figure 5-28: K/Rb vs Rb plot of the UAG in the Burnt Lake area. Symbols as in Figure 5-20.**



**Figure 5-29: K/Rb vs U plot of the UAG in the Burnt Lake area. Symbols as in Figure 5-20.**



### 5.6.1 Rare Earth Element Patterns

Analytical procedures for rare earth element (REE) analysis are given in Appendix I, and data are listed in Table 5-7. Chondrite-normalized REE patterns for the Upper Aillik Group are illustrated on Figures 5-30 to 5-32.

In general, unmineralized Upper Aillik Group felsic volcanic rocks (discussed in Chapter 3) have very enriched REE contents (up to ~ 1000x chondrite LREE elsewhere but only 200 to 400X near Burnt Lake; Figure 5-30) and usually intense negative Eu anomalies (Wilton et al., 1986, Wilton and Wardle, 1987). With respect to the uranium mineralized rocks at Burnt Lake (Figure 5-31), REE patterns are the same (i.e. enriched and intense negative Eu anomalies) as those of the unmineralized host rocks. The similarities in REE patterns suggest that the mineralizing fluids were chemically similar to the hosting felsic volcanic rocks or at least had achieved a degree of equilibrium with these rocks. All of which supports the idea that syn- to slightly post-volcanic leaching produced the uranium mineralization in the samples plotted.

In contrast, REE patterns for samples from the Emben Main Showing (Figure 5-32) are flat and enriched in Eu (i.e. a much smaller negative Eu anomaly). Of the four samples plotted on this diagram, W84-79E, which has the largest Eu depletion, contains the least U (82 ppm); whereas W84-79A, with the highest U concentration (10,680 ppm), has a decreased Eu

anomaly and also contains the greatest enrichments in REE (especially MREE). The other samples are intermediate (*i.e.* 79A has 129 ppm U; 79A1 has 1399 ppm U). This indicates that with increased U contents there is an increase in the LREE/HREE ratio. These pattern types are reminiscent of those in the Makkovik area that were linked to granite-related, phosphate complex-bearing, hydrothermal fluids (MacDougall and Wilton, 1987; Wilton and Wardle, 1987; Wilton *et al.*, 1986).

**Table 5-7: Rare earth element data for the Upper Aillik Group in the Burnt Lake Area.**

EL(ppm)	LM85-14	LM85-32	LM85-37	LM85-60	W84-65A	W84-65A.1
LA	62.1	107.9	107.2	89.8	108.6	292.6
CE	139.5	211.8	227.0	185.0	231.8	602.7
PR	11.7	16.9	19.1	16.2	19.7	55.4
ND	52.9	73.2	87.0	67.6	92.6	239.5
SM	10.6	11.7	15.0	10.5	16.2	40.6
EU	0.2	0.0	0.7	0.0	0.2	0.9
GD	9.3	8.5	11.4	6.6	10.5	32.8
DY	11.9	7.4	11.0	4.7	8.8	26.0
ER	6.9	4.5	7.2	2.7	3.7	11.2
YB	6.5	4.1	6.7	1.9	3.1	6.0
EL(ppm)	W84-65B	W84-79	W84-79A	W84-79A.1	W84-79E	
LA	118.7	134.6	162.1	106.6	42.3	
CE	287.7	480.5	320.3	287.2	95.8	
PR	24.3	62.4	33.9	32.7	8.9	
ND	106.6	290.7	264.2	173.7	39.8	
SM	20.5	77.6	32.9	40.0	12.5	
EU	0.0	2.0	3.9	2.2	0.2	
GD	15.8	65.3	29.9	41.1	13.7	
DY	14.1	48.4	29.3	39.0	20.8	
ER	6.5	17.4	15.5	18.1	13.3	
YB	3.3	10.3	10.9	10.0	14.4	

**Table 5-7: (Continued).**

EL(ppm)	EMS86-TR3A	EMS86TR3B	EMS86-TR4B	EMS86-TR6	EMS86TR5B
LA	6.7	26.8	67.2	56.2	89.8
CE	23.1	73.9	147.2	132.1	224.0
PR	2.8	9.6	17.6	17.5	27.7
ND	13.9	42.8	77.0	77.3	128.6
SM	3.2	11.8	32.2	30.6	50.3
EU	0.0	0.0	1.7	1.1	3.1
GD	4.2	11.5	45.2	42.2	67.7
DY	6.3	13.9	58.6	47.7	85.8
ER	4.0	7.3	26.0	21.3	46.1
YB	6.2	6.7	21.3	18.7	40.3

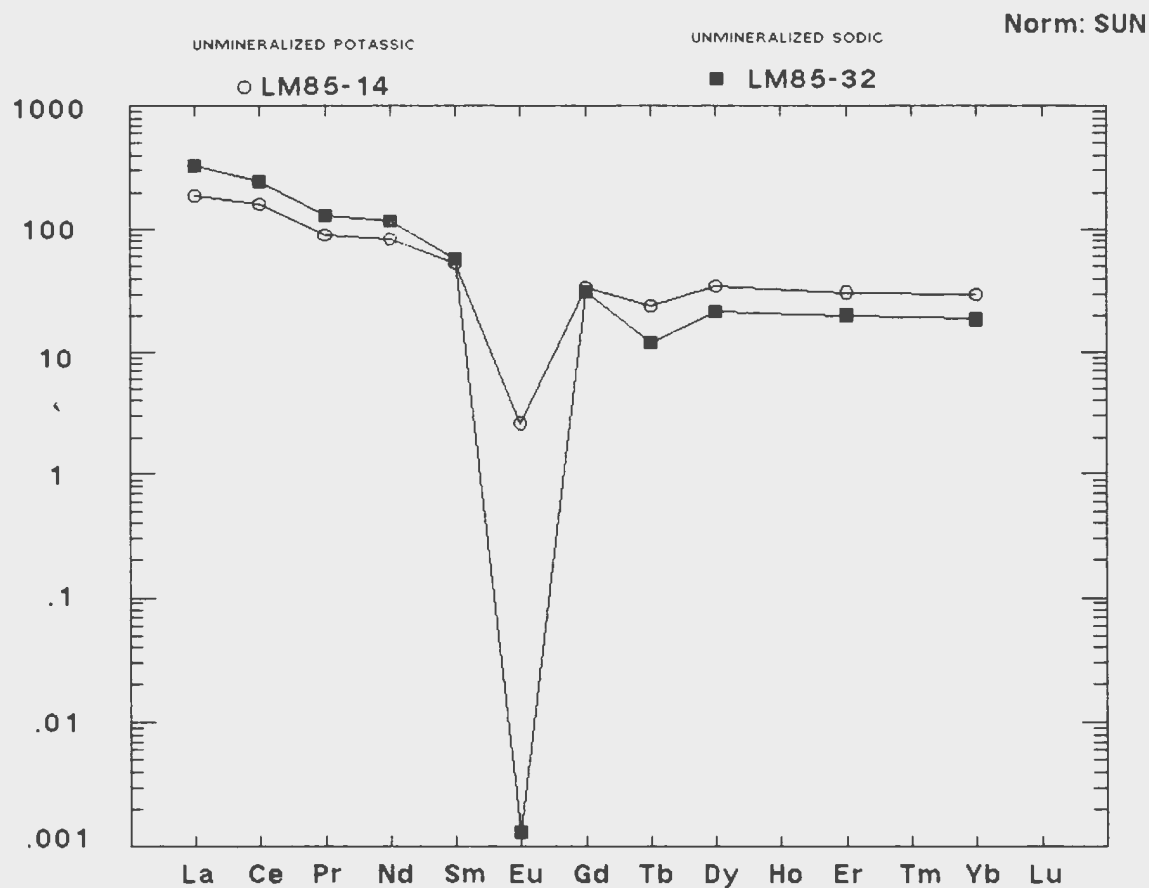


**Figure 5-30: SUN-normalized REE patterns for non-mineralized felsic volcanic rocks of the UAG in the Burnt Lake area.**

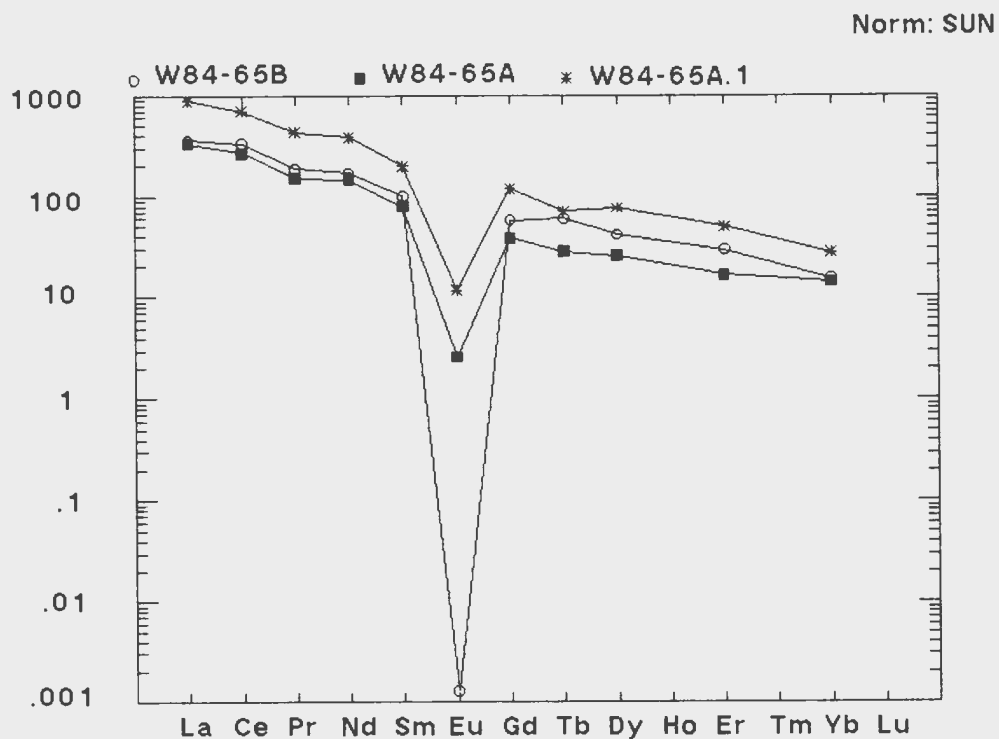


**Figure 5-31: SUN-normalized REE patterns for mineralized felsic volcanic rocks of the UAG in the Burnt Lake area.**

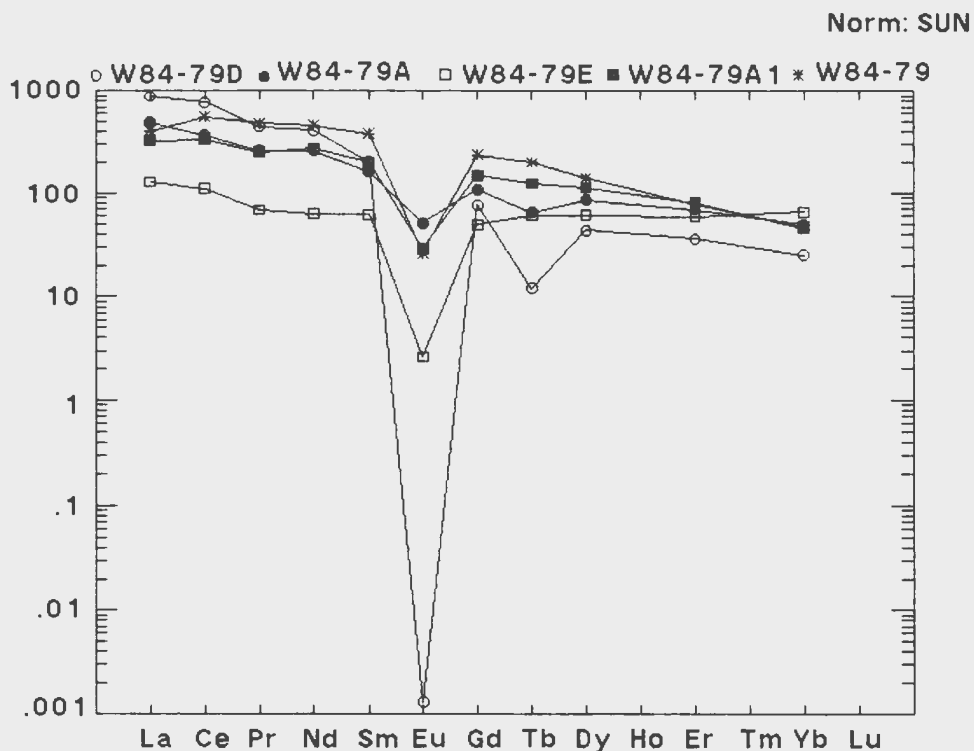


**Figure 5-32: SUN-normalized REE patterns for samples from the Emben Main Showing (both mineralized and non-mineralized).**

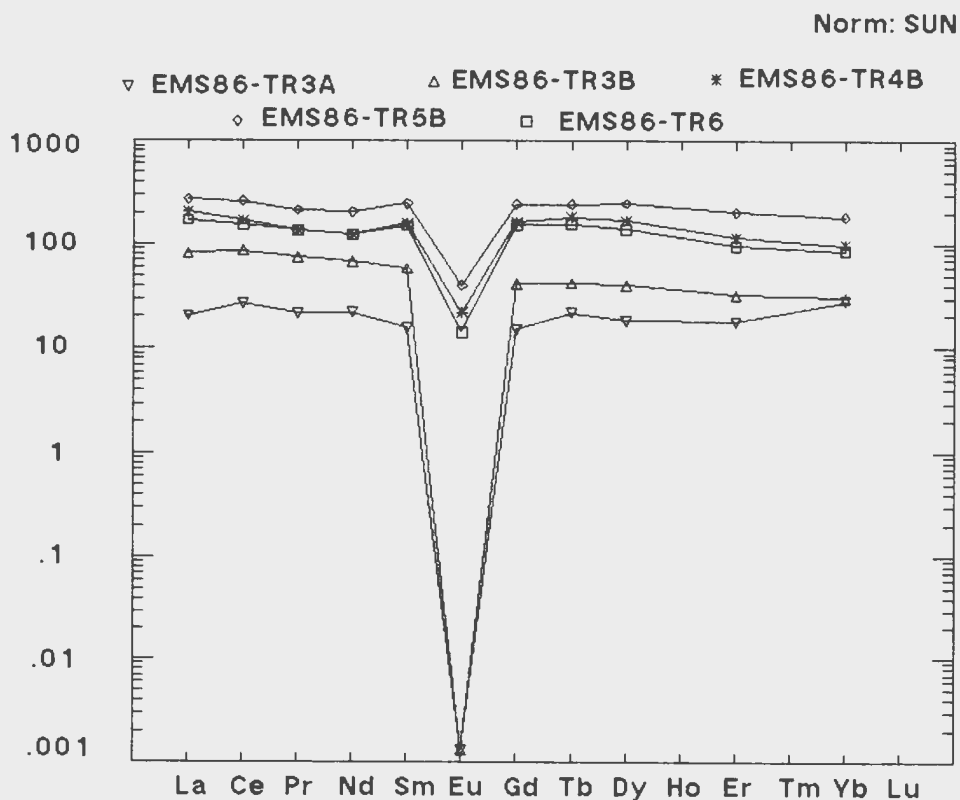


**Figure 5-33: SUN-normalized REE patterns for samples from the Emben South Showing.**

## 5.7 Pb Isotope Data

Galena separates were collected from four trenches at the Burnt Lake Showings (viz. two samples from the Burnt Lake Southwest Zone; one sample each from the Burnt Lake Northwest and Burnt Lake Main Zones) and one from the Emben South Showing.

Model ages and  $\mu$  values (from Stacey and Kramers (1975) average crustal model) for the five samples are listed in Table 5-6 (from Wilton 1991a). The Emben South sample (EMS86-TR5) and the Burnt Lake Main sample (LM85-TR13) have completely uranogenic  $^{206}\text{Pb}/^{204}\text{Pb}$  ratios of 108 and 762,

respectively. The  $^{207}\text{Pb}/^{206}\text{Pb}$  model ages of these samples are 2218 Ma for the Emben South sample and 2341 Ma for the Burnt Lake Main sample (Wilton, 1991). The two samples from the Burnt Lake Southwest zone (LM85-TR17 and LM85-TR18) have unrealistically low model ages (656 and 771 Ma) and have elevated  $\mu$  values (8.869 and 8.894) and therefore probably contain abundant radiogenic Pb derived from the uranium occurrences. The sample from the Burnt Lake northwest zone (BL86-6) has a more reasonable Stacey and Kramer's  $\mu$  value and model age of 1906 Ma. Zartman and Doe's (1981) lower crust model age for this sample hosted by 1860 Ma Upper Aillik Group is 1651 Ma. This younger age is very close to that of the TransLabrador Batholith which includes the Burnt Lake Granite (ca. 1650 Ma, Kerr and Krogh, 1990), thus suggesting that some of the galena mineralization (BL86-6) might be related directly to magmatic fluids from the granite.

**TABLE 5-8: Pb isotope ratios, calculated  $\mu$  and model ages (using Stacey and Kramer's (1975) model) for galena separates from the Burnt Lake area.**

SAMPLE AGE	206Pb/204Pb	207Pb/204Pb	208Pb/204Pb	$\mu$	MODEL
BL86-6	14.893	14.993	34.500	8.676	1906 Ma
LM85-TR17	17.077	15.335	34.545	8.869	656 Ma
LM85-TR18	16.918	15.327	34.545	8.894	771 Ma
LM85-TR13	762.02	126.80	36.074	----	2341 Ma
EMS86-TR5B	108.20	29.089	34.807	----	2281 Ma

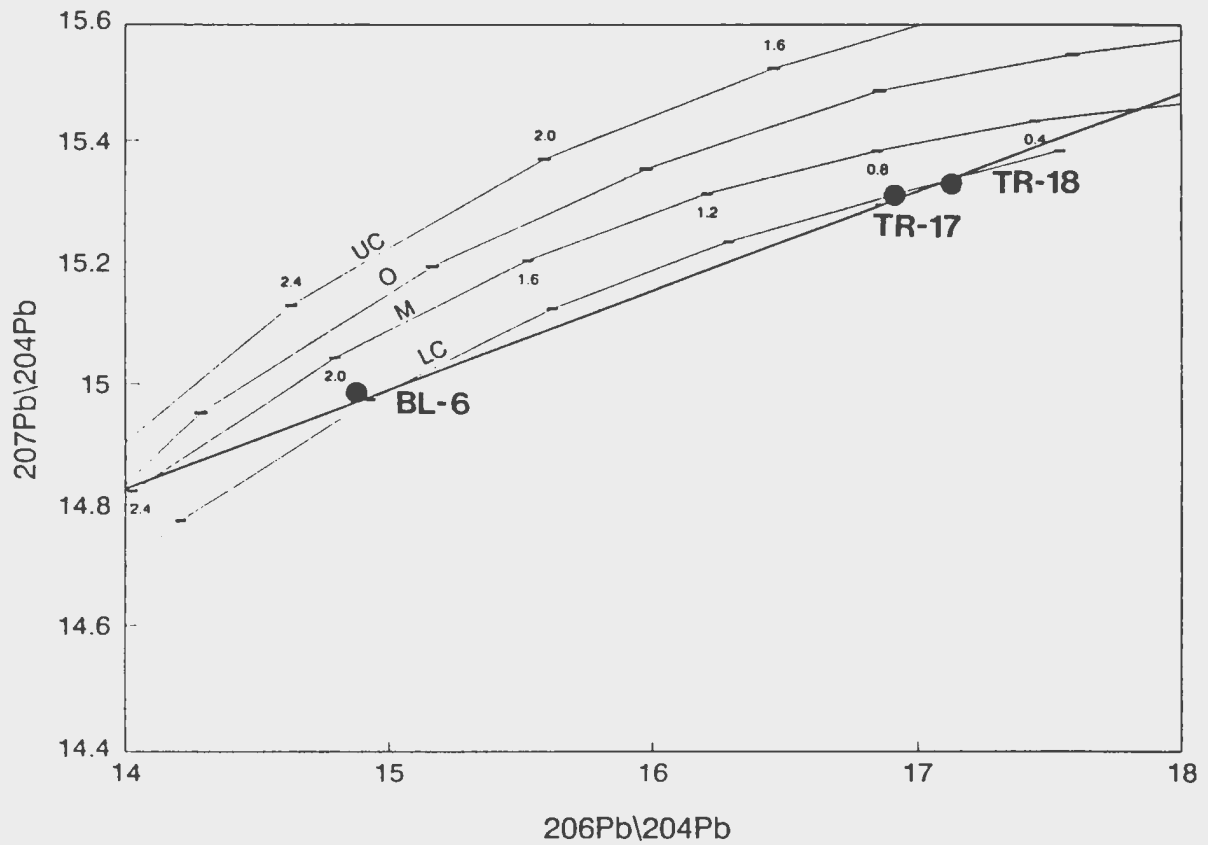


**Figure 5-34:**  $^{207}\text{Pb}/^{204}\text{Pb}$  vs.  $^{206}\text{Pb}/^{204}\text{Pb}$  diagram for three galena separates from the Burnt Lake radioactive occurrences. The straight line regressed through the points is a Model-2 Yorkfit (York, 1969). The plotted curves are Zartman and Doe's (1981) Version II model growth curves (after Wilton, 1991).

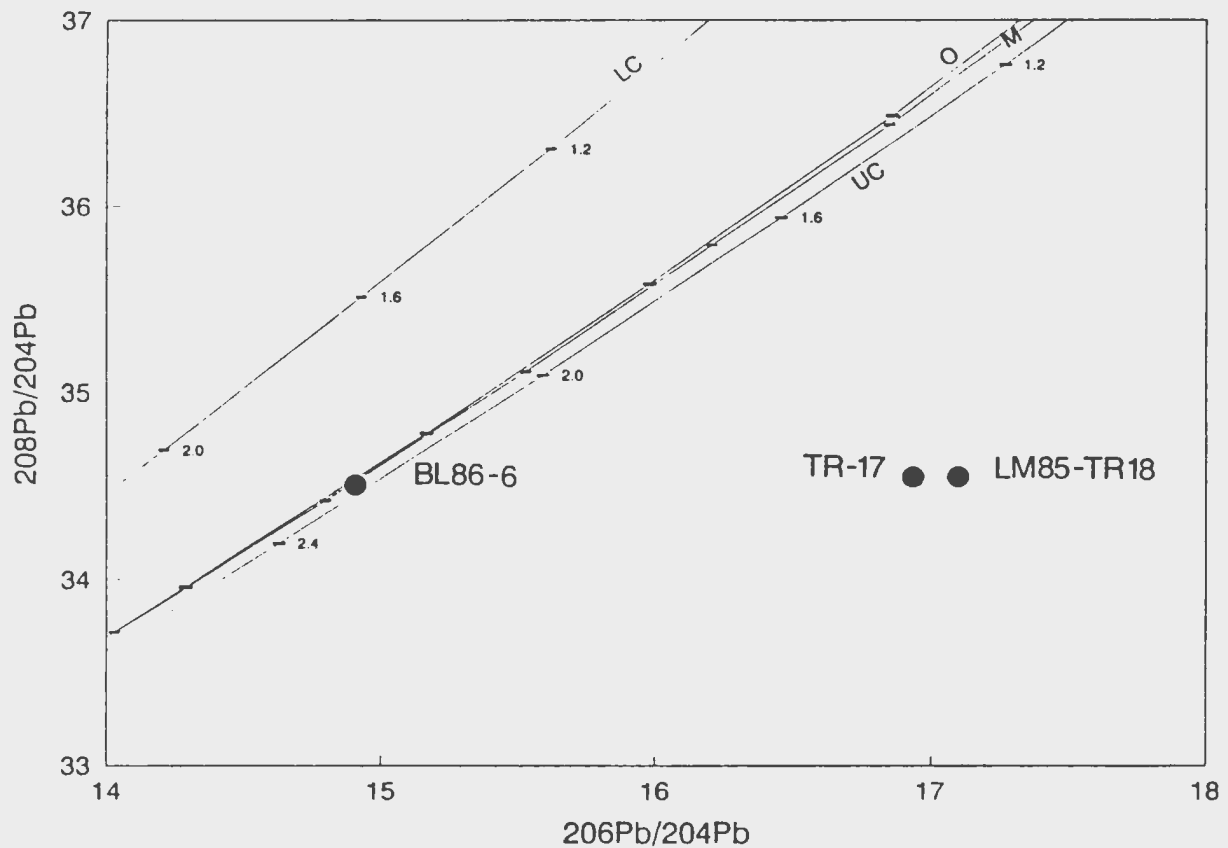


Figure 5-35:  $^{208}\text{Pb}/^{204}\text{Pb}$  vs.  $^{206}\text{Pb}/^{204}\text{Pb}$  diagram for three galena separates from the Burnt Lake radioactive occurrences. The plotted curves are Zartman and Doe's (1981) Version II model growth curves (after Wilton, 1991).



### 5.8 Sulphur Isotope Data

Separates of sulphide minerals were collected from mineralized showings at both Burnt Lake and Emben. The mineral separates were hand picked, crushed and analysed at the Ottawa-Carleton Centre for Geoscience Studies - Geological Survey of Canada (OCCGS-GSC) stable isotope facility in Ottawa, Ontario. The data obtained are given in Table 5-9 and show a broad range in values. Since  $\delta^{34}\text{S}$  values of sulphides can be very sensitive to  $f\text{O}_2$  and pH (Ohmoto, 1979), the large negative  $\delta^{34}\text{S}$  values may be explained by elevated  $f\text{O}_2$  (as suggested by the mineral assemblages given earlier). The data was used to estimate temperatures using the equilibrium factors of Kajiwara and Krouse (1971) for coexisting sulphide minerals. The isotopic equilibrium temperature calculated for the sphalerite-pyrite pair in sample BL86-2A gave a temperature of  $114^\circ\text{C}$  and is a reasonable estimate for deposition from hydrothermal solutions. Sample BL86-6 gave an estimated temperature of  $293^\circ\text{C}$  which is reasonable for magmatic solutions. The Emben samples (EMS86-TR5B) which gave an estimated temperature of  $354^\circ\text{C}$  can also be related to a magmatic source. The molybdenite separate from Emben South gave a  $\delta^{32}\text{S}/\delta^{34}\text{S}$  of -18.6 which closely resembles a sedimentary source for the sulfur, while the molybdenite sample from the Burnt Lake Granite (LM85-163) gave a reasonable magmatic source value of + 3.4.

**Table 5-9: Sulphur isotope data for mineral separates from the Burnt Lake and Emben Showings.**

Sample No.	Description	% Yield Mineral	$\delta^{32}\text{S}/\delta^{34}\text{S}$
BL86-2A(PY)	Pyrite	87	0.2
BL86-2A(SP)	Sphalerite	36	-1.8
BL86-6(GN)	Galena	75	-9.6
BL86-6(SP)	Sphalerite	32	-7.1 (R -8.9) *
BL86-8(SP)	Sphalerite	79	-2.2
BL86-11	Galena	68	-10.7
EMS86-TR5B(PY)	Pyrite	90	-11.8
EMS86-TR5B(GN)	Galena	65	-14.6
EMS85-TR-1B	Molybdenite	84	-18.6
LM85-163	Molybdenite	71	3.4
BH11-290.5	Galena	98	-6.3

\* (R = repeat)

### 5.9 Summary of the Radioactive Zones

The major characteristics of each mineralized suite from the Burnt Lake study area are shown in Table 5-10. Generally, the timing of mineralization is poorly constrained and only an estimate is given for each zone.

**Table 5-10: General characteristics of the five mineralized rock suites in the Burnt Lake area.**

	BURNT LAKE (POTASSIC)	BURNT LAKE (SODIC)	EMBEN SOUTH
AGE (Timing of Mineralization)	1855/1650 Ma	1800-1740 Ma	1800-1740 Ma
HOST ROCKS	Porphyritic rhyolite, breccia	Tuffaceous rocks, breccias	Mafic dykes
CHEMICAL FEATURES	Enrichments in Pb, Zn, Mn, CaO Ga, K <sub>2</sub> O, Rb, Sr, U, Y, Cu, Mo As, Ag, Au, Ce Depletions in SiO <sub>2</sub> , Na <sub>2</sub> O, P <sub>2</sub> O <sub>5</sub> MgO, Nb, Th	Enrichments in Na <sub>2</sub> O, U, Pb, FeO, TiO <sub>2</sub> , Cu, V, Zr, As, Rb, Ba, Ga, Nb, Y, Ag Depletions in SiO <sub>2</sub> , K <sub>2</sub> O P <sub>2</sub> O <sub>5</sub>	Enrichments in FeO, TiO <sub>2</sub> , P <sub>2</sub> O <sub>5</sub> Pb, Zn, Cu, Mo, U, Ga, Ni Co, Cd, Ag, As, Th, Rb, Y, Nb Depletions in SiO <sub>2</sub> , Al <sub>2</sub> O <sub>3</sub> , K <sub>2</sub> O Na <sub>2</sub> O, MgO
METALLIC MINERAL ASSEMBLAGE	U, Gn, Sp, Cp, Py, Hem, Mte	U, Gn, Cp, Hem, Mte	U, Gn, Sp, Cp, Py
GRANOPHILE MINERALS	Mo, Fl		Mo, Fl, Sh
ALTERATION ASSEMBLAGES	secondary microcline hematization	albitization of feldspars sodic pyroxenes and amph. hematization chlorite and epidote	sodic pyroxenes
ACCESSORY MINERALS	sphene, zircon, ilmenite apatite, monazite, barite	sphene, zircon, ilmenite apatite, monazite, barite	zircon
PITCHBLEND ASSOCIATION	amphiboles and pyroxenes sphene, zircon, ilmenite apatite, monazite, Ti-Fe-Mn inclusions in qtz, veinlets inclusions in pyrite, hematite	sphene, pyroxenes and amph. ilmenite, Ti-Fe-Mn oxide galena + chalcopryrite inclusions in qtz, veinlets V-rich mineral (carnitite)	sodic pyroxenes inclusions in plagioclase
COMPLEXING AGENT	carbonate, phosphate or fluoride complexes	sodium bearing uranyl carbonate complex	phosphate or fluoride complexes
ENVIRONMENT OF DEPOSITION	Syngenetic leaching of host volcanic rocks	Epigenetic magmatic hydrothermal	Remobilization during granite intrusion
PB ISOTOPES	1650 Ma - Granite Related	Uranogenic	Uranogenic

Table 5-10 (Continued)

	EMBEN MAIN	AURORA RIVER
AGE (Timing of Mineralization)	1800-1740 Ma	1800-1740 Ma
HOST ROCKS	Tuffaceous-sedimentary rocks	Sheared andesite/rhyolite t
CHEMICAL FEATURES	Enrichments in Na <sub>2</sub> O, U, Y, Ga Pb, Th, As, Ag, Au, Rb, Nb  Depletions in SiO <sub>2</sub> , K <sub>2</sub> O, P <sub>2</sub> O <sub>5</sub> MgO	Enrichments in U, Pb, Na <sub>2</sub> O V, Ba, Ga, Nb, Zr, Y, Bi, A SiO <sub>2</sub> , P <sub>2</sub> O <sub>5</sub> Depletions in K <sub>2</sub> O, Al <sub>2</sub> O <sub>3</sub> , F MgO, Rb, Sr, Cr, Ni, Co
METALLIC MINERAL ASSEMBLAGE	U, Hem, Mte	U, Hem
GRANOPHILE MINERALS		
ALTERATION ASSEMBLAGES	hematization	hematization chlorite, tremolite, epidot sericite, qtz-carb veins
ACCESSORY MINERALS	sphene, ilmenite garnet, barite	
PITCHBLEND ASSOCIATION	fracture fillings inclusions in plagioclase Ti-Fe-Mn oxides	fracture fillings/veinlets oxidation of iron
COMPLEXING AGENT	uranyl carbonate complex	Uranyl carbonate
ENVIRONMENT OF DEPOSITION	-----	-----
PB ISOTOPES	-----	-----

## CHAPTER 6

## DISCUSSION AND CONCLUSIONS

## 6.1 Uranium Ore Genesis

The conditions under which uranium is transported in and eventually deposited from hydrothermal solutions are variable and depend on a combination of factors. Generally, a hydrothermal environment suitable for uranium mineralization must have the following characteristics: highly oxidized solutions; source(s) of leachable uranium; suitable complexing agents to transport uranium; a reductant and/or an increase in pH to precipitate uranium; and a hydrologic setting in which to operate.

When the uranium is held within the crystal structure of rock-forming or accessory minerals, it must first be released from the the crystal lattice through metamorphism or hydrothermal alteration. After the uranium is released from these minerals it will quickly co-precipitate with secondary oxides or is adsorbed on these oxides or on secondary clay minerals. Mobilization of uranium occurs when the loosely held metal is dissolved by oxidizing solutions which sometimes requires fracture-induced permeability.

Uranium is soluble in the hexavalent state (U+6) in the form of uranyl complexes. The dominant complexing agent

depends primarily on the concentration of the complexing anion which is in turn influenced by the temperature, pressure, composition and pH of the hydrothermal fluid (Romberger, 1984). The complexing agents may be derived from the hydrothermal solutions or from the host rocks themselves. At temperatures  $<300^{\circ}\text{C}$  and under acidic conditions the most important complexing agent is phosphate. With as little as 0.1 ppm P in solution, most of the complexes will form as  $\text{UO}_2(\text{HPO}_4)_2^{2-}$  (Romberger, 1984). Fluoride complexes are only important in near neutral solutions while carbonate complexes are dominant at pH values above 7. Chloride and sulphate complexes are generally weak even at high concentrations of these anions. Hydroxide complexes are quite stable for neutral solutions, although the activity of the hydroxyl ion is small. Uranyl hydroxide complexes increase in stability as the temperature increases. Therefore, the dominant complexing agent is likely to be variable during the physiochemical evolution of the hydrothermal fluid.

The predominant uranium complex in hydrothermal solutions is dependent on the concentration of the complexing anion which is in turn dependent on the temperature and pH of the solution. Other factors that influence the solubility of uranium in a hydrothermal system are pressure, oxidation state, Eh, activity of the complexing anion, and partial pressure of volatiles (i.e. carbon dioxide).

Deposition of uranium from hydrothermal solutions is

caused either by a reduction from hexavalent state to the tetravalent state, or by an increase in the pH, which occurs as solutions react with the wallrock or as a result of volatile loss during boiling of the hydrothermal fluids (Romberger, 1984). Precipitation is usually accomplished by reaction with iron, sulfur or organic compounds. Uranium may also precipitate when the activity of the complexing anion is decreased by dilution of the hydrothermal solution or by precipitation of gangue minerals. Precipitation of fluorite, calcite and apatite as a result of wall rock reaction and decreasing solubility would reduce the activity of these complexing agents and further promote uranium deposition. Other mechanisms that precipitate uranium from solution are changes in the pressure and temperature, reduction due to the formation of metallo-organic compounds, or a lowering of the Eh of a system.

The oxidizing solutions may have a meteoric or formational water origin (i.e. oxygenated) or be derived from fluids released during metamorphic or magmatic processes that have maintained a high oxygen fugacity. Typically, uranium is concentrated in residual magmatic fluids as a result of the low partitioning of uranium into the crystallizing solid phases (Langmuir, 1978). Common sites of uranium in igneous rocks are mafic silicate minerals (e.g. biotite and hornblende) or refractory minerals (e.g. zircon, apatite, sphene and monazite). Uranium is also concentrated in magmas

through volatile and alkali transfer. Devitrification of volcanic glasses by alkaline solutions can also provide a source of uranium (Zielinski, 1979).

Uranium enrichments will usually occur when a volatile phase is exsolved (i.e. boiling) from a magma; for example in a highly siliceous melt that is low in alkalies. Uranium may also be concentrated as disseminations in silicate minerals when volatiles are dissolved in the melt; e.g. an undersaturated, peralkaline melt.

A common source of uranium is from alkaline volcanism wherein radioelement concentration occurs in the final stages of the magmatic cycle. During crystallization-fractionation in an alkaline magma, there can be a build up of an incompatible element-enriched volatile phase. Uranium is typically concentrated in the residual magmatic fluids because of low partitioning coefficients between the crystallizing phases and the magma. Subsequent eruption would deposit thick sequences of ash tuffs and rhyolite porphyries enriched in U, Th and K. Uranium is usually concentrated in the matrices and glasses rather than in the major mineral phases of these volcanic rocks (Sorensen, 1970). As the massive ignimbritic deposits become compacted and locally welded, a considerable quantity of alkaline and high oxygen fugacity fluid would be expelled. Ionic exchange occurs during hydrothermal alteration of the cooling volcanic pile, and it is during this alteration of the volcanic pile that uranium is released from the



volcanic glass and is enriched in the aqueous phase (Zielinski, 1982). Generally accompanying alkali metasomatism is the release of U, Na, K, Sr, Ba, Be, W, Sn, Nb, Li, F and Cl during devitrification and alteration and this is considered the source for later enrichments of these elements. REE contents of accessory minerals (i.e. allanite, monazite, magnetite, zircon and uraninite) are also depleted during metasomatism.

## **6.2 Ore Forming Models**

Uranium mineralization in the Burnt Lake area has characteristics common to many uranium deposits elsewhere in the world. The geological setting and characteristics of ore formation are discussed below.

The predominantly felsic volcanic rocks of the Upper Aillik Group were deposited in a subaerial rift-related environment. Others have suggested (e.g. Wardle and Bailey, 1980) that the transition from basic volcanism to felsic volcanism in the Aillik Group was a result of different tectonic conditions ranging from rifting to ensialic orogeny. However, the apparent calc-alkaline affinity in these felsic rocks was chemically altered by wide-spread and efficient alkali metasomatism (White and Martin, 1980). Alkali metasomatism is commonly associated with uranium mineralization in felsic volcanic and igneous rocks throughout

the world (Smellie and Laurikko, 1984; Stuckless and Troeng, 1984; Cathelineau, 1983; White and Martin, 1980; Kontak, 1980; Leroy, 1978; Smirnov, 1977; Hoeve, 1974; Zinchenko and Rakovich, 1972).

Uranium mineralization in the Burnt Lake area is found in a variety of host rocks and resulted from a combination of syngenetic and epigenetic processes. The ultimate source(s) of uranium was igneous, however, several physiochemical modifications lead to the local concentration and deposition as uraninite.

**Stage I:** This involved the build up of an incompatible element-enriched volatile component during the fractionation of a calc-alkaline magma. Subsequent eruption deposited thick sequences of ash tuffs and rhyolite porphyries that were enriched in these incompatible elements (Figure 6-1). Uranium was concentrated in the matrices and glasses rather than in the normal silicate mineral phases of these volcanic rocks. As the massive ignimbritic deposits became compacted and locally welded, considerable amounts of alkaline and high oxygen fugacity fluids were expelled. At this time, devitrification of the glasses and matrices of the felsic tuffs was effected by these alkaline solutions and uranium was released into solution.

Leaching of devitrified volcanic glasses was accompanied by a gain of K, Al and Ti and depletion of Na, Si and P in the

host rocks. Alkali exchange is common during the hydration of volcanic glasses (Scott, 1971) and is usually associated with an inverse alkali relationship (cation exchange). Metasomatism involved a simple ( $\text{Na}^+ - \text{K}^+$ ) cation exchange from a K-enriched solution, while intense metasomatic alteration involved K+Al substituting for Si. White and Martin (1980) considered the uranium at Burnt Lake to have been transported as a sodium-bearing uranyl carbonate or halide complex, however, the close association of uraninite and sphene in the Burnt Lake area may indicate that the mineralizing solutions were also enriched in Ca and Ti.

The source of the oxidizing hydrothermal fluids would be meteoric or magmatic as a result of volatile exsolution (boiling). Circulation and convection of the aqueous fluid would have been set in motion by the heat dissipating from an underlying cooling magma chamber.

Precipitation of the dissolved uranium ions from the oxidized hydrothermal fluids would result from reaction with relatively reduced country (now host) rock. Disseminated pyrite and magnetite are common in unmineralized country rock, whilst the mineralized zones are commonly associated with red hematitic alteration. The oxidation of magnetite to hematite would cause a decrease in the  $f\text{O}_2$  of the hydrothermal fluids and promote precipitation of the uraninite as discrete disseminated grains. Uranium is also commonly associated with the accessory minerals zircon, sphene and apatite or a secondary

Fe-Mn-Ti oxide. This Fe-Mn-Ti secondary oxide associated with uraninite is considered to be an alteration product of biotite and sphene (Zielinski, 1978) and indicates U mobilization and reprecipitation with Fe-Mn-Ti oxides occurred along fissures and as grain coatings.

At the Skuppesavon deposit in Sweden (Smellie and Laurikko, 1984) the uranium mineralization superseded the main metasomatic events and is confined to fine disseminations of uraninite concentrated throughout the rock. Smellie and Laurikko (1984) noted that the main metasomatic minerals such as chlorite, riebeckite and aegirine augite showed no significant uranium enrichments and they therefore concluded that the uranium, present mainly as uraninite and uranotitanates, precipitated within the pre-existing metasomatites. In other words, as a result of local redox reactions the uranium precipitated in those parts of the metasomatites containing the greatest percentage of mafic mineral phases.

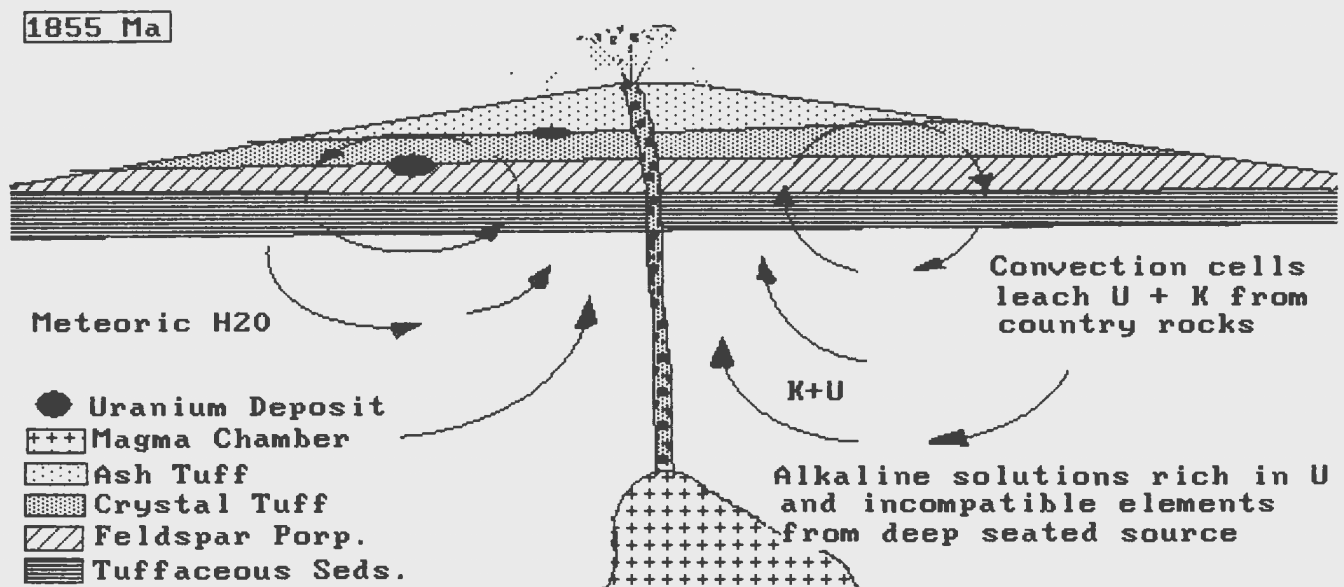


Figure 6-1: Schematic diagram representing a syngenetic model for uranium mineralization within the Upper Aillik Group in the Burnt Lake area.

**Stage II:** Epigenetic uranium mineralization occurred during a long period of metamorphism and igneous intrusion during the Makkovikian Orogeny ca. 1800-1720 Ma (Gower and Ryan, 1986)(Figure 6-2). The post-tectonic Makkovikian intrusion in the area (i.e. Freshsteak granitoid) has an Rb/Sr date of  $1798 \pm 28$  Ma (Kerr and Krogh, 1990) which corresponds to Kontak's (1980) U/Pb age of 1770 Ma for uraninites from Burnt Lake. Uranium mineralization at Burnt Lake was accompanied by wide-spread and efficient alkali metasomatism characterized by enrichments of  $\text{Na}_2\text{O}$ ,  $\text{Al}_2\text{O}_3$  and  $\text{TiO}_2$  and depletions in  $\text{K}_2\text{O}$ ,  $\text{SiO}_2$  and  $\text{P}_2\text{O}_5$ . During fractionation of the posttectonic granitoid, a metal-bearing, volatile-rich fluid evolved and was expelled into the overlying volcanic and sedimentary sequence. The Na-metasomatic event that preceded and accompanied the uranium mineralization is recognized by the complete to partial albitization of feldspars and replacement of the matrices by albite, as well as by the presence of the metasomatic silicate phases of chlorite, riebeckite and aegirine augite. The host rocks are all sodium metasomatites, that is they are enriched in Na and depleted in K. Generally, the uraniferous phase was preceded by a Na and/or Ca-rich metasomatic phase. The mineralizing solutions followed structural weaknesses (faults, lithological contacts or dykes) until favourable conditions of temperature, pressure, oxidation and redox potential and pH resulted in the precipitation of uraninite.

The Emben Main showing was formed near the contacts of a small gabbro dyke. The dyke itself is not mineralized rather it caused fracture induced permeability within the surrounding host rocks in which to localize later mineralizing solutions. Both the mineralized and unmineralized rocks are strongly Na-metasomatized, accompanied by  $\text{Na}_2\text{O}$  enrichments and  $\text{K}_2\text{O}$  and  $\text{SiO}_2$  depletions. This supposes that the uraniferous phase was preceded by a Na-metasomatic phase. The hydrothermal fluids were activated during metamorphism and were enriched in Ca and Ti, resulting in the association of uraninite with sphene. Uraninite also commonly occurs as veinlets or is concentrated along fractures associated with hematization. REE patterns for the Emben Main showing are similar to those in the Makkovik area that were linked to granite-related, phosphate complex-bearing, hydrothermal fluids (MacDougall, 1988; Wilton and Wardle, 1986; Wilton *et al.*, 1986).

The Emben South zone has undergone strong alkali metasomatism involving  $\text{Na}_2\text{O}$  enrichments and  $\text{K}_2\text{O}$  depletions. The introduction of Ca-, Ti-, P- and Fe-rich solutions coeval and subsequent to uraninite precipitation has resulted in the association of uraninite and sphene, ilmenite, calcic amphiboles and pyroxenes. The presence of abundant apatite reflects the probability that uraninite was transported as a phosphate complex. The association of fluorite with molybdenite mineralization suggests that Mo was transported predominantly as a fluoride complex while fluids were expelled

from the volatile phase of the posttectonic granite. The metamafic dykes which host the mineralization had a direct influence on ore deposition by providing a possible REDOX boundary or acting as a conduit or channel for uraniferous hydrothermal solutions being expelled from the evolving granite. This spatial relationship between diabase dykes and uranium mineralization is evident at the Litljuthatten orebody in Sweden (Stuckless and Troeng, 1984). Minatidis (1976) suggested that the mafic dykes in the Emben area could have been the source of the radioactive metal but also suggested that the source could have been the crustal rock via metamorphism at depth.

The Aurora River uraniferous phase was preceded by a Na + Ca metasomatic phase as indicated by the high contents of  $\text{Na}_2\text{O}$  and  $\text{CaO}$  in both mineralized and unmineralized andesitic rocks. Hydrothermal fluids were activated during metamorphism and were enriched in U, V,  $\text{SiO}_2$ ,  $\text{TiO}_2$  and  $\text{Al}_2\text{O}_3$ . Passage through the rocks was accomplished by way of structural weaknesses such as lithological boundaries and fault zones.



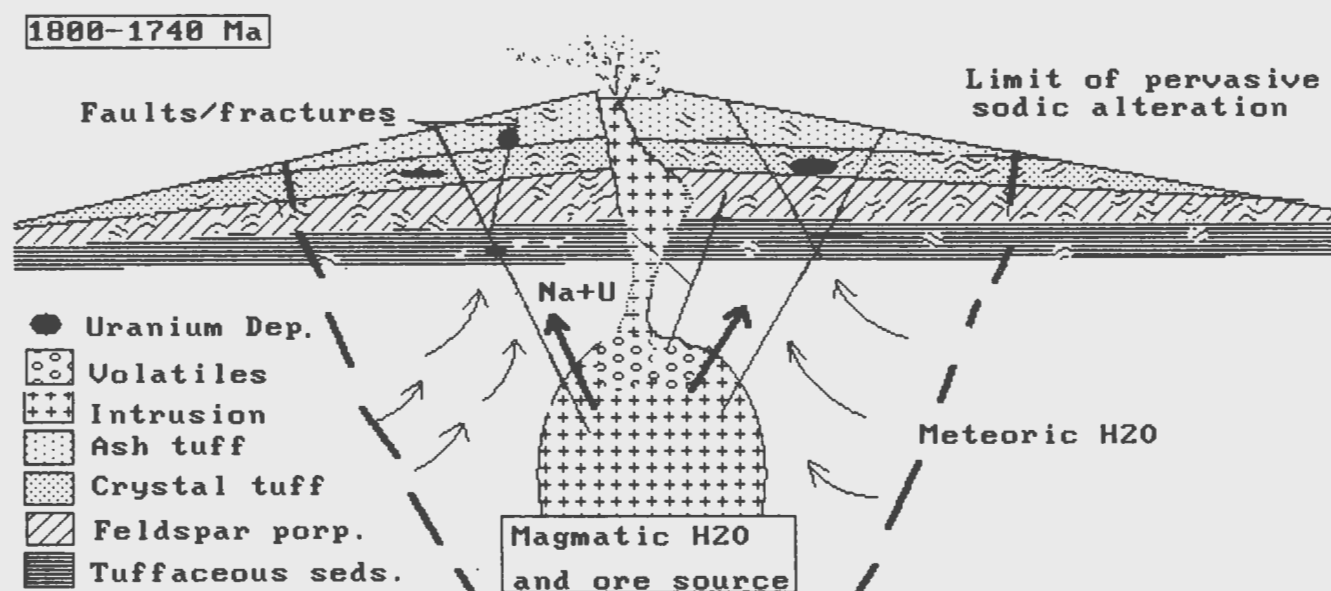
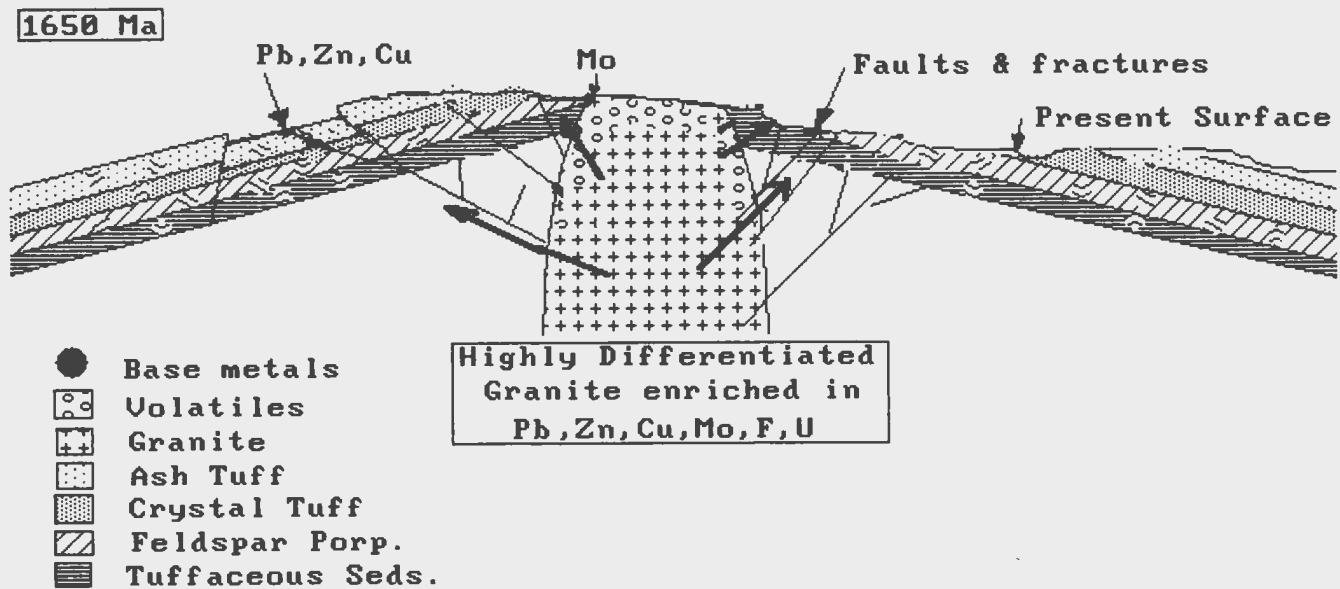


Figure 6-2: Schematic diagram representing an epigenetic model for uranium mineralization within the Upper Aillik Group in the Burnt Lake Area.

**Stage III:** During fractionation of the 1650 Ma Burnt Lake Granite a metal-bearing, volatile-rich fluid evolved and was expelled into the overlying and adjacent volcanic sequence (Figure 6-3). The hydrothermal fluids were enriched in the incompatible elements of K, Rb, Mn, Ca, Pb, Zn, Mo and Ga. The potassic metasomatism and mineralization was controlled by regional fractures and permeable lithological horizons. Whole-rock geochemistry indicates an increase in  $K_2O$ ,  $CaO$ ,  $MnO$ ,  $Pb$ ,  $Zn$ ,  $Mo$ ,  $Rb$ ,  $Ga$  and  $U$  with a decrease in  $Na_2O$  and  $SiO_2$  within the host rocks. The uranium mineralization associated with this metasomatic event is not correlated with the granophile mineralization but is probably remnant of the earlier Stage I mineralization.  $Pb$  isotope data from this rock suite indicates a model age of 1651 Ma which relates the galena mineralization to the post-tectonic Burnt Lake Granite.



**Figure 6-3: Schematic diagram representing a model for base metal mineralization within the Upper Aillik Group in the Burnt Lake Area.**

### 6.3 Conclusions

The Burnt Lake area is underlain by the dominantly calcalkaline felsic volcanic and volcanoclastic rocks of the Upper Aillik Group. These rocks were deposited during subduction related volcanic activity at ca. 1855 Ma. The volcanic rocks were subjected to polyphase deformation during the Makkovikian Orogeny (ca. 1700 - 1720 Ma) and were later overprinted during the Grenville Orogeny (ca. 1000 Ma). Metamorphic grade is from lower to middle greenschist facies. Granitoid rocks are represented by the synkinematic Makkovikian plutonic suite (ca. 1800 Ma) and the post-tectonic Burnt Lake Granite which is part of the regional Trans-Labrador batholith (ca. 1650 Ma).

The post-tectonic Burnt Lake Granite is a high level leucocratic granite which exhibits geochemical trends and endocontact molybdenite mineralization characteristic of specialized granites. The Burnt Lake Granite also shows a regular zonation pattern of silica towards its western intrusive (molybdenite-bearing) contact with the Upper Aillik Group felsic volcanic rocks. Rb/Sr data from the Burnt Lake Granite give an age of 1650 Ma, however, the isotopic ratios were disturbed by later fluids whereby Rb was removed and/or Sr was added.

Detailed studies of uranium occurrences in the Burnt Lake area have characterized the showings into five main suites.

These are (1) the Burnt Lake sodic, (2) the Burnt Lake potassic, (3) the Emben Main, (4) the Emben South and (5) the Aurora River suites.

(1). The Burnt Lake potassic occurrences were formed by syn- to slightly post-volcanic metasomatic alteration along with contemporaneous leaching and deposition of uranium in reducing environments. The K-metasomatic event is reflected in the whole-rock chemistry which indicates an increase in  $K_2O$  and U and a decrease in  $SiO_2$  and  $Na_2O$ . The similarities in REE patterns between the mineralized and unmineralized rocks suggest that the mineralizing fluids were chemically similar to the hosting felsic volcanic rocks or at least had achieved a degree of equilibrium with these rocks. Hydrothermal solution movement, responsible for alkali metasomatism and uranium mineralization, was initiated and maintained by a deep-seated heat source adjacent to vent areas with fluid movement and alterations taking place along more permeable tuffaceous horizons.

(2). The Burnt Lake sodic occurrences were formed as a result of metamorphism and igneous activity during the Makkovikian Orogeny between 1800-1770 Ma. The Na-metasomatic event was initiated during intrusion of post-tectonic granitoids and was accompanied by  $Na_2O$  enrichments and  $K_2O$  and  $SiO_2$  depletions.

(3). The Emben Main showing was formed as a result of Na-metasomatism accompanied by  $Na_2O$  enrichments and  $K_2O$  and  $SiO_2$

depletions. REE patterns for the Emben Main showing are reminiscent of those in the Makkovik area that were linked to granite-related, phosphate complex-bearing, hydrothermal fluids. The uraninite mineralization has been dated at ca. 1300 Ma, therefore, remobilization and reconcentration of uranium probably occurred during the Grenville Orogeny.

(4). The Emben South uraniferous occurrence was preceded by strong alkali metasomatism involving  $\text{Na}_2\text{O}$  enrichments and  $\text{K}_2\text{O}$  depletions. Uraniferous volatile-rich solutions were expelled during fractionation of the post-tectonic granite and permeated along mafic dykes which acted as a channel or a REDOX boundary for the hydrothermal solutions. Ca-, Ti-, P- and Fe-rich solutions coeval or subsequent to uraninite precipitation have resulted in the association of uraninite and sphene, ilmenite, calcic amphiboles and pyroxenes. The presence of abundant apatite reflects the probability that uraninite was transported as a phosphate complex. The association of the granophile minerals fluorite, molybdenite, chalcopyrite and sphalerite attests to the granite related mineralization. Later remobilization and reconcentration of uranium during the Grenville orogeny has possibly increased the grade at this showing.

(5). Uranium-rich solutions activated during regional metamorphism (Makkovikian Orogeny - 1800-1770 Ma) permeated

along structural weaknesses and precipitated in favourable horizons of carbonate-rich andesites. The Aurora River uraniferous phase was preceded by a sodic and calcic metasomatic phase.

(6). Another period of mineralization was initiated during intrusion of the Burnt Lake Granite which is considered to be a small pluton within the Trans Labrador Batholith. During fractionation of the granite a metal-bearing, volatile-rich fluid evolved and was expelled into the overlying and adjacent volcanic sequence. The potassic metasomatism and mineralization was controlled by regional fractures and permeable lithological horizons. The K-metasomatic event was accompanied by an increase in  $K_2O$ ,  $CaO$ ,  $Pb$  and  $Zn$  and a decrease in  $Na_2O$  and  $SiO_2$ .  $Pb$  isotope data from this rock suite indicates a model age of 1651 Ma which relates the galena mineralization to the post-tectonic Burnt Lake Granite.

To summarize, the Burnt Lake area has had a complex evolutionary history of sedimentary, volcanic and igneous activity. Uranium mineralization occurred as a result of syn- to slightly post-volcanic metasomatic alteration (K) which resulted in contemporaneous leaching and deposition of uranium in reducing environments during deposition of the Upper Aillik Group in the Hudsonian Orogeny. Epigenetic uranium mineralization is associated with intense sodic metasomatism

which was initiated during the terminal phase of the Makkovikian Orogeny. Granophile mineralization associated with potash metasomatism occurred during the later stages of fractionation of the Burnt Lake Granite during the Labradorian Orogeny. Remobilization and concentration of uranium associated with structural weaknesses can be related to the Grenville Orogeny. Finally, Pb and Rb/Sr isotopic signatures have been disturbed by varying degrees during the Grenvillian, thus further complicating the understanding.



## REFERENCES

- Bailey, D.G., 1978. The geology of the Walker-MacLean Lake area (13K/9, 13J/12), Central Mineral Belt, Labrador. Nfld. Dept of Mines and Energy, Rept. 78-1, pp. 1-8.
- Bailey, D.G., 1979. Geology of the Walker-MacLean Lake area, 13K/9, 13J/12, Central Mineral Belt, Labrador. Nfld. Dept. of Mines and Energy, Rept. 78-3, 17p..
- Bailey, D. G., 1981. Kaipokok Bay - Big River Labrador. Nfld. Dept. of Mines and Energy, Map 81-18, 1:100,000.
- Bailey, J. C., 1977. Fluorine in granitic rocks and melts: A Review. Chem. Geol., v. 19, pp.1-42.
- Beavan, A.P., 1958. The Labrador uranium area. Proc. of the Geol. Assoc. of Can., v. 10, pp. 137-145.
- Beavan, A.P., 1968. Report on Exploration in the Kaipokok Bay -Big River Joint Venture Area, 1967: Annual Report, BRINEX Ltd.
- Brummer, J.J., and Mann, E.L., 1961. Geology of the Seal Lake area, Labrador. Geol. Soc. of Amer. Bull., v. 72, pp. 1361-1382.
- Bundrock, G., 1970. Geological Observations in the Michelin, Emben and Shoal Lake Areas. Unpub. BRINEX Ltd. Rept..
- Cathelineau, M., 1983. Potassic alteration in French hydrothermal uranium deposits. Mineral. Deposita, v. 18, pp. 89-97.
- Christie, A.M., Roscoe, S.M. and Fahrig, W.F., 1953. Preliminary map of the Central Labrador Coast, Nfld. with descriptive notes. Geol. Sur. of Can., Pap. 53-14, 3 p..
- Cote, R., 1980. Reconnaissance Geology and Prospecting of the Aurora - McLean - Burnt - Emben Lakes Area, Area A, Labrador. Unpub. BRINEX Ltd. Rept..
- Daly, R.A., 1902. The geology of the northeast coast of Labrador. Bull. of Com. Zoo., Harvard, v. 38, Geol. Series, v. 5, no.5, pp. 205-269.

- Davidson, G.I. and Gentile, F., 1978. Reconnaissance Investigation of Emben, Winter-Bernard Lakes, Marsha Lake and Pitch Lake Prospects, Area A and Active Pond Area, Area B, Labrador. Unpub. BRINEX Ltd. Rept..
- Doak, R.S. and MacCallum, I.M., 1970. Boulder tracing and allied work in the Kaipokok River area. Unpublished BRINEX report on file with Nfld. Dept. of Mines and Energy, Mineral Development Division.
- Douglas, G.V., 1953. Notes on localities visited on the Labrador coast in 1946 and 1947. Geol. Surv. of Can., Pap. 53-1, 67p..
- Easton, R.M., 1986. Geochronology of the Grenville Province. In The Grenville Province, ed. J.M. Moore et al.. Geol. Assoc. Can. Spec. Pap. 31, pp. 127-173.
- Ermanovics, I.F., and Raudsepp, M., 1979. Geology of the Hopedale block of eastern Nain Province, Labrador. Geol. Surv. of Can., Pap. 79-1B, pp. 341-348.
- Evans, D., 1980. Geology and petrochemistry of the Kitts and Michelin uranium deposits and related prospects, Central Mineral Belt, Labrador. Unpub. Ph.D. thesis, Queen's Univ., Kingston, Ont., 311p..
- Evans, E.L., 1952. Native copper discoveries in the Seal Lake area, Labrador. Proc. Geol. Assoc. of Can., v.5, pp.111-116.
- Fahrig, W.F., 1959. Snegamook Lake, west half. Geol. Surv. of Can., Map 1079A.
- Fahrig, W.F., and Larochelle, A., 1972. Paleomagnetism of the Michael Gabbro and possible evidence of the rotation of the Makkovik Subprovince. Can. Jour. of Earth Sci., v. 9, pp. 1287-1296.
- Fryer, B. J., 1977. Rare earth evidence in iron formation for changing oxidation states. Geochim. Cosmo. Acta, v. 41, pp. 361-367.
- Gandhi, S.S., 1968. General geological observations on Aillik-Makkovik Area, Labrador; Report on exploration in Aillik-Makkovik area during 1967. Unpub. BRINEX Ltd. Rept..
- Gandhi, S.S., Grasty, R.L. and Grieve, R.A.F., 1969. The geology and geochemistry of the Makkovik Bay area, Labrador. Can. Jour. of Earth Sci., v. 6, pp. 1019-1035.

- Gandhi, S.S., 1978. Geological setting and genetic aspects of uranium occurrences in the Kaipokok Bay - Big River area, Labrador. *Econ. Geol.* v. 73, pp. 1492-1522.
- Gandhi, S.S., 1984. Uranium in early Proterozoic Aillik Group, Labrador. *In* Proterozoic unconformity and stratabound uranium deposits. ed. Ferguson, J.. IAEA, Vienna, Tech. Doc. 315, pp. 35-68.
- Gandhi, S.S., 1986. Uranium in early Proterozoic Aillik Group, Labrador. *In* Uranium deposits of Canada, CIM Spec. Vol 33, p.p. 70-82.
- Gandhi, S.S., Grasty, R. L., and Grieve, R.A.F., 1959. The geology and geochronology of the Makkovik Bay area, Labrador. *Can. Jour. of Earth Sci.*, v. 6, pp. 1019-1034.
- Gandhi, S.S., Krogh, T.E., and Corfu, F., 1988. U-Pb zircon and titanite dates on two granitic intrusions of the Makkovik Orogen and a peralkaline granite of the Red Wine Intrusive Complex, central Labrador. *Geol. Assoc. of Can., Prog. with Abst.*, 13, p. A42.
- Gower, C. F., Flanagan, M.J., Kerr, A., and Bailey, D.G., 1982. Geology of the Kaipokok Bay - Big River area, Central Mineral Belt, Labrador. *Nfld. Dept. of Mines and Energy Rept.* 82-7, 77 p..
- Gower, C.F., and Owen, V., 1984. Pre-Grenvillian and Grenvillian lithotectonic regions in eastern Labrador - correlations with the Sveconorwegian Orogenic Belt in Sweden. *Can. Jour. of Earth Sci.*, v. 21, pp. 678-693.
- Gower, C.F., Ryan, A.B., Bailey, D.G., and Thomas, A., 1980. The position of the Grenville Front in eastern and central Labrador. *Can. Jour. of Earth Sci.*, v. 17, pp. 784-788.
- Gower, C.F., and Ryan, A.B., 1986. Proterozoic evolution of the Grenville Province and adjacent Makkovik Province in eastern-central Labrador. *In* The Grenville Province, *Geol. Assoc. Can. Spec. Pap.* 33, pp. 281-296.
- Gower, C.F., and Ryan, A.B., 1987. Two stage felsic volcanism in the Lower Proterozoic Upper Aillik Group, Labrador, Canada: Its relationship to syn- and post-kinematic plutonism. *Jour. Geol. Soc. Lond., Spec. Pub. No.* 33, pp. 201-210.

- Grant, N.K., Voner, F.R., Marzano, M.S., Hickman, M.H., and Ermanovics, I.F., 1983. A summary of Rb-Sr isotope studies in the Archean Hopedale Block and the adjacent Proterozoic Makkovik Subprovince, Labrador: Rept. 5. Geol. Sur. of Can., Pap. 83-1B, pp. 127-134.
- Hanson, G. N., 1980. Rare earth elements in petrogenetic studies of igneous systems. Ann. Rev. Earth Plan. Sci., v.8, pp. 371-406.
- Harder, D.G., 1981. Reevaluation of the Emben (Mathew Ben) Showings, Area A, Labrador. Unpub. BRINEX Ltd. Rept., 49p..
- Henman, L.M., McNutt, R.H., and Krogh, T.E., 1986. Geological significance of U-Pb and Rb-Sr ages for two pre-tectonic granites from the Central Metasedimentary Belt, Ontario; In The Grenville Province, Geol. Assoc. of Can. Spec. Pap. 33, pp. 209-221.
- Hildreth, W., 1981. Gradients in silicic magma chambers: Implications for lithospheric magmatism. Jour. Geophys. Res., v. 86, pp. 10153-10192.
- Hoffman, P.F., 1988. United plates of America, the birth of a craton: Early Proterozoic assembly and growth of Laurentia. Ann. Rev. Earth Plan. Sci., v. 16, pp. 543-603.
- Hoeve, J., 1974. Soda metasomatism and radioactive mineralization in the Vastervik area, southeastern Sweden. unpub. Ph.D. thesis, Free Univ., Amsterdam, The Netherlands.
- Hughes, C.J., 1973. Spilites, keratophyres, and the igneous spectrum. Geol. Mag., v. 109, pp. 513-527.
- Hum, P., 1984. Labrador Areas A and B, 1984, summary of field investigations. Unpub. BRINEX Ltd. Rept., Brinco Document No. 634.
- Hum, P., 1985. Burnt Lake Prospect, Labrador, first year assessment report. Unpub. BRINEX Ltd. Rept., Brinco Mining Document No. 727.
- Irvine, T.N., and Baragar, W.R.A., 1971. A guide to the chemical classification of the common volcanic rocks. Can. Jour. of Earth Sci., v.8, pp. 523-548.
- Janecek, J., 1969. Investigation of Emben (Mathew Ben) Radioactive Showings during 1969. Unpub. BRINEX Ltd. Rept..

- Jensen, L.S., 1976. A new cation plot for classifying subalkalic volcanic rocks. Ont. Dept. Mines, Misc. Pap. 66, 22p.
- Kerr, A., 1986. Plutonic rocks of the eastern Central Mineral Belt: general geology and description of regional granitoid units. Nfld. Dept. of Mines and Energy Rept. 86-1, pp. 89-100.
- Kerr, A., 1987. Plutonic rocks of the eastern Central Mineral Belt: lithogeochemical patterns and identification of potential specialized granitoids. Nfld. Dept. of Mines and Energy Rept. 87-1, pp. 161-181.
- Kerr, A., 1988. Geochemical characteristics and mineral potential of specialized granitoid plutons in the Trans-Labrador Batholith, eastern Labrador. Nfld. Dept. of Mines, Rept. 88-1, pp. 15-36.
- Kerr, A., 1990. Early Proterozoic granitoid magmatism and crustal evolution in the Makkovik Province of Labrador: A geochemical and isotopic study. Unpub. PhD. thesis, Memorial University of Newfoundland, 528p..
- Kerr, A., and Fryer, B.J., 1989. Neodymium isotopic signatures of Proterozoic igneous rocks and the subsurface distribution of Precambrian crustal provinces in eastern Labrador. Geol. Assoc. Can. Prog. with Abst., v. 14, p. A125.
- Kerr, A. and Krogh, T., 1990. The Trans-Labrador granitoid belt in the Makkovik Province: New geochronological and isotopic data and their geological implications. Nfld. Dept. of Mines and Energy, Report 90-1, pp. 237-249.
- Kerrick, R., 1989. Lithophile element systematics of gold vein deposits in Archean greenstone belts: Implications for source processes. Econ. Geol. v. \*\* , pp. 508-519.
- Kerrick, R., Fryer, B.J., King, R.W., Willmore, L.M., and van Hees, E., 1987. Crustal outgassing and LILE enrichment in major lithosphere structures, Archean Abitibi greenstone belt. Can. Min. Pet., v. 97, pp. 156-168.
- King, A.F., 1963. Geology of the Cape Makkovik Peninsula, Aillik, Labrador. Unpub. MSc. thesis, Memorial University of Nfld., 114p.
- Kontak, D.J., 1978. Investigation of four uranium showings in the Central Mineral Belt, Labrador. In Report of Activities for 1977, Nfld. Dept. of Mines and Energy, Mineral Development Division, Rept. 78-1, pp. 27-43.

- Kontak, D.J., 1980. Geology, geochronology and uranium mineralization in the Central Mineral Belt of Labrador, Canada. Unpub. MSc. thesis, Univ. of Alberta, Edmonton, Alberta. 378p..
- Krajewski, J., 1976. Geological Map of MacLean Lake. Unpub. BRINEX Ltd. Map.
- Krajewski, J., Turner, D., Turner, M.A., 1977. Surface exploration and diamond drilling results of the Burnt Lake Prospect, Annual Report 1977, Brinco Document No. G77021.
- Kranck, E. H., 1939. Bedrock geology of the seaboard region of Newfoundland and Labrador. Geol. Sur. of Nfld., Bull. 19, 44p..
- Kranck, E. H., 1953. Bedrock geology of the seaboard of Labrador between Domino Run and Hopedale, Newfoundland. Geol. Sur. of Can., Bull. 26, 41p..
- Langmuir, D.L., 1978. Uranium solution-mineral equilibria at low temperatures with applications to sedimentary ore deposits. Geochim. et Cosmochim. Acta, v. 42, pp. 547-570.
- Leroy, J., 1978. The Margnac and Fanay uranium deposits of the La Crouzille district (western Massif Central, France): Geologic and fluid inclusion studies. Econ. Geol. v. 73, pp. 1611-1634.
- Lieber, O. M., 1860. Notes on the geology of the coast of Labrador. Report of the United States Coast Survey for 1860.
- Longerich, H.P., and Veinott, G., 1986. Study of precision and accuracy of XRF data obtained in the Dept. Earth Sciences/Centre for Earth Resources Research, Memorial University. Unpub. MUN Rept., 23p.
- Ludwig, K.R., 1989. ISOPLOT for MS-DOS - A plotting and regression program for radiogenic-isotope data, for IBM-PC compatible computers, Version 1.10. USGS Open-File Rept. 88-557 (revised 1989.06.26), 43p..
- MacDougall, C.S., 1988. A metallogenic study of polymetallic granophile mineralization within the early Proterozoic Upper Aillik Group, Round Pond area, Central Mineral Belt, Labrador. Unpub. MSc. thesis, Memorial University of Nfld., 245p.

- MacDougall, C.S., and Wilton, D.H.C., 1987a. Middle Proterozoic granite-related mineralization in the Round Pond area, Labrador. Geol. Surv. of Can. Rept. 87-1A, pp. 457-466.
- MacDougall, C.S., and Wilton, D.H.C., 1987b. A new zinc showing with associated precious metals, in the Round Pond area, near Makkovik, Labrador. Nfld. Dept. of Mines, Open File Report 130/3 (110), 9p..
- MacDougall, C.S., and Wilton, D.H.C., 1988. Geology of radioactive zones in the Round Pond area, Labrador. Geol. Surv. of Can. Rept. 88-1C, pp. 271-275.
- MacKenzie L.M., and Wilton, D.H.C., 1987a. Uranium, molybdenum and base metal sulphide mineralization in the Burnt Lake area, central Labrador; three different styles of ore formation. Geol. Surv. of Can. Rept. 87-1A, pp. 467-476.
- MacKenzie L.M., and Wilton, D.H.C., 1987b. Metallogeny of the Burnt Lake area, Labrador; four different styles of mineralization. CIM Bull., v. 80, p.85.
- MacKenzie L.M., and Wilton, D.H.C., 1988. The Grenville Province boundary in the Burnt Lake area, Labrador Central Mineral Belt. Geol. Surv. of Can. Rept. 88-1C, pp. 233-237.
- MacPherson, H.G., 1954. Report on the Kaipokok River concession area, Labrador. Unpub. AMCO Ltd. rept., 13p..
- Marten, B.E., 1975. Geology of the Letitia Lake area, Labrador. Nfld. Dept. of Mines and Energy Rept. 75-1, pp. 75-86.
- Marten, B.E., 1977. The relationship between the Aillik Group and the Hopedale gneiss, Kaipokok Bay, Labrador. Unpub. Ph.D. thesis, Memorial University of Newfoundland., St. John's, Nfld., 389p.
- Meschede, M., 1986. A method of discrimination between different types of mid-ocean basalts and continental tholeiites with the Nb-Zr-Y diagram. Chem. Geol. v. 56, pp. 207-218.
- Minatidas, D.G., 1976. A comparative study of trace element geochemistry and mineralogy of some uranium deposits of Labrador, and evaluation of some uranium exploration techniques in a glacial terrain. Unpub. M.Sc. thesis, Memorial University of Nfld., St. John's, Nfld.

- Muecke, G.K., and Clarke, D.B., 1981. Geochemical Evolution of the South Mountain Batholith, Nova Scotia: rare earth element evidence. *Can. Mineral.*, v. 19, pp. 133-145.
- Mutschler, F. E., Wright, E. G., Ludington, S., Abbott, J. T., 1981. Granite molybdenite systems. *Econ. Geol.*, v. 76, pp. 874-897.
- Nie, N.H., Hull, C.H., Jenkins, J.G., Steinbrenner, K., and Bent, D.H., 1975. SPSS. Statistical package for the social sciences. Second Edition, McGraw-Hill, 675 p.
- North J.W., and Wilton, D.H.C., 1988 Stratigraphy of the Warren Creek Formation, Moran Lake Group, Labrador Central Mineral Belt. *Geol. Surv. of Can. Rept.* 88-1C, pp. 123-128.
- O'Conner, J.T., 1965. A classification of quartz-rich igneous rocks based on feldspar ratios. *U.S. Geol. Surv. Prof. Pap.* 525-B.
- Owen, J.V., Rivers, T., and Gower, C.F., 1986. The Grenville Front on the Labrador coast. *Geol. Assoc. of Can. Spec. Pap.* pp. 95-106.
- Packard, A. S., 1891. The Labrador coast. New York, N.D.C. Hodges (publisher), 513 p..
- Payette, C. and Martin, R. F., 1986. The glass inclusions and mineralogy of rhyolites, Upper Aillik Group, Labrador. Unpub. Rept., *Geol. Surv. of Canada*, Project 27 ST.2323-3-5-0058, 98p..
- Pearce, J.A., and Cann, J.R., 1973. Tectonic setting of basic volcanic rocks determined using trace element analyses. *Earth Plan. Sci. Lett.*, v. 19, pp. 290-300.
- Pearce, J.A., Harris, N.B.W., and Tindle, A.G., 1984. Trace element discrimination diagrams for the tectonic interpretation of granitic rocks. *Jour. of Pet.*, v. 25, pp. 956-983.
- Piloski, M.J., 1955. Geological Report on Aillik-Shoal Lake area. Unpub. BRINEX Report G56016, Appendix 1, 9p..
- Rivers, T., and Chown, E.H., 1986. The Grenville Orogen in eastern Quebec and western Labrador - definition, identification and tectonometamorphic relationships of autochthonous, parautochthonous and allochthonous terranes. *In* The Grenville Province, *Geol. Assoc. Can. Spec. Pap.* 33, pp. 31-50.



- Romberger, S. B., 1984. Transport and deposition of uranium at temperatures up to 300 C: geological implications. in Uranium Geochemistry, Mineralogy, Geology, Exploration, and Resources, eds. B. DeVivo, F. Ippolito, G. Capaldi, and P.R. Simpson. Inst. of Min. and Metall., pp. 12-17.
- Roscoe, S.M. and Emslie, R.F., 1973. Kasheshibaw Lake. Geol. Sur. of Can., Map 1342A.
- Ryan, A.B., 1977. Molybdenite: Some background information and a review of mineralization on the Aillik Peninsula, Labrador. Unpub. Rept Nfld. Dept. of Mines (File 130/3 (74)). 15p..
- Ryan, A.B., 1984. Regional geology of the central part of the Central Mineral Belt, Labrador. Nfld. Dept. of Mines and Energy Mem. 3, 185p..
- Ryan, A.B., Baragar, W.R.A., and Kontak, D.J., 1987. Geochemistry, tectonic setting, and mineralization of high-potassium Middle Proterozoic rocks in central Labrador, Canada. In press, IGCP 217 Symposium Vol. 15p..
- Ryan, A.B., Kay, A., and Ermanovics I.F., 1983. Notes to accompany maps 83-38 to 83-41 showing the geology of the Makkovik Subprovince between Kaipokok Bay and Bay of Islands, Labrador. Nfld. Dept. of Mines Rept., 21p.
- Scharer, U., Krogh, T.E., Wardle, R.J., Ryan, B., and Gandhi, S.S., 1988. U-Pb ages of early to middle Proterozoic volcanism and metamorphism in the Makkovik Orogen, Labrador. Can. Jour. of Earth Sci., v. 25, pp. 1098-1107.
- Scharer, U., Krogh, T., and Gower, C.F., 1986. Age and evolution of the Grenville Province in eastern Labrador, from U/Pb systematics in accessory minerals. Cont. Min. Pet., v.94, pp. 438-451.
- Scott, R.B., 1971. Alkali exchange during devitrification and hydration of glasses in ignimbrite cooling units. Jour. of Geol., v. 79, pp. 100-110.
- Sharpley, F.J., 1978. BRINEX/UG Canada joint venture areas A and B: Geology and uranium exploration of the Melody Hill prospect. Unpub. BRINEX Rept..
- Sharpley, F.J. and Cote, P., 1980. Geology and uranium exploration of the Musong North, Aurora River extension, Aurora River, Burnt Brook Prospects and Andrew zone, Area A, Labrador. Unpub. BRINEX Rept.

- Simpson, A.M., 1988. Geochemical signatures and dispersal patterns of trace and rare earth elements in till from the Burnt Lake area, Labrador. Unpub. BSc. thesis, Memorial University of Nfld., 119p..
- Smellie, J.A.T. and Laurikko, J., 1984. Skuppesavon, northern Sweden: A uranium mineralization associated with alkali metasomatism. Mineral. Deposita, v. 19, pp.183-192.
- Smirnov, V.I., 1977. Deposits of uranium. in Ore deposits of the USSR. Vol. II. ed. V.I. Smirnov. Pitman Publ.
- Smith, D.K., 1984. Uranium mineralogy. in Uranium Geochemistry, Mineralogy, Geology, Exploration, and Resources, eds. B. DeVivo, F. Ippolito, G. Capaldi, and P.R. Simpson. Inst. of Min. and Metall., pp. 43-88.
- Smyth, W.R., Marten, B.E., and Ryan, A.B., 1975. Geological mapping in the Central Mineral Belt, Labrador; redefinition of the Croteau Group. Nfld. Dept. Mines and Energy, Rept. 75-1, pp. 51-74.
- Smyth, W.R., Marten, B.E., and Ryan, A.B., 1978. A major Aphebian-Helikian unconformity within the Central Mineral Belt of Labrador; definition of new groups and metallogenic implications Can. Jour. of Earth Sci., pp. 1954-1966.
- Sorensen, H., 1977. Features of the distribution of uranium in igneous rocks - uranium deposits associated with igneous rocks. In. Recognition and evaluation of uraniferous areas. Int. Atomic Energy Agency, Vienna.
- Stacey, J.S., and Kramers, J.D., 1975. Approximation of terrestrial lead isotope evolution by a two-stage model. Earth and Plan. Sci. Lett., v. 26, pp. 207-221.
- Stemprok, M., 1980. Differentiation of some elements by ore-bearing granites. Metallization Associated with Acid Volcanism, v. 3, pp. 393-403.
- Stevenson, I.M., 1970. Rigolet and Groswater Bay map-areas, Newfoundland (Labrador). Geol. Sur. of Can., Pap. 69-48, 24p..
- Stewart, J.W. 1983. BP Minerals - Billiton joint venture, Florence Lake, Labrador, Summer 1983, BP Minerals Ltd. Preliminary Report. Unpub. Rept. BP Minerals Ltd., 11p..

- Stockwell, C.H. 1963a: Second report on structural provinces, orogenies, and time-classification of rocks of the Canadian Precambrian Shield. Geol. Sur. of Can., Pap. 62-17, pp. 123-133.
- 1963b: Third report on structural provinces, orogenies and time-classification of the Canadian Precambrian Shield. Geol. Sur. of Can., Pap. 63-17, pp. 125-131.
- Stockwell, C.H., 1964. Fourth report on structural provinces, orogenies and time-classification of rocks of the Canadian Precambrian Shield. Geol. Sur. of Can., Pap. 64-17, pp. 1-21.
- Stockwell, C.H., 1973. Revised Precambrian time-scale for the Canadian Shield. Geol. Sur. of Can., Pap. 75-52, 4p..
- Streckheisen, A., 1976. To each plutonic rock its proper name. Earth Sci. Rev., v. 12, pp. 1-33.
- Strong, D.F., 1981. Ore deposits models- 5: A model for granophile mineral deposits. Geoscience Canada, v. 8, pp. 155-161.
- Stuckless, J.S. and Troeng, B., 1984. Uranium mineralization in response to regional metamorphism at Lilljuthatten, Sweden. Econ. Geol., v. 79, pp. 509-528.
- Sutton, J.S. 1970. Geological report - area West of Florence Lake, Uqjoktok Area, Labrador. Unpub. BRINEX Ltd. Rept., 8p..
- Sutton, J.S., 1972. The Precambrian gneisses and supracrustal rocks of the western shore of Kaipokok Bay, Labrador, Newfoundland. Can. Jour. of Earth Sci., v.9, pp. 1677-1692.
- Sutton, J.S., Marten, B.E., and Clark, A.M.S., 1971. Structural history of the Kaipokok Bay area, Labrador, Newfoundland. Proc. of the Geol. Assoc. of Can., v.24, pp.103-106.
- Sutton, J.S., Marten, B.E., Clark, A.M.S. and Knight I., 1972. Correlation of Precambrian supracrustal rocks of coastal Labrador and southwestern Greenland. Nature, v. 238, pp. 122-123.
- Swinden, H.S., Lane, T. E., and Thorpe, R.I., 1988. Lead-isotope compositions of galena in carbonate-hosted deposits of western Newfoundland: evidence for diverse lead sources. Can. Jour. of Earth Sci., v. 25, pp. 593-602.

- Taylor, F.C., 1971. A revision of Precambrian structural provinces in northeastern Quebec and northern Labrador. *Can. Jour. of Earth Sci.*, v. 8, pp. 579-584.
- Taylor, F.C., 1972. Reconnaissance geology of a part of the Precambrian Shield, northeastern Quebec and northern Labrador, Part III. *Geol. Surv. of Can.*, Pap. 71-48.
- Taylor, F.C., 1979. Reconnaissance geology of a part of the Precambrian Shield, northeastern Quebec, northern Labrador and Northwest Territories. *Geol. Surv. of Can. Mem.* 393, 99p..
- Taylor, R.P., Strong, D.F., and Fryer, B.J., 1981. Volatile control of contrasting trace element distributions in peralkaline granitic and volcanic rocks. *Can. Min. Pet.*, v. 77, pp. 267-271.
- Taylor, R.P., and Fryer, B.J., 1982. Rare earth element geochemistry as an aid to interpreting hydrothermal ore deposits. In *Metallization associated with acid magmatism*, v. 6.
- Taylor, R.P., and Fryer, B.J., 1983. Rare earth element lithogeochemistry of granitoid mineral deposits. *Can. Min. Metall. Bull.*, v. 76, No. 850, pp. 74-84.
- Taylor, R.P. and Strong, D.F., 1985. Granite-related mineral deposits: Geology, petrogenesis and tectonic setting. Extended Abstracts of papers presented at the CIM conference in Halifax, 1985 CIM Geology Division.
- Taylor, S.R., and McLennan, S.M., 1981. The composition and evolution of the continental crust: rare earth element evidence from sedimentary rocks. *Phil. Trans. Roy. Soc. Lon.*, v. A301, pp. 381-399.
- Thomas, A., 1981. Geology of the southwestern margin of the Central Mineral Belt, Labrador. *Nfld. Dept. of Mines and Energy Rept.* 81-4, 40p..
- Thomas, A., 1983. Geology of the Letitia Lake - Wapustan Lake area. *Nfld. Dept. of Mines and Energy Map* 83-31.
- Thomas, A., Nunn, G.A.G., and Krogh, T.E., 1986. The Labradorian Orogeny: evidence for a newly identified 1600 to 1700 Ma orogenic event in Grenville Province crystalline rocks from central Labrador. In *The Grenville Province*, *Geol. Assoc. Can. Spec. Pap.* 33, pp. 175-190.

- Tischendorf, G., 1977. Geochemical and petrographic characteristics of silicic magmatic rocks associated with rare-earth mineralization. In Mineralization Associated with Acid Magmatism, v. 23, pp. 41-96.
- Turekian, K. K., and Wedepohl, K. H., 1961. Distribution of the elements in the earth's crust. Geol. Soc. Amer. Bull., v. 72, pp. 175-192.
- Tuach, J., Davenport, P.H., Dickson, W.L. and Strong, D.F., 1986. Geochemical trends in the Ackley granite, southeast, Newfoundland: Their relevance to magmatic/metallogenic processes in high-silica granitoid systems. Can. Jour. of Earth Sci., v. 23, pp. 747-765.
- Wagenbauer, H.A., Riley, C.A. and Dawe, C., 1983. Geochemical Laboratory - descriptions of analytical procedures. In Current Research, compiled and edited by M.J. Murry, P.D. Saunders, W.D. Boyce and R.V. Gibbons, Newfoundland Department of Mines and Energy, Mineral Development Division Report 83-1, pages 133-137.
- Walraven, F., Kleemann, G. J., and Allsopp, H. L., 1986. Disturbance of trace element and isotope systems and its bearing on mineralization in acid rocks of the Bushveld Complex, South Africa. In High heat production (HHP) granites, hydrothermal circulation and ore genesis, CIMM Spec. Vol., pp. 393-408.
- Wanless, R.K., and Loveridge, W.D., 1978. Rubidium - Strontium isotopic age studies, Report 2 (Canadian Shield). Geol. Surv. of Can. Pap. 77-14.
- Wanless, R. K., Stevens, R. D., Lachance, G. R., and Delabio, R. N., 1970. Age determinations and geological studies, K-Ar isotopic ages, Report 9. Geol. Sur. of Can., Pap. 69-2A, pp. 73-74.
- Wardle, R.J., and Bailey, D.G., 1980. Contrasting sedimentary-volcanic regimes in the Lower Proterozoic of Labrador. Geol. Assoc. of Can. program, v. 5, p. 87.
- Wardle, R.J., and Bailey, D.G., 1981. Early Proterozoic sequences in Labrador. In Proterozoic Basins of Canada. Geol. Surv. of Can., Pap. 81-10, pp. 331-359.
- Wardle, R.J., Rivers, T., Gower, C.F., Nunn, G.A.G., and Thomas, A., 1986. The northeastern Grenville Province: new insights. In The Grenville Province, Geol. Assoc. Can. Spec. Pap. 33, pp. 13-30.

- Wardle, R.J., and Wilton, D., 1985. Reconnaissance sampling for precious metals in the Kaipokok Bay - Big River area, Labrador. Nfld. Dept. of Mines and Energy Open File Lab 1679, 17p..
- Wardle, R.J., and Wilton, D., 1988. Reconnaissance studies in the Seal - Letitia Lake area, Labrador. Nfld. Dept. of Mines Rept. of Act. for 1988, pp. 35-36.
- Watson-White, M.V.W., 1976. A petrological study of acid volcanic rocks of the Aillik Series, Labrador. Unpub. MSc. thesis, McGill Univ., Montreal, 92p..
- White, A.J.R. and Chappel, B.W., 1983. Granitoid types and their distribution in the Lachlan Fold Belt, Southeastern Australia. Geol. Soc. of Amer., Mem. 159, pp. 21-54.
- White, M.V.W., and Martin R.F., 1980. The metasomatic changes that accompany uranium mineralization in the nonorogenic rhyolites of the upper Aillik Group, Labrador. Can. Min., v. 18, pp. 459-479.
- Windley, B.F., 1984. The Evolving Continents, 2<sup>nd</sup> Edition. John Wiley & Sons, Toronto. 399p..
- Williams, H., and Hatcher, R.D. Jr., 1982. Suspect terranes and accretionary history of the Appalachian Orogen. Geology, v.10, pp. 530-536.
- Wilton, D.H.C., 1989c. Final report on metallogeny of the Labrador Central Mineral Belt. Unpub. Rept. to the Geol. Surv. Can., Contract Serial No. 23233-8-0936/01-55, 310p..
- Wilton, D.H.C., 1991a. Metallogeny of the Labrador Central Mineral Belt. Geol. Surv. of Can. Pap., (in press).
- Wilton, D.H.C., 1991b. Metallogenic and Tectonic Implications of Pb isotope data for galena separates from the Labrador Central Mineral Belt. Econ. Geol., (in press).
- Wilton, D.H.C., Longerich, H.P., and Fryer, B.J., 1988. The application of inductively coupled plasma-mass spectrometry (ICP-MS) determinations of inter and intra element isotope ratios to radiogenic isotope tracer studies and geochronology. Geol. Assoc. of Can., Prog. with Abst., v. 13, p. A135.
- Wilton, D.H.C., Longerich, H.P., and Fryer, B.J., 1990. Metallogenic significance of ICP-MS-derived trace element and Pb isotope data on uraninite separates from the Labrador Central Mineral Belt. (in press).

- Wilton, D.H.C., MacDougall, C.S., and MacKenzie, L.M., 1985a. Preliminary report on the metallogeny of portions of the Central Mineral Belt, Labrador. Nfld. Dept. of Mines and Energy Prelim. Rept. of Act. for 1985, pp. 14-20
- Wilton, D.H.C., MacDougall, C.S., and MacKenzie, L.M., 1985b. Preliminary report on field work during 1985 in the Central Mineral Belt of Labrador. Unpub. Rept. for the Geol. Surv. of Can., Contract No. OST84-00524. 31p..
- Wilton, D.H.C., MacDougall, C.S., and MacKenzie, L.M., 1986a. Final Report on 1985 field work in the Central Mineral Belt, Labrador; ERDA Agreement II-2, Metallogeny of the Central Mineral Belt. Unpub. Rept. submitted to Geol. Surv. Can., 149p..
- Wilton, D.H.C., MacDougall, C.S., and MacKenzie, L.M., 1986b. Interim report on progress of research during 1985 in the Central Mineral Belt of Labrador. Unpub. Contract Rept. for the Geol. Surv. of Can., 17p..
- Wilton, D.H.C., MacDougall, C.S., MacKenzie, L.M., and North J.W., 1986. Preliminary report on field work completed during 1986 in the Central Mineral Belt of Labrador. Unpub. Rept. for Geol. Surv. of Can., 59p.
- Wilton, D.H.C., MacDougall, C.S., MacKenzie, L.M., and North J.W., 1987a. Precious-metal contents in samples from the eastern Central Mineral Belt, Labrador. Nfld. Dept. Mines Open File Lab (724), 39p.
- Wilton, D.H.C., MacDougall, C.S., MacKenzie, L.M., and North J.W., 1987b. Final report on field work completed during 1986 in the Central Mineral Belt of Labrador. Unpub. Rept. (Contract No. 23233-6-0196/01-ST) for Geol. Surv. of Can., 121p.
- Wilton, D.H.C., MacDougall, C.S., MacKenzie, L.M., and Pumphrey, C., 1988. Stratigraphy and metallogeny of the Moran Lake Group, northeast of Moran Lake. Geol. Surv. of Can. Rept. 88-1C, pp. 277-282.
- Wilton, D.H.C., and Wardle, R.J., 1987. Two contrasting granophile and non-granophile metallogenic styles in the early Proterozoic Upper Aillik Group, Central Mineral Belt, Labrador. Mineralium Deposita, v. 22, pp. 198-206.
- Winchester, J.A., and Floyd, P.A., 1977. Geochemical discrimination of different magma series and their differentiation products using immobile elements. Chem. Geol., v.20, pp. 325-343.

- Wynne-Edwards, H.R., 1972. The Grenville Province. in Variations in tectonic styles in Canada. Geol. Assoc. of Can. Pap. 11, pp. 263-334.
- York, D., 1969. Least-squares fitting of a straight line with correlated errors. Earth Plan. Sci. Lett., v. 5, pp. 320-324.
- Zartman, R.E., and Doe, B.R., 1981. Plumbotectonics - The model. Tectonophysics, v. 75, pp. 135-162.
- Zielinski, R.A., 1979. Uranium mobility during interaction of rhyolitic obsidian, perlite and felsite with alkaline carbonate solutions. T=120 C, P=210 Kg/cm<sup>2</sup>. Chem. Geol. v. 14.
- Zielinski, R.A., 1982. The mobility of uranium and other elements during alteration of rhyolite ash to montmorillonite: a case study in the Troublesome Formation, Colorado, U.S.A.. Chem. Geol., v. 35, pp. 185-204.
- Zinchenko, V.A., and Radovich, F.I., 1972. Migration of matter during processes of sodium metasomatism and the formation of uranium ores; uranium ores of the sodium-uranium formation. Akad. Nauk. Ukr. RSR. Dopov. v. 11, pp. 973-976.



**APPENDIX I****ANALYTICAL METHODS****Sample Preparation**

Grab samples weighing 1-2 kg were collected from mineralized and unmineralized outcrops for geochemical analysis. Weathered rinds were removed using a rotary diamond blade table saw. The samples were broken into chips using a hammer on a steel plate, crushed in a steel jaw crusher, and then pulverized in a tungsten-carbide puck mill, producing a -100 mesh whole rock powder. A standard consisting of silica sand was pulverized using the same procedure. The powder was then split into quarters until there was enough powder to fill a 125 ml plastic sample bottle.

**Major Element Analysis**

Major element oxides (except for  $P_2O_5$  and LOI) were determined by atomic absorption spectrometry. Sample preparation followed the methods of Langmuir and Paus (1968). Table 1 lists precision of the method. The elements were analyzed on a Perkin-Elmer Model 370 atomic absorption spectrometer with digital readout. Occasionally aqua-regia dissolution was required for sulphide-rich samples. Iron is reported as total  $Fe_2O_3$ . Loss on ignition (LOI), which reflects volatile content of the sample, was determined by weighing (accurately to  $10^{-4}$  g) a portion of the sample into a porcelain crucible, heating the crucible to  $1050^{\circ}C$  for at least two hours,

cooling it in a desiccator, and then weighing the de-volatized sample to determine the percent loss of volatiles.

$P_2O_5$  was analyzed with a Bausch and Lomb Spectronic 20 Colourimeter (ie. colourimetrically), based on a modification of the method outlined by Shapiro and Brannock (1962).

Table 1: Precision of Major Element Analyses based on four analyses of standard G-2. (Published value from Flanagan (1970)).

Element	Published			Range	
	Value	Mean	S.D.	Low	High
SiO <sub>2</sub>	69.11	69.70	0.57	68.50	69.96
Al <sub>2</sub> O <sub>3</sub>	15.40	15.10	0.24	14.75	15.60
Fe <sub>2</sub> O <sub>3</sub>	2.65	2.60	0.02	2.64	2.74
MgO	0.76	0.80	0.005	0.75	0.82
CaO	1.94	2.00	0.10	1.92	2.14
Na <sub>2</sub> O	4.07	4.30	0.02	4.07	4.21
K <sub>2</sub> O	4.51	4.56	0.02	4.50	4.57
TiO <sub>2</sub>	0.50	0.50	0.01	0.47	0.51
MnO	0.03	0.03	0.00	-	-

#### Trace Element Analyses

The trace elements were determined by X-Ray Fluorescence techniques on pressed, whole rock powder pellets using a Phillips 1450 automatic X-Ray fluorescence spectrometer with a rhodium tube.

The pellets were made from a homogenized powder containing 10g of sample and 1-1.5g of binding material (Union Carbide Phenolic Resin TR-16933). The powder was pressed at 30 tons psi for a minute, and then baked for ten minutes at 200<sup>0</sup> C. Data reduction was done with a Hewlett-Packard 9845B mini-computer.

Precision and accuracy for trace element analyses are given in Table 2 using the standards as listed.

Table 2: Precision and accuracy of trace elements analyses  
(from Longerich and Veinott, 1986).

Standard G-2	Determined	Accepted	%RSD	N
TiO <sub>2</sub>	0.49	0.48	1.0	10
V	36	36	10.9	10
Cr	10	8	28.3	10
Ni	8	4	17.9	10
Cu	25	10	4.1	10
Zn	88	84	2.6	10
Ga	23	23	6.8	10
Rb	171	170	0.6	10
Sr	459	480	1.4	10
Y	15	11	12.4	10
Zr	304	300	1.0	10
Nb	13	13	9.3	10
Ba	1864	1900	1.7	10
La	130	92	3.7	10
Ce	155	160	23.7	10
Pb	35	30	15.4	10
Th	20	25	34.8	10
U	0	2	300.0	10

Analyses for Mo and Ag were performed by Chemex Labs Ltd. of Vancouver, using a semi-quantitative, multi-element ICP analysis. The analytical technique involves digestion of 0.5 g of material

in nitric acid - aqua regia followed by ICP analysis. Since digestion is incomplete for many minerals, values reported for Al, Sb, Ba, Be, Ca, Cr, Ga, La, Mg, K, Na, Sr, Tl, Ti, W and V can be considered as partial analyses. In the case where elements have been duplicated by both XRF and ICP analysis, the XRF values are used. ICP detection limits are listed in Table 3.

Table 3: ICP trace element analysis detection limits (from Chemex Labs Ltd.).

Ag	0.2 ppm	Cu	1 ppm	K	0.01%
Al	0.01%	Fe	0.01%	Sb	5 ppm
As	5 ppm	Ga	10 ppm	Sr	1 ppm
Ba	1 ppm	La	10 ppm	Tl	10 ppm
Be	0.5 ppm	Pb	2 ppm	Ti	0.01%
Bi	2 ppm	Mg	0.01%	W	10 ppm
Cd	0.5 ppm	Mn	1 ppm	U	10 ppm
Ca	0.01%	Mo	1 ppm	V	1 ppm
Cr	1 ppm	Ni	1 ppm	Zn	10 ppm
Co	1 ppm	P	10 ppm		

Analyses for gold were also performed by Chemex Labs Ltd. using fire assay preconcentration of 10 gm of sample followed by atomic absorption spectrometry. The detection limit for gold is 5 ppb.

#### **Rare Earth Element Analyses**

The rare earth element analyses were carried out using the thin film X-Ray fluorescence technique as outlined by Fryer (1977). A 1-2 g sample was dissolved in HF and the resultant solution was put through columns containing ion exchange resin. Calibrated

elutions of 2N HCL concentrated the REE's into the final solution.  $H_2SO_4$  was added to remove Ba and the solution was dried on ion filter paper. This paper was then analysed by X-Ray Fluorescence spectrometry (see above).

The data are assumed to be accurate to  $\pm 5-10\%$  or  $\pm 0.1$  ppm, whichever is greater.

## Upper Aillik Group

Sample Name Rock Type	BL86-1A unit 4b	BL86-1B unit 4b	BL86-2B unit 4b	BL86-5 unit 4b	BL86-23 unit 4b
(wt%) SiO <sub>2</sub>	81.20	79.30	64.80	76.90	76.50
TiO <sub>2</sub>	0.12	0.16	0.24	0.32	0.16
Al <sub>2</sub> O <sub>3</sub>	8.05	9.31	17.20	11.50	10.90
Fe <sub>2</sub> O <sub>3</sub>	0.00	0.00	0.00	0.00	0.00
FeO	1.56	1.25	1.56	1.48	2.18
MnO	0.02	0.02	0.07	0.07	0.05
MgO	0.14	0.02	0.12	0.45	0.06
CaO	0.18	0.06	0.38	0.28	1.26
Na <sub>2</sub> O	1.26	0.46	1.73	5.33	6.64
K <sub>2</sub> O	5.57	8.13	13.40	2.82	0.07
P <sub>2</sub> O <sub>5</sub>	0.02	0.02	0.05	0.03	0.01
LOI	0.10	0.37	0.47	0.19	0.95
TOTAL	98.39	99.24	100.19	99.54	99.02
(ppm) Cr	0	0	9	0	0
Ni	0	0	0	0	0
Co	41	48	24	40	0
V	17	4	144	84	3
Cu	4	37	33	5	2
Pb	27	37	49	41	24
Zn	68	1692	19	67	29
Bi	0.00	8.00	0.00	0.00	0.00
Mo	1.00	92.00	9.00	0.00	0.00
As	5.00	15.00	30.00	0.00	0.00
Ag	0.2	3.0	0.2	0.2	0.0
Au	0.0	20.0	0.0	0.0	0.0
K	46237	67487	111233	23409	581
Rb	101	179	275	68	0
Ba	324	353	2215	117	0
Sr	22	6	15	9	26
Ga	11	14	23	21	32
Nb	32.0	28.0	21.0	33.0	34.0
Zr	226	207	139	195	650
Ti	719	959	1439	1918	959
Y	54	59	30	59	101
Th	24.00	19.00	1.00	31.00	24.00
U	2.00	13.00	75.00	15.00	11.00
La	127.00	88.00	11.00	181.00	0.00
Ce	201.00	183.00	41.00	247.00	0.00

Sample Name	BL86-30B	LM85-2	LM85-14	LM85-32	LM85-37
Rock Type	unit 4b	unit 4b	unit 4b(a)	unit 4b	unit 4b
(wt%)					
SiO <sub>2</sub>	73.10	73.30	85.10	75.70	74.60
TiO <sub>2</sub>	0.20	0.20	0.48	0.16	0.32
Al <sub>2</sub> O <sub>3</sub>	11.90	11.90	7.28	11.80	12.80
Fe <sub>2</sub> O <sub>3</sub>	0.00	0.00	0.00	0.00	0.00
FeO	1.43	2.01	1.94	1.75	2.99
MnO	0.06	0.03	0.08	0.01	0.06
MgO	0.04	0.03	0.13	0.02	0.28
CaO	0.06	0.24	0.32	0.00	0.52
Na <sub>2</sub> O	0.61	0.84	4.19	1.64	5.75
K <sub>2</sub> O	10.54	9.98	0.26	8.10	2.68
P <sub>2</sub> O <sub>5</sub>	0.01	0.05	0.03	0.02	0.03
LOI	0.35	0.08	0.21	0.09	0.15
TOTAL	98.46	98.88	100.24	99.49	100.46
(ppm)					
Cr	0	0	0	0	0
Ni	0	0	0	0	0
Co	43	0	0	0	0
V	43	109	189	10	9
Cu	18	4	4	6	6
Pb	22	27	174	27	36
Zn	98	2	141	14	31
Bi	0.00	0.00	0.00	0.00	0.00
Mo	3.00	0.00	0.00	0.00	0.00
As	20.00	0.00	0.00	0.00	0.00
Ag	0.2	0.0	0.0	0.0	0.0
Au	0.0	0.0	0.0	0.0	0.0
K	87493	82844	2158	67238	22247
Rb	230	217	9	231	51
Ba	0	68	0	140	853
Sr	4	4	17	12	60
Ga	16	15	17	21	23
Nb	29.0	29.0	57.0	21.0	33.0
Zr	286	288	507	231	513
Ti	1199	1199	2878	959	1918
Y	45	58	79	48	73
Th	34.00	27.00	29.00	33.00	31.00
U	31.00	0.00	10.00	0.00	4.00
La	0.00	0.00	0.00	0.00	0.00
Ce	0.00	0.00	0.00	0.00	0.00

Sample Name	LM85-41B	LM85-45	LM85-52	LM85-84	LM85-85
Rock Type	unit 4b	unit 4b	unit 4b	unit 4b	unit 4b
(wt%) SiO <sub>2</sub>	70.90	77.50	76.80	75.70	72.40
TiO <sub>2</sub>	0.20	0.12	0.12	0.20	0.24
Al <sub>2</sub> O <sub>3</sub>	11.90	11.40	10.60	12.00	14.10
Fe <sub>2</sub> O <sub>3</sub>	0.00	0.00	0.00	0.00	0.00
FeO	2.61	1.57	2.15	1.75	1.70
MnO	0.82	0.01	0.05	0.03	0.04
MgO	1.10	0.01	0.05	0.06	0.53
CaO	4.00	0.26	0.68	0.20	1.20
Na <sub>2</sub> O	4.44	2.21	4.95	2.43	4.16
K <sub>2</sub> O	3.91	6.86	3.37	7.57	4.88
P <sub>2</sub> O <sub>5</sub>	0.02	0.02	0.02	0.02	0.06
LOI	0.20	0.12	0.54	0.15	0.60
TOTAL	100.39	100.25	99.57	100.2	100.1
(ppm) Cr	0	0	0	0	0
Ni	0	0	0	0	0
Co	21	0	0	0	0
V	23	1	6	50	13
Cu	10	7	1	3	6
Pb	97	39	30	35	36
Zn	260	0	146	5	17
Bi	0.00	0.00	0.00	0.00	0.00
Mo	0.00	0.00	0.00	0.00	0.00
As	0.00	0.00	0.00	0.00	0.00
Ag	0.0	0.0	0.0	0.0	0.0
Au	0.0	0.0	0.0	0.0	0.0
K	32457	56945	27974	62839	40509
Rb	89	154	80	146	146
Ba	543	328	4	114	717
Sr	44	82	27	20	269
Ga	22	17	28	20	17
Nb	35.0	35.0	42.0	27.0	20.0
Zr	265	210	715	211	158
Ti	1199	719	719	1199	1439
Y	59	65	101	51	36
Th	35.00	34.00	24.00	38.00	21.00
U	1.00	6.00	1.00	3.00	5.00
La	0.00	0.00	0.00	0.00	0.00
Ce	0.00	0.00	0.00	0.00	0.00



Sample Name	BL86-26	BL86-28	BL86-17B	BL86-18D	BL86-19B
Rock Type	unit 4b	unit 4b	andesite	andesite	andesite
(wt%) SiO <sub>2</sub>	70.40	76.30	52.00	46.60	48.80
TiO <sub>2</sub>	0.28	0.08	0.88	0.92	0.92
Al <sub>2</sub> O <sub>3</sub>	15.00	10.50	14.00	14.00	15.20
Fe <sub>2</sub> O <sub>3</sub>	0.00	0.00	10.47	11.30	11.48
FeO	1.98	1.66	0.00	0.00	0.00
MnO	0.02	0.01	0.16	0.16	0.17
MgO	0.05	0.00	7.47	6.38	5.25
CaO	0.72	0.00	7.28	7.84	9.98
Na <sub>2</sub> O	5.46	2.07	4.28	5.13	4.82
K <sub>2</sub> O	5.40	6.59	1.85	2.61	0.84
P <sub>2</sub> O <sub>5</sub>	0.04	0.00	0.17	0.12	0.19
LOI	0.22	0.90	1.09	4.77	4.57
TOTAL	99.79	98.2	99.65	99.83	99.22
(ppm) Cr	0	0	115	44	96
Ni	0	0	62	45	62
Co	37	59	39	40	38
V	20	13	213	218	205
Cu	42	4	11	0	2
Pb	14	12	2	4	9
Zn	2	0	94	165	121
Bi	0.00	0.00	0.00	0.00	0.00
Mo	0.00	53.00	0.00	0.00	0.00
As	5.00	30.00	10.00	20.00	20.00
Ag	0.2	0.2	0.0	0.0	0.0
Au	0.0	0.0	0.0	0.0	0.0
K	44825	54704	15357	21666	6973
Rb	65	145	80	111	36
Ba	0	0	894	958	468
Sr	124	22	383	346	589
Ga	25	18	13	10	12
Nb	29.0	29.0	8.0	6.0	6.0
Zr	306	262	60	55	53
Ti	1679	480	5276	5515	5515
Y	59	32	33	27	25
Th	34.00	25.00	0.00	0.00	0.00
U	10.00	18.00	0.00	0.00	0.00
La	0.00	0.00	0.00	0.00	0.00
Ce	0.00	0.00	0.00	0.00	0.00

Sample Name	BL86-20B	BL86-21B	BL86-12	BL86-24	BL86-27
Rock Type	andesite	andesite	unit 4d	unit 4d	unit 4d
(wt%) SiO <sub>2</sub>	51.60	54.80	76.20	72.30	76.50
TiO <sub>2</sub>	0.72	1.08	0.20	0.44	0.20
Al <sub>2</sub> O <sub>3</sub>	11.60	12.40	11.20	12.50	10.80
Fe <sub>2</sub> O <sub>3</sub>	7.56	11.52	0.00	0.00	0.00
FeO	0.00	0.00	1.57	3.28	1.30
MnO	0.16	0.15	0.01	0.06	0.06
MgO	3.53	6.43	0.01	0.16	0.09
CaO	10.56	6.14	0.20	0.66	0.12
Na <sub>2</sub> O	6.54	6.30	2.30	3.73	1.96
K <sub>2</sub> O	0.09	0.09	6.63	6.15	7.81
P <sub>2</sub> O <sub>5</sub>	0.29	0.26	0.03	0.07	0.03
LOI	5.94	0.57	0.16	0.08	0.29
TOTAL	98.59	99.74	98.68	99.8	99.31
(ppm) Cr	45	53	0	10	0
Ni	24	50	0	0	0
Co	10	24	49	42	46
V	210	203	5	109	136
Cu	7	4	3	3	4
Pb	55	0	30	49	31
Zn	73	185	0	38	0
Bi	0.00	0.00	0.00	0.00	0.00
Mo	0.00	0.00	0.00	0.00	0.00
As	10.00	10.00	5.00	10.00	10.00
Ag	0.2	0.0	0.2	0.2	0.2
Au	0.0	0.0	0.0	0.0	0.0
K	747	747	55036	51051	64831
Rb	0	0	160	135	177
Ba	0	0	0	0	0
Sr	208	248	19	19	5
Ga	16	14	21	20	14
Nb	4.0	4.0	25.0	35.0	20.0
Zr	35	69	157	366	268
Ti	4316	6475	1199	2638	1199
Y	23	24	39	59	51
Th	2.00	5.00	38.00	25.00	15.00
U	25.00	7.00	19.00	17.00	28.00
La	0.00	0.00	81.00	0.00	0.00
Ce	0.00	0.00	0.00	0.00	0.00

Sample Name	BL86-30A	LM85-11	LM85-33	LM85-40	BL86-29
Rock Type	unit 4d	unit 4d	unit 4d	unit 4d	unit 4b
(wt%) SiO <sub>2</sub>	75.40	74.80	73.60	74.30	74.50
TiO <sub>2</sub>	0.12	0.20	0.32	0.20	0.20
Al <sub>2</sub> O <sub>3</sub>	11.80	12.50	12.40	12.30	12.00
Fe <sub>2</sub> O <sub>3</sub>	0.00	0.00	0.00	0.00	0.00
FeO	1.69	1.48	2.61	2.85	1.76
MnO	0.02	0.04	0.04	0.01	0.04
MgO	0.01	0.24	0.05	0.02	0.02
CaO	0.02	0.22	0.38	0.10	0.20
Na <sub>2</sub> O	3.04	3.68	2.58	2.76	2.04
K <sub>2</sub> O	6.47	5.02	7.65	7.08	7.86
P <sub>2</sub> O <sub>5</sub>	0.02	0.03	0.02	0.03	0.03
LOI	0.11	0.26	0.17	0.19	0.18
TOTAL	98.89	98.57	100.11	100.16	99.03
(ppm) Cr	0	0	0	0	0
Ni	0	0	0	0	0
Co	36	51	0	0	42
V	34	9	8	0	78
Cu	5	6	5	3	3
Pb	19	55	34	41	31
Zn	8	61	9	23	76
Bi	0.00	0.00	0.00	0.00	0.00
Mo	0.00	0.00	0.00	0.00	0.00
As	10.00	0.00	0.00	0.00	5.00
Ag	0.2	0.0	0.0	0.0	0.2
Au	0.0	0.0	0.0	0.0	0.0
K	53707	41671	63503	58771	65246
Rb	151	147	140	177	181
Ba	0	217	971	218	0
Sr	6	16	48	15	6
Ga	20	18	24	22	21
Nb	27.0	33.0	31.0	29.0	27.0
Zr	224	320	484	513	252
Ti	719	1199	1918	1199	1199
Y	37	68	70	63	42
Th	24.00	37.00	30.00	23.00	27.00
U	12.00	2.00	14.00	5.00	35.00
La	0.00	0.00	0.00	0.00	0.00
Ce	0.00	0.00	0.00	0.00	0.00

Sample Name	LM85-91	LM85-64	BL86-18B	BL86-22	BL86-25
Rock Type	unit 4b	unit 4b	unit 4b	unit 2	unit 4e
(wt%) SiO <sub>2</sub>	75.20	71.20	75.80	69.40	73.60
TiO <sub>2</sub>	0.24	0.32	0.32	0.48	0.28
Al <sub>2</sub> O <sub>3</sub>	10.80	12.80	11.40	14.10	12.40
Fe <sub>2</sub> O <sub>3</sub>	0.00	0.00	2.65	0.00	0.00
FeO	1.64	3.41	0.00	3.47	2.05
MnO	0.05	0.01	0.00	0.04	0.03
MgO	0.05	0.01	0.00	0.16	0.03
CaO	0.04	0.02	0.26	0.78	0.12
Na <sub>2</sub> O	0.73	2.47	3.26	6.57	0.49
K <sub>2</sub> O	8.99	8.30	5.68	3.15	10.73
P <sub>2</sub> O <sub>5</sub>	0.02	0.03	0.04	0.07	0.03
LOI	0.67	0.10	0.14	0.46	0.13
TOTAL	98.61	99.05	99.55	99.07	100.12
(ppm) Cr	0	0	0	0	0
Ni	0	0	0	0	0
Co	0	0	39	0	32
V	10	1	5	16	20
Cu	3	5	3	6	5
Pb	76	94	14	12	13
Zn	2	79	0	57	0
Bi	0.00	0.00	0.00	0.00	0.00
Mo	0.00	0.00	0.00	0.00	3.00
As	0.00	0.00	5.00	0.00	5.00
Ag	0.0	0.0	0.2	0.0	0.2
Au	0.0	0.0	0.0	0.0	0.0
K	74626	68898	47150	26148	89070
Rb	236	211	107	47	22
Ba	1447	45	1058	0	0
Sr	12	24	34	120	6
Ga	15	29	15	21	18
Nb	23.0	41.0	22.0	15.0	22.0
Zr	363	686	346	317	394
Ti	1439	1918	1918	2878	1679
Y	35	75	43	29	37
Th	22.00	18.00	12.00	6.00	28.00
U	4.00	11.00	8.00	7.00	15.00
La	0.00	0.00	0.00	0.00	0.00
Ce	0.00	0.00	0.00	0.00	0.00

Sample Name		EMS85-TR1B	EM86-1	EM86-WB	EMS86-TR1D	EMS86-TR1E
Rock Type		unit 1a	unit 1a	unit 1a	unit 1d	unit 1d
(wt%)	SiO <sub>2</sub>	71.60	70.30	77.40	53.10	55.00
	TiO <sub>2</sub>	0.12	0.16	0.08	2.48	2.56
	Al <sub>2</sub> O <sub>3</sub>	11.70	15.40	11.90	13.30	13.30
	Fe <sub>2</sub> O <sub>3</sub>	0.00	0.00	0.00	0.00	0.00
	FeO	1.69	1.65	1.92	14.82	12.91
	MnO	0.06	0.06	0.03	0.04	0.27
	MgO	0.06	0.09	0.03	1.57	0.98
	CaO	3.78	1.34	0.20	3.10	3.56
	Na <sub>2</sub> O	7.13	9.20	7.05	8.29	8.51
	K <sub>2</sub> O	0.15	0.14	0.87	0.33	0.14
	P <sub>2</sub> O <sub>5</sub>	0.05	0.02	0.01	1.25	1.38
	LOI	1.47	0.30	0.18	0.04	0.03
	TOTAL	98	98.84	99.88	100.25	97.98
(ppm)	Cr	0	0	0	9	3
	Ni	0	0	0	13	17
	Co	30	42	48	41	26
	V	48	45	188	256	238
	Cu	134	1	2	7	5
	Pb	192	27	28	118	37
	Zn	366	0	13	245	116
	Bi	0.00	0.00	0.00	0.00	0.00
	Mo	2122.00	0.00	0.00	0.00	0.00
	As	10.00	0.00	0.00	35.00	30.00
	Ag	5.2	0.4	0.0	0.2	0.6
	Au	10.0	0.0	0.0	0.0	0.0
	K	1245	1162	7222	2739	1162
	Rb	5	3	19	24	7
	Ba	0	0	0	47	33
	Sr	62	47	6	138	141
	Ga	41	36	25	23	27
	Nb	22.0	43.0	26.0	76.0	103.0
	Zr	476	293	360	529	536
	Ti	719	959	480	14868	15347
	Y	112	81	29	184	241
	Th	56.00	8.00	13.00	0.00	0.00
	U	89.00	33.00	24.00	38.00	37.00
	La	56.00	0.00	0.00	0.00	0.00
	Ce	945.00	0.00	0.00	0.00	0.00

Sample Name		EMS86-TR5A	EMS86-TR3A
Rock Type		unit 1d	unit 1b
(wt%)	SiO <sub>2</sub>	48.80	61.80
	TiO <sub>2</sub>	2.16	0.24
	Al <sub>2</sub> O <sub>3</sub>	13.10	12.10
	Fe <sub>2</sub> O <sub>3</sub>	0.00	0.00
	FeO	13.54	7.71
	MnO	0.40	0.34
	MgO	3.78	2.37
	CaO	6.80	4.74
	Na <sub>2</sub> O	6.80	9.28
	K <sub>2</sub> O	0.82	0.09
	P <sub>2</sub> O <sub>5</sub>	1.65	0.05
	LOI	0.10	0.20
	TOTAL	99.34	99.78
(ppm)	Cr	87	28
	Ni	23	18
	Co	27	17
	V	285	445
	Cu	9	9
	Pb	85	23
	Zn	803	289
	Bi	0.00	0.00
	Mo	0.00	0.00
	As	35.00	0.00
	Ag	0.2	0.2
	Au	0.0	0.0
	K	6807	747
	Rb	68	1
	Ba	0	0
	Sr	367	36
	Ga	21	39
	Nb	29.0	22.0
	Zr	153	537
	Ti	12949	1439
	Y	108	78
	Th	6.00	10.00
	U	34.00	25.00
	La	0.00	0.00
	Ce	0.00	0.00

Sample Name	BH9-072.0	BH10-290.0	BH14-342.1	LM85-63	LM85-67
Rock Type	unit 4a	unit 4a	unit 4a	unit 4a	unit 4a
(ppm)					
Cr	0	0	0	9	4
Ni	0	0	0	0	0
Co	24	20	30	0	0
V	19	100	51	3	5
Cu	3	7	2	0	0
Pb	48	7	24	47	26
Zn	32	59	36	32	64
Bi	0.00	0.00	0.00	0.00	0.00
Mo	0.00	0.00	0.00	0.00	0.00
As	5.00	10.00	0.00	0.00	0.00
Ag	0.2	0.2	0.2	0.0	0.0
Au	0.0	0.0	0.0	0.0	0.0
K	0	0	0	0	0
Rb	1	187	2	227	44
Ba	0	0	0	160	43
Sr	10	630	11	18	36
Ga	23	18	23	14	32
Nb	33.0	26.0	25.0	24.0	42.0
Zr	252	219	360	310	336
Ti	839	4197	1559	2578	1019
Y	63	53	48	46	100
Th	32.00	13.00	31.00	5.00	23.00
U	46.00	27.00	26.00	10.00	7.00
La	85.00	62.00	93.00	38.00	147.00
Ce	0.00	0.00	0.00	0.00	0.00

Sample Name	LM85-68	LM85-74	BH-2-265.8	BH5-364.5	BL86-45
Rock Type	unit 4a	unit 4a	unit 4b	unit 4b	unit 4b
(ppm)					
Cr	4	17	0	0	3
Ni	0	0	0	0	0
Co	41	0	24	32	0
V	92	42	13	182	9
Cu	4	0	3	6	0
Pb	25	24	13	24	8
Zn	1	0	0	239	116
Bi	0.00	0.00	0.00	0.00	0.00
Mo	1.00	0.00	0.00	0.00	0.00
As	0.00	0.00	0.00	0.00	0.00
Ag	0.2	0.0	0.0	0.2	0.0
Au	0.0	0.0	0.0	0.0	0.0
K	0	0	0	0	0
Rb	199	168	0	4	228
Ba	253	239	0	0	314
Sr	4	31	16	10	14
Ga	18	14	23	19	18
Nb	28.0	23.0	31.0	34.0	23.0
Zr	269	333	286	348	274
Ti	1079	899	1259	1379	1139
Y	48	31	45	54	60
Th	28.00	20.00	19.00	27.00	27.00
U	0.00	7.00	34.00	19.00	9.00
La	106.00	58.00	60.00	67.00	99.00
Ce	179.00	0.00	0.00	0.00	0.00

Sample Name	BL86-46	LM-Tr-6-4b	LM85-TR9	LM85-TR28	LM85-1
Rock Type	unit 4b	unit 4b(a)	unit 4b	unit 4b	unit 4b
(ppm)					
Cr	0	10	0	0	13
Ni	0	0	0	0	0
Co	0	23	36	38	0
V	59	495	80	119	425
Cu	0	4	7	15	0
Pb	10	45	23	28	10
Zn	28	94	40	10	46
Bi	0.00	0.00	0.00	0.00	0.00
Mo	0.00	0.00	1.00	0.00	0.00
As	0.00	0.00	0.00	0.00	0.00
Ag	0.0	0.2	0.2	0.2	0.0
Au	0.0	0.0	0.0	0.0	0.0
K	0	0	0	0	0
Rb	212	4	202	93	0
Ba	117	78	114	243	4
Sr	8	5	15	13	4
Ga	18	22	11	20	23
Nb	21.0	29.0	29.0	31.0	25.0
Zr	247	404	275	271	418
Ti	1259	1799	959	1199	1199
Y	48	46	42	47	32
Th	19.00	29.00	33.00	25.00	26.00
U	8.00	58.00	15.00	35.00	28.00
La	106.00	86.00	167.00	117.00	86.00
Ce	0.00	133.00	253.00	180.00	0.00

Sample Name	LM85-5b	LM85-6	LM85-35	LM85-41a	LM85-42
Rock Type	unit 4b	unit 4b(e)	unit 4b	unit 4b	unit 4b
(ppm)					
Cr	0	0	0	0	0
Ni	0	0	0	0	0
Co	0	0	0	23	31
V	69	3	5	14	13
Cu	8	5	2	12	9
Pb	58	42	32	64	39
Zn	10	0	0	80	0
Bi	0.00	0.00	0.00	0.00	0.00
Mo	0.00	0.00	0.00	0.00	10.00
As	0.00	0.00	0.00	0.00	0.00
Ag	0.0	0.0	0.0	0.2	0.2
Au	0.0	0.0	0.0	0.0	0.0
K	0	0	0	0	0
Rb	119	202	285	87	130
Ba	28	273	165	391	421
Sr	22	48	15	36	15
Ga	23	15	21	19	21
Nb	28.0	26.0	34.0	28.0	30.0
Zr	383	276	357	243	533
Ti	1259	899	1499	779	1379
Y	40	48	71	47	54
Th	41.00	30.00	35.00	35.00	20.00
U	10.00	5.00	5.00	0.00	5.00
La	0.00	0.00	97.00	51.00	116.00
Ce	0.00	0.00	156.00	62.00	185.00



## 320

Sample Name	LM85-49	LM85-50	LM85-60m	LM85-71	LM85-78
Rock Type	unit 4b	unit 4b	unit 4b	unit 4b(a)	unit 4b
(ppm)					
Cr	3	0	0	11	0
Ni	0	0	0	0	0
Co	0	0	0	0	0
V	14	0	62	1335	0
Cu	0	0	4	10	0
Pb	14	11	34	65	12
Zn	0	0	62	23	3
Bi	0.00	0.00	0.00	0.00	0.00
Mo	0.00	0.00	0.00	0.00	0.00
As	0.00	0.00	0.00	0.00	0.00
Ag	0.0	0.0	0.0	0.0	0.0
Au	0.0	0.0	0.0	0.0	0.0
K	0	0	0	0	0
Rb	207	273	111	10	112
Ba	79	41	110	0	537
Sr	9	8	17	36	48
Ga	24	15	16	23	23
Nb	35.0	43.0	25.0	18.0	32.0
Zr	318	1571	601	281	544
Ti	1079	1139	839	1439	1259
Y	73	147	70	38	78
Th	35.00	45.00	37.00	33.00	16.00
U	11.00	13.00	23.00	76.00	4.00
La	153.00	241.00	73.00	31.00	59.00
Ce	0.00	0.00	71.00	0.00	0.00

Sample Name	LM85-82	LM85-90	LM85-96	LM85-102	LM85-108
Rock Type	unit 4b(a)	unit 4b	unit 4b	unit 4b	unit 4b
(ppm)					
Cr	0	0	0	0	0
Ni	0	0	0	0	0
Co	0	19	0	0	0
V	153	10	4	2	7
Cu	54	3	0	4	9
Pb	69	66	24	29	7
Zn	39	0	17	5	91
Bi	0.00	0.00	0.00	0.00	0.00
Mo	0.00	1.00	0.00	0.00	0.00
As	0.00	0.00	0.00	0.00	0.00
Ag	0.0	0.0	0.0	0.0	0.0
Au	0.0	0.0	0.0	0.0	0.0
K	0	0	0	0	0
Rb	3	100	235	227	82
Ba	0	432	91	0	60
Sr	10	56	9	15	16
Ga	50	21	17	26	26
Nb	50.0	30.0	26.0	39.0	44.0
Zr	756	249	268	550	775
Ti	2758	659	1019	1499	839
Y	36	50	53	69	109
Th	63.00	38.00	22.00	32.00	2.00
U	32.00	4.00	7.00	9.00	7.00
La	104.00	78.00	99.00	109.00	66.00
Ce	0.00	144.00	0.00	0.00	0.00

## 321

Sample Name	LM85-109	LM85-124	LM85-128	LM85-161	LM85-15
Rock Type	unit 4b	unit 4b	unit 4b	unit 4b	unit 4b
(ppm) Cr	0	0	0	5	0
Ni	1	0	0	0	0
Co	0	0	0	0	38
V	1	7	35	8	117
Cu	3	8	0	0	43
Pb	20	40	9	13	46
Zn	29	8	5	0	0
Bi	0.00	0.00	0.00	0.00	0
Mo	0.00	0.00	0.00	0.00	9
As	0.00	0.00	0.00	0.00	0
Ag	0.0	0.0	0.0	0.0	0.2
Au	0.0	0.0	0.0	0.0	0
K	0	0	0	0	0
Rb	65	33	100	187	141
Ba	0	0	167	59	867
Sr	13	75	30	16	229
Ga	33	29	28	15	16
Nb	29.0	46.0	35.0	27.0	52
Zr	682	360	858	191	314
Ti	719	1019	899	779	1679
Y	123	80	82	64	46
Th	36.00	28.00	16.00	24.00	26
U	11.00	15.00	4.00	6.00	0
La	40.00	85.00	51.00	49.00	70
Ce	0.00	0.00	0.00	0.00	105

Sample Name	LM85-E3	LM85-E5	LM85-E6a	LM85-E6b	LM85-53
Rock Type	unit 1a	unit 1a	unit 1a	unit 1a	unit 2
(ppm) Cr	4	0	4	0	12
Ni	8	0	0	0	0
Co	0	0	0	0	0
V	13	0	27	0	25
Cu	0	0	1	0	0
Pb	15	31	44	11	39
Zn	47	94	19	0	31
Bi	0.00	0.00	0.00	0.00	0.00
Mo	0.00	0.00	0.00	0.00	0.00
As	0.00	0.00	0.00	0.00	0.00
Ag	0.0	0.0	0.0	0.0	0.0
Au	0.0	0.0	0.0	0.0	0.0
K	0	0	0	0	0
Rb	3	2	5	219	86
Ba	13	0	0	102	639
Sr	18	7	19	9	60
Ga	48	35	30	19	19
Nb	72.0	65.0	51.0	35.0	10.0
Zr	563	536	417	275	130
Ti	0	0	0	0	2218
Y	268	70	57	67	24
Th	37.00	30.00	9.00	219.00	12.00
U	10.00	18.00	50.00	2.00	3.00
La	179.00	81.00	34.00	23.00	37.00
Ce	102.00	0.00	44.00	49.00	0.00

Sample Name	LM85-114a	LM85-114b	LM85-118	LM85-131	LM85-140
Rock Type	unit 2	unit 2	unit 2	unit 2	unit 2
(ppm)					
Cr	0	63	30	0	0
Ni	0	40	0	0	0
Co	0	0	0	0	0
V	11	47	11	30	1
Cu	4	0	2	6	0
Pb	12	11	12	39	8
Zn	0	140	29	19	40
Bi	0.00	0.00	0.00	0.00	0.00
Mo	0.00	0.00	0.00	0.00	0.00
As	0.00	0.00	0.00	0.00	0.00
Ag	0.0	0.0	0.0	0.0	0.0
Au	0.0	0.0	0.0	0.0	0.0
K	0	0	0	0	0
Rb	283	52	137	21	146
Ba	0	351	2040	0	1715
Sr	48	138	83	48	78
Ga	24	21	18	21	12
Nb	14.0	12.0	11.0	16.0	13.0
Zr	135	171	76	273	323
Ti	2218	2998	1379	2938	1139
Y	28	50	22	26	42
Th	10.00	9.00	11.00	17.00	8.00
U	3.00	5.00	8.00	69.00	4.00
La	51.00	34.00	8.00	30.00	41.00
Ce	0.00	0.00	0.00	0.00	0.00

Sample Name	LM85-150	LM85-170	LM85-54	LM85-125	LM85-162
Rock Type	unit 2	unit 2	unit 3	unit 3	unit 3
(ppm)					
Cr	52	11	29	27	74
Ni	5	0	0	2	13
Co	0	0	25	0	0
V	51	48	34	21	19
Cu	4	61	3	0	0
Pb	10	42	35	21	10
Zn	46	89	95	42	42
Bi	0.00	0.00	0.00	0.00	0.00
Mo	0.00	0.00	1.00	0.00	0.00
As	0.00	0.00	20.00	0.00	0.00
Ag	0.0	0.0	0.2	0.0	0.0
Au	0.0	0.0	0.0	0.0	0.0
K	0	0	0	0	0
Rb	45	2	48	85	232
Ba	0	0	142	1459	1000
Sr	139	375	112	213	169
Ga	19	14	23	16	20
Nb	13.0	8.0	12.0	10.0	10.0
Zr	182	153	165	186	408
Ti	2998	1679	2638	2098	3057
Y	28	23	39	24	34
Th	12.00	7.00	31.00	10.00	14.00
U	6.00	0.00	0.00	7.00	6.00
La	15.00	12.00	53.00	31.00	17.00
Ce	0.00	0.00	145.00	0.00	0.00

Sample Name	LM85-171	BL86-32B	BL86-33b	LM85-7	LM85-39
Rock Type	unit 3	unit 4d(5a	unit 4d	unit 4d	unit 4d
(ppm)					
Cr	55	5	8	0	0
Ni	8	0	0	0	0
Co	0	0	0	0	57
V	36	39	31	0	0
Cu	5	0	0	3	3
Pb	11	47	18	26	49
Zn	60	22	4	3	36
Bi	0.00	0.00	0.00	0.00	0.00
Mo	0.00	0.00	0.00	0.00	1.00
As	0.00	0.00	0.00	0.00	10.00
Ag	0.0	0.0	0.0	0.0	0.2
Au	0.0	0.0	0.0	0.0	0.0
K	0	0	0	0	0
Rb	145	181	201	119	229
Ba	0	82	264	300	96
Sr	144	9	16	7	18
Ga	16	13	17	18	23
Nb	13.0	22.0	27.0	22.0	34.0
Zr	147	250	249	213	542
Ti	2218	1139	1319	959	1379
Y	34	40	51	58	80
Th	41.00	22.00	24.00	28.00	23.00
U	8.00	30.00	9.00	1.00	4.00
La	53.00	88.00	93.00	0.00	140.00
Ce	0.00	0.00	0.00	0.00	136.00

Sample Name	LM85-51	LM85-79	LM85-94	LM85-85b	LM85-86
Rock Type	unit 4d	unit 4d	unit 4c	unit 4a	unit 4a
(ppm)					
Cr	0	0	0	0	0
Ni	0	0	0	0	0
Co	0	0	23	0	0
V	0	9	7	15	11
Cu	0	2	4	4	10
Pb	35	26	30	50	19
Zn	22	3	0	6	6
Bi	0.00	0.00	0.00	0.00	0.00
Mo	0.00	0.00	0.00	0.00	0.00
As	0.00	0.00	0.00	0.00	0.00
Ag	0.0	0.0	0.0	0.0	0.0
Au	0.0	0.0	0.0	0.0	0.0
K	0	0	0	0	0
Rb	153	153	233	270	306
Ba	177	0	324	539	0
Sr	17	10	23	21	18
Ga	25	25	17	17	17
Nb	28.0	30.0	30.0	28.0	28.0
Zr	644	465	220	308	322
Ti	1619	1379	899	1439	1559
Y	68	58	53	46	51
Th	16.00	26.00	44.00	38.00	27.00
U	2.00	9.00	0.00	2.00	13.00
La	99.00	70.00	64.00	77.00	68.00
Ce	0.00	0.00	92.00	119.00	0.00

Sample Name	LM85-130	LM85-136	LM85-110
Rock Type	unit 4a	unit 4a	unit 4e
(ppm)			
Cr	1	0	0
Ni	0	0	0
Co	0	0	0
V	37	8	9
Cu	0	7	2
Pb	1	32	13
Zn	8	0	223
Bi	0.00	0.00	0.00
Mo	0.00	0.00	0.00
As	0.00	0.00	0.00
Ag	0.0	0.0	0.0
Au	0.0	0.0	0.0
K	0	0	0
Rb	0	97	182
Ba	30	0	0
Sr	66	25	9
Ga	18	23	21
Nb	22.0	31.0	64.0
Zr	224	500	1022
Ti	1799	899	1019
Y	37	54	62
Th	11.00	15.00	27.00
U	3.00	6.00	12.00
La	82.00	82.00	97.00
Ce	0.00	0.00	0.00

## Upper Aillik Group - Mineralized Rocks

Sample Name	BL86-3	BL86-8	LM85-TR26	LM85-TR3A
Rock Type	4a	4a	4a	4b(a)
(wt. %)				
SiO <sub>2</sub>	77.30	74.10	76.30	76.20
TiO <sub>2</sub>	0.12	0.20	0.20	0.24
Al <sub>2</sub> O <sub>3</sub>	12.00	12.90	11.50	10.90
FeO	0.91	1.40	1.28	2.25
MnO	0.07	0.14	0.16	0.13
MgO	0.25	0.46	0.30	0.08
CaO	0.52	0.44	0.78	0.42
Na <sub>2</sub> O	7.08	7.70	6.97	7.24
K <sub>2</sub> O	0.11	0.13	0.11	0.08
P <sub>2</sub> O <sub>5</sub>	0.04	0.05	0.08	0.07
LOI	0.25	0.37	0.50	0.33
TOTAL	98.75	98.05	98.32	98.19
(ppm)				
Cr	0	0	0	7
Ni	0	0	0	0
Co	33	25	35	54
V	109	256	278	547
Cu	42	5	0	9
Pb	77	230	358	339
Zn	18	1274	151	58
Bi	0.00	0.00	0.00	0.00
Cd	0.00	0.00	0.00	0.00
Mo	0.00	5.00	10.00	1.00
As	5.00	5.00	10.00	10.00
Ag	0.6	0.6	0.2	0.6
Au	0.0	0.0	0.0	0.0
K	913	1079	913	664
Rb	5	7	5	4
Ba	271	0	54	154
Sr	5	75	38	21
Ga	28	28	25	21
Nb	23.0	20.0	26.0	34.0
Zr	262	312	309	428
Ti	719	1199	1199	1439
Y	52	47	57	72
Th	23.00	33.00	34.00	41.00
U	181.00	540.00	760.00	1233.00
La	200.00	102.00	178.00	119.00
Ce	201.00	0.00	235.00	186.00

Sample Name		LM85-TR4A	L85-TR6-3A	LM85-TR13	LM85-TR14A
Rock Type		4b(a)	4b(a)	4b(a)	4b(a)
(wt. %)	SiO <sub>2</sub>	78.70	78.80	69.60	69.80
	TiO <sub>2</sub>	0.20	0.20	0.40	0.20
	Al <sub>2</sub> O <sub>3</sub>	11.00	10.70	9.70	14.90
	FeO	0.95	1.58	6.82	2.28
	MnO	0.03	0.04	0.11	0.05
	MgO	0.05	0.10	0.27	0.19
	CaO	0.20	0.28	0.62	0.54
	Na <sub>2</sub> O	6.87	6.94	8.48	9.46
	K <sub>2</sub> O	0.12	0.16	0.09	0.18
	P <sub>2</sub> O <sub>5</sub>	0.06	0.04	0.02	0.01
	LOI	0.18	0.20	1.15	0.79
	TOTAL	98.47	99.22	98.02	98.65
(ppm)	Cr	0	8	178	9
	Ni	0	0	0	0
	Co	41	29	24	33
	V	170	450	3960	693
	Cu	3	0	207	599
	Pb	304	275	1541	1941
	Zn	146	121	132	89
	Bi	0.00	0.00	0.00	14.00
	Cd	0.00	0.00	0.00	0.00
	Mo	0.00	0.00	0.00	1.00
	As	0.00	10.00	30.00	40.00
	Ag	0.2	0.0	2.8	6.6
	Au	0.0	0.0	15.0	0.0
	K	996	1328	747	1494
	Rb	3	4	11	24
	Ba	227	300	681	488
	Sr	15	21	50	69
	Ga	18	18	27	30
	Nb	32.0	31.0	55.0	34.0
	Zr	420	484	1002	508
	Ti	1199	1199	2398	1199
	Y	74	85	175	102
	Th	36.00	41.00	19.00	61.00
	U	880.00	925.00	6792.00	8438.00
	La	106.00	92.00	84.00	113.00
	Ce	183.00	116.00	135.00	279.00

Sample Name		BL86-10	BL86-16	BL86-2A	BL86-4
Rock Type		4b(a)	4b(a)	4b	4b
(wt. %)	SiO <sub>2</sub>	68.50	77.40	67.50	62.50
	TiO <sub>2</sub>	0.32	0.16	0.36	0.40
	Al <sub>2</sub> O <sub>3</sub>	14.40	11.60	13.20	13.90
	FeO	2.78	1.16	3.94	5.56
	MnO	0.20	0.10	0.07	0.39
	MgC	0.69	0.30	0.05	0.53
	CaO	0.78	0.70	0.22	1.40
	Na <sub>2</sub> O	8.08	7.10	2.23	5.32
	K <sub>2</sub> O	1.92	0.13	9.00	7.69
	P <sub>2</sub> O <sub>5</sub>	0.05	0.01	0.04	0.04
	LOI	0.42	0.37	1.74	0.57
	TOTAL	98.45	99.1	98.79	98.92
(ppm)	Cr	0	0	0	0
	Ni	0	0	0	0
	Co	34	31	70	20
	V	7533	501	81	698
	Cu	250	1192	164	4
	Pb	377	1472	2127	385
	Zn	821	87	4352	1040
	Bi	0.00	0.00	2.00	0.00
	Cd	0.00	0.00	0.00	0.00
	Mo	0.00	0.00	273.00	0.00
	As	5.00	15.00	75.00	15.00
	Ag	2.0	26.0	7.8	1.0
	Au	0.0	70.0	195.0	0.0
	K	15938	1079	74709	63835
	Rb	55	57	216	172
	Ba	0	74	1108	785
	Sr	10	19	30	22
	Ga	25	28	38	24
	Nb	40.0	22.0	44.0	41.0
	Zr	488	491	350	642
	Ti	1918	959	2158	2398
	Y	106	40	91	105
	Th	28.00	2.00	35.00	26.00
	U	1251.00	5315.00	1156.00	912.00
	La	111.00	43.00	148.00	113.00
	Ce	0.00	159.00	352.00	222.00



Sample Name	BL86-6	LM85-TR5A	LM85-TR5B	LM85-TR7A
Rock Type	4b	4b	4b	4b
(wt. %)				
SiO <sub>2</sub>	64.50	70.10	68.60	71.10
TiO <sub>2</sub>	0.16	0.24	0.28	0.56
Al <sub>2</sub> O <sub>3</sub>	9.90	15.50	16.00	13.00
FeO	1.30	1.17	0.93	2.50
MnO	0.42	0.04	0.08	0.06
MgO	0.03	0.16	0.23	0.21
CaO	3.54	0.20	0.10	0.26
Na <sub>2</sub> O	1.48	5.49	5.36	5.23
K <sub>2</sub> O	6.91	6.56	7.10	4.98
P <sub>2</sub> O <sub>5</sub>	0.02	0.05	0.06	0.04
LOI	1.85	0.49	0.42	0.68
TOTAL	90.25	100.13	99.26	98.9
(ppm)				
Cr	0	0	0	14
Ni	0	0	0	0
Co	26	20	30	40
V	33	223	212	409
Cu	109	5	2	0
Pb	11084	311	765	914
Zn	38876	390	988	306
B	0.00	2.00	2.00	2.00
Cd	0.00	0.50	1.50	0.00
Mo	0.00	1.00	2.00	10.00
As	10.00	10.00	10.00	20.00
Ag	5.2	0.2	0.6	0.6
Au	120.0	0.0	0.0	0.0
K	57360	54455	58937	41339
Rb	173	145	161	122
Ba	321	113	345	521
Sr	65	11	12	27
Ga	127	25	24	27
Nb	23.0	46.0	36.0	106.0
Zr	274	643	306	406
Ti	959	1439	1679	3357
Y	62	69	118	141
Th	22.00	71.00	52.00	104.00
U	709.00	998.00	1517.00	3600.00
La	0.00	151.00	236.00	54.00
Ce	194.00	180.00	415.00	158.00

Sample Name		LM85-TR12A	LM85-TR17	LM85-TR18A	LM85-TR23A
Rock Type		4b	4a	4b	4b
(wt. %)	SiO <sub>2</sub>	76.20	72.90	65.90	76.70
	TiO <sub>2</sub>	0.20	0.32	0.36	0.16
	Al <sub>2</sub> O <sub>3</sub>	8.70	11.90	13.50	11.60
	FeO	2.74	3.29	3.00	1.19
	MnO	0.13	0.24	0.06	0.08
	MgO	0.46	0.27	0.15	0.11
	CaO	1.26	0.78	0.26	0.30
	Na <sub>2</sub> O	3.06	5.58	1.14	2.74
	K <sub>2</sub> O	4.95	2.48	10.68	6.91
	P <sub>2</sub> O <sub>5</sub>	0.01	0.10	0.05	0.04
	LOI	0.85	0.55	1.86	0.68
	TOTAL	98.86	98.78	97.29	100.64
(ppm)	Cr	23	29	0	3
	Ni	1	0	0	0
	Co	31	29	55	55
	V	581	328	211	322
	Cu	124	67	186	0
	Pb	4189	890	5045	527
	Zn	412	2309	13122	125
	Bi	22.00	0.00	2.00	0.00
	Cd	1.50	7.50	34.00	0.00
	Mo	3.00	101.00	1830.00	14.00
	As	80.00	20.00	120.00	10.00
	Ag	0.8	2.0	18.2	0.4
	Au	45.0	0.0	390.0	0.0
	K	41090	20586	88655	57360
	Rb	160	63	254	153
	Ba	867	987	449	111
	Sr	67	25	0	13
	Ga	32	29	63	19
	Nb	31.0	32.0	74.0	33.0
	Zr	536	283	494	360
	Ti	1199	1918	2158	959
	Y	222	71	105	69
	Th	4.00	38.00	87.00	30.00
	U	17251.00	492.00	2247.00	1255.00
	La	57.00	98.00	14.00	112.00
	Ce	249.00	200.00	784.00	227.00

Sample Name		LM85-60	BL86-9	BL86-11	BL86-1C
Rock Type		4b	4b	4b	4c
(wt. %)	SiO <sub>2</sub>	78.80	74.00	77.60	55.80
	TiO <sub>2</sub>	0.20	0.20	0.24	0.56
	Al <sub>2</sub> O <sub>3</sub>	10.30	12.20	9.33	15.30
	FeO	1.96	1.34	1.78	3.26
	MnO	0.06	0.08	0.08	1.40
	MgO	0.19	0.40	0.19	2.01
	CaO	0.18	0.16	0.40	4.76
	Na <sub>2</sub> O	2.89	5.35	2.00	7.77
	K <sub>2</sub> O	5.33	3.80	6.44	1.54
	P <sub>2</sub> O <sub>5</sub>	0.01	0.03	0.02	0.15
	LOI	0.14	0.55	0.19	3.00
	TOTAL	100.28	98.26	98.47	95.91
(ppm)	Cr	1	0	0	14
	Ni	0	0	0	13
	Co	0	26	30	29
	V	341	316	235	186
	Cu	4	3	2	29
	Pb	63	322	170	2153
	Zn	40	144	220	8202
	Bi	0.00	0.00	0.00	0.00
	Cd	0.00	0.00	0.00	0.00
	Mo	0.00	0.00	0.00	308.00
	As	0.00	15.00	5.00	20.00
	Ag	0.0	0.4	0.8	4.0
	Au	0.0	0.0	0.0	0.0
	K	44244	31544	53458	12784
	Rb	120	103	154	122
	Ba	28	0	0	1255
	Sr	8	3	6	119
	Ga	19	22	11	60
	Nb	30.0	26.0	39.0	58.0
	Zr	339	263	452	363
	Ti	1199	1199	1439	3357
	Y	32	32	135	154
	Th	32.00	29.00	31.00	81.00
	U	178.00	872.00	539.00	1107.00
	La	0.00	82.00	67.00	76.00
	Ce	0.00	0.00	0.00	382.00

Sample Name Rock Type		BL86-7 4c	LM85-TR25 4c	LM85-TR29 4d	BL86-17A andesite
(wt. %)	SiO <sub>2</sub>	71.30	74.30	76.30	53.60
	TiO <sub>2</sub>	0.32	0.24	0.20	0.80
	Al <sub>2</sub> O <sub>3</sub>	11.80	12.60	10.80	12.90
	FeO	2.10	2.31	1.69	5.93
	MnO	0.17	0.07	0.07	0.08
	MgO	0.67	0.21	0.18	3.15
	CaO	1.10	0.36	0.38	9.28
	Na <sub>2</sub> O	4.41	6.97	2.79	7.15
	K <sub>2</sub> O	5.49	1.83	5.86	0.30
	P <sub>2</sub> O <sub>5</sub>	0.05	0.07	0.04	0.66
	LOI	0.85	0.17	0.20	4.66
	TOTAL	98.49	99.39	98.7	98.51
(ppm)	Cr	5	17	9	64
	Ni	0	0	0	18
	Co	27	23	32	12
	V	2052	887	482	1481
	Cu	2	0	9	20
	Pb	227	194	181	83
	Zn	57	0	306	20
	Bi	0.00	0.00	0.00	0.00
	Cd	0.00	0.00	1.00	0.00
	Mo	0.00	1.00	2.00	0.00
	As	10.00	0.00	0.00	20.00
	Ag	0.4	0.2	0.2	0.4
	Au	0.0	5.0	0.0	0.0
	K	45572	15191	48644	2490
	Rb	143	44	120	15
	Ba	0	265	315	204
	Sr	37	19	32	95
	Ga	25	30	16	17
	Nb	31.0	37.0	28.0	11.0
	Zr	316	401	453	153
	Ti	1918	1439	1199	4796
	Y	77	42	65	53
	Th	30.00	19.00	32.00	103.00
	U	424.00	880.00	491.00	711.00
	La	90.00	122.00	88.00	0.00
	Ce	0.00	217.00	86.00	0.00

Sample Name	BL86-18A	BL86-18C	BL86-19A	BL86-19C
Rock Type	andesite	andesite	andesite	andesite
(wt. %)				
SiO <sub>2</sub>	56.30	56.30	54.80	55.60
TiO <sub>2</sub>	0.64	0.80	0.64	0.68
Al <sub>2</sub> O <sub>3</sub>	11.70	12.20	10.80	11.50
FeO	7.94	8.87	10.30	8.81
MnO	0.16	0.16	0.19	0.20
MgO	3.69	4.03	5.55	5.17
CaO	7.68	7.22	8.38	9.50
Na <sub>2</sub> O	6.46	6.64	5.58	5.28
K <sub>2</sub> O	0.14	0.18	0.11	0.38
P <sub>2</sub> O <sub>5</sub>	0.21	0.21	0.13	0.29
LOI	1.11	0.71	2.08	2.77
TOTAL	96.03	97.32	98.56	100.18
(ppm)				
Cr	44	38	37	49
Ni	24	29	33	33
Co	11	10	10	13
V	691	827	591	493
Cu	13	23	15	10
Pb	386	159	329	166
Zn	146	145	194	169
Bi	0.00	0.00	0.00	0.00
Cd	0.00	0.00	0.00	0.00
Mo	0.00	0.00	0.00	0.00
As	20.00	20.00	20.00	25.00
Ag	0.0	0.0	0.2	0.6
Au	0.0	0.0	0.0	0.0
K	1162	1494	913	3154
Rb	28	15	16	22
Ba	332	483	252	2808
Sr	79	137	283	543
Ga	17	11	14	12
Nb	11.0	9.0	11.0	9.0
Zr	241	220	197	177
Ti	3837	4796	3837	4077
Y	68	37	54	41
Th	0.00	0.00	0.00	0.00
U	2119.00	761.00	946.00	859.00
La	0.00	0.00	0.00	0.00
Ce	0.00	0.00	0.00	0.00

Sample Name	BL86-20A	BL86-21A	EM85-TR1A	EM85-TR1B
Rock Type	andesite	andesite	1a	1a
(wt. %) SiO <sub>2</sub>	44.60	56.30	66.90	77.70
TiO <sub>2</sub>	1.08	1.36	0.24	0.20
Al <sub>2</sub> O <sub>3</sub>	12.90	14.00	15.80	10.90
FeO	11.89	8.40	4.68	1.94
MnO	0.15	0.10	0.04	0.04
MgO	2.92	2.53	0.11	0.10
CaO	10.62	6.48	0.50	0.28
Na <sub>2</sub> O	6.44	7.34	10.38	7.03
K <sub>2</sub> O	0.70	0.26	0.22	0.09
P <sub>2</sub> O <sub>5</sub>	0.67	0.44	0.05	0.06
LOI	6.94	2.08	0.10	0.15
TOTAL	98.91	98.59	99.54	98.77
(ppm) Cr	72	72	29	0
Ni	24	38	0	0
Co	20	19	17	57
V	558	390	1249	279
Cu	0	0	0	8
Pb	655	1280	359	185
Zn	67	111	158	81
Bi	0.00	0.00	2.00	0.00
Cd	0.00	0.00	0.50	0.00
Mo	0.00	0.00	1.00	220.00
As	25.00	30.00	0.00	0.00
Ag	0.0	0.0	0.2	0.4
Au	0.0	0.0	0.0	15.0
K	5811	2158	1826	747
Rb	71	84	5	2
Ba	0	0	34	0
Sr	364	328	20	12
Ga	16	27	45	26
Nb	10.0	5.0	49.0	27.0
Zr	95	407	1051	490
Ti	6475	8153	1439	1199
Y	62	34	132	53
Th	0.00	0.00	64.00	23.00
U	2880.00	5955.00	1527.00	260.00
La	0.00	0.00	205.00	166.00
Ce	0.00	0.00	267.00	300.00

Sample Name		EM85-TR2A	EM85-TR3B	EM85-TR4	EM86-CS
Rock Type		1a	1a	1b	1b
(wt. %)	SiO <sub>2</sub>	65.90	78.20	79.50	78.10
	TiO <sub>2</sub>	0.16	0.12	0.12	0.12
	Al <sub>2</sub> O <sub>3</sub>	17.90	10.60	9.95	10.90
	FeO	1.60	2.08	1.88	0.70
	MnO	0.12	0.06	0.04	0.05
	MgO	0.04	0.15	0.06	0.01
	CaO	1.82	0.08	0.46	0.58
	Na <sub>2</sub> O	10.10	6.37	5.82	6.86
	K <sub>2</sub> O	0.14	0.05	0.13	0.16
	P <sub>2</sub> O <sub>5</sub>	0.05	0.04	0.04	0.00
	LOI	0.38	0.38	0.21	0.57
	TOTAL	98.39	98.36	98.42	98.13
(ppm)	Cr	4	3	0	0
	Ni	0	0	0	0
	Co	19	24	30	41
	V	263	360	205	39
	Cu	11	4	19	61
	Pb	685	168	180	3923
	Zn	58	56	206	41
	Bi	2.00	0.00	0.00	24.00
	Cd	0.00	0.00	0.50	0.00
	Mo	1.00	2.00	2.00	0.00
	As	10.00	0.00	0.00	5.00
	Ag	7.0	0.2	0.2	50.0
	Au	70.0	215.0	10.0	230.0
	K	1162	415	1079	1328
	Rb	5	3	8	26
	Ba	0	0	0	0
	Sr	74	12	27	31
	Ga	45	25	27	55
	Nb	39.0	33.0	31.0	40.0
	Zr	749	640	515	397
	Ti	959	719	719	719
	Y	107	42	79	168
	Th	48.00	24.00	30.00	56.00
	U	1462.00	226.00	359.00	2253.00
	La	83.00	127.00	191.00	0.00
	Ce	100.00	156.00	215.00	0.00

Sample Name		EM86-TR1	EM86-TR3	EM86-WS	EMS85-TR1A
Rock Type		1a	1a	1a	1c
(wt. %)	SiO <sub>2</sub>	66.60	75.70	63.80	55.60
	TiO <sub>2</sub>	0.20	0.20	1.28	2.20
	Al <sub>2</sub> O <sub>3</sub>	16.80	12.50	15.00	9.70
	FeO	2.44	1.22	5.87	12.05
	MnO	0.02	0.04	0.04	0.24
	MgO	0.02	0.22	0.09	0.67
	CaO	0.12	0.62	0.52	4.56
	Na <sub>2</sub> O	11.15	7.20	10.65	8.12
	K <sub>2</sub> O	0.13	0.15	0.20	0.10
	P <sub>2</sub> O <sub>5</sub>	0.02	0.04	0.01	1.53
	LOI	0.21	0.43	0.34	0.81
	TOTAL	97.98	98.46	99.88	96.92
(ppm)	Cr	0	1	8	12
	Ni	0	0	0	30
	Co	34	35	53	48
	V	851	213	1600	394
	Cu	0	4	0	392
	Pb	237	86	809	4902
	Zn	132	30	149	1223
	Bi	0.00	0.00	2.00	24.00
	Cd	0.00	0.00	0.00	4.00
	Mo	3.00	22.00	0.00	14.00
	As	0.00	5.00	10.00	70.00
	Ag	0.2	0.6	0.0	5.6
	Au	0.0	0.0	0.0	0.0
	K	1079	1245	1660	830
	Rb	9	5	22	42
	Ba	8	19	0	41
	Sr	20	88	41	209
	Ga	51	21	44	51
	Nb	31.0	32.0	207.0	167.0
	Zr	1194	383	847	650
	Ti	1199	1199	7674	13189
	Y	56	58	131	709
	Th	27.00	12.00	178.00	73.00
	U	669.00	135.00	1903.00	20269.00
	La	0.00	0.00	0.00	142.00
	Ce	0.00	0.00	0.00	489.00



Sample Name		EMS86-TR1A	EMS86-TR1B	EMS86-TR1C	EMS86-TR3B
Rock Type		1b	1c	1c	1a
(wt. %)	SiO <sub>2</sub>	66.70	56.70	53.60	72.30
	TiO <sub>2</sub>	0.04	2.32	2.56	0.00
	Al <sub>2</sub> O <sub>3</sub>	17.80	14.20	13.00	10.40
	FeO	1.65	9.58	13.25	0.71
	MnO	0.06	0.35	0.16	0.02
	MgO	0.18	0.44	0.57	0.00
	CaO	0.66	3.00	4.32	4.46
	Na <sub>2</sub> O	10.96	9.24	8.57	6.20
	K <sub>2</sub> O	0.13	0.10	0.08	0.10
	P <sub>2</sub> O <sub>5</sub>	0.10	1.06	1.23	0.02
	LOI	0.21	0.06	0.21	2.53
	TOTAL	98.67	98.00	98.61	96.82
(ppm)	Cr	0	5	12	0
	Ni	0	0	16	0
	Co	27	25	20	25
	V	101	213	293	5
	Cu	0	24	1	413
	Pb	137	2534	95	557
	Zn	59	3549	245	2213
	Bi	0.00	0.00	0.00	2.00
	Cd	0.00	0.00	0.00	6.50
	Mo	0.00	0.00	0.00	2763.00
	As	0.00	20.00	25.00	0.00
	Ag	0.2	8.6	0.4	8.6
	Au	0.0	0.0	0.0	10.0
	K	1079	830	664	830
	Rb	3	7	5	4
	Ba	0	18	15	0
	Sr	29	138	156	74
	Ga	58	18	23	42
	Nb	31.0	230.0	118.0	18.0
	Zr	1186	288	578	380
	Ti	240	13908	15347	0
	Y	117	151	282	85
	Th	32.00	0.00	11.00	52.00
	U	412.00	334.00	119.00	267.00
	La	0.00	0.00	0.00	0.00
	Ce	0.00	0.00	0.00	0.00

Sample Name		EMS86-TR4A	EMS86-TR4B	EMS86-TR5B	EMS86-TR6
Rock Type		1b	1c	1c	1c
(wt. %)	SiO <sub>2</sub>	64.50	58.80	55.50	38.80
	TiO <sub>2</sub>	0.44	1.20	2.20	1.96
	Al <sub>2</sub> O <sub>3</sub>	16.60	14.50	10.80	9.19
	FeO	3.46	5.83	9.30	24.44
	MnO	0.08	0.12	0.14	0.12
	MgO	0.27	0.29	0.53	0.13
	CaO	1.10	4.48	5.38	3.16
	Na <sub>2</sub> O	10.66	9.53	9.03	6.07
	K <sub>2</sub> O	0.16	0.17	0.08	0.09
	P <sub>2</sub> O <sub>5</sub>	0.15	2.27	1.78	1.63
	LOI	0.33	0.29	0.44	8.11
	TOTAL	98.14	98.13	96.22	96.13
(ppm)	Cr	1	34	0	0
	Ni	21	31	35	40
	Co	10	20	18	367
	V	632	973	380	504
	Cu	23	363	52	1072
	Pb	279	1663	5963	5826
	Zn	76	244	3155	20125
	Bi	2.00	8.00	44.00	6.00
	Cd	0.00	0.00	5.00	53.00
	Mo	3.00	0.00	418.00	1415.00
	As	5.00	0.00	40.00	90.00
	Ag	1.2	32.0	13.6	22.0
	Au	0.0	55.0	0.0	30.0
	K	1328	1411	664	747
	Rb	25	50	146	52
	Ba	0	0	0	0
	Sr	53	345	234	227
	Ga	56	59	84	89
	Nb	53.0	123.0	227.0	176.0
	Zr	1060	502	684	462
	Ti	2638	7194	13189	11750
	Y	301	431	576	377
	Th	37.00	79.00	54.00	52.00
	U	1700.00	3494.00	12126.00	4311.00
	La	0.00	0.00	0.00	0.00
	Ce	0.00	0.00	0.00	0.00

Sample Name		EMS86-TR7	ES85-TR1AB
Rock Type		1c	1b
(wt. %)	SiO <sub>2</sub>	56.30	62.60
	TiO <sub>2</sub>	2.40	1.36
	Al <sub>2</sub> O <sub>3</sub>	12.30	15.00
	FeO	9.50	4.31
	MnO	0.09	0.17
	MgO	0.24	0.35
	CaO	3.78	2.62
	Na <sub>2</sub> O	9.30	10.04
	K <sub>2</sub> O	0.07	0.15
	P <sub>2</sub> O <sub>5</sub>	1.29	0.95
	LOI	1.15	0.51
	TOTAL	97.48	98.54
(ppm)	Cr	0	0
	Ni	15	25
	Co	33	28
	V	326	149
	Cu	432	0
	Pb	418	4771
	Zn	486	637
	Bi	0.00	24.00
	Cd	0.50	2.00
	Mo	110.00	6.00
	As	0.00	60.00
	Ag	2.4	0.4
	Au	0.0	0.0
	K	581	1245
	Rb	15	40
	Ba	0	35
	Sr	128	125
	Ga	43	82
	Nb	181.0	278.0
	Zr	498	246
	Ti	14388	8153
	Y	269	112
	Th	8.00	85.00
	U	1263.00	17850.00
	La	0.00	62.00
	Ce	0.00	471.00

Sample Name	BH1-164.8	BH5-246.6	BH9-161.9	BH11-355.2
Rock Type	4a	4a	4a	4a
(ppm)				
Cr	20	0	0	0
Ni	0	0	0	0
Co	34	26	11	19
V	369	404	28	65
Cu	40	11	13	101
Pb	22	42	274	2064
Zn	41	195	2292	8048
Bi	0.00	0.00	0.00	10.00
Cd	0.00	0.00	7.50	17.50
Mo	414.00	0.00	10.00	0.00
As	15.00	0.00	10.00	10.00
Ag	0.6	0.4	0.4	4.0
Au	0.0	0.0	0.0	0.0
K	0	0	0	0
Rb	102	2	1	65
Ba	0	0	0	0
Sr	19	28	53	73
Ga	24	21	23	48
Nb	23.0	23.0	48.0	27.0
Zr	242	411	288	386
Ti	4376	1259	1079	899
Y	38	52	56	65
Th	26.00	25.00	26.00	36.00
U	115.00	66.00	21.00	1753.00
La	13.00	91.00	57.00	178.00
Ce	0.00	0.00	0.00	0.00

Sample Name	BH10-191.0	BH11-194.8	L85-TR6-3B	L85-TR6-4A
Rock Type	4a	4a	4b(a)	4b(a)
(ppm)				
Cr	0	25	32	4
Ni	0	0	0	0
Co	29	43	25	33
V	215	583	1148	426
Cu	8	34	2	0
Pb	116	96	104	286
Zn	90	110	54	166
Bi	0.00	0.00	0.00	2.00
Cd	0.00	0.00	0.00	0.00
Mo	0.00	563.00	0.00	1.00
As	0.00	5.00	0.00	10.00
Ag	0.2	0.4	0.2	0.4
Au	0.0	0.0	0.0	0.0
K	0	0	0	0
Rb	32	18	4	124
Ba	0	0	13	440
Sr	38	30	6	17
Ga	30	25	18	14
Nb	24.0	22.0	26.0	32.0
Zr	449	251	535	418
Ti	1139	3117	2398	1559
Y	66	22	56	85
Th	36.00	31.00	18.00	46.00
U	284.00	357.00	456.00	970.00
La	80.00	127.00	106.00	101.00
Ce	0.00	0.00	193.00	140.00

## 340

Sample Name	BL86-34a	BH1-167.1	BH3-42.0	BH9-202.6
Rock Type	4b(a)	4b	4b	4b
(ppm)				
Cr	9	17	0	0
Ni	0	2	0	0
Co	0	29	36	36
V	326	108	127	28
Cu	1	14	6	11
Pb	29	30	25	210
Zn	132	200	247	845
Bi	0.00	0.00	0.00	0.00
Cd	0.00	0.00	0.00	2.50
Mo	0.00	17.00	0.00	0.00
As	0.00	5.00	0.00	5.00
Ag	0.0	0.2	0.2	0.2
Au	0.0	0.0	0.0	0.0
K	0	0	0	0
Rb	162	95	239	1
Ba	373	0	0	0
Sr	19	19	29	25
Ga	12	25	15	25
Nb	19.0	30.0	29.0	30.0
Zr	250	284	381	251
Ti	1019	2698	1319	839
Y	41	66	68	46
Th	16.00	33.00	49.00	33.00
U	34.00	70.00	29.00	68.00
La	80.00	88.00	155.00	114.00
Ce	0.00	0.00	0.00	0.00

Sample Name	BH11-230.3	BH11-290.5	LM85-TR14B	LM85-TR1A
Rock Type	4b	4b	4b	4b
(ppm)				
Cr	0	0	14	4
Ni	0	0	0	0
Co	34	58	29	40
V	126	15	863	581
Cu	9	24	74	6
Pb	61	297	324	94
Zn	143	11295	38	161
Bi	0.00	2.00	2.00	0.00
Cd	0.00	27.00	0.00	0.00
Mo	0.00	0.00	0.00	1.00
As	5.00	25.00	0.00	0.00
Ag	0.2	0.2	0.4	0.4
Au	0.0	0.0	0.0	0.0
K	0	0	0	0
Rb	136	5	5	2
Ba	0	0	0	471
Sr	50	28	11	18
Ga	24	29	26	26
Nb	33.0	57.0	26.0	32.0
Zr	315	278	566	418
Ti	1918	1559	2518	1739
Y	49	66	31	64
Th	31.00	40.00	35.00	31.00
U	41.00	471.00	768.00	95.00
La	86.00	153.00	108.00	118.00
Ce	0.00	0.00	103.00	150.00

## 341

Sample Name	BH1-164.8	BH5-246.6	BH9-161.9	BH11-355.2
Rock Type	4a	4a	4a	4a
(ppm)				
Cr	20	0	0	0
Ni	0	0	0	0
Co	34	26	11	19
V	369	404	28	65
Cu	40	11	13	101
Pb	22	42	274	2064
Zn	41	195	2292	8048
Bi	0.00	0.00	0.00	10.00
Cd	0.00	0.00	7.50	17.50
Mo	414.00	0.00	10.00	0.00
As	15.00	0.00	10.00	10.00
Ag	0.6	0.4	0.4	4.0
Au	0.0	0.0	0.0	0.0
K	0	0	0	0
Rb	102	2	1	65
Ba	0	0	0	0
Sr	19	28	53	73
Ga	24	21	23	48
Nb	23.0	23.0	48.0	27.0
Zr	242	411	288	386
Ti	4376	1259	1079	899
Y	38	52	56	65
Th	26.00	25.00	26.00	36.00
U	115.00	66.00	21.00	1753.00
La	13.00	91.00	57.00	178.00
Ce	0.00	0.00	0.00	0.00

Sample Name	BH10-191.0	BH11-194.8	L85-TR6-3B	L85-TR6-4A
Rock Type	4a	4a	4b(a)	4b(a)
(ppm)				
Cr	0	25	32	4
Ni	0	0	0	0
Co	29	43	25	33
V	215	583	1148	426
Cu	8	34	2	0
Pb	116	96	104	286
Zn	90	110	54	166
Bi	0.00	0.00	0.00	2.00
Cd	0.00	0.00	0.00	0.00
Mo	0.00	563.00	0.00	1.00
As	0.00	5.00	0.00	10.00
Ag	0.2	0.4	0.2	0.4
Au	0.0	0.0	0.0	0.0
K	0	0	0	0
Rb	32	18	4	124
Ba	0	0	13	440
Sr	38	30	6	17
Ga	30	25	18	14
Nb	24.0	22.0	26.0	32.0
Zr	449	251	535	418
Ti	1139	3117	2398	1559
Y	66	22	56	85
Th	36.00	31.00	18.00	46.00
U	284.00	357.00	456.00	970.00
La	80.00	127.00	106.00	101.00
Ce	0.00	0.00	193.00	140.00

## 342

Sample Name	BH10-141.8	L85-TR6-1A	LM85-TR10	LM85-E.1
Rock Type	4d	4d	4d	1a
(ppm) Cr	0	14	12	0
Ni	0	0	0	1
Co	20	26	23	0
V	554	854	718	638
Cu	5	0	2	5
Pb	55	215	138	394
Zn	187	100	136	109
Bi	0.00	0.00	0.00	0.00
Cd	0.50	0.00	0.00	0.00
Mo	0.00	0.00	0.00	0.00
As	0.00	10.00	0.00	0.00
Ag	0.2	0.2	0.2	0.0
Au	0.0	0.0	0.0	0.0
K	0	0	0	0
Rb	104	4	48	12
Ba	0	243	433	23
Sr	12	13	13	43
Ga	27	20	25	46
Nb	31.0	25.0	26.0	89.0
Zr	495	481	453	1621
Ti	1619	1799	959	0
Y	67	73	51	149
Th	19.00	27.00	35.00	65.00
U	33.00	885.00	231.00	711.00
La	83.00	90.00	109.00	194.00
Ce	0.00	181.00	168.00	50.00

Sample Name	LM85-TR2B	LM85-TR4B	LM85-TR8	LM85-TR8B-A
Rock Type	4b	4b	4b	4b
(ppm) Cr	13	0	1	5
Ni	0	0	3	0
Co	28	19	28	29
V	408	248	319	417
Cu	6	8	1	5
Pb	327	82	130	234
Zn	515	11	293	144
Bi	0.00	0.00	0.00	0.00
Cd	0.00	0.00	0.00	0.00
Mo	1.00	0.00	0.00	0.00
As	0.00	0.00	0.00	0.00
Ag	0.0	0.4	0.2	0.2
Au	0.0	0.0	0.0	0.0
K	0	0	0	0
Rb	2	6	21	109
Ba	328	29	45	127
Sr	21	9	7	13
Ga	22	22	30	19
Nb	32.0	25.0	51.0	45.0
Zr	312	453	413	571
Ti	1799	1019	1439	1739
Y	40	33	178	70
Th	28.00	30.00	29.00	40.00
U	40.00	348.00	435.00	848.00
La	128.00	16.00	106.00	152.00
Ce	170.00	43.00	147.00	199.00

## Burnt Lake Area Granitoids

Sample Name	BL86-13	BL86-14	BL86-15	BL86-32a	BL86-33a
Unit	5a	5a	5a	5a	5a
(wt %)					
SiO <sub>2</sub>	74.40	75.50	79.10	74.20	76.20
TiO <sub>2</sub>	0.12	0.12	0.12	0.04	0.04
Al <sub>2</sub> O <sub>3</sub>	12.40	12.30	12.00	12.90	12.60
Fe <sub>2</sub> O <sub>3</sub>	0.14	0.14	0.08	0.08	0.06
FeO	0.72	0.71	0.38	0.41	0.30
MnO	0.03	0.01	0.05	0.02	0.01
MgO	0.12	0.11	0.46	0.07	0.03
CaO	0.70	0.62	4.84	0.98	0.40
Na <sub>2</sub> O	3.67	3.53	4.84	4.27	4.57
K <sub>2</sub> O	4.93	5.08	2.91	4.83	4.36
P <sub>2</sub> O <sub>5</sub>	0.02	0.02	0.01	0.01	0.00
LOI	0.26	0.41	0.23	0.19	0.16
	-----	-----	-----	-----	-----
TOTAL	97.60	98.62	100.22	98.04	98.76
(ppm)					
Cr	0	0	0	4	2
Ni	0	0	0	0	0
Co	26	19	40	n.a.	n.a.
V	5	5	5	0	0
Cu	3	9	4	0	0
Pb	43	27	29	28	13
Zn	6	0	0	0	0
Mo	0.00	27.00	55.00	n.a.	n.a.
As	0.00	0.00	0.00	n.a.	n.a.
Ag	0.2	0.0	0.0	n.a.	n.a.
K	40925	42171	24157	40095	36194
Rb	253	217	90	241	247
Ba	n.a.	n.a.	n.a.	52	34
Sr	75	60	146	23	19
Ga	19	19	18	20	17
Nb	26.0	29.0	26.0	46.0	36.0
Zr	114	89	69	70	74
Ti	719	719	719	240	240
Y	34	25	15	31	24
Th	40.00	30.00	25.00	22.00	24.00
U	26.00	17.00	19.00	27.00	18.00
F	n.a.	n.a.	n.a.	n.a.	n.a.
La	51.00	2.00	0.00	0.00	0.00
NORM					
Qtz	32.19	33.68	33.18	29.05	32.04
Or	29.14	30.03	17.20	28.55	25.77
Ab	31.05	29.87	40.95	36.13	38.67
An	2.80	2.72	2.43	1.77	0.99
Di	0.46	0.20	3.48	1.61	0.86
Ol	--	--	--	--	--
Hy	1.13	1.17	--	--	0.08
Mt	0.21	0.20	0.11	0.12	0.08



Sample Name	BL86-35	BL86-36	BL86-38	BL86-37	LM85-134
Unit	5b	5b	5b	5b	5b
(wt %)					
SiO <sub>2</sub>	58.00	74.70	47.30	39.40	61.90
TiO <sub>2</sub>	0.76	0.12	1.24	1.92	0.92
Al <sub>2</sub> O <sub>3</sub>	17.00	13.60	18.80	15.20	15.10
Fe <sub>2</sub> O <sub>3</sub>	1.02	1.02	1.72	3.09	1.27
FeO	5.21	5.21	8.76	15.74	6.47
MnO	0.11	0.00	0.14	0.17	0.12
MgO	2.53	0.02	4.58	8.53	0.41
CaO	4.70	0.18	8.12	8.64	2.14
Na <sub>2</sub> O	4.15	3.22	3.54	2.22	4.71
K <sub>2</sub> O	3.60	6.98	2.37	0.83	5.32
P <sub>2</sub> O <sub>5</sub>	0.45	0.02	0.82	0.06	0.11
LOI	0.50	0.10	0.69	0.95	0.19
	-----	-----	-----	-----	-----
TOTAL	98.61	99.01	99.06	98.50	99.38
(ppm)					
Cr	0	0	0	0	0
Ni	0	0	0	0	0
Co	n.a.	n.a.	n.a.	n.a.	n.a.
V	100	1	153	639	16
Cu	24	5	7	77	134
Pb	10	12	9	0	49
Zn	59	0	81	103	89
Mo	n.a.	n.a.	n.a.	n.a.	n.a.
As	n.a.	n.a.	n.a.	n.a.	n.a.
Ag	n.a.	n.a.	n.a.	n.a.	n.a.
K	29885	57943	19674	6890	44163
Rb	97	99	69	99	113
Ba	n.a.	n.a.	1491	n.a.	1
Sr	469	31	665	477	171
Ga	19	15	22	19	20
Nb	10.0	7.0	14.0	6.0	22.0
Zr	147	12	96	53	1748
Ti	4556	719	7434	11510	5515
Y	23	7	35	24	74
Th	11.00	11.00	0.00	0.00	42.00
U	9.00	11.00	1.00	14.00	9.00
F	n.a.	n.a.	n.a.	n.a.	n.a.
La	43.00	0.00	41.00	0.00	405.20
NORM					
Qtz	4.71	25.01	--	--	6.11
Or	21.28	41.26	14.01	4.91	31.44
Ab	35.11	27.24	23.20	7.22	39.85
An	17.13	0.76	28.41	29.06	4.35
Di	2.70	--	5.41	11.13	4.87
Ol	--	--	15.95	28.95	--
Hy	12.62	8.57	--	--	8.00
Mt	1.48	1.48	2.49	4.48	1.84

Sample Name		BL86-41	BL86-42	BL86-43	GEO-1	GEO-2
Unit		5c	5c	5c	5a	5a
(wt %)	SiO <sub>2</sub>	57.90	47.80	45.80	72.00	72.00
	TiO <sub>2</sub>	1.04	1.32	2.24	0.28	0.28
	Al <sub>2</sub> O <sub>3</sub>	17.00	15.10	14.40	14.20	14.30
	Fe <sub>2</sub> O <sub>3</sub>	1.02	1.76	2.52	0.32	0.32
	FeO	5.22	8.95	12.84	1.64	1.64
	MnO	0.13	0.28	0.19	0.04	0.03
	MgO	2.33	7.56	6.03	0.36	0.33
	CaO	4.80	8.86	9.86	1.08	1.08
	Na <sub>2</sub> O	4.52	3.17	2.81	3.89	3.78
	K <sub>2</sub> O	3.10	1.28	0.63	5.01	5.57
	P <sub>2</sub> O <sub>5</sub>	0.39	0.17	0.15	0.08	0.05
	LOI	0.30	0.09	16.79	0.46	0.51
		-----	-----	-----	-----	-----
	TOTAL	98.33	98.16	99.12	99.55	100.07
(ppm)	Cr	0	34	0	0	0
	Ni	0	33	0	0	0
	Co	n.a.	n.a.	n.a.	n.a.	n.a.
	V	116	168	509	1	2
	Cu	13	43	15	4	3
	Pb	16	11	0	45	23
	Zn	77	178	113	31	34
	Mo	n.a.	n.a.	n.a.	n.a.	n.a.
	As	n.a.	n.a.	n.a.	n.a.	n.a.
	Ag	n.a.	n.a.	n.a.	n.a.	n.a.
	K	25734	10626	5230	41590	46238
	Rb	70	8	10	194	163
	Ba	n.a.	n.a.	n.a.	718	842
	Sr	600	733	670	122	118
	Ga	19	19	19	20	18
	Nb	15.0	5.0	4.0	18.0	16.0
	Zr	130	77	100	254	313
	Ti	6235	7913	13429	1679	1679
	Y	36	25	25	26	24
	Th	15.00	0.00	0.00	34.00	15.00
	U	15.00	9.00	10.00	2.00	0.00
	F	n.a.	n.a.	n.a.	340.00	310.00
	La	55.00	4.00	0.00	59.40	62.80
	NORM					
	Qtz	4.71	--	--	26.50	24.96
	Or	18.32	7.57	3.72	29.61	32.92
	Ab	38.24	25.53	23.78	32.91	31.98
	An	16.95	23.20	24.82	4.84	5.03
	Di	3.60	16.07	19.25	--	--
	Ol	--	17.73	16.86	--	--
	Hy	11.27	--	0.78	3.25	3.16
	Mt	1.48	2.54	3.65	0.47	0.47

Sample Name		LM85-151	LM85-165	LM85-166	LM85-167	LM85-106
Unit		5a	5a	5a	5a	6
(wt %)	SiO <sub>2</sub>	63.50	76.90	72.60	76.20	45.70
	TiO <sub>2</sub>	0.12	0.08	0.20	0.08	1.64
	Al <sub>2</sub> O <sub>3</sub>	19.20	12.60	14.10	12.70	13.90
	Fe <sub>2</sub> O <sub>3</sub>	0.22	0.14	0.26	0.13	2.33
	FeO	1.10	0.71	1.31	0.67	11.85
	MnO	0.04	0.04	0.06	0.02	0.20
	MgO	0.48	0.08	0.35	0.11	6.27
	CaO	1.08	0.71	1.20	0.72	7.02
	Na <sub>2</sub> O	6.26	4.11	4.30	3.94	2.10
	K <sub>2</sub> O	6.29	4.16	4.69	4.74	4.52
	P <sub>2</sub> O <sub>5</sub>	0.05	0.00	0.02	0.01	0.18
	LOI	0.70	0.44	0.48	0.41	3.52
	TOTAL	99.15	100.06	99.71	99.81	100.55
<hr/>						
(ppm)	Cr	0	0	0	0	139
	Ni	0	0	26	0	63
	Co	n.a.	n.a.	n.a.	n.a.	48
	V	0	0	4	0	333
	Cu	5	4	4	5	0
	Pb	36	52	33	32	30
	Zn	0	0	22	0	234
	Mo	n.a.	n.a.	n.a.	n.a.	0.00
	As	n.a.	n.a.	n.a.	n.a.	10.00
	Ag	n.a.	n.a.	n.a.	n.a.	0.2
	K	52215	34533	38933	39348	37522
	Rb	130	219	141	213	199
	Ba	1743	0	3	252	700
	Sr	242	38	229	89	95
	Ga	21	20	18	22	16
	Nb	23.0	36.0	19.0	36.0	7.0
	Zr	163	98	160	100	147
	Ti	719	480	1199	480	9832
	Y	32	16	23	22	44
	Th	43.00	58.00	22.00	45.00	12.00
	U	0.00	5.00	0.00	10.00	7.00
	F	550.00	80.00	180.00	90.00	n.a.
	La	39.00	11.10	40.70	23.00	6.00
<hr/>						
NORM						
	Qtz	--	34.91	25.81	33.11	--
	Or	37.18	24.59	27.72	28.02	26.72
	Ab	52.97	34.77	36.38	33.34	6.83
	An	5.03	3.52	5.32	2.97	15.15
	Di	--	--	0.42	0.46	15.36
	Ol	1.90	--	--	--	18.81
	Hy	0.35	1.34	2.63	1.07	--
	Mt	0.31	0.20	0.37	0.19	3.37

Sample Name		LM85-157	LM85-168	LM85-174	LM85-176	LM85-17C
Unit		7	5a	5a	5a	peg
(wt %)	SiO <sub>2</sub>	46.60	75.20	68.60	76.40	77.80
	TiO <sub>2</sub>	0.24	0.16	0.24	0.08	0.08
	Al <sub>2</sub> O <sub>3</sub>	8.86	13.20	15.40	12.70	12.50
	Fe <sub>2</sub> O <sub>3</sub>	1.59	0.21	0.38	0.09	0.15
	FeO	8.13	1.08	1.95	0.46	0.78
	MnO	0.17	0.03	0.07	0.01	0.00
	MgO	18.80	0.19	0.62	0.08	0.08
	CaO	13.60	0.84	1.88	0.58	0.40
	Na <sub>2</sub> O	0.85	3.71	4.50	4.16	6.57
	K <sub>2</sub> O	0.70	5.14	4.64	4.55	0.33
	P <sub>2</sub> O <sub>5</sub>	0.07	0.03	0.08	0.00	0.01
	LOI	1.11	0.41	0.40	0.27	0.63
	TOTAL	99.63	100.32	98.99	99.43	99.42
(ppm)	Cr	1207	0	0	0	0
	Ni	207	0	0	21	0
	Co	51	n.a.	n.a.	n.a.	n.a.
	V	121	0	23	52	0
	Cu	115	2	8	0	36
	Pb	19	40	0	19	53
	Zn	47	20	28	33	0
	Mo	0.00	n.a.	n.a.	n.a.	n.a.
	As	0.00	n.a.	n.a.	n.a.	n.a.
	Ag	0.2	n.a.	n.a.	n.a.	n.a.
	K	5811	42669	38518	37771	2739
	Rb	29	231	128	148	12
	Ba	218	0	0	434	0
	Sr	323	95	346	155	133
	Ga	0	22	21	17	22
	Nb	4.0	32.0	22.0	20.0	37.0
	Zr	25	190	241	117	52
	Ti	1439	959	1439	480	480
	Y	12	30	35	30	5
	Th	7.00	33.00	128.00	16.00	6.00
	U	10.00	0.00	0.00	7.00	1.00
	F	n.a.	n.a.	n.a.	n.a.	n.a.
	La	0.00	25.80	49.50	30.00	0.90
	NORM					
	Qtz	--	31.22	18.72	33.20	36.84
	Or	4.14	30.38	27.42	26.89	1.95
	Ab	3.33	31.39	38.07	35.20	55.59
	An	18.29	3.97	8.12	2.55	1.92
	Di	38.91	--	0.58	0.29	--
	Ol	29.83	--	--	--	--
	Hy	--	2.07	4.26	0.71	1.37
	Mt	2.31	0.31	0.56	0.13	0.22

Sample Name	LM85-21a	LM85-23	LM85-34	LM85-164
Unit	5a	5a	5a	5a
(wt %)				
SiO <sub>2</sub>	76.70	75.50	74.90	76.80
TiO <sub>2</sub>	0.04	0.16	0.08	0.08
Al <sub>2</sub> O <sub>3</sub>	13.20	13.40	13.50	12.80
Fe <sub>2</sub> O <sub>3</sub>	0.12	0.18	0.11	0.11
FeO	0.59	0.90	0.57	0.57
MnO	0.02	0.03	0.01	0.02
MgO	0.09	0.15	0.10	0.10
CaO	0.24	0.68	0.92	0.68
Na <sub>2</sub> O	4.59	3.71	3.99	3.86
K <sub>2</sub> O	4.60	5.02	4.60	5.10
P <sub>2</sub> O <sub>5</sub>	0.01	0.03	0.02	0.00
LOI	0.24	0.52	0.28	0.41
	-----	-----	-----	-----
TOTAL	100.50	100.38	99.15	100.60
(ppm)				
Cr	0	0	0	0
Ni	0	0	0	0
Co	n.a.	n.a.	n.a.	n.a.
V	0	0	0	0
Cu	8	2	5	4
Pb	28	44	36	38
Zn	0	15	0	0
Mo	n.a.	n.a.	n.a.	n.a.
As	n.a.	n.a.	n.a.	n.a.
Ag	n.a.	n.a.	n.a.	n.a.
K	38186	41673	38186	42337
Rb	189	243	162	198
Ba	65	0	3	0
Sr	32	81	110	92
Ga	23	23	21	18
Nb	45.0	34.0	8.0	30.0
Zr	82	147	92	101
Ti	240	959	480	480
Y	40	29	14	18
Th	36.00	29.00	32.00	49.00
U	11.00	15.00	2.00	13.00
F	n.a.	n.a.	n.a.	n.a.
La	0.00	23.30	16.40	16.00
NORM				
Qtz	31.34	32.52	31.60	33.01
Or	27.19	29.67	27.19	30.14
Ab	38.84	31.39	33.76	32.66
An	1.13	3.18	4.43	2.54
Di	--	--	--	0.72
Ol	--	--	--	--
Hy	1.18	1.67	1.18	0.74
Mt	0.17	0.26	0.11	0.16

Sample Name	BL86-40	LM85-17B	LM85-21b	LM85-148	LM85-24
Unit	5b	5a	5a	5a	5a
(ppm) Cr	0	0	0	0	0
Ni	0	0	0	0	0
Co	n.a.	n.a.	n.a.	n.a.	33
V	6	0	0	157	1
Cu	0	6	9	13	8
Pb	13	32	43	1	27
Zn	29	0	0	68	0
Mo	n.a.	n.a.	n.a.	n.a.	1.00
As	n.a.	n.a.	n.a.	n.a.	0.00
Ag	n.a.	n.a.	n.a.	n.a.	0.2
Rb	132	219	182	140	119
Ba	875	0	14	0	305
Sr	170	28	19	392	110
Ga	18	19	22	18	16
Nb	13.0	30.0	48.0	12.0	5.0
Zr	776	64	89	162	67
Y	39	13	18	33	4
Th	11.00	18.00	47.00	16.00	7.00
U	7.00	7.00	6.00	8.00	3.00
La	117.00	4.60	4.60	37.00	6.60

Sample Name	LM85-107	LM85-26
Unit	6	peg
(ppm) Cr	133	0
Ni	56	0
Co	31	n.a.
V	310	0
Cu	10	5
Pb	12	25
Zn	116	0
Mo	0.00	n.a.
As	30.00	n.a.
Ag	0.2	n.a.
Rb	74	43
Ba	467	42
Sr	109	52
Ga	14	9
Nb	10.0	21.0
Zr	149	52
Y	44	23
Th	7.00	27.00
U	0.00	0.00
La	4.00	11.00

## REE data for the Burnt Lake Area Granitoids

Sample Name	LM85-134	GEO-1	GEO-2	LM85-165	LM85-166
Unit	5b	5a	5a	5a	5a
(wt %)					
SiO <sub>2</sub>	61.90	72.00	72.00	76.90	72.60
REES					
(ppm)					
La	405.20	59.40	62.80	11.10	40.70
Ce	782.20	118.50	126.80	21.40	82.00
Pr	61.40	10.40	10.00	1.80	7.60
Nd	282.10	41.70	43.80	7.00	29.20
Sm	36.70	6.60	6.60	1.60	4.70
Eu	0.00	0.50	0.60	0.00	0.30
Gd	18.10	4.80	5.70	1.80	3.90
Tb	0.30	1.00	0.70	0.70	0.90
Dy	12.30	5.00	5.20	3.00	4.50
Ho	1.60	0.80	0.80	0.80	1.10
Er	6.80	3.20	2.60	2.30	2.70
Tm	22.80	21.80	22.30	22.00	22.30
Yb	4.10	3.10	2.50	2.90	3.00
Lu	1.00	0.20	0.50	0.50	0.50

Sample Name	LM85-167	LM85-168	LM85-174	LM85-17C	LM85-23
Unit	5a	5a	5a	peg	5a
(wt %)					
SiO <sub>2</sub>	76.20	75.20	68.60	77.80	75.50
REES					
(ppm)					
La	23.00	25.80	49.50	0.90	23.30
Ce	51.10	63.80	105.30	1.20	57.40
Pr	3.60	4.30	9.30	0.00	4.10
Nd	14.60	18.20	41.30	0.60	17.90
Sm	2.70	3.90	7.10	0.00	3.40
Eu	0.20	0.30	0.80	0.20	0.30
Gd	2.30	3.80	5.50	0.40	4.00
Tb	0.50	1.00	0.60	0.30	0.40
Dy	3.60	5.20	5.80	1.20	4.70
Ho	0.80	0.90	0.70	0.50	0.90
Er	3.00	3.70	4.00	1.00	4.00
Tm	22.10	21.60	20.90	14.70	22.30
Yb	2.90	4.20	3.20	1.40	5.10
Lu	0.40	0.80	0.70	0.00	1.00

## REE data for the Burnt Lake Area Granitoids

Sample Name		LM85-34	LM85-164	LM85-17B	LM85-21b	LM85-24
Unit		5a	5a	5a	5a	peg
(wt %)	SiO <sub>2</sub>	74.90	76.80	na	na	na
	REES					
(ppm)	La	16.40	16.00	4.60	4.60	6.60
	Ce	40.80	40.00	11.50	10.80	10.80
	Pr	3.10	3.20	0.60	1.00	0.90
	Nd	12.70	9.40	4.40	5.00	3.50
	Sm	2.80	1.80	1.00	1.60	0.70
	Eu	0.30	0.00	0.00	0.10	0.00
	Gd	2.40	1.70	1.30	1.80	0.70
	Tb	0.60	0.80	0.70	0.70	0.20
	Dy	3.80	2.50	2.40	3.40	0.70
	Ho	1.00	0.30	0.50	1.10	0.10
	Er	2.10	2.30	1.90	2.30	0.50
	Tm	22.00	22.20	22.10	20.60	13.90
	Yb	1.30	2.40	2.10	3.00	0.40
	Lu	0.20	0.30	0.20	0.50	0.00

Sample Name		LM85-26
Unit		peg
(wt %)	SiO <sub>2</sub>	na
	REES	
(ppm)	La	11.00
	Ce	29.30
	Pr	2.30
	Nd	11.50
	Sm	2.70
	Eu	0.10
	Gd	3.40
	Tb	0.80
	Dy	4.70
	Ho	0.60
	Er	2.80
	Tm	20.30
	Yb	2.60
	Lu	0.40



## APPENDIX II

SUMMARY DESCRIPTIONS OF ROCK SAMPLES  
USED IN CHEMICAL ANALYSIS

<u>SAMPLE NO.</u>	<u>ROCK UNIT</u>	<u>DESCRIPTION</u>
LM85-1	4b	Whitish, sucrosic felsic quartz-crystal tuff with a strong mineral lineation.
LM85-2	4b	Coarse-grained quartz-feldspar porphyry.
LM85-5b	4d	Brecciated, coarse-grained feldspar porphyry with 50% feldspar phenocrysts.
LM85-6	4b	Pink and grey, feldspar $\pm$ quartz porphyry.
LM85-7a	4d	Feldspar porphyry.
LM85-11b	4d	Coarse-grained feldspar porphyry with alignment of phenocrysts.
LM85-14	4b(a)	Sucrosic, feldspar $\pm$ quartz porphyry with atoll rim around feldspar phenocrysts.
LM85-15	4b	Pink, quartz porphyry with green mafic veinlets; containing micas, minor pyrite and magnetite.
LM85-17b	5a	Buff coloured fine-grained granite with minor mafic specks and hematite.
LM85-17c	peg	Coarse-grained feldspar+quartz pegmatite with hematite staining.
LM85-21a	4b, 5a	Contact between sugary felsic tuff and leucocratic granite; minor pyrite.
LM85-21b	5a	Pink to brown, fine-grained leucocratic granite with minor quartz veins and trace pyrite.
LM85-23	5a	Fine-grained granite with 10% mafics.

LM85-24	5a	Fine-grained granite with minor mafics and trace pyrite.
LM85-26	peg	Coarse-grained quartz+feldspar pegmatite with some greenish chlorite alteration and minor pyrite.
LM85-32	4b	Slightly porphyritic felsic tuff with reddish brown matrix with quartz and mafic fragments.
LM85-33	4d	Pink-grey feldspar porphyry.
LM85-34	5a	Fine-grained leucocratic granite.
LM85-35	4b	Grey-brown porphyritic rhyolite with 10% white feldspar and 1-2% blue quartz eyes.
LM85-37	4b	Coarse-grained porphyritic rhyolite with 25% rounded feldspar phenocrysts; mafic veinlets and greenish chlorite alteration.
LM85-39	4d	Feldspar porphyry with 20% white subrounded feldspar phenocrysts and a sugary grey-blue matrix.
LM85-40	4d	Coarse-grained feldspar porphyry with 25-30% white feldspar phenocrysts; matrix is sugary blue-grey.
LM85-41a	4b	Quartz porphyry with minor feldspar phenocrysts.
LM85-41b	4b	Sugary feldspar+quartz porphyry; rusty.
LM85-42	4b	Slightly porphyritic rhyolite.
LM85-45	4b	Brownish-grey laminated slightly porphyritic felsic tuff.
LM85-49	4b	Coarse-grained porphyritic rhyolite and fine-grained ash tuff.
LM85-50	4b	Quartz porphyry with 15-20% blue qtz phenos in a pink-grey matrix; 2% white feldspar and small mafic fragments.

LM85-51	4d	Coarse-grained feldspar porphyry with 20% white euhedral feldspar and 2% blue quartz in a blue-grey matrix.
LM85-52	4b	Quartz-feldspar porphyry.
LM85-53	2	Volcaniclastic siltstone and sandstone.
LM85-54	3	Well-bedded maroon volcaniclastic siltstone.
LM85-60	4b	Banded quartz porphyry with 10-15% quartz and minor feldspar in a pink-grey matrix; mafic veinlets and trace pyrite.
LM85-60m	4b	Pink sugary quartz porphyry with 5% quartz phenocrysts; mafic veinlets and disseminated pyrite.
LM85-63	4a	Banded non-porphyritic tuff.
LM85-64	4b	Feldspar-quartz porphyry with 10% pink euhedral feldspar and <5% blue quartz in a fine-grained grey matrix.
LM85-67	4a	Grey recrystallized slightly banded and foliated porphyritic rhyolite.
LM85-68	4a	Sugary felsic ash tuff with 10% small quartz and feldspar phenos in a pink-grey matrix; trace pyrite.
LM85-71	4b(a)	Sugary, sparsely quartz porphyritic tuff with possible lithic fragments and minor pyrite.
LM85-74	4a	Streaky, sugary banded tuff with minor quartz and glass shards.
LM85-78	4b	Welded, banded quartz-feldspar porphyry with mafic veinlets.
LM85-79	4d	Quartz-feldspar porphyry with 10% pink feldspar and 5% blue quartz in a grey matrix; weak alignment.
LM85-82	4b(a)	Fine-grained pink sugary rhyolite with mafic streaks; diss. pyrite.

LM85-84	4b	Quartz-feldspar porphyry with a pink grey matrix; 10% mafics.
LM85-85b	4b(a)	Banded felsic tuff with minor quartz phenocrysts and a strong fabric.
LM85-86	4a	Reddish sparsely porphyritic magnetite and pyrite-bearing ash tuff.
LM85-90	4b	Quartz porphyry with blue stretched quartz eyes in a pink matrix.
LM85-91	4b	Quartz-feldspar porphyry.
LM85-94	4d	Feldspar porphyry with a pink-grey matrix.
LM85-96	4b	Coarse-grained quartz-feldspar porphyry with a pink matrix.
LM85-102	4b	Feldspar-quartz porphyry/welded tuff pink to blue matrix; magnetite.
LM85-106	6	Metadiabase dyke.
LM85-107	6	Metadiabase dyke.
LM85-108	4b	Quartz porphyry with a glassy dark siliceous matrix.
LM85-109	4b	Blue-pink recrystallized, slightly brecciated quartz porphyry with magnetite.
LM85-110	4e	Prophyllitized, sericitized pink-green quartz breccia.
LM85-114a	2	Dark bluish-grey volcanoclastic siltstone.
LM85-114b	2	Maroon volcanoclastic siltstone.
LM85-118	2	Well bedded pink-green volcanoclastic sandstone.
LM85-124	4b	Micaceous quartz-feldspar porphyry.
LM85-125	3	Sheared maroon volcanoclastic siltstone.
LM85-128	4b	Foliated quartz-feldspar porphyry.

LM85-130	4a	Banded slightly porphyritic felsic tuff in a pink and green matrix with mafic banding.
LM85-131	2	Banded volcaniclastic sandstone.
LM85-134	4b	Foliated biotite-hornblende granite.
LM85-136	4b	Quartz-feldspar porphyry with a distinctive foliation and lineation.
LM85-140	2	Blue-grey banded volcaniclastic sandstone.
LM85-148	5a	Foliated granite.
LM85-150	2	Banded blue-grey volcaniclastic siltstone.
LM85-151	5a	Fine to medium grained porphyritic granite, minor pyrite and chlorite alteration.
LM85-157	7	Coarse-grained gabbro.
LM85-161	4b	Pink, welded felsic tuff.
LM85-162	3	Maroon volcaniclastic siltstone.
LM85-164	5a	Pink, fine-grained leucocratic granite with local epidote veinlets.
LM85-165	5a	Tan to grey, medium-grained leucocratic granite.
LM85-166	5a	Pink, medium grained leucocratic granite with local chlorite alteration.
LM85-167	5a	Pink, fine-grained leucocratic granite with local concentration of muscovite and pyrite.
LM85-168	5a	Pink to tan, fine-grained leucocratic granite with local rusty fractures.
LM85-170	2	Pink-yellow-green banded volcaniclastic siltstone.
LM85-171	3	Maroon volcaniclastic siltstone.

LM85-174	5a	Pink, medium-grained leucocratic granite.
LM85-175	5a	Foliated medium-grained granite.
LM85-GEO1	5a	Medium-grained biotite granite.
LM85-GEO2	5a	Foliated medium grained biotite granite.
BH1-153.3	4a	Pyritiferous ash tuff.
BH1-164.8	4a	Pyritiferous ash tuff.
BH1-167.1	4b	Pyritiferous quartz-feldspar porphyry.
BH2-265.8	4b	Medium grained quartz-feldspar porphyry.
BH3-042.0	4b	Coarse grained quartz-feldspar porphyry.
BH5-246.6	4a	Sucrosic banded ash flow tuff.
BH5-364.5	4b	Sucrosic quartz-feldspar porphyry.
BH9-072.0	4a	Banded ash-flow tuff.
BH9-161.9	4a	Pyritiferous sucrosic ash tuff.
BH9-202.6	4b	Pyritiferous quartz porphyry.
BH10-141.8	4d	Coarse grained feldspar porphyry.
BH10-191.0	4a	Banded ash flow tuff.
BH10-290.0	4a	Felsic ash tuff with carbonate and amphibole veins.
BH11-194.8	4a	Fine grained ash flow tuff.
BH11-230.3	4b	Sucrosic quartz porphyritic rhyolite.
BH11-290.5	4b	Sucrosic quartz porphyry with disseminated sphalerite.
BH11-355.2	4a	Biotite-bearing ash tuff.
BH14-342.1	4a	Felsic ash tuff with minor quartz phenocrysts.

LM85-TR1A	4b	Hematized quartz porphyry.
LM85-TR2B	4b	Hematized, pink-grey, quartz-feldspar porphyry.
LM85-TR3A	4b(a)	Hematized, coarse grained quartz-feldspar porphyry.
LM85-TR4A	4a(b)	Hematized banded ash tuff.
LM85-TR4B	4b	Banded porphyritic rhyolite.
LM85-TR5A	4b	Quartz-feldspar porphyry with fine grained ash tuff lenses.
LM85-TR5B	4b	Quartz-feldspar porphyry with felsic ash tuff layers.
LM85-TR6-1A	4d	Feldspar porphyry with 50% feldspar phenocrysts.
LM85-TR6-3A	4b(a)	Hematized and brecciated banded quartz-feldspar porphyry with felsic ash layers.
LM85-TR6-3B	4b	Brecciated quartz-feldspar porphyry.
LM85-TR6-4A	4b	Hematized feldspar-quartz porphyry.
LM85-TR6-4B	4b(a)	Hematized and brecciated quartz-feldspar porphyry with ash tuff lenses.
LM85-TR7A	4b	Hematized quartz-feldspar porphyry with felsic ash lenses.
LM85-TR8	4b	Hematized and brecciated quartz-feldspar porphyry.
LM85-TR8B-A	4a	Fine grained ash tuff with mafic rich bands.
LM85-TR9B	4b	Pyritiferous sucrosic quartz-feldspar porphyry.
LM85-TR10	4d(a)	Feldspar porphyry with pink and grey ash layers.
LM85-TR12A	4b	Hematized quartz-feldspar porphyry.
LM85-TR13A	4b(a)	Hematized and brecciated felsic crystal tuff.

LM85-TR14A	4b(a)	Hematized and brecciated felsic crystal tuff with mafic banding and ash layers.
LM85-TR14B	4b(a)	same as 14A.
LM85-TR17	4a	Hematized banded ash-flow tuff.
LM85-TR18A	4b	Hematized felsic crystal tuff with mafic bands and pods.
LM85-TR23A	4b	Hematized quartz-feldspar porphyry with mafic pods.
LM85-TR25	4c	Lapilli tuff with 30% elongated feldspar phenocrysts.
LM85-TR26	4a	Pink-grey felsic ash tuff.
LM85-TR28	4b	Quartz-feldspar porphyry with mafic pods and veinlets.
LM85-TR29	4d	Feldspar porphyry with 15% feldspar phenocrysts in a pink to grey matrix.
BL86-1A	4b	Quartz porphyry.
BL86-1B	4b	Quartz-porphyry with disseminated galena, pyrite and magnetite.
BL86-1C	4c	Hematized quartz-feldspar porphyry with carbonate veins containing amphiboles.
BL86-2A	4b	Coarse grained quartz-feldspar porphyry with galena, sphalerite and pyrite.
BL86-2B	4b	Quartz-feldspar porphyry with pegmatitic carbonate and amphiboles.
BL86-3	4a	Rusty gossan.
BL86-4	4b	Hematized coarse-grained feldspar + quartz porphyry with disseminated magnetite.
BL86-5	4b	Hematized coarse grained feldspar + quartz porphyry with trace pyrite.



BL86-6	4b	Hematized quartz porphyry with stringers of galena, sphalerite and bornite.
BL86-7	4c	Lapilli tuff with coarse amphiboles.
BL86-8	4a	Hematized, sucrosic felsic crystal tuff.
BL86-9	4b	Hematized quartz-feldspar porphyry.
BL86-10	4a	Banded ash flow tuff.
BL86-11	4b	Brecciated felsic volcanic.
BL86-12	4d	Coarse grained feldspar porphyry.
BL86-13	5a	Fine-grained leucocratic granite.
BL86-14	5a	Fine-grained leucocratic granite with minor disseminated molybdenite.
BL86-15	5a	Fine-grained leucocratic granite with minor disseminated molybdenite.
BL86-16	4b(a)	Hematized quartz-feldspar porphyry.
BL86-17A	4f	Hematized and brecciated andesite.
BL86-17B	4f	Composite sample of quartz vein and tremolite banded andesite.
BL86-18A	4f	Hematized andesite.
BL86-18B	4b	Quartz-feldspar porphyry.
BL86-18C	4f	Tremolite banded andesite.
BL86-18D	4f	Sheared and chloritized andesite.
BL86-19A	4f	Hematized and sheared andesite cut by thin quartz-carbonate veins.
BL86-19B	4f	Sheared andesite.
BL86-19C	4f	Quartz-carbonate veins with large pods of specular hematite.
BL86-20A	4f	Composite sample of hematized andesite and rhyolite.

BL86-20B	4f	Brecciated andesite and rhyolite with thin quartz-carbonate veins.
BL86-21A	4f	Fine-grained hematized andesite.
BL86-21B	4f	Andesite with tremolite bands cut by quartz-carbonate veins with specular hematite.
BL86-22	2	Blue-gray volcanoclastic siltstone and sandstone.
BL86-23	4b	Fine grained quartz-feldspar porphyry.
BL86-24	4d	Coarse grained feldspar porphyry.
BL86-25	4e	Felsic volcanic breccia.
BL86-26	4b	Medium-grained quartz-feldspar porphyry.
BL86-27	4d	Coarse-grained feldspar porphyry with mafic pods.
BL86-28	4b	Pyritiferous quartz porphyry.
BL86-29	4b	Medium grained quartz-feldspar porphyry.
BL86-30A	4d	Coarse grained feldspar $\pm$ quartz porphyry.
BL86-30B	4b	Medium grained quartz porphyry.
BL86-32A	5a	Medium grained leucocratic granite.
BL86-32B	4d(5a)	Feldspar porphyry near contact with leucocratic granite.
BL86-33A	5a	Medium-grained leucocratic granite.
BL86-33B	4d	Feldspar porphyry near contact with leucocratic granite.
BL86-34A	4b(a)	Quartz-feldspar porphyry with ash tuff lenses.
BL86-35	4b	Medium to coarse grained granite.
BL86-36	4b	Pink to white, coarse grained granite.

BL86-37	4b	Coarse-grained gabbro.
BL86-38	4b	Coarse-grained gabbro.
BL86-40	4b	Coarse-grained biotite-hornblende granite.
BL86-41	4c	Coarse-grained biotite granite.
BL86-42	4c	Coarse grained biotite-hornblende granite.
BL86-43	4c	Medium grained granite.
BL86-45	4b	Fine grained quartz-feldspar porphyry.
BL86-46	4b	Quartz-feldspar porphyry.
EMS85-TR1A	6	Radioactive aerigine veinlets hosted in a biotite-feldspar dyke.
EMS85-TR1B	1	Sucrosic banded rhyolite.
EMS85-TR1A(B)	6	Biotite-feldspar dyke.
LM85-E1	1	Grey felsic volcanic sediment with disseminated pyrite and magnetite.
LM85-E3	1	Sucrosic brownish arkosic sandstone with mafic veinlets.
LM85-E5	1	Sucrosic brownish arkosic sandstone with mafic pods.
LM85-E6A	1	Pink to grey sucrosic arkosic sediment.
LM85-E6B	1	Banded volcanic sediment.
LM85-EMTR1A	1	Reddish medium grained tuffaceous sediment.
LM85-EMTR1B	1	Sucrosic banded arkosic sediment.
LM85-EMTR2A	1	Hematized sucrosic tuffaceous sediment.
LM85-EMTR3B	1	Banded rhyolite.

LM85-EMTR4	1	Hematized banded rhyolite.
EM86-1	1	Banded rhyolite.
EM86-CS	1	Sucrosic banded rhyolite with magnetite rich laminations.
EM86-TR1	1	Hematized banded arkosic sandstone.
EM86-TR3	1	Pink to brownish grey sucrosic banded arkosic sandstone.
EM86-WB	1	Sucrosic banded rhyolite, magnetite laminations define bedding.
EM86-WS	1	same as EM86-WB.
EMS86-TR1A	1	Felsic volcanic lapilli tuff or volcanic conglomerate.
EMS86-TR1B	6	Biotite-feldspar mafic dyke.
EMS86-TR1C	6	Same as 1B.
EMS86-TR1D	6	Same as 1B.
EMS86-TR1E	6(1)	Contact between a biotite-feldspar dyke and felsic volcanic host.
EMS86-TR3A	6	Aegirine veinlets.
EMS86-TR3B	1	Sucrosic felsic tuff with disseminated molybdenite and fluorite.
EMS86-TR4A	6(1)	Composite sample of biotite-feldspar dyke and felsic volcanic host.
EMS86-TR4B	6	Biotite-feldspar dyke contact with trace fluorite.
EMS86-TR5A	6	Biotite-feldspar dyke with trace fluorite.
EMS86-TR5B	6	Radioactive biotite-feldspar dyke with galena.
EMS86-TR6	6(1)	Contact between sulphide-bearing mafic dyke and felsic volcanic host rock.

EMS86-TR7

6

Brecciated sulphide rich zone in a  
mafic dyke.

## APPENDIX III

## DIAMOND DRILL RECORD

Property: Burnt Lake, Labrador  
 Map Area: 13J/12  
 Logged By: L. MacKenzie  
 Total Depth: 84.58 m

DDH No: 77.1  
 Location: L48W  
 Dip: 45°  
 Azimuth: 330°N

Footage		Description
From	To	
0	0.7	Overburden.
0.7	2.4	Amphibolite dyke: foliated.
2.4	5.0	Felsic crystal tuff: 10-15% euhedral feldspar phenocrysts 2-5 mm; 10% elliptical blue quartz eyes 1-3mm; minor pyrite.
5.0	6.0	Feldspar porphyry: 20% euhedral feldspar phenocrysts, 5-10 mm in size with minor 1-3 mm blue quartz eyes.
6.0	9.8	Felsic crystal tuff: 10-20% elliptical blue quartz eyes; <5% euhedral feldspar phenocrysts; trace disseminated pyrite throughout; common thin greenish amphibolite dyklets.
9.8	12.1	Quartz porphyry: 15-20% elliptical 1-5 mm quartz phenocrysts in a reddish to grey matrix; common mafic veinlets.
12.1	21.5	Felsic crystal tuff: 10-15% euhedral feldspar phenocrysts; 10% blue quartz phenocrysts 1-5 mm size; trace disseminated pyrite throughout; at 15.5-16.1m phenocrysts are highly stretched.
21.5	22.2	Feldspar porphyry: 20-25% euhedral feldspar phenocrysts; minor blue quartz eyes in a reddish brown matrix.
22.2	25.4	Felsic crystal tuff: 5-10% euhedral feldspar phenocrysts and 10% blue quartz eyes, 1-4 mm in a pink-grey matrix; trace disseminated pyrite; common mafic veinlets.
25.4	27.1	Amphibolite dyke - crenulated.

Footage		Description
From	To	
27.1	28.5	Feldspar porphyry: 15-20% euhedral feldspar phenocrysts; 3-5% blue quartz eyes.
28.5	30.1	Felsic crystal tuff: 10% euhedral feldspar phenocrysts; minor blue quartz eyes in a pink to grey matrix; minor pyrite.
30.1	31.9	Mafic tuff: banded with dark mafic clots or fragments.
31.9	34.1	Feldspar porphyry: 20-25% euhedral feldspar phenocrysts; <5% blue quartz; very altered; strong deformation (mylonite?); brecciated with an ash matrix.
34.1	34.4	Metadiorite dyke.
34.4	40.9	Felsic crystal tuff: altered with common mafic clots and veinlets.
40.9	48.7	Felsic crystal tuff: 10-15% blue quartz; minor euhedral feldspar phenocrysts; disseminated pyrite throughout.
48.7	50.3	Fine grained reddish brown ash tuff with common mafic specks and veinlets.
50.3	50.8	Fragmental felsic crystal tuff - banded and crenulated.
50.8	51.5	Feldspar porphyry.
51.5	57.9	Felsic crystal tuff: 5-10% euhedral to subrounded feldspar phenocrysts 2-5 mm; 5-10% blue quartz 1-4 mm in size. Common mafic fragments and greenish alteration (chlorite) in matrix; locally phenocrysts are replaced by black rim (magnetite).
57.9	84.6	Feldspar porphyry: 20-25% euhedral feldspar 2-6 mm size; up to 10% blue quartz eyes 1-3 mm in a reddish to grey matrix.

## DIAMOND DRILL RECORD

Property: Burnt Lake, Labrador  
 Map Area: 13J/12  
 Logged By: L. MacKenzie  
 Total Depth: 124.4 m

DDH No: 77.10  
 Location:  
 Dip: 45°  
 Azimuth: 318°N

Footage		Description
From	To	
0	2.2	Overburden.
2.2	13.7	Felsic crystal tuff: 5-10% feldspar phenocrysts, <5% elongated quartz in a pink to green-grey matrix; abundant hematized veinlets and thin chlorite veinlets; rimming of feldspar phenocrysts with hematite or chlorite.
13.7	17.1	Feldspar porphyry: 10-15% feldspar 0.5 to 1.2 cm in a purple matrix.
17.1	17.5	Green amphibolite dyke; crenulated.
17.5	30.5	Feldspar porphyry: 10-15% euhedral feldspar phenocrysts in a reddish brown to green matrix; feldspars are variably altered by chlorite; rare blue elliptical quartz eyes.
30.5	40.2	Felsic crystal tuff: 5% feldspar 2-5 mm; 5% quartz 1 mm (up to 1 cm); minor chlorite veinlets; minor thin amphibolite dykelets.
40.2	55.3	Lapilli tuff (brecciated zone) - fragments of felsic crystal tuff in a reddish matrix; green pods; minor black fragments.
55.3	61.7	Felsic ash tuff: sugary white to grey matrix with hematite specks; locally banded (1-2 mm bands); white grey to green and thin mafic veinlets.
		Radioactive Zone up to 400 cps from 48.9-56.9m
61.7	62.5	Green to black amphibolite dyke.



Footage		Description
From	To	
62.5	76.2	Felsic crystal tuff: 5% euhedral feldspar phenocrysts; wavy bands 1-2 mm wide wrap around phenocrysts; narrow amphibolite dykelets.
76.2	79.2	Feldspar porphyry: 5-10% feldspar 3-10 mm in a purple matrix.
79.2	89.9	Felsic crystal tuff: sugary; green to pink matrix; minor small phenocrysts with wavy bands; minor thin amphibolite dykelets.
89.9	93.7	Brecciated amphibolite dyke intercalated with felsic ash tuff.
93.7	108.9	Felsic crystal tuff: 1-10% phenocrysts banded; variable welded textures, local felsic ash lenses; orange rusty stain on fractures; minor thin amphibolite dykelets.
108.9	110.2	Black amphibolite dyke.
110.2	124.4	Mixed Zone - brecciated dyke + calcite; local pegmatite veins intermixed with felsic ash.

EOH

## DIAMOND DRILL RECORD

Property: Burnt Lake, Labrador  
 Map Area: 13J/12  
 Logged By: L. MacKenzie  
 Total Depth: 121.65 m

DDH No: 77.11  
 Location:  
 Dip: 45°  
 Azimuth: 0°

Footage		Description
From	To	
0	1.8	Overburden.
1.8	4.8	Lapilli tuff: greenish-grey to pink in color with 30% elongated white feldspar phenocrysts, 1-10mm in size, minor quartz phenocrysts and mafic pods.
4.8	6.1	Felsic ash tuff: greenish-grey in color with a pinkish tinge, fine to medium grained with alternating pink and grey bands of felsic ash tuff 2-5 cm wide with 2-3%, 1-2mm size quartz phenocrysts; locally brecciated.
7.7	8.0	Black foliated amphibolite dyke.
8.0	15.5	Felsic ash tuff: greenish-grey to pink in color, fine grained with 2-3%, 1-2mm quartz phenocrysts, faint banding is locally evident.
15.5	23.7	Lapilli tuff: greenish-grey to pink with 20% white feldspar fragments in a greenish matrix.
23.7	48.2	Felsic ash tuff: greenish-grey to pink in color, fine to medium grained, with 2-3% blue quartz and chlorite eyes 1-2mm in size. Occ brecciated and fragmental areas.
48.2	58.7	Feldspar porphyry: grey to pink in color with 10-15% euhedral feldspar phenocrysts 1-10 mm in size, minor blue quartz eyes, 1-2 mm.
58.7	110.1	Felsic ash tuff: greenish-grey to pink, fine to medium grained, generally massive, however fragments are present locally, and faint banding is sometimes present, minor < 2% blue quartz eyes, 1-2mm in size, local enrichment of mafic pods and veinlets, trace disseminated pyrite.

Footage		Description
From	To	
		Radioactive Zone up to 1000 cps from 106.3 - 113.3m
110.1	118.9	Feldspar porphyry: reddish to grey in color, generally massive with 10% euhedral feldspar phenocrysts , 2-10mm in size, local brecciation.
118.9	121.6	Felsic ash tuff: grey in color with 2-3% blue quartz eyes.

EOH

## DIAMOND DRILL RECORD

Property: Burnt Lake, Labrador  
 Map Area: 13J/12  
 Logged By: L. MacKenzie  
 Total Depth: 121.9

DDH No: 77-12  
 Location: L33W  
 Dip: 45°  
 Azimuth: 318°N

Footage		Description
From	To	
0	0.8	Overburden.
0.8	3.3	Feldspar porphyry: 5-10% feldspar phenocrysts; 3% quartz in a red and grey matrix.
3.3	4.3	Felsic crystal tuff: minor quartz ± feldspar phenocrysts; pink matrix; abundant mafic veinlets.
4.3	5.3	Black to green amphibolite dyke.
5.3	11.4	Lapilli tuff: 20-30% elongated 1-2 cm feldspar phenocrysts; minor quartz in a pink-grey matrix; chlorite alteration of phenocrysts.
11.4	17.2	Felsic crystal tuff: minor phenocrysts in a tuffaceous matrix.
17.2	18.2	Green amphibolite dyke.
18.2	30.5	Lapilli tuff: 20% 0.5 to 1 cm sized elongated chloritic fragments; 2-3% quartz in a reddish matrix; intercalated with thin grey-brown ash layers.
30.5	42.3	Felsic crystal tuff: minor greenish chloritic fragments; <1% quartz in a greenish matrix.  Radioactive Zone up to 1000 cps from 30.5-39.5m
42.3	56.4	Felsic crystal tuff: 5% minor greenish chlorite fragments; 1% quartz phenocrysts 1-4 mm in a grey-pink matrix; local brecciated areas.
56.4	59.2	Feldspar porphyry: 5-10% whitish feldspar phenocrysts; 2-3% quartz in a dark purplish grey matrix.

Footage		Description
From	To	
59.2	61.4	Amphibolite dyke.
61.4	71.0	Feldspar porphyry: 5-10% 0.5 to 1 cm size feldspar phenocrysts in a dark purplish-grey matrix; abundant hematite and chlorite veinlets.
71.0	73.8	Felsic ash tuff: Grey-green-pink colour; fine-grained abundant mafic specs.
73.8	74.8	Amphibolite dyke.
74.8	78.0	Felsic ash tuff: grey-green to pink, fine grained.
78.0	79.3	Feldspar porphyry: dark purplish colour; locally welded.
79.3	80.5	Amphibolite dyke.
80.5	92.6	Lapilli tuff: green to pink to purple; minor large chloritic fragments; minor quartz phenocrysts.
92.6	93.0	Dark green amphibolite dyke.
93.0	97.6	Lapilli tuff: 2-10%, 2-10 mm euhedral feldspar phenocrysts in a pink to green to grey matrix; rare large 3 cm chloritic fragments.
97.6	97.9	Greenish Amphibolite dyke.
97.9	103.7	Lapilli tuff.
103.7	104.0	Greenish amphibolite dyke.
104.0	109.8	Lapilli tuff: phenocrysts are becoming much more altered by chlorite; eutaxitic texture of phenocrysts.
109.8	111.9	Felsic crystal tuff: dark grey matrix; only minor feldspar phenocrysts.

Footage		Description
From	To	
111.9	113.1	Ash flow tuff: dark blue-grey matrix with thin chloritic veinlets.
113.1	118.2	Grades into a Felsic crystal tuff; pink to grey matrix.
118.2	120.7	Light green amphibolite dyke.
120.7	121.9	Felsic crystal tuff.

EOH

## DIAMOND DRILL RECORD

Property: Burnt Lake, Labrador  
 Map Area: 13J/12  
 Logged By: L. MacKenzie  
 Total Depth: 119.80 m

DDH No: 77.13  
 Location:  
 Dip: 45°  
 Azimuth: 000°N

Footage		Description
From	To	
0	6.1	Overburden
6.1	7.2	Felsic crystal tuff: dark grey in color with 5% feldspar phenocrysts and 1% blue quartz eyes in a fine grained tuffaceous matrix.
7.2	10.4	Feldspar porphyry: greenish-grey with a pinkish tinge, 5-10% dark colored feldspar phenocrysts rimmed in black (magnetite?) 2-12 mm in size.
10.4	12.0	Feldspar porphyry: pink to purple in color with 10% euhedral feldspar phenocrysts, 1-10mm in size.
12.6	12.8	Green amphibolite dyke.
12.0	18.6	Felsic crystal tuff: reddish-orange to dark red-grey in color with < 5% feldspar and quartz phenocrysts 1-5mm in size.
18.6	19.6	Breccia: black fragments in a fine grained grey matrix.
19.6	23.8	Felsic ash tuff: greenish-grey to pink felsic ash tuff with mafic pods and veinlets occurring locally.
23.8	55.4	Lapilli tuff: pink and greenish-grey matrix with 10-20% chloritic pods and veinlets, very altered, elongated chloritic fragments up to 4 cm in size and are greenish-black in color in a quartz crystal ash matrix.
55.4	55.6	Amphibolite dyke.
55.6	66.5	Felsic ash tuff: brownish-red in color with rare phenocrysts, common cross-cutting mafic veinlets.

Footage		Description
From	To	
		(65.2-65.9; 10% pyrite associated with mafic clots)
66.5	67.4	Amphibolite dyke.
67.4	109.8	Lapilli tuff: greenish-grey to pink with 40% chloritic fragments, locally brecciated and hematized, minor quartz phenocrysts and rusty stains.
		(Radioactive Zone with up to 1000 cps from 62.1 to 73.6m )
109.8	119.8	Felsic crystal tuff: greenish-grey to red felsic crystal tuff.

EOH



## DIAMOND DRILL RECORD

Property: Burnt Lake, Labrador  
 Map Area: 13J/12  
 Logged By: L. MacKenzie  
 Total Depth: 106.6 m

DDH No: 77.14  
 Location:  
 Dip: 45°  
 Azimuth: 318°N

Footage		Description
From	To	
0	1.2	Overburden.
1.2	5.1	Feldspar porphyry: 5-10% 3 to 7 mm feldspar phenocrysts; ~1% quartz in a reddish grey to purple matrix.
5.1	7.8	Amphibolite dyke.
7.8	34.1	Feldspar porphyry: minor mafic specks and pods in a reddish-grey to purple matrix; locally feldspars have been altered to chlorite (rimming phenocrysts).
34.1	35.9	Amphibolite dyke.
35.9	47.3	Felsic crystal tuff: reddish-grey matrix; 2-3% feldspar; <1% quartz; orange coloured staining of feldspar and matrix.
47.3	55.9	Feldspar porphyry: 10-15% euhedral feldspar phenocrysts up to 1 cm; rare stretched quartz phenocrysts up to 0.5 cm; locally contains mafic specks in a dark grey to purple matrix.
55.9	75.0	Felsic crystal tuff: minor feldspar + quartz phenocrysts in a pink-greenish matrix; local thin felsic ash lenses; chlorite alteration is increasing with depth as rimming of phenocrysts and as thin veinlets.
75.0	76.4	Greenish amphibolite dyke.
76.4	92.4	Felsic ash tuff: banded (1 mm to 1 cm bands); minor feldspar phenocrysts in hematized areas within a grey-green-reddish matrix. (Radioactive Zone up to 400 cps from 66.5-88.4m)

Footage		Description
From	To	
92.4	93.2	Greenish amphibolite dyke.
93.2	99.8	Felsic ash tuff: sugary quartz-rich with a green to pink tint; minor magnetite pods.
99.8	100.5	Green amphibolite dyke.
100.5	103.9	Felsic crystal tuff: 2-3% dark green altered feldspar; 1% blue quartz eyes in a red to grey matrix with abundant mafic veinlets.
103.9	105.5	Banded felsic ash tuff: banding wraps around rare feldspar phenocrysts.
105.5	106.6	Feldspar porphyry: 5-10% euhedral feldspar phenocrysts; 2-3% blue quartz in a red-grey to purple matrix.

EOH

**APPENDIX IV****Scanning Electron Microscope Ore Mineral Identification**

Polished, carbon-coated thin sections were examined with a Hitachi S570 scanning electron microscope at an accelerating voltage of 15 Kv. Backscattered electron imaging was obtained with a GW Electronic type 113 solid state Backscattered Electron Detector. X-ray analysis was performed on beam spot mode with a Tracer Northern 5500 Energy Dispersive X-ray Analyzer equipped with a spectral resolution of 145 eV. Detector/sample positioning was set at 30° take-off angle.

Backscattered electron images were recorded on Polaroid type 665 positive/negative film.

## APPENDIX V

## Rb/Sr Geochronological Techniques

The analyses were carried out at the Department of Earth Sciences of Memorial University using the same methods outlined by Taylor and Fryer (1983). Rb and Sr analyses were completed using whole rock pressed powder pellets and X-Ray Fluorescence techniques outlined in Appendix I. Rb and Sr concentrations of mineral separates were analysed by ICP-MS techniques outlined in Appendix I.

Sr was separated by standard ion exchange methods and Sr isotopic compositions were measured on a Micromass 30B solid-source mass spectrometer, with computer-controlled magnetic peak switching. The ion beam was collected in a Faraday cup collector. Data was processed using a Hewlett-Packard 2114A computer and a Hewlett-Packard 9845B mini-computer.

The estimated error for Rb and Sr concentrations is  $\pm 1\%$  and for the Rb/Sr ratio is  $\pm 0.5$  ppm. Data was reduced using Ludwig's (1989) ISOPLOT isotope plotting program which uses the regression method of York (1969) and the decay constant ( $1.42 \times 10^{-11} \text{ yr}^{-1}$ ) from Steiger and Jager (1977).

**APPENDIX VI****Pb Isotopes**

Pb isotope data for five mineral separates from the Burnt Lake area within the CMB are listed in Table 5-8. The analyses were completed by Geospec Consultants Ltd. of Edmonton, Alberta. The analyses were done on a Micromass MM-30 mass spectrometer using the methodology as outlined by Swinden et al. (1988). The galena grains were handpicked from vein samples. The grains were large enough to be seen by the naked eye. Also listed in Table 5-8 are Stacey and Kramers (1975) model Pb ages and u as determined by Ludwig's (1989) ISOPLOT radiogenic isotope plotting program. Model ages and model u are also calculated using the Version II Plumbotectonics model curves of Zartman and Doe (1981).

## References Cited in Appendices

- Fryer, B.J., 1977. Rare earth evidence in iron formation for changing oxidation states. *Geochim. Cosmochim. Acta*, v. 41, pp. 361-367.
- Flanagan, F.J., 1970. Sources of geochemical standards - II. *Geochim. Cosmochim. Acta*, v. 34, pp. 121-125.
- Langmhyr, F.J., and Paus, P.E., 1968. The analysis of inorganic siliceous materials by atomic absorption spectrophotometry and the hydrofluoric acid decomposition technique. Pt. I. The analysis of silicate rocks. *Anal. Chimica Acta*, v. 43, pp. 397-408.
- Longerich, H.P., and Veinott, G., 1986. Study of precision and accuracy of XRF data obtained in the Department of Earth Sciences and Centre for Earth Resources Research at Memorial University of Newfoundland. Unpub. Rept., Dept. of Earth Sciences, Memorial University of Newfoundland, 20p.
- Ludwig, K.R., 1989. ISOPLOT for MS-DOS - A plotting and regression program for radiogenic-isotope data, for IBM-PC compatible computers, Version 1.10. USGS Open-File Rept. 88-557 (revised 1989.06.26), 43p..
- Shapiro, L., and Brannock, W.W., 1962. Rapid analysis of silicate, carbonate and phosphate rocks. *U.S. Geol. Sur. Bull.*, 1144A, pp. 31-33.
- Stacey, J.S., and Kramers, J.D., 1975. Approximation of terrestrial lead isotope evolution by a two stage model. *Earth and Plan. Sci. Lett.*, v. 26, pp. 207-221.
- Swinden, H.S., Lane, T.E., and Thorpe, R.I., 1988. Lead-isotope compositions of galena in carbonate-hosted deposits of western Newfoundland: evidence for diverse lead sources. *Can. Jour. Earth Sci.*, v. 25, pp. 593-602.
- Zartman, R.E., and Doe, B.R., 1981. Plumbotectonics - The model. *Tectonophysics*, v. 75, pp. 135-162.

TR5

2

2

TR1

3

2

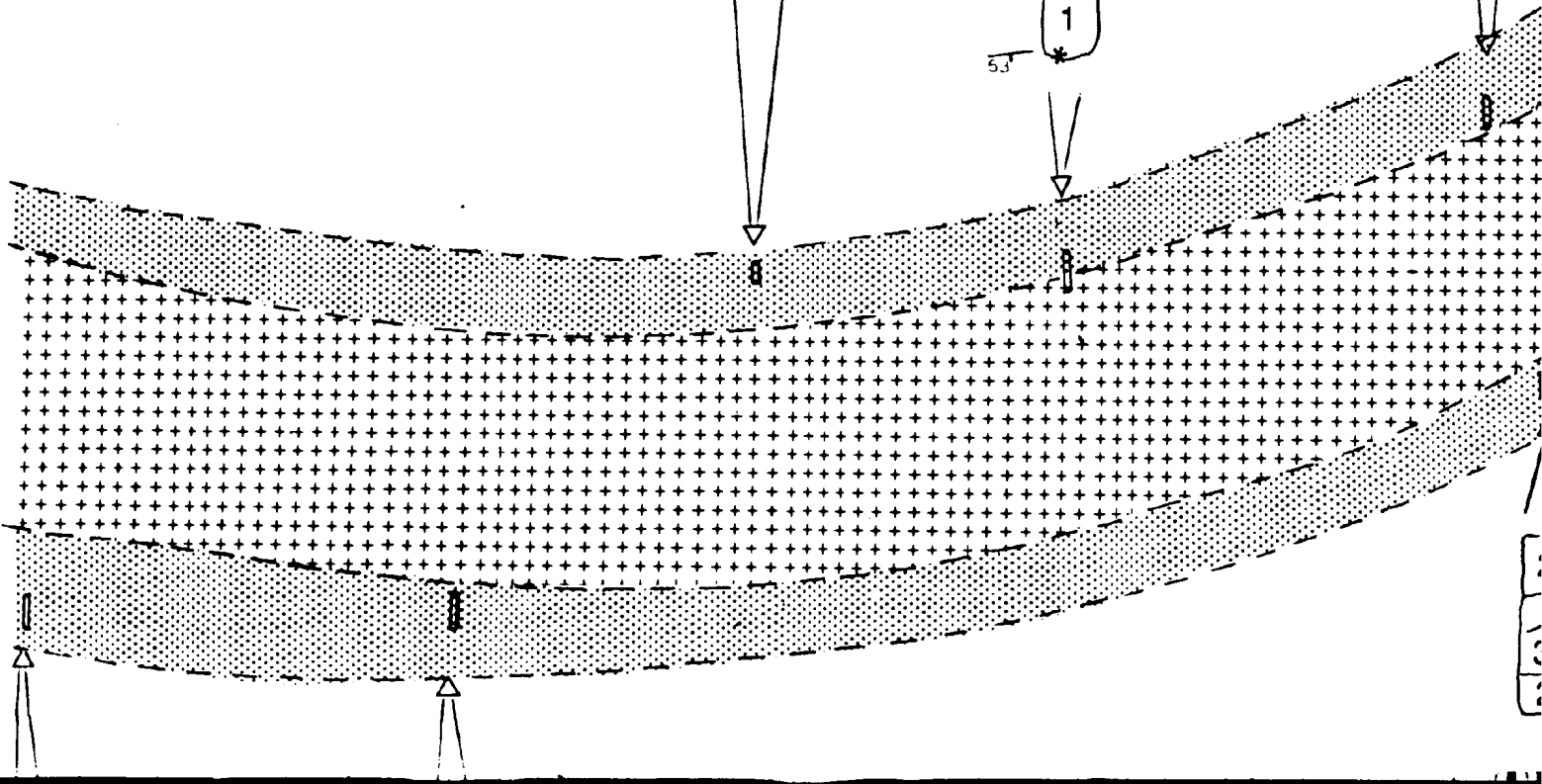
1

TR2

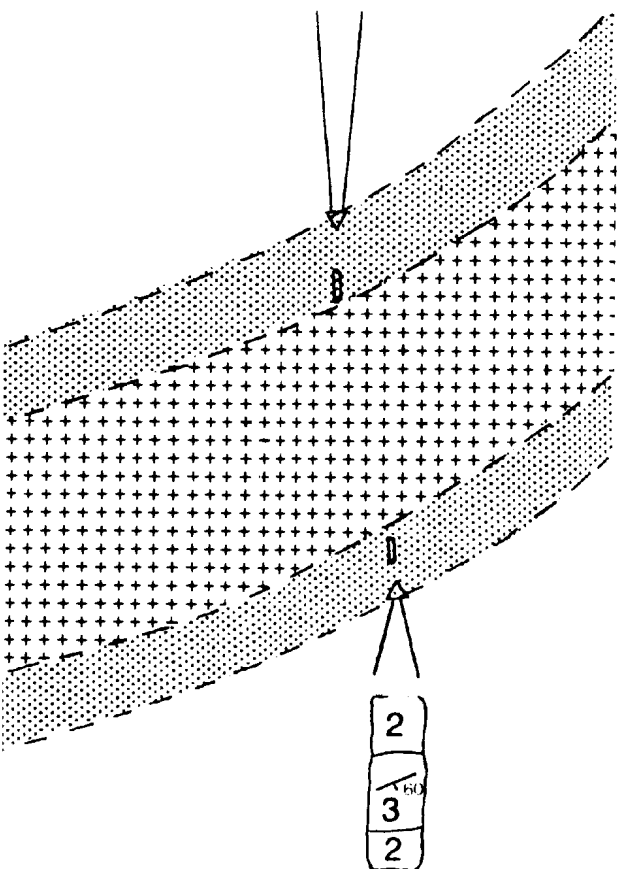
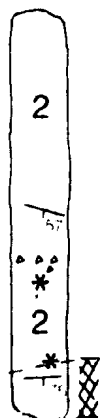
3

2

1



TR5



## TRENCH LEGEND

- 1 Mixed Rhyolite and A
- 2 Andesite
- 3 Feldspar  $\pm$  Quartz P

### Symbols

Geological Boundary

Banding

Foliation

Lineation

Hematized Radioact

Breccia Zone

Shear Zone

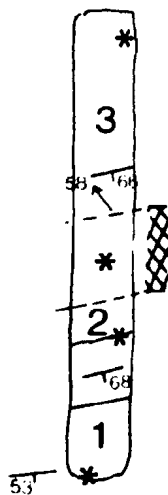
Sample Location



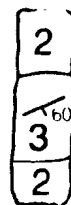
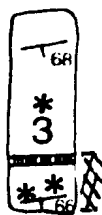
TR5



TR1



TR2



# TRENCH LEGEND

- 1 Mixed Rhyolite and Andesite
- 2 Andesite
- 3 Feldspar ± Quartz Porphyry

## Symbols

Geological Boundary

Banding

Foliation

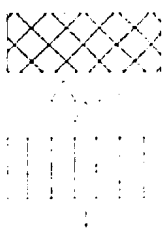
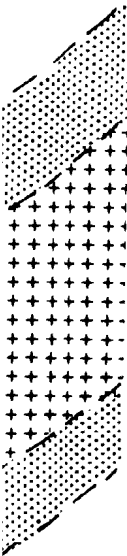
Lineation

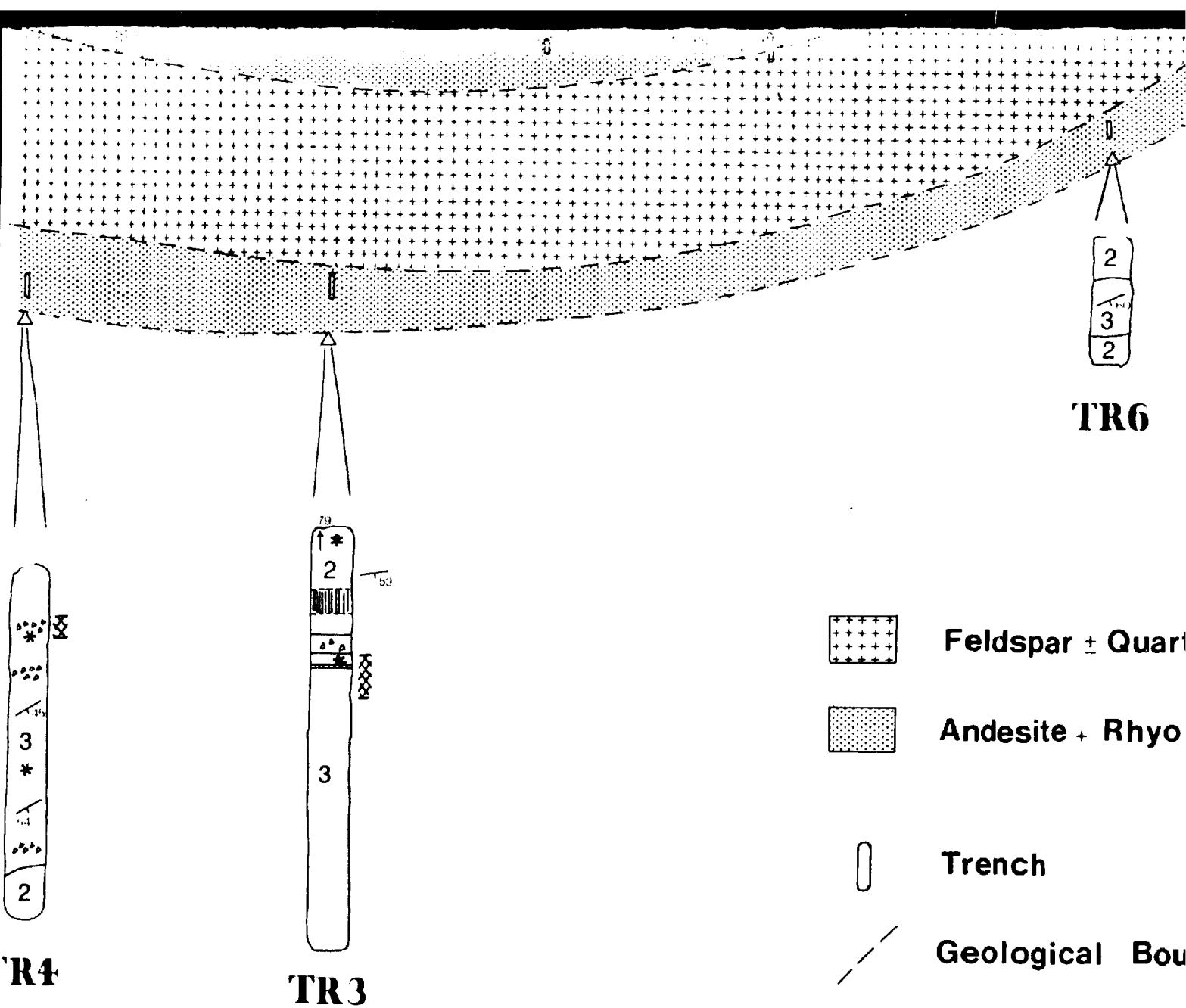
Hematized Radioactive Zone

Breccia Zone

Shear Zone

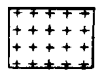
Sample Location





Sheet Zone  
Sample Location

TR6



**Feldspar ± Quartz Porphyry**



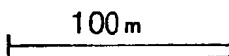
**Andesite + Rhyolite**



**Trench**



**Geological Boundary**



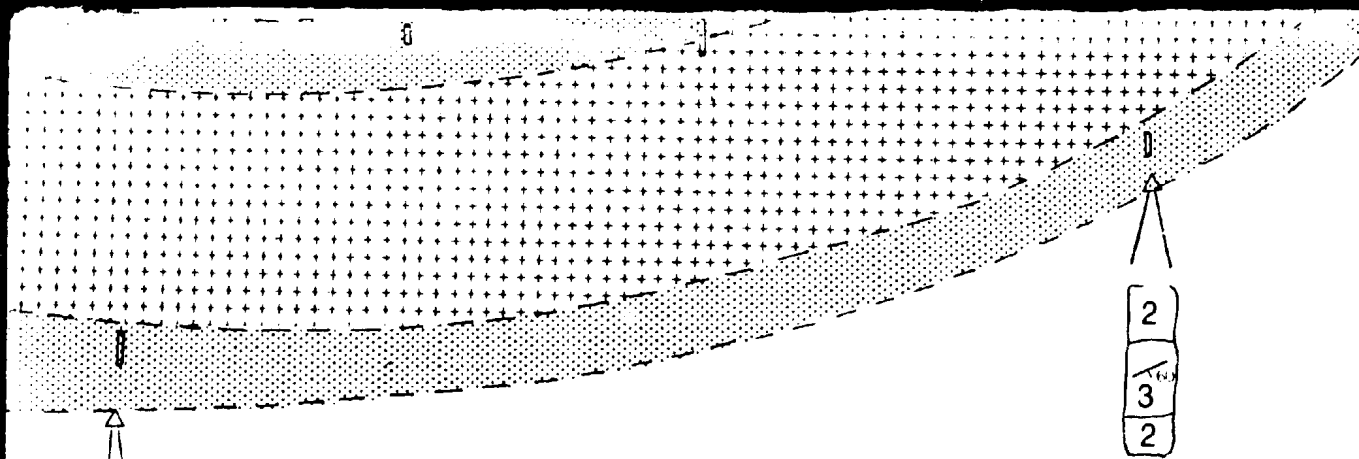
Geology of the  
Aurora River  
Radioactive Showings

Drawn by: LMK

Date:

Scale:

Map:



**TR6**



**Feldspar ± Quartz Porphyry**



**Andesite + Rhyolite**



**Trench**



**Geological Boundary**

**TR3**

100m

Shear Zone

Sample Location

Quartz Porphyry

Yolite

Boundary

Geology of the  
Aurora River  
Radioactive Showings

Drawn by: LMK

Date: April, 1990

Scale:

Map: 3



● LM-50

● BL-26

● TR-23A

● M-82

● LM-78

● LM-79

● LM-74

● LM-68

LM-71●

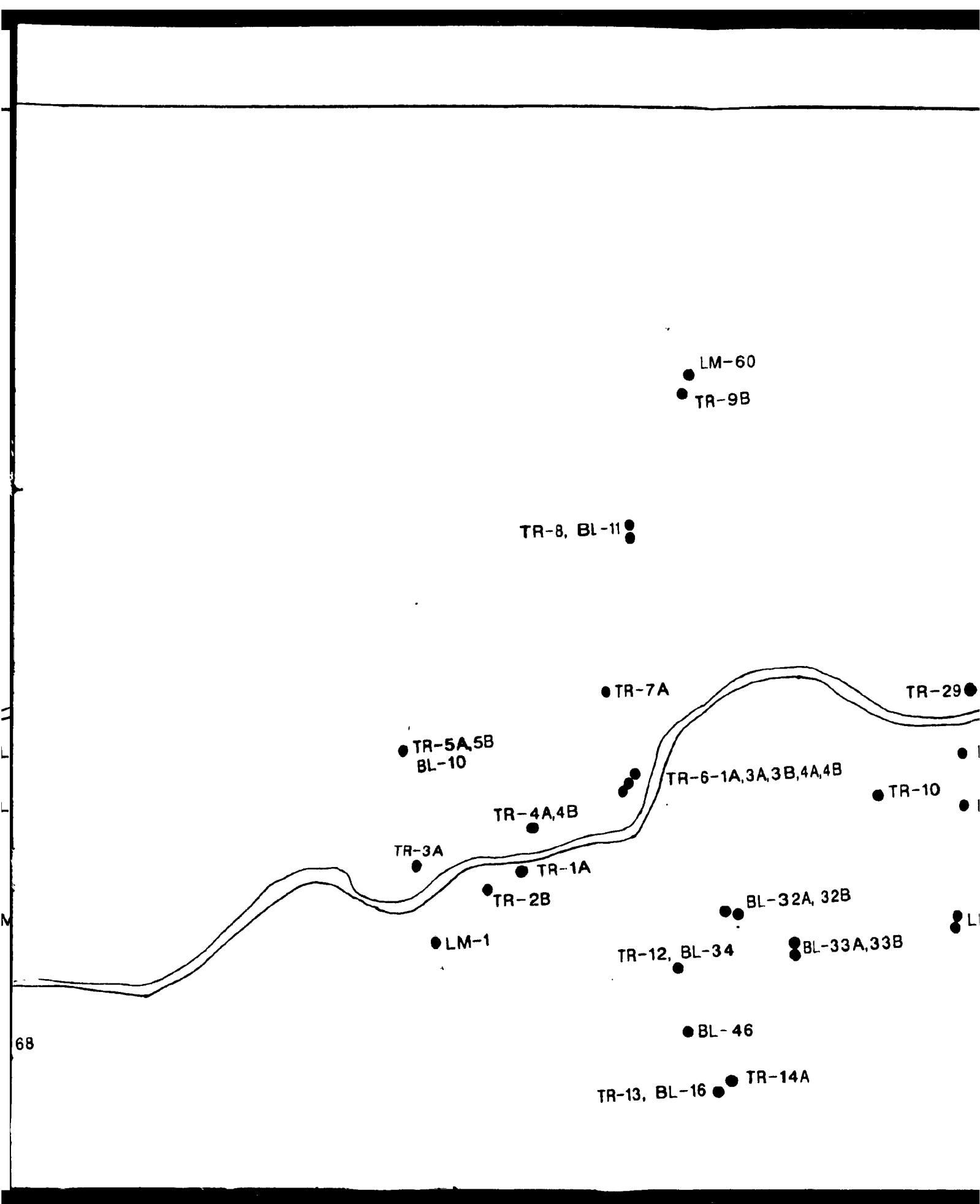
● LM-82

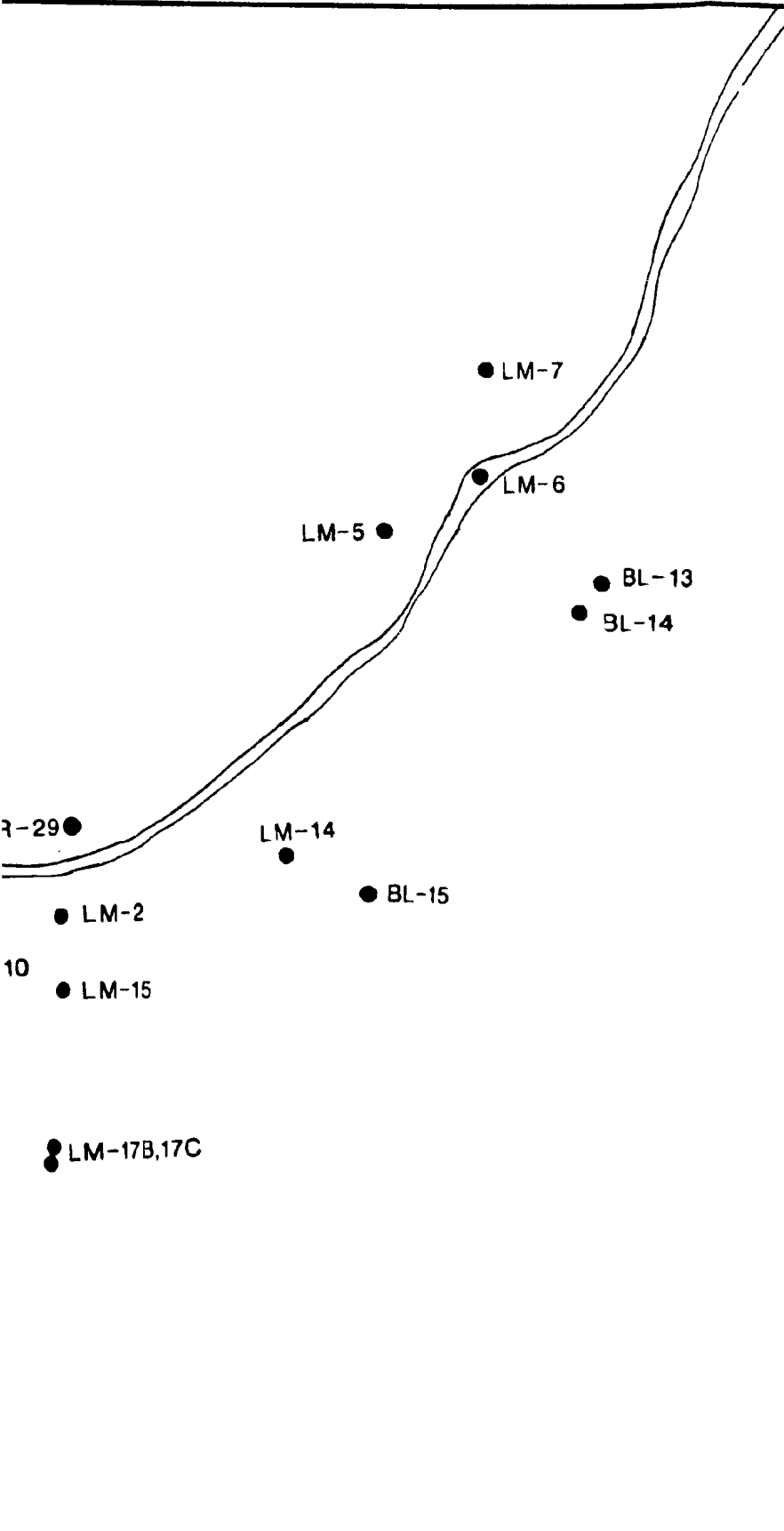
● TR 28

● 30A 300

A-50







R-29

LM-7

LM-6

LM-5

BL-13

BL-14

LM-14

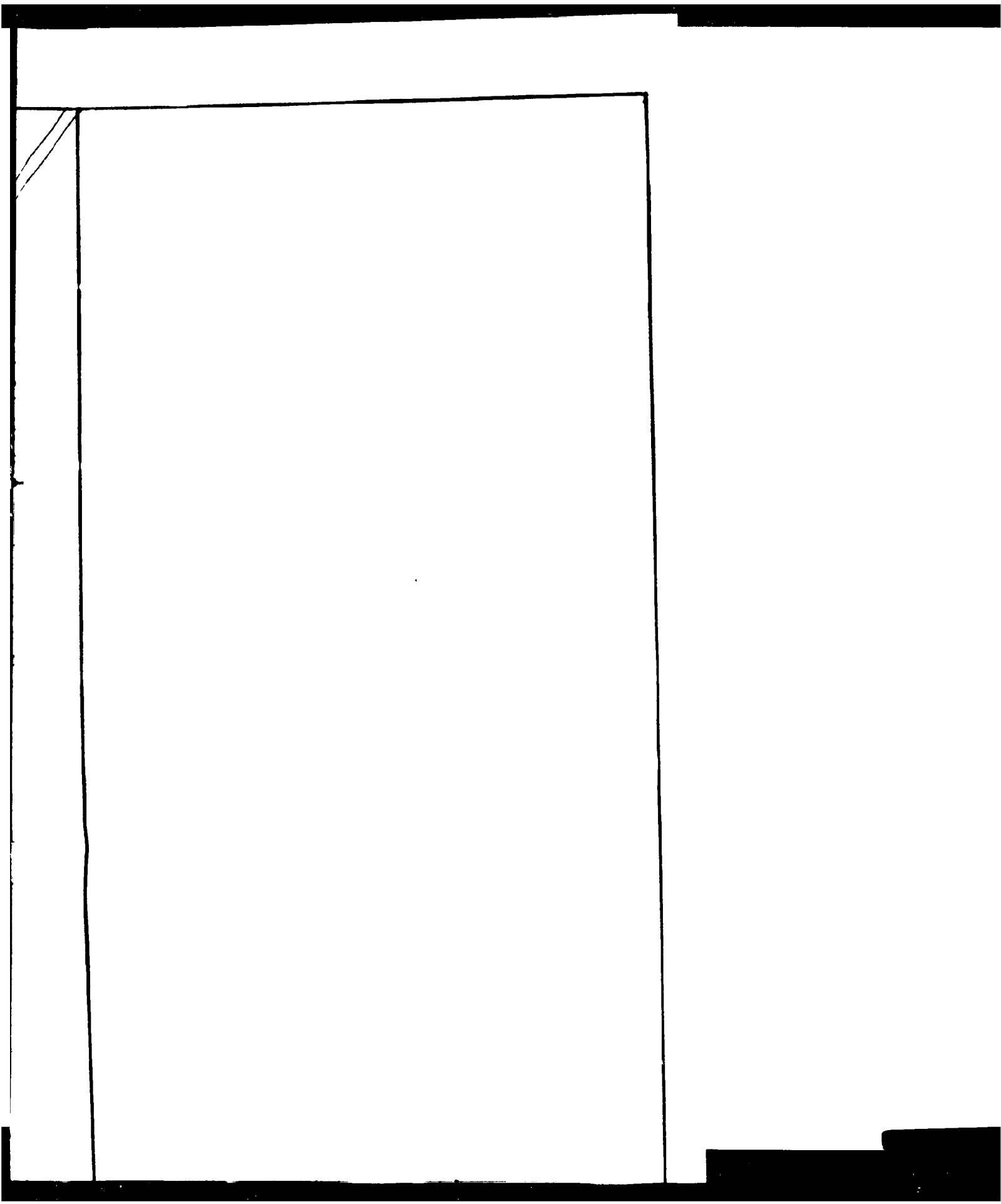
BL-15

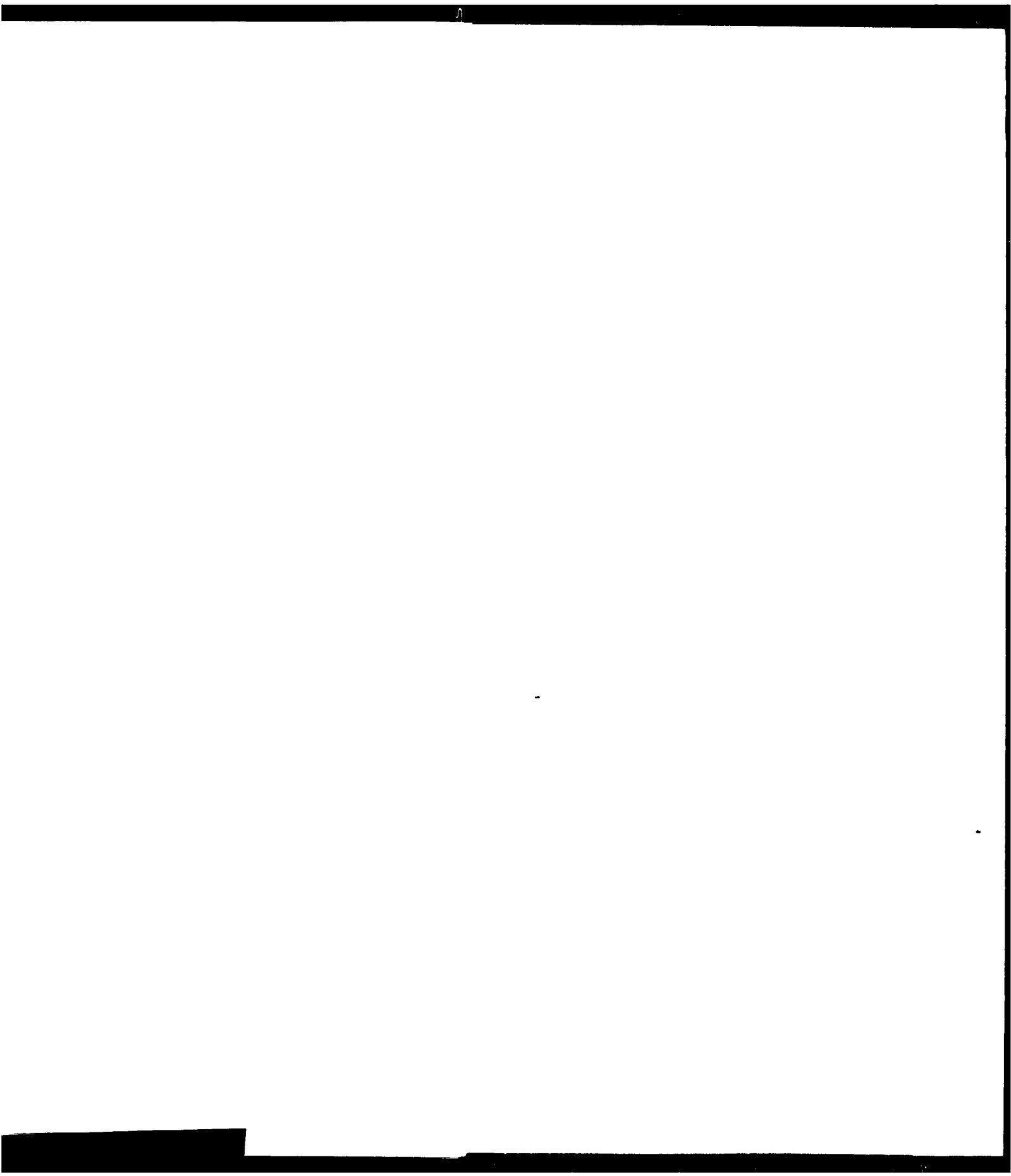
LM-2

10

LM-15

LM-17B,17C





● BL-26  
BL-5 ● TR-23A ● BL-6

● BL-45

● LM-84

● BL-4      BL-27 ●      BL-28 ●  
● TR-25, I

BL-3





● LM-68

LM-71 ●

● LM-82

● TR-28

● BL-30A,30B

BL-9 ●

● BL-29

BL-28

● TR-26, BL-8

● TR-25, BL-7

● LM-1

TR-12, BL-34 ●

● BL 33A, 33

● BL-46

TR-13, BL-16 ● TR-14A

LM-

LM-21A, 21B ●



● LM-23

# LEGEND

LM-2 = LM85-2

BL-6 = BL86-6

BURNT LAKE RADIOACTIVE

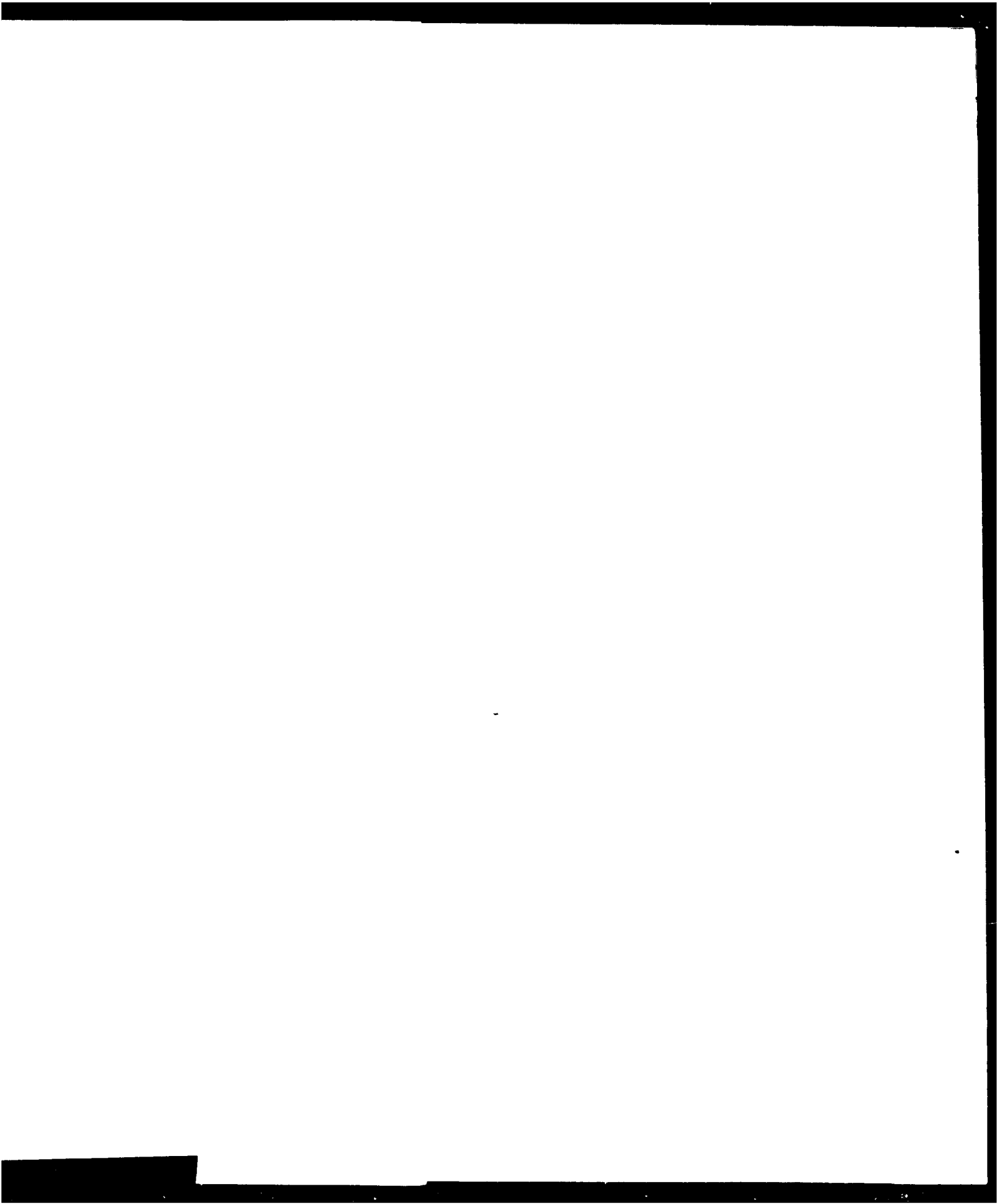


LEGEND

LM-2 = LM85-2

BL-6 = BL86-6

BURNT LAKE RADIOACTIVE ZONE





BL-3

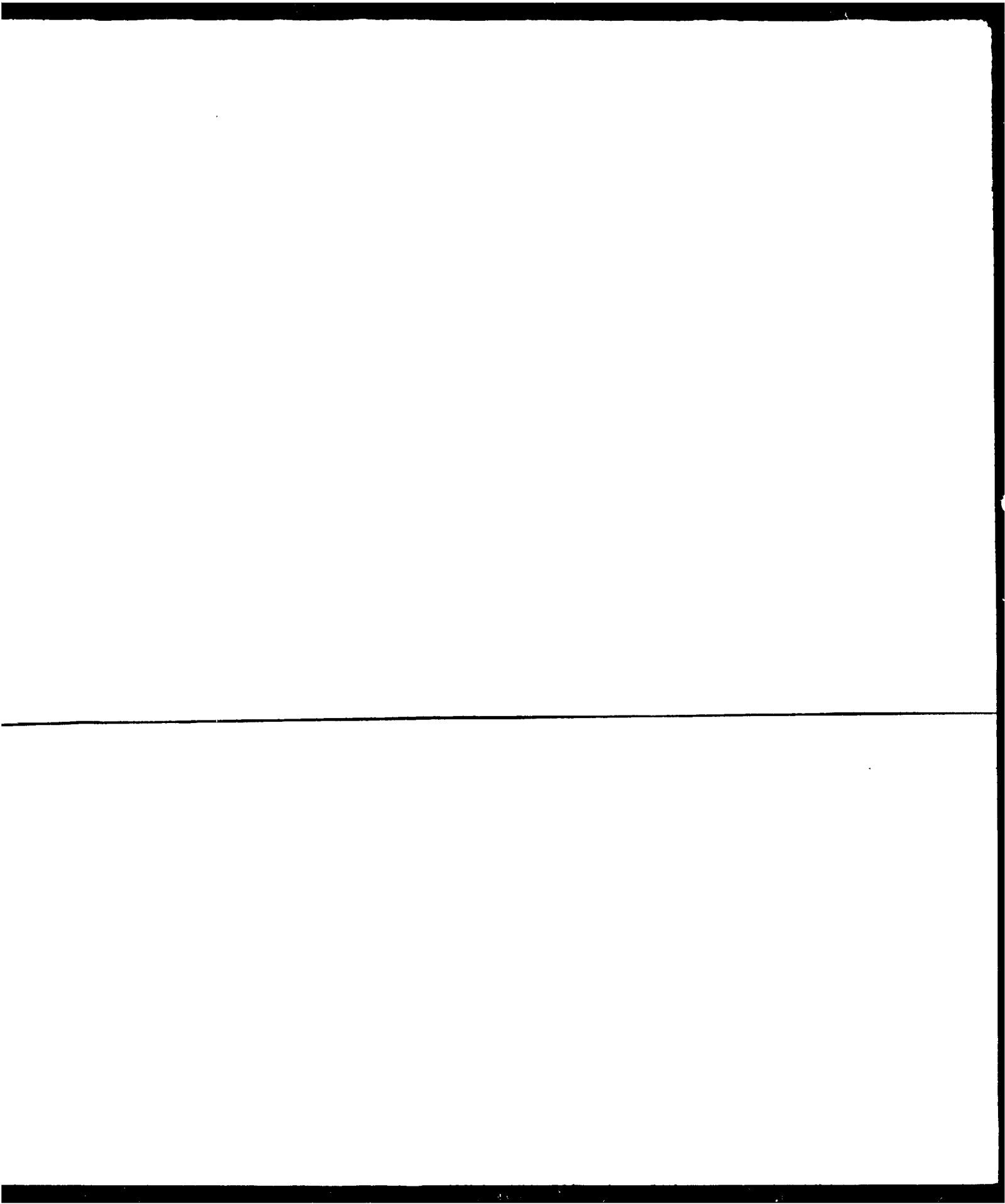


BL-25 ●

● TR-18A, BL-2A, 2B

● TR-17, BL1A, 1B, 1C

● BL-24





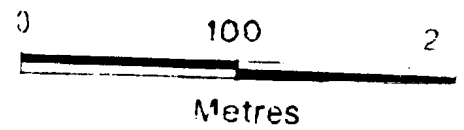
BURNT LAKE RADIOACTIVE

SAMPLE LOCATION MAP

SCALE: 1:3,000

DATE: APR 11

MAP 2B



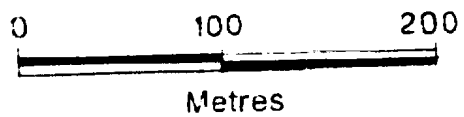
BURNT LAKE RADIOACTIVE ZONE

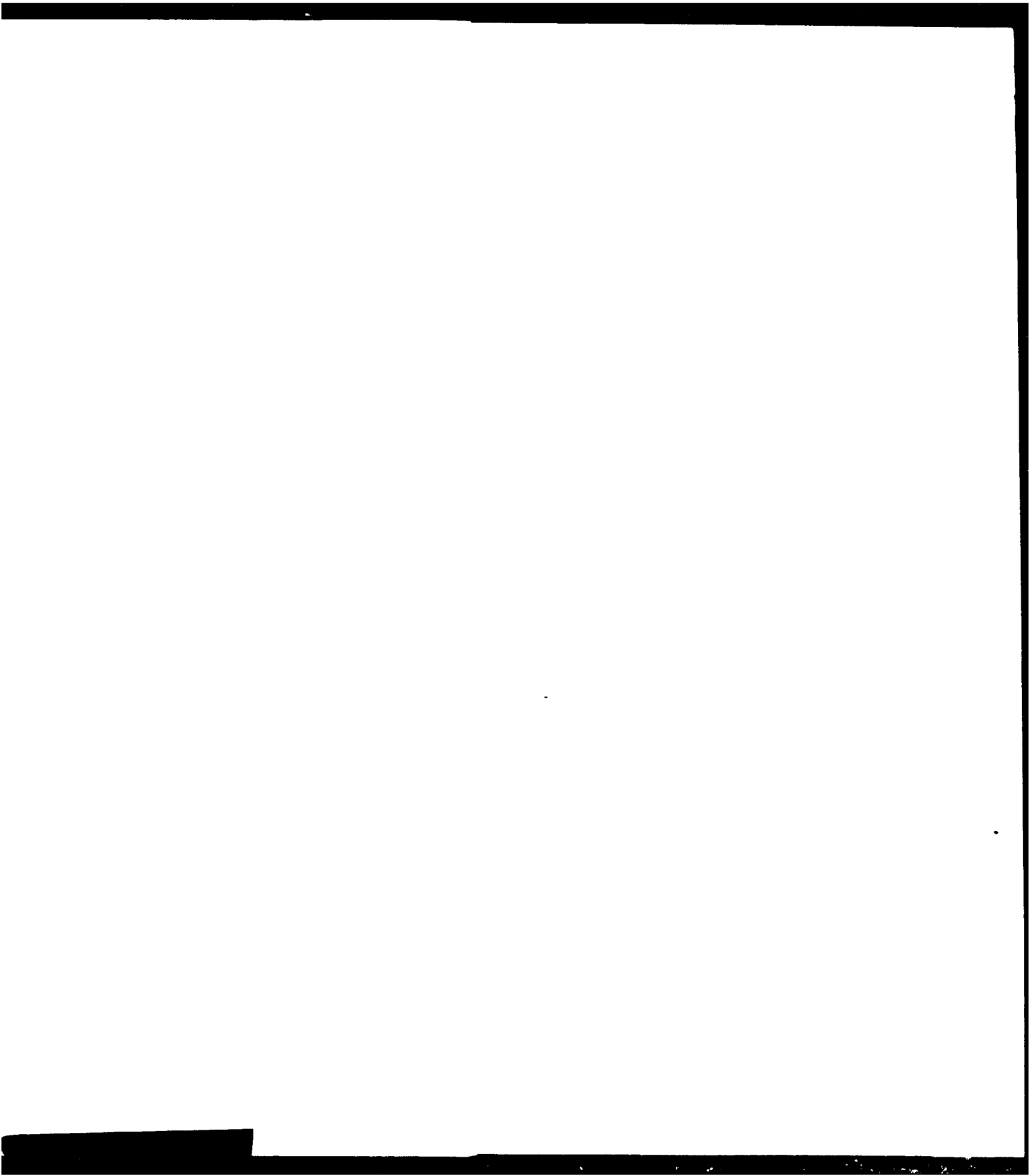
SAMPLE LOCATION MAP

SCALE: 1:3,000

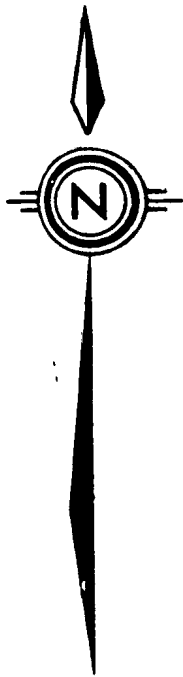
DATE: APRIL, 1991

MAP 2B

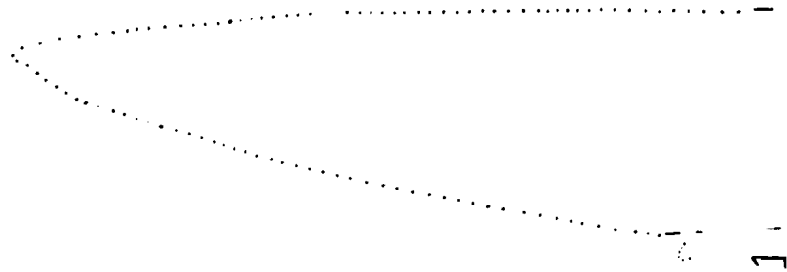


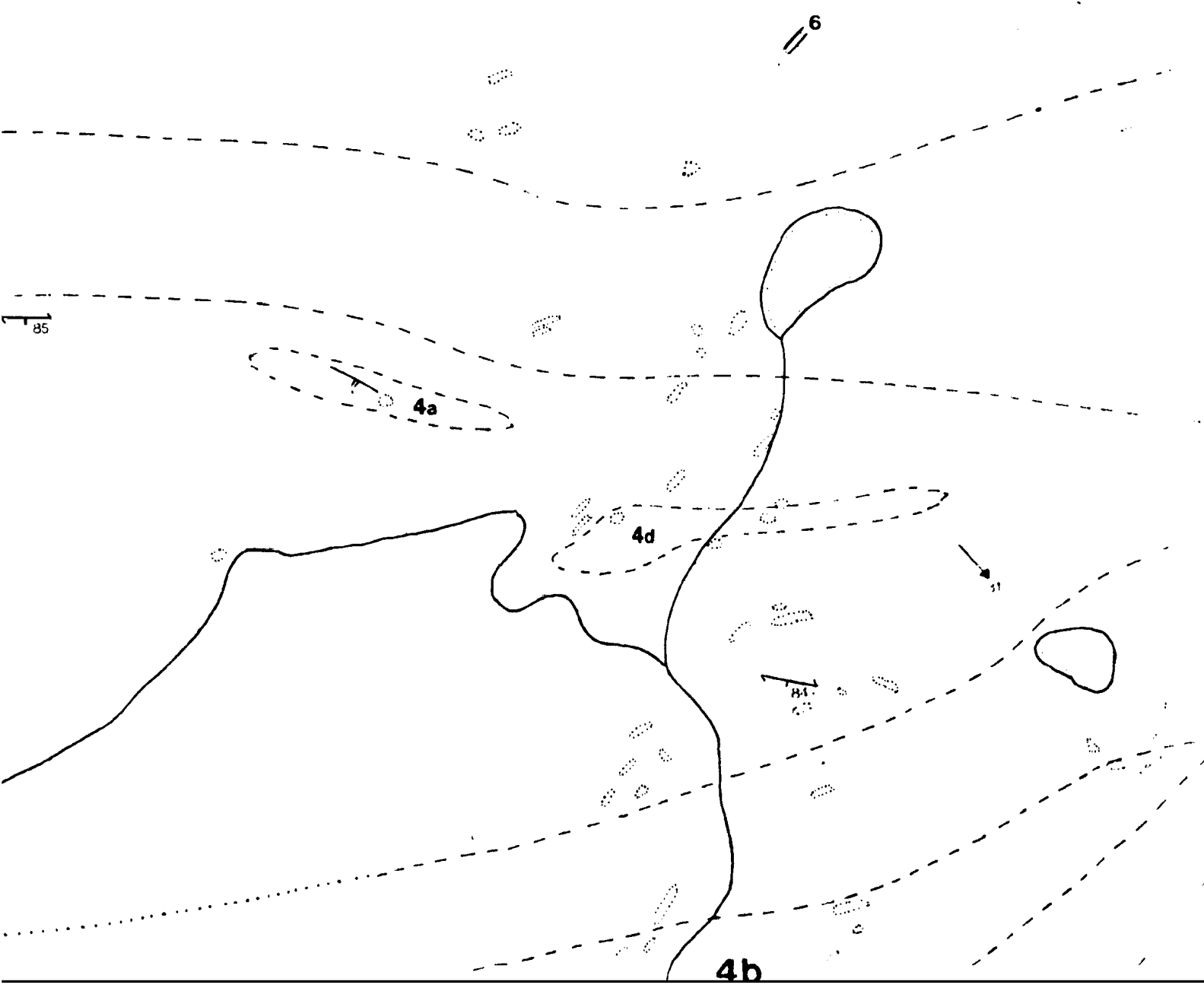


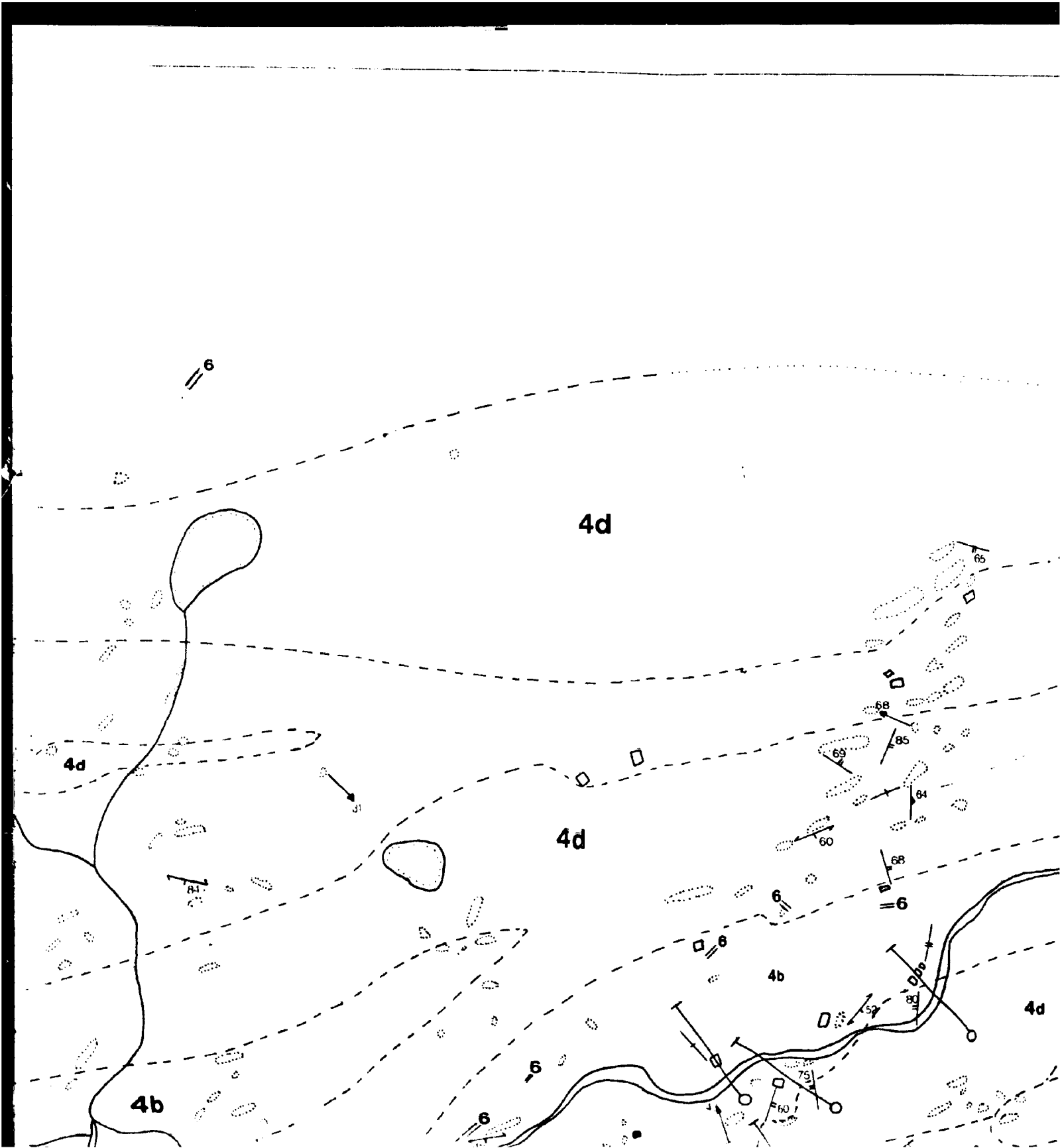




4b





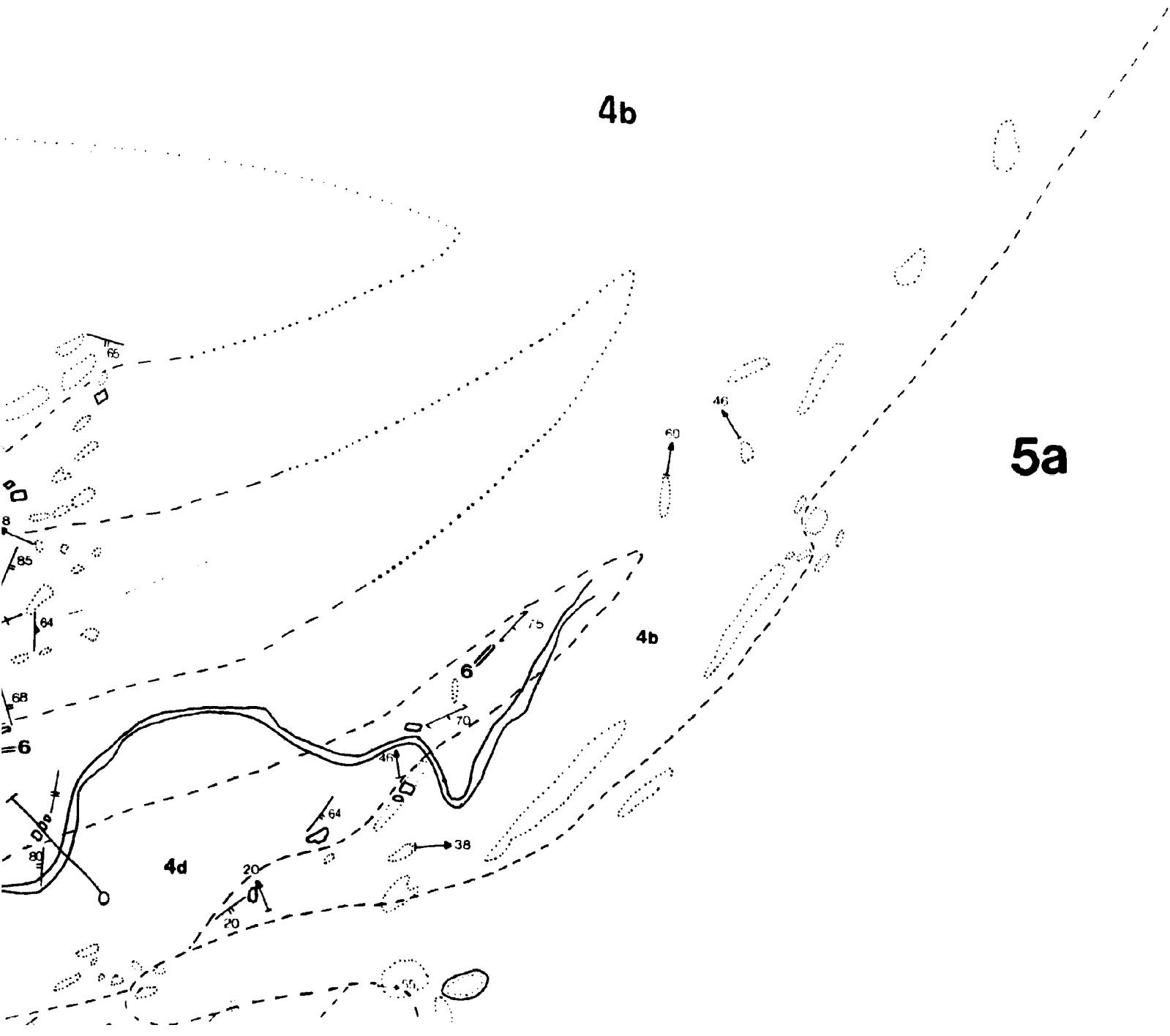


4b

5a

4b

4d



4b

5a

4c

4b

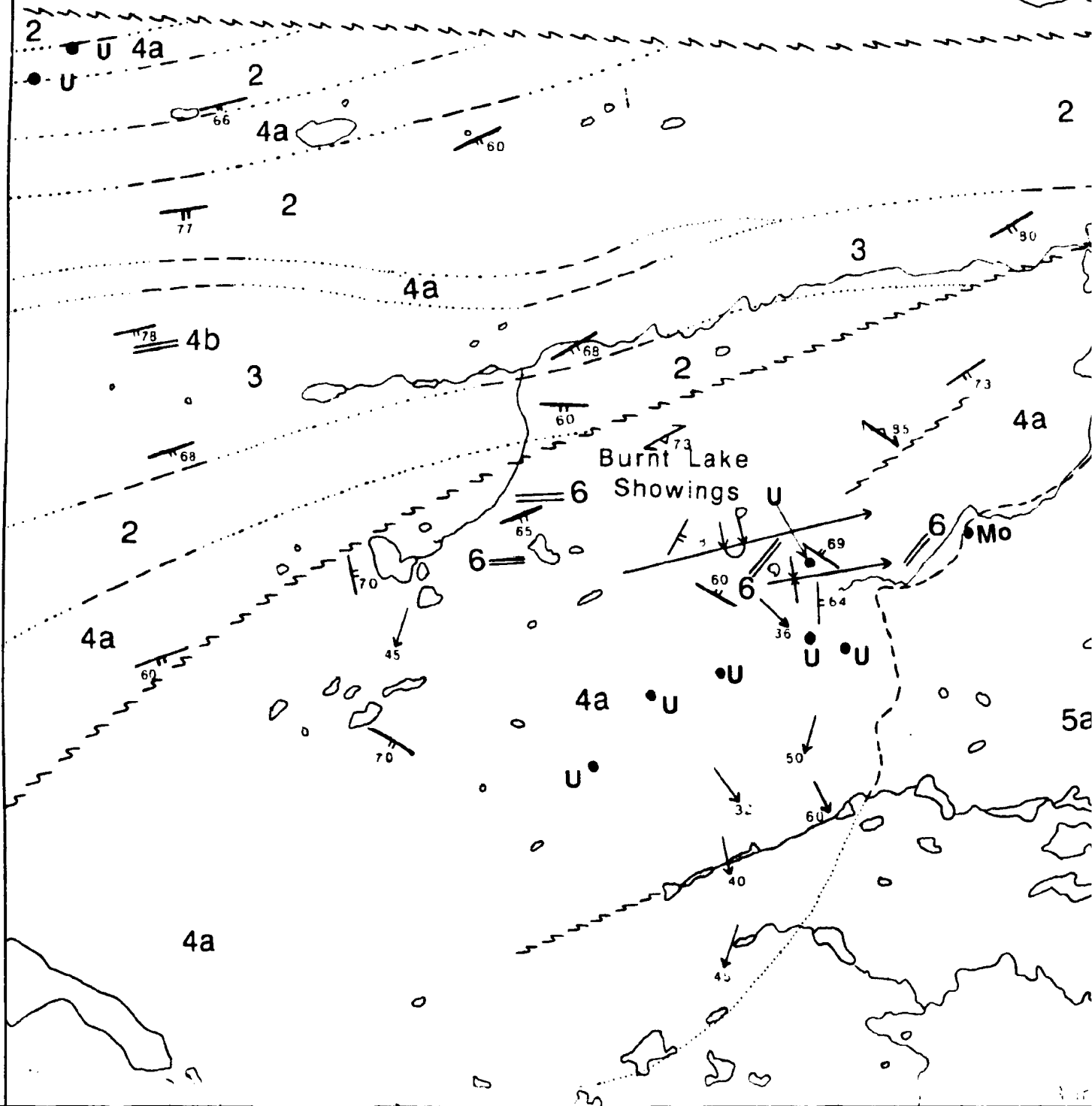


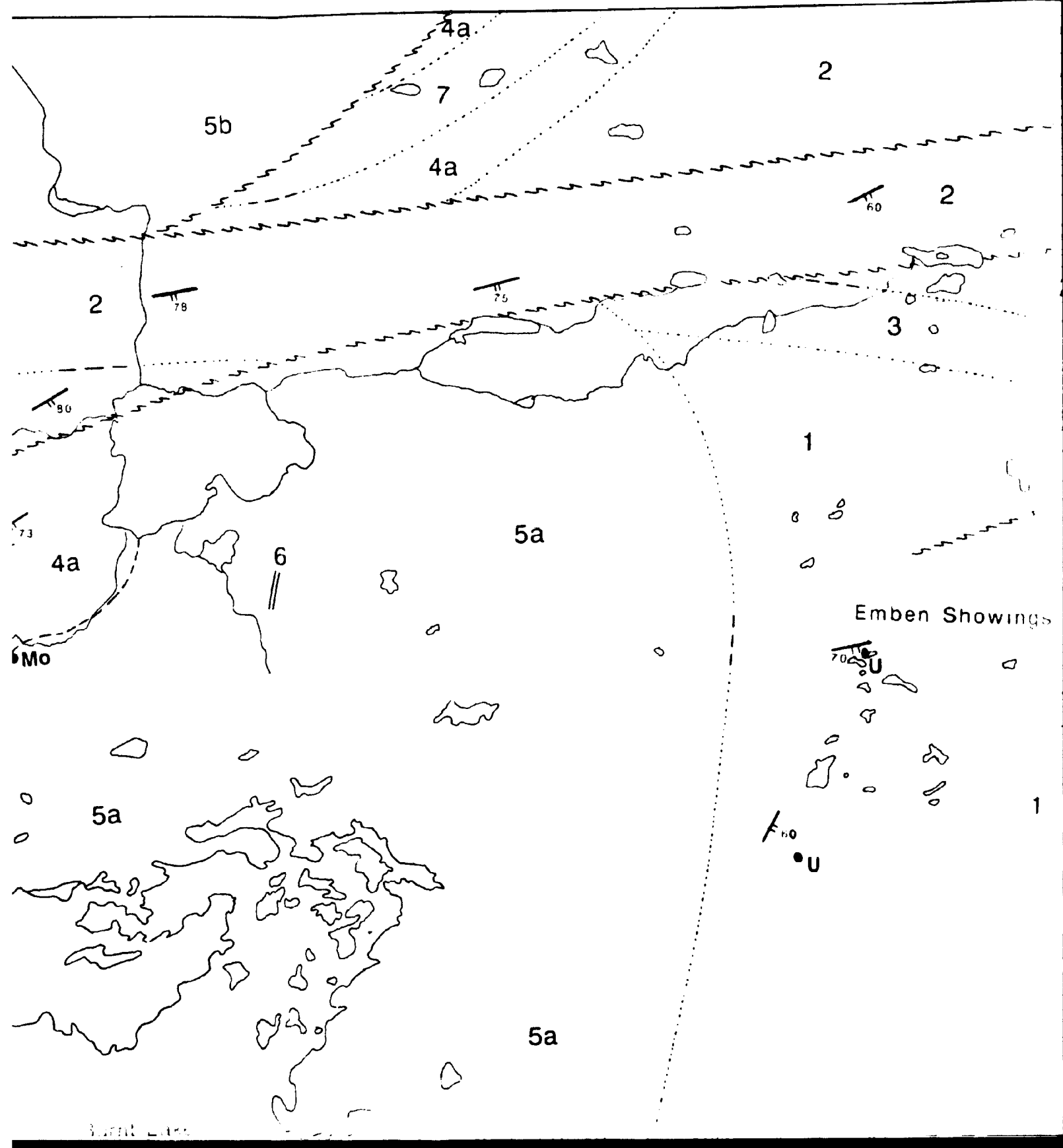
[REDACTED]

[REDACTED]

59° 46'  
54° 41'

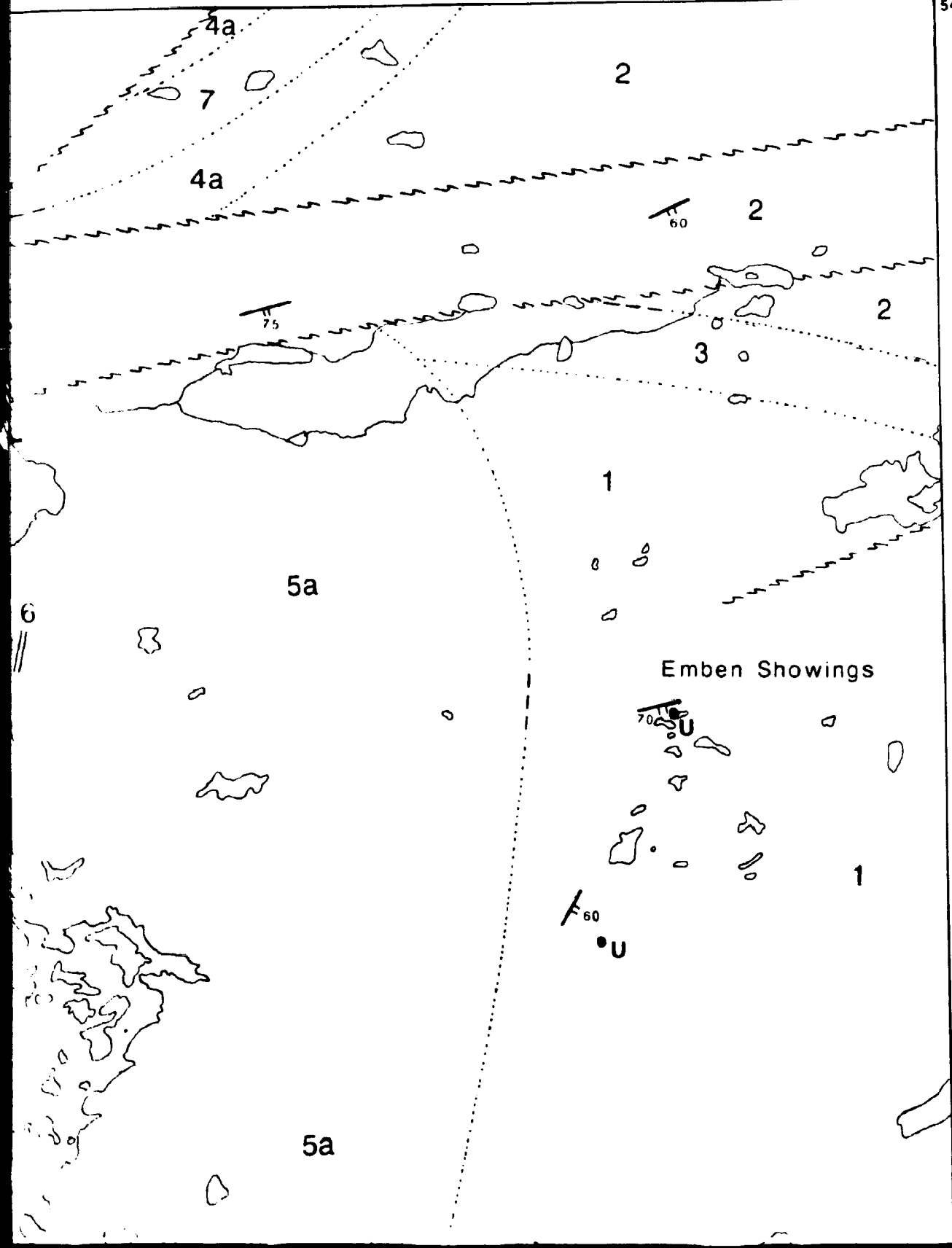
**Aurora River Showings**







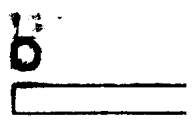
59° 35' 54° 41'



- 7** Michae Gal minor diab
- 6** Metadabas
- 5** 5a Medium and granite hornblende
- 4** 4a Pink to porphyries breccia m
- 3** Red to mar
- 2** Pink, grey minor rhyo
- 1** Pink to grey rhyolite

**Syncline**  
 Geologic boundary is  
 Fault (defined, approx)  
 Bedding (tops known)  
 Schistosity, cleavage  
 Lineation  
 Mineral occurrence

# **GEOLOGY (**



## Legend

Michae Gabbro medium to coarse grained gabbro  
minor diabase diorite

Metadiabase and metadiorite dykes

5a Medium to fine grained leucogranite quartz monzonite  
and granite 5b Medium to coarse grained pink  
hornblende biotite granite 5c Hornblende biotite granite

4a Pink to grey quartz-feldspar porphyries, minor  
porphyries, volcanoclastic felsic sandstone, pyroclastic  
breccia, minor lapilli tuff

Red to maroon volcanoclastic siltstone and sandstone

Pink, grey and green volcanoclastic siltstone sandstone  
minor rhyolite tuff and breccia

Pink to grey arkosic sandstone, minor massive porphyritic  
rhyolite

## Symbols

Syncline

Syncline (overturned)

gic boundary (approximate, assumed).....

(defined, approximate, assumed).....

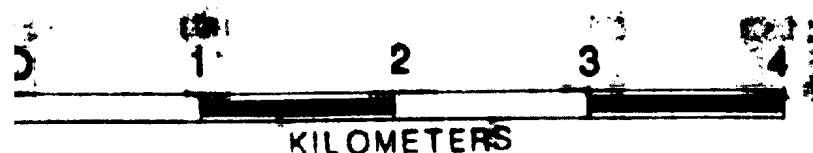
ng (tops known, tops unknown).....

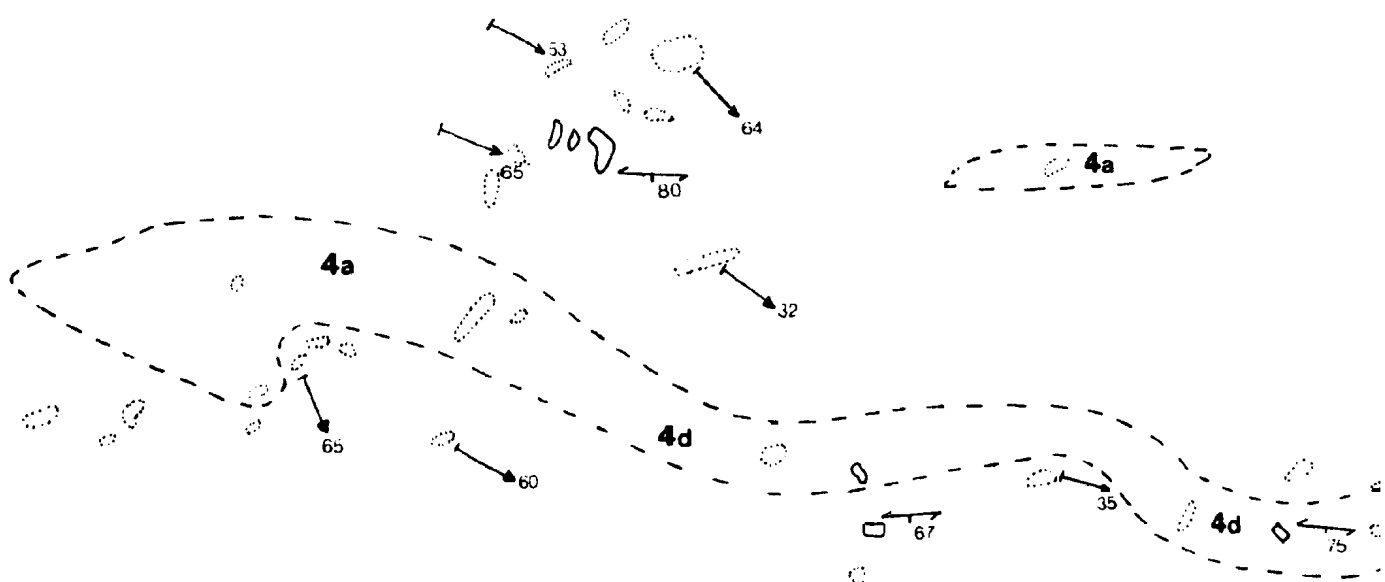
osity, cleavage (inclined, vertical).....

ion.....

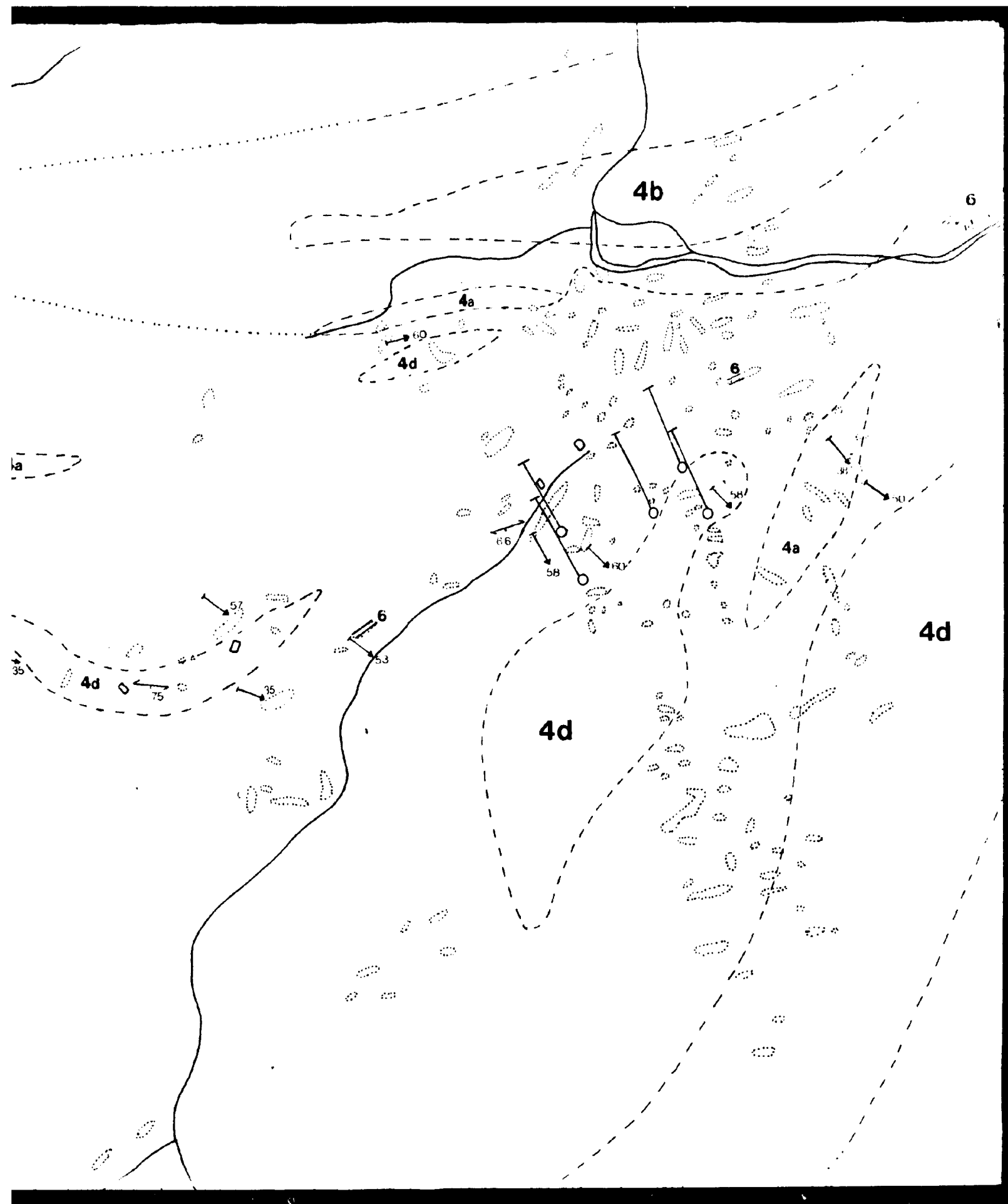
at occurrence.....

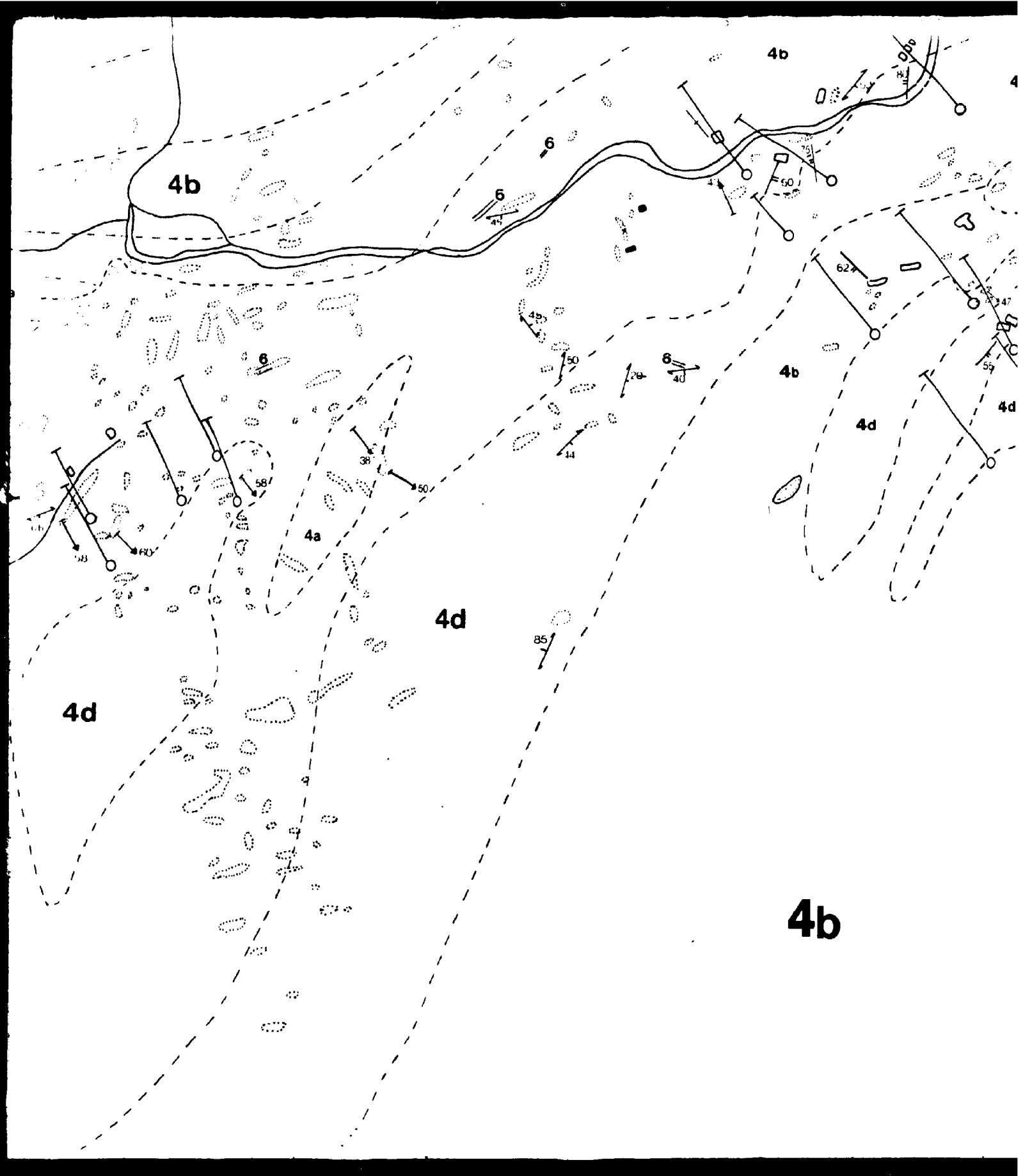
## GEOLOGY OF THE BURNT LAKE AREA, LABRADOR

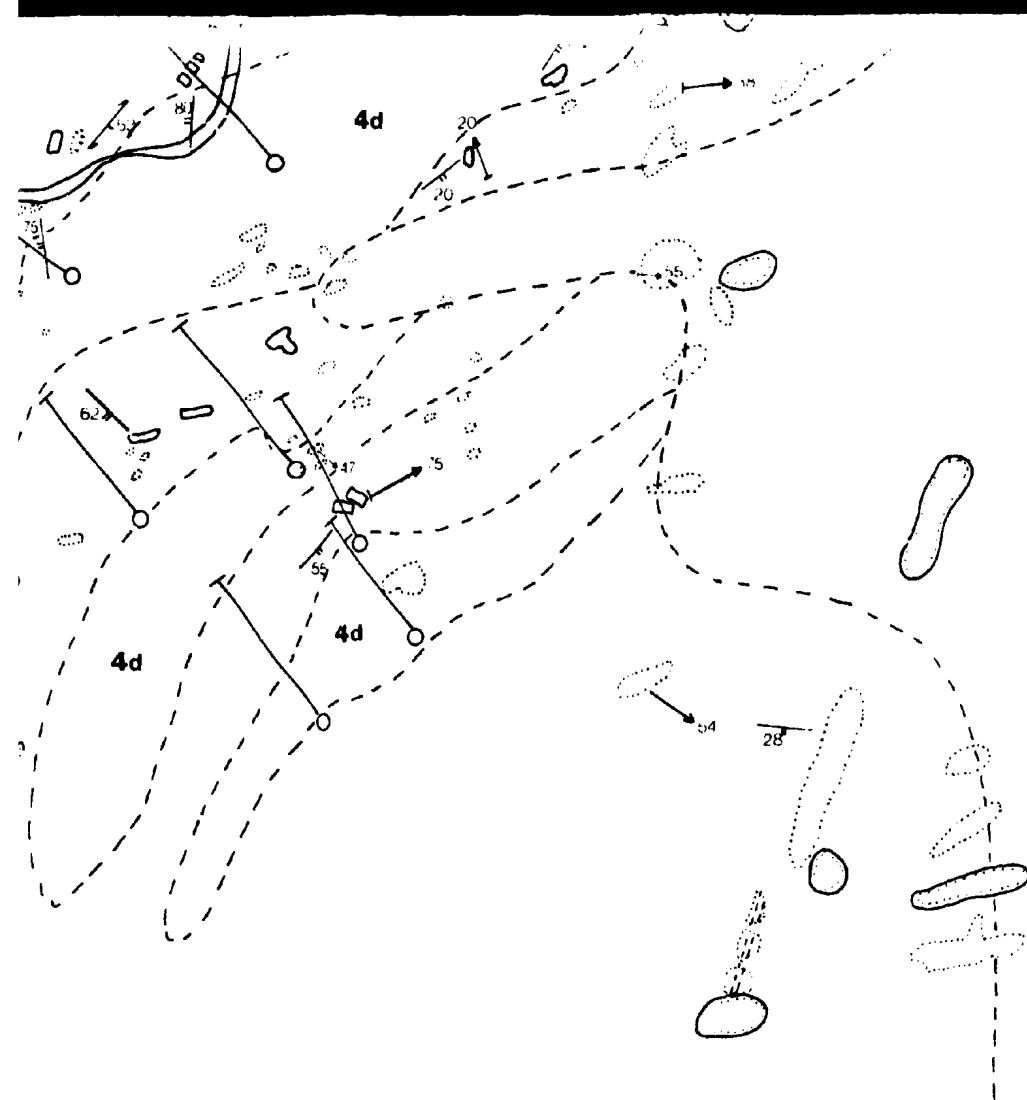




**4b**







**5a**

## LEGEND

### Helikian

- 6 - Metadiabase and Metadiorite Dykes
- 5 - Burnt Lake Granite

### Aphebian

#### Aillik group

- 4a - Felsic Ash Flow Tuff (banded)
- 4b - Felsic Crystal Tuff (includes Quartz porphyry and Quartz - Feldspar porphyry)
- 4c - Lapilli Tuff
- 4d - Feldspar Porphyry (with minor quartz)

### Mineral Occurrence

- U - uranium
- Py - pyrite
- Gn - galena
- Sp - sphalerite
- Mo - molybdenum
- Fl - fluorite
- peg - pegmatite



**5a**

**LEGEND**

**Helikian**

- 6 - Metadiabase and Metadiorite Dykes
- 5 - Burnt Lake Granite

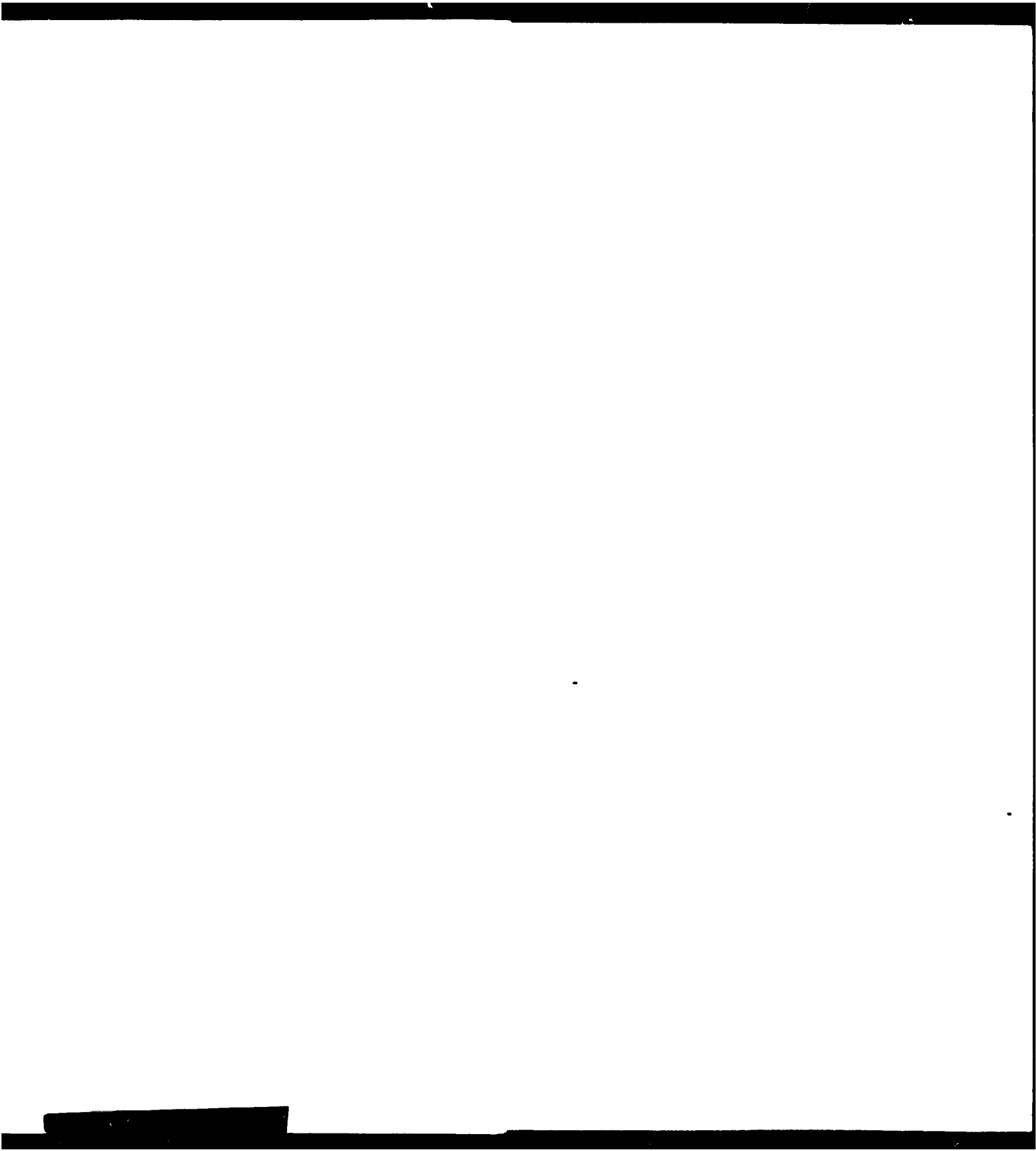
**Aphebian**

**Aillik group**

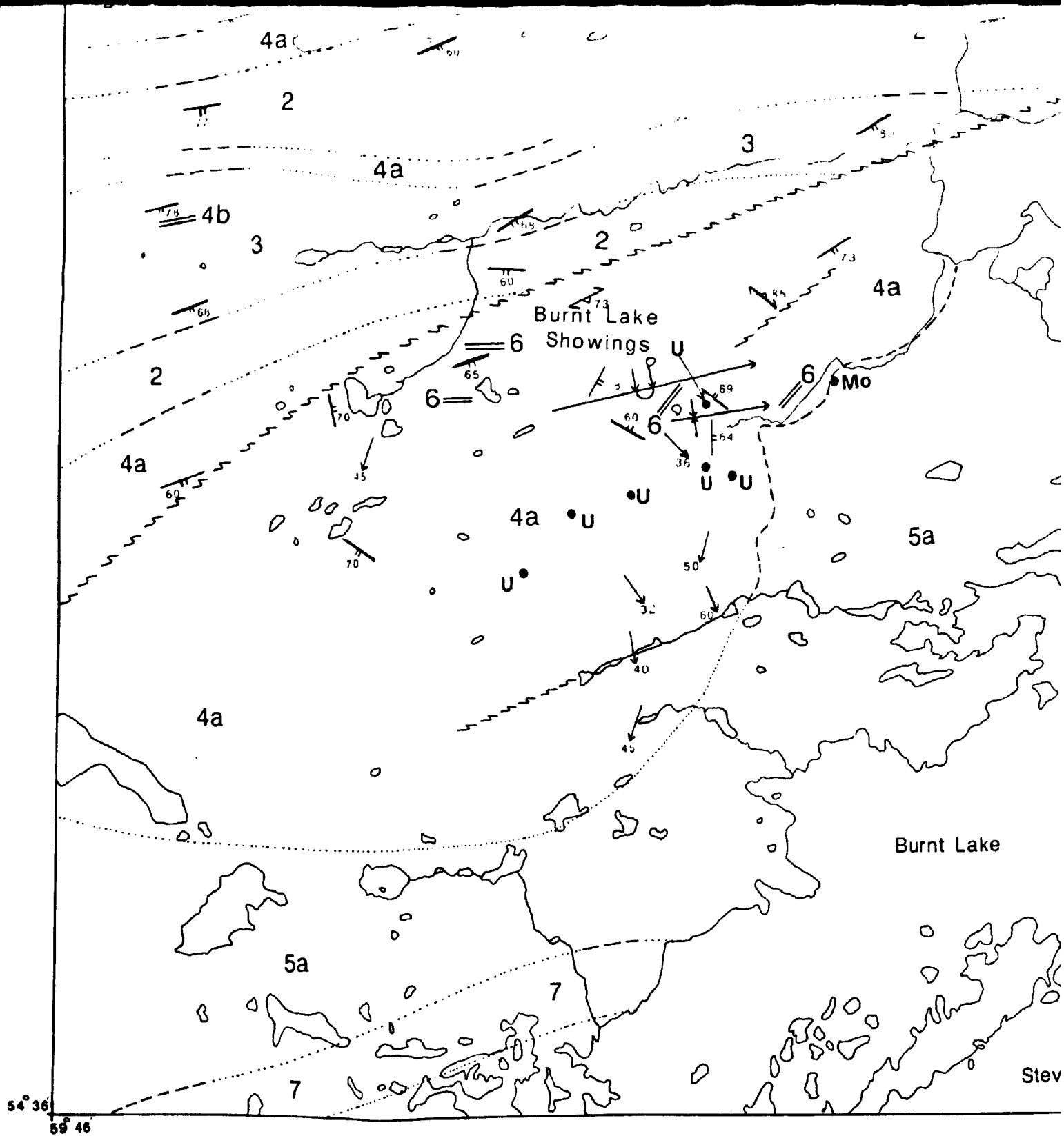
- 4a - Felsic Ash Flow Tuff (banded)
- 4b - Felsic Crystal Tuff (includes Quartz porphyry - and Quartz - Feldspar porphyry)
- 4c - Lapilli Tuff
- 4d - Feldspar Porphyry (with minor quartz)

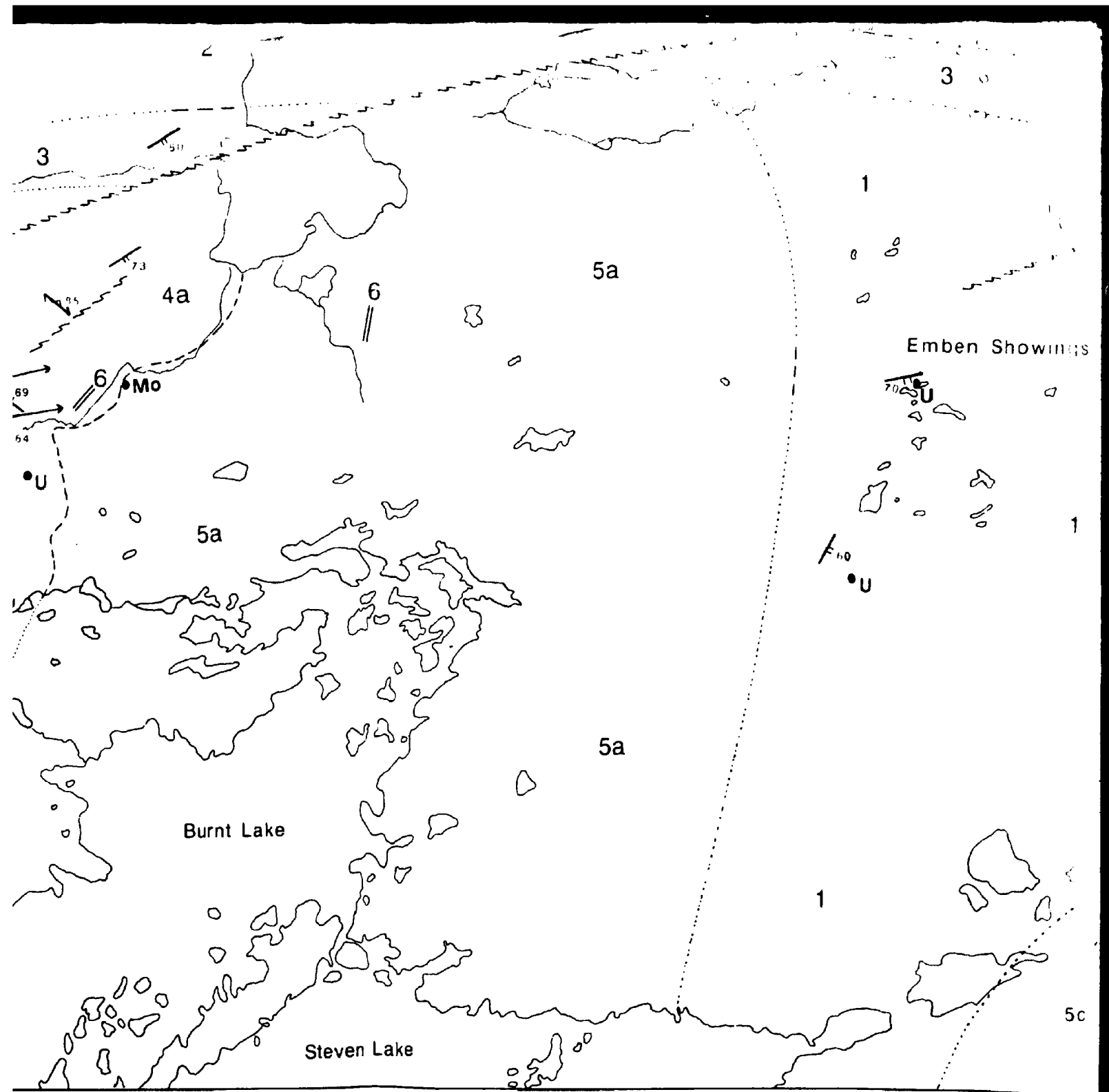
**Mineral Occurrence**

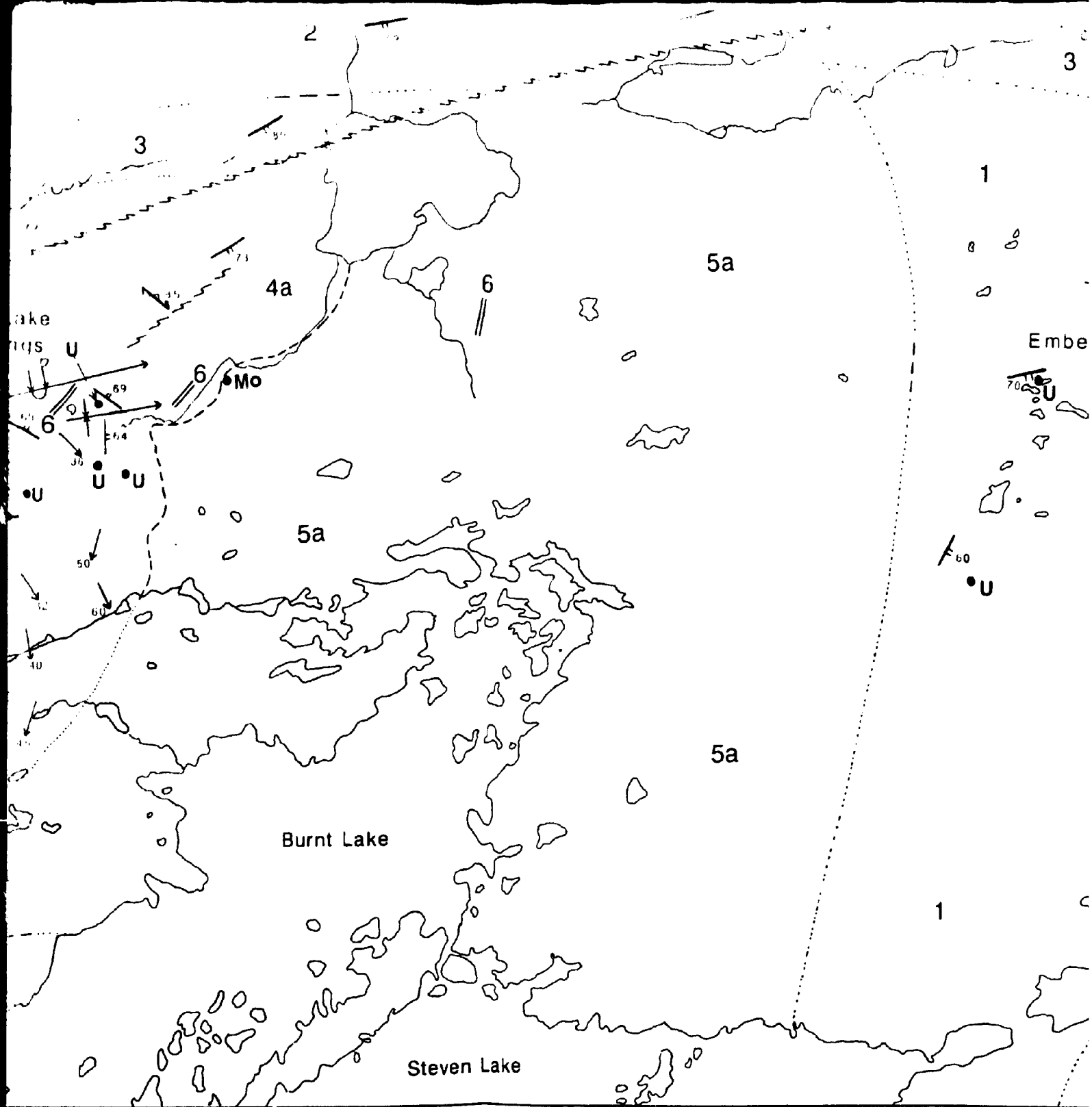
- U - uranium
- Py - pyrite
- Gn - galena
- Sp - sphalerite
- Mo - molybdenum
- Fl - fluorite
- peg - pegmatite

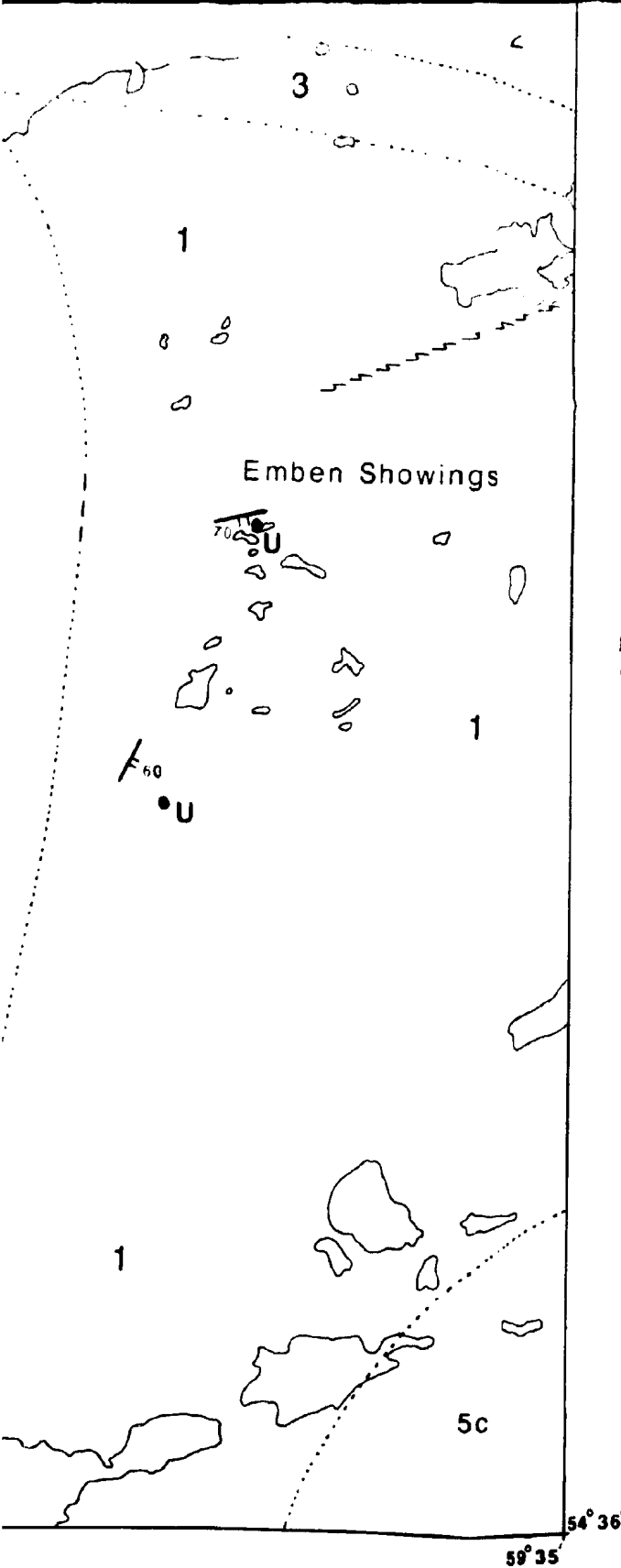






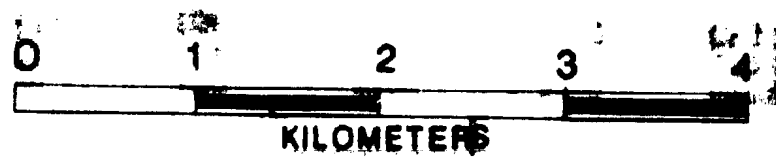






- 6** Metatuff and metatuffite type
- 5** 5a Medium to fine grained leucogranite quartz monzonite and granite. 5b Medium to coarse grained pink hornblende-biotite granite. 5c Hornblende-biotite granite.
- 4** 4a Pink to grey quartz-feldspar porphyries, minor amphiboles, volcaniclastic siltstone sandstone, breccia, minor apophyllite.
- 3** Red to maroon volcaniclastic siltstone and sandstone.
- 2** Pink, grey and green volcaniclastic siltstone sandstone, minor rhyolite tuff and breccia.
- 1** Pink to grey arkosic sandstone, minor massive porphyritic rhyolite.
- Symbols**
- Syncline      Syncline (overturned)
- Geologic boundary (approximate, assumed) .....
- Fault (defined, approximate, assumed) .....
- Bedding (tops known, tops unknown) .....
- Schistosity, cleavage (inclined, vertical) .....
- Lineation .....
- Mineral occurrence .....

# GEOLOGY OF THE BURNT LAKE AREA, LABRADOR



L.M. MacKenzie

Map 1

March 1986

4b

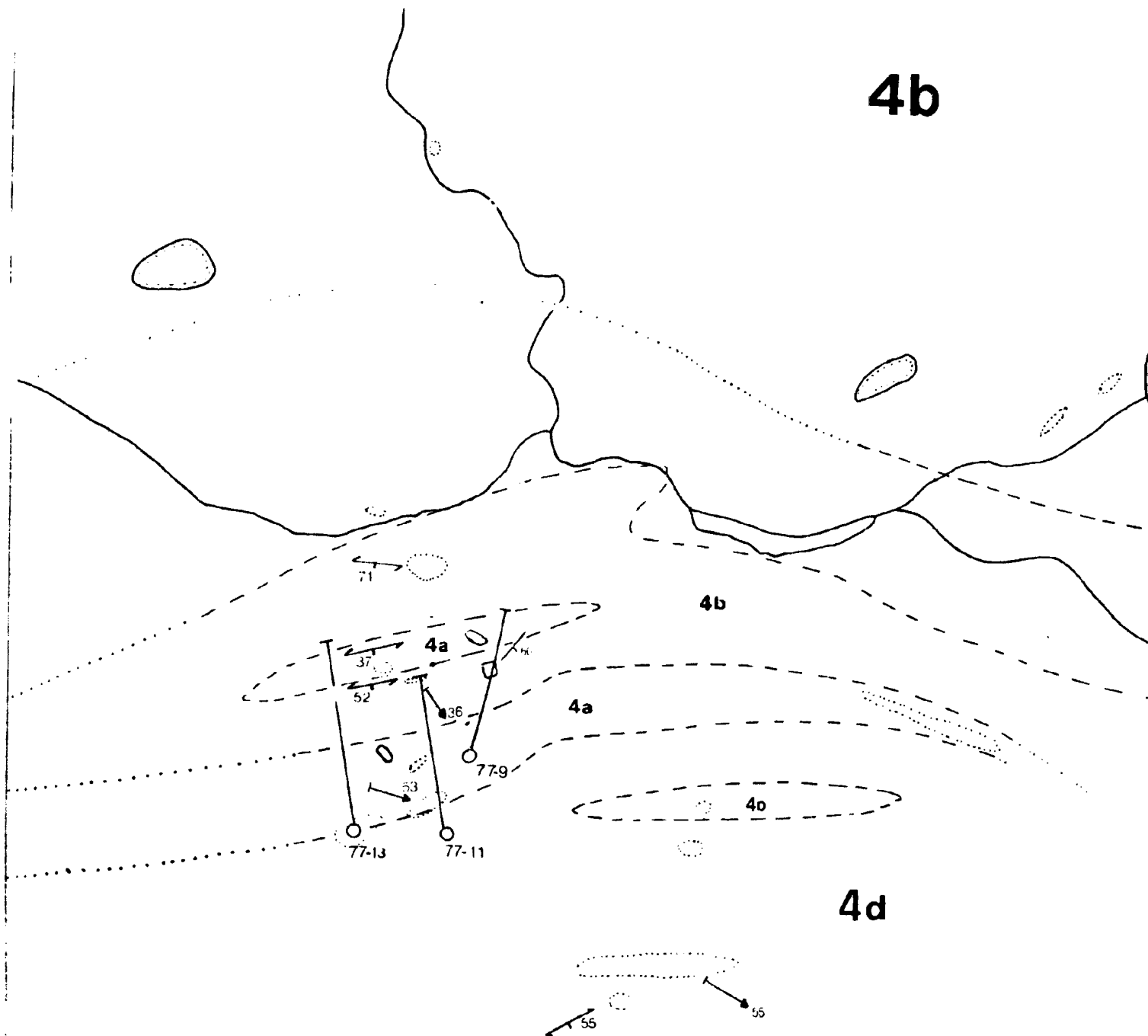
4b

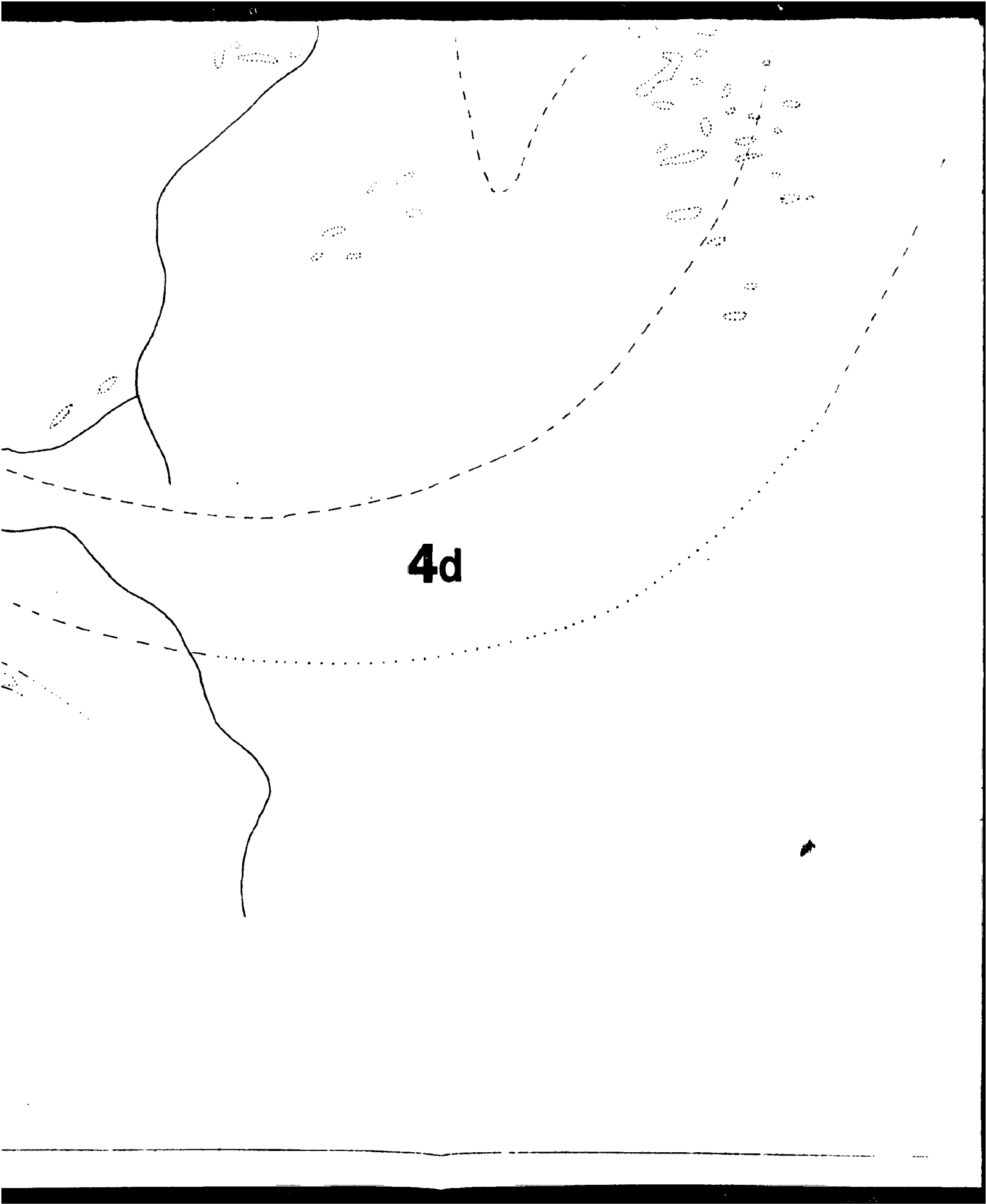
4a

4a

4b

4d





4b

d



Helikian

- 6 - Metadiabase and Metadiorite Dykes
- 5 - Burnt Lake Granite

Aphebian














Aillik group

- 4a - Felsic Ash Flow Tuff (banded)
- 4b - Felsic Crystal Tuff (includes Quartz porphyry and Quartz - Feldspar porphyry)
- 4c - Lapilli Tuff
- 4d - Feldspar Porphyry (with minor quartz)

Mineral Occurrence

- U - uranium
- Py - pyrite
- Gn - galena
- Sp - sphalerite
- Mo - molybdenum
- Fl - fluorite
- peg - pegmatite

Symbols

-  Fault (approximate, assumed)
-  Outcrop
-  Geological Contact (approximate)
-  Bedding and Banding
-  Schistosity
-  Lineation
-  Synform, Antiform Axial Tension
-  Diamond Drill Hole
-  Trench
-  Pond
-  Stream
-  Camp Building
-  Sample Location

Geology and Mineral Occurrence  
of the Burnt Lake Radioactive  
Showings

Drawn by: LMK

Date

Scale: 1:3000

Map



#### Helikian

- 6 - Metadiabase and Metadiorite Dykes
- 5 - Burnt Lake Granite

#### Aphebian

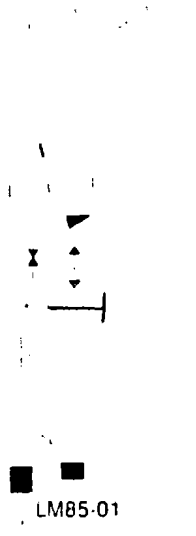
#### Aillik group

- 4a - Felsic Ash Flow Tuff (banded)
- 4b - Felsic Crystal Tuff (includes Quartz porphyry - and Quartz - Feldspar porphyry)
- 4c - Lapilli Tuff
- 4d - Feldspar Porphyry (with minor quartz)

#### Mineral Occurrence

- U - uranium
- Py - pyrite
- Gn - galena
- Sp - sphalerite
- Mo - molybdenum
- Fl - fluorite
- peg - pegmatite

#### Symbols

- 
- Fault (approximate, assumed)
  - Outcrop
  - Geological Contact (approximate, assumed)
  - Bedding and Banding
  - Schistosity
  - Lineation
  - Synform, Antiform Axial Trace
  - Diamond Drill Hole
  - Trench
  - Pond
  - Stream
  - Camp Building
  - Sample Location
- LM85-01

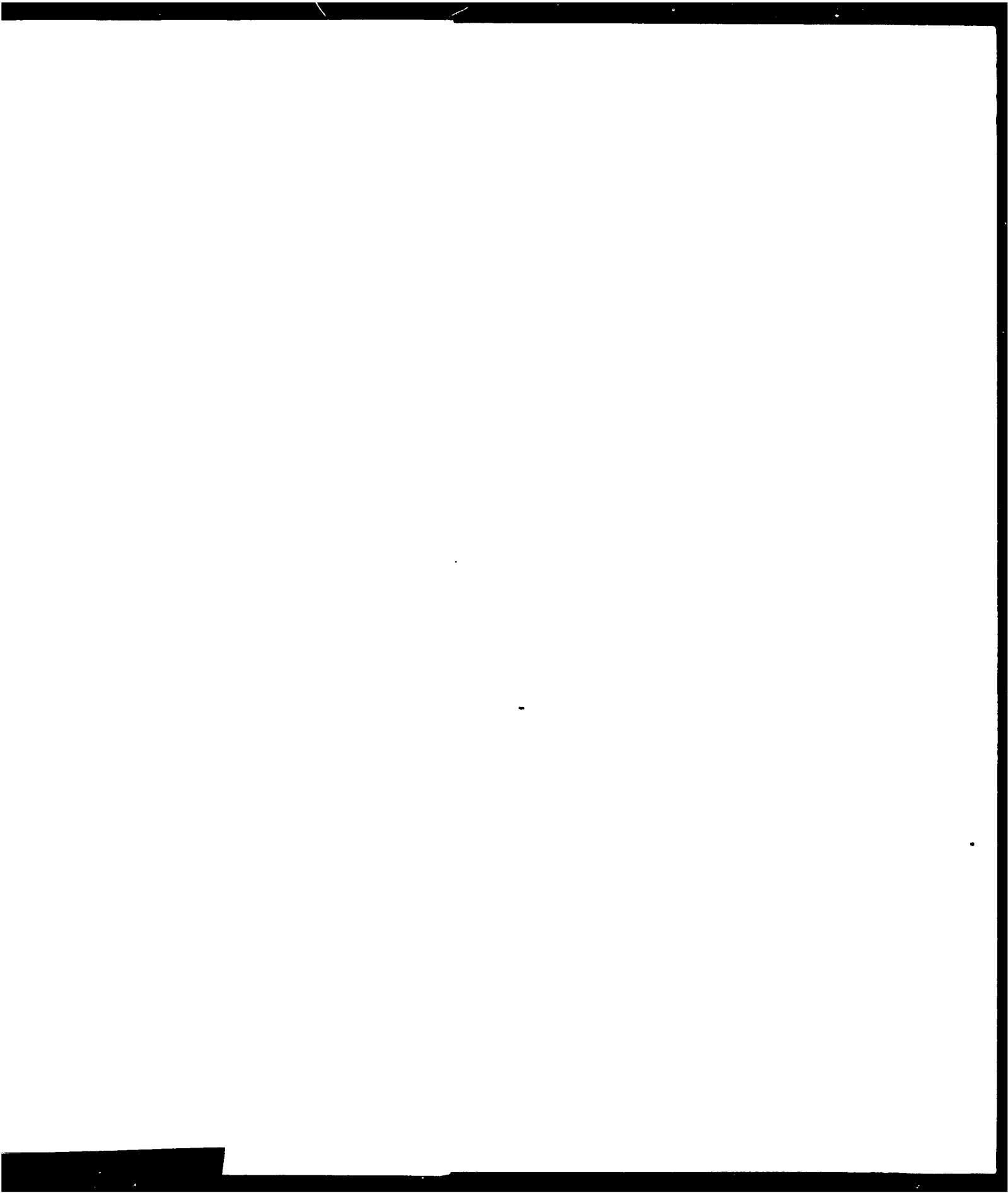
## Geology and Mineral Occurrences of the Burnt Lake Radioactive Showings

Drawn by: LMK

Date: April, 1990

Scale: 1:3000

Map: 2



MCLEAN LAKE

AR

BL36

134

133

135

132 131

130 129

128

127

126

125

124

123

155

BL35

BL37

BL40

BL38

BL39

136

137

138

118

139

117

116

119

140

115

114

113

112

110

109

108

107

106

105

104

103

102

101

100

99

98

97

96

95

94

93

92

91

90

89

88

87

86

85

84

83

82

81

80

79

78

77

76

75

74

73

72

71

70

69

68

67

66

65

64

63

62

61

60

59

58

57

56

55

54

53

52

51

50

49

48

47

46

45

44

43

42

41

40

39

38

37

36

35

34

33

32

31

30

29

28

27

26

25

24

23

22

21

20

19

18

17

16

15

14

13

12

11

10

9

8

7

6

5

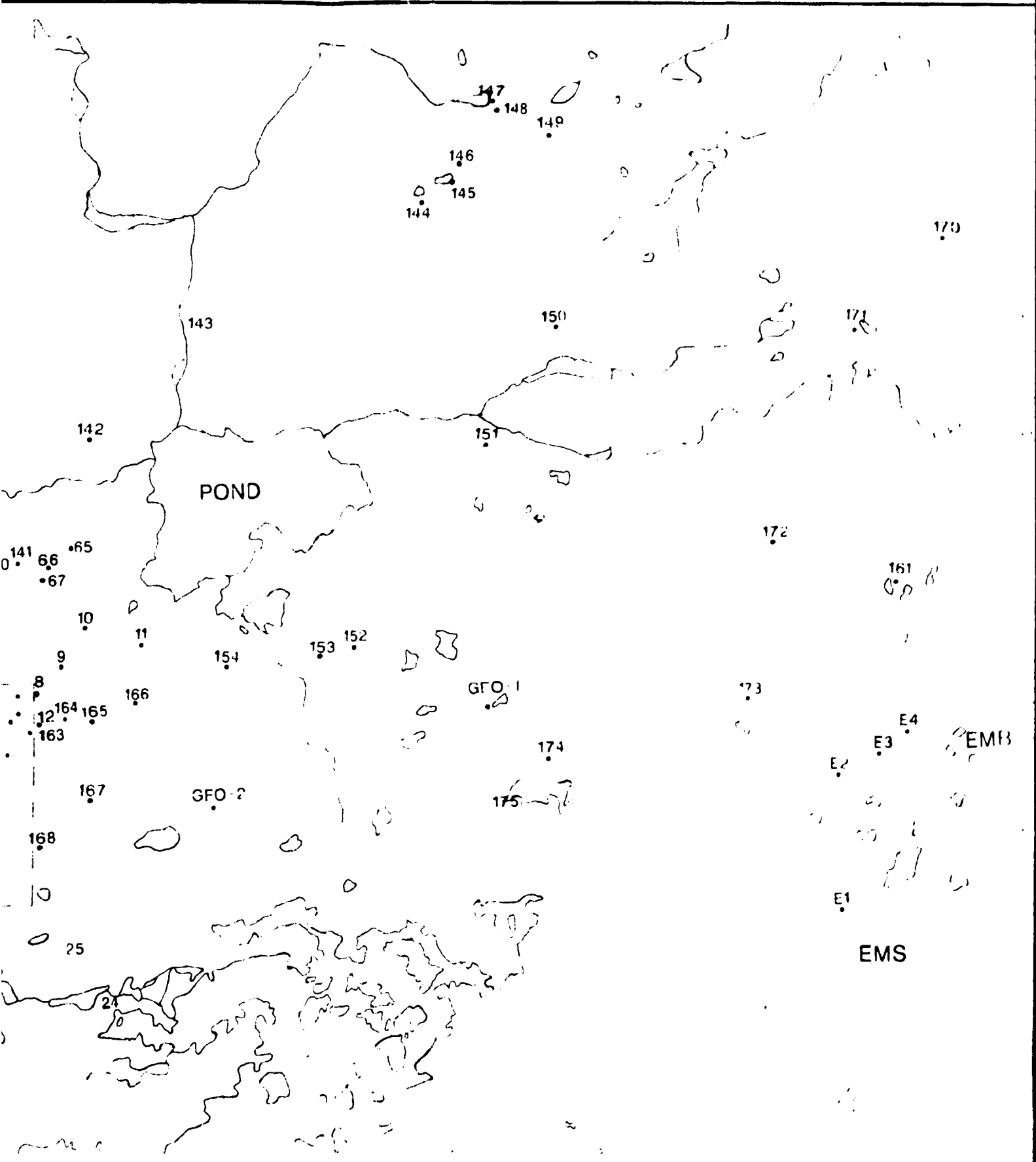
4

3

2

1

MAP 2B



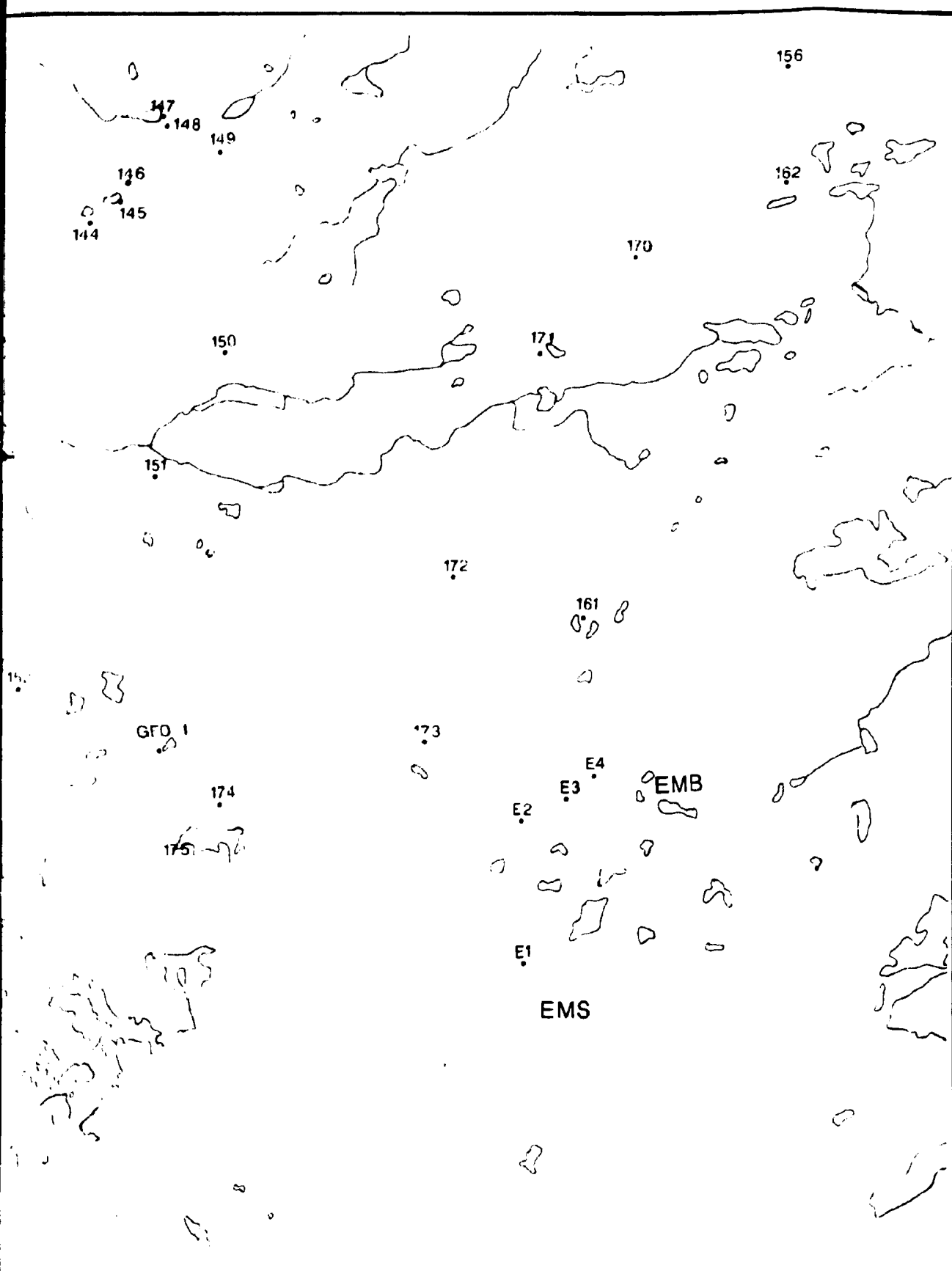
POND

GFO-1

GFO-2

EMS

EMB



# LEGE

- 181 = LM
- BL43 =
- E2 = LM
- TR7 = L
- EMB = E
- EMS = E
- AR = /

BUF

CENTR

## LEGEND

181 = LM85-181

BL43 = BL86-43

E2 = LM85-E2

TR7 = LM85-TR7

EMB = EMBEN MAIN

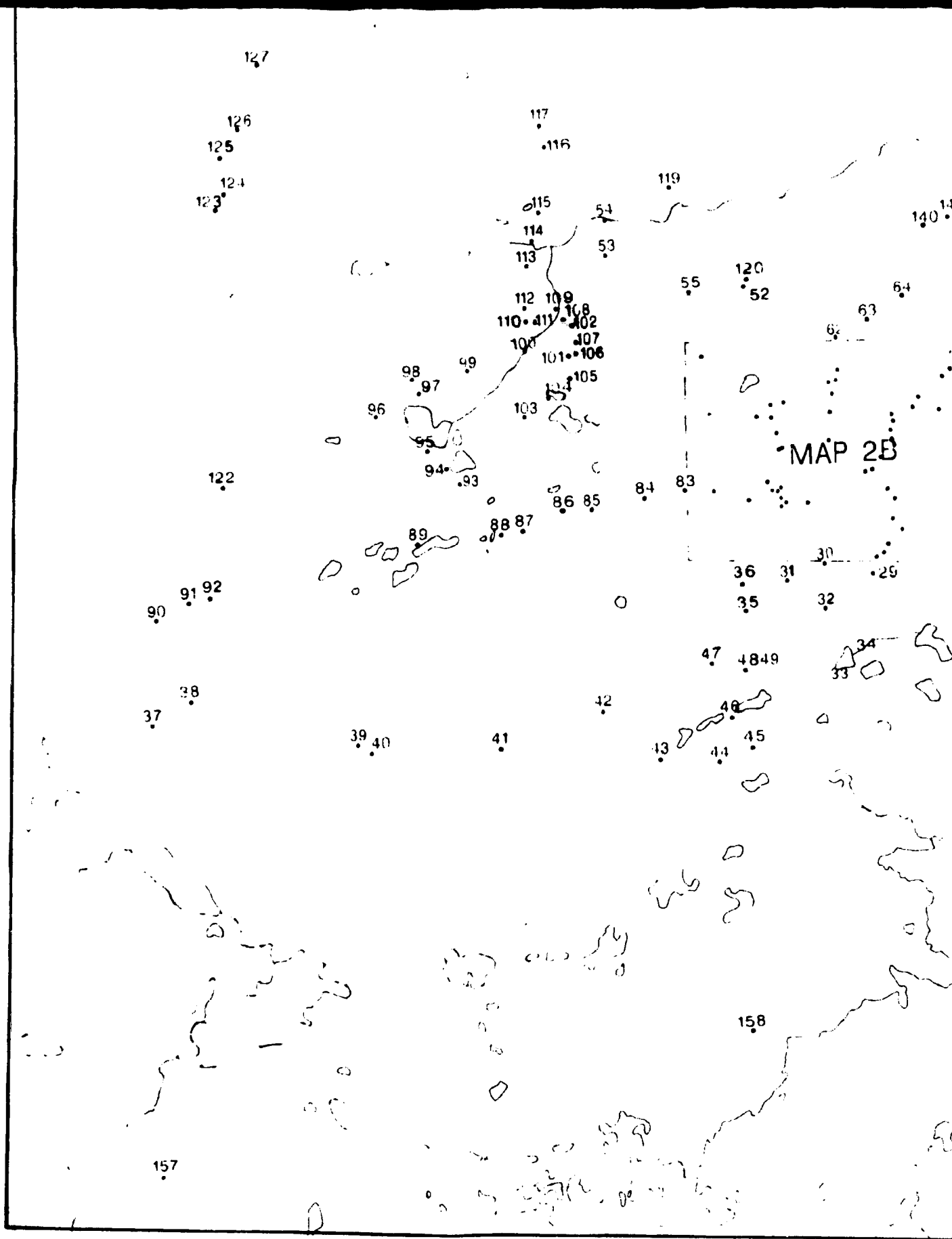
EMS = EMBEN SOUTH

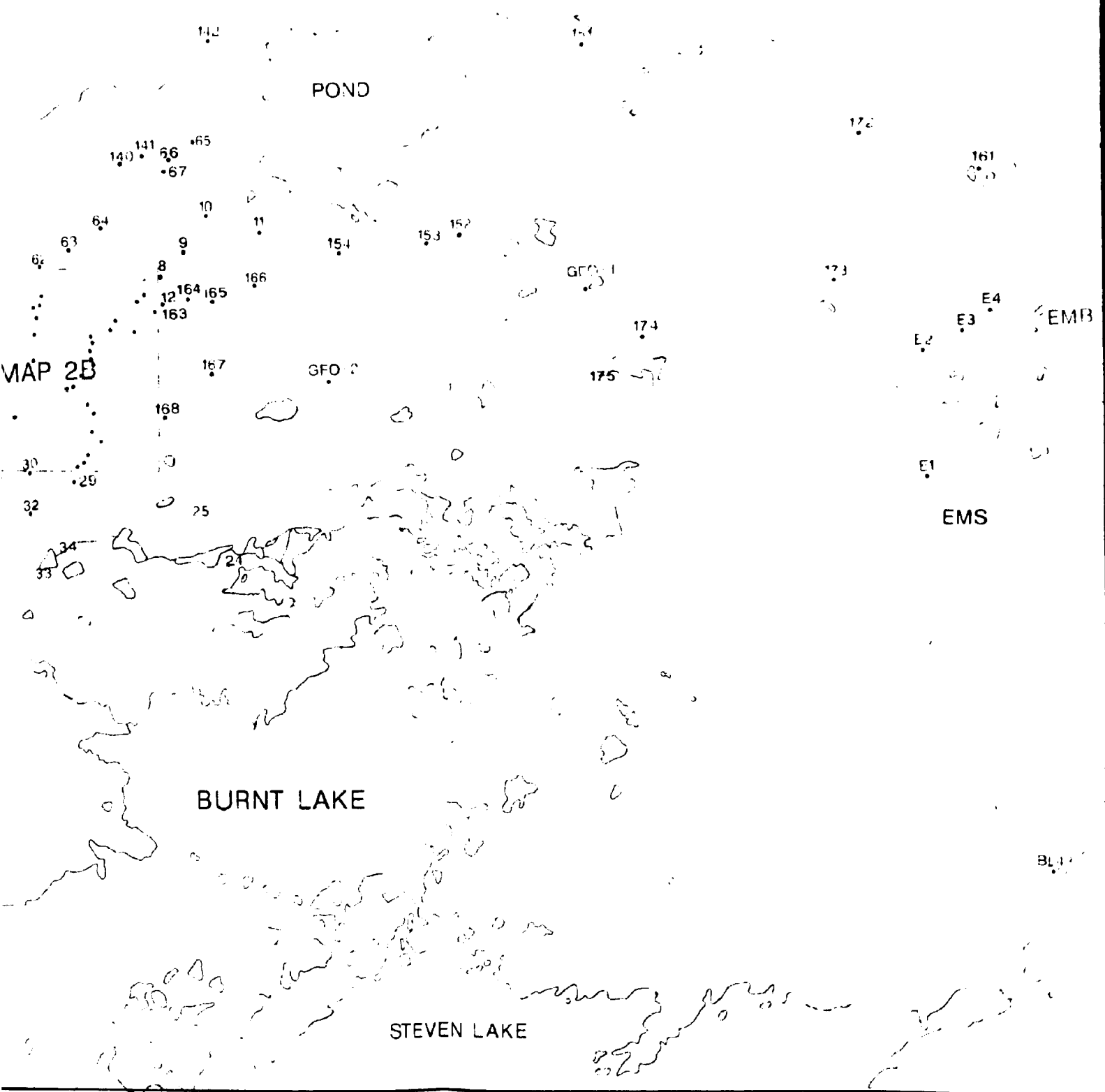
AR = AURORA RIVER

BURNT LAKE AREA

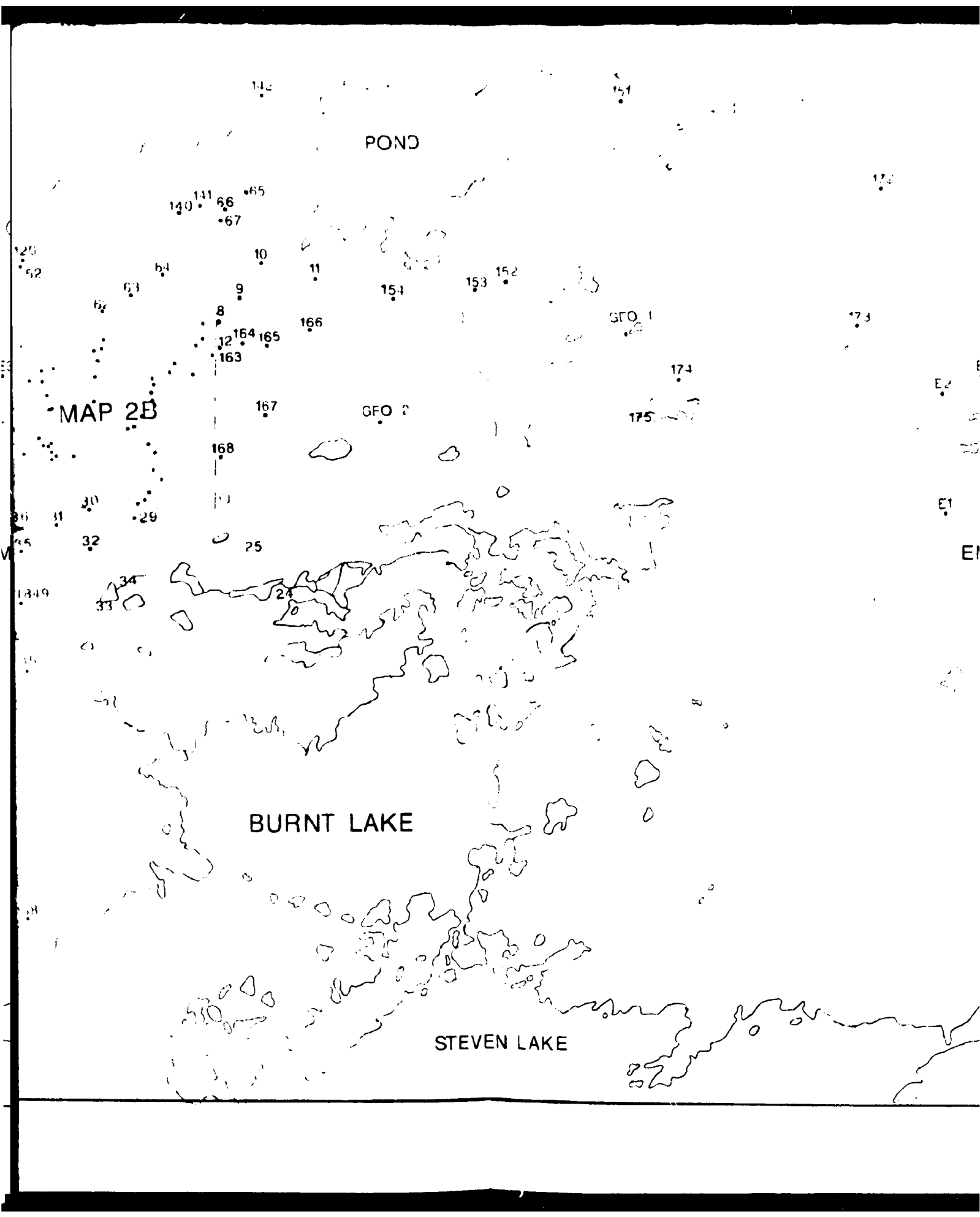
CENTRAL MINERAL BELT

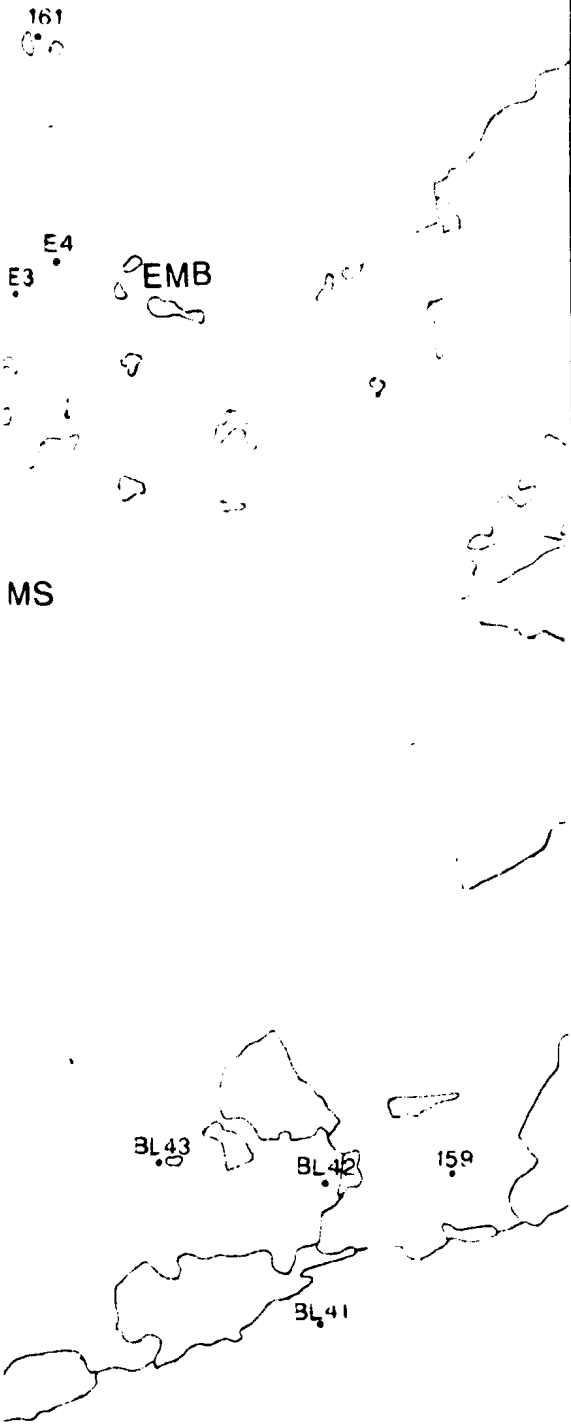
LABRADOR











## LEGEND

181 LM85-181

BL43 - BL86-43

E2 = LM85-E2

TR7 = LM85-TR7

EMB = EMBEN MAIN

EMS = EMBEN SOUTH

AR = AURORA RIVER

BURNT LAKE AREA  
CENTRAL MINERAL BELT  
LABRADOR

SAMPLE LOCATION MAP

SCALE: 1:30,000

DATE: APRIL, 1991

MAP 1B



